Polyphase Induction Motors

Analysis, Design, and Application

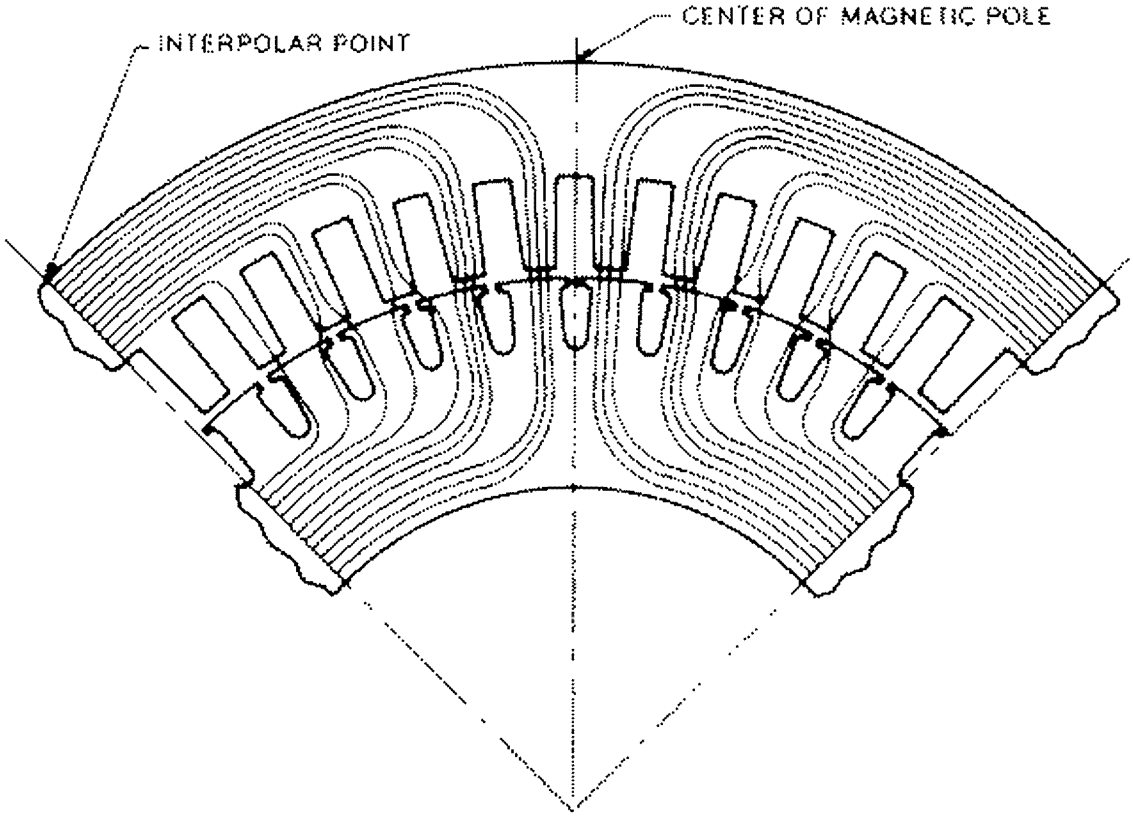
INTERPOLAR POINT
CENTER OF MAGNETIC POLE

Paul L. Cochran

CRC Press
Taylor & Francis Group

Polyphase Induction Motors

ELECTRICAL ENGINEERING AND ELECTRONICS

A Series of Reference Books and Textbooks

EXECUTIVE EDITORS

Marlin O. Thurston
Department of
Electrical Engineering
The Ohio State University
Columbus, Ohio

William Middendorf
Department of
Electrical and Computer Engineering
University of Cincinnati
Cincinnati, Ohio

EDITORIAL BOARD

Maurice Bellanger
Télécommunications, Radioelectriques, et
Téléphoniques (TRT)
Le Plessis-Robinson, France

J. Lewis Blackburn
Bothell, Washington

Sing T. Bow
Department of Electrical Engineering
The Pennsylvania State University
University Park, Pennsylvania

Norman B. Fuqua
Reliability Analysis Center
Griffiss Air Force Base, New York

Charles A. Harper
Westinghouse Electric Corporation
and Technology Seminars, Inc.
Timonium, Maryland

Naim A. Kheir
Department of Electrical and
Systems Engineering
Oakland University
Rochester, Michigan

Lionel M. Levinson
General Electric Company
Schenectady, New York

V. Rajagopalan
Department of Engineering
Université du Québec
à Trois-Rivières
Trois-Rivières, Quebec, Canada

Earl Swartzlander
TRW Defense Systems Group
Redondo Beach, California

Spyros G. Tzafestas
Department of Electrical Engineering
National Technical University
of Athens
Athens, Greece

Sakae Yamamura
Central Research Institute of
the Electric Power Industry
Tokyo, Japan

1. Rational Fault Analysis, *edited by Richard Saeks and S. R. Liberty*
2. Nonparametric Methods in Communications, *edited by P. Papantoni-Kazakos and Dimitri Kazakos*
3. Interactive Pattern Recognition, *Yi-tzuu Chien*
4. Solid-State Electronics, *Lawrence E. Murr*
5. Electronic, Magnetic, and Thermal Properties of Solid Materials, *Klaus Schröder*
6. Magnetic-Bubble Memory Technology, *Hsu Chang*
7. Transformer and Inductor Design Handbook, *Colonel Wm. T. McLyman*
8. Electromagnetics: Classical and Modern Theory and Applications, *Samuel Seely and Alexander D. Poularikas*
9. One-Dimensional Digital Signal Processing, *Chi-Tsong Chen*
10. Interconnected Dynamical Systems, *Raymond A. DeCarlo and Richard Saeks*
11. Modern Digital Control Systems, *Raymond G. Jacquot*
12. Hybrid Circuit Design and Manufacture, *Roydn D. Jones*
13. Magnetic Core Selection for Transformers and Inductors: A User's Guide to Practice and Specification, *Colonel Wm. T. McLyman*
14. Static and Rotating Electromagnetic Devices, *Richard H. Engelmann*
15. Energy-Efficient Electric Motors: Selection and Application, *John C. Andreas*
16. Electromagnetic Compossibility, *Heinz M. Schlicke*
17. Electronics: Models, Analysis, and Systems, *James G. Gottling*
18. Digital Filter Design Handbook, *Fred J. Taylor*
19. Multivariable Control: An Introduction, *P. K. Sinha*
20. Flexible Circuits: Design and Applications, *Steve Gurley, with contributions by Carl A. Edstrom, Jr., Ray D. Greenway, and William P. Kelly*
21. Circuit Interruption: Theory and Techniques, *Thomas E. Browne, Jr.*
22. Switch Mode Power Conversion: Basic Theory and Design, *K. Kit Sum*
23. Pattern Recognition: Applications to Large Data-Set Problems, *Sing-Tze Bow*
24. Custom-Specific Integrated Circuits: Design and Fabrication, *Stanley L. Hurst*
25. Digital Circuits: Logic and Design, *Ronald C. Emery*
26. Large-Scale Control Systems: Theories and Techniques, *Magdi S. Mahmoud, Mohamed F. Hassan, and Mohamed G. Darwish*
27. Microprocessor Software Project Management, *Eli T. Fathi and Cedric V. W. Armstrong (Sponsored by Ontario Centre for Microelectronics)*
28. Low Frequency Electromagnetic Design, *Michael P. Perry*
29. Multidimensional Systems: Techniques and Applications, *edited by Spyros G. Tzafestas*
30. AC Motors for High-Performance Applications: Analysis and Control, *Sakae Yamamura*

31. Ceramic Materials for Electronics: Processing, Properties, and Applications, *edited by Relva C. Buchanan*
32. Microcomputer Bus Structures and Bus Interface Design, *Arthur L. Dexter*
33. End User's Guide to Innovative Flexible Circuit Packaging, *Jay J. Miniet*
34. Reliability Engineering for Electronic Design, *Norman B. Fuqua*
35. Design Fundamentals for Low-Voltage Distribution and Control, *Frank W. Kussy and Jack L. Warren*
36. Encapsulation of Electronic Devices and Components, *Edward R. Salmon*
37. Protective Relaying: Principles and Applications, *J. Lewis Blackburn*
38. Testing Active and Passive Electronic Components, *Richard F. Powell*
39. Adaptive Control Systems: Techniques and Applications, *V. V. Chalam*
40. Computer-Aided Analysis of Power Electronic Systems, *Venkatachari Rajagopalan*
41. Integrated Circuit Quality and Reliability, *Eugene R. Hnatek*
42. Systolic Signal Processing Systems, *edited by Earl E. Swartzlander, Jr.*
43. Adaptive Digital Filters and Signal Analysis, *Maurice G. Bellanger*
44. Electronic Ceramics: Properties, Configuration, and Applications, *edited by Lionel M. Levinson*
45. Computer Systems Engineering Management, *Robert S. Alford*
46. Systems Modeling and Computer Simulation, *edited by Naim A. Kheir*
47. Rigid-Flex Printed Wiring Design for Production Readiness, *Walter S. Rigling*
48. Analog Methods for Computer-Aided Circuit Analysis and Diagnosis, *edited by Takao Ozawa*
49. Transformer and Inductor Design Handbook, Second Edition, Revised and Expanded, *Colonel Wm. T. McLyman*
50. Power System Grounding and Transients: An Introduction, *A. P. Sakis Meliopoulos*
51. Signal Processing Handbook, *edited by C. H. Chen*
52. Electronic Product Design for Automated Manufacturing, *H. Richard Stillwell*
53. Dynamic Models and Discrete Event Simulation, *William Delaney and Erminia Vaccari*
54. FET Technology and Application: An Introduction, *Edwin S. Oxner*
55. Digital Speech Processing, Synthesis, and Recognition, *Sadaoki Furui*
56. VLSI RISC Architecture and Organization, *Stephen B. Furber*
57. Surface Mount and Related Technologies, *Gerald Ginsberg*
58. Uninterruptible Power Supplies: Power Conditioners For Critical Equipment, *David C. Griffith*
59. Polyphase Induction Motors: Analysis, Design, and Application, *Paul L. Cochran*

Additional Volumes in Preparation

Battery Technology Handbook, *edited by H. A. Kiehne*

High-Voltage Engineering: Theory and Practice, *edited by Mohamed Khalifa*

Linear Circuits and Systems, *Nubuo Nagai*

Electrical Engineering-Electronics Software

1. Transformer and Inductor Design Software for the IBM PC, *Colonel Wm. T. McLyman*
2. Transformer and Inductor Design Software for the Macintosh, *Colonel Wm. T. McLyman*
3. Digital Filter Design Software for the IBM PC, *Fred J. Taylor and Thanos Stouraitis*

Polyphase Induction Motors

Analysis, Design, and Application

PAUL L. COCHRAN
Schenectady, New York

Marcel Dekker, Inc. • New York and Basel

Library of Congress Cataloging-in-Publication Data

Cochran, Paul L.
Polyphase induction motors : analysis, design, and application /
p. cm.
Bibliography: p.
Includes index.
1. Electric motors, induction--Design and construction.
I. Title.
TK2785.C58 1989
621.46--dc20
ISBN 0-8247-8043-4 89-32538

This book is printed on acid-free paper.

Copyright © 1989 by MARCEL DEKKER, INC. All Rights Reserved

Neither this book nor any part may be reproduced or transmitted in any form or by any means, electronic or mechanical, including photocopying, microfilming, and recording, or by any information storage and retrieval system, without permission in writing from the publisher.

MARCEL DEKKER, INC.
270 Madison Avenue, New York, New York 10016

Current printing (last digit):
10 9 8 7 6 5 4 3 2 1

PRINTED IN THE UNITED STATES OF AMERICA

To my wife, Ruth, whose encouragement and support have made this book possible.

Preface

Two motivations prompted the writing of this book: first, to acclaim the simple, technological elegance of the widely used polyphase induction motor and its frequently unrecognized importance to modern industry and the economic well-being of society; and second, to collect into one volume a significant core of knowledge about polyphase induction motors. This information will be especially useful to young engineers and other technicians whose careers have started within the past two decades, a time when the dissemination of such knowledge has not been emphasized.

Present-day society is very dependent on (but frequently oblivious to) the polyphase induction motor. The technical community is aware that these ubiquitous machines are the "workhorses" of society but appears to take them for granted. I have been concerned, for some time, about the adequate propagation of the art and science of induction-motor technology. For the past 25 years, various engineering colleges have, for the most part, taught electrical machine courses with insufficient time being allocated to ensure reasonable comprehension of the subject matter. This is understandable, considering the huge proliferation of solid-state and other subject matter that has occurred during this period and the need of colleges to include relevant subject matter in an already crowded curriculum. However, decreased attention given to the rotating-machine, and in particular the induction motor, has had its effect.

Therefore, as would be expected, recent engineering graduates have considerably less background in the basic fundamentals of rotating machines than did their predecessors. Fortunately, the day-to-day working equations required for analysis, design, and application problems were recognized and retained in use. This was largely due to the early wave of applying digital computers to engineering that occurred throughout the country in the 1950s and 1960s. However, the practicing engineers who were responsible for this initial computerization have retired; since then, there has been an increasing and troubling dependence on the computer as the repository of technical knowledge. The present extent of dependence on computers, at the expense of broad knowledge of basic fundamentals, is apparent when a major computer must be shut down for a day or two. To varying degrees, this dependence occurs across the motor industry, including application-engineering firms, motor manufacturers, and user industries. The problem has been improved, to some extent, by the use of in-house technical courses conducted by senior engineers; for the most part, this has proven helpful.

The book addresses the three major divisions of technical knowledge, which include analysis, design, and application. Pertinent aspects of polyphase induction motors are considered, and the treatment is sufficiently extensive and deep to cover the subject matter. In the division of analysis, for example, four algorithms are used: the complete equivalent circuit, the simplified equivalent circuit, the vector diagram, and the circle diagram. The relationships among these various algorithms are stressed. The book begins by discussing fundamental laws, such as Ampère's law and Faraday's law, and derives the important equations and relationships that are required to analyze, design, and apply polyphase induction motors. Equations are derived using the worldwide SI system of units; however, the resulting working equations are also expressed in the "practical" system of units, which is still commonly used in the United States. Considerable attention has been given to consistency in notation and in identification of units for the various equations, and each equation has been identified by number for subsequent reference.

Numerical examples are used frequently throughout the book to illustrate working equations. Also, the text is written to be appreciated and used at several technical levels. Thus, the emphasis on fundamentals and on the derivation of all working equations should be of considerable use to engineering students, as well as to practicing engineers and engineering managers. The chapters that discuss stator windings, rotor windings, stator core, rotor core, insulation, and application have considerable descriptive information for those whose work requires a more general approach. Accordingly, the book can be used as a text for electrical engineering courses (at the senior or graduate level); and as a reference for design and application engineers, engineering and maintenance offices of user industries, and for engineering and power production offices of electric utility companies.

I am grateful to the General Electric Company for permission to use the various photographs that appear throughout the book. It was also necessary to consult many professional and trade journals. Accordingly, I am grateful to General Electric for permission to use the Main Library at the Schenectady plant, and the Whitney Library, at the Corporate Research and Development Center, in Niskayuna. Likewise, I also thank Union College, in Schenectady, for permission to use the Schaffer Library. I am also very appreciative of the generous help provided by Paul G. Cummings (retired), Harrison C. Bicknell, and Edward L. Owen, of General Electric. Furthermore,

I wish to express my sincere thanks to the staff of Marcel Dekker, Inc., for their suggestions and cooperation. Finally, I am very grateful to my wife, Ruth, for her considerable help in proofreading, and in other special ways, during the preparation of this book.

Paul L. Cochran

Contents

Preface v

1 INTRODUCTION 1

1.1 The Economic Need for Drive Motors 1
1.2 The Dominance of Polyphase Induction Motors 2
1.3 Distribution of Ratings 3
1.4 The Future of Polyphase Induction Motors 4

2 AMPÈRE'S LAW AND FARADAY'S LAW 5

2.1 Introduction 5
2.2 Ampère's Law 5
2.3 Faraday's Law 7

3 MOTOR ACTION 13

3.1 The Three Requirements for Motor Action in an Induction Motor 13
3.2 First Requirement: Rotating Magnetic Field 14
3.3 Second Requirement: Axial Current Flow in the Rotor Circuit 18
3.4 Third Requirement: In-Phase Relationship Between Flux Wave and Rotor-Current Wave 24
3.5 Production of Torque 28

4 BACKGROUND OF THE EQUIVALENT CIRCUIT 33

4.1 Introduction 33
4.2 One-Phase Representation 34
4.3 Physical Model of the Phase 35
4.4 Determination of the Equivalent T Network 36
4.5 Effect of Core Loss on the Equivalent Circuit 41
4.6 Effect of Turns Ratio on the Equivalent Circuit 43
4.7 Use of Actual Units for Equivalent-Circuit Calculations 46
4.8 Use of Per Unit Quantities for Equivalent-Circuit Calculations 50

5 ANALYSIS OF THE EQUIVALENT CIRCUIT 59

5.1 Introduction 59
5.2 Formulation of the Equivalent Circuit 60
5.3 Determination of the Stator and Rotor Phase Currents 64
5.4 Determination of the Power Output 67
5.5 Determination of Efficiency and Power Factor at Full Load 70
5.6 Determination of Efficiency and Power Factor at Part Load 76
5.7 Derivation of the General Torque Equation 81
5.8 Maximum Torque 85
5.9 Starting Torque 90
5.10 Starting Current 92
5.11 The Speed-Torque Curve 93
5.12 The Speed-Current Curve 95

6 THE SIMPLIFIED EQUIVALENT CIRCUIT 97

6.1 Background 98
6.2 Determination of the Phase Current 98
6.3 Determination of the Power Output 101
6.4 Determination of the Torque Output 104
6.5 Maximum Torque 105
6.6 Starting Torque 109
6.7 Numerical Example Using the Simplified Equivalent Circuit 111
6.8 Comparison of Results of Calculations by Use of the Two Circuits 117

6.9 Improvement of Simplified Equivalent-Circuit Results by Use of Adjusted Voltage 119
6.10 Comments on Choice of Equivalent Circuit 120

7 THE VECTOR DIAGRAM 123

7.1 Inference of the Vector Diagram from the Equivalent Circuit 123
7.2 Construction of the Vector Diagram 126
7.3 Interpretation of the Vector Diagram 127
7.4 Analysis of Power Transformation by Use of the Vector Diagram 128
7.5 Determining Performance from the Vector Diagram 131
7.6 Example of Calculating Performance from the Vector Diagram 138

8 THE CIRCLE DIAGRAM 141

8.1 Status of the Circle Diagram 142
8.2 Locus of the Current in a Series Circuit with Fixed Inductance and for Which the Resistance Is Varied 142
8.3 Concept of the Conventional Polyphase Induction Motor Circle Diagram 145
8.4 Determination of the Conventional Diagram from Test Data 147
8.5 Interpretation of the Conventional Diagram 150
8.6 Starting Torque from the Conventional Diagram 151
8.7 Maximum Torque from the Conventional Diagram 152
8.8 Maximum Power from the Conventional Diagram 153
8.9 Maximum Power Factor from the Conventional Diagram 153
8.10 Operating-Point Performance from the Conventional Diagram 154
8.11 Limitations of the Conventional Diagram 158
8.12 Concept of the Adjusted Circle Diagram 160
8.13 Numerical Example of Use of the Adjusted Diagram 162
8.14 Determination of Adjusted-Diagram Construction Data from Test Data 162
8.15 Construction of the Adjusted Diagram 166
8.16 Determination of Maximum Torque and Starting Torque from the Adjusted Diagram 169

8.17 Determination of Performance at Rated Load from the Adjusted Diagram 170
8.18 Comparison of Performance at Rated Load as Calculated by the Adjusted Diagram 176

9 STATOR WINDINGS 177

9.1 Function and Importance of the Stator Winding 178
9.2 Stator Coils 179
9.3 Eddy-Current Losses in the Copper Within the Slot 197
9.4 Additional Winding Losses Due to Circulating Currents in the Strands 205
9.5 Slot Factor 209
9.6 Numerical Example of Calculation of Eddy-Current Loss and Strand Loss in a Stator Winding 210
9.7 Induced Voltage in the Stator Coil 217
9.8 Coil-Pitch Factor 220
9.9 Use of the Coil-Pitch Factor in Controlling Harmonics 223
9.10 Distribution Factor 225
9.11 Use of the Distribution Factor in Controlling Harmonics 229
9.12 Voltage Induced in the Stator Phase Winding 231
9.13 Integral-Slot Windings 232
9.14 Fractional-Slot Windings 236
9.15 Generalized Rules for Determining Stator Winding Configurations 238
9.16 Unbalanced Windings 242
9.17 Stator Connection Diagrams 245
9.18 Magnetic Pull or Radial Decentering Force 246
9.19 Numerical Example of Calculation of Unbalanced Magnetic Pull 257
9.20 Temporary Operation with Damaged Stator Coils 259

10 ROTOR WINDINGS 263

10.1 Function and Importance of the Rotor Winding 264
10.2 General Types of Rotor Windings 265
10.3 Squirrel-Cage Rotor Windings 266
10.4 Wound-Rotor Windings 330

11 DIELECTRICS AND INSULATION 357

11.1 Function, Scope, and Importance of Insulation 358
11.2 Relative Aspect of Insulators and Conductors 360

11.3 Methodology Used in Understanding and in Applying Insulation 361
11.4 Electrostatic Background of Dielectrics 362
11.5 Capacitors and Capacitance 365
11.6 Physical Behavior of Dielectric Materials 371
11.7 Factors Affecting Insulation Strength 388
11.8 Corona 396
11.9 Capacitance to Ground 398
11.10 Charging Current and Charging Volt-Amperes for High-Potential Testing 401
11.11 Numerical Example of Calculation of Phase-Winding Capacitance to Ground, Charging Current, and Charging Volt-Amperes 402
11.12 Winding Surges 405
11.13 Temperature Classes of Insulation 419
11.14 Insulation Resistance Testing 420
11.15 Creepage, Tracking, and Arc Resistance 424
11.16 Application of Insulation to Windings 424

12 MAGNETOMOTIVE FORCES ACTING ACROSS THE AIR GAP 427

12.1 Introduction 428
12.2 Magnetomotive Force Produced by One Stator Coil 429
12.3 Magnetomotive Force Produced by a Pair of Coil Groups of Opposite Polarity 434
12.4 Magnetomotive Force Produced by One Phase 436
12.5 Magnetomotive Force Produced by the Complete Stator Winding 438
12.6 Example of the Graphical Construction of the Magnetomotive-Force Wave Produced by a Three-Phase Stator Winding 441
12.7 The Equivalent Circuit with the Space Harmonics Considered 445
12.8 Magnetizing Current 446
12.9 Various Types of Harmonics Present in the Air Gap 449
12.10 Perturbations on the Speed-Torque Curve 453
12.11 Electromagnetically Induced Noise and Vibration 466
12.12 Additional Effects of Harmonics 477

13 REACTANCE 479

13.1 Effect of Reactance on Polyphase Induction Motor Size and Performance 480
13.2 Separation of Total Winding Reactance into Leakage Reactance and Magnetizing Reactance 481
13.3 Magnetizing Reactance 484
13.4 Components of Leakage Reactance 486
13.5 Stator-Slot Leakage Reactance of a Rectangular Slot 487
13.6 Stator-Slot Leakage Reactance of a Nonrectangular Slot 497
13.7 Rotor-Slot Leakage Reactance of a Phase-Wound Rotor 499
13.8 Rotor-Slot Leakage Reactance of a Squirrel-Cage Rotor with Rectangular Slots 502
13.9 Rotor-Slot Leakage Reactance of a Single-Cage Rotor with Nonrectangular Slots 503
13.10 Rotor-Slot Leakage Reactance of a Multiple-Cage Rotor 505
13.11 End-Turn Leakage Reactance 508
13.12 Differential Leakage Reactance 519
13.13 Skew Leakage Reactance 527
13.14 Numerical Example of Running-Reactance Calculation 529
13.15 Blocked-Rotor Reactance 536
13.16 Numerical Example of Blocked-Rotor Reactance Calculation 540

14 THE MAGNETIC CIRCUIT 549

14.1 Function and Role of the Magnetic Circuit 550
14.2 Diamagnetism and Paramagnetism 550
14.3 Ferromagnetic Materials 551
14.4 Magnetic Saturation 552
14.5 Magnetic Hysteresis Loss 553
14.6 Eddy-Current Loss 558
14.7 No-Load Core Loss 562
14.8 Load Loss 564
14.9 Core Structure 567
14.10 Effect of Slot and Air-Duct Openings and the Use of Carter's Coefficient 582
14.11 Calculation of the Magnetic Circuit 585

15 APPLICATION OF INDUCTION MOTORS 599

15.1 The Role of Application 600
15.2 Installation 601
15.3 Methods of Power Transmission 602
15.4 Methods of Starting Squirrel-Cage Induction Motors 614
15.5 Wound-Rotor Motor Starting 624
15.6 Methods of Speed Control 627
15.7 Acceleration 644
15.8 Braking 653
15.9 Power Requirement for a Duty-Cycle Application 658

LIST OF SYMBOLS 661

BIBLIOGRAPHY 665

Index 671

1

Introduction

1.1 The Economic Need for Drive Motors 1

1.2 The Dominance of Polyphase Induction Motors 2

1.3 Distribution of Ratings 3

1.4 The Future of Polyphase Induction Motors 4

1.1 THE ECONOMIC NEED FOR DRIVE MOTORS

The economic well-being of a society, in the long run, is obviously related to its capability to produce goods and services. The capability of a society to produce goods and, to some extent, to produce services, is directly related to its capability to control and use energy effectively. One measure of the quantity of energy, which is available for producing goods and services, is the quantity of electrical energy, in kilowatt-hours, which is generated during a given period. Although much of this energy is required for residential and commercial use, a considerable amount is left for industrial use for the production of goods. There are some industrial processes, such as electrolysis, electric welding, and industrial space heating, as well as lighting, for which electrical energy is used directly. However, much of the electrical energy that is used for the production of goods must be converted to mechanical energy, first in the form of rotating shafts. Such conversion of electrical energy into mechanical energy is the function of electric drive motors. Since power is the rate of energy transfer, drive motors can also be regarded as converters of electrical power to mechanical power. Accordingly, such motors are rated in horsepower, at a specific speed.

1.2 THE DOMINANCE OF POLYPHASE INDUCTION MOTORS

As will be shown in Chapter 3, the electromagnetic requirements for producing motor action are to have two magnetomotive forces, which have components in space quadrature and in time phase. These requirements have been accomplished in three different motor configurations—dc motors, synchronous motors, and induction motors—to provide electrical drives for industry. A dc motor requires a source of dc power to excite the stationary field winding and to supply dc power to the rotating armature winding, through the brushes and commutator. Thus the original cost and the maintenance cost per horsepower are greater for this type of motor than for the other two types mentioned above. Although the dc motor has very good speed-control characteristics, its significantly greater total cost per horsepower has limited its industrial application to a small percentage of total drive-motor horsepower.

A synchronous motor requires a source of dc power to excite the rotating field winding, through the brushes and collector rings. For many synchronous motors, for which fine control of the field winding is not required, the field is excited by a rotating alternator, the output of which is rectified by a rotating rectifier bank. However, in either case, the original cost is greater and the maintenance cost per horsepower is generally greater than for an induction motor of the same horsepower rating. Although the synchronous motor can be designed, at an increase in cost, to exhibit a leading power factor (i. e., to deliver positive reactive volt-amperes to the ac bus), the application of synchronous motors is limited primarily to driven equipment that cannot be permitted a change in speed upon a change in load.

A polyphase induction motor requires only a source of polyphase power. Polyphase voltage, impressed on the stator winding of such a motor, produces a synchronously rotating magnetomotive-force wave which, in turn, produces a synchronously rotating flux wave. Since the flux wave is traveling at a greater angular velocity than is the rotor structure, the relative motion results in a voltage being induced in the rotor winding. This induced voltage will cause a corresponding rotor current to flow in each phase of the rotor winding, the direction of which is such as to oppose the original influencing agent, the stator bus. The currents in the rotor phases will combine to produce a rotor-current wave, which rotates at an angular velocity that is equal to the difference in velocity between the synchronous flux wave and the rotor structure. The sum of the angular velocity of this rotating rotor-current wave and of the angular velocity of the rotor structure is equal to the synchronous speed. Thus the rotating flux wave, produced by the stator winding, and the rotating rotor-current wave, developed in the rotor winding, are traveling at the same speed as seen from a point on the stator. As shown in Chapter 3, the rotor current interacts with the stator flux to produce a torque on the rotor structure. Accordingly, the rotor will accelerate until the torque produced by the motor is just equal to the load torque. For the usual application, this will occur at a rotor speed that is slightly less than synchronous speed. The simplicity and inherently high reliability of the polyphase induction motor has generally made it the drive motor of choice throughout the industry and has earned it the reputation of being society's "workhorse."

1.3 DISTRIBUTION OF RATINGS

Polyphase induction motors span a range of ratings, from 1/2 hp to as large a power rating as the local electrical distribution system can accommodate. The federal government owns four induction motors, each with a power rating of 45,000 hp and a synchronous speed of 720 rpm. Each of these machines has a short-time rating of 54,000 hp for 1 hour. Insofar as the author is aware, these four machines have the largest power ratings of any motor built to date. The federal government also owns induction motors with a power rating of 41,500 hp and a synchronous speed of 514 rpm. This motor design develops approximately 30% more torque, at full speed, and is physically larger than the 45,000-hp design.

As might be expected, there is an inverse relationship between a given power rating and the corresponding number of induction motors which are in use throughout the country. Table 1.1 shows an estimate of the polyphase induction motor population above 5 hp in the United States as of 1986. It is apparent from the table that the total number of induction motors with ratings greater than 5 hp is greater than 15,000,000. It is also estimated that these units have a total power rating of about 575,000,000 hp. This is approximately equal to 2.5 hp for each person living in the United States, and this does not include induction motors rated 5 hp or less. Most such motors are used in industry, to produce goods for consumption. Thus more than 2.5 hp

TABLE 1.1 Estimated Population of Polyphase Induction Motors in the United States

Horsepower rating[a]	Population[b]
5.1-20	10,000,000
21-50	3,300,000
51-125	1,700,000
126 and above	400,000

[a] Ratings of 5 hp or less are not included.

[b] Populations are based on 1986.

of industrial motors per person is required to provide for our economic well-being at the level that existed in 1986. Because of diversity among loads, all of the motor horsepower will not be in operation at any one time, so that the total motor load on the electric utilities will be less than this amount.

It is also of interest to note the amount of motor horsepower that is required for the generation of electric power. Various kinds of ancillary equipment, such as pumps, fans, and so on, are required in the operation of fossil-fuel and nuclear power plants. Typically, the total connected motor load of such auxiliaries is about 10% of the gross output of the plant. Thus for a 500,000-kW plant, the connected auxiliary-motor load is approximately equal to $(500,000)(0.10)/0.746 = 67,000$ hp. The magnitude of power ratings for individual motors varies from a few horsepower for motor-operated valves to as much as 10,000 hp for certain pumps. Again, because of diversity, not all of this connected load of auxiliary motors will be in operation at any given time.

1.4 THE FUTURE OF POLYPHASE INDUCTION MOTORS

The polyphase induction motor, the discovery of which was announced by Tesla in 1887, occurred at such a time as to have a tremendous effect on the economic and the industrial history of this country. The relative ease with which electric power could be transmitted and distributed by virtue of alternating current, and the availability of a reliable ac drive motor, made the conversion of electric power to mechanical power a relatively simple operation. This, in large measure, made possible the enormous expansion of industry that has occurred during the twentieth century.

The polyphase induction motor has been greatly improved in the years following 1887, and more improvement will occur in the future. However, its simple technological elegance and its inherent reliability will continue to make it as important in the foreseeable future as it has been in the past. As long as there is a need to convert electrical power to mechanical power by use of a rotating shaft, there will be a need for this machine. To state the long-term outlook for the polyphase induction motor in terms of the buzzwords of the day: It will be as important to a high-tech society as it has been to a smokestack society.

2

Ampère's Law and Faraday's Law

2.1 Introduction 5

2.2 Ampère's Law 5

2.3 Faraday's Law 7

2.1 INTRODUCTION

The nineteenth century was a fruitful period for scientific progress, much of which laid the fundamental foundation for the rapid development of the industrial art experienced during the second half of that century and the ensuing twentieth century. Prime among nineteenth-century scientific progress was the work of Ampère and Faraday. Standing on the shoulders of such predecessors, Tesla announced the invention of the polyphase induction motor in 1887. Since this book concerns the polyphase induction motor, it is appropriate that the first technical topic to be considered be the two fundamental laws that determine its electromagnetic operation: Ampère's law and Faraday's law.

2.2 AMPÈRE'S LAW

In 1820, Oersted published the qualitative observation that an electric current in a conductor will cause a compass to deflect. This appears to be the first significant documentation of the physical relationship between a magnetic field and a current-carrying conductor. Subsequently, during the same year, Bivot and Savart published the first quantitative relationship of the force between a magnet and a current-carrying conductor located in the vicinity of the field of that magnet. However, a more general analysis was done by Ampère, who published a series of papers, beginning in September 1820, on the quantitative relationship between a magnetic field and the flow of an electric charge. From this work has come a fundamental physical relationship, important to the domain of electric motor action, known as Ampère's law.

Assume that a conductor carrying a current i is located within a uniform magnetic field of flux density B, as shown in Fig. 2.1. For such a configuration, Ampère's law may be stated as

$$dF = Bi\, d\ell \sin\gamma \quad \text{newtons} \tag{2.1}$$

where dF is the incremental force exerted on an incremental length $d\ell$ of the conductor. The units of the terms expressed in Eq. (2.1) are

F = force, newtons
B = flux density of the magnetic field, webers/meter^2
i = current flow in the conductor, amperes
ℓ = conductor length, meters
γ = angle between the direction of the magnetic field and the direction of the current i

The direction of the force exerted on the current-carrying conductor, by the magnetic field, can be intuitively determined by superimposing the circumferentially directed flux field, produced by the current flow, upon the already existing flux field, as shown in Fig. 2.2. It is apparent that the flux ϕ_I produced by the current-carrying conductor tends to cancel the flux ϕ_F of the magnetic field on the right side of the conductor and to reinforce it on the left side. Thus, intuitively, the conductor should experience a force exerted on it, which is directed to the right. This is, in fact, what has been experimentally determined, as stated by Ampère's law in eq. (2.1).

Ampère's law may be stated in a more general form by remembering that the vector cross product of two vectors, A and B, produces a third vector equal to AB sin γ, where γ is the angle between the vector directions of A and B and where the direction of the new vector is perpendicular to the plane

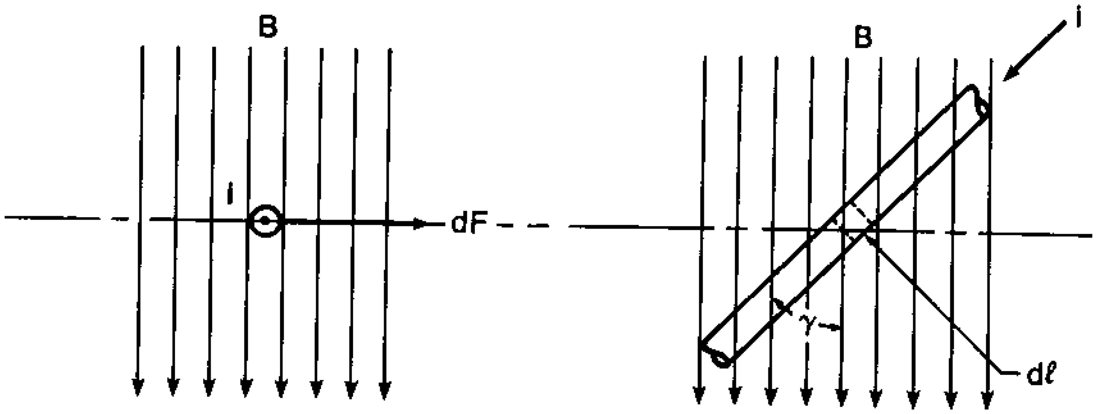

FIGURE 2.1 Incremental force on a current-carrying conductor in a magnetic field.

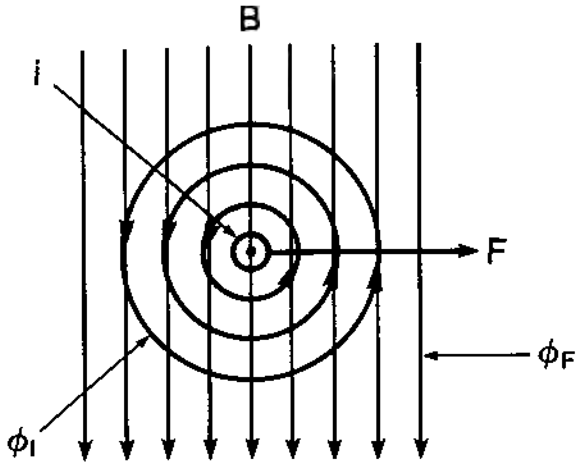

FIGURE 2.2 Magnetic field of a conductor superimposed on an already existing magnetic field.

defined by vectors A and B. The new vector will point in the direction determined by the advance of a right-hand screw as vector A is rotated into vector B through the angle between them. Then eq. (2.1) may be written as

$$dF = d\ell\,(i \times B) \quad \text{newtons} \tag{2.2}$$

However, since the current i consists of the flow of electrical charges which are assumed to be limited to the confines of the conductor and since the conductor direction is expressed by ℓ (and, differentially, by $d\ell$), eq. (2.2) may be written in a more useful form as

$$dF = i(d\ell \times B) \quad \text{newtons} \tag{2.3}$$

2.3 FARADAY'S LAW

Several contemporaries of Ampère reasoned that if an electric current would result in the production of a magnetic field, it should be expected that a magnetic field would result in the production of a current. In 1831, Faraday discovered what was, in effect, this relationship. He determined that a bar magnet which was moved rapidly through a coil, or loop of wire, would produce a voltage within that coil and that the magnitude of the induced voltage was proportional to the time rate of change of the magnetic flux linking the coil. If the coil of wire was closed upon itself to form a conducting circuit, the induced voltage would, of course, cause a corresponding current to flow. The direction, or polarity, of the induced voltage was found experimentally to be such as to oppose the mechanical motion causing the voltage, consistent with the principle of conservation of energy. If the coil or loop is closed upon itself so that current can flow, the current will flow in such a direction as to produce a force, by Ampère's law, which opposes the original

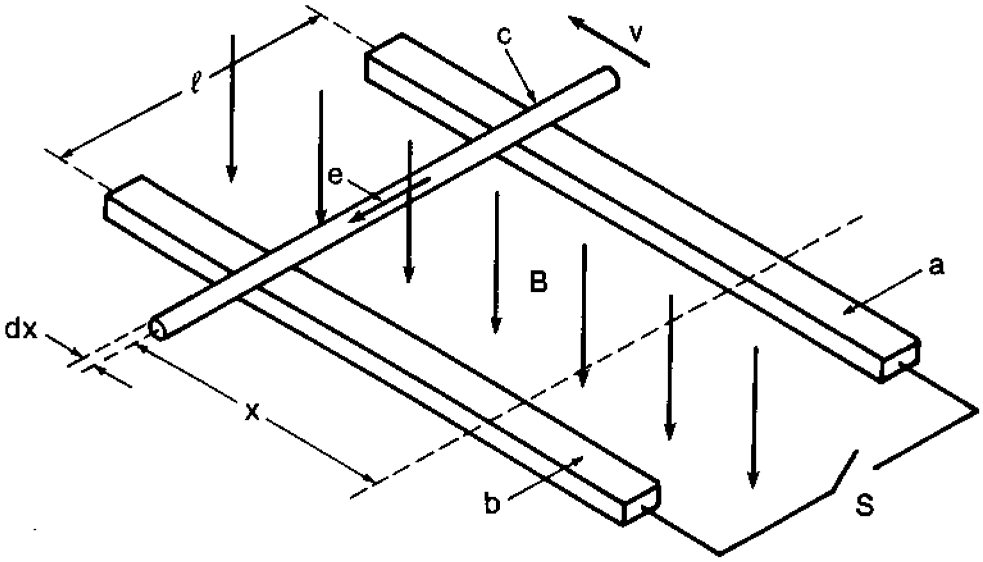

FIGURE 2.3 Voltage induced in a conductor moving relative to a magnetic field.

motion. Thus the epochal phenomenon of electromagnetic induction, which has proven so significant to the development of subsequent electrical technology, was discovered at about the same time as Ampère's law. Both Ampère's law and Faraday's law are fundamental to the operation of rotating electrical machinery, including induction motors, as well as to much else in present-day electrical technology.

Faraday's law may be quantitatively stated in several forms, three of which will be considered. The first form to be considered is formulated on the basis of relative motion between a magnetic field and a conductor positioned such as to have a component normal to the direction of the field, as shown in Fig. 2.3. Let a and b be two parallel tracks or ways on which a conductor c is positioned. Let the plane formed by the conductor and the two ways supporting it be normal to the direction of a magnetic field, of flux density B. If the conductor is moved to the left at a velocity v, a voltage will be induced in the conductor in the direction shown and its instantaneous value will be

$$e = B\ell v \quad \text{volts} \tag{2.4}$$

where

e = induced voltage, volts
B = flux density, webers/meters^2
ℓ = length of the conductor, perpendicular to B, meters
v = velocity of conductor, perpendicular to both B and ℓ, meters/second

It is not required that the velocity v or that the flux density B be constant in magnitude. The instantaneous value of the induced voltage will be proportional to the product of their instantaneous values. Also, although the physical system in Fig. 2.3 is set up on the basis of the magnetic field being fixed in space and the conductor moving to the left, relative to it, the same instantaneous value and direction of induced voltage will result if the conductor is fixed in space and the magnetic field is moving to the right, at a velocity of v.

The results expressed in eq. (2.4) might have been expected from consideration of the principle of conservation of energy and of Ampère's law. Let the two ways or tracks that support the conductor c be made from a conducting material and let the switch S be closed, permitting current to flow in the conductor. Then, as the conductor is moved to the left, a current i will flow and will be in the same direction as the induced voltage. The value of the energy developed in the circuit in a time of dt seconds is equal to

$$dw_1 = ei\,dt \quad \text{joules} \tag{2.5}$$

However, the current flowing in the conductor produces a force which, from Ampère's law, is directed to the right and which opposes the original force which is causing the motion to the left. The magnitude of this opposition force is

$$F = Bi\ell \quad \text{newtons} \tag{2.6}$$

The product of this force and the incremental distance dx meters, traveled in the incremental time dt seconds, is equal to the work done in moving the conductor through the distance dx meters, or

$$dw_2 = Bi\ell\,dx \quad \text{joules} \tag{2.7}$$

From the principle of conservation of energy, dw_1 and dw_2 must be equal in magnitude if there are no other losses in the system. Then

$$ei\,dt = Bi\ell\,dx \quad \text{joules} \tag{2.8}$$

Rearranging eq. (2.8) gives us

$$e = B\ell\frac{dx}{dt} = B\ell v \quad \text{volts} \tag{2.9}$$

which is identical to eq. (2.4).

Faraday's law may be quantitatively stated in a somewhat more general form by considering the rate of change of magnetic flux which links a coil or conductor loop. Consider Fig. 2.4. Let a conducting loop consist of two

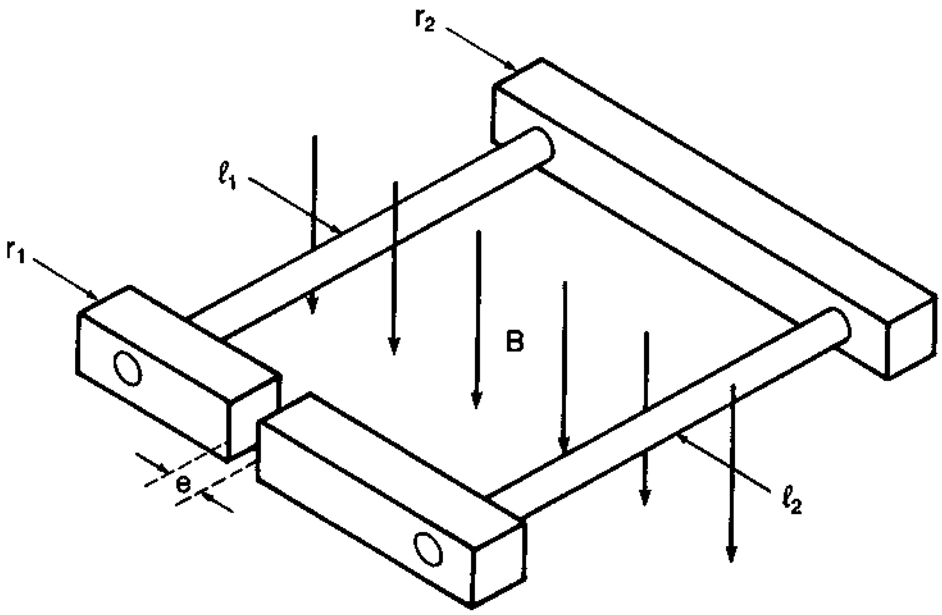

FIGURE 2.4 Voltage induced in a conducting loop by a varying magnetic field.

parallel bars that terminate into two additional parts at each end of the bars, all made of conducting material, somewhat typical of two squirrel-cage induction motor rotor bars located one pole pitch apart. Also, let a magnetic field of flux density B flow through the confines of this loop. The total flux through the loop is then

$$\phi = \int_S B \, dA \quad \text{webers} \tag{2.10}$$

where ϕ is the flux linking the loop in webers and A is the cross-sectional area normal to the direction of flux flow in meters^2. The surface integral is taken in the plane of the loop, normal to the direction of B and within the confines of the perimeter of the loop. Then if the quantity of flux ϕ through the loop is changing with time, the instantaneous value of the voltage induced in the loop is

$$e = -\frac{d\phi}{dt} \quad \text{volts} \tag{2.11}$$

Further, if there is a discrete number of turns N forming the loop, typical of a stator coil or of a wound rotor coil, and if all of the turns enclosed the same flux ϕ, the instantaneous value of the voltage induced in the N-turn loop is

$$e = -N \frac{d\phi}{dt} \quad \text{volts} \tag{2.12}$$

Equivalence between the two forms in which eqs. (2.4) and (2.11) express Faraday's law is apparent by noting that ℓv has dimensions of meters^2/second and is numerically equal to the area swept over by the moving conductor in unit time. Thus ℓv multiplied by B is equal to the total change in flux experienced by the conductor in unit time. The phase relationship between the flux through the coil and the voltage induced in that coil, in eq. (2.11) or (2.12), is expressed by the equation. The induced voltage is equal to -1 multiplied by the time derivative of the flux through the coil and this establishes the phase relationship. On the other hand, the phase relationship between the flux field and the induced voltage in a conductor moving through it is determined by an examination of the physical relationships involved. In Fig. 2.3, the direction of the induced voltage and of the current when switch S is closed are such as to cause a counteracting force to be produced, in accordance with Ampère's law, and to be in such a direction as to oppose the original force causing the motion.

The last and most general form to be considered in which Faraday's law may be expressed is that given by Maxwell and included as one of his four equations. Equation (2.11) is an experimentally determined relationship which states that a change in magnetic flux through a coil or loop will cause an induced voltage e to appear across the terminals of that coil or loop, such as is shown in Fig. 2.5. However, as will be seen, this voltage is developed throughout the length of the loop. The existence of an induced voltage also implies the existence of an induced electric field in the vicinity of the loop. The induced voltage e is obtained by summing the electric field intensity

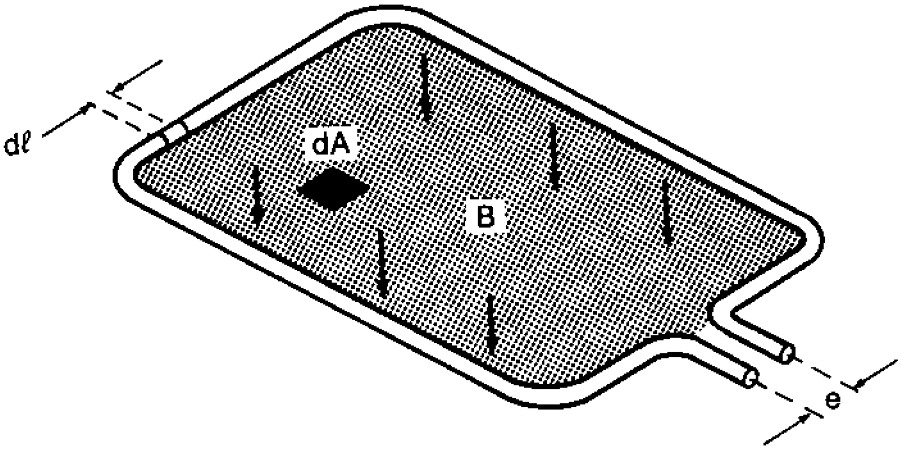

FIGURE 2.5 Incremental consideration of voltage induced in a conducting loop.

around the periphery of the loop. The voltage then appears across the two terminals of the loop, which may be regarded as the beginning and end points of the path of integration. The fundamental relationship between voltage and electric field intensity is

$$e = \int E \, d\ell \quad \text{volts} \tag{2.13}$$

where

e = induced voltage, volts
E = electric field intensity, volts/meter
ℓ = length around the loop, meters

Then, substituting the expression for the voltage e from eq. (2.13) into Faraday's experimentally determined law, as stated in eq. (2.11), we have

$$\int E \, d\ell = - \frac{d\phi}{dt} \quad \text{volts} \tag{2.14}$$

Magnetic flux ϕ is expressed in more fundamental terms as the surface integral of the flux density B, as formulated in eq. (2.10). If the surface integral of B is substituted for ϕ in eq. (2.14),

$$\int E \, d\ell = - \frac{d \int B \, dA}{dt} \quad \text{volts} \tag{2.15}$$

where the surface integral is taken over the surface formed by the plane of the coil and bounded by the perimeter of the coil and where the line integral is taken around the periphery of the coil. For an N-turn coil, typical of a rotating machine winding, the line integral is taken once for each turn, which increases the induced voltage N times. When Faraday's law is expressed in the form shown in eq. (2.15), it may be used for a very wide range of physical applications.

3

Motor Action

3.1 The Three Requirements for Motor Action in an Induction Motor 13
3.2 First Requirement: Rotating Magnetic Field 14
3.3 Second Requirement: Axial Current Flow in the Rotor Circuit 18
3.4 Third Requirement: In-Phase Relationship Between Flux Wave and Rotor-Current Wave 24
3.5 Production of Torque 28

3.1 THE THREE REQUIREMENTS FOR MOTOR ACTION IN AN INDUCTION MOTOR

It is apparent from Ampère's law that if a magnetic field and a current-carrying conductor are placed in such a spatial relationship as to have components mutually perpendicular to each other, a useful force may be obtained in a direction perpendicular to both. Further, if this force appears as a tangential force near the periphery of a circumferential structure capable of rotating on a shaft through its center, such as a rotor, a useful torque will be produced. Such an action constitutes a conversion from electrical to mechanical energy and is known as motor action.

Figure 3.1 illustrates one example of the configuration described above for which, for simplification, only a small sector of the complete stator, rotor, and air gap are shown. If a magnetic field is produced by either the stator or the rotor (in Fig. 3.1, the stator), if mutual flux of that magnetic field links both the stator and the rotor magnetic circuits and if at the same time, a current is made to flow through conductors near the air-gap

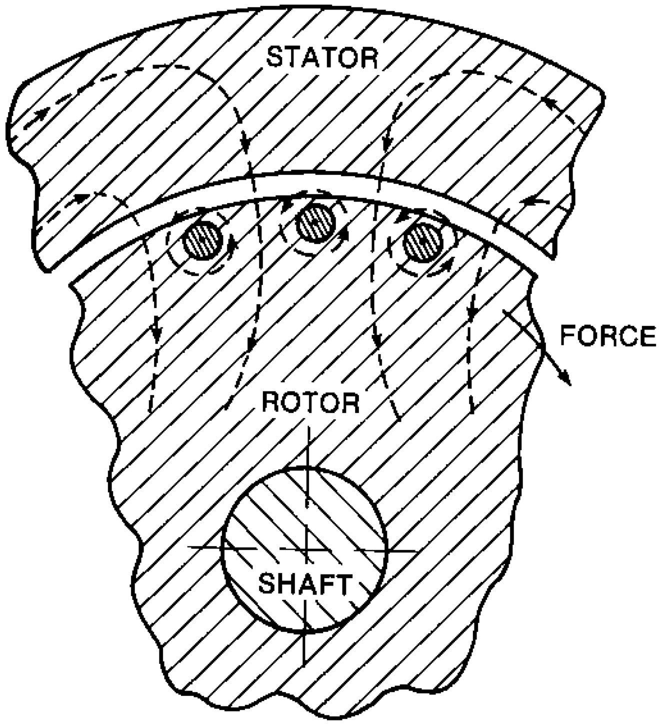

FIGURE 3.1 Simplified motor action.

surface of the other member (in Fig. 3.1, the rotor), a force is then exerted (in Fig. 3.1, to the right) near the rotor surface. Since the force is tangential to the rotor surface and since it is applied to a lever arm of approximately half of the rotor diameter, a useful torque will be produced about the shaft and the rotor body will tend to rotate (in Fig. 3.1, in a clockwise direction). Thus there are three electrical requirements for producing motor torque: (1) a rotating magnetic flux field across the air gap, produced by either the stator or the rotor, which links both the stator and the rotor, (2) current flow through axial conducting paths near the air-gap surface of the other member, and (3) the proper phase relationship between the air-gap flux and the current if they are time-varying quantities. How these three requirements are met by polyphase induction motors to produce motor action will now be considered, the first of which will be the production of a magnetic flux field across the air gap, which rotates around the stator bore at a constant angular velocity.

3.2 FIRST REQUIREMENT: ROTATING MAGNETIC FIELD

If q different windings are displaced $2\pi/q$ electrical radians apart around the stator bore, and if q different voltage sources, each lagging the preceding one by $2\pi/q$ radians in time, are applied with one voltage source across each winding, a rotating magnetic field will be produced which travels around the stator bore at the angular velocity of

$$\omega = 2\pi f \quad \text{electrical radians/second} \tag{3.1}$$

where f is the frequency of the applied voltage in hertz. For a three-phase stator winding, three separate but essentially identical phase windings are located around the stator bore, $2\pi/3$ electrical radians, or 120 electrical degrees, apart in space and the phase voltage which is impressed across each winding is displaced $2\pi/3$ electrical radians, or 120 electrical degrees, apart in time. It will be noted now, and discussed later, that it is usual practice to have the 120 electrical degrees allocated to each phase winding, for every 360 electrical degrees of stator bore, to consist of two sections, or groups of coils, electrically connected together.

To understand how a three-phase voltage source can act upon a stator with three separate phase windings to produce a rotating magnetomotive-force wave, consider Fig. 3.2. This figure shows a conceptual representation of a simplified, three-phase stator winding with the magnetic axis of

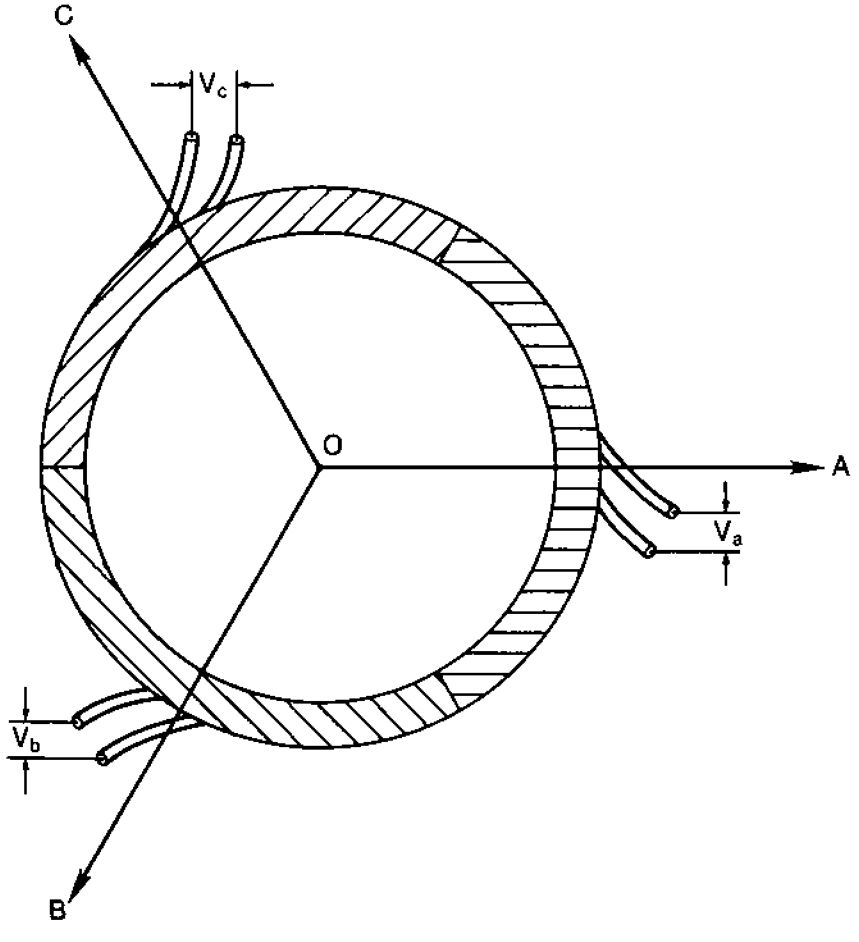

FIGURE 3.2 Conceptual representation of a three-phase stator winding.

each winding 120 electrical degrees apart, along lines OA, OB, and OC, respectively. Let a separate single-phase ac voltage source be applied to each of the three windings, such that each winding produces a sinusoidally alternating magnetic field, with a maximum value of H ampere-turns/meter. If the voltage source is a balanced three-phase system and if time reference is taken such as to have zero time correspond to the instant that winding A is experiencing its maximum field strength, the alternating field strength of three individual phase windings may be expressed, respectively, as

$$h_A = H \cos \omega t \qquad \text{ampere-turns/meter} \tag{3.2}$$

$$h_B = H \cos(\omega t - 120) \qquad \text{ampere-turns/meter} \tag{3.3}$$

$$h_C = H \cos(\omega t - 240) \qquad \text{ampere-turns/meter} \tag{3.4}$$

It will be assumed that the spatial distribution of the magnetomotive-force wave in ampere-turns of each of the phase windings is sinusoidal, which is a reasonable approximation of an actual machine, as will be seen subsequently. Let point a, in Fig. 3.2, be located α electrical degrees from the magnetic axis of phase A. Then, for maximum field strength in each of the phase windings, the magnetic field strength at point a, caused by all three phases, is

$$\begin{aligned} H_a &= H \cos \alpha + H \cos(\alpha - 120) \\ &\quad + H \cos(\alpha - 240) \qquad \text{ampere-turns/meter} \end{aligned} \tag{3.5}$$

However, the actual field strength of each phase is a function of time as stated in eqs. (3.2), (3.3), and (3.4). Hence the actual field strength at point a, at a particular instant of time, is

$$\begin{aligned} H_a &= H \cos \alpha \cos \omega t + H \cos(\alpha - 120) \cos(\omega t - 120) \\ &\quad + H \cos(\alpha - 240) \cos(\omega t - 240) \qquad \text{ampere-turns/meter} \end{aligned} \tag{3.6}$$

Upon simplifying, we obtain

$$\begin{aligned} H_a &= \frac{H}{2} [3 \cos(\alpha - \omega t) + \cos(\alpha + \omega t) + \cos(\alpha + \omega t - 120) \\ &\quad + \cos(\alpha + \omega t - 240)] \qquad \text{ampere-turns/meter} \end{aligned} \tag{3.7}$$

Since

$$\cos(\alpha + \omega t) + \cos(\alpha + \omega t - 120) + \cos(\alpha + \omega t - 240) = 0 \qquad \text{numeric} \tag{3.8}$$

eq. (3.7) reduces

$$H_a = \frac{3H}{2} \cos(\alpha - \omega t) \quad \text{ampere-turns/meter} \tag{3.9}$$

Also,

$$\cos \psi = \sin\left(\frac{\pi}{2} - \psi\right) \quad \text{numeric} \tag{3.10}$$

and then

$$H_a = \frac{3H}{2} \sin\left(\omega t + \frac{\pi}{2} - \alpha\right) \quad \text{ampere-turns/meter} \tag{3.11}$$

Equation (3.11) shows that the field strength has a sinusoidal space distribution at any given instant of time, consistent with the initial assumption. It also shows that at any point a, the field strength varies sinusoidally with time. Finally, if α is set equal to ωt, such that point a rotates around the stator bore at synchronous speed, eq. (3.11) reduces to

$$H_a = \frac{3H}{2} \quad \text{ampere-turns/meter} \tag{3.12}$$

That is, the magnetic field strength produced by the three-phase stator winding is constant in magnitude as it rotates around the stator bore at the angular velocity of ω radians/second.

The magnetic field strength of 3/2H ampere-turns/meter is a vector quantity which is the gradient, in the direction of H, of the magnetomotive force F produced by current flowing in the three-phase winding. This magnetomotive force, which is a potential field, will cause a useful amount of magnetic flux ϕ to flow if a suitable magnetic circuit is provided which has a sufficiently small value of reluctance (or a sufficiently large value of permeance), in accordance with

$$\phi = \frac{F}{R} \quad \text{webers} \tag{3.13}$$

where F is the magnetomotive force in ampere-turns and R is the reluctance of the magnetic circuit in ampere-turns/weber (or in 1/henry).

Figure 3.3 shows a simplified two-pole rotor and stator core, assumed to be made of magnetic steel, which provides a low-reluctance circuit for the flow of magnetic flux. If the radial dimension of the air gap is small, as is typical of induction motors, a useful amount of flux per pole ϕ_p will result

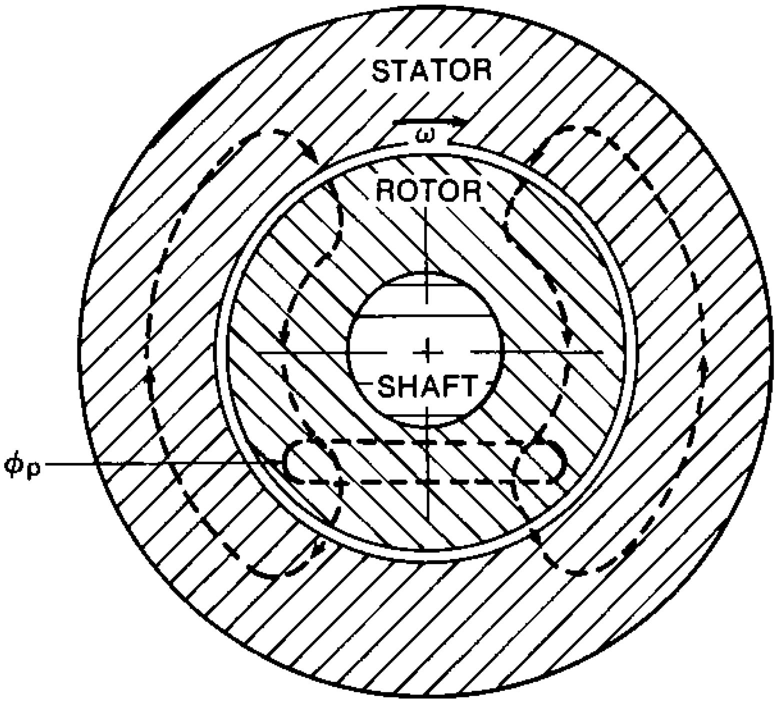

FIGURE 3.3 Rotating magnetic flux-flow pattern in a stator and rotor core.

and will flow in the general pattern shown in the figure. This pattern of flux flow will, of course, also rotate around the core structure at an angular velocity of ω radians/second, relative to the stator. This is the first of the three aforementioned requirements for polyphase induction motors to produce motor action, that is, a rotating magnetic flux field, produced by the stator, the flux of which links both the stator and rotor core.

3.3 SECOND REQUIREMENT: AXIAL CURRENT FLOW IN THE ROTOR CIRCUIT

The second of the three requirements for polyphase induction motors to produce motor action is current flow through axial conducting paths near the air-gap surface of the rotor. This requirement will be considered sufficiently at this time to understand the concept. The axial flow of such current near the rotor surface presumes the existence of a corresponding induced electromotive force (EMF), or voltage, which causes the current to flow. Accordingly, the basis of this induced voltage must now be sought.

As discussed above, the three-phase two-pole conceptual stator winding shown in Fig. 3.2 produces a magnetomotive force that is constant in magnitude and rotates around the air gap at a constant angular velocity of ω radians/second. This magnetomotive force causes magnetic flux to flow through the stator and rotor magnetic cores in the general pattern shown in Fig. 3.3, which flux also rotates around the air gap at ω radians/second.

This flux flow results in some type of spatial distribution of the air-gap flux density B_g, from pole to pole, along the air gap which, again, rotates around the air gap at ω radians/second. If, as will be considered later, there are several stator coils per phase, per pole, the spatial distribution of the rotating air-gap flux density B_g will approach a sinusoidal distribution, as shown in Fig. 3.4.

Squirrel-cage rotor windings are formed by axially placed, evenly spaced bars located around the periphery of the magnetic core of the rotor, near the air-gap surface. The bars are made from electrically conducting materials such as copper, brass, or aluminum. They are terminated at end rings made of similar materials, located circumferentially around each end of the rotor, which provide paths for current flow from one axial bar to another within the squirrel-cage winding. Figure 3.4 conceptually shows 12 axially positioned rotor bars, evenly distributed along 360 electrical degrees, each bar of which is displaced 30 electrical degrees from the preceding one. Although a greater number of bars would normally be used in practice, 12 is a sufficient number to illustrate the concept.

If the rotor is initially blocked from rotating, the air-gap flux-density wave will pass each rotor bar at an angular velocity of ω electrical radians/second. The number of revolutions per second (rps) made by the flux wave, for a two-pole winding, is

$$\text{rps} = \frac{\omega}{2\pi} \quad \text{revolutions/second} \tag{3.14}$$

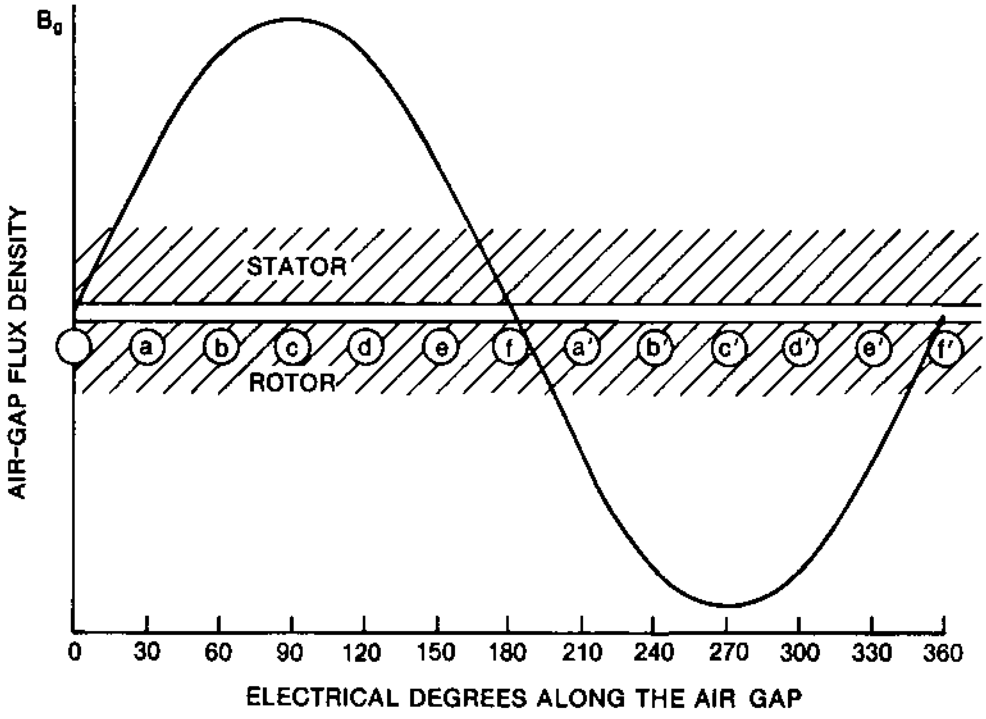

FIGURE 3.4 Air-gap flux wave rotating relative to rotor bars.

The circumferential distances around the air gap is

$$\text{air-gap circumference} = \pi d \quad \text{meters} \tag{3.15}$$

where d is the diameter of stator bore in meters. Then the tangential velocity with which the flux wave passes the blocked-rotor bars is

$$v = \frac{\omega}{2\pi}\pi d = \frac{\omega d}{2} \quad \text{meters/second} \tag{3.16}$$

Remembering the form in which Faraday's law was written in eq. (2.4), and setting $B = B_g$ yields

$$e = B_g \ell v \quad \text{volts} \tag{3.17}$$

Substituting the value of v given in eq. (3.16) into eq. (3.17) gives the instantaneous voltage induced in a given rotor bar, as

$$e = B_g \ell \frac{\omega d}{2} \quad \text{volts} \tag{3.18}$$

where ℓ is the active length of the rotor bar in meters. Since B_g is varying sinusoidally with time, as seen from a point on the stationary rotor, the air-gap flux-density wave shown in Fig. 3.4 may be represented as

$$B_g = B_{gm} \sin \omega t \quad \text{webers/meter}^2 \tag{3.19}$$

where B_{gm} is the maximum value of air-gap flux density in webers/meter^2. Then the instantaneous voltage induced in a bar of the stationary rotor is

$$e = \frac{B_{gm} \ell \omega d}{2} \sin \omega t \quad \text{volts} \tag{3.20}$$

Since the two dimensions, d and ℓ, are fixed and since the angular velocity ω is assumed to be constant, the instantaneous value of the induced voltage e is proportional to the instantaneous value of the air-gap flux density B_g. If two rotor bars in Fig. 3.4, such as a and a', which are separated by one pole pitch or 180 electrical degrees, are considered, it is apparent that each is under the influence of air-gap flux, which is equal in magnitude but opposite in polarity, or sign, from the other. Thus the voltages induced in the two bars will be equal in magnitude but will be in opposite directions along the two bars. Using the convention that a positive value of B_g corresponds to flux flowing from the stator core and into the rotor core and the convention that a positive value of e corresponds to a voltage directed out of the plane of the paper in Fig. 3.4, the voltage induced in bar a will be positive and the voltage induced in bar a' will be negative. Accordingly, the two voltages will add around the conducting path consisting of the rotor bar a, rotor bar a', and the corresponding end-ring segments which complete the loop. The magnitude of the induced voltage around the loop of what, in effect, is a full-pitch rotor coil is then equal to twice that of eq. (3.20).

It is necessary, however, to note the angular relationship of the two rotor bars, considered individually, to that of the rotor coil formed jointly by them, so that the time variation of the voltage induced in the blocked-rotor coil may be properly defined. The voltage induced in a bar is directly proportional to the air-gap flux at that point on the flux wave which is passing the stationary bar at that instant. Thus for the angular reference used in Fig. 3.4, the time variation of the induced voltage in a bar is represented by a sine function. However, the position of a coil in space is defined by the position of its axis, which is located midway between the two coil sides which form that coil. Then the axis of coil aa' lags bar a by 90 electrical degrees. Accordingly, using the same time reference, some specific point on the induced voltage wave of the coil, such as the maximum positive value, will lag the corresponding point on the induced voltage wave of bar a by 90 electrical degrees or $\pi/2$ electrical radians. From the above and from the trigonometric relationship

$$\sin\left(\alpha - \frac{\pi}{2}\right) = -\cos\alpha \quad \text{numeric} \tag{3.21}$$

the time variation of the voltage induced in the stationary rotor coil is represented by the function $-\cos\omega t$, using the same time reference as for B_g in Fig. 3.4. Thus, from consideration of the two paragraphs above, the voltage induced in the stationary rotor coil, formed by bar a and a', is

$$e_{aa'} = -B_{gm}\ell\omega d\cos\omega t \quad \text{volts} \tag{3.22}$$

If the maximum air-gap flux density is B_{gm}, the average air-gap density, averaged over one pole pitch of 180 degrees or π electrical radians along the air gap, is

$$B_{gav} = \frac{\int_0^\pi B_{gm}\sin\alpha\, d\alpha}{\pi} = -\frac{B_{gm}}{\pi}\cos\alpha\Big|_0^\pi = \frac{2B_{gm}}{\pi} \quad \text{webers/meter}^2 \tag{3.23}$$

The stator bore area per pole A_p is

$$A_p = \frac{\pi \ell d}{p} \quad \text{meters}^2 \tag{3.24}$$

where p is the number of poles for which the stator is wound. Then, for a two-pole stator,

$$A_p = \frac{\pi \ell d}{2} \quad \text{meters} \tag{3.25}$$

The flux per pole is equal to B_{gav} multiplied by A_p, or

$$\phi_p = \frac{2B_{gm}}{\pi} \frac{\pi \ell d}{2} = B_{gm} \, d\ell \quad \text{webers} \tag{3.26}$$

Incorporating eq. (3.26) into eq. (3.22), we have

$$e_{aa'} = -\omega\phi_p \cos \omega t \quad \text{volts} \tag{3.27}$$

Equation (3.27) was derived from the first form in which Faraday's law was stated in eq. (2.4), for pedagogical reasons. However, the voltage induced in a stationary rotor coil may be derived more simply from the form in which Faraday's law is stated in eq. (2.11). The air-gap flux density, as a function of time, is given in eq. (3.19), as

$$B_g = B_{gm} \sin \omega t \quad \text{webers/meter}^2 \tag{3.28}$$

This equation may be converted to flux per pole, as a function of time, by remembering that the value of flux per pole ϕ_p, corresponding to a maximum air-gap flux density of B_{gm} for the two-pole machine being considered, was shown in eq. (3.26) to be equal to B_{gm} multiplied by $d\ell$. In a similar manner, the flux per pole ϕ_p, at any given instant of time, is equal to the corresponding air-gap flux density at that instant of time B_g, multiplied by $d\ell$. Then if both sides of eq. (3.28) are multiplied by $d\ell$, the equation becomes

$$\phi = \phi_p \sin \omega t \quad \text{webers} \tag{3.29}$$

Substituting eq. (3.29) into eq. (2.11), where coil aa' is the conducting loop being considered through which the flux per pole ϕ_p is changing with time, we obtain

$$e_{aa'} = -\frac{d(\phi_p \sin \omega t)}{dt} = -\omega\phi_p \cos \omega t \quad \text{volts} \tag{3.30}$$

which is identical to eq. (3.27).

To return to Fig. 3.4, it is apparent that 1/12 of a cycle later in time after the induced voltage in bar pairs a and a' have reached a maximum value, the air-gap flux-density wave will have traveled 30 electrical degrees along the air gap and that rotor-bar pairs b and b' will be under the influence of the same magnitude and polarity of flux density as discussed previously for bar pairs a and a'. Accordingly, bar pairs b and b' will experience the same induced voltage as did bar pairs a and a', but this will occur 1/12 of a cycle later in time. Rotor-bar pairs c and c' will experience the same induced voltage as did bar pairs a and a', but this will occur 1/6 of a cycle later. Also, rotor-bar pairs d and d' will experience the same induced voltage as did rotor-bar pairs a and a', but this will occur 1/4 of a cycle later in time. Continuing this process for rotor-bar pairs e and e', f and f', a' and a, and so on, it is seen that the maximum value of the voltage induced in the various rotor-bar pairs located 180 electrical degrees apart occur successively, each pair after the preceding pair, and that this effect travels around the blocked-rotor periphery at an angular velocity of ω radians/second.

The voltage induced in the loop consisting of a pair of rotor bars located 180 electrical degrees apart, such as a and a', will cause a corresponding current to flow in this pair of bars. The magnitude of this current will be limited by the resistance and leakage reactance exhibited by the rotor coil. The impedance of rotor and stator windings of polyphase induction motors will be considered in detail later. It is sufficient, at this time, to assign a value of resistance and leakage reactance, r' and x', respectively, attributable to the pair of rotor bars and the included segments of end rings, which are a part of the total resistance and leakage reactance per phase of the rotor winding. Then the instantaneous value of the current in bar pairs a and a' is

$$i_{aa'} = \frac{e_{aa'}}{r' + jx'} \quad \text{amperes} \tag{3.31}$$

and the bar current will lag the bar voltage in time by an angle θ_2' such that

$$\phi_2' = \tan^{-1} \frac{X'}{r'} \quad \text{radians} \tag{3.32}$$

Using eq. (3.27) to express the induced voltage e_{aa}' in eq. (3.31), we obtain

$$i_{aa'} = \frac{-\omega\phi_p}{\sqrt{(r')^2 + (X')^2}} \cos(\omega t - \theta_2') \quad \text{amperes} \tag{3.33}$$

In a similar manner to that used for visualizing the voltage sequentially induced in the various pairs of rotor bars spaced 180 electrical degrees apart, the current in each of these pairs of bars will successively reach a maximum value 1/12 of a cycle after the preceding pair. Thus all 12 possible combinations of pairs of bars, located one pole pitch apart, successively reach their maximum current values in (12)(1/12) = 1 cycle. Accordingly, this current effect travels around the blocked-rotor periphery at an angular velocity of ω radians/second and, as seen from eq. (3.33), lags the corresponding induced voltage effect by θ_2' electrical radians. This is the second of the three aforementioned requirements for polyphase induction motors to produce motor action (i.e., current flow through axial conducting paths near the air-gap surface of the rotor).

3.4 THIRD REQUIREMENT: IN-PHASE RELATIONSHIP BETWEEN FLUX WAVE AND ROTOR-CURRENT WAVE

In the two requirements discussed previously for polyphase induction motors to produce motor action, we considered two quantities, air-gap flux density and rotor-bar current, both of which were found to vary with time as seen from a point on the blocked rotor. Thus there is need for the third requirement, which is that the proper phase relationship must exist between these two quantities, so that a net unidirectional force will be exerted on the rotor bar, in accordance with Ampère's law.

In eq. (3.33), the current in the squirrel-cage rotor coil, consisting of bars a and a', is expressed as a function of time. However, since the electromagnetic force produced by Ampère's law is exerted on individual rotor bars, it is desirable to determine the expression for the current in the individual rotor bar as a function of time. The direction of the current is in one direction (out of the plane of the paper) in bar a and in the opposite direction (into the plane of the paper) in bar a', in Fig. 3.4. As discussed previously, the angular position of coil aa' is defined by the angular position of its magnetic axis. The axis of the coil is 90 electrical degrees behind bar a and is 90 electrical degrees ahead of bar a', and eq. (3.33) correctly expresses the time variation of the coil current as reckoned by the angular position of its axis. The maximum value of the current in bar a is, of course, equal in magnitude to that of coil aa', of which it is a part. Since

$$\sin\alpha = -\cos\left(\alpha + \frac{\pi}{2}\right) \quad \text{numeric} \tag{3.34}$$

the current in bar a may be expressed as

$$i_a = \frac{\omega\phi}{\sqrt{(r')^2 + (x')^2}} \sin(\omega t - \theta_2') \quad \text{amperes} \tag{3.35}$$

Examination of eqs. (3.19) and (3.35) shows that the maximum value of current in rotor bar a lags the maximum value of the air-gap-density wave by the angle θ_2', which is the power factor angle of the blocked-rotor circuit. The air-gap flux-density wave rotates around the air gap at the angular velocity of ω radians/second. Also, each rotor bar in the blocked rotor successively reaches its maximum value of current after the preceding one, and this rotor-bar current-wave effect rotates around the periphery of the rotor at the angular velocity of ω radians/second. Then the phase displacement between the air-gap flux density and the rotor-bar current is equal to the angle θ_2' for the blocked-rotor condition. Since θ_2', the blocked-rotor circuit power-factor angle, is always less than 90 degrees, there will always be a component of one of the two quantities in phase with the other quantity. Accordingly, a net unidirectional force will be exerted on each bar of the blocked rotor, causing the rotor to tend to rotate about the centerline of the shaft.

Up to this point, the rotor has been assumed to be blocked. If this block is removed, so that the rotor is free to rotate, the torque due to the net unidirectional force on the rotor bars, multiplied by a lever arm approximately equal to the radius of the rotor, will accelerate the rotational inertia of the rotor and that of any connected load. Let the rotor speed, at any instant of time, be

$$n = \text{rotor speed relative to stator} \quad \text{rpm} \tag{3.36}$$

As stated above, the air-gap flux field rotates around the air gap at an angular velocity of ω radian/second, as seen from a fixed point on the stator. Since

$$\omega = 2\pi f \quad \text{radians/second} \tag{3.37}$$

it will rotate through 2π electrical radians, or the span of one pair of poles, for each cycle of the stator power supply. Then the rotational speed of the air-gap flux field, for a stator wound for p poles, is

$$n_s = \frac{60f}{p/2} \quad \text{rpm} \tag{3.38}$$

and this speed is called the synchronous speed of the machine.

The difference in speed between synchronous speed and the actual rotor speed, at any instant of time, is equal to s, the slip. Expressed in per unit of synchronous speed, slip is equal to

$$s = \frac{n_s - n}{n_s} \quad \text{per unit} \tag{3.39}$$

At a rotor speed of n, corresponding to a per unit slip of s, a fixed point on the rotor will see the stator synchronous wave at a rotational speed equal to the difference between synchronous speed and the rotor speed, or

$$n_s - n = sn_s \quad \text{rpm} \tag{3.40}$$

Then ω_2, the angular velocity of the stator synchronous wave relative to the moving rotor bars, is equal to

$$\omega_2 = s\omega \quad \text{radians/second} \tag{3.41}$$

Accordingly, eq. (3.29), the expression for the flux per pole, as a function of time, is equal to

$$\phi = \phi_p \sin s\omega t \quad \text{webers} \tag{3.42}$$

for a fixed point on the moving rotor. The voltage induced in coil aa' is then

$$e_{aa'} = \frac{d(\phi_p \sin s\omega t)}{dt} = -s\omega\phi_p \cos s\omega t \quad \text{volts} \tag{3.43}$$

and the corresponding current in coil aa' is

$$i_{aa'} = \frac{-s\omega\phi_p}{\sqrt{(r')^2 + (sx')^2}} \cos(s\omega t - \theta_2) \quad \text{amperes} \tag{3.44}$$

where

$$\theta_2 = \tan^{-1} \frac{sx'}{r'} \quad \text{radians} \tag{3.45}$$

Based on analogous reasoning to that for eq. (3.35), the current in an individual bar may be expressed as

$$i_a = \frac{s\omega\phi_p \sin(s\omega t - \theta_2)}{\sqrt{(r')^2 + (sx')^2}} \quad \text{amperes} \tag{3.46}$$

By dividing the numerator and denominator of eq. (3.46) by s, it may be rewritten as

$$i_a = \frac{\omega\phi_p \sin(s\omega t - \theta_2)}{\sqrt{(r'/s)^2 + (x')^2}} \quad \text{amperes} \tag{3.47}$$

Comparison of eqs. (3.42) and (3.47) shows that relative to a fixed point on the rotor, the air-gap flux wave and the rotor-bar current wave rotate at an angular velocity of $s\omega$ radians/second and that the rotor-bar current wave lags the flux wave by θ_2 radians, the power-factor angle of the rotating rotor circuit. As can be seen from eq. (3.47), the rotor circuit impedance will change during the acceleration period, since the magnitude of the slip s changes with rotor speed. However, the phase angle θ_2 is always less than 90 electrical degrees, even at very low rotor speed, and it tends to decrease as the rotor speed increases. Accordingly, there will always be a component of the rotor-bar current in phase with the air-gap flux, producing a net unidirectional torque that will accelerate the rotor to full speed and will cause it to drive the connected load at full speed. This is the third of the three aforementioned requirements for a polyphase induction motor to produce motor action, that is, the proper phase relationship between the air-gap flux and the rotor-bar current, if they are time-varying quantities.

Before leaving the subject of phase relationship, it is interesting to note that a fixed point on the stator will see the rotor-bar current at a rotational speed equal to the sum of n, the speed of the rotor structure, and $n_s - n$, the speed of the rotor-bar current wave relative to a fixed point on the rotor structure, or

$$\text{rotor-bar current-wave speed, at the stator} = n + (n_s - n) = n_s \quad \text{rpm} \tag{3.48}$$

Thus at any rotor rotational speed n, the air-gap flux wave and the rotor-bar current wave will continue to rotate at an angular velocity of ω radians/second, as seen from a fixed point on the stator and, again, the rotor-bar current will lag the air-gap flux wave by θ_2 radians.

3.5 PRODUCTION OF TORQUE

The force exerted on the rotor bar of a polyphase induction motor, from Ampère's law, is equal to

$$F_a = B_g i_a \ell \quad \text{newtons} \tag{3.49}$$

Each rotor bar is located near the periphery of the rotor structure and, accordingly, the force exerted on each bar will act upon a lever arm approximately equal to the radius of the rotor. Then the torque developed by a bar is

$$T_a = \frac{B_g i_a \ell d}{2} \quad \text{newton-meters} \tag{3.50}$$

As discussed above, both the air-gap flux density B_g and the rotor-bar current i_a are time-varying quantities. Since torque is produced by the rotor-bar current interacting with the flux-density wave in the air gap, the appropriate time variation is that seen from a fixed point on the rotor. If each side of eq. (3.42) is divided by ℓd, then

$$\frac{\phi}{\ell d} = \frac{\phi_p}{\ell d} \sin s\omega t \quad \text{webers/meter}^2 \tag{3.51}$$

However, it was determined previously that for a two-pole stator, $\phi/\ell d = B_g$ and that $\phi_p/\ell d = B_{gm}$. Accordingly, eq. (3.51) can be written as

$$B_g = B_{gm} \sin s\omega t \quad \text{webers/meter}^2 \tag{3.52}$$

Substituting eqs. (3.47) and (3.52) into eq. (3.50) yields

$$T_a = \left(\frac{\ell d}{2} B_{gm} \sin s\omega t\right)\left[\frac{\omega\phi_p \sin(s\omega t - \theta_2)}{\sqrt{(r'/s)^2 + (x')^2}}\right] \quad \text{newton-meters} \tag{3.53}$$

or

$$T_a = \left(\frac{\phi_p}{2} \sin s\omega t\right)\left[\frac{\phi_p \omega}{\sqrt{(r'/s)^2 + (x')^2}} \sin(s\omega t - \theta_2)\right] \quad \text{newton-meters} \tag{3.54}$$

Rearranging eq. (3.54) yields

$$T_a = \frac{\omega\phi_p^2}{2Z_2'} \sin s\omega t \sin(s\omega t - \theta_2) \quad \text{newton-meters} \tag{3.55}$$

where

$$Z_2' = \sqrt{(r'/s)^2 + (x')^2} \quad \text{ohms} \tag{3.56}$$

Let

$$K_a = \frac{\omega\phi_p^2}{2Z_2'} \quad \text{newton-meters} \tag{3.57}$$

Then

$$T_a = K_a \sin s\omega t \sin(s\omega t - \theta_2) \quad \text{newton-meters} \tag{3.58}$$

Expanding eq. (3.58) gives us

$$T_a = \frac{K_a}{2} \left[\cos(s\omega t - s\omega t + \theta_2) - \cos(s\omega t + s\omega t - \theta_2)\right] \quad \text{newton-meters} \tag{3.59}$$

which reduces to

$$T_a = \frac{K_a}{2} \left[\cos \theta_2 - \cos(2s\omega t - \theta_2)\right] \quad \text{newton-meters} \tag{3.60}$$

An examination of eq. (3.60) shows that the torque produced by an individual rotor bar consists of two components, a constant term equal to $K_a/2 \cos\theta_2$, and a second term of double-slip frequency equal to $-K_a/2 \cos(2s\omega t - \theta_2)$. Thus the average torque produced by a bar is proportional to the rotor circuit power factor, and its instantaneous value oscillates, at two times slip frequency, about an offset axis equal to the constant term. The blocked-rotor power factor of the rotor circuit will depend on specific facts of the design and rating of the machine, such as the specified starting

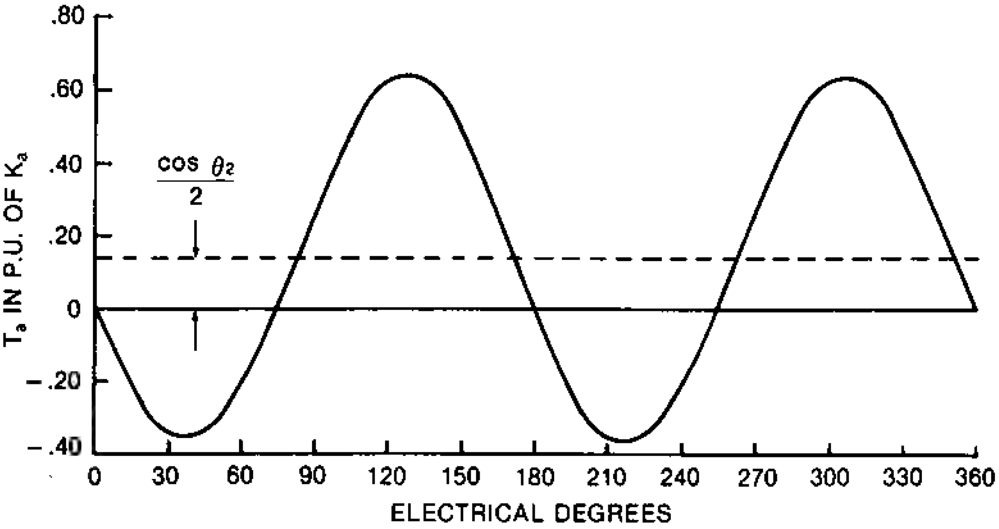

FIGURE 3.5 Blocked-rotor torque produced by one individual rotor bar.

torque. However, it will normally be greater than 0.282, which corresponds to a blocked-rotor value of θ_2 equal to 73.6 degrees. Figure 3.5 shows a plot of the starting torque produced by a bar, for $\cos\theta_2 = 0.282$. In this plot, the torque is normalized in per unit of K_a. Since the slip s is equal to 1.0 under blocked-rotor condition, the frequency of alternation of the bar torque is equal to twice line frequency, as is apparent from eq. (3.60) and Fig. 3.5.

As the rotor accelerates to full speed, the value of the slip will decrease from unity to a small value, such as 0.01 to 0.03 per unit. Accordingly, the frequency of the torque developed by a rotor bar will decrease to the range of 0.5 to 2.0 Hz at full-load, full-speed conditions. Also, the rotor-circuit power factor $\cos\theta_2$ is very close to 1.0 at full load and full speed, since the slip is small and, as is apparent from eq. (3.45), the angle θ_2 is correspondingly small. This causes the offset axis of the alternating bar torque, determined by the first term of eq. (3.60), to be essentially equal to the maximum value of the alternating component of torque, as determined by the second term of eq. (3.60). Accordingly, the instantaneous value of the bar torque is essentially positive at all points. Figure 3.6 shows a plot of the torque produced by a rotor bar for $\theta_2 = 1.0$, which corresponds closely to conditions of full speed and full load. Again, the torque is normalized in per unit of K_a.

Inspection of eq. (3.60), Fig. 3.5, and Fig. 3.6 would intuitively indicate that the average torque produced by a rotor bar over one slip cycle, or during $2\pi/s\omega$ seconds, is

$$T_{aav} = \frac{K_a}{2}\cos\theta_2 \quad \text{newton-meters} \tag{3.61}$$

This can be shown analytically by integrating eq. (3.60) with respect to time, within limits of one slip cycle, to obtain the area under the curve and then by dividing this integral by the time corresponding to one slip cycle, to obtain the average value of T_a.

$$T_{aav} = \frac{K_a/2}{2\pi/s\omega}\int_0^{2\pi/s\omega} [\cos\theta_2 - \cos(2s\omega t - \theta_2)]\,dt \quad \text{newton-meters} \tag{3.62}$$

$$T_{aav} = \frac{K_a s\omega}{4\pi}\left[t\cos\theta_2 - \frac{\sin(2s\omega t - \theta_2)}{2s\omega}\right]\Bigg|_0^{2\pi/s\omega} \quad \text{newton-meters} \tag{3.63}$$

$$T_{aav} = \frac{K_a}{2}\cos\theta_2 \quad \text{newton-meters} \tag{3.64}$$

Since all of the bars of a given rotor are identical and are distributed symmetrically around the periphery of the rotor, the individual bar torques act in mechanical coordination to rotate the rotor about the center of the shaft. Thus the unidirectional component of the various bar torques combine to form a larger, unidirectional torque and the alternating component of the various bar torques sum to zero. Accordingly, a unidirectional torque is developed to accelerate the rotor and then to drive the connected load in the region of full speed.

The large proportion of polyphase induction motors in use have squirrel-cage rotors, for which the axial conducting bars are terminated into circumferential conducting end rings at each end of the rotor structure. However, some polyphase induction motors in service have phase-wound rotors. For such wound-rotor motors, a single bar in each rotor slot is

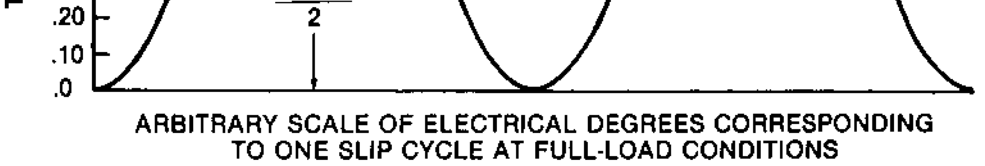

FIGURE 3.6 Full-speed torque produced by one individual rotor bar.

replaced by two different coil sides located in the same slot. Nevertheless, the fundamentals of torque production are the same for the two types of motors.

As will be discussed subsequently, torque is actually calculated from a consideration of the electrical losses produced in the rotor circuit. This is possible because, as shown in eq. (3.64), torque is proportional to cos θ_2, the rotor-circuit power factor.

4

Background of the Equivalent Circuit

4.1 Introduction 33

4.2 One-Phase Representation 34

4.3 Physical Model of the Phase 35

4.4 Determination of the Equivalent T Network 36

- 4.4.1 Test 1 37
- 4.4.2 Test 2 37
- 4.4.3 Test 3 38
- 4.4.4 Transformation of physical model test data into T-network impedances 38
- 4.4.5 Hypothetical example 39

4.5 Effect of Core Loss on the Equivalent Circuit 41

4.6 Effect of Turns Ratio on the Equivalent Circuit 43

4.7 Use of Actual Units for Equivalent-Circuit Calculations 46

- 4.7.1 Example of use of actual units 47

4.8 Use of Per Unit Quantities for Equivalent-Circuit Calculations 50

- 4.8.1 Example of use of per unit quantities 54

4.1 INTRODUCTION

Three algorithms used for analyzing the operation and performance of polyphase induction motors are the equivalent circuit, the vector diagram, and the circle diagram. All three are not independent systems, however, as the vector diagram is essentially derived from the equivalent circuit and represents the voltage and current vector relationships for one phase of the machine, as depicted by the equivalent circuit. The circle diagram is less frequently used than in previous years. It is, nevertheless, useful in visualizing various quantities, such as certain losses and torque, and how these quantities vary with changes in operation, such as changes in load. The circle diagram requires some effort to construct, and since it is a graphical method, is subject to construction and scale inaccuracies. However, use of computer calculating and graphical capabilities can reduce this problem.

The equivalent circuit will be the first method to be used in analyzing the operation and performance of the polyphase induction motor. In Chapter 1 it was determined that rotor-bar current resulted from voltage which was induced in the rotor bars by a rotating magnetic field, produced by the stator. Thus the polyphase induction motor operates by transformer action between the primary member, the stator, and the secondary member, the rotor. Accordingly, the machine may be analyzed as a polyphase transformer for which the secondary is capable of rotating and for which the secondary load impedance is a function of the speed of rotation. This is the approach used in the equivalent-circuit method, which will now be considered.

4.2 ONE-PHASE REPRESENTATION

Three-phase stator and rotor windings will be considered in detail subsequently. However, it will be noted, at this time, that the stator coils of each phase are connected in series, or series-parallel, to produce each phase winding and that the magnetic axis of each of the otherwise identical phase windings is displaced from that of the other two phases by 120 electrical degrees in space. Thus each stator phase winding is a specific two-terminal circuit which is symmetrically displaced from, but otherwise electrically identical to, the other two phase windings. Accordingly, only one stator phase winding need be considered for analysis. Since the descriptive comments above also apply to the rotor phase winding of a wound-rotor induction motor, only one of its rotor phase windings need be considered for analysis.

Under the influence of the rotating magnetic field of the stator, the influenced rotor bars and corresponding segments of end rings of squirrel-cage rotors form into appropriate current-conducting coils to provide phase windings that mimic the behavior of the rotor phase windings of wound-rotor machines. As will be considered subsequently, the phase-impedance parameters of a squirrel-cage phase winding may be accurately calculated. Also, at a given instant of time, the phase winding may be regarded as having two terminal points, similar to a wound-rotor phase winding, and these terminals may be considered short circuited in normal operation. Then, as for a wound-rotor machine, only one rotor phase winding need be considered for analysis for a squirrel-cage machine.

4.3 PHYSICAL MODEL OF THE PHASE

One phase of an iron-core polyphase two-winding transformer (i.e., a transformer with a primary and a secondary winding for each phase and with no tertiary winding) may be represented by the simplified physical model shown in Fig. 4.1. This suggests that a similar simplified physical model might be used to represent one phase of a polyphase induction motor since, as discussed above, such a machine can be considered as a polyphase transformer. There are two significant differences, however, which are (1) that the polyphase induction motor has an air gap which is in series with the magnetic steel to form the magnetic circuit for the mutual flux and (2) that the polyphase induction motor has a secondary winding which rotates relative to the stator. The series air gap in the magnetic circuit can be modeled by having an equivalent air gap in the physical model. As was shown in eq. (3.47) for an individual rotor bar, and as will be shown in Chapter 5 for the entire rotor phase winding, rotation of the rotor results

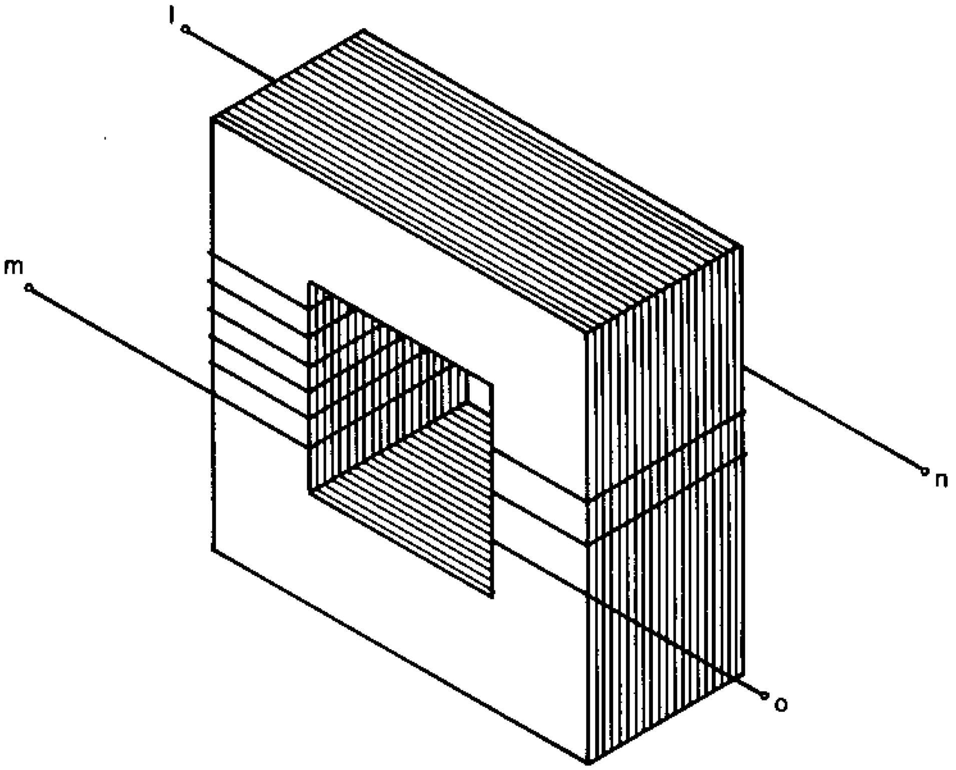

FIGURE 4.1 Simplified physical model of a two-winding iron-core transformer.

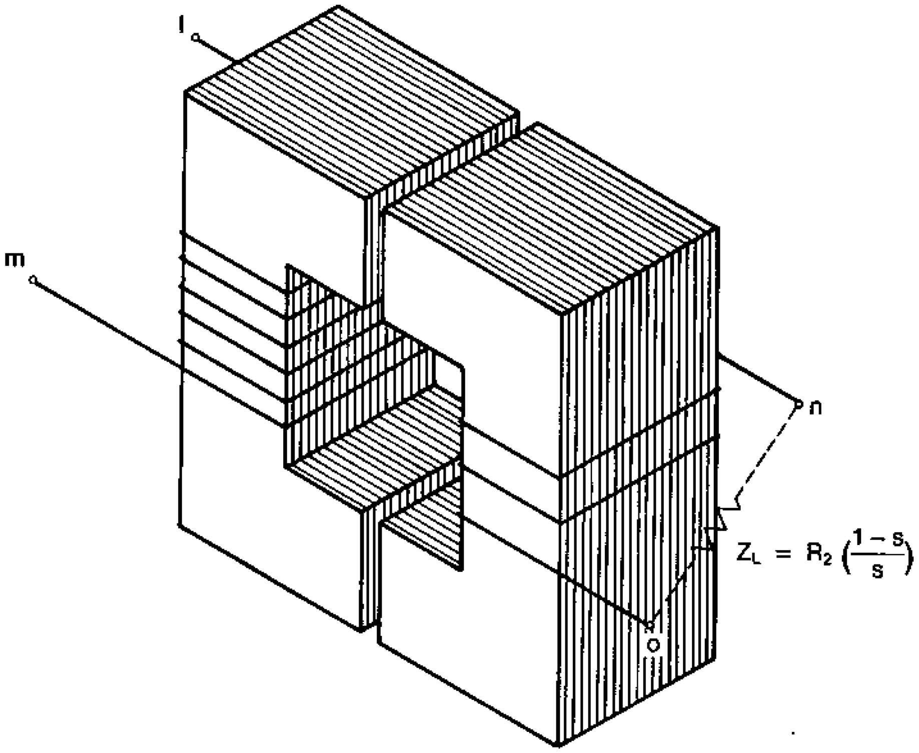

FIGURE 4.2 Simplified physical model of a polyphase induction motor.

in R_2, the ohmic resistance of the rotor phase winding, being divided by s, the slip, to give R_2/s. Since

$$\frac{R_2}{s} = R_2 + \frac{1 - s}{s} R_2 \quad \text{ohms} \tag{4.1}$$

then rotation of the secondary, for the physical model, is effectively equivalent to the secondary winding being connected to an external load of Z_L, equal to

$$Z_L = \frac{1 - s}{s} R_2 \quad \text{ohms} \tag{4.2}$$

The corresponding physical model of one phase of a polyphase induction motor is then as shown in Fig. 4.2.

4.4 DETERMINATION OF THE EQUIVALENT T NETWORK

A three- or a four-terminal network can be replaced by an equivalent circuit consisting of a T or a Π section if the impedance elements of that network are linear and bilateral and if no energy sources exist internal to the network.

The model shown in Fig. 4.2 meets these requirements and can therefore be represented by an equivalent circuit consisting of a T section, such as shown in Fig. 4.3.

To determine the equivalent circuit between input terminals 1 and 2 and output terminals 3 and 4, let the three impedances, Z_A, Z_B, and Z_C of the equivalent circuit, be found by performing electrical tests on the physical model shown in Fig. 4.2 or, theoretically, on one phase of the machine. Since there are three unknowns, it is necessary to perform three such independent tests in order to obtain three independent equations involving three unknowns.

4.4.1 Test 1

With secondary terminals n and o of the model open-circuited, measure the impedance across primary terminals ℓ and m, using the appropriate frequency, such as 60 Hz. By inspection of Fig. 4.3, the result corresponds to the sum of Z_A and Z_C of the equivalent circuit. Then

$$Z_A + Z_C = k_1 \quad \text{ohms} \tag{4.3}$$

where k_1 is the measured complex impedance across the primary winding of the model, with the secondary winding open-circuited.

4.4.2 Test 2

With secondary terminals n and o of the model short-circuited, measure the impedance across primary terminals ℓ and m, using the same frequency as for Test 1. By inspection of Fig. 4.3, the resulting equation involving the equivalent-circuit parameters is

$$Z_A + \frac{Z_B Z_C}{Z_B + Z_C} = k_2 \quad \text{ohms} \tag{4.4}$$

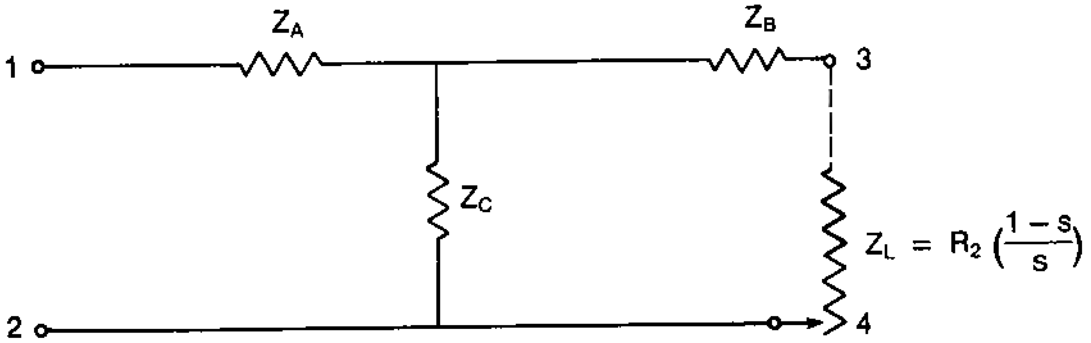

FIGURE 4.3 T-section equivalent circuit of one phase of a polyphase induction motor.

where k_2 is the measured complex impedance across the primary winding of the model, with the secondary winding short-circuited.

4.4.3 Test 3

With primary terminals ℓ and m of the model open circuited and with Z_L disconnected, measure the impedance across secondary terminals n and o, using the same frequency as for Test 1 and Test 2. By inspection of Fig. 4.3, this test would correspond to the sum of $Z_B + Z_C$. Then

$$Z_B + Z_C = k_3 \quad \text{ohms} \tag{4.5}$$

where k_3 is the measured complex impedance across the secondary winding of the model, with Z_L disconnected and with the primary winding open circuited.

4.4.4 Transformation of Physical Model Test Data into T-Network Impedances

Equations (4.3), (4.4), and (4.5) form a set of three independent equations with three unknown quantities, Z_A, Z_B, and Z_C. This set can then be solved for each unknown in terms of the three known quantities, k_1, k_2, and k_3. First, subtract eq. (4.4) from eq. (4.3), to give

$$Z_C - \frac{Z_B Z_C}{Z_B + Z_C} = k_1 - k_2 \quad \text{ohms} \tag{4.6}$$

From inspection of eq. (4.5),

$$Z_B + Z_C = k_3 \quad \text{ohms} \tag{4.7}$$

and

$$Z_C = k_3 - Z_B \quad \text{ohms} \tag{4.8}$$

Substituting eqs. (4.7) and (4.8) into eq. (4.6) yields

$$k_3 - Z_B - \frac{Z_B(k_3 - Z_B)}{k_3} = k_1 - k_2 \quad \text{ohms} \tag{4.9}$$

Multiplying eq. (4.9) by k_3 gives us

$$k_3^2 - k_3 Z_B - Z_B(k_3 - Z_B) = (k_1 - k_2)k_3 \quad \text{ohms}^2 \tag{4.10}$$

Rearranging eq. (4.10), we have

$$Z_B^2 - 2k_3 Z_B + k_3^2 - k_3(k_1 - k_2) = 0 \quad \text{ohms}^2 \tag{4.11}$$

Equation (4.11) is a quadratic equation with Z_B as the variable. Solving for Z_B yields

$$Z_B = k_3 \mp \sqrt{k_3(k_1 - k_2)} \quad \text{ohms} \tag{4.12}$$

Substituting eq. (4.12), the solution for Z_B, into eq. (4.8), we obtain

$$Z_C = k_3 - \left[k_3 \mp \sqrt{k_3(k_1 - k_2)}\right] = \pm\sqrt{k_3(k_1 - k_2)} \quad \text{ohms} \tag{4.13}$$

Finally, substituting eq. (4.13), the solution for Z_C, into eq. (4.3) gives us

$$Z_A \pm \sqrt{k_3(k_1 - k_2)} = k_1 \quad \text{ohms} \tag{4.14}$$

Rearranging yields

$$Z_A = k_1 \mp \sqrt{k_3(k_1 - k_2)} \quad \text{ohms} \tag{4.15}$$

4.4.5 Hypothetical Example

A hypothetical example will illustrate the transformation of test results of a physical model into equivalent T-network impedances. Let the test results, in per unit on the model's own volt-ampere rating, be

$$k_1 = 0.025 + j3.10 = 3.10/\underline{89.54^\circ} \quad \text{per unit} \tag{4.16}$$

$$k_2 = 0.053 + j0.197 = 0.204/\underline{74.94^\circ} \quad \text{per unit} \tag{4.17}$$

$$k_3 = 0.030 + j3.10 = 3.10/\underline{89.45^\circ} \quad \text{per unit} \tag{4.18}$$

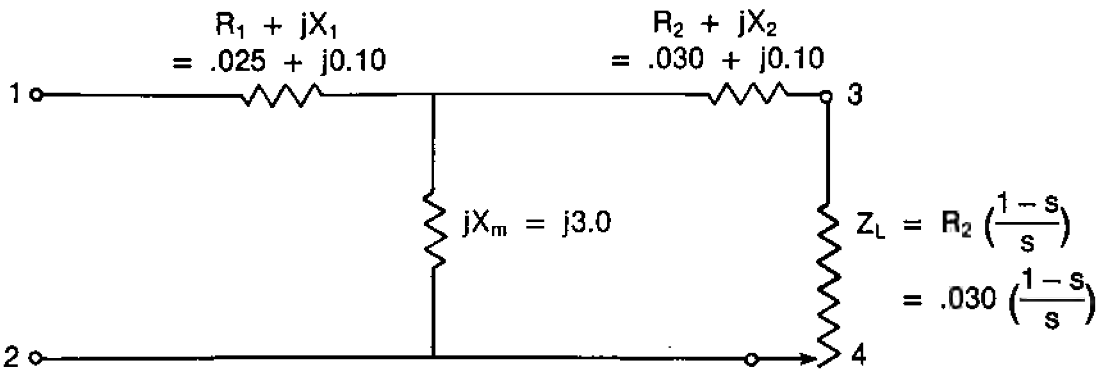

FIGURE 4.4 Equivalent circuit resulting from three hypothetical tests on a physical model.

To calculate the equivalent-circuit impedance Z_A, we use the equation

$$Z_A = k_1 \mp \sqrt{(k_1 - k_2)k_3} \quad \text{ohms or per unit} \tag{4.19}$$

Substituting the test data into eq. (4.19) gives us

$$Z_A = 3.10\underline{/89.54^\circ} \mp \sqrt{(3.10\underline{/89.54^\circ} - 0.204\underline{/74.94^\circ})(3.10\underline{/89.45^\circ})} \quad \text{per unit} \tag{4.20}$$

Upon simplification we have

$$Z_A = 0.025 + j0.10 \quad \text{per unit} \tag{4.21}$$

To calculate the equivalent-circuit impedance Z_B, we use the formula

$$Z_B = k_3 \mp \sqrt{(k_1 - k_2)k_3} \quad \text{ohms or per unit} \tag{4.22}$$

Substituting the test data into eq. (4.22) yields

$$Z_B = 3.10\underline{/89.45^\circ} \mp \sqrt{(3.10\underline{/89.54^\circ} - 0.204\underline{/74.94^\circ})(3.10\underline{/89.45^\circ})} \quad \text{per unit} \tag{4.23}$$

Upon simplification we have

$$Z_B = 0.030 + j0.10 \quad \text{per unit} \tag{4.24}$$

To calculate the equivalent-circuit impedance Z_C, we use the equation

$$Z_C = \pm\sqrt{(k_1 - k_2)k_3} \quad \text{ohms or per unit} \tag{4.25}$$

Substituting the test data into eq. (4.25) gives us

$$Z_C = \pm\sqrt{(3.10\underline{/89.54^\circ} - 0.204\underline{/74.94^\circ})(3.10\underline{/89.45^\circ})} \quad \text{per unit} \tag{4.26}$$

Upon simplification we obtain

$$Z_C = j3.0 \quad \text{per unit} \tag{4.27}$$

Then the resulting equivalent circuit is as shown in Fig. 4.4. The stator and rotor winding resistances are equal to 0.025 p.u. and 0.030 p.u., respectively, the stator and rotor winding leakage reactances are each equal to 0.10 p.u. and the magnetizing reactance is equal to 3.0 p.u. in this example. Although the impedance parameters of polyphase induction motors vary widely with rating and application, those shown in the hypothetical example of Fig. 4.4 are in the range of such parameters for a general-purpose induction motor of moderate size, with the parameters expressed in per unit on the machine's own input volt-ampere base. This numerical example is intended only to illustrate the relationship between the physical model of one phase of an induction machine and the resulting equivalent circuit which is used for analysis. In actual practice, as will become apparent later, the parameters of the equivalent circuit are calculated at the design stage from the geometry and the winding details of the machine under consideration. This allows the equivalent circuit to be used in calculating the performance of the machine at the design stage and prior to its manufacture.

4.5 EFFECT OF CORE LOSS ON THE EQUIVALENT CIRCUIT

The vector relationship of the magnetizing current, the energy component of primary current which sustains core loss and the induced voltages, is shown in Fig. 4.5 for an iron-core transformer at no-load condition. All quantities are effective values and are defined as

E_1 = induced voltage in the primary phase winding, volts/phase

E_2 = induced voltage in the secondary phase winding, volts/phase

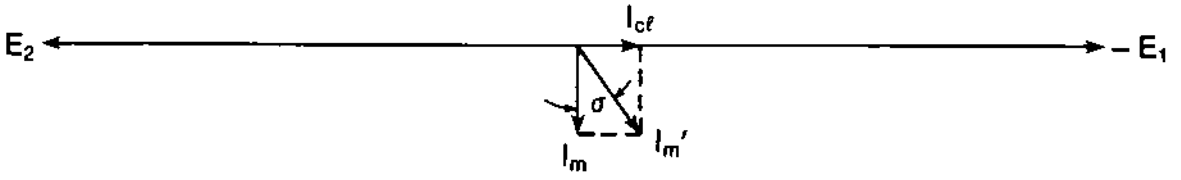

FIGURE 4.5 Vector diagram of excitation current components and of induced voltage of an iron-core transformer.

$I_{c\ell}$ = energy component of current in the primary phase winding which sustains core loss, amperes/phase

I_m = magnetizing component of current in the primary phase winding, amperes/phase

I_m' = vector sum of energy component $I_{c\ell}$ and magnetizing current I_m in the primary phase winding, amperes/phase

For such a transformer, the magnetizing current I_m is equal to a small percentage of full-load phase current, it being in the region of 5%. For an induction motor, however, the magnetizing current is equal to a significant percentage of rated phase current, typically ranging from 25 to 40%, and even more for low-speed machines. For both iron-core transformers and induction motors, the core loss varies with the rating but is of the order of 1 to 2% of the kVA rating of the unit. Accordingly, the value of $I_{c\ell}$ is approximately equal for the two machines in percent. The angle σ between I_m and I_m' is then considerably larger for the transformer than for the induction motor. Although σ varies with rating, it is typically of the order of 15 to 20 degrees for transformers and of the order of 2 to 3 degrees for induction motors.

Because of the considerably larger value of the angle σ which is present in transformers, a resistance in parallel with the magnetizing reactance X_m is usually added to the transformer equivalent circuit. The magnitude of this resistance is set equal to $R_{c\ell}$, such that $I_{c\ell}^2 R_{c\ell}$ equals the core loss attributable to one phase of the transformer under rated-voltage conditions. The original induction motor equivalent circuit, as suggested by Steinmetz, also had a corresponding resistance branch in parallel with X_m. However, because of the small value of the angle σ which actually exists in induction motors, no significant error results in the magnitude and angle of the magnetizing current if the resistance branch is omitted. Accordingly, this resistance branch is not usually added to the induction motor equivalent circuit, and the circuit shown in Fig. 4.3 has become the one in general use for most induction motor calculations in this country. In Chapter 5 an alternative way to account for the core-loss component, together with other components of loss, will be used.

4.6 EFFECT OF TURNS RATIO ON THE EQUIVALENT CIRCUIT

For an actual machine, the number of effective turns in series in the stator phase winding is, in general, not equal to the number of equivalent turns in series in the rotor phase winding. Accordingly, for both the physical model shown in Fig. 4.2 and the equivalent circuit shown in Fig. 4.3, the voltage induced in the primary winding by the mutual flux (i.e., by magnetizing current I_m flowing through the magnetizing reactance X_m of the equivalent circuit) will be different from that induced in the secondary phase winding. From Faraday's law, eq. (2.12),

$$e = -N \frac{d\phi}{dt} \quad \text{volts} \tag{4.28}$$

Then the voltage induced in the stator phase winding, due to the rate of change of the mutual flux, as determined by the supply bus frequency, is

$$e_1 = -N_1' \frac{d\phi_g}{dt} \quad \text{volts} \tag{4.29}$$

where

e_1 = voltage induced in the stator phase winding, volts

N_1' = effective turns in series in the stator phase winding, turns

ϕ_g = mutual flux, webers

The corresponding voltage induced in the rotor phase winding is

$$e_2 = -N_2' \frac{d\phi_g}{dt} \quad \text{volts} \tag{4.30}$$

where e_2 is the voltage induced in the rotor phase winding in volts and N_2' is the equivalent turns in series in the rotor phase winding, in turns. The rate of change of the mutual flux, $d\phi_g/dt$, is the same for both eqs. (4.29) and (4.30) when both are viewed from either the stationary stator or the rotating rotor. Solving for this quantity in each of the equations and equating the resulting expressions, we have

$$\frac{e_1}{N_1'} = \frac{e_2}{N_2'} \quad \text{volts/turn} \tag{4.31}$$

Solving for e_1 yields

$$e_1 = \frac{N_1'}{N_2'} e_2 \quad \text{volts} \tag{4.32}$$

The induced voltages e_1 and e_2 are instantaneous voltages as expressed in eqs. (4.31) and (4.32). Since the two voltages are proportional for all instantaneous values, including their maximum values, and since they both vary sinusoidally at the same frequency, when both are viewed from the stator or from the rotor, eq. (4.32) may also be written in rms, or effective, values as E_1 and E_2. Then

$$E_1 = \frac{N_1'}{N_2'} E_2 \quad \text{volts} \tag{4.33}$$

Equation (4.33) holds for the physical model and for the resulting equivalent circuit, when the voltages are expressed in volts and not in per unit or percent. Accordingly, the rotor induced voltage, and all other rotor voltages, must be multiplied by the turns ratio N_1'/N_2' when the rotor voltage is referred to the stator in an equivalent circuit for which actual units of volts are used. It is convenient to use the symbol a for the turns ratio, or

$$a = \frac{N_1'}{N_2'} \quad \text{numeric} \tag{4.34}$$

and

$$E_1 = aE_2 \quad \text{volts} \tag{4.35}$$

Let voltage be applied to the stator of a polyphase induction motor with either a squirrel-cage rotor or a wound rotor, the rotor phase circuits of which are closed. A current will then flow through each phase of the stator and the rotor phase windings. The rotor phase current, reacting on the mutual flux, will produce a torque on the rotor structure in accordance with Ampère's law. This torque will accelerate the rotor structure to full speed, after which the machine will operate as a drive motor. While operating as a drive motor, the rotor phase current I_2, flowing in the rotor phase winding, will produce a magnetomotive force of $N_2'I_2$ ampere turns, which tends to reduce the mutual flux ϕ_g and the resulting induced voltages E_1 and E_2. A reduction of E_1 will cause more stator current to flow, since the net stator phase voltage acting in the stator phase winding is equal to the applied bus voltage, less the induced voltage E_1. The stator current will increase until an equilibrium is established and the additional stator ampere turns just balance the rotor demagnetizing ampere turns $N_2'I_2$, or

$$N_1'I_1' = N_2'I_2 \quad \text{ampere-turns} \tag{4.36}$$

where I_1' is the component of stator phase current required to overcome the demagnetizing effect of rotor current I_2 in amperes. Solving for I_1' gives us

$$I_1' = \frac{N_2'}{N_1'} I_2 \quad \text{amperes} \tag{4.37}$$

and from eq. (4.34), we have

$$I_1' = \frac{1}{a} I_2 \quad \text{amperes} \tag{4.38}$$

Accordingly, the rotor current must be divided by the turns ratio N_1'/N_2' when the rotor current is referred to the stator in an equivalent circuit, for which actual units of amperes are used.

The impedance of the rotor of the equivalent circuit may be expressed as

$$Z_2 = \frac{E_2}{I_2} \quad \text{ohms} \tag{4.39}$$

Remembering from the above that when referring rotor voltage to the stator, it is multiplied by the turns ratio a, and when referring the rotor current to the stator, it is divided by a

$$Z_2' = \frac{aE_2}{I_2/a} = \frac{a^2 E_2}{I_2} \quad \text{ohms} \tag{4.40}$$

where Z_2' is the rotor equivalent-circuit impedance referred to the stator. Then

$$Z_2' = a^2 Z_2 \quad \text{ohms} \tag{4.41}$$

and it follows that

$$R_2' = a^2 R_2 \quad \text{ohms} \tag{4.42}$$

$$X_2' = a^2 X_2 \quad \text{ohms} \tag{4.43}$$

where R_2' is the rotor equivalent-circuit resistance referred to the stator and X_2' is the rotor equivalent-circuit leakage reactance referred to the stator. Thus the rotor impedance must be multiplied by the turns ratio raised to the second power, or by a^2, when the rotor impedance is referred to the stator in an equivalent-circuit calculation for which actual units of ohms are used.

4.7 USE OF ACTUAL UNITS FOR EQUIVALENT-CIRCUIT CALCULATIONS

When performing equivalent-circuit calculations, it is desirable to transfer all stator quantities to the rotor side or, conversely, to transfer all rotor quantities to the stator side and, thereby, eliminate further concern with the turns ratio during the circuit calculation. Although either side may be used, it is more convenient, in many cases, to work with the rotor quantities referred to the stator side. For example, the stator winding is electrically connected to the voltage supply bus, through a circuit breaker or a motor starter. If the regulation, or short-circuit kVA, of the supply bus is known, the voltage dip during starting may be calculated directly, along with other quantities, if the rotor quantities are referred to the stator. Also, the power factor of an induction motor is defined and calculated from the viewpoint of the stator terminals.

After the calculations are performed and numerical results are available, any specific quantity that involves volts, amperes, or ohms may be referred back to its actual rotor value by multiplying by the appropriate turns-ratio coefficient. The rotor phase current of a wound-rotor motor, for example, should be multiplied by the coefficient a to refer it back to the actual rotor phase current value. The rotor phase current was tacitly multiplied by 1/a when the decision was made to perform the calculation on the stator side, which automatically required that the rotor current be referred

TABLE 4.1 Procedure for Using Actual Units Referred to the Stator

Quantity	To refer rotor quantities to the stator side for calculation, multiply by:	After calculation, to refer rotor quantities back to the rotor, multiply by:
Voltage (volts/phase)	a	$1/a$
Current (amperes/phase)	$1/a$	a
Impedance (ohms/phase)	a^2	$1/a^2$

TABLE 4.2 Procedure for Using Actual Units Referred to the Rotor

Quantity	To refer stator quantities to the rotor side for calculation, multiply by:	After calculation, to refer stator quantities back to the stator, multiply by:
Voltage (volts/phase)	$1/a$	a
Current (amperes/phase)	a	$1/a$
Impedance (ohms/phase)	$1/a^2$	a^2

to the stator side during the calculation. Accordingly, the calculated value of rotor phase current must be multiplied by the coefficient a, after circuit calculations are completed, in order to obtain the value of amperes as seen in the actual rotor phase winding of the machine. Tables 4.1 and 4.2 summarize the procedure for handling actual units of volts, amperes, and ohms when making calculations with the equivalent circuit.

Calculated performance quantities, such as I^2R, slip, torque, and so on, constitute valid results, as calculated, without consideration as to which side of the equivalent circuit the original quantities of volts, amperes, and ohms were referred. This is because the turns ratio cancels, as a factor, in the expression. For example, the rotor I^2R calculated from the equivalent circuit may be used directly after calculation. If, in this case, the rotor circuit quantities were referred to the stator side, the actual rotor ohmic resistance was multiplied by $(1/a)^2$ and it was tacitly understood that the rotor current was multiplied by a. Then, for the resulting expression of rotor copper loss,

$$(aI_2)^2 \frac{R_2}{a^2} = I_2^2R_2 \quad \text{watts} \tag{4.44}$$

4.7.1 Example of Use of Actual Units

Use of the stator-to-rotor turns ratio when using actual units of volts, amperes, and ohms will be illustrated with an example. Consider a 1500-hp polyphase wound-rotor induction motor with a stator wound for 4000 V line to line, and with stator and rotor winding parameters as follows:

Parameter	Magnitude (ohms/phase)
Stator resistance	0.143, referred to the stator
Stator leakage resistance	1.03, referred to the stator
Magnetizing reactance	59.4, referred to the stator
Rotor resistance	0.096, referred to the rotor
Rotor leakage reactance	0.601, referred to the rotor

The ratio of the effective turns in series of the stator phase winding to that of the rotor phase winding, or the value of a, is equal to 1.33 and both the stator and rotor windings are connected in wye. The equivalent circuit for one phase of the motor, similar to that shown in Fig. 4.4, but with the parameters above, is shown in Fig. 4.6.

Let it be required to (1) determine the voltage between the rotor-circuit slip rings, at blocked-rotor conditions, with the brushes lifted (i.e., with the rotor winding open-circuited between points 3 and 4 in Fig. 4.6) and with full voltage applied to the stator winding, and to (2) determine the rotor current corresponding to a slip of 0.012 per unit with the brushes of the three different rotor phases short circuited (i.e., with no additional external resistance in the rotor circuit).

To determine requirement 1, the open-circuited rotor voltage under blocked-rotor conditions is equal to the voltage across X_m. With the rotor circuit open circuited,

$$I_1 = \frac{V_1}{R_1 + j(x_1 + X_m)} \quad \text{amperes/phase} \tag{4.45}$$

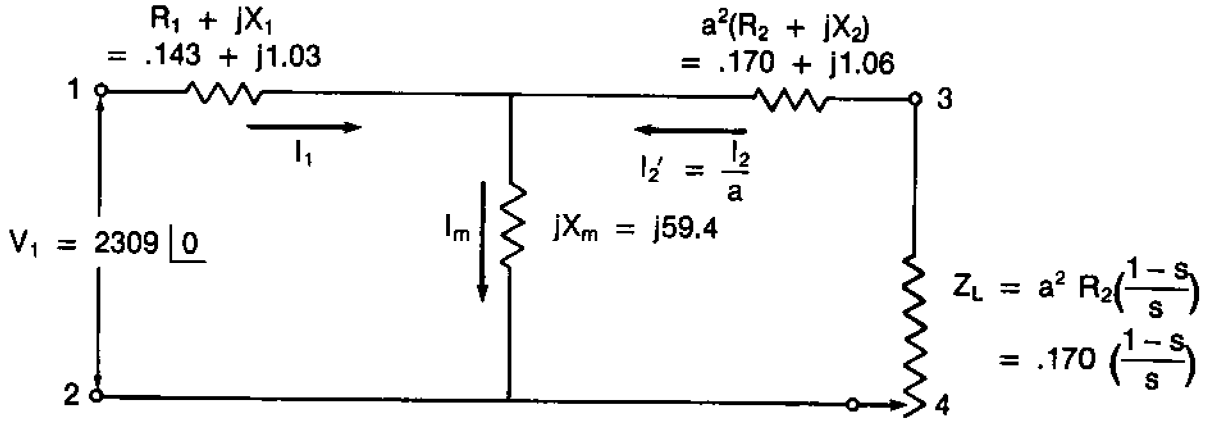

FIGURE 4.6 Polyphase induction motor equivalent circuit with parameters in actual units.

or for the parameters in Fig. 4.6,

$$I_1 = \frac{2309\underline{/0^\circ}}{0.143 + j60.43} = \frac{2309\underline{/0^\circ}}{60.43\underline{/89.9^\circ}} = 38.2\underline{/-89.9^\circ} \quad \text{amperes/phase} \tag{4.46}$$

Then the magnitude of open-circuit voltage, referred to the stator, is

$$V_2' = I_1 X_m \quad \text{volts/phase} \tag{4.47}$$

or for the parameter in Fig. 4.6,

$$V_2' = (38.2)(59.4) = 2269 \quad \text{volts/phase} \tag{4.48}$$

To refer this voltage back to the rotor,

$$V_2' = aV_2 \quad \text{volts/phase} \tag{4.49}$$

or

$$V_2 = \frac{1}{a} V_2' \quad \text{volts/phase} \tag{4.50}$$

and the actual rotor phase voltage is

$$V_2 = \left(\frac{1}{1.33}\right)(2269) = 1706 \quad \text{volts/phase} \tag{4.51}$$

However, the voltage between slip rings is a line-to-line voltage. Therefore, for this wye-connected rotor winding, the voltage between slip rings is

$$V_{\underline{2}(L-L)} = \left(\sqrt{3}\right)(1706) = 2955 \quad \text{volts, line to line} \tag{4.52}$$

To determine requirement 2, it is necessary to calculate the rotor current corresponding to 0.012 per unit slip, with the slip rings shorted. Writing Kirchhoff's voltage equation around the rotor and stator loops and letting $I_2/a = I_2'$, we have

$$I_1(0.143 + j1.03) + (I_1 + I_2')(j59.4) = 2309\underline{/0^\circ} \quad \text{volts/phase} \tag{4.53}$$

$$I_2'\left(\frac{0.170}{0.012} + j1.06\right) + (I_2' + I_1)(j59.4) = 0 \quad \text{volts/phase} \tag{4.54}$$

Rearranging eqs. (4.53) and (4.54), putting the complex quantities into polar form, and using the simplified polar notation, $A\epsilon^{j\theta} = A/\underline{\theta}$ yields

$$(60.4/\underline{89.9^\circ})I_1 + (59.4/\underline{90^\circ})I_2' = 2309/\underline{0^\circ} \quad \text{volts/phase} \tag{4.55}$$

$$(59.4/\underline{90^\circ})I_1 + (62.1/\underline{76.8^\circ})I_2' = 0 \quad \text{volts/phase} \tag{4.56}$$

Solving for I_2', we have

$$I_2' = \frac{\begin{vmatrix} 60.4/\underline{89.9^\circ} & 2309/\underline{0^\circ} \\ 59.4/\underline{90^\circ} & 0 \end{vmatrix}}{\begin{vmatrix} 60.4/\underline{89.9^\circ} & 59.4/\underline{90^\circ} \\ 59.4/\underline{90^\circ} & 62.1/\underline{76.8^\circ} \end{vmatrix}} = 157.3/\underline{172^\circ} \quad \text{amperes/phase} \tag{4.57}$$

To refer this current back to the rotor, we use

$$I_2' = \frac{I_2}{a} \quad \text{amperes/phase} \tag{4.58}$$

or

$$I_2 = aI_2' \quad \text{amperes/phase} \tag{4.59}$$

$$I_2 = (1.33)(157.3/\underline{172^\circ}) = 209/\underline{172^\circ} \quad \text{amperes/phase} \tag{4.60}$$

Thus the rotor phase current is equal to 209 A when the shaft load is of such a magnitude that the slip is equal to 0.012 p.u.

4.8 USE OF PER UNIT QUANTITIES FOR EQUIVALENT-CIRCUIT CALCULATIONS

It is frequently useful to convert quantities that involve volts, amperes, and ohms to per unit quantities before performing equivalent-circuit calculations. This permits using quantities whose magnitudes are in the general region of unity. Also, when quantities are in per unit, the person performing the calculation will have a more intuitive feeling for the relative magnitude of each quantity.

To establish the per unit system, a three-phase volt-ampere base $(VA)_b$ and a line-to-line voltage base E_{L-L} is selected. Normal voltage, normal current, and normal impedance are then defined as follows:

$$\text{normal voltage} = E_n = \frac{E_{L-L}}{\sqrt{3}} \quad \text{volts} \tag{4.61}$$

$$\text{normal current} = I_n = \frac{(VA)_b}{\sqrt{3}\,E_{L-L}} \quad \text{amperes} \tag{4.62}$$

$$\text{normal impedance} = Z_n = \frac{E_n}{I_n} = \frac{E^2_{L-L}}{(VA)_b} \quad \text{ohms} \tag{4.63}$$

The per unit value of a specific voltage, current, or impedance is equal to the actual value divided by the normal value. For example, if the actual value of the stator leakage reactance is equal to 0.251 Ω per phase and the value of normal impedance Z_n is equal to 2.90 Ω, the per unit value of the stator leakage reactance is then equal to 0.251/2.90 = 0.087 p.u.

Any three-phase volt-ampere base and any line-to-line voltage base may be selected for use in performing calculations on the equivalent circuit, (1) provided that the resulting per unit values are converted back to actual units at the conclusion of the calculation, or (2) provided that the volt-ampere base and the voltage base are made known to anyone who might want to use the resulting per unit values.

Although any volt-ampere base and any voltage base may be used, some are more convenient and more applicable than others and are therefore preferable. Two such preferable bases are (1) the machine's own rated volt-ampere output, and (2) the machine's own rated volt-ampere input, with the voltage base being the stator line-to-line voltage for both. The output volt-ampere rating is equal to the nameplate horsepower rating, converted to volt-amperes, or

$$(VA)_{bo} = 746\ \text{hp} \quad \text{volt-amperes} \tag{4.64}$$

Normal current, on an output base, is

$$I_{no} = \frac{746\,\text{hp}}{\sqrt{3}\,E_{L-L}} \quad \text{amperes} \tag{4.65}$$

and normal impedance is

$$Z_{no} = \frac{E^2_{L-L}}{746\ \text{hp}} \quad \text{ohms} \tag{4.66}$$

The horsepower rating and the stator line-to-line voltage are both stamped on the machine's nameplate and are therefore available to all who have access to the machine. From this standpoint, the machine's own volt-ampere output constitutes a desirable per unit base. However, the machine's own volt-ampere input has the advantage that when used with the stator voltage as the corresponding voltage base, normal current is equal to the actual stator current of the machine at rated load.

The input volt-ampere rating is equal to the nameplate horsepower rating, converted to volt-amperes and divided by full-load power factor and full-load efficiency, or

$$(\mathrm{VA})_{\mathrm{bi}} = \frac{746\ \mathrm{hp}}{(\mathrm{PF})(\eta)} \quad \text{volt-amperes} \tag{4.67}$$

where PF is the full-load power factor, in per unit, and η is the full-load efficiency, in per unit. Then normal current, on an input base, is

$$I_{\mathrm{ni}} = \frac{746\ \mathrm{hp}}{\sqrt{3}\,E_{\mathrm{L-L}}(\mathrm{PF})(\eta)} \quad \text{amperes} \tag{4.68}$$

and normal impedance is

$$Z_{\mathrm{ni}} = \frac{(E_{\mathrm{L-L}})^2(\mathrm{PF})(\eta)}{746\ \mathrm{hp}} \quad \text{ohms} \tag{4.69}$$

An inspection of eqs. (4.65) and (4.68) shows that for the same horsepower and stator voltage ratings, the ratio of normal current for the two volt-ampere bases is

$$\frac{I_{\mathrm{ni}}}{I_{\mathrm{no}}} = \frac{1}{(\mathrm{PF})(\eta)} \quad \text{numeric} \tag{4.70}$$

Since PF and η are always less than 1.0, normal current for the input base is greater than that for the output base, for the same machine. Since the actual current is divided by base current, to give per unit current, full-load stator current is equal to 1.0 per unit on an input basis, and if the machine has a rated power factor of 0.90 and a rated efficiency of 0.94, for example, full-load stator current is equal to $1.0/(0.90)(0.94) = 1.182$ per unit on an output basis, for the same actual amperes.

In a similar manner, an inspection of eqs. (4.66) and (4.69) shows that for the same horsepower and stator voltage ratings, the ratio of normal impedance for the two volt-ampere bases is

TABLE 4.3 Procedure for Calculating Normal Values for the Per Unit System

Type of VA base	Value of VA base	Value of voltage base	Normal volts	Normal amperes	Normal ohms
Any VA base	$(VA)_b$	E_{L-L}	$\frac{E_{L-L}}{\sqrt{3}}$	$\frac{(VA)_b}{\sqrt{3}\,E_{L-L}}$	$\frac{(E_{L-L})^2}{(VA)_b}$
Rated VA output	746 hp	E_{L-L}	$\frac{E_{L-L}}{\sqrt{3}}$	$\frac{746\text{ hp}}{\sqrt{3}\,E_{L-L}}$	$\frac{(E_{L-L})^2}{746\text{ hp}}$
Rated VA input	$\frac{746\text{ hp}}{(PF)(\eta)}$	E_{L-L}	$\frac{E_{L-L}}{\sqrt{3}}$	$\frac{746\text{ hp}}{\sqrt{3}\,E_{L-L}(PF)(\eta)}$	$\frac{(E_{L-L})^2(PF)(\eta)}{746\text{ hp}}$

$$\frac{Z_{ni}}{Z_{no}} = (PF)(\eta) \quad \text{numeric} \tag{4.71}$$

Again, since rated power factor and rated efficiency are always less than 1.0, normal impedance for the input base is less than that for the output base, for the same machine. Since the actual ohmic value of the impedance is divided by normal impedance, to give per unit impedance, an element of impedance, such as the stator leakage reactance, will be greater on an input base than on an output base. The procedure for establishing normal voltage, normal current, and normal impedance is summarized in Table 4.3.

4.8.1 Example of Use of Per Unit Quantities

Use of the per unit system will be illustrated by use of the previous example of the 1500-hp 4000-V polyphase wound-rotor induction motor used to illustrate the use of turns ratio, for which the parameters have been given previously. Since power factor and efficiency are not known, the machine's output will be selected as the kVA base. Then, to determine normal volts, from Table 4.3,

$$E_n = \frac{E_{L-L}}{\sqrt{3}} = \frac{4000}{\sqrt{3}} = 2309 \quad \text{volts/phase} \tag{4.72}$$

and to determine normal amperes,

$$I_n = \frac{746\ \text{hp}}{\sqrt{3}\,E_{L-L}} = \frac{(746)(1500)}{(\sqrt{3})(4000)} = 161.5 \quad \text{amperes/phase} \tag{4.73}$$

and to determine normal ohms,

$$Z_n = \frac{(E_{L-L})^2}{746\ \text{hp}} = \frac{(4000)^2}{(746)(1500)} = 14.3 \quad \text{ohms/phase} \tag{4.74}$$

Normal ohms may also be determined from the ratio of normal volts to normal amperes, as

$$Z_n = \frac{E_n}{I_n} = \frac{2309}{161.5} = 14.3 \quad \text{ohms/phase} \tag{4.75}$$

The ohmic values of the machine parameters referred to the stator for the previous example can be converted to per unit by dividing by normal ohms. Then

Parameter	Ohmic value, referred to the stator (ohms/phase)	Per unit value, referred to the stator (p.u.)
Stator resistance	0.143	0.010
Stator leakage reactance	1.03	0.072
Magnetizing reactance	59.4	4.154
Rotor resistance	0.170	0.012
Rotor leakage reactance	1.06	0.074

The equivalent circuit of one phase of the machine with per unit parameters all referred to the stator, is shown in Fig. 4.7.

To determine requirement 1, the voltage between slip rings at blocked-rotor condition, with the brushes lifted and with full voltage applied to the stator winding, it is first necessary to determine the voltage across X_m. With the rotor open circuited between points 3 and 4 (i.e., with the brushes lifted),

$$I_1 = \frac{V_1}{R_1 + j(X_1 + X_m)} = \frac{1.0/\underline{0^\circ}}{0.010 + j4.226} \quad \text{per unit} \tag{4.76}$$

Putting all quantities into polar form, we have

$$I_1 = \frac{1.0/\underline{0^\circ}}{4.226/\underline{89.9^\circ}} = 0.2366/\underline{-89.9^\circ} \quad \text{per unit} \tag{4.77}$$

The magnitude of the open-circuited voltage, referred to the stator, is

$$V_2' = I_1 X_m \quad \text{per unit} \tag{4.78}$$

or

$$V_2' = (0.2366)(4.154) = 0.9828 \quad \text{per unit} \tag{4.79}$$

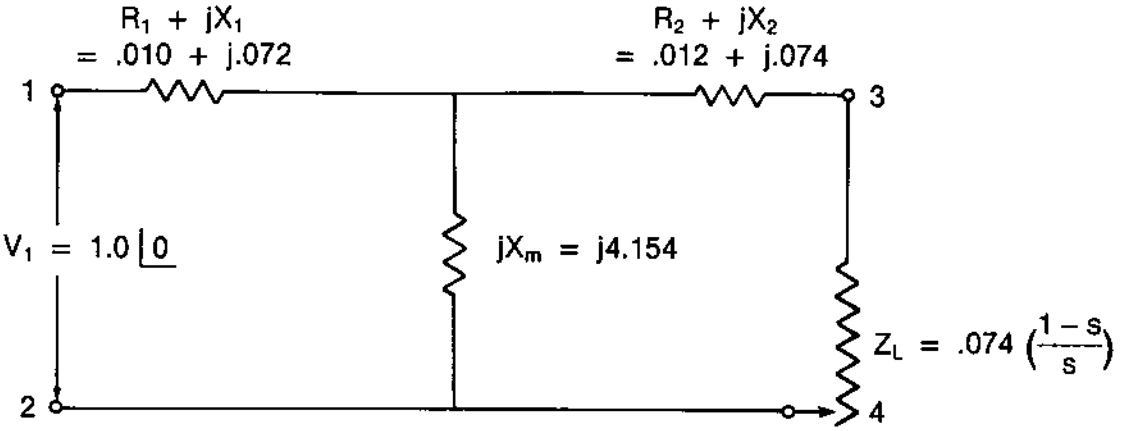

FIGURE 4.7 Polyphase induction motor equivalent circuit with parameters in per unit.

To transfer from per unit to actual volts, the value above must be multiplied by normal volts or V_n.

$$V_2' = (2309)(0.9828) = 2269 \quad \text{volts/phase} \tag{4.80}$$

To refer V_2' back to the rotor, it must be divided by the turns ratio, or

$$V_2 = \frac{2269}{1.33} = 1706 \quad \text{volts/phase} \tag{4.81}$$

Since the value above is a phase voltage and since the desired voltage between slip rings is a line-to-line voltage,

$$V_{2(L-L)} = (\sqrt{3})(1706) = 2955 \quad \text{volts, line to line} \tag{4.82}$$

which agrees with that value calculated in eq. (4.52).

To determine requirement 2, or the rotor current corresponding to 0.012 per unit slip, it is necessary to write Kirchhoff's voltage equations around the rotor and stator loops of the circuit in Fig. 4.7 and then to solve for I_2'. Writing the voltage equation for the stator loop, we have

$$(0.010 + j0.072)I_1 + (I_1 + I_2')(j4.154) = 1.0\underline{/0^\circ} \quad \text{per unit} \tag{4.83}$$

Writing the voltage equation for the rotor loop with the slip set at s = 0.012 per unit gives us

$$(I_1 + I_2')(j4.154) + \left(\frac{0.012}{0.012} + j0.074\right)I_2' = 0 \quad \text{per unit} \tag{4.84}$$

Simplifying eqs. (4.83) and (4.84) yields

$$(4.226/\underline{89.9^\circ})I_1 + (4.154/\underline{90^\circ})I_2' = 1.0/\underline{0^\circ} \quad \text{per unit} \tag{4.85}$$

$$(4.154/\underline{90^\circ})I_1 + (4.340/\underline{76.8^\circ})I_2' = 0 \quad \text{per unit} \tag{4.86}$$

Solving for I_2', we have

$$I_2' = \frac{\begin{vmatrix} 4.226/\underline{89.9^\circ} & 1.0/\underline{0^\circ} \\ 4.154/\underline{90^\circ} & 0 \end{vmatrix}}{\begin{vmatrix} 4.226/\underline{89.9^\circ} & 4.154/\underline{90^\circ} \\ 4.154/\underline{90^\circ} & 4.340/\underline{76.8^\circ} \end{vmatrix}} = 0.974/\underline{172^\circ} \quad \text{per unit} \tag{4.87}$$

To transfer from per unit to amperes, this value of I_2' must be multiplied by normal amperes. Then

$$I_2' = (161.5)(0.974)/\underline{172^\circ}) = 157.3/\underline{172^\circ} \quad \text{amperes/phase} \tag{4.88}$$

To refer I_2' back to the rotor, we use

$$I_2 = aI_2' \quad \text{amperes/phase} \tag{4.89}$$

Substituting the appropriate values into eq. (4.89) gives us

$$I_2 = (1.33)(157.3)/\underline{172^\circ}) = 209/\underline{172^\circ} \quad \text{amperes/phase} \tag{4.90}$$

or the rotor phase current is equal to 209 A when the shaft load is such that the slip is equal to 0.012 p.u. This value of I_2 agrees with that calculated in eq. (4.60).

5

Analysis of the Equivalent Circuit

5.1 Introduction 59
5.2 Formulation of the Equivalent Circuit 60
5.3 Determination of the Stator and Rotor Phase Currents 64
5.4 Determination of the Power Output 67
5.5 Determination of Efficiency and Power Factor at Full Load 70
5.6 Determination of Efficiency and Power Factor at Part Load 76
5.7 Derivation of the General Torque Equation 81
5.8 Maximum Torque 85
5.9 Starting Torque 90
5.10 Starting Current 92
5.11 The Speed-Torque Curve 93
5.12 The Speed-Current Curve 95

5.1 INTRODUCTION

In the preceding chapter it was shown that one phase of a polyphase induction motor can be represented electrically by a T-section equivalent circuit such as that shown in Fig. 4.3. This algorithm has been found to be very important in analyzing the behavior of the polyphase induction motor and in predicting its performance. The stator and rotor phase resistance and leakage reactance and the phase magnetizing reactance can be calculated from the geometry and the winding details of either the actual or the contemplated machine. When these calculated values are assigned to the corresponding impedances of the equivalent circuit, the stator and rotor currents can then be calculated for any desired speed or load condition. Stator and rotor copper losses can, of course, be calculated from the equivalent circuit. If the other components of losses (i.e., core loss, load loss, and friction and windage) are also known, essentially all of the usual performance characteristics, such as speed-torque characteristics, speed-current characteristics, efficiency, power factor, and so on, can be calculated. However, as will subsequently be shown, an iterative process may be necessary to obtain accurate values for some of the performance characteristics, since the components of loss, except for the rotor and stator resistance losses, are not modeled in the basic equivalent circuit.

It should be noted that stator leakage reactance X_1, rotor leakage reactance X_2, and rotor resistance R_2 are not constants, strictly speaking, for all conditions of operations in the actual machine and, therefore, in the equivalent circuit. As discussed later, some of the ferrous paths for leakage flux tend to saturate at lower speeds, during acceleration, because of the saturating effect of the large current flowing in the actual stator and rotor windings at such speeds. This has the effect of reducing the permeance, or of increasing the reluctance, of the leakage flux paths, which results in less leakage flux per ampere and hence less leakage inductance. Also, since the frequency of rotor-bar current approaches 60 Hz at low speeds, the bar current tends to be crowded to the upper part of the rotor bars. This, in turn, produces two rotor-bar effects. The first effect is an increase in effective resistance of the rotor bar and, therefore, of the rotor phase resistance at lower speeds. The second effect is a reduction in the effective height of the rotor bar, which reduces the rotor-slot leakage inductance, further reducing the rotor phase leakage reactance at lower speeds.

The blocked-rotor leakage reactance and the full-speed leakage reactance are both calculated from the geometry and the winding details of the machine. Also, the rotor-bar effective resistance is calculated for the blocked-rotor condition and the full-speed condition, as well as for any intermediate speeds that might be desired. In making numerical calculations, it is only necessary to insert the proper numerical values of these quantities into the equivalent circuit, depending on the operating conditions for which the numerical calculations are intended.

5.2 FORMULATION OF THE EQUIVALENT CIRCUIT

Assume that the rotor winding of a polyphase induction motor is open-circuited and that bus voltage is applied to the stator winding terminals. Then the only magnetomotive forces acting are those produced by the current flowing in the stator winding. The portion of the T-section equivalent circuit that represents this condition is shown in Fig. 5.1.

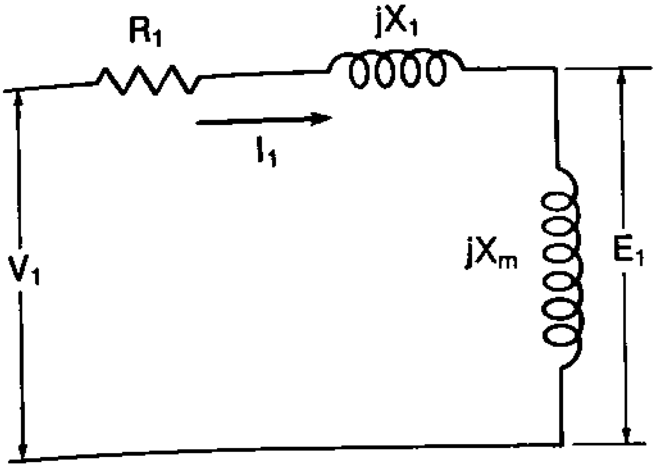

FIGURE 5.1 Equivalent circuit that represents the stator with an open-circuited rotor winding.

The bus voltage V_1 impressed across the stator terminals will cause a current I_1 to flow in each phase of the stator winding, the magnitude of which is equal to

$$I_1 = \frac{V_1}{R_1 + j(X_1 + X_m)} \quad \text{amperes/phase} \tag{5.1}$$

This current produces a rotating magnetomotive-force wave in the stator winding of the machine which, as shown earlier, produces a rotating air-gap flux wave. From the viewpoint of the equivalent circuit, the current flows through, and excites, the magnetizing reactance X_m associated with the mutual flux ϕ_m, which, in turn, flows through the magnetic circuit of the machine. The component of stator current that flows through the magnetizing reactance X_m is the magnetizing current I_m, one definition of which is

$$I_m = \frac{V_1}{R_1 + j(X_1 + X_m)} \quad \text{amperes/phase} \tag{5.2}$$

For the condition of an open-circuited rotor winding, it is apparent that $I_1 = I_m$. In the actual machine, the air-gap flux wave, which is sustained by I_m, rotates at an angular velocity of ω radians/second, as seen by the stator, and induces a voltage E_1 in the windings. From the viewpoint of the equivalent circuit, the magnitude of this induced voltage is equal to the bus voltage impressed on the stator terminals V_1, less the voltage drop caused by the current flowing through the stator winding resistance R_1 and stator winding leakage reactance X_1.

It is necessary, however, that the instantaneous polarity of the induced voltage be consistent with the circuit constraints that are placed on it. For V_1, the voltage impressed across the stator circuit, to be considered a voltage rise relative to the circuit, the induced voltage in the stator circuit E_1 should be considered a voltage drop relative to the stator circuit. Further, as will soon become apparent, the induced voltage in the rotor circuit E_2, which is equal to E_1 in magnitude and angle when referred to the stator, should be considered a voltage rise relative to the rotor circuit. Then, writing Kirchhoff's voltage equation for the circuit in Fig. 5.1, we have

$$V_1 - I_1(R_1 + jX_1) - (-E_1) = 0 \quad \text{volts/phase} \tag{5.3}$$

The wave shape of the generated voltage E_1 in the actual machine is the same as that of the bus voltage impressed across the stator winding terminals V_1, in general, except as the impedance drop affects it. Factors that cause harmonics in the space distribution of the air-gap flux wave, such as slot harmonics, for example, produce voltages of fundamental frequency in the stator winding, and such effects are included in the stator leakage reactance. This subject will be considered subsequently when zigzag and belt leakage reactances are studied as components of leakage reactance.

Assume that the rotor winding of the machine is now closed and that bus voltage is applied to the terminals of the stator winding. The rotating flux wave, produced by current flowing in the stator winding, will induce a voltage in the rotor winding, and since the rotor winding is closed, rotor current will flow and the rotor structure will rotate due to the torque produced. The actual voltage induced in the rotor winding E_2 is equal to E_1 at blocked-rotor conditions. In general, it is equal to E_1, multiplied by the rotor slip s. As defined in eq. (3.39), per unit slip is equal to the difference in speed between the rotating stator magnetomotive-force wave and the rotor structure, divided by the speed of the stator wave. In equation form,

$$s = \frac{n_s - n}{n_s} \quad \text{per unit} \tag{5.4}$$

with the quantities as originally defined. Then the actual voltage induced in the rotor winding is equal to

$$E_2 = sE_1 \quad \text{volts/phase} \tag{5.5}$$

The resulting current flowing in the rotor circuit is

$$I_2 = \frac{E_2}{R_2 + jX_{s2}} = \frac{sE_1}{R_2 + jX_{s2}} \quad \text{amperes/phase} \tag{5.6}$$

where R_2 is the rotor winding resistance, in ohms/phase, and X_{s2} is the rotor winding leakage reactance at slip frequency, in ohms/phase. Since, as stated above, the rotor slip s is defined as the difference in speed between synchronous speed and the speed of the rotor structure, expressed in per unit of synchronous speed, the actual rotor frequency f_2 is equal to

$$f_2 = sf_1 \quad \text{hertz} \tag{5.7}$$

Accordingly, if X_2 is the leakage reactance of the rotor winding, in ohms/phase, at a rotor circuit frequency of 60 Hz, the rotor winding leakage reactance at any value of slip s is

$$X_{s2} = sX_2 \quad \text{ohms/phase} \tag{5.8}$$

Equation (5.6) may then be written as

$$I_2 = \frac{sE_1}{R_2 + jsX_2} = \frac{sE_1}{\sqrt{(R_2)^2 + (sX_2)^2}} \quad \text{amperes/phase} \tag{5.9}$$

Dividing the numerator and denominator of eq. (5.9) by s yields

$$I_2 = \frac{E_1}{R_2/s + jX_2} = \frac{E_1}{\sqrt{(R_2/s)^2 + (X_2)^2}} \quad \text{amperes/phase} \tag{5.10}$$

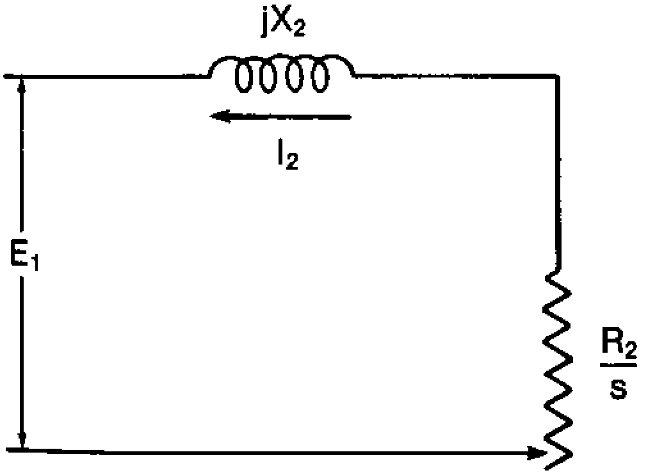

FIGURE 5.2 Equivalent circuit that represents the rotor circuit.

Then the equivalent circuit for this equation, which represents one phase of the rotor winding, is shown in Fig. 5.2. Combining Fig. 5.1, the equivalent circuit for one phase of the stator winding, with Fig. 5.2, the equivalent circuit for one phase of the rotor winding, at the common point of the induced voltage E_1, forms the equivalent circuit of one phase of the entire polyphase induction motor. It is usual practice to refer the impedance values to the stator side, when working with the equivalent circuit, and in the following, that is assumed unless otherwise stated.

5.3 DETERMINATION OF THE STATOR AND ROTOR PHASE CURRENTS

First we write the Kirchhoff voltage equations around the two loops of the equivalent circuit in Fig. 5.3:

$$I_1(R_1 + jX_1) + (I_1 + I_2)jX_m = V_1 \quad \text{volts/phase} \tag{5.11}$$

$$(I_2 + I_1)jX_m + I_2\left(\frac{R_2}{s} + jX_2\right) = 0 \quad \text{volts/phase} \tag{5.12}$$

Rearranging the two equations above gives us

$$[R_1 + j(X_1 + X_m)]I_1 + jX_mI_2 = V_1 \quad \text{volts/phase} \tag{5.13}$$

$$jX_mI_1 + \left[\frac{R_2}{s} + j(X_2 + X_m 0\right]I_2 = 0 \quad \text{volts/phase} \tag{5.14}$$

Solving for I_1, we obtain

$$I_1 = \frac{\begin{vmatrix} V_1 & jX_m \\ 0 & \dfrac{R_2}{s} + j(X_2 + X_m) \end{vmatrix}}{\begin{vmatrix} R_1 + j(X_1 + X_m) & jX_m \\ jX_m & \dfrac{R_2}{s} + j(X_2 + X_m) \end{vmatrix}} \quad \text{amperes/phase} \tag{5.15}$$

$$I_1 = \frac{V_1[R_2/s + j(X_2 + X_m)]}{[R_1 + j(X_1 + X_m)][R_2/s + j(X_2 + X_m)] - (jX_m)^2} \quad \text{amperes/phase} \tag{5.16}$$

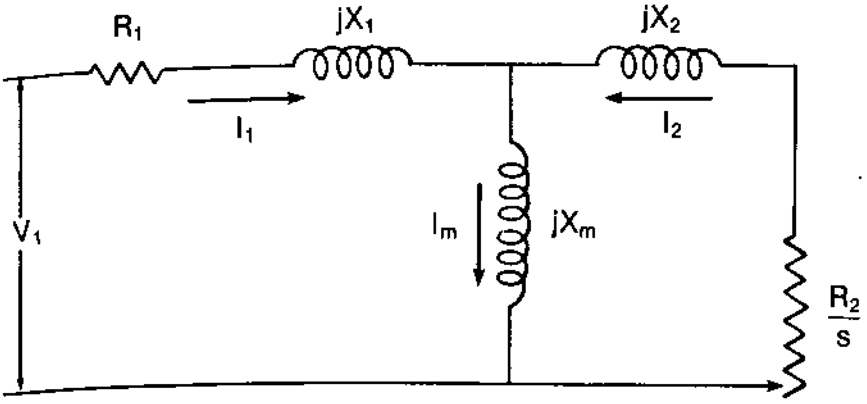

FIGURE 5.3 Equivalent circuit of one phase of the polyphase induction motor.

Rearranging eq. (5.16) by collecting the real parts together and the imaginary parts together, we obtain

$$I_1 = \frac{V_1[R_2/s + j(X_2 + X_m)]}{[R_1(R_2/s) - X_1X_2 - X_m(X_1 + X_2)] + j[(R_2/s)(X_1 + X_m) + R_1(X_2 + X_m)]}$$

amperes/phase (5.17)

Equation (5.17) can be written as follows if only the magnitude of the current is desired:

$$I_1 = \frac{V_1\sqrt{(R_2/s)^2 + (X_2 + X_m)^2}}{\sqrt{[R_1(R_2/s) - X_1X_2 - X_m(X_1 + X_2)]^2 + [(R_2/s)(X_1 + X_m) + R_1(X_2 + X_m)]^2}}$$

amperes/phase (5.18)

If both the magnitude and angle are desired, I_1 may be calculated by use of eq. (5.16). This equation can be rearranged, as shown below, to improve the ease with which such complex quantity calculations may be made.

$$I_1 = \frac{V_1}{R_1 + j(X_1 + X_m) - (jX_m)^2/[R_2/s + j(X_2 + X_m)]} \quad \text{amperes/phase} \tag{5.19}$$

Solving for I_2, we have

$$I_2 = \frac{\begin{vmatrix} R_1 + j(X_1 + X_m) & V_1 \\ jX_m & 0 \end{vmatrix}}{\begin{vmatrix} R_1 + j(X_1 + X_m) & jX_m \\ jX_m & \dfrac{R_2}{s} + j(X_2 + X_m) \end{vmatrix}} \quad \text{amperes/phase} \qquad (5.20)$$

$$I_2 = \frac{-jV_1X_m}{[R_1 + j(X_1 + X_m)][R_2/s + j(X_2 + X_m)] - (jX_m)^2} \quad \text{amperes/phase} \qquad (5.21)$$

Rearranging eq. (5.21) by grouping the real parts together and the imaginary parts together and then dividing the numerator and the denominator by the imaginary operator j gives us

$$I_2 = \frac{-V_1X_m}{[(R_2/s)(X_1 + X_m) + R_1(X_2 + X_m)] + j[-R_1(R_2/s) + X_1X_2 + X_m(X_1 + X_2)]}$$
$$\text{amperes/phase} \qquad (5.22)$$

Again, eq. (5.22) may be written as shown below if only the magnitude of the current is desired.

$$I_2 = \frac{-V_1X_m}{\sqrt{[R_2/s(X_1 + X_m) + R_1(X_2 + X_m)]^2 + [-R_1R_2/s + X_1X_2 + X_m(X_1 + X_2)]^2}}$$
$$\text{amperes/phase} \qquad (5.23)$$

One definition of the magnetizing current I_m was given in eq. (5.2). Another definition can be obtained directly from the equivalent circuit. From an inspection of Fig. 5.3, it is apparent that

$$I_m = I_1 + I_2 \quad \text{amperes/phase} \qquad (5.24)$$

Inserting the expressions for I_1 and I_2 from eqs. (5.16) and (5.21), respectively, into eq. (5.24) and simplifying gives us

$$I_m = \frac{V_1(R_2/s + jX_2)}{[R_1 + j(X_1 + X_m)][R_2/s + j(X_2 + X_m)] - (jX_m)^2} \quad \text{amperes/phase} \tag{5.25}$$

5.4 DETERMINATION OF THE POWER OUTPUT

From the equivalent circuit, the gross power developed in each phase of the rotor is equal to

$$P_{g2} = I_2^2 \frac{R_2}{s} \quad \text{watts/phase} \tag{5.26}$$

and the gross power developed by the rotor, for a three-phase machine, is equal to

$$P_{g2} = 3I_2^2 \frac{R_2}{s} \quad \text{watts} \tag{5.27}$$

However, the electrical losses developed in the rotor circuit and the mechanical losses developed by the rotor, due to rotation of the rotor structure, must be subtracted from eq. (5.27) in order to obtain the net power delivered to the coupling, sheave, or sprocket on the drive shaft.

The predominate part of the electrical losses that occur in the rotor circuit, under load conditions, are the I^2R losses in each of the rotor phase windings, and these losses are modeled in the equivalent circuit. As will be considered subsequently, core loss consists of a fundamental component due to hysteresis losses and eddy-current losses, caused by fundamental frequency flux change in the magnetic steel, and of a high-frequency component due to various harmonics of the magnetomotive-force wave and of permeance variations, caused by such factors as slot openings in the magnetic punchings. The actual rate of flux change in the rotor is of the order of 1 Hz and, accordingly, the fundamental component of core loss is essentially nonexistent in the rotor core. A portion of the high-frequency component of core loss does occur on, or near, the surface of the rotor and is usually called rotor-surface loss. This component of loss represents only a minor part of the total core loss in the machine and, accordingly, it has been the practice to consider that all of the core loss occurs in the stator when calculating efficiency and power factor. Such a practice results in very insignificant, if any, error and results in simpler calculations. Accordingly, the rotor-winding resistance losses are the only electrical losses which are customarily considered to occur in the rotor and, as stated above, they are modeled in the equivalent circuit.

Equation (5.27) may be rewritten as

$$P_{g2} = 3I_2^2R_2 + 3I_2^2R_2 \frac{1 - s}{s} \quad \text{watts} \tag{5.28}$$

The first term of eq. (5.28) clearly represents the I^2R losses in the three separate, but identical, rotor phase windings, and the second term represents the gross power developed by the rotor, less the rotor I^2R losses, and is designated as P_2. Thus

$$P_2 = P_{g2} - 3I_2^2R_2 \quad \text{watts} \tag{5.29}$$

Then

$$P_2 = 3I_2^2R_2 \frac{1 - s}{s} \quad \text{watts} \tag{5.30}$$

where the term $R_2(1 - s)/s$ is called the equivalent load resistance and has units of ohms. Accordingly, the equivalent circuit, shown in Fig. 5.3, may be rearranged as shown in Fig. 5.4, which is consistent with that shown in Fig. 4.4.

Mechanical losses, caused by rotation of the rotor body, are sufficiently significant that their effect must be considered. Rotation of the rotor structure results in the production of friction and windage losses which equal 1% or more of the output rating of the machine. The friction power losses correspond to the time rate of energy losses that occur in the bearing assemblies and for wound-rotor machines, also at the contact surface between the collector rings, at the terminals of the rotor phase windings, and the mating brushes. Such frictional losses are manifest as heat energy, and the time rate at which this energy is produced represents a power loss that must be subtracted from the total power developed by the rotor. It should be noted that, not infrequently, the brush friction loss is lumped with the rotor I^2R loss. This presents no problem, since that loss is also subtracted from P_{g2}.

Similarly, fan blades mounted on the rotor structure or on the shaft, as well as other salient protrusions on the rotor body, produce a localized increase in air pressure and impart a localized turbulence to the air. Ventilation, and the accompanying windage losses, are considered later. It is necessary to note at this time, though, that the windage losses above must also be subtracted from the total power developed by the rotor. Friction losses and windage losses are grouped into one component of machine power loss which is designated as F & W, with units of watts or kilowatts. Then

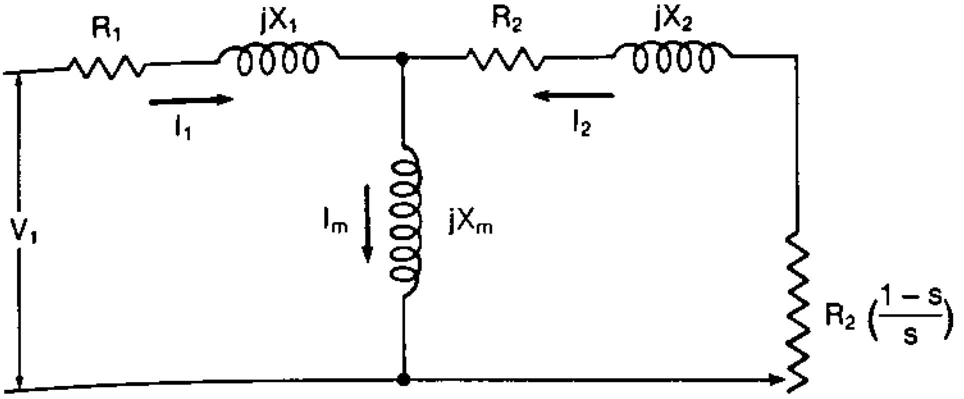

FIGURE 5.4 Equivalent circuit of one phase of the polyphase induction motor with equivalent load resistance.

F&W must be subtracted from P_2, in eq. (5.30), in order to obtain the net output power P_o, which is available at the shaft to drive the external load. Then

$$P_o = 3I_2^2R_2\frac{1-s}{s} - F\&W \quad \text{watts} \tag{5.31}$$

Since there are 746 W in 1 U.S. horsepower unit, eq. (5.31) may be written as

$$HP_o = \left(\frac{3}{746}\right)I_2^2R_2\frac{1-s}{s} - \frac{F\&W}{746} \quad \text{horsepower} \tag{5.32}$$

The power output may be expressed in terms of the stator and rotor winding parameters of the machine by substituting the expression for I_2, as given in eq. (5.23), into eq. (5.32). Then

$$HP_o = \frac{(3/746)V_1^2X_m^2R_2[(1-s)/s]}{[(R_2/s)(X_1+X_m)+R_1(X_2+X_m)]^2+[-(R_1R_2/s)+X_1X_2+X_m(X_1+X_2)]^2} - \frac{F\&W}{746} \quad \text{horsepower} \tag{5.33}$$

The values of rotor and stator winding leakage reactance to be used in eq. (5.33) are the "running" values, since the stator and rotor currents are in the region of 1.0 p.u. or less. The value of rotor winding resistance to use in eqs. (5.32) and (5.33) is usually the running value. The exception to this is that for low-speed operation of wound-rotor induction motors for which the rotor-circuit frequency is a significant percentage of the stator frequency, the value of the rotor winding resistance should be that corresponding to the rotor-circuit frequency.

It should be noted that the horsepower output, as defined in eqs. (5.32) and (5.33), is based on the horsepower unit as it is defined in the United States, which is equal to 746 W. In the SI system of units, the horsepower unit is equal to 735.5 W and is therefore approximately 1.40% less than the horsepower unit normally used in the United States.

5.5 DETERMINATION OF EFFICIENCY AND POWER FACTOR AT FULL LOAD

The three components of machine loss—core loss, load loss, and friction and windage—can be calculated at the design stage for a machine yet to be built, using empirical equations. They can also be determined by measurement of a similar machine that might be available. Similarly, the stator and rotor phase winding resistance can be calculated or measured. It is necessary, however, to know the magnitude of the stator and rotor currents in order to calculate the resulting I^2R losses. The equivalent circuit is usually used to make such calculations.

As stated earlier, load loss, core loss, and friction and windage are not modeled in the basic equivalent circuit. Although a shunt resistance, in parallel with X_m, may be used to model core loss and a series resistance may be used to model load loss, the use of such supplemental resistances is fraught with some risk. Unlike the equivalent-circuit winding resistance, leakage reactance, and magnetizing reactance, which represent similar physical conditions in the actual stator and rotor windings, load-loss and core-loss resistances do not have a similar one-to-one correspondence to the physical phenomena which they supposedly represent. If the equivalent circuit with such supplemental resistances is used for transient calculations, false results may be obtained. It is for such reasons that supplemental resistances to represent core loss and load loss have not found general acceptance in the United States. Because the machine loss components above are not normally modeled, it is necessary to perform an iterative process when using the equivalent circuit to calculate power factor.

The procedure for calculating efficiency and power factor, as well as for other quantities, can best be shown by an example. The power output for a specific value of slip will be calculated first. Then the efficiency and power factor will be calculated for this value of power output. Consider a 1000-hp 4000-V 1800-rpm three-phase 60-Hz squirrel-cage induction motor with parameters as given in Table 5.1. The same set of parameters will be used in subsequent examples so that calculated results can be compared when various algorithms are used.

Power output may be easily calculated if the rotor current I_2 is known. From eq. (5.21),

$$I_2 = \frac{-jV_1X_m}{[R_1 + j(X_1 + X_m)][R_2/s + j(X_2 + X_m)] - (jX_m)^2} \quad \text{amperes/phase} \tag{5.34}$$

Substituting the appropriate parameters from Table 5.1 into eq. (5.34) yields

$$I_2 = \frac{(-2309/\underline{0^\circ})(75.1/\underline{90^\circ})}{(-0.2145 + j76.81)(0.236/0.0124 + j76.6) - (75.1/\underline{90^\circ})^2}$$

$$= 115.9/\underline{170.8^\circ} \quad \text{amperes/phase} \tag{5.35}$$

From eq. (5.32), the shaft power is equal to

$$HP_o = \left(\frac{3}{746}\right)I_2^2R_2\frac{1 - s}{s} - \frac{F\&W}{746} \quad \text{horsepower} \tag{5.36}$$

TABLE 5.1 Parameters of a 1000-hp Squirrel-Cage Induction Motor

Parameter	Running value	Blocked-rotor value	Units
R_1	0.2145[a]	0.2145[a]	ohms/phase
R_2	0.2360[a]	—	ohms/phase
$R_{2\ell}$	—	0.4900[a]	ohms/phase
X_1	1.714	—	ohms/phase
$X_{1\ell}$	—	1.714	ohms/phase
X_2	1.502	—	ohms/phase
$X_{2\ell}$	—	1.006	ohms/phase
X_m	75.10	75.10	ohms/phase
s	0.0124	1.000	per unit
CL	7500	—	watts/machine
LL	8000	—	watts/machine
F&W	11,500	—	watts/machine
V_1	2309	2309	volts/phase

[a] The value of resistance is that which corresponds to full-load winding temperatures.

Substituting the appropriate quantities from Table 5.1 into eq. (5.36) yields

$$HP_o = \left(\frac{3}{746}\right)(115.9)^2(0.236)\left(\frac{1 - 0.0124}{0.0124}\right) - \frac{11{,}500}{746}$$

$$= 1000 \quad \text{horsepower} \tag{5.37}$$

Thus the value of slip of s = 0.0124 is full-load slip and the value of I_2 calculated in eq. (5.35), using this value of slip, is the full-load value of rotor current.

The full-load value of stator current, from eq. (5.19), is

$$I_1 = \frac{V_1}{R_1 + j(X_1 + X_m) - (jX_m)^2/[R_2/s + j(X_2 + X_m)]} \quad \text{amperes/phase} \tag{5.38}$$

Again, substituting the appropriate quantities from Table 5.1 into eq. (5.38), we have

$$I_1 = \frac{2309\underline{/0^\circ}}{0.2145 + j76.81 - (75.1\underline{/90^\circ})^2/(0.236/0.0124 + j76.6)}$$

$$= 121.7\underline{/-23.1^\circ} \quad \text{amperes/phase} \tag{5.39}$$

Friction and windage loss is correctly represented by additional shaft load, and the full-load value of slip includes the effect of this component of loss. Hence the effect of friction and windage on full-load stator and rotor current has been considered. Stator and rotor winding I^2R loss is modeled in the equivalent circuit, for purposes of calculating the energy component of stator current and hence the power factor. On the other hand, core loss and load loss are not modeled in the normal equivalent circuit and, accordingly, an additional step is necessary in order to determine the current component corresponding to these losses in the total stator current. This is accomplished by starting with the stator current as calculated closely, but not exactly, from the equivalent circuit in eq. (5.39) and by adding to this value an amount equal to the current component that sustains core loss and load loss.

As mentioned earlier, core loss consists of two components, one component called fundamental core loss and a second component called high-frequency core loss. Fundamental core loss consists of hysteresis and eddy-current losses in the stator core due primarily to flux changes associated with impressed line frequency. The higher-frequency core loss is caused by higher-frequency eddy-current losses in parts of the stator and rotor cores adjacent to the air gap, due to various harmonics in the air-gap flux wave. Thus core loss in the actual machine is associated with the mutual flux, and accordingly, core loss in the equivalent circuit should be computed at the voltage across the magnetizing reactance X_m. Load loss consists of the additional loss in the loaded machine which is not accounted for by normal stator and rotor I^2R losses, core loss, and friction and windage losses. This loss is caused primarily by the rotating flux wave inducing eddy currents in various machine parts, by additional losses in the stator and rotor windings induced by slot leakage flux, and by any air-gap harmonic losses not accounted for in the other components of loss. Accordingly, load loss in the actual machine is associated with the rotating magnetomotive force and flux waves and with leakage flux in the stator and rotor core slots. The voltage across the magnetizing reactance, X_m, in the equivalent circuit is the voltage most central to this activity, and accordingly, load loss should be computed at this voltage.

Because of the foregoing considerations, it is necessary to know the value of the generated voltage E_1, expressed as a voltage drop across the magnetizing reactance of the equivalent circuit, in order to calculate the value of ΔI_1, the current that sustains core loss and load loss. The generated voltage may be calculated very closely, at this point in the example, by subtracting the stator winding impedance drop, at rated load, from the impressed stator voltage V_1. This is accomplished by using the value of rated stator current calculated in eq. (5.39), which is nearly, but not precisely, correct and the tabulated values of stator impedance and stator voltage from Table 5.1. This exercise has been done separately in Table 5.2, for this numerical example, so as not to interrupt the continuity of thought in calculating rated power factor and, at the same time, to retain the procedure for future use.

From eq. (5.39), the stator current as calculated from the equivalent circuit is

$$I_1 = 121.7/\underline{-23.1^\circ} \quad \text{amperes/phase} \qquad (5.40)$$

and its in-phase and reactive components, relative to the stator phase voltage, are

$$I_1 = 111.94 - j47.75 \quad \text{amperes/phase} \qquad (5.41)$$

From Table 5.2 the component of stator current that sustains core loss and load loss is equal to

$$\Delta I_1 = 2.34/\underline{-4.73^\circ} \quad \text{amperes/phase} \qquad (5.42)$$

and the in-phase and reactive components are

$$\Delta I_1 = 2.33 - j0.19 \quad \text{amperes/phase} \qquad (5.43)$$

TABLE 5.2 Procedure for Determining ΔI_1 at Rated Load Applied to the 1000-hp Motor Example

Action	Steps
Determine normal values of volts, amperes, and ohms on an output base for the 1000-hp motor example in Table 5.1	Rated motor output base = 746 kW Rated line-to-line voltage = 4000 V Normal volts = $4000/\sqrt{3} = 2309$ V/phase Normal amperes = $(746)(1000/\sqrt{3})(4000) =$ 107.7 A/phase Normal ohms = normal volts/normal amperes = $2309/107.7 = 21.44\ \Omega$/phase
Convert stator impedance to per unit on an output base	$R_1 = 0.2145/21.44 = 0.010$ p.u. $X_1 = 1.714/21.44 = 0.080$ p.u.
Convert stator current from eq. (5.39) to per unit on an output base	$I_1 = 121.7\underline{/-23.1^\circ}/107.7 = 1.13\underline{/-23.1^\circ}$ p.u
Calculate generated voltage, expressed as a voltage drop $-E_1$, in the stator circuit, in per unit	$-E_1 = V_1 - I_1(R_1 + jX\ )$ p.u. $-E_1 = 1.0\underline{/0^\circ} - (1.13\underline{/-23.1^\circ})(0.01 + j0.08)$ p.u. $-E_1 = 0.957\underline{/-4.73^\circ}$ p.u.
Convert $-E_1$ to actual volts	$-E_1 = (2309)(0.957\underline{/-4.73^\circ}) = 2210\underline{/-4.73^\circ}$ V/phase
Calculate ΔI_1 in magnitude and angle at full load	Since ΔI_1 is in phase with $-E_1$: (ΔI_1)(magnitude of E_1) = (CL + LL)/3 W/phase $(\Delta I_1)(2210) = 15{,}500/3$ W/phase $\Delta I_1 = 2.34$ A/phase Since the angle of ΔI_1 is the same as that of $-E_1$: $\Delta I_1 = 2.34\underline{/-4.73\ }$ A/phase

Then, adding eqs. (5.41) and (5.43), the corrected value of stator phase current is

$$I_1 = 111.94 + 2.33 - j(47.75 + 0.19) = 123.9\underline{/-22.7^\circ} \quad \text{amperes/phase} \tag{5.44}$$

Rated power factor is defined as

$$\text{PF} = \frac{\text{kW}_1}{3I_1V_1} \quad \text{per unit} \tag{5.45}$$

For this example, the full-load power factor is equal to

$$\text{PF} = \frac{746 + (3)(123.9)^2(0.2145)/1000 + (3)(115.9)^2(0.236)/1000 + 7.5 + 8.0 + 11.5}{(3)(123.9)(2309/1000)}$$

$$= 0.923 \quad \text{per unit} \tag{5.46}$$

As a check on the value calculated above, full-load power factor may also be calculated as the cosine of the angle θ_1, between stator phase voltage and stator phase current, at rated load, or

$$\text{PF} = \cos \theta_1 \quad \text{per unit} \tag{5.47}$$

The stator phase voltage was taken as angle reference, (i.e., $V_1 = 2309\underline{/0^\circ}$). On that basis, the adjusted stator phase current was calculated in eq. (5.44) as $I_1 = 123.9\underline{/-22.7^\circ}$. Thus $\theta_1 = -22.7$ and

$$\text{PF} = \cos(-22.7) = 0.923 \quad \text{per unit} \tag{5.48}$$

which agrees with eq. (5.46).

Efficiency is equal to the ratio of mechanical power out of the shaft to electrical power into the stator winding, or

$$\eta = \frac{P_o}{P_i} = \frac{P_o}{P_o + \Sigma \text{ losses}} \quad \text{per unit} \tag{5.49}$$

Then, for the subject machine, full-load efficiency is equal to

$$\eta = \frac{746}{746 + (9.88 + 9.51 + 7.5 + 8.0 + 11.5)}$$

$$= 0.941 \quad \text{per unit} \tag{5.50}$$

5.6 DETERMINATION OF EFFICIENCY AND POWER FACTOR AT PART LOAD

It is normal commercial practice for the manufacturer to provide efficiency and power factor at one-fourth, one-half, and three-fourths load for use by the customer. Such fractional-load values may be determined as indicated above for full load, except that the values for use in eqs. (5.45) and (5.49) are calculated for the partial load being considered and the losses are adjusted for that particular load. The part-load calculations for core loss, load loss, and friction and windage are, necessarily, somewhat arbitrary. Core loss is assumed to be constant, which assumes that the stator bus voltage remains constant and that the stator impedance drop is independent of changes in load. Load loss is assumed to vary as the second power of the load, which is a close approximation in the region of full load, but which becomes increasingly less accurate as the load is decreased. Friction and windage losses are assumed to be constant, which neglects the effect of change in shaft load on bearing friction loss. Also, windage loss varies as the third power of rotor speed, so that small changes in rotor speed, due to a change in slip, will result in somewhat greater changes in windage loss. However, on balance, the above-mentioned arbitrary practices for determining part-load losses give reasonable and satisfactory results. Using the convention above, core loss, load loss, and friction and windage losses at three-fourths load, based on the full-load values of the example above, have been calculated and are tabulated in Table 5.3.

Although there are commercially accepted practices for simply determining core loss, load loss, and friction and windage losses at part load, the stator and rotor currents, at such loads, must be calculated before the stator and rotor I^2R losses can be determined. Alternative approximate methods for calculating stator and rotor current are available and, to some extent, are used. However, for accurate results, part-load currents and I^2R losses should be determined in the same way that full-load values are determined.

To calculate stator and rotor phase currents from eqs. (5.19) and (5.21) at part load, the slip must be known for the load being considered. Slip is essentially proportional to total shaft power output, which provides a method for obtaining an approximate value at any part load. However, the exact value may be determined by solving eq. (5.33) for slip, at the particular power output being considered, i.e.,

$$HP_0 = \frac{(3/746)V_1^2X_m^2R_2[(1 - s)/s]}{[(R_2/s)(X_1 + X_m) + R_1(X_2 + X_m)]^2 + [-R_1R_2/s + X_1X_2 + X_m(X_1 + X_2)]^2} - \frac{F\&W}{746} \quad \text{horsepower} \tag{5.51}$$

TABLE 5.3 Conventional Proportioning of the Nonresistive Losses at Part Load for the Example

Per unit load	Core loss (kW)	Load loss (kW)	Friction and windage (kW)
1.0	7.50	8.00	11.50
0.75	7.50	4.50	11.50
0.50	7.50	2.00	11.50
0.25	7.50	0.50	11.50

If this equation is set equal to (0.75)(1000) = 750 hp and the winding parameters from Table 5.1 are substituted into the equation, it may be solved for the slip s which corresponds to that value of power output. Thus

$$750 = \frac{(3/746)(2309)^2(75.1)^2(0.236)[(1-s)/s]}{[(0.236/s)(76.81)+(0.2145)(76.60)]^2+[(0.2145)(0.236)/s+(1.502)(1.704)+(75.1)(3.216)]^2}$$

$$-\frac{11,500}{746} \quad \text{horsepower} \tag{5.52}$$

Equation (5.52) reduces to

$$97,700s^2 - 36,780s + 329 = 0 \quad \text{numeric} \tag{5.53}$$

Applying the quadratic formula and discarding the extraneous root, we obtain

$$s = \frac{36,780 \pm \sqrt{13.528 \times 10^8 - 1.29 \times 10^8}}{(2)(97,700)}$$

$$= 0.00921 \quad \text{per unit} \tag{5.54}$$

Equation (5.21) gives I_2 in terms of the winding parameters of the machine and of slip, that is,

$$I_2 = \frac{-jV_1X_m}{[R_1 + j(X_1 + X_m)][R_2/s + j(X_2 + X_m)] - (jX_m)^2} \quad \text{amperes/phase} \tag{5.55}$$

Using the value of slip calculated in eq. (5.54) and the values of the winding parameters given in Table 5.1, we obtain

$$I_2 = \frac{(2309/\underline{0^\circ})(75.1/\underline{90^\circ})}{(0.2145 + j76.81)(0.236/0.00921 + j76.6) - (75.1)/\underline{90^\circ})^2}$$

$$= 86.6/\underline{173.2^\circ} \quad \text{amperes/phase} \tag{5.56}$$

To verify the shaft horsepower at the value of slip calculated in eq. (5.54) and at the value of current calculated in eq. (5.56), substitute these quantities into eq. (5.32):

$$HP_o = \left(\frac{3}{746}\right)I_2^2R_2\frac{1 - s}{s} - \frac{F\&W}{746} \quad \text{horsepower} \tag{5.57}$$

$$= \left(\frac{3}{746}\right)(86.6)^2(0.236)\left(\frac{1 - 0.00921}{0.00921}\right) - \frac{11,500}{746}$$

$$= 750 \quad \text{horsepower} \tag{5.58}$$

We calculate the stator current at three-fourths load from eq. (5.19), or

$$I_1 = \frac{V_1}{R_1 + j(X_1 + X_m) - (jX_m)^2/[R_2/s + j(X_2 + X_m)]} \quad \text{amperes/phase} \tag{5.59}$$

Substituting the value of slip calculated in eq. (5.54) and the values of the winding parameters given in Table 5.1 into eq. (5.59) yields

$$I_1 = \frac{2309/\underline{0^\circ})}{0.2145 + j76.81 - (75.1/\underline{90^\circ})^2/[0.236/0.00921 + j76.60]}$$

$$= 93.3/\underline{-25.4^\circ} \quad \text{amperes/phase} \tag{5.60}$$

and the in-phase and reactive components are equal to

$$I_1 = 93.3/\underline{-25.4^\circ} = 84.28 - j40.02 \quad \text{amperes/phase} \tag{5.61}$$

The additional component of stator current ΔI_1, which sustains core loss and load loss at three-fourths load, is determined as a separate exercise in Table 5.4. From that table, the value of ΔI_1, at three-fourths load, is

TABLE 5.4 Procedure for Determining ΔI_1 at Three-Fourths Load Applied to the 1000-hp Motor Example

Action	Steps
Determine normal values of volts, amperes, and ohms on an output base for the 1000-hp motor example in Table 5.1	Refer to Table 5.2, where this has been done
Convert stator impedance to per unit on an output base	Refer to Table 5.2, where this has been done
Convert stator current from eq. (5.60) to per unit on an output base	$I_1 = 93.3\underline{/-25.4^\circ}/107.7 = 0.866\underline{/-25.4^\circ}$ p.u.
Calculate generated voltage, expressed as a voltage drop $-E_1$, in the stator circuit, in per unit	$-E_1 = V_1 - I_1(R_1 + jX_1)$ p.u. $-E_1 = 1.0\underline{/0^\circ} - (0.866\underline{/-25.4^\circ})(0.01 + j0.08)$ p.u. $-E_1 = 0.964\underline{/-3.51^\circ}$ p.u.
Convert $-E_1$ to actual volts	$-E_1 = (2309)(0.964\underline{/-3.51^\circ}) = 2226\underline{/-3.51^\circ}$ p.u.
Calculate ΔI_1 in magnitude and angle at 3/4 load	$(\Delta I_1)(\text{magnitude of } E_1) = (CL + LL)/3$ W/phase $(\Delta I_1)(2226) = (7500 + 4500)/3$ W/phase $\Delta I_1 = 1.80$ A/phase Since the angle of ΔI_1 is the same as that of $-E_1$, $\Delta I_1 = 1.80\underline{/-3.51^\circ}$ A/phase

$$\Delta I_1 = 1.80\underline{/-3.51^\circ} \quad \text{amperes/phase} \tag{5.62}$$

Resolving it into the in-phase and reactive components, relative to the stator voltage V_1, gives us

$$\Delta I_1 = 1.797 - j0.11 \quad \text{amperes/phase} \tag{5.63}$$

Adding eqs. (5.61) and (5.63), the corrected value of stator phase current at 0.75 p.u. load is

$$I_1 = 86.08 - j40.13 = 95.0\underline{/-25.0^\circ} \quad \text{amperes/phase} \tag{5.64}$$

Calculating the stator winding I^2R, using the current value given in eq. (5.64), we have

$$I_1^2R_1 = \frac{(3)(95.0)^2(0.2145)}{1000} = 5.81 \quad \text{kilowatts} \tag{5.65}$$

and calculating the rotor winding I^2R, using the current value given in eq. (5.56), yields

$$I_2^2R_2 = \frac{(3)(86.6)^2(0.236)}{1000} = 5.31 \quad \text{kilowatts} \tag{5.66}$$

Power factor at 0.75 p.u. load is equal to

$$PF = \frac{kW_1}{3I_1V_1} \quad \text{per unit} \tag{5.67}$$

where kW_1 and I_1 are the values for this load condition. Inserting the appropriate values into eq. (5.67), the 0.75 p.u. power factor is

$$PF = \frac{(746)(0.750) + 5.81 + 5.31 + 7.50 + 4.50 + 11.5}{(3)(95.0)(2309/1000)}$$

$$= 0.903 \quad \text{per unit} \tag{5.68}$$

From eq. (5.64), the angle between the stator phase current and voltage is $\theta_1 = -25.0^\circ$. The cosine of this angle provides a check on the value of power factor, as calculated by eq. (5.68). Then

$$\cos(-25.0) = 0.906 \quad \text{per unit} \tag{5.69}$$

which agrees with eq. (5.68) to within 0.003 p.u. Efficiency, at part load, is equal to

$$\eta = \frac{P_o}{P_i} \quad \text{per unit} \tag{5.70}$$

where P_o and P_i corresponds to 0.75 p.u. load conditions for this example. Inserting the corresponding values into eq. (5.70), the 0.75 p.u. load efficiency is

$$\eta = \frac{(746)(0.750)}{(746)(0.750) + 5.81 + 5.31 + 7.50 + 4.50 + 11.5}$$

$$= 0.942 \quad \text{per unit} \tag{5.71}$$

Proceeding in a similar manner and using the appropriate part-load values, power factor and efficiency may be calculated for any part-load condition.

5.7 DERIVATION OF THE GENERAL TORQUE EQUATION

It was shown previously that if a magnetic field and a current-carrying conductor were so positioned as to have components mutually perpendicular to each other, a useful force would be obtained in a direction perpendicular to both. Also, if this force appeared as a tangential force near the periphery of a rotor structure, a useful torque would be produced. Torque is the very essence of motor action and is an important machine quantity. The motor output torque characteristics must be matched with the load torque requirements of the driven equipment for a successful application and hence torque is a basic application consideration. Motor torque will now be derived from the power produced by, and the speed of, the rotor. The relationship between rotor power, speed, and torque is

$$P_2 = \omega_2 T \quad \text{watts} \tag{5.72}$$

where ω_2 is the angular speed of rotation in radians/second, and T is the torque produced by the machine in newton-meters. Equation (5.72) may be written as

$$P_2 = 2\pi n T \quad \text{watts} \tag{5.73}$$

where n is the speed of rotation in revolutions/second. In terms of synchronous speed n_s and slip s, the speed of rotation can be written as

$$n = \frac{n_s}{60}(1 - s) \quad \text{revolutions/second} \tag{5.74}$$

Substituting eq. (5.74) into eq. (5.73) yields

$$P_2 = 2\pi \frac{n_s}{60}(1 - s)T \quad \text{watts} \tag{5.75}$$

Solving for T gives us

$$T = \frac{60}{2\pi}\left[\frac{1}{n_s(1 - s)}\right]P_2 \quad \text{newton-meters} \tag{5.76}$$

Substituting eq. (5.30) into eq. (5.76), we have

$$T = \frac{60}{2\pi}\left[\frac{1}{n_s(1 - s)}\right]\left[3I_2^2R_2 \frac{(1 - s)}{s}\right] \quad \text{newton-meters} \tag{5.77}$$

Simplifying yields

$$T = \frac{90}{\pi}\frac{1}{n_s}\left(I_2^2 \frac{R_2}{s}\right) \quad \text{newton-meters} \tag{5.78}$$

In the United States, torque units of pound-feet are in more general industrial use than are newton-meters. Remembering that 1.0 lb-ft = 1.356 N-m, we obtain

$$T = \frac{90}{\pi}\left(\frac{1}{1.356}\right)\left(\frac{1}{n_s} \; I_2^2 \frac{R_2}{s}\right) \quad \text{pound-feet} \tag{5.79}$$

and upon simplifying, we have

$$T = \frac{21.1}{n_s}\left(I_2^2 \frac{R_2}{s}\right) \quad \text{pound-feet} \tag{5.80}$$

To express the torque equation in terms of the winding parameters of the machine, substitute eq. (5.23) into eq. (5.80). Then

$$T = \frac{(21.1/n_s)(V_1^2 X_m^2 R_2/s)}{[(R_2/s)(X_1 + X_m) + R_1(X_2 + X_m)]^2 + [-R_1 R_2/s + X_1 X_2 + X_m(X_1 + X_2)]^2} \quad \text{pound-feet} \qquad (5.81)$$

Equations (5.80) and (5.81) show that torque is proportional to the rotor winding loss, or to $I_2^2 R_2/s$. This could be expected and is compatible with eq. (3.64), which shows that torque is proportional to $\cos\theta_2$, the rotor circuit power factor. Equation (5.81) is, of course, the same equation as eq. (5.80), except that the machine parameters have been substituted for I_2.

Equations (5.80) and (5.81) represent the torque produced by the machine, including that required to overcome friction and windage losses. To obtain the net shaft torque, the torque required to overcome friction and windage losses must be subtracted from the total torque produced. The relationship between torque, power, and speed in the foot-pound-second system of units is

$$\text{hp} = \frac{2\pi n T}{33{,}000} \quad \text{horsepower} \qquad (5.82)$$

Solving for torque gives us

$$T = 5252\,\frac{\text{hp}}{n} \quad \text{pound-feet} \qquad (5.83)$$

Using watts instead of horsepower as the unit of power, we have

$$T = \left(\frac{5252}{746}\right)\frac{\text{watts}}{n} = \frac{7.04(\text{watts})}{n} \quad \text{pound-feet} \qquad (5.84)$$

Hence the torque required to overcome friction and windage losses, with the machine operating in the region of rated speed, is

$$T_{F\&W} = \frac{7.04(F\&W)}{n} = \frac{7.04(F\&W)}{n_s(1 - s)} \quad \text{pound-feet} \qquad (5.85)$$

and the net shaft torque is then equal to

$$T_o = \frac{21.1}{n_s} I_2^2 \frac{R_2}{s} - \frac{7.04(F\&W)}{n_s(1 - s)} \quad \text{pound-feet} \qquad (5.86)$$

or in terms of the winding parameters of the machine, the net shaft torque is equal to

$$T_o = \frac{(21.1/n_s)(V_1^2 X_m^2 R_2/s)}{[(R_2/s)(X_1 + X_m) + R_1(X_2 + X_m)]^2 + [-R_1R_2/s + X_1X_2 + X_m(X_1 + X_2)]^2} - \frac{7.04(F\&W)}{n_s(1 - s)} \quad \text{pound-feet} \qquad (5.87)$$

Either eq. (5.86) or (5.87) may be used to calculate the shaft torque, depending on whether or not the rotor current has been calculated. For the example represented by the parameters in Table 5.1, for which the current has been calculated in eq. (5.35), the net full-load torque can be determined from eq. (5.86) as

$$T_o = \frac{(21.1)(115.9)^2(0.236/0.0124)}{1800} - \frac{(7.04)(11{,}500)}{(1800)(1 - 0.0124)} = 2952 \quad \text{pound-feet} \qquad (5.88)$$

If the rotor current has not been calculated previously, the full-load net torque can be calculated directly by substituting the winding parameters from Table 5.1 into eq. (5.87). Thus

$$T_o = \frac{(21.1/1800)(2309)^2(75.1)^2(0.236/0.0124)}{[(0.236/0.0124)(76.81) + (0.2145)(76.6)]^2 + [-(0.2145)(0.236/0.0124) + (1.714)(1.502) + (75.1)(3.22)]^2} - \frac{(7.04)(11{,}500)}{(1800)(1 - 0.0124)} \quad \text{pound-feet} \qquad (5.89)$$

or

$$T_o = 2952 \quad \text{pound-feet} \qquad (5.90)$$

Some comments are in order concerning the second term of eq. (5.89), that is, the expression for the torque expended to overcome the friction and windage losses. This term requires that such losses be known. This will have been calculated for full-speed operation of the machine, which is the mode of operation for squirrel-cage machines. However, wound-rotor machines may operate at various speeds for prolonged periods. The error introduced by the probable accuracy by which the machine parameters are known in eq. (5.87) is of the same order as the error introduced by use of full-speed friction and windage at reduced speed. However, if it is required that an accurate value of output torque be known for some specific, reduced speed, it is probably desirable to calculate friction and windage losses at that reduced speed and to use it in eq. (5.86) or (5.87). Friction and windage power losses vary approximately as the cube of the speed, except for very low speeds. Accordingly, the torque required to overcome these losses varies as the square of the speed, except at very low speeds.

It should be noted further that the term for friction and windage, as defined in eq. (5.84), is accurate only in the region of full speed. Indeed, the expression is not defined at very low speeds because speed n is a term in the denominator. The actual friction and windage losses of the machine are low at lower speeds. However, these losses may be greater than that indicated by the cubic variation with speed. This is because of an increase in the proportion of friction loss relative to the windage loss at lower speeds.

5.8 MAXIMUM TORQUE

If a polyphase induction motor has been operating at some given load point and the external load is then increased by some increment, the speed of the rotor will decrease and the slip will increase. An increase in slip will cause the voltage generated in the rotor circuit to increase, in accordance with eq. (5.5). This will tend to increase the rotor current and hence the torque produced by the machine. However, an increase in slip will also increase the leakage reactance component of the rotor impedance, in accordance with eq. (5.8). This will tend to decrease the rotor current and hence the torque. The net effect of these two opposing interactions is that the torque produced by the machine does increase with increasing external load and increasing slip, until a maximum value of torque is reached, after which the motor becomes unstable as the load and slip are increased further. The point at which this effect starts to occur is called the maximum or breakdown torque of the machine.

The value of slip at which maximum torque occurs can be determined from the general torque equation, as given in eq. (5.87). If this torque equation is differentiated with respect to slip s, equated to zero, and then solved for s, the slip at which maximum torque occurs will be obtained. For this procedure, the second term in eq. (5.87), which considers the torque required to overcome friction and windage losses, should be ignored when differentiating the equation. The equation to be differentiated is then

$$T = \frac{(21.1/n_s)(V_1^2 X_m^2 R_2/s)}{[(R_2/s)(X_1 + X_m) + R_1(X_2 + X_m)]^2 + [-R_1R_2/s + X_1X_2 + X_m(X_1 + X_2)]^2} \quad \text{pound-feet} \qquad (5.91)$$

To simplify the mathematical manipulation, the following substitutions will be made for terms that are constant relative to the differentiation.

$$A = R_2(X_1 + X_m)$$

$$B = R_1(X_2 + X_m)$$

$$C = R_1R_2$$

$$D = X_1X_2 + X_m(X_1 + X_2)$$

$$K = \frac{21.1}{n_s} V_1^2X_m^2 R_2$$

Then, making the substitutions above and multiplying the numerator and denominator by s, we have

$$T = \frac{K}{(s)(A/s + B)^2 + (s)(-C/s + D)^2} \quad \text{pound-feet} \qquad (5.92)$$

Differentiating eq. (5.92) with respect to s yields

$$\frac{dT}{ds} = \frac{-K[2s(A/s + B)(-A/s^2) + (A/s + B)^2 + 2s(-C/s + D)(C/s^2) + (-C/s + D)^2]}{[(s)(A/s + B)^2 + (s)(-C/s + D)^2]^2}$$

$$= 0 \qquad (5.93)$$

or

$$-K[-2(A + Bs)(A/s^2) + A^2/s^2 + B^2 + 2(AB/s) + 2(-C + Ds)(C/s^2)$$
$$+ C^2/s^2 + D^2 - 2(CD/s)] = 0 \qquad (5.94)$$

Simplifying gives

$$\frac{A^2 + C^2}{s^2} = B^2 + D^2 \qquad (5.95)$$

or

$$s^2 = \frac{A^2 + C^2}{B^2 + D^2} \qquad (5.96)$$

and

$$s = \left(\frac{A^2 + C^2}{B^2 + D^2}\right)^{1/2} \quad \text{per unit} \qquad (5.97)$$

Upon resubstituting the winding parameters for A, B, C, and D and simplifying, we have

$$s_m = \left\{\frac{R_2^2(X_1 + X_m)^2 + R_1^2R_2^2}{R_1^2(X_2 + X_m)^2 + [X_1X_2 + X_m(X_1 + X_2)]^2}\right\}^{1/2} \quad \text{per unit} \qquad (5.98)$$

which gives the value of slip at which maximum torque occurs in terms of the impedance parameters of the machine

The term R_2 may be factored out of the radical in eq. (5.98), to give

$$s_m = R_2\left\{\frac{(X_1 + X_m)^2 + R_1^2}{R_1^2(X_2 + X_m)^2 + [X_1X_2 + X_m(X_1 + X_2)]^2}\right\}^{1/2} \quad \text{per unit} \qquad (5.99)$$

It is apparent from this equation that the slip at which maximum torque occurs is directly proportional to the rotor resistance; that is, the greater the rotor resistance, the proportionally greater is the slip at which maximum torque occurs. However, the magnitude of the maximum torque is independent of the value of rotor resistance. This is apparent from a consideration of eq. (5.87). In that equation, rotor resistance R_2 and slip s occur as the ratio R_2/s. Hence if s_m and R_2 are directly proportional, as stated in eq. (5.99), the ratio R_2/s remains constant at the speed at which maximum torque occurs, and the other winding parameters determine the value of maximum torque.

For any given case, the value of s_m can be calculated from eq. (5.99) and this value of slip then substituted into eq. (5.87) to calculate the maximum torque. It is more convenient, however, initially to combine eq. (5.99) with eq. (5.87) to derive the equation for maximum torque in terms of the winding parameters. Equation (5.99) may be rearranged as

$$\frac{R_2}{s_m} = \left\{\frac{R_1^2(X_2 + X_m)^2 + [X_1X_2 + X_m(X_1 + X_2)]^2}{(X_1 + X_m)^2 + R_1^2}\right\}^{1/2} \quad \text{ohms} \qquad (5.100)$$

Make the substitution

$$\frac{R_2}{s_n} = \frac{M}{N} \quad \text{ohms} \tag{5.101}$$

where

$$M = \sqrt{R_1^2(X_2 + X_m)^2 + [X_1X_2 + X_m(X_1 + X_2)]^2} \quad \text{ohms}^2 \tag{5.102}$$

and

$$N = \sqrt{(X_1 + X_m)^2 + R_1^2} \quad \text{ohms} \tag{5.103}$$

Neglecting the friction and windage term in the general torque equation, given in eq. (5.87), gives us

$$T = \frac{(21.1/n_s)(V_1^2X_m^2R_2/s)}{[(R_2/s)(X_1+X_m)+R_1(X_2+X_m)]^2+[-R_1R_2/s+X_1X_2+X_m(X_1+X_2)]^2} \quad \text{pound-feet} \tag{5.104}$$

Rearranging eq. (5.104) yields

$$T = \frac{(21.2/n_s)V_1^2X_m^2R_2/s)}{(R_2/s)^2[R_1^2+(X_1+X_m)^2]+2R_1X_m^2(R_2/s)+R_1^2(X_2+X_m)^2+[X_1X_2+X_m(X_1+X_2]^2} \quad \text{pound-feet} \tag{5.105}$$

Substituting eqs. (5.101), (5.102), and (5.103) into eq. (5.105) and then simplifying, we obtain

$$T_m = \frac{(21.1/n_s)(V_1^2X_m^2)}{2(MN + R_1X_m^2)} \quad \text{pound-feet} \tag{5.106}$$

Resubstituting eqs. (5.102) and (5.103) into eq. (5.106) in order to have the equation expressed in terms of winding constants, gives us

$$T_m = \frac{(1/2)(21.1/n_s)(V_1^2 X_m^2)}{\sqrt{[R_1^2(X_2+X_m)^2 + [X_1X_2+X_m(X_1+X_2)]^2][(X_1+X_m)^2+R_1^2]} + R_1X_m^2}$$

pound-feet (5.107)

This is the exact equation for maximum torque of a polyphase induction motor, as derived from the complete equivalent circuit. A corresponding but less accurate equation will subsequently be derived from the simplified equivalent circuit.

If the full-speed friction and windage losses are known, these losses can be converted to a torque at the speed at which maximum torque occurs, and the resulting loss torque subtracted from eq. (5.107). This is accomplished by multiplying eq. (5.85) by the cube of the ratio of the speed at which maximum torque occurs to rated speed and then subtracting the value of loss torque from eq. (5.107). Such a refinement is not normally used, however. This is because maximum torque is usually in the range 200 to 300% of rated torque, whereas the torque required to overcome friction and windage losses is usually less than 2%. Neglecting friction and windage torque will cause less percentage change, in the usual case, than that caused by the probable error in the accuracy by which the impedance parameters are known.

The slip at which maximum torque occurs and the maximum torque will be calculated using the parameters for the example given in Table 5.1. From eq. (5.99), the slip at maximum torque is equal to

$$s_m = R_2 \left\{ \frac{(X_1 + X_m)^2 + R_1^2}{R_1^2(X_2 + X_m)^2 + [X_1X_2 + X_m(X_1 + X_2)]^2} \right\}^{1/2} \quad \text{per unit} \qquad (5.108)$$

Inserting the winding parameters from Table 5.1 into eq. (5.108) gives us

$$s_m = 0.236 \left\{ \frac{(76.81)^2 + (0.2145)^2}{(0.2145)^2(76.5)^2 + [(1.714)(1.502) + (75.1)(3.216)]^2} \right\}^{1/2}$$

$$= 0.0741 \quad \text{per unit} \qquad (5.109)$$

From eq. (5.107), the magnitude of maximum torque is equal to

$$T_m = \frac{(1/2)(21.1/n_s)(V_1^2 X_m^2)}{\sqrt{\{R_1^2(X_2 + X_m)^2 + [X_1 X_2 + X_m(X_1 + X_2)]^2\}[(X_1 + X_m)^2 + R_1^2]} + R_1 X_m^2} \quad \text{pound-feet} \qquad (5.110)$$

Again, inserting the winding parameters from Table 5.1 into eq. (5.110), we have

$$T_m = \frac{(1/2)(21.1/1800)(2309)^2(75.1)^2}{\sqrt{\{(0.2145)^2(76.5)^2 + [(1.714)(1.502) + (75.1)(3.216)]^2\}[(76.81)^2 + (0.2145)^2]} + (0.2145)(75.1)^2} \quad \text{pound-feet} \qquad (5.111)$$

or

$$T_m = 8814 \quad \text{pound-feet} \qquad (5.112)$$

5.9 STARTING TORQUE

If voltage is impressed across the stator winding of a quiescent, polyphase induction motor, a torque is produced which tends to cause rotation of the rotor and connected load. At zero speed, the slip is equal to 1.0. Then, setting s = 1 in eq. (5.80), the starting torque is

$$T_{st} = \frac{21.1}{n_s} I_2^2 R_2 \quad \text{pound-feet} \qquad (5.113)$$

An inspection of this equation shows that starting torque is proportional to the rotor winding losses at blocked-rotor condition. This fact presents an apparent dilemma in the design of induction motors. It is obviously necessary to have sufficient starting torque to meet the requirements of the application. On the other hand, it is important to keep the rotor-winding losses, at full-speed operation, as low as reasonably possible, because of efficiency and heating considerations. Fortunately, as will be discussed subsequently, this apparent dilemma is resolved for squirrel-cage motors by use of rotor bars which are designed to exhibit high resistance when the rotor-circuit frequency is in the region of 60 Hz, or at high slip, and to exhibit low resistance when the rotor-circuit frequency is low, or at low slip.

Starting torque, in terms of the winding parameters of the machine, may be obtained by setting s = 1 in eq. (5.81) and by remembering that the blocked-rotor values of rotor phase resistance and of rotor and stator phase leakage reactance should be used. Then

$$T_{st} = \frac{(21.1/n_s)V_1^2 X_m^2 R_{2\ell}}{[R_{2\ell}(X_{1\ell} + X_m) + R_1(X_{2\ell} + X_m)]^2 + [-R_1 R_{2\ell} + X_{1\ell}X_{2\ell} + X_m(X_{1\ell} + X_{2\ell})]^2} \quad \text{pound-feet} \tag{5.114}$$

Inserting the winding parameters from Table 5.1 into eq. (5.114) gives us

$$T_{st} = \frac{(21.1/1800)(2309)^2(75.1)^2(0.490)}{[(0.490)(76.81) + (0.2145)(76.1)]^2 + [-0.2145)(0.490) + (1.714)(1.006) + (75.1)(2.72)]^2} \quad \text{pound-feet} \tag{5.115}$$

or

$$T_{st} = 3811 \quad \text{pound-feet} \tag{5.116}$$

The rotor phase windings of wound-rotor motors are brought out to collector rings for external connection of resistance. This permits using whatever value of resistance that might be required in the rotor circuit at startup, and then decreasing the external rotor resistance to whatever value that is required for subsequent operation. To determine what amount of total rotor resistance should be in the rotor circuit of a wound-rotor motor, in order to cause maximum torque to coincide with starting torque, set s = 1 in eq. (5.108) and solve for R_2. Then

$$1.0 = R_2' \left\{ \frac{(X_1 + X_m)^2 + R_1^2}{R_1^2(X_2 + X_m)^2 + [X_1X_2 + X_m(X_1 + X_2)]^2} \right\}^{1/2} \quad \text{per unit} \tag{5.117}$$

Solving for R_2', we have

$$R_2' = \left\{ \frac{R_1^2(X_2 + X_m)^2 + [X_1X_2 + X_m(X_1 + X_2)]^2}{(X_1 + X_m)^2 + R_1^2} \right\}^{1/2} \quad \text{ohms/phase} \tag{5.118}$$

The value of R_2' above is total rotor circuit resistance, which includes the sum of the rotor winding resistance/phase and the external resistance/phase. To obtain the amount of external rotor resistance to add per phase, the rotor winding resistance/phase must be subtracted from eq. (5.118).

The previously mentioned increase in rotor winding resistance, caused by current crowding in the rotor bar at blocked-rotor conditions, is somewhat different for wound-rotor machines than for squirrel-cage machines. Two reasons for this difference are (1) that there are usually several separate conductors per slot in the wound-rotor machine instead of one solid bar, and (2) that a major portion of the total rotor resistance may be external to the machine in wound-rotor machines. However, the decrease in winding leakage reactance, due to saturation of some ferrous leakage flux paths, may be similar to that for squirrel-cage motors if insufficient external rotor resistance is added, at startup, to limit the current to a value below which saturation does not occur. Accordingly, if blocked-rotor winding parameters are known to be different from running parameters for a given wound-rotor machine undergoing a given starting procedure, the blocked-rotor parameters should be used in eq. (5.118).

5.10 STARTING CURRENT

Starting current, or blocked-rotor current, is the symmetrical, alternating current that occurs just after bus voltage is applied to the stator terminals and just as rotation of the rotor is imminent. It may be calculated by setting s = 1 in eq. (5.19) and by remembering that at such high slip and high current conditions, the blocked-rotor values of rotor resistance and of stator and rotor leakage reactance should be used. Then

$$I_\ell = \frac{V_1}{R_1 + j(X_{1\ell} + X_m) - (jX_m)^2/[R_{2\ell} + j(X_{2\ell} + X_m)]} \quad \text{amperes/phase} \tag{5.119}$$

To calculate the magnitude of starting current for the example motor, substitute the appropriate values from Table 5.1 into eq. (5.119).

$$I_\ell = \frac{2309\underline{/0^\circ}}{0.2145 + j(1.714 + 75.1) - (75.1\underline{/90^\circ})^2/[0.490 + j(1.006 + 75.1)]}$$

$$= 825.2\underline{/-75.5^\circ} \quad \text{amperes/phase} \tag{5.120}$$

5.11 THE SPEED-TORQUE CURVE

As has been shown, starting torque, maximum torque, and full-load torque may be calculated from eq. (5.87) by using a value of slip equal to 1, s_m, and rated, respectively. Obviously, the torque corresponding to any value of slip, from unity to essentially zero, may also be calculated by eq. (5.87). It is normal practice to plot speed versus torque with torque as one axis and speed, instead of slip, as the other. Such a curve is the locus of all corresponding points of speed and torque for a given design and appropriately, is called the speed-torque curve. As will be considered later, torque is an important quantity in applying a polyphase induction motor to the driven equipment. Accordingly, the speed-torque curve has become a significant application tool in matching the drive motor to the driven equipment.

The detail of the speed-torque curve will, of course, vary with the winding parameters of the specific design being considered, in accordance with eq. (5.87). The curve in Fig. 5.5 illustrates the general appearance of the speed-torque curve of a medium-sized squirrel-cage motor. In this curve, speed is considered the independent variable, along the abscissa, and torque is considered a function of speed, along the ordinate. It is not unusual, however, to find the axes selected to represent speed and torque, reversed from that shown in Fig. 5.5. The effect of certain harmonics, which may cause perturbations on the speed-torque curve, will be considered subsequently, and such effects are not shown in Fig. 5.5.

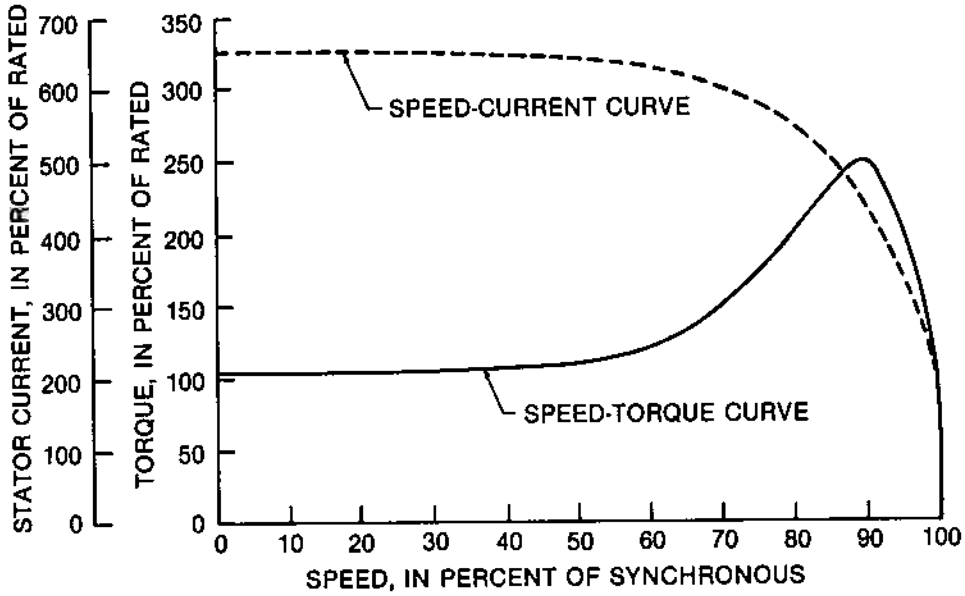

FIGURE 5.5 Speed-torque curve and speed-current curve of a squirrel-cage induction motor.

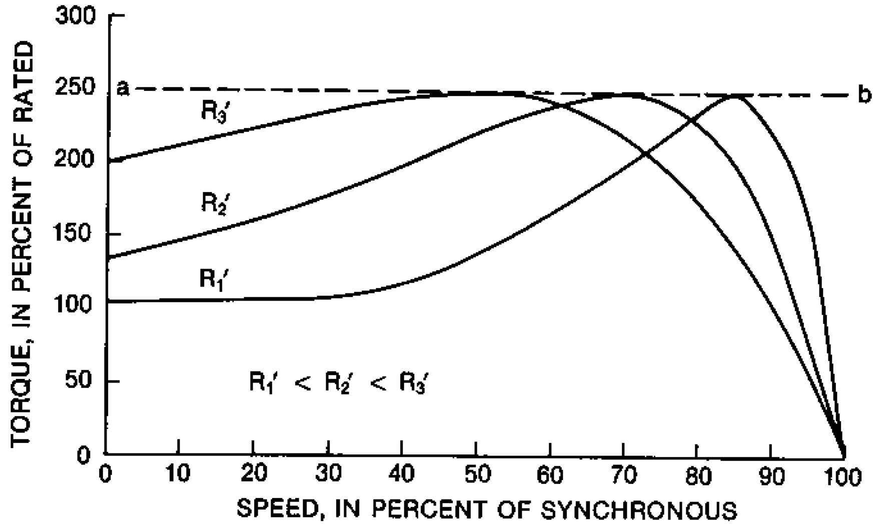

FIGURE 5.6 Speed-torque curve of a wound-rotor induction motor with several different values of total rotor-circuit resistance.

If the slip rings of a wound-rotor motor are shorted, (i.e., if no external resistance is inserted into the rotor circuit), the resulting speed-torque characteristic will, in general, resemble that of a squirrel-cage motor but will typically have less starting torque. However, a wound-rotor motor is not normally operated without external resistance in the rotor circuit. It is normal practice to have considerable external resistance inserted during acceleration. This is done to reduce the kVA requirements on the stator bus and, at the same time, to develop adequate starting torque. Subsequent to acceleration, the external resistance is set to match the speed and torque requirements of the driven equipment.

The speed-torque curve of a wound-rotor motor is illustrated in Fig. 5.6. Since, as shown in eq. (5.99), the slip at which maximum torque occurs is proportional to the total rotor-circuit resistance, the amount of external rotor resistance inserted into the rotor circuit will affect the speed at which maximum torque occurs. Figure 5.6 shows several different curves, each corresponding to a different value of total rotor resistance and, for this family of curves, $R_1' < R_2' < R_3'$

The magnitude of maximum torque is independent of the magnitude of rotor resistance for wound-rotor motors as it is for squirrel-cage motors. However, the magnitude of maximum torque may not fall strictly along a line parallel to the abscissa of the speed-torque curve, such as line ab in Fig. 5.6, as the external rotor resistance is varied. One reason for this is that the external resistor, connected in series with the rotor phase winding, is not a completely pure resistance but does contain some amount of reactance. Then, as more and more external resistance is added to the rotor circuit, an increasing amount of additional reactance may inadvertently be added. The exact amount of this additional reactance varies with the particular resistor being used, ranging from essentially none to an amount that produces a noticeable effect. This additional reactance, to the extent that it does occur, tends to decrease slightly the magnitude of maximum torque.

Another reason for a slight decrease in maximum torque at lower speeds in a wound-rotor motor is because of an increase in the eddy-current component of core loss in the magnetic core of the rotor at such speeds. Near full speed, the frequency of flux change in the rotor core is small, varying from less than 1 Hz to only a few hertz. However, at low-speed operation, it will approach line frequency. Since this loss occurs on the rotor side of the air gap, it subtracts from the torque produced by the rotor, leaving less net torque available at the shaft. This effect is small, in any case, and will not exceed a small percentage.

As mentioned earlier, the magnitude of leakage reactance is not constant at all speeds and operating conditions. For squirrel-cage motors which are accelerating to full speed, the current flow is high at lower speeds, as can be seen in Fig. 5.5. For squirrel-cage motors, the current during acceleration can reach six to seven times rated value, which is sufficient to cause some amount of saturation of the ferromagnetic leakage flux paths. As discussed earlier, this has the effect of reducing the leakage reactance of the machine, which increases the magnitude of maximum torque. Wound-rotor motors operate at reduced speeds by insertion of additional external resistance into the rotor winding, which thereby increases the slip. This also has the effect of limiting the current magnitude so that reduction in leakage reactance due to saturation of ferromagnetic leakage flux paths at reduced speeds, is less probable for wound-rotor motors.

However, if the individual turns of the rotor winding are simply made of deep, insulated bars which are not properly stranded, it is possible that leakage flux across the rotor slot can tend to crowd the rotor-bar current toward the top of the bar, at the rotor-circuit frequencies occurring at lower speed. This can effectively reduce the rotor-bar height and tend to reduce the rotor-slot leakage reactance and hence increase the magnitude of maximum torque. Many wound-rotor windings, though, have two different coil sides occupying each rotor slot with each coil side probably consisting of several strands, even if there is only one turn per coil side. Accordingly, this effect is not very great for wound-rotor motors.

5.12 THE SPEED-CURRENT CURVE

Stator phase current is calculated from eq. (5.19) using the winding parameters, stator phase voltage, and slip. Since stator current is a function of slip, it is also a function of speed. Accordingly, the stator phase current of a squirrel-cage motor may be calculated, as a function of speed, during the acceleration period. Such a curve is illustrated in Fig. 5.5.

The speed-current curve is constructed from several different current values, calculated from a range of corresponding speeds. The values of rotor resistance and leakage reactance used in eq. (5.19) should correspond to that for the particular speed being considered.

6

The Simplified Equivalent Circuit

6.1 Background 98

6.2 Determination of the Phase Current 98

6.3 Determination of the Power Output 101

6.4 Determination of the Torque Output 104

6.5 Maximum Torque 105

6.6 Starting Torque 109

6.7 Numerical Example Using the Simplified Equivalent Circuit 111

- 6.7.1 Calculation of slip and power output 111
- 6.7.2 Calculation of torque output 112
- 6.7.3 Calculation of maximum torque 113
- 6.7.4 Calculation of starting torque 114
- 6.7.5 Calculation of line current 114
- 6.7.6 Calculation of blocked-rotor current 115
- 6.7.7 Calculation of power factor and efficiency 115

6.8 Comparison of Results of Calculations by Use of the Two Circuits 117

6.9 Improvement of Simplified Equivalent-Circuit Results by Use of Adjusted Voltage 119

6.10 Comments on Choice of Equivalent Circuit 120

6.1 BACKGROUND

The equations derived from the equivalent circuit shown in Fig. 5.4 provide a basis for accurate analysis, and such equations should, in general, be used. Hand calculators, desk calculators, and digital computers provide for easy handling of such equations. However, during the period of rapid development of induction motor lore, which extended from about 1890 to about 1950, calculations were performed primarily by use of slide rules and tables of logarithms. Thus during that period in the development of the induction motor, there was a motivation to simplify equations in order to simplify calculations. It is not surprising, then, that the simplified equivalent circuit shown in Fig. 6.1 came into use to some extent. This circuit resulted in simpler equations, but at the expense of accuracy in results and of less precise analog representation of the actual machine. In the simplified equivalent circuit, as in the complete equivalent circuit, the circuit quantities are all referred either to the stator side or to the rotor side, by applying the turns ratio. Unless otherwise stated, they are assumed below to be referred to the stator side.

6.2 DETERMINATION OF THE PHASE CURRENT

Two points concerning current flow are apparent from observing Fig. 6.1, both of which introduce approximations into the results derived from the simplified equivalent circuit and both of which depart from the true physical conditions that exist in the actual machine. The first point is that the magnetizing reactance X_m is assumed to be shunted across the stator bus, and the voltage impressed across it is not subject to the varying impedance drop caused by a varying stator current flowing through the stator winding impedance. Thus X_m is effectively removed from the circuit in terms of affecting the behavior of the rest of the circuit. The second point is that the series current I' is assumed to flow through both the rotor and the stator phase windings. This requires that the current flowing in the rotor phase winding and in the stator phase winding be equal in magnitude and in phase angle, which they are not, of course. Also, since there is no representation of the voltage drop caused by magnetizing current flowing through the stator winding impedance, the rotor voltage is in error by a few percent in the simplified circuit unless an additional adjustment is made to compensate for this deficiency.

The relationship among current, voltage, and impedance may be determined, by inspection of Fig. 6.1, as

$$I' = \frac{-V_1}{R_1 + R_2/s + j(X_1 + X_2)} = \frac{-V_1}{\sqrt{(R_1 + R_2/s)^2 + (X_1 + X_2)^2}} \quad \text{amperes/phase} \qquad (6.1)$$

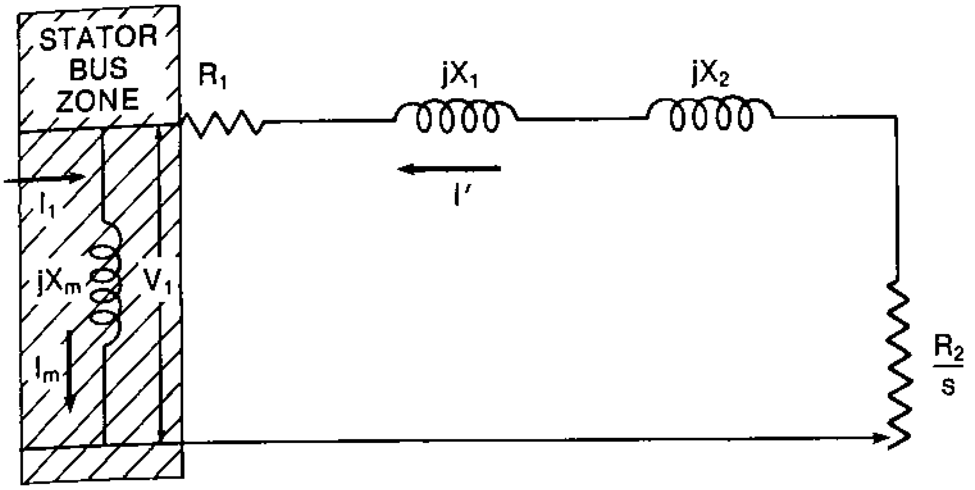

FIGURE 6.1 Simplified equivalent circuit of the polyphase induction motor.

and

$$I_m = \frac{V_1}{jX_m} = \frac{-jV_1}{X_m} \quad \text{amperes/phase} \tag{6.2}$$

To obtain the total phase current in the actual machine, we use the formula

$$I_1 = I_m - I' \quad \text{amperes/phase} \tag{6.3}$$

Substituting eqs. (6.1) and (6.2) into eq. (6.3) yields

$$I_1 = -\frac{jV_1}{X_m} + \frac{V_1}{R_1 + R_2/s + j(X_1 + X_2)} \quad \text{amperes/phase} \tag{6.4}$$

It should be noted that although I_1 in eq. (6.4) is the input current to the machine, it is not the current flowing in the stator winding of the circuit, as described in Fig. 6.1. This, again, demonstrates an inconsistency between the actual machine and the simplified equivalent-circuit model of the machine.

The current I' in eq. (6.1) is the current that flows through the rotor winding, including R_2/s, in the simplified circuit, and which produces the torque developed in the rotor. Consider the corresponding rotor current which flows through the rotor winding of the complete circuit, in eq. (5.22).

$$I_2 = \frac{-V_1X_m}{[(R_2/s)(X_1 + X_m) + R_1(X_2 + X_m)] + j[-R_1R_2/s + X_1X_2 + X_m(X_1 + X_2)]}$$

$$\text{amperes/phase} \tag{6.5}$$

It is apparent that if the magnetizing branch containing X_m is removed from the complete equivalent circuit in Fig. 5.4, the resulting circuit is equal to that of Fig. 6.1, to the right of the stator-voltage bus. Accordingly, it would be intuitively expected that the equations derived from the complete equivalent circuit, if properly acted upon mathematically to remove X_m, should transform into the equations derived from the simplified circuit. The numerator and denominator of eq. (6.5) may be divided by X_m without affecting the equation. Then, for the rotor current I_2,

$$I_2 = \frac{-V_1}{[(R_2/s)(X_1/X_m + 1) + R_1(X_2/X_m + 1)] + j[-R_1R_2/X_m s + X_1X_2/X_m + (X_1 + X_2)]}$$

amperes/phase (6.6)

In the limit as X_m approaches infinity, I_2 will approach I', since the complete equivalent circuit has been transformed into the simplified equivalent circuit, to the right of the stator-voltage bus zone.

$$\lim_{X_m \to \infty} \frac{-V_1}{[(R_2/s)(X_1/X_m + 1) + R_1(X_2/X_m + 1)] + j[-R_1R_2/X_m s + X_1X_2/X_m + (X_1 + X_2)]}$$

$$= \frac{-V_1}{R_2/s + R_1 + j(X_1 + X_2)} = \frac{-V_1}{\sqrt{(R_1 + R_2/s)^2 + (X_1 + X_2)^2}}$$

amperes/phase (6.7)

which is identical to eq. (6.1).

Further, it would be intuitively expected that the stator current in eq. (5.17), which was derived from the complete equivalent circuit, would also approach I' as X_m approaches infinity, since the simplified equivalent circuit assumes that the current I' flows through the stator winding as well as the rotor winding. The stator current, derived from the complete equivalent circuit, is

$$I_1 = \frac{V_1[R_2/s + j(X_2 + X_m)]}{[R_1R_2/s - X_1X_2 - X_m(X_1 + X_2)] + j[(R_2/s)(X_1 + X_m) + R_1(X_2 + X_m)]}$$

amperes/phase (6.8)

Dividing the numerator and denominator of eq. (6.8) by X_m, we obtain

$$I_1 = \frac{V_1[R_2/X_m s + j(X_2/X_m + 1)]}{[R_1R_2/X_m s - X_1X_2/X_m - (X_1 + X_2)] + j[(R_2/s)(X_1/X_m + 1) + R_1(X_2/X_m + 1)]}$$

amperes/phase (6.9)

Taking the limit of eq. (6.9) as X_m approaches infinity gives us

$$\lim_{X \to \infty} \frac{V_1[R_2/X_m s + j(X_2/X_m + 1)]}{[R_1R_2/X_m s - X_1X_2/X_m - (X_1 + X_2)] + j[(R_2/s)(X_1/X_m + 1) + R_1(X_2/X_m + 1)]}$$

$$= \frac{jV_1}{-(X_1 + X_2) + j(R_2/s + R_1)} = \frac{V_1}{(R_1 + R_2/s) + j(X_1 + X_2)}$$

amperes/phase (6.10)

which, as anticipated, is identical to the expression for I'.

The expression for the magnitizing current I_m derived from the complete equivalent circuit will not transform to that derived from the simplified equivalent circuit. This is because the magnetizing reactance X_m is shunted across the constant voltage of the stator bus and hence is effectively removed from the circuit to the right of the stator-bus zone. It is also for this reason that for the simplified circuit, the actual input current to the machine, such as might appear on the nameplate, must be obtained by vectorially adding the magnetizing current, calculated as $-jV_1/X_m$, to I', as indicated in eqs. (6.3) and (6.4).

6.3 DETERMINATION OF THE POWER OUTPUT

The current I' flows through the rotor circuit in the simplified equivalent circuit in Fig. 6.1 and produces the power developed in the rotor. Then the gross power developed in each phase of the rotor is equal to

$$P_{g2} = (I')^2 \frac{R_2}{s} \quad \text{watts/phase} \tag{6.11}$$

and for the three phases is equal to

$$P_{g2} = 3(I')^2 \frac{R_2}{s} \quad \text{watts} \tag{6.12}$$

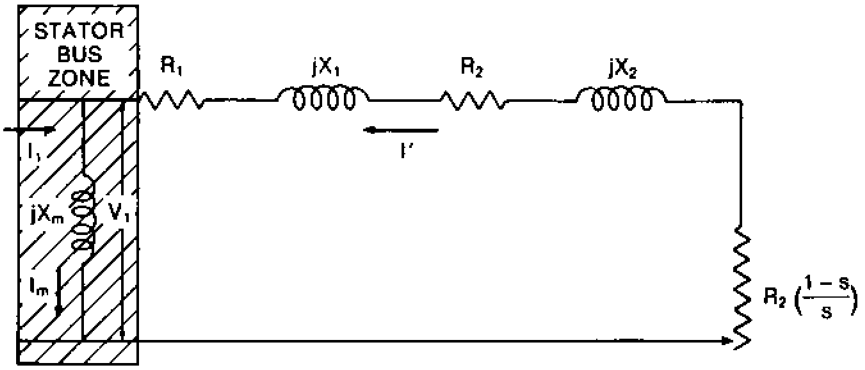

FIGURE 6.2 Simplified equivalent circuit of the polyphase induction motor, showing the equivalent load resistance.

Rewriting eq. (6.12) to isolate the rotor winding resistance loss, $3(I')^2R_2$, yields

$$P_{g2} = 3(I')^2R_2 + 3(I')^2R_2\,\frac{1-s}{s} \quad \text{watts} \tag{6.13}$$

The net power developed by the rotor is then

$$P_2 = 3(I')^2R_2\,\frac{1-s}{s} \quad \text{watts} \tag{6.14}$$

where, as for eq. (5.30), the term $R_2(1-s)/s$ is called the equivalent load resistance and has units of ohms. The simplified equivalent circuit of Fig. 6.1 is rearranged to show the equivalent load resistance in Fig. 6.2.

As discussed in Chapter 5, the power required to overcome friction and windage losses must be subtracted from P_2 in eq. (6.14) to obtain the net output power P_o which is available at the shaft of the machine. Then

$$P_o = 3(I')^2R_2\,\frac{1-s}{s} - F\&W \quad \text{watts} \tag{6.15}$$

The current I' flowing in the rotor circuit, in terms of the winding parameters, is given in eq. (6.1) as

$$I' = \frac{-V_1}{R_1 + R_2/s + j(X_1+X_2)} = \frac{-V_1}{\sqrt{(R_1+R_2/s)^2 + (X_1+X_2)^2}} \quad \text{amperes/phase} \tag{6.16}$$

Substituting eq. (6.16) into eq. (6.15) to give the net output power in terms of the winding parameters gives us

$$P_o = \frac{3V_1^2 R_2[(1 - s)/s]}{(R_1 + R_2/s)^2 + (X_1 + X_2)^2} - F\&W \quad \text{watts} \tag{6.17}$$

or, in terms of horsepower,

$$HP_1 = \frac{(3/746)V_1^2 R_2[(1 - s)/s]}{(R_1 + R_2/s)^2 + (X_1 + X_2)^2} - \frac{F\&W}{746} \quad \text{horsepower} \tag{6.18}$$

The corresponding equation for net output power derived from the complete equivalent circuit, as given in eq. (5.33), will transform into eq. (6.18), in the limit, if the magnetizing reactance is allowed to approach infinity. The expression for net output power as derived from the complete equivalent circuit is

$$HP_o = \frac{(3/746)V_1^2 X_m^2 R_2[(1 - s)/s]}{[(R_2/s)(X_1 + X_m) + R_1(X_2 + X_m)]^2 + [-R_1R_2/s + X_1X_2 + X_m(X_1 + X_2)]^2} - \frac{F\&W}{746} \quad \text{horsepower} \tag{6.19}$$

Dividing the numerator and denominator of eq. (6.19) by X_m^2 yields

$$HP_o = \frac{(3/746)V_1^2 R_2[(1 - s)/s]}{[(R_2/s)(X_1/X_m + 1) + R_1(X_2/X_m + 1)]^2 + [-R_1R_2/sX_m + X_1X_2/X_m + (X_1 + X_2)]^2} - \frac{F\&W}{746} \quad \text{horsepower} \tag{6.20}$$

Taking the limit of eq. (6.20) as X_m approaches infinity gives us

$$\lim_{X_m \to \infty} \frac{(3/746)V_1^2 R_2[(1 - s)/s]}{[(R_2/s)(X_1/X_m + 1) + R_1(X_2/X_m + 1)]^2 + [-R_1R_2/sX_m + X_1X_2/X_m + (X_1 + X_2)]^2} - \frac{F\&W}{746} = \frac{(3/746)V_1^2 R_2[(1 - s)/s]}{(R_2/s + R_1)^2 + (X_1 + X_2)^2} - \frac{F\&W}{746} \quad \text{horsepower} \tag{6.21}$$

which is identical to eq. (6.18).

6.4 DETERMINATION OF THE TORQUE OUTPUT

It is shown in eq. (5.78) that the total torque developed by the rotor, including the net shaft torque and the torque required to overcome friction and windage losses, is equal to

$$T = \frac{90}{\pi}\frac{1}{n_s} I_2^2 \frac{R_2}{s} \quad \text{newton-meters} \tag{6.22}$$

or, in terms of pound-feet,

$$T = \frac{21.1}{n_s} I_2^2 \frac{R_2}{s} \quad \text{pound-feet} \tag{6.23}$$

and the net shaft torque is equal to

$$T_o = \frac{21.1}{n_s} I_2^2 \frac{R_2}{s} - \frac{7.04(F\&W)}{n_s(1-s)} \quad \text{pound-feet} \tag{6.24}$$

Remembering that I' in eq. (6.1) is the simplified-circuit version of rotor current and substituting that expression for I' into eq. (6.24) yields

$$T_o = \frac{(21.1)/n_s)V_1^2(R_2/s)}{(R_1 + R_2/s)^2 + (X_1 + X_2)^2} - \frac{7.04(F\&W)}{n_s(1-s)} \quad \text{pound-feet} \tag{6.25}$$

This is the general torque output equation, as derived from the simplified equivalent circuit.

The corresponding equation for output, or eq. (5.87), derived from the complete circuit is

$$T_o = \frac{(21.1/n_s)V_1^2X_m^2(R_2/s)}{[(R_2/s)(X_1 + X_m) + R_1(X_2 + X_m)]^2 + [-R_1R_2/s + X_1X_2 + X_m(X_1 + X_2)]^2} - \frac{7.04(F\&W)}{n_s(1-s)} \quad \text{pound-feet} \tag{6.26}$$

Equation (6.26) will transform, in the limit, to eq. (6.25) as X_m approaches infinity. Dividing the numerator and denominator of eq. (6.26) by X_m^2 gives us

$$T_o = \frac{(21.1/n_s)V_1^2(R_2/s)}{[(R_2/s)(X_1/X_m + 1) + R_1(X_2/X_m + 1)]^2 + [-R_1R_2/sX_m + X_1X_2/X_m + X_1 + X_2]^2} - \frac{7.04(F\&W)}{n_s(1 - s)} \quad \text{pound-feet} \tag{6.27}$$

and taking the limit as X_m approaches infinity, we obtain

$$\lim_{X_m \to \infty} \frac{(21.1/n_s)V_1^2(R_2/s)}{[(R_2/s)(X_1/X_m + 1) + R_1(X_2/X_m + 1)]^2 + [-R_1R_2/sX_m + X_1X_2/X_m + X_1 + X_2]^2} - \frac{7.04(F\&W)}{n_s(1 - s)} = \frac{(21.1/n_s)V_1^2(R_2/s)}{(R_2/s + R_1)^2 + (X_1 + X_2)^2} - \frac{7.04(F\&W)}{n_s(1 - s)}$$

$$\text{pound-feet} \tag{6.28}$$

which is identical to eq. (6.25).

6.5 MAXIMUM TORQUE

The slip at which maximum torque occurs can be derived for the simplified equivalent circuit by differentiating eq. (6.25) with respect to slip s, equating the resulting expression to zero, and solving for s. In the differentiation, the second term of eq. (6.25), which corrects for the torque required to overcome friction and windage losses, should be ignored. Then the equation to be differentiated is

$$T = \frac{(21.1/n_s)V_1^2(R_2/s)}{(R_1 + R_2/s)^2 + (X_1 + X_2)^2} \quad \text{pound-feet} \tag{6.29}$$

Equation (6.29) may be written as

$$T = \frac{(21.1/n_s)V_1^2R_2}{s(R_1 + R_2/s)^2 + s(X_1 + X_2)^2} \quad \text{pound-feet} \tag{6.30}$$

Differentiating eq. (6.30) with respect to slip s and equating to zero gives us

$$\frac{dT}{ds} = \frac{21.1V_1^2\{-R_2[2s(R_1 + R_2/s)(-R_2/s^2) + (R_1 + R_2/s)^2 + (X_1 + X_2)^2]\}}{n_s[s(R_1 + R_2/s)^2 + s(X_1 + X_2)^2]^2} = 0 \tag{6.31}$$

or

$$-2\left(\frac{R_1R_2}{s}\right) - 2\left(\frac{R_2}{s}\right)^2 + R_1^2 + \left(\frac{R_2}{s}\right)^2 + 2\left(\frac{R_1R_2}{s}\right) + (X_1 + X_2)^2 = 0 \tag{6.32}$$

Simplifying yields

$$\left(\frac{R_2}{s}\right)^2 = R_1^2 + (X_1 + X_2)^2 \tag{6.33}$$

and

$$s_m = \frac{R_2}{\sqrt{R_1^2 + (X_1 + X_2)^2}} \quad \text{per unit} \tag{6.34}$$

which is the slip at which maximum torque occurs for the simplified equivalent circuit.

The corresponding equation for the slip at maximum torque, or eq. (5.99), derived from the complete equivalent circuit, is

$$s_m = R_2\left\{\frac{R_1^2 + (X_1 + X_m)^2}{R_1^2(X_2 + X_m)^2 + [X_1X_2 + X_m(X_1 + X_2)]^2}\right\}^{1/2} \quad \text{per unit} \tag{6.35}$$

Again, eq. (6.35) will transform, in the limit, to eq. (6.34) as X_m approaches infinity. Dividing the numerator and denominator by X_m, we obtain

$$s_m = R_2\left\{\frac{(R_1/X_m)^2 + (X_1/X_m + 1)^2}{R_1^2(X_2/X_m + 1)^2 + [X_1X_2/X_m + (X_1 + X_2)]^2}\right\}^{1/2} \quad \text{per unit} . \tag{6.36}$$

and taking the limit as X_m approaches infinity, we have

$$\lim_{X_m \to \infty} R_2 \left\{ \frac{(R_1/X_m)^2 + (X_1/X_m + 1)^2}{R_1^2(X_2/X_m + 1)^2 + [X_1X_2/X_m + (X_1 + X_2)]^2} \right\}^{1/2}$$

$$= \frac{R_2}{\sqrt{R_1^2 + (X_1 + X_2)^2}} \quad \text{per unit} \tag{6.37}$$

which is identical to eq. (6.34).

Equation (6.25) is the general torque output equation as derived from the simplified equivalent circuit. Neglecting for the present time the second term of this equation, which corrects for the power required to overcome friction and windage losses, we have

$$T = \frac{(21.1/n_s)V_1^2(R_2/s)}{(R_1 + R_2/s)^2 + (X_1 + X_2)^2} \quad \text{pound-feet} \tag{6.38}$$

The expression for maximum torque can be derived by substituting into eq. (6.38) the value of slip given in eq. (6.34). Rearranging eq. (6.34) to solve for R_2/s gives us

$$\frac{R_2}{s_m} = \sqrt{R_1^2 + (X_1 + X_2)^2} \quad \text{ohms} \tag{6.39}$$

Substituting this expression for R_2/s into eq. (6.38) and expanding yields

$$T_m = \frac{(21.1/n_s)V_1^2\sqrt{R_1^2 + (X_1 + X_2)^2}}{R_1^2 + R_1^2 + (X_1 + X_2)^2 + 2R_1\sqrt{R_1^2 + (X_1 + X_2)^2} + (X_1 + X_2)^2} \quad \text{pound-feet} \tag{6.40}$$

or

$$T_m = \frac{(21.1/n_s)V_1^2\sqrt{R_1^2 + (X_1 + X_2)^2}}{2[R_1^2 + (X_1 + X_2)^2 + R_1\sqrt{R_1^2 + (X_1 + X_2)^2}]} \quad \text{pound-feet} \tag{6.41}$$

Dividing numerator and denominator by $\sqrt{R_1^2 + (X_1 + X_2)^2}$, we obtain

$$T_m = \frac{(21.1/n_s)V_1^2}{2[\sqrt{R_1^2 + (X_1 + X_2)^2} + R_1]} \quad \text{pound-feet} \qquad (6.42)$$

Equation (6.42) is the equation for maximum torque associated with the simplified equivalent circuit.

It would also be expected that eq. (5.107), the equation for maximum torque associated with the complete equivalent circuit, will transform to eq. (6.42), in the limit, as X_m approaches infinity. To verify that, consider the general equation for maximum torque derived from the complete equivalent circuit.

$$T_m = \frac{(1/2)(21.1/n_s)V_1^2 X_m^2}{\sqrt{\{R_1^2(X_2 + X_m)^2 + [X_1X_2 + X_m(X_1 + X_2)]^2\}\{(X_1 + X_m)^2 + R_1^2\}} + R_1X_m^2}$$

$$\text{pound-feet} \qquad (6.43)$$

Dividing the numerator and denominator of eq. (5.43) by X_m^2 and taking the limit as X_m approaches infinity gives us

$$T_m = \lim_{X_m \to \infty} \frac{(1/2)(21.1/n_s)V_1^2}{\sqrt{\{R_1^2(X_2/X_m + 1)^2 + [X_1X_2/X_m + (X_1 + X_2)]^2\}\{(X_1/X_m + 1)^2 + (R_1/X_m)^2\}} + R_1}$$

$$\text{pound-feet} \qquad (6.44)$$

or

$$T_m = \frac{(21.1/n_s)V_1^2}{2[\sqrt{R_1^2 + (X_1 + X_2)^2} + R_1]} \quad \text{pound-feet} \qquad (6.45)$$

which is identical to eq. (6.42).

The equation for maximum torque, eq. (6.42), derived from the simplified equivalent circuit, as well as the corresponding equation, eq. (5.107), derived from the complete equivalent circuit, give the torque developed by the rotor, including that required to overcome friction and windage. To determine the net shaft torque available at the coupling, sheave, or sprocket, the torque required to overcome friction and windage losses should be subtracted, as discussed for eq. (5.107). However, this correction is small, being of the order of 1% or so, whereas the magnitude of maximum torque is of the order of 200 to 300%. The winding parameters determine the magnitude of maximum torque, and the probable error in the accuracy by which these parameters are known is considerably greater than the error resulting from neglecting to correct for the torque to overcome friction and windage losses. Then as a practical matter, this correction may be neglected with justification, except for very unusual cases.

6.6 STARTING TORQUE

From eq. (6.25), the net torque developed by the rotor, in terms of the winding parameters, is equal to

$$T_o = \frac{(21.1/n_s)V_1^2(R_2/s)}{(R_1 + R_2/s)^2 + (X_1 + X_2)^2} - \frac{7.04(F\&W)}{n_s(1-s)} \quad \text{pound-feet} \tag{6.46}$$

Starting torque is obtained from this equation by setting $s = 1$, by using the blocked-rotor values of rotor resistance and rotor and stator leakage reactances, and by neglecting the second term of eq. (6.46), since there is no friction and windage losses until after the rotor starts to rotate. Then

$$T_{st} = \frac{(21.1/n_s)V_1^2 R_{2\ell}}{(R_1 + R_{2\ell})^2 + (X_{1\ell} + X_{2\ell})^2} \quad \text{pound-feet} \tag{6.47}$$

The corresponding equation for starting torque, eq. (5.114), derived from the complete equivalent circuit, is

$$T_{st} = \frac{(21.1/n_s)V_1^2 X_m^2 R_{2\ell}}{[R_{2\ell}(X_{1\ell} + X_m) + R_1(X_{2\ell} + X_m)]^2 + [-R_1R_{2\ell} + X_{1\ell}X_{2\ell} + X_m(X_{1\ell} + X_{2\ell})]^2} \quad \text{pound-feet} \tag{6.48}$$

Equation (6.48) will transform, in the limit, to eq. (6.47) as X_m approaches infinity. This may be shown by dividing the numerator and denominator by X_m^2.

$$T_{st} = \frac{(21.1/n_s)V_1^2R_{2\ell}}{[R_{2\ell}(X_{1\ell}/X_m + 1) + R_1(X_{2\ell}/X_m + 1)]^2 + [-R_1R_{2\ell}/X_m + X_{1\ell}X_{2\ell}/X_m + (X_{1\ell} + X_{2\ell})]^2} \quad \text{pound-feet} \qquad (6.49)$$

and taking the limit as X_m approaches infinity gives us

$$\lim_{X_m \to \infty} \frac{(21.1/n_s)V_1^2R_{2\ell}}{[R_{2\ell}(X_{1\ell}/X_m + 1) + R_1(X_{2\ell}/X_m + 1)]^2 + [-R_1R_{2\ell}/X_m + X_{1\ell}X_{2\ell}/X_m + (X_{1\ell} + X_{2\ell})]^2}$$

$$= \frac{(21.1/n_s)V_1^2R_{2\ell}}{(R_{2\ell} + R_1)^2 + (X_{1\ell} + X_{2\ell})^2} \quad \text{pound-feet} \qquad (6.50)$$

which is identical to eq. (6.47).

As discussed in Chapter 5, for wound-rotor motors, maximum torque can be made to coincide with starting torque if the appropriate magnitude of external rotor resistance is added to the rotor circuit. The slip at maximum torque derived from the simplified circuit in eq. (6.34) is

$$s_m = \frac{R_2}{\sqrt{R_1^2 + (X_1 + X_2)^2}} \quad \text{numeric} \qquad (6.51)$$

Setting $s_m = 1$ and solving for R_2 yields

$$R_2' = \sqrt{R_1^2 + (X_1 + X_2)^2} \quad \text{ohms/phase} \qquad (6.52)$$

The value of R_2' above is the total value of rotor resistance/phase. The external rotor resistance to be added is equal to R_2' less the rotor winding resistance/phase.

It is apparent that eq. (5.118), the corresponding rotor resistance equation, which causes maximum torque to coincide with starting torque, derived from the complete equivalent circuit will transform to eq. (6.52), in the limit, as X_m approaches infinity. A similar transformation was shown to occur for s_m for the same equation.

6.7 NUMERICAL EXAMPLE USING THE SIMPLIFIED EQUIVALENT CIRCUIT

6.7.1 Calculation of Slip and Power Output

The 1000-hp 4000-V 1800-rpm three-phase, 60-Hz squirrel-cage motor with the winding parameter and losses shown in Table 5.1 will be used as an example of calculating with equations derived from the simplified equivalent circuit. However, the value of slip at rated load, given in Table 5.1, resulted from calculations made with the complete equivalent circuit and, accordingly, slip must be recalculated using the simplified equivalent circuit.

To calculate rated slip, the equation for power output is set equal to 1000 hp, or rated power output, and the equation solved for the variable s. The equation for power output, derived from the simplified circuit, was shown to be

$$HP_o = \frac{(3/746)V_1^2 R_2[(1 - s/s]}{(R_1 + R_2/s)^2 + (X_1 + X_2)^2} - \frac{F\&W}{746} \quad \text{horsepower} \qquad (6.53)$$

Substituting the values of the winding parameters and of rated voltage from Table 5.1 into eq. (6.53) yields

$$1000 = \frac{(3/746)(2309)^2(0.236)[(1 - s)/s]}{(0.2145 + 0.236/s)^2 + (1.714 + 1.502)^2} - \frac{11,500}{746} \quad \text{horsepower} \qquad (6.54)$$

Rearranging the equation and solving for s, we obtain

$$3.0842s^2 - 0.9797s + 0.01118 = 0 \quad \text{numeric} \qquad (6.55)$$

Utilizing the quadratic formula and discarding the extraneous root gives us

$$s = \frac{0.9797 \pm \sqrt{(0.9797)^2 - (4)(3.0842)(0.01118)}}{(2)(3.0842)} = 0.01185 \quad \text{numeric} \qquad (6.56)$$

The foregoing value of calculated slip may be used to calculate the rotor current, and then this value of rotor current may be used to calculate the power output, as a check. From eq. (6.1), the current flowing through the rotor winding is

$$I' = \frac{-V_1}{R_1 + R_2/s + j(X_1 + X_2)} \quad \text{amperes/phase} \qquad (6.57)$$

Substituting the appropriate constants from Table 5.1 into this equation yields

$$I' = \frac{-2309/\underline{0^\circ}}{0.2145 + 0.236/0.01185 + j3.216} = 113.27/\underline{170.9^\circ} \quad \text{amperes/phase} \qquad (6.58)$$

From eq. (6.15), the output power in terms of rotor current is equal to

$$P_o = \frac{3}{746}(I')^2 R_2 \frac{1-s}{s} - \frac{F\&W}{746} \quad \text{horsepower} \qquad (6.59)$$

Then substituting the calculated value of rotor current from eq. (6.58), the value of calculated slip from eq. (6.56), and the value of friction and windage losses from Table 5.1 into eq. (6.59), we obtain

$$\begin{aligned} P_o &= \left(\frac{3}{746}\right)(113.27)^2(0.236)\left(\frac{1 - 0.01185}{0.01185}\right) - \frac{11,500}{746} \\ &= 1015.4 - 15.4 = 1000 \quad \text{horsepower} \end{aligned} \qquad (6.60)$$

which agrees with the power rating of the motor.

6.7.2 Calculation of Torque Output

Torque output, or net torque, is the torque developed by the rotor less the torque required to overcome friction and windage losses, and is the actual torque available at the coupling, sheave, or sprocket of the machine. Net torque as derived from the simplified equivalent circuit was shown in eq. (6.25) to be

$$T_o = \frac{(21.1/n_s)V_1^2(R_2/s)}{(R_1 + R_2/s)^2 + (X_1 + X_2)^2} - \frac{7.04(F\&W)}{n_s(1-s)} \quad \text{pound-feet} \qquad (6.61)$$

Substituting the value of the appropriate winding parameters and machine losses from Table 5.1 and the value of slip calculated in eq. (6.56) into eq. (6.61), we have

$$T_o = \frac{(21.1/1800)(2309)^2(0.236/0.01185)}{(0.2145 + 0.236/0.01185)^2 + (3.216)^2} - \frac{(7.04)(11,500)}{(1800)(1 - 0.01185)} = 2951 \text{ pound-feet} \qquad (6.62)$$

6.7.3 Calculation of Maximum Torque

The slip at which maximum torque occurs, eq. (6.34), derived from the simplified equivalent circuit, was shown to be

$$s_m = \frac{R_2}{\sqrt{R_1^2 + (X_1 + X_2)^2}} \quad \text{numeric} \qquad (6.63)$$

For the numerical example given in Table 5.1, we obtain

$$s_m = \frac{0.236}{\sqrt{(0.2145)^2 + (3.216)^2}} = 0.0732 \quad \text{numeric} \qquad (6.64)$$

Substituting this value of slip, together with the values of the appropriate winding constants of rated voltage and of synchronous speed from Table 5.1, into eq. (6.61) gives us

$$T_m = \frac{(21.1/1800)(2309)^2(0.236/0.0732)}{(0.2145 + 0.236/0.0732)^2 + (3.216)^2} = 9089 \quad \text{pound-feet} \qquad (6.65)$$

Again, the second term of eq. (6.61), which corrects for the torque required to overcome friction and windage losses, is intentionally omitted in eq. (6.65) because its magnitude is insignificant relative to the magnitude of maximum torque and would represent a correction which is less than the probable error by which the magnitudes of the winding parameters are known.

Maximum torque may also be calculated directly from the equation for maximum torque, eq. (6.42), derived from the simplified equivalent torque, or

$$T_m = \frac{21.1}{n_s} \frac{V_1^2}{2[\sqrt{R_1^2 + (X_1 + X_2)^2} + R_1]} \quad \text{pound-feet} \qquad (6.66)$$

Substituting the required constants from Table 5.1 into eq. (6.66) yields

$$T_m = \left(\frac{21.1}{1800}\right)\frac{(2309)^2}{2[\sqrt{(0.2145)^2 + (3.216)^2} + 0.2145]} = 9089 \quad \text{pound-feet} \tag{6.67}$$

which agrees with the value calculated in eq. (6.65).

6.7.4 Calculation of Starting Torque

From eq. (6.47), the equation for starting torque, derived from the simplified circuit, is

$$T_{st} = \frac{(21.1/n_s)V_1^2 R_{2\ell}}{(R_1 + R_{2\ell})^2 + (X_{1\ell} + X_{2\ell})^2} \quad \text{pound-feet} \tag{6.68}$$

Inserting the values of the appropriate constants from Table 5.1 into eq. (6.68) and remembering that for starting torque, the blocked-rotor values of the winding constants are to be used, we obtain

$$T_{st} = \frac{(21.1/1800)(2309)^2(0.490)}{(0.2145 + 0.490)^2 + (1.714 + 1.006)^2} = 3879 \quad \text{pound-feet} \tag{6.69}$$

6.7.5 Calculation of Line Current

Because the simplified equivalent circuit relocates the magnetizing reactance to the left of the stator winding impedance, to simplify calculations, this circuit portrays the same current I' flowing through the stator and rotor windings. If a more accurate value of stator current is required, such as for determining the input current to the machine or for calculating the stator winding I^2R loss, the magnetizing current I_m must be added vectorially to the current I'. Equation (6.4) accomplishes the vector addition of I' and I_m as

$$I_1 = \frac{-jV_1}{X_m} + \frac{V_1}{R_1 + R_2/s + j(X_1 + X_2)} \quad \text{amperes/phase} \tag{6.70}$$

Substituting the values of the required constants from Table 5.1 into eq. (6.70), we have

$$I_1 = \frac{2309\underline{/-90^\circ}}{75.1} + \frac{2309\underline{/0^\circ}}{0.2145 + 0.236/0.01185 + j3.216} = 121.9\underline{/-23.5^\circ}$$

amperes/phase (6.71)

This is the value of line current as calculated from the simplified equivalent circuit. It does not have the correction for the additional component of current which sustains core loss and load loss to compensate for the fact that these losses are not modeled in the equivalent circuit. The more accurate value of line current, with the current components above included, is given in eq. (6.77).

6.7.6 Calculation of Blocked-Rotor Current

The blocked-rotor current is also called the starting current. As derived from the simplified equivalent circuit, it is calculated by setting $s = 1$ in eq. (6.70) and by remembering that the blocked-rotor value of rotor resistance and of rotor and stator leakage reactance should be used. Then

$$I_\ell = \frac{-jV_1}{X_m} + \frac{V_1}{(R_1 + R_{2\ell}) + j(X_{1\ell} + X_{2\ell})} \quad \text{amperes/phase} \qquad (6.72)$$

Substituting the values of the winding constants from Table 5.1 into eq. (6.72) gives us

$$I_\ell = \frac{2309\underline{/-90^\circ}}{75.1} + \frac{2309\underline{/0^\circ}}{(0.2145 + 0.490) + j(1.714 + 1.006)} = 852\underline{/-76.0^\circ}$$

amperes/phase (6.73)

6.7.7 Calculation of Power Factor and Efficiency

As is true for the complete equivalent circuit, core loss and load loss are not modeled in the simplified equivalent circuit. An additional step is required in order to represent these losses in the in-phase component of stator current. Since magnetizing current has been added to the current I' in eq. (6.71) that current is nearly equal to full-load current input to the machine, except for the loss components of current mentioned above. Resolving the current in eq. (6.71) into its in-phase and reactive components yields

$$I_1 = 121.9\underline{/-23.5^\circ} = 111.8 - j48.6 \quad \text{amperes/phase} \qquad (6.74)$$

The in-phase component of stator current that sustains core loss and load loss for the simplified equivalent circuit is equal to

$$\Delta I_1 = \frac{CL + LL}{3} \frac{\sqrt{3}}{E_{LL}} \quad \text{amperes/phase} \tag{6.75}$$

since the magnetizing reactance X_m is shunted across the stator bus for this circuit. Substituting the values of the losses and of rated voltage from Table 5.1 into eq. (6.75), we obtain

$$\Delta I_1 = \left(\frac{7500 + 8000}{3}\right)\left(\frac{\sqrt{3}}{4000}\right) = 2.24 \quad \text{amperes/phase} \tag{6.76}$$

Adding eqs. (6.74) and (6.76) gives us

$$I_1 = 111.8 - j48.6 + 2.24 = 124\underline{/-23.1^\circ} \quad \text{amperes/phase} \tag{6.77}$$

The rated power factor for an induction motor is equal to

$$PF = \frac{kW_1}{kVA_1} = \frac{kW_0 + \Sigma \text{ losses}}{3I_1V_1} \quad \text{numeric} \tag{6.78}$$

Substituting the values of I_1, V_1, and the losses into eq. (6.78) yields

$$PF = \frac{746 + (3)(124)^2(0.2145)/1000 + (3)(113.3)^2(0.236)/1000 + 7.5 + 8.0 + 11.5}{(3)(124)(2309)/1000} = 0.922$$

$$\text{per unit} \tag{6.79}$$

Also, power factor is defined as the cosine of the angle between the stator phase current and stator phase voltage, and this relationship may be used as a check. From eq. (6.77), the phase angle is equal to -23.1 degrees, since the stator phase voltage has been used as angle reference. Then

$$\cos(-23.1) = 0.920 \quad \text{numeric} \tag{6.80}$$

which is close to that calculated in eq. (6.79).

Efficiency is equal to the ratio of net mechanical power output at the shaft to the electrical power input at the stator terminals:

$$\eta = \frac{P_o}{P_i} \quad \text{per unit} \tag{6.81}$$

Inserting the appropriate values for this example into eq. (6.81) gives us

$$\eta = \frac{746}{746 + 9.89 + 9.09 + 7.5 + 8.0 + 11.5} = 0.942 \quad \text{per unit} \tag{6.82}$$

6.8 COMPARISON OF RESULTS OF CALCULATIONS BY USE OF THE TWO CIRCUITS

Characteristics of the 1000-hp three-phase 60-Hz 4000-V squirrel-cage induction motor example have been calculated by use of the complete equivalent circuit in Chapter 5 and by use of the simplified equivalent circuit in this chapter. The results of these calculations are tabulated in Table 6.1 for comparison.

On first observation, it would appear that reasonable agreement exists between the two sets of results calculated by the two methods. However, it must be remembered that for the complete equivalent circuit, the calculated value of slip is equal to 0.0124 per unit and for the simplified equivalent circuit, it is equal to 0.01185 per unit. Thus these two sets of results are associated with values of full-load slip that differ by 4.4% in value. Both sets of results apply to the same physical machine, with the same winding parameters. However, the complete equivalent circuit will yield the more accurate results, since it more accurately represents the actual machine. Then the basic problem concerning calculated performance results of the simplified circuit, for this example, is that the calculated value of full-load slip is too small by over 4%.

The curve of slip versus power, in the region of full load, has a high rate of change of power, with respect to slip, for an incremental change in slip. If the value of full-load slip 0.01185, calculated from the simplified circuit, is substituted into the power output equation, eq. (5.33), derived from the complete circuit, the calculated power output is equal to 951 hp, instead of the rated value of 1000 hp as indicated by the tabulation. Similarly, if this value of slip is also substituted into the torque output equation, eq. (5.87), the calculated torque output is equal to 2805 lb-ft, instead of 2951 lb-ft as shown in the tabulation. Accordingly, if the motor is loaded until the slip just equals 0.01185 p.u., the full-load slip calculated by the simplified circuit, the actual shaft power is 95% of rated instead of 100%. Also, the input current to the stator should be about 118 A per phase, and not the 124 A per phase indicated in the tabulation, at this value of slip.

TABLE 6.1 Comparison of Calculated Results for the 1000-hp Motor Example, Using the Complete Circuit, the Simplified Circuit with Rated Voltage V_1 Applied, and the Simplified Circuit with Adjusted Voltage V_1' Applied

Symbol	Quantity	Complete circuit	Simplified circuit[a]	Simplified circuit[b]	Units
s	Slip	0.0124	0.01185	0.01247	per unit
P_o	Power output	1000	1000	1000	hp
T_o	Torque output	2952	2951	2952	lb-ft
s_m	Slip at maximum torque	0.0741	0.0732	0.0732	per unit
T_m	Maximum torque	8814	9089	8677	lb-ft
T_{st}	Starting torque	3811	3879	3703	lb-ft
PF	Power factor	0.923	0.922	0.923	per unit
η	Efficiency	0.941	0.942	0.941	per unit
I_2, I'	Rotor current	$115.9\underline{/170.8^\circ}$	$113.3\underline{/170.9^\circ}$	$116.2\underline{/170.7^\circ}$	amperes/phase
I_1	Stator current	$123.9\underline{/-22.7^\circ}$	$124\underline{/-23.1^\circ}$	$126.7\underline{/-22.6^\circ}$	amperes/phase
I_ℓ	Blocked-rotor current	$825\underline{/-75.7^\circ}$	$852\underline{/-76^\circ}$	$832\underline{/-76^\circ}$	amperes/phase
n_r	Full-load speed	1777.7	1778.7	1777.6	rpm

[a] Calculations were made with V_1 applied to the circuit.

[b] Calculations were made with adjusted voltage V_1', from eq. (6.85), applied to the circuit

6.9 IMPROVEMENT OF SIMPLIFIED EQUIVALENT-CIRCUIT RESULTS BY USE OF ADJUSTED VOLTAGE

The accuracy of the results from the simplified equivalent circuit can be improved by an obvious and easily made adjustment which causes the equations to represent more closely the actual physical conditions in the machine. As stated earlier, the simplified circuit does not allow for the voltage drop caused by magnetizing current flowing through the stator winding impedance. Accordingly, if the voltage V_1 is replaced with the adjusted voltage V_1', obtained by vectorially subtracting this impedance drop from V_1, in the various performance equations derived from the simplified circuit, the resulting equations will give more accurate results, in general. The adjusted voltage is calculated as

$$V_1' = V_1 - I_m(R_1 + jX_1) \quad \text{volts/phase} \tag{6.83}$$

From eq. (6.2), for the simplified circuit, we obtain

$$I_m = \frac{V_1}{jX_m} \quad \text{amperes/phase} \tag{6.84}$$

Substituting eq. (6.84) into eq. (6.83) yields

$$V_1' = V_1 - \frac{V_1}{jX_m}(R_1 + jX_1) \quad \text{volts/phase} \tag{6.85}$$

Inserting the appropriate values for the example in Table 5.1 into eq. (6.85), to calculate the adjusted voltage for the example gives us

$$V_1' = 2309\underline{/0^\circ} - \frac{2309\,\underline{/0^\circ}}{75.1\underline{/90^\circ}}(0.2145 + j1.714) = 2256\underline{/0.2^\circ} \quad \text{volts/phase} \tag{6.86}$$

If the calculations performed in eq. (6.53) through eq. (6.82) are repeated, using $V_1' = 2256\underline{/0.2^\circ}$ in place of $V_1 = 2309\underline{/0^\circ}$, wherever V_1 occurs in the equations, a new set of performance values will be obtained. This has been done and the resulting values are also tabulated in Table 6.1.

An inspection of Table 6.1 shows close agreement between the values calculated from the simplified circuit and from the complete circuit. Since the calculated value of full-load slip for the simplified circuit, using the adjusted voltage V_1' is very close to that for the complete circuit, it is apparent that the full-load set point on the slip-power curve and the slip-torque curve is very close to being identical for the two corresponding sets of calculations. Accordingly, these two sets of values can be compared on a more equivalent and meaningful basis than if a greater difference existed in the calculated full-load slip values, as is the case when comparing the simplified circuit with the impressed voltage V_1.

It will be noted in Table 6.1 that the calculated values of maximum torque and of starting torque are optimistic, or greater, for the simplified circuit with V_1 applied compared to the complete circuit. On the other hand, both maximum torque and starting torque are pessimistic, or less, for the simplified circuit with the adjusted voltage V_1' applied compared to the complete circuit. Both maximum torque and starting torque are important performance characteristics for applying drive motors to match the load requirements of the driven equipment. In some installations, such torque characteristics can be critical and, accordingly, it is not prudent to employ a method of calculation that tends to give optimistic values.

The magnitude of line current input to the stator of a polyphase induction motor is also equal to

$$I_1 = \frac{746\ \text{hp}}{\sqrt{3}\,E_{LL}(\eta)(PF)} \quad \text{amperes/phase} \tag{6.87}$$

Then, for the numerical example,

$$I_1 = \frac{(746)(1000)}{(\sqrt{3})(4000)(0.941)(0.923)} = 124 \quad \text{amperes/phase} \tag{6.88}$$

An inspection of Table 6.1 indicates that the input current I_1 is about 2% higher when calculated by the simplified circuit with the adjusted voltage V_1' applied compared to the corresponding current calculated by the complete circuit. The full-load slip is essentially equal for the two calculations and, accordingly, they represent essentially identical load conditions on the actual machine. Thus the difference in calculated input current is attributable to the intrinsic limitation of the simplified network to represent the machine accurately, for a specific load condition compared to the more complete network. Incidentally, if the calculation using the simplified circuit with voltage V_1 applied was repeated, but for a value of slip equal to 0.0124 per unit instead of 0.01185 p.u., the resulting input current would be over 4% greater than that shown in Table 6.1.

6.10 COMMENTS ON CHOICE OF EQUIVALENT CIRCUIT

Since both the complete and the simplified equivalent circuit have been considered, this is an appropriate point at which to comment on the choice of circuit for use in making calculations. The complete equivalent circuit should, in general, be used for making calculations since it more fully represents the actual machine than does the simplified circuit. It will consistently yield more accurate values for steady-state performance of the machine, and since the magnetizing reactance branch X_m is positioned at a location in the complete circuit corresponding to the generated voltage in the actual machine, this circuit will also consistently yield more accurate values for transient performance. With the availability of hand and desk calculators, personal computers, access terminals to mainframe computers, and so on, the earlier, historic motivation for developing and using the simplified circuit have essentially ceased to exist. If, for some reason, however, the simplified circuit should be used, it would appear that the adjusted voltage V_1', determined in accordance with eq. (6.85), should be substituted for V_1 wherever V_1 appears in the performance equations derived from that circuit.

7

The Vector Diagram

7.1 Inference of the Vector Diagram from the Equivalent Circuit 123

7.2 Construction of the Vector Diagram 126

7.3 Interpretation of the Vector Diagram 127

7.4 Analysis of Power Transformation by Use of the Vector Diagram 128

7.5 Determining Performance from the Vector Diagram 131

- 7.5.1 Power output 131
- 7.5.2 Torque output 132
- 7.5.3 Power factor and efficiency 137

7.6 Example of Calculating Performance from the Vector Diagram 138

- 7.6.1 Rated power output 138
- 7.6.2 Rated torque output 138
- 7.6.3 Rated power factor 139
- 7.6.4 Rated efficiency 139

7.1 INFERENCE OF THE VECTOR DIAGRAM FROM THE EQUIVALENT CIRCUIT

In the previous chapters, the complete equivalent circuit has been developed for, and applied to, the analysis of the polyphase induction motor. The complete equivalent circuit is a four-terminal T-section network which models one phase of the physical machine to an extent compatible with making accurate and reliable performance calculations. This circuit is, in effect, a mathematical model for one phase of the actual machine, and the current and voltage values which are obtained from calculations using this circuit are complex phase quantities which include both magnitude and angle. If the calculated values of current and voltage are plotted on polar coordinate paper, a vector diagram of one phase of the machine results which shows both magnitude and phase angle of each quantity. This will now be done for the 1000-hp squirrel-cage motor used previously as an example for equivalent-circuit calculations.

All of the current and voltage quantities for the example required for the vector diagram have been calculated previously except for the magnetizing current I_m and the induced voltage E_1. The magnetizing current may be calculated from eq. (5.25), which was derived from the equivalent circuit. Also, it may be calculated from the complex values of I_1 and I_2 by remembering that I_m is equal to the vector sum of these two currents, as is apparent by inspection of the equivalent circuit. However, ΔI_1, the previously added component of stator current which sustains core loss and load loss, must be subtracted from I_1 before making the vector addition. This is because core loss and load loss are not modeled in the equivalent circuit. In constructing the vector diagram, ΔI_1 will be reinserted in the correct vector position, to produce the correct total value of I_1. Then

$$I_m = (I_1 - \Delta I_1) + I_2 \quad \text{amperes/phase} \tag{7.1}$$

Substituting the calculated values of I_1 from eq. (5.44), of I_2 from eq. (5.35), and of ΔI_1 from (5.42) into eq. (7.1), we have

$$I_m = (123.9/\underline{-22.7^\circ} - 2.34/\underline{-4.7^\circ}) + 115.9/\underline{170.8^\circ} = 29.3/\underline{-94.8^\circ} = 29.3/\underline{265.2^\circ} \quad \text{amperes/phase} \tag{7.2}$$

From eq. (5.3), the induced voltage is determined as

$$V_1 - I_1(R_1 + jX_1) + E_1 = 0 \quad \text{volts/phase} \tag{7.3}$$

Rearranging eq. (5.3) and remembering that $E_1 = E_2$, when E_2 is referred to the stator

$$E_1 = E_2 = -[V_1 - I_1(R_1 + jX_1)] \quad \text{volts/phase} \tag{7.4}$$

Substituting the appropriate quantities from the numerical example into eq. (7.4) yields

$$E_1 = E_2 = -[2309/\underline{0^\circ} - (123.9/\underline{-22.7^\circ})(0.2145 + j1.714)] = 2211/\underline{175.2^\circ} \quad \text{volts/phase} \tag{7.5}$$

It is interesting to observe that the preliminary value of E_1, calculated in Table 5.2, is very close to the value calculated in eq. (7.5). It should be noted that the vector I_m leads the vectors E_1 and E_2 by 90 degrees. Since the mutual flux ϕ_m is in phase with the magnetizing current which produces it, ϕ_m also leads E_1 and E_2 by 90 degrees.

All of the current and voltage quantities associated with the vector diagram may now be tabulated in Table 7.1 for use in constructing the vector diagram for the example. If the complex quantities in Table 7.1 are plotted on polar coordinate paper, the vector diagram for the 1000-hp motor example is the result (Fig. 7.1). In the induction motor vector diagram, all quantities are referred to the stator, by use of the turns ratio, and all angular velocities are as viewed from the stator. These complex quantities, expressed as two-dimensional vectors, are occasionally called phasors.

From the above it is apparent that the existence of the vector diagram of the polyphase induction motor may be inferred from the existence, and the solution, of the equivalent circuit for that machine. In fact, one point of view concerning the vector diagram is that it is only an organized, graphical representation of the currents and voltages, as vector quantities, obtained by solution of the equivalent circuit. However, another point of view is that it is worthy of consideration, based on its own merits, and that it can provide additional insight into machine performance. For example, it is useful in visualizing some of the interrelationships between the various quantities

TABLE 7.1 Vector Diagram Quantities for the 1000-hp Squirrel-Cage Motor Example

Symbol	Description	Value
I_1	Stator phase current	$123.9\underline{/-22.7^\circ}$ amperes/phase
ΔI_1	CL and LL current increment	$2.34\underline{/-4.8^\circ}$ amperes/phase
I_2	Rotor phase current	$115.9\underline{/170.8^\circ}$ amperes/phase
I_m	Magnetizing current	$29.3\underline{/265.2^\circ}$ amperes/phase
V_1	Impressed stator phase voltage	$2309\underline{/0^\circ}$ volts/phase
E_1	Induced stator phase voltage	$2211\underline{/175.2^\circ}$ volts/phase
E_2	Induced rotor phase voltage	$2211\underline{/175.2^\circ}$ volts/phase
I_1R_1	Stator resistance voltage drop	$26.6\underline{/-22.7^\circ}$ volts/phase
jI_1X_1	Stator reactance voltage drop	$212.4\underline{/67.3^\circ}$ volts/phase
$I_2(R_2/s)$	Total in-phase rotor voltage drop	$2206\underline{/170.8^\circ}$ volts/phase
jI_2X_2	Rotor reactance voltage drop	$174.1\underline{/80.8^\circ}$ volts/phase

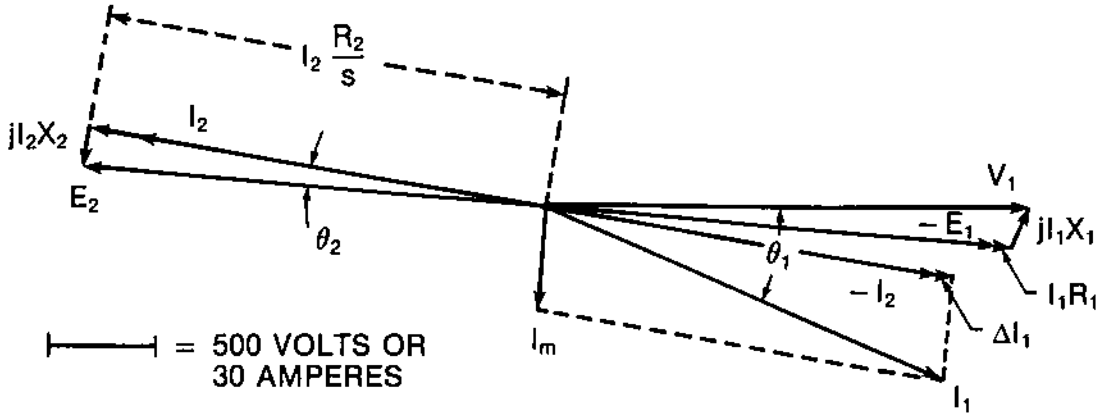
$I_2 \frac{R_2}{s}$
I_2
jI_2X_2
E_2
θ_2
V_1
$-E_1$
jI_1X_1
θ_1
$-I_2$
I_1R_1
ΔI_1
I_m
I_1
= 500 VOLTS OR
30 AMPERES

FIGURE 7.1 Vector representation of currents and voltages obtained from the equivalent-circuit solution of the 1000-hp squirrel-cage induction motor.

involved and in demonstrating the effect on these quantities when one of them, such as the leakage reactance or the magnetizing reactance, is changed in a given design.

7.2 CONSTRUCTION OF THE VECTOR DIAGRAM

Since the magnitudes of all rotor quantities are referred to the stator by the turns ratio and since their angular velocities are as viewed from the stator, the vector diagram shows the rotor and stator vector quantities in comparable magnitudes and angular positions. The rotor and stator vector quantities maintain their relative angular positions as they rotate at an angular velocity of ω radians/second in a counterclockwise direction. Thus the vector diagram may be regarded as an instantaneous picture of this set of rotating vectors. In constructing the vector diagram, the impressed stator

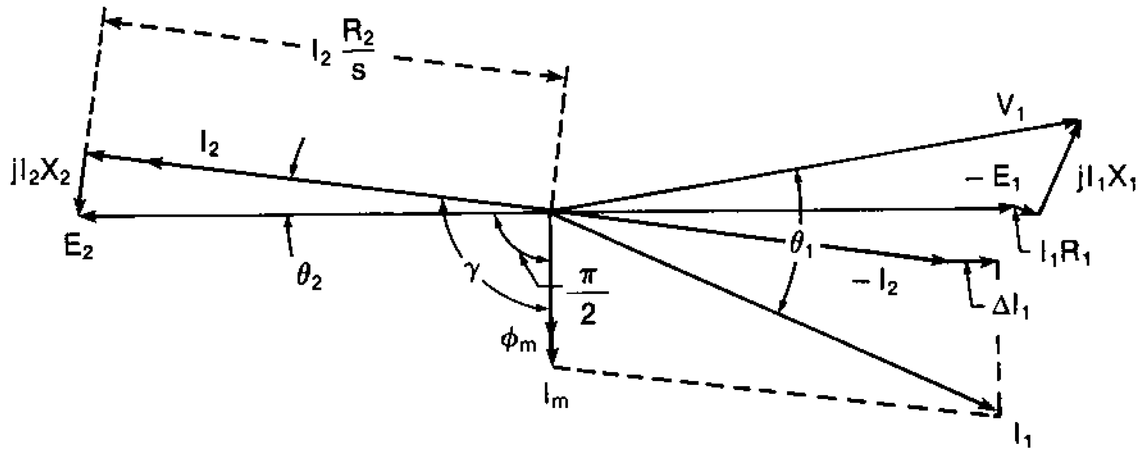
$I_2 \frac{R_2}{s}$
I_2
jI_2X_2
E_2
θ_2
γ
$\frac{\pi}{2}$
ϕ_m
I_m
V_1
$-E_1$
jI_1X_1
θ_1
I_1R_1
$-I_2$
ΔI_1
I_1

FIGURE 7.2 Vector diagram of one phase of a polyphase induction motor.

phase voltage is taken as time, or angle, reference. The angular position of this vector is arbitrarily set at 0 radians and the angular positions of the remaining vectors are thereby determined by their angular positions relative to the stator voltage vector. Figure 7.2 shows the vector diagram of the polyphase induction motor, with the quantities expressed in general terms. In this figure, the magnitudes of I_1R_1 and ΔI_1 are intentionally distorted to make them appear larger than they would actually occur, for ease of observing their relative angular positions.

7.3 INTERPRETATION OF THE VECTOR DIAGRAM

If the rotor winding of the machine is open circuited and voltage is applied to the stator winding, magnetizing current I_m will flow in the stator circuit and will produce a magnetic flux wave that rotates at ω radians/second. This rotating flux wave will induce the voltages E_1 and E_2 in the stator and rotor winding, respectively. If the rotor winding is then closed, a current will flow in the rotor circuit and produce a torque that will cause the rotor structure and connected load to accelerate until the torque produced by the machine just equals the load torque plus a torque required to overcome the friction and windage losses. After the rotor has accelerated to full speed, the machine will operate at a slip corresponding to the shaft load, plus friction and windage losses, and a current I_2, corresponding to that load, will flow in the rotor circuit. The resulting rotor magnetomotive force $N_2'I_2$ will react against a corresponding stator magnetomotive force $N_1'(-I_2)$, where N_2' and N_1' are the effective turns per phase in the rotor and stator, respectively. Thus a load will cause a current to flow in the rotor circuit, which will cause a corresponding load component of current to flow in the stator circuit. Further, since the rotor quantities are presumed to be referred to the stator in the vector diagram, by application of the turns ratio, the load component of stator current $-I_2$ will be equal in magnitude to the rotor current I_2. Also, as discussed previously, there will be a third component of stator current ΔI_1, in phase with the induced voltage, which sustains core loss and load loss. Then the stator phase current is equal to the vector sum of I_m, $-I_2$, and ΔI_1, or

$$I_1 = I_m - I_2 + \Delta I_1 \quad \text{amperes/phase} \tag{7.6}$$

The vector relationship among I_m, I_2, $-I_2$, ΔI_1, and I_1 is shown in Fig. 7.2. The stator current I_1 lags the voltage V_1 impressed on the stator winding by the angle θ_1 and the stator circuit power factor is equal to cos θ_1.

The voltage E_2 induced in the rotor winding lags the magnetizing current I_m and the mutual flux ϕ_m by $\pi/2$ radians. All of the generated rotor voltage E_2 is required to overcome the rotor circuit impedance drop, in accordance with eq. (5.10) and Fig. 5.2. Then

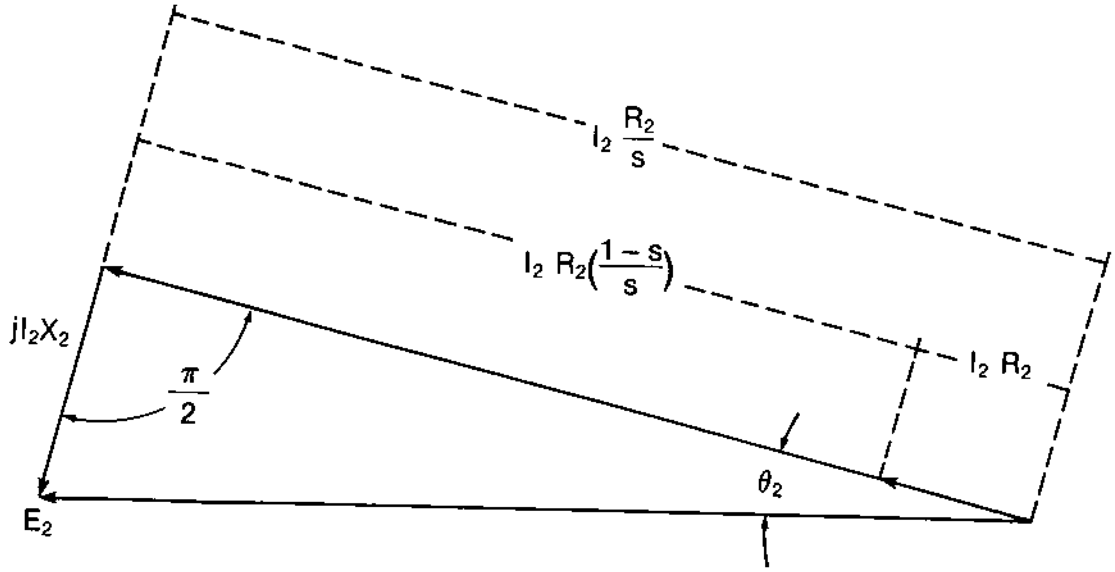

FIGURE 7.3 Vector diagram of rotor voltages of one phase of a polyphase induction motor.

$$E_2 = E_1 = I_2\left(\frac{R_2}{s} + jX_2\right) \quad \text{volts/phase} \tag{7.7}$$

The vector voltage triangle in Fig. 7.2, the sides of which are formed by E_2, I_2R_2/s, and jI_2X_2, is shown in larger scale in Fig. 7.3.

The voltage component $I_2R_2[(1 - s)/s]$ corresponds to the voltage drop in the rotor circuit caused by the rotor current I_2 flowing through the equivalent load resistance $R_2[(1 - s)/s]$. As shown earlier, the voltage components I_2R_2 and jI_2X_2 correspond respectively to the voltage drops across the actual rotor winding resistance and the rotor winding leakage reactance referred to the stator. The relationship between the rotor circuit voltages in the vector diagram and the corresponding equivalent circuit current and impedances can be seen in Fig. 5.4. The rotor current I_2 is in phase with the voltage drop $I_2(R_2/s)$, as shown in Fig. 7.2, and the rotor current lags the generated voltage E_2 by the angle θ_2. The rotor circuit power factor is then equal to cos θ_2.

7.4 ANALYSIS OF POWER TRANSFORMATION BY USE OF THE VECTOR DIAGRAM

Electric motors are machines that convert electrical energy into mechanical energy or, in terms of the time rate at which energy is transferred, electrical power into mechanical power. The vector dot, or scalar, product of the voltage and current vectors at a given point in the equivalent circuit is equal to the power in the corresponding part of the actual machine. Accordingly, the vector diagram is useful in determining the various components of power expenditure or transformation throughout the entire machine. Figure 7.4 shows the current and voltage vectors in the stator circuit, together with additional definition of the angles between these vectors.

The electrical power input to one phase of the stator is equal to

$$P_1 = V_1 I_1 \cos \theta_1 \quad \text{watts/phase} \tag{7.8}$$

Representing this relationship in terms of the vector dot product of V_1 and I_1, we have

$$P_1 = V_1 \cdot I_1 = [V_1][I_1] \cos \theta_1 \quad \text{watts/phase} \tag{7.9}$$

where $[V_1]$ and $[I_1]$ indicate the magnitude of V_1 and I_1, respectively. Since the dot, or scalar, multiplication obeys the distributive law, the vector V_1 may be replaced by the sum of its vector components. Then, from Fig. 7.4,

$$P_1 = (-E_1 + I_1 R_1 + jI_1 X_1) \cdot I_1 \quad \text{watts/phase} \tag{7.10}$$

or

$$P_1 = -E_1 \cdot I_1 + [I_1 R_1][I_1] \cos o + [I_1 X_1][I_1] \cos \frac{\pi}{2} \quad \text{watts/phase} \tag{7.11}$$

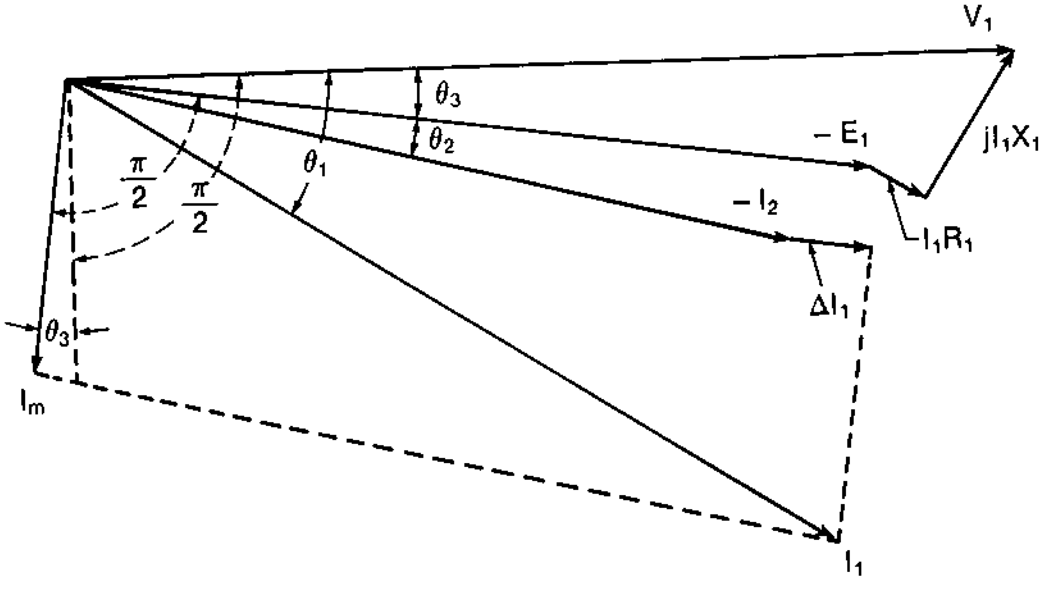

FIGURE 7.4 Vector diagram of stator voltages and currents of one phase of a polyphase induction motor.

where the first term was intentionally left unevaluated as a scalar quantity. Equation (7.11) may be written as

$$P_1 = -E_1 \cdot I_1 + I_1^2 R_1 + 0 \quad \text{watts/phase} \tag{7.12}$$

Similarly, the vector I_1, in the first term of eq. (7.12) may be replaced by the sum of its vector components, shown in Fig. 7.4. Then

$$P_1 = -E_1 \cdot (I_m - I_2 + \Delta I_1) + I_1^2 R_1 \quad \text{watts/phase} \tag{7.13}$$

Performing the multiplication indicated gives us

$$P_1 = [-E_1][I_m] \cos \frac{\pi}{2} + [-E_1][-I_2] \cos \theta_2 + [-E_1][\Delta I_1] \cos o + I_1^2 R_1 \quad \text{watts/phase} \tag{7.14}$$

Rewriting eq. (7.14) and remembering that $E_1 = E_2$ yields

$$P_1 = 0 + [E_2][I_2] \cos \theta_2 + [-E_1][\Delta I_1] \cos o + I_1^2 R_1 \quad \text{watts/phase} \tag{7.15}$$

The interpretation of eq. (7.15), in terms of the components of power expended or transferred within the machine, is as follows:

P_1 = power transferred across the air gap + core loss and load loss, sustained by the current ΔI_1 + stator winding copper loss watts/phase (7.16)

In a similar manner, the power transferred across the air gap, $[E_2][I_2] \cos \theta_2$, may be analyzed. Then

$$P_{g2} = [E_2][I_2] \cos \theta_2 = E_2 \cdot I_2 \quad \text{watts/phase} \tag{7.17}$$

Replacing E_2 by the sum of its vector components from Fig. 7.3, we have

$$P_{g2} = \left(I_2 R_2 \frac{1-s}{s} + I_2 R_2 + jI_2 X_2\right) \cdot I_2 \quad \text{watts/phase} \tag{7.18}$$

Performing the multiplication indicated, we obtain

$$P_{g2} = \left(I_2 R_2 \frac{1-s}{s}\right)[I_2] \cos o + [I_2 R_2][I_2] \cos o + [I_2 X_2][I_2] \cos \frac{\pi}{2} \quad \text{watts/phase} \tag{7.19}$$

or

$$P_{g2} = I_2^2 R_2 \frac{1 - s}{s} + I_2^2 R_2 + 0 \quad \text{watts/phase} \tag{7.20}$$

Similarly, the interpretation of eq. (7.20), in terms of the components of power expended or transferred, is as follows:

P_{g2} = total shaft power (including net shaft power + friction and windage losses) + rotor winding copper loss watts/phase (7.21)

7.5 DETERMINING PERFORMANCE FROM THE VECTOR DIAGRAM

In the usual circumstance, the winding parameters are calculated or otherwise determined and using these parameters the machine performance is determined from the equations derived previously from the equivalent circuit. Accordingly, the vector diagram is not, necessarily, involved in the calculation of performance of a polyphase induction motor. However, since the vector diagram provides the magnitude and angle of the various voltages and currents for one phase of the machine at a certain value of slip, usually rated, it can be used to determine performance at that particular value of slip. Obviously, performance characteristics associated with values of slip other than rated, such as starting torque or maximum torque for example, cannot be determined directly from a vector diagram for rated load conditions. A vector diagram can, of course, be constructed for any value of slip desired, including blocked-rotor or maximum torque conditions, if there is any reason for doing so and if the necessary data are available. Equations for operating characteristics which can be determined from the vector diagram are given below.

7.5.1 Power Output

From eqs. (7.20) and (7.21), the total power transferred across the air gap, or the gross power developed in the rotor, for each phase of the motor is equal to

$$P_{g2} = I_2^2 R_2 \frac{1 - s}{s} + I_2^2 R_2 \quad \text{watts/phase} \tag{7.22}$$

and for all three phases

$$P_{g2} = 3I_2^2 R_2 \frac{1 - s}{s} + 3I_2^2 R_2 \quad \text{watts} \tag{7.23}$$

The total shaft power developed by the rotor is equal to P_{g2} less the rotor winding $I_2^2R_2$ losses, or

$$P_2 = 3I_2^2R_2\frac{1-s}{s} \quad \text{watts} \tag{7.24}$$

Equation (7.24) includes all power loading on the shaft, including the component of load required to overcome friction and windage losses. Hence the net power available at the coupling, sheave, or sprocket is

$$P_o = 3I_2^2R_2\frac{1-s}{s} - \text{F\&W} \quad \text{watts} \tag{7.25}$$

which is identical to eq. (5.31). In units of horsepower, the net shaft power is

$$HP_o = \left(\frac{3}{746}\right)I_2^2R_2\frac{1-s}{s} - \frac{\text{F\&W}}{746} \quad \text{horsepower} \tag{7.26}$$

which is identical to eq. (5.32).

7.5.2 Torque Output

Motor power is equal to

$$P = \omega T \quad \text{watts} \tag{7.27}$$

where ω is angular velocity of the rotor, in units of radians/second, and T is total shaft torque, in units of newton-meters. Solving for torque gives us

$$T = \frac{P}{\omega} \quad \text{newton-meters} \tag{7.28}$$

Substituting eq. (7.24) into eq. (7.28) yields

$$T = \frac{3I_2^2R_2}{\omega}\frac{1-s}{s} \quad \text{newton-meters} \tag{7.29}$$

Remembering that

$$\omega = 2\pi\frac{n}{60} \quad \text{radians/second} \tag{7.30}$$

then

$$T = \frac{3I_2^2R_2}{2\pi n/60}\,\frac{1-s}{s} \quad \text{newton-meters} \tag{7.31}$$

Simplifying, we obtain

$$T = \frac{28.65}{n}\,I_2^2R^2\,\frac{1-s}{s} \quad \text{newton-meters} \tag{7.32}$$

The speed of rotation of the rotor can be expressed in terms of synchronous speed n_s and slip s as

$$n = n_s(1-s) \quad \text{rpm} \tag{7.33}$$

Replacing n in eq. (7.32) with the expression in eq. (7.33), we have

$$T = \frac{28.65}{n_s}\,I_2^2\,\frac{R_2}{s} \quad \text{newton-meters} \tag{7.34}$$

Since 1.356 N-m equal 1 lb-ft,

$$T = \frac{28.65}{1.356n_s}\,I_2^2\,\frac{R_2}{s} = \frac{21.1}{n_s}\,I_2^2\,\frac{R_2}{s} \quad \text{pound-feet} \tag{7.35}$$

Equation (7.35) includes the net shaft torque output and the torque required to overcome the retarding effect of friction and windage losses. From eq. (5.85), the torque required to overcome friction and windage losses is

$$T_{F\&W} = \frac{7.04(F\&W)}{n_s(1-s)} \quad \text{pound-feet} \tag{7.36}$$

Then the net motor torque available to the external load is

$$T_o = \frac{21.1}{n_s}\,I_2^2\,\frac{R_2}{s} - \frac{7.04(F\&W)}{n_s(1-s)} \quad \text{pound-feet} \tag{7.37}$$

which is identical to eq. (5.86).

Torque may also be derived by another method involving the vector diagram which more fully illustrates the vector nature of torque. Torque, in newton-meters, is equal to force, in newtons, multiplied by a lever arm in meters. Thus eq. (2.1), which expresses Ampère's law in terms of force, may be converted to an expression of torque by multiplying each side of the equation by d/2, the radius of the rotor, and then by 2, since there are two sets of rotor bars, 180 electrical degrees apart, reacting on the mutual flux to produce torque in an actual motor. Then, for a rotor with an active length of ℓ meters and a diameter of d meters, the resulting equation is

$$T = BI_2 \ell d \sin \gamma \quad \text{newton-meters} \tag{7.38}$$

where γ is the angle between the direction of B and the direction of I_2. This equation may be written as

$$T = \phi_m I_2 \sin \gamma \quad \text{newton-meters} \tag{7.39}$$

where

ϕ_m = mutual flux, in webers
I_2 = rotor current, in amperes/phase
γ = angle between the direction of ϕ_m and the direction of I_2

T is another vector which is perpendicular to the plane formed by the directions of ϕ_m and I_2 and which has a positive direction formed by the advance of a right-handed screw as ϕ_m is rotated into I_2. Equation (7.39) may be written, in vector notation, as the vector product of the two quantities ϕ_m and I_2.

$$T = \phi_m \times I_2 \quad \text{newton-meters} \tag{7.40}$$

It is interesting to verify that eqs. (7.39) and (7.40) do, indeed, have units of newton-meters. The mutual flux ϕ_m has units of webers, which are equal to units of volt-seconds. The current I_2 has units of amperes, such that the product of $\phi_m I_2$ has units of volt-seconds, multiplied by amperes, or of watt-seconds. One watt-second equals 1 joule, which equals 1 newton-meter. Equation (7.40) is applicable to several different types of electric motors if I_2 is understood to be the current flowing in the armature winding of the motor, whether that member be the rotor or the stator. In applying the equation to polyphase induction motors, it is understood that the armature is the rotor member and that I_2 is the phase current flowing in that member.

From Fig. 7.2,

$$\gamma = \theta_2 + \frac{\pi}{2} \quad \text{radians} \tag{7.41}$$

Substituting eq. (7.41) into eq. (7.39) gives us

$$T = \phi_m I_2 \sin\left(\theta_2 + \frac{\pi}{2}\right) \quad \text{newton-meters} \tag{7.42}$$

Expanding the trigonometric term $\sin(\theta_2 + \pi/2)$ yields

$$T = \phi_m I_2 \left(\sin \frac{\pi}{2} \cos \theta_2 + \cos \frac{\pi}{2} \sin \theta_2\right) \quad \text{newton-meters} \tag{7.43}$$

which reduces to

$$T = \phi_m I_2 \cos \theta_2 \quad \text{newton-meters} \tag{7.44}$$

Since the three different rotor phase currents react on the mutual flux and produce torque simultaneously, the torque produced by the machine is

$$T = 3\phi_m I_2 \cos \theta_2 \quad \text{newton-meters} \tag{7.45}$$

Let the magnetizing inductance of the machine be defined as

$$L_m = \frac{\phi_m}{I_m} \quad \text{henrys} \tag{7.46}$$

so that

$$\phi_m = L_m I_m \quad \text{webers} \tag{7.47}$$

Also, from Fig. 7.3,

$$\cos \theta_2 = \frac{I_2(R_2/s)}{E_2} \quad \text{numeric} \tag{7.48}$$

However,

$$E_2 = I_m X_m = I_m \omega L_m \quad \text{volts/phase} \tag{7.49}$$

Substituting eq. (7.49) into eq. (7.48) gives us

$$\cos \theta_2 = \frac{I_2(R_2/s)}{I_m \omega L_m} \quad \text{numeric} \tag{7.50}$$

and substituting eqs. (7.47) and (7.50) into eq. (7.45), we have

$$T = (3)(L_m I_m)(I_2) \frac{I_2(R_2/s)}{I_m \omega L_m} \quad \text{newton-meters} \tag{7.51}$$

which reduces to

$$T = \frac{3}{\omega} I_2^2 \frac{R_2}{s} \quad \text{newton-meters} \tag{7.52}$$

Replacing ω in eq. (7.52) with its equivalent from eq. (7.30), we obtain

$$T = \frac{(3)(60)}{2\pi n} I_2^2 \frac{R_2}{s} \quad \text{newton-meters} \tag{7.53}$$

or

$$T = \frac{28.65}{n} I_2^2 \frac{R_2}{s} \quad \text{newton-meters} \tag{7.54}$$

Since 1.356 N-m equal 1 lb-ft,

$$T = \frac{28.65}{1.356n} I_2^2 \frac{R_2}{s} = \frac{21.1}{n} I_2^2 \frac{R_2}{s} \quad \text{pound-feet} \tag{7.55}$$

Equation (7.55) is the total torque associated with the total power transferred across the air gap. To determine the net shaft torque delivered to the external load, the torque required to overcome the losses associated with the rotor winding resistance and with friction and windage must be subtracted. To subtract the torque required to overcome the rotor winding resistance loss, subtract $I_2^2R_2$ from $I_2^2(R_2/s)$. Then

$$T' = \frac{21.1}{n}\left(I_2^2 \frac{R_2}{s} - I_2^2 R_2\right) = \frac{21.1}{n} I_2^2 R_2 \frac{1 - s}{s} \quad \text{pound-feet} \tag{7.56}$$

To subtract the torque required to overcome the friction and windage losses, subtract eq. (7.36) from eq. (7.56):

$$T_o = \frac{21.1}{n} I_2^2 \frac{R_2}{s} \frac{1 - s}{s} - \frac{7.04(F\&W)}{n_s(1 - s)} \quad \text{pound-feet} \tag{7.57}$$

Finally, replace n, the speed of rotation, with its equivalent from eq. (7.33):

$$T_o = \frac{21.1}{n_s(1 - s)}\left(I_2^2 R_2 \frac{1 - s}{s}\right) - \frac{7.04(F\&W)}{n_s(1 - s)} \quad \text{pound-feet} \tag{7.58}$$

which, after simplifying, is

$$T_o = \frac{21.1}{n_s} I_2^2 \frac{R_2}{s} - \frac{7.04(F\&W)}{n_s(1 - s)} \quad \text{pound-feet} \tag{7.59}$$

and eq. (7.59) is identical to eq. (7.37).

7.5.3 Power Factor and Efficiency

Rated power factor of the machine is equal to the cosine of the angle between the bus voltage impressed on the stator phase winding and the resulting stator phase current, at rated load. From Fig. 7.3,

$$PF = \cos\theta_1 \quad \text{per unit} \tag{7.60}$$

Thus rated power factor can be determined from the vector diagram to the same degree of accuracy that the angle of stator phase current is known on that diagram.

By definition, rated efficiency of the machine is equal to the ratio of net shaft power output to electrical power input to the stator winding at rated load. Accordingly,

$$\eta = \frac{P_o}{3I_1V_1\cos\theta_1} \quad \text{per unit} \tag{7.61}$$

The value of slip, and hence the value of rotor current, should always be so determined as to include friction and windage losses, as well as the net shaft output. The vector diagram itself includes the effect of resistance losses in the stator and rotor phase windings. The current increment ΔI_1, which sustains core loss and load loss, includes the effect of these losses in the vector diagram. Thus rated efficiency can be determined from the vector diagram to a degree of accuracy determined by the accuracy by which the quantities in eq. (7.61) are known in the vector diagram. However, different quantities are used in eq. (7.61) than in the more basic calculation of efficiency in eq. (5.49), in which efficiency is calculated by summing the losses. Therefore, the accumulated effect of rounding off to, say, three significant figures when performing the calculations would be different for the two methods. Accordingly, the results from the two methods would probably differ slightly in the third significant figure.

7.6 EXAMPLE OF CALCULATING PERFORMANCE FROM THE VECTOR DIAGRAM

The performance characteristics at rated load will be calculated for the 1000-hp numerical example using the equations just derived from the vector diagram and the vector quantities tabulated in Table 7.1, from which the vector diagram in Fig. 7.1 was constructed. In addition to the vector quantities in Table 7.1, it will be assumed that the values of full-load slip, rotor-winding resistance, and friction and windage losses have been determined by test or by other means. Then $s = 0.0124$ p.u., $R_2 = 0.236\ \Omega$ per phase, and $F\&W = 11{,}500$ W.

7.6.1 Rated Power Output

From eq. (7.26),

$$HP_o = \frac{3}{746} I_2^2 R_2 \frac{1 - s}{s} - \frac{F\&W}{746} \quad \text{horsepower} \tag{7.62}$$

Inserting the magnitudes of the vector quantities from Table 7.1 and the values of slip, rotor winding resistance, and friction and windage losses from the preceding paragraph into eq. (7.62) gives us

$$HP_o = \left(\frac{3}{746}\right)(115.9)^2(0.236)\left(\frac{1 - 0.0124}{0.0124}\right) - \frac{11{,}500}{746} = 1000 \quad \text{horsepower} \tag{7.63}$$

which agrees with the horsepower rating of the numerical example.

7.6.2 Rated Torque Output

From eq. (7.37) or (7.59),

$$T_o = \frac{21.1}{n_s} I_2^2 \frac{R_2}{s} - \frac{7.04(F\&W)}{n_s(1 - s)} \quad \text{pound-feet} \tag{7.64}$$

Inserting the appropriate values from Table 7.1 and from the additional information above, and remembering that the numerical example is a four-pole machine, for which $n_s = 1800$ rpm, we obtain

$$T_o = \left(\frac{21.1}{1800}\right)(115.9)^2\left(\frac{0.236}{0.0124}\right) - \frac{(7.04)(11,500)}{(1800)(1 - 0.124)} = 2952 \quad \text{pound-feet} \tag{7.65}$$

7.6.3 Rated Power Factor

From eq. (7.60),

$$PF = \cos \theta_1$$

From the table of vector quantities in Table 7.1, the angle of I_1 with respect to the stator phase voltage V_1, which has been taken as angle reference, is -22.7 degrees. Then

$$PF = \cos(-22.7^\circ) = 0.923 \quad \text{per unit} \tag{7.66}$$

7.6.4 Rated Efficiency

From eq. (7.61),

$$\eta = \frac{P_o}{3I_1V_1 \cos \theta_1} \quad \text{per unit} \tag{7.67}$$

Inserting the magnitudes of the vector quantities I_1 and V_1 and the value of the angle between them from Table 7.1 into eq. (7.67) and remembering that rated output is 1000 hp, which is equal to 746,000 W, we obtain

$$\eta = \frac{746,000}{(3)(123.9)(2309)[\cos(-22.9^\circ)]} = 0.942 \quad \text{per unit} \tag{7.68}$$

8

The Circle Diagram

8.1 Status of the Circle Diagram 142

8.2 Locus of the Current in a Series Circuit with Fixed Inductance and for Which the Resistance Is Varied 142

8.3 Concept of the Conventional Polyphase Induction Motor Circle Diagram 145

8.4 Determination of the Conventional Diagram from Test Data 147

8.5 Interpretation of the Conventional Diagram 150

8.6 Starting Torque from the Conventional Diagram 151

8.7 Maximum Torque from the Conventional Diagram 152

8.8 Maximum Power from the Conventional Diagram 153

8.9 Maximum Power Factor from the Conventional Diagram 153

8.10 Operating-Point Performance from the Conventional Diagram 154

8.11 Limitations of the Conventional Diagram 158

8.12 Concept of the Adjusted Circle Diagram 160

8.13 Numerical Example of Use of the Adjusted Diagram 162

8.14 Determination of Adjusted-Diagram Construction Data from Test Data 162

8.15 Construction of the Adjusted Diagram 166

8.16 Determination of Maximum Torque and Starting Torque from the Adjusted Diagram 169

8.17 Determination of Performance at Rated Load from the Adjusted Diagram 170

8.18 Comparison of Performance at Rated Load as Calculated by the Adjusted Diagram 176

8.1 STATUS OF THE CIRCLE DIAGRAM

The third algorithm to be considered for analyzing and determining the performance of polyphase induction motors is the circle diagram. Behrend and Heyland individually arrived at this concept at about the same time, in the mid-1890s. The circle diagram is much less frequently used than earlier in the history of induction motor lore. This is probably due to the fact that the equivalent circuit has the capability to yield more accurate results than the circle diagram and does not require that any graphical construction be done. Nevertheless, the circle diagram will provide the general performance of the machine, with reasonable accuracy with a minimum of data and will, at the same time, easily permit the design engineer and the application engineer to visualize the operating points of such characteristics as maximum torque, maximum power output, and maximum power factor. The circle diagram has both inherent inaccuracies and construction inaccuracies. The inherent inaccuracies will be discussed subsequently. The construction inaccuracies depend, of course, upon the care taken by the person doing the work and upon the scale that is chosen. However, construction requirements for the circle diagram are well within the capability of presently available desk computers, so that this source of inaccuracy can be eliminated by use of such equipment.

8.2 LOCUS OF THE CURRENT IN A SERIES CIRCUIT WITH FIXED INDUCTANCE AND FOR WHICH THE RESISTANCE IS VARIED

Consider a series circuit, consisting of resistance and inductive reactance, for which the reactance is considered constant and for which the resistance may be varied (see Fig. 8.1). The current in this circuit is equal to

$$I = \frac{V}{R + jX} \quad \text{amperes} \tag{8.1}$$

The term V/j2X may be added and subtracted from the right-hand side of eq. (8.1) without changing the equation. Then

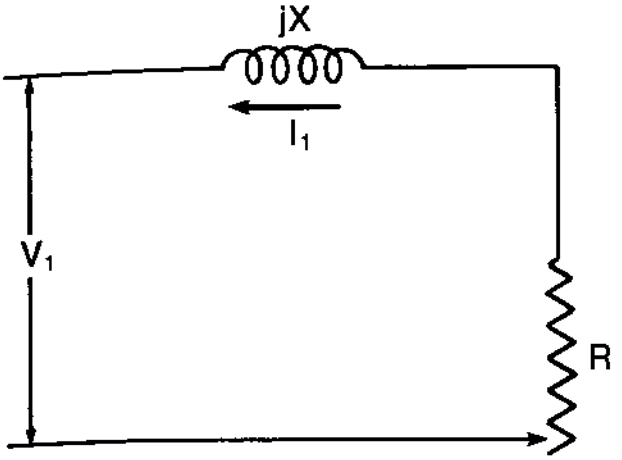

FIGURE 8.1 Series circuit with fixed inductive reactance and variable resistance.

$$I = \frac{V}{j2X} + \frac{V}{R + jX} - \frac{V}{j2X} \quad \text{amperes} \tag{8.2}$$

Combining the last two terms on the right-hand side of the equation gives us

$$I = \frac{V}{j2X} + \frac{V[j2X - (R + jX)]}{(j2X)(R + jX)} \quad \text{amperes} \tag{8.3}$$

Rearranging yields

$$I = \frac{V}{j2X} + \frac{V(-R + jX)}{(j2X)(R + jX)} \quad \text{amperes} \tag{8.4}$$

Multiplying the numerator and denominator by the operator j

$$I = \frac{-jV}{2X} - \frac{jV}{2X}\,\frac{-R + jX}{R + jX} = \frac{-jV}{2X} + \frac{jV}{2X}\,\frac{R - jX}{R + jX} \quad \text{amperes} \tag{8.5}$$

Multiplying the numerator and denominator of the last term of eq. (8.5) by the term R - jX gives us

$$I = \frac{-jV}{2X} + \frac{jV}{2X}\,\frac{(R - jX)^2}{R^2 + X^2} = \frac{-jV}{2X} + \frac{jV}{2X}\left[\frac{R - jX}{(R^2 + X^2)^{1/2}}\right]^2 \tag{8.6}$$

or

$$I = \frac{-jV}{2X} + \frac{jV}{2X}(\cos\theta - j\sin\theta)^2 \quad \text{amperes} \tag{8.7}$$

where

$$\theta = \tan^{-1}\left(-\frac{X}{R}\right) \quad \text{numeric} \tag{8.8}$$

and where cos θ is the power factor of the circuit in Fig. 8.1. Since, from DeMoivre's theorem,

$$(\cos\theta - j\sin\theta)^2 = \cos 2\theta - j\sin 2\theta \quad \text{numeric} \tag{8.9}$$

eq. (8.7) may be written as

$$\begin{aligned} I &= -j\frac{V}{2X} + j\frac{V}{2X}(\cos 2\theta - j\sin 2\theta) \\ &= \frac{-jV}{2X} + \frac{V}{2X}(\sin 2\theta + j\cos 2\theta) \quad \text{amperes} \end{aligned} \tag{8.10}$$

Equation (8.10) defines a vector, I, in terms of complex coordinates and the terminal point of I describes a locus that is a circle. If I is plotted on a

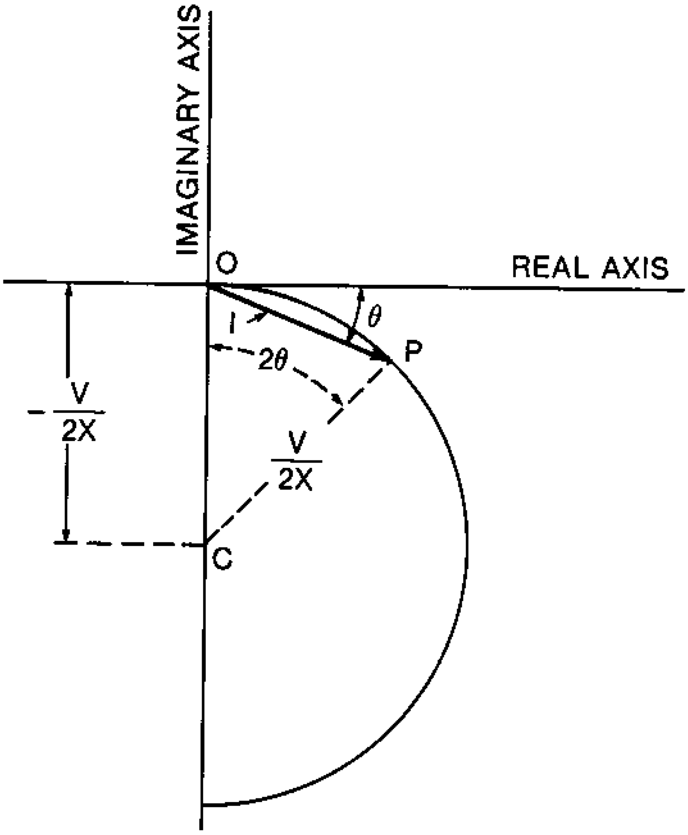

FIGURE 8.2 Locus of current, as resistance is varied, for series circuit with fixed inductive reactance.

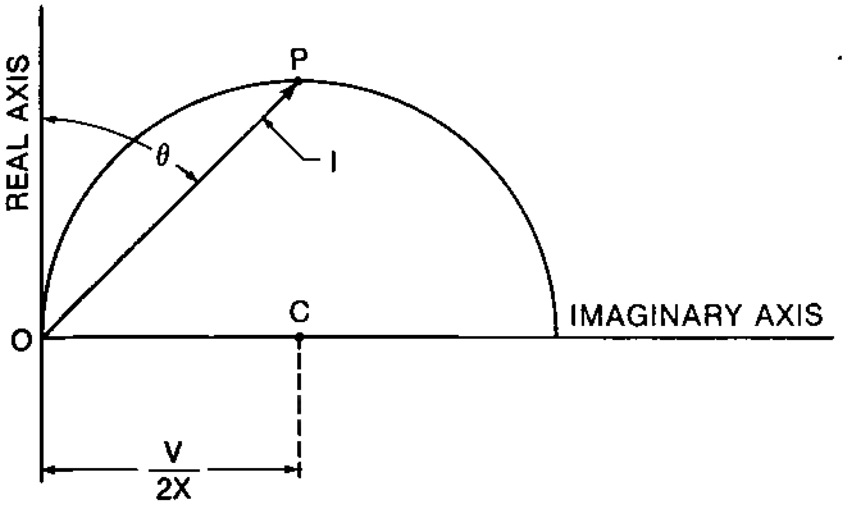

FIGURE 8.3 Locus of current shown in Fig. 8.2, with coordinate system rotated $\pi/2$ radians counterclockwise.

complex coordinate system, as the resistance is varied, the resulting locus is shown in Fig. 8.2. It is interesting to note that the locus of I is for a circuit with inductive reactance, and if the circuit in Fig. 8.1 had a fixed value of capacitive instead of inductive reactance, the locus of I would have been in the upper right-hand quadrant.

The complex coordinate system in Fig. 8.2 may be rotated $\pi/2$ radians counterclockwise, for convenience, without changing any of the relationships described above (see Fig. 8.3). Several comments can be made concerning Figs. 8.2 and 8.3. The real and the imaginary axes both have dimensions of amperes, or per unit current, if plotted in per unit. The radius of the circle is equal to V/2X and the center of the circle is located at -V/2X on the imaginary axis. As the resistance of the circuit in Fig. 8.1 is decreased from a high value to a lower value, the vector OP representing the circuit current I rotates in a clockwise direction through an angle θ, and the vector CP, which represents the radius of the circle, rotates through an angle of 2θ with a constant magnitude of V/2X amperes.

8.3 CONCEPT OF THE CONVENTIONAL POLYPHASE INDUCTION MOTOR CIRCLE DIAGRAM

The similarity between the circuit in Fig. 8.1 and the circuit to the right of the stator bus zone in Fig. 6.1, the simplified equivalent circuit for the polyphase induction motor, is apparent. If R in Fig. 8.1 is set equal to $R_1 + R_2/s$ in Fig. 6.1 and if X in Fig. 8.1 is set equal to $X_1 + X_2$ in Fig. 6.1, the two circuits are identical. Thus the variation of the circuit current, I', in Fig. 6.1 will follow the circular locus illustrated in Fig. 8.3. One limit of this variation is when θ approaches zero, as R approaches a large value relative to X. This is similar to the state of the motor while operating in the region of full speed and full load, with a small value of slip s. The other limit of this variation is when θ approaches $\pi/2$ radians. This is similar to the state of the motor as it approaches, but does not reach, a zero value of $R_1 + R_2/s$ at blocked-rotor conditions, with slip equal to unity.

For the circle diagram to represent the input current to the motor, the magnetizing current I_m must be vectorially added to the current I shown in Fig. 8.3. The current I' flowing in the simplified equivalent circuit is essentially the rotor current referred to the stator. Correspondingly, the current OP in Fig. 8.3, should be considered the equivalent stator current which will produce the same magnitude of magnetomotive force, in ampere turns, as the actual rotor phase current flowing in the actual rotor phase winding. The magnetizing current I_m should be vectorially added to the current represented by the vector OP, in accordance with Fig. 6.1, in order to equal the total input phase current from the stator bus to the motor. However, as will be discussed subsequently, the circle diagram more correctly utilizes the no-load current, instead of the magnetizing current, for this purpose. Figure 8.4 shows the resulting conventional circle diagram for the polyphase induction motor.

In Fig. 8.4, the stator input current is shown as the vector from point A, the point of intersection of the real and imaginary axes, to points on the semicircular locus. For example, vectors AO, AP, and AB represent, respectively, the no-load current, the full-load current, and the blocked-rotor current. Since these points are on the semicircle and since the corresponding motor input current can be measured, in magnitude and in angle, the circle diagram can be constructed from electrical test data for

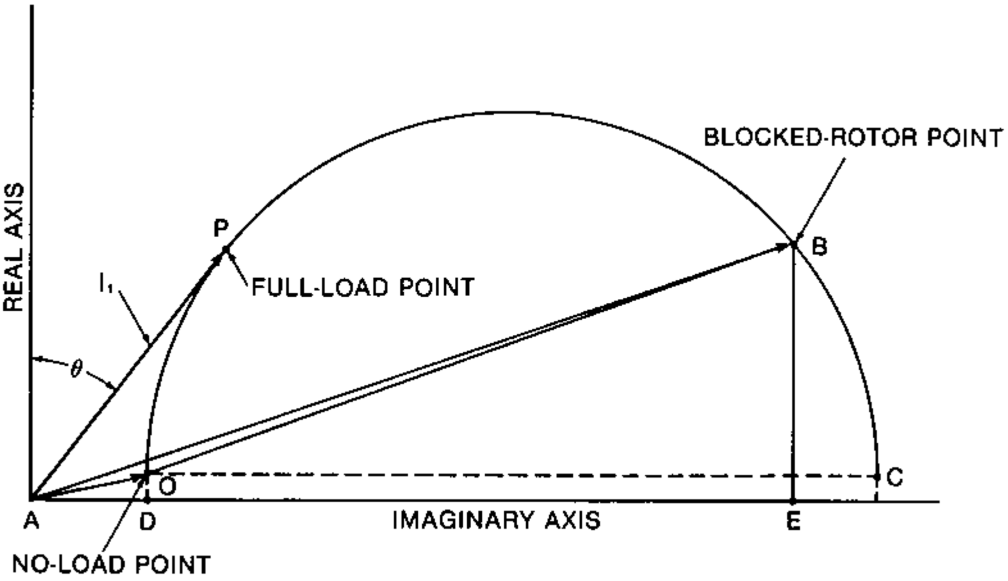

FIGURE 8.4 Extension of current locus in Fig. 8.3 to locus of input current of the polyphase induction motor.

two of the points. The no-load point must be one of the two points, in order to know the magnitude and angle of the vector AO. The blocked-rotor point is typically the other point, as the magnitude of the vector AB is six, or more, times the magnitude of AP, the full-load current and will facilitate accuracy in the construction process. Such construction is made easier if it is being done manually, by remembering that, from plane geometry, the two chords OB and BC intersect at right angles. However, the construction can be done by use of a computer, utilizing its calculating and graphic capabilities.

8.4 DETERMINATION OF THE CONVENTIONAL DIAGRAM FROM TEST DATA

The no-load current is determined by disconnecting the coupling, sheave, or sprocket from any driven equipment, applying rated voltage to the stator winding, and measuring the stator phase current and total power input to the stator winding. For a wound-rotor motor, the brushes of the various phases should be shorted together at the brush-rigging connections while conducting this test. At no-load operation, the total losses are equal to the sum of core loss, friction and windage losses, and the I^2R loss in each of the three stator phase windings due to no-load current. The rotor winding I^2R loss at no-load conditions is too small to be significant. Then

$$P_n = CL + F\&W + 3I_n^2R_1 \quad \text{watts} \tag{8.11}$$

where P_n is the total no-load losses in watts and I_n is the no-load stator phase current in amperes. The total no-load volt ampere input to the motor is equal to

$$(VA)_n = 3I_nV_1 \quad \text{volt-amperes} \tag{8.12}$$

Thus the no-load power factor is

$$(PF)_n = \frac{P_n}{(VA)_n} = \frac{CL + F\&W + 3I_n^2R_1}{3I_nV_1} \quad \text{numeric} \tag{8.13}$$

and the phase angle θ_n of the no-load current is equal to

$$\theta_n = \cos^{-1}\frac{P_n}{(VA)_n} \quad \text{degrees} \tag{8.14}$$

The test value of the stator current that corresponds to the no-load operating point, vector AO in Fig. 8.4, is then $I_n \angle \theta_n$. The in-phase or energy component of load current, which is represented by the vector OD for one phase and which sustains one-third of the core loss, friction and windage losses, and no-load copper loss in the stator winding, is determined by the relationship

$$OD = I_n \cos\theta_n \quad \text{amperes/phase} \tag{8.15}$$

or by the relationship

$$OD = \frac{P_n}{3V_1} \quad \text{amperes/phase} \tag{8.16}$$

The no-load operating point O may be located, when constructing the circle diagram, by laying out the no-load current I_n at the angle θ_n or by using the no-load current I_n and the value of OD from eq. (8.15) or (8.16) to construct the triangle AOD.

The blocked-rotor current is determined by mechanically blocking the rotor from rotating, applying voltage to the stator winding, and measuring the stator phase current and total power input to the machine. As indicated above for the no-load test, for a wound-rotor motor, the brushes of the various phases should also be shorted together at the brush-rigging connections when conducting the blocked-rotor test. At blocked-rotor conditions, the resistance component of impedance is small and the flow of current is limited primarily by leakage reactance. Because of this, the magnitude of current input to the motor is approximately six times that at rated-load conditions. Accordingly, the rate at which heat energy is produced in the windings, due to the I^2R losses, is 35 to 40 times the normal rate. This requires that caution be observed so that the motor windings do not overheat during full-voltage application, while performing the blocked-rotor test. This makes it necessary to determine the current and power values at the rated-voltage point as rapidly as reasonable possible. Another possible problem occasionally encountered with full-voltage testing is that for large motors, the kVA demand on the local power distribution system is significant and many local systems may be inadequate to support this type of test for motors with significant power ratings.

An alternative test procedure is to perform the blocked-rotor test by determining test points at lower voltage and terminating the testing at as high a voltage as is practical for the local power system conditions. The full-voltage value of current and power is then determined by a logical extension of the curve of current versus voltage and of the curve of power versus voltage obtained from lower-voltage test points. This procedure is fraught with the possibility of some inaccuracy in the results, however, if the test points are not continued to a sufficiently high applied stator voltage, and correspondingly high locked-rotor current, to approach normal saturation. If the test value of blocked-rotor leakage reactance is determined at an applied voltage, and resulting current, significantly lower than the rated value, the leakage flux densities will be correspondingly lower. This will result in less than normal saturation of the iron paths of leakage flux. Thus the ratio of leakage flux to current will be greater than it should be if full voltage had been applied, which will result in a test value of blocked-rotor reactance which is greater than the true value.

At blocked-rotor condition, the stator impedance drop resulting from the large value of stator current flowing through the stator-winding impedance is typically 50% or more of the applied voltage. This causes the voltage across the magnetizing reactance X_m to be 50% or less of rated voltage. Since core loss varies approximately as the second power (actually, slightly less than the second power) of the magnetizing voltage, the core loss is a small fraction of that at rated conditions. Although there is some core loss in the rotor core, because of the fundamental frequency of flux change in the rotor, this is not large, because of the reduced voltage across the magnetizing reactance. Also, since the rotor structure is not rotating, the friction and windage losses are equal to zero. On the other hand, the stator I^2R losses are typically 35 to 40 times normal and the rotor I^2R losses are typically 50 to 60 times normal. The proportionally greater increase of rotor I^2R loss, compared to that of the stator, results from the fact that, at blocked-rotor conditions, the ac resistance of the rotor winding is greater than the dc resistance, because of the effect of current crowding to the top of the solid rotor bar at fundamental line frequency. Accordingly, all of the power input to the machine at blocked-rotor condition is used to supply stator and rotor winding I^2R, except for a very small component, equal to a fraction of 1% of the total, which is to supply core loss. The error introduced by neglecting core loss is certainly less than the accuracy by which the other losses are known and it is conventional wisdom to neglect this component of loss at the blocked-rotor test point.

The power input to the motor, under blocked-rotor conditions, is

$$P_\ell = 3I_\ell^2 R_1 + 3I_{2\ell}^2 R_{2\ell} \quad \text{watts} \tag{8.17}$$

where the quantities are as defined previously, with the subscript ℓ denoting blocked-rotor values for those quantities that change under this condition. The total blocked-rotor volt ampere input to the motor is equal to

$$(VA)_\ell = 3I_\ell V_1 \quad \text{volt-amperes} \tag{8.18}$$

and the blocked-rotor power factor is

$$(PF)_\ell = \frac{3I_\ell^2R_1 + 3I_{2\ell}^2R_{2\ell}}{3I_\ell V_1} = \frac{I_\ell^2R_1 + I_{2\ell}^2R_{2\ell}}{I_\ell V_1} \quad \text{numeric} \tag{8.19}$$

The phase angle θ_ℓ of the blocked-rotor current is equal to

$$\theta_\ell = \cos^{-1}\frac{P_\ell}{(VA)_\ell} \quad \text{degrees} \tag{8.20}$$

From the above, the test value of the stator current which corresponds to the blocked-rotor operating point, vector AB in Fig. 7.4, is $I_\ell \underline{/\theta_\ell}$.

The energy component of blocked-rotor current, which is represented by the vector BE and which sustains the I^2R losses in the rotor and stator windings, is determined by

$$BE = I_\ell \cos\theta_\ell \quad \text{amperes/phase} \tag{8.21}$$

or by

$$BE = \frac{P_\ell}{3V_1} \quad \text{amperes/phase} \tag{8.22}$$

Again, the blocked-rotor operating point B may be located, when constructing the circle diagram, by laying out the blocked-rotor current I_ℓ at the angle θ_ℓ or by using the blocked-rotor current and the value of BE from eq. (8.21) or (8.22) to construct the triangle ABE.

8.5 INTERPRETATION OF THE CONVENTIONAL DIAGRAM

As discussed above, the conventional polyphase induction motor circle diagram may be constructed from test data determined at the no-load and the blocked-rotor operating points. Figure 8.5 shows such a construction, together with interpretation of the resulting diagram. The diagram is drawn to an appropriate current scale, and all vector lines on the diagram represent phase amperes (or per unit current) to that scale. Vertical components of current, which are parallel to the phase voltage impressed across the stator winding, are energy components, and horizontal components of current, which are parallel to the imaginary axis, are reactive components. Accordingly, vertical components of current, multiplied by stator phase voltage,

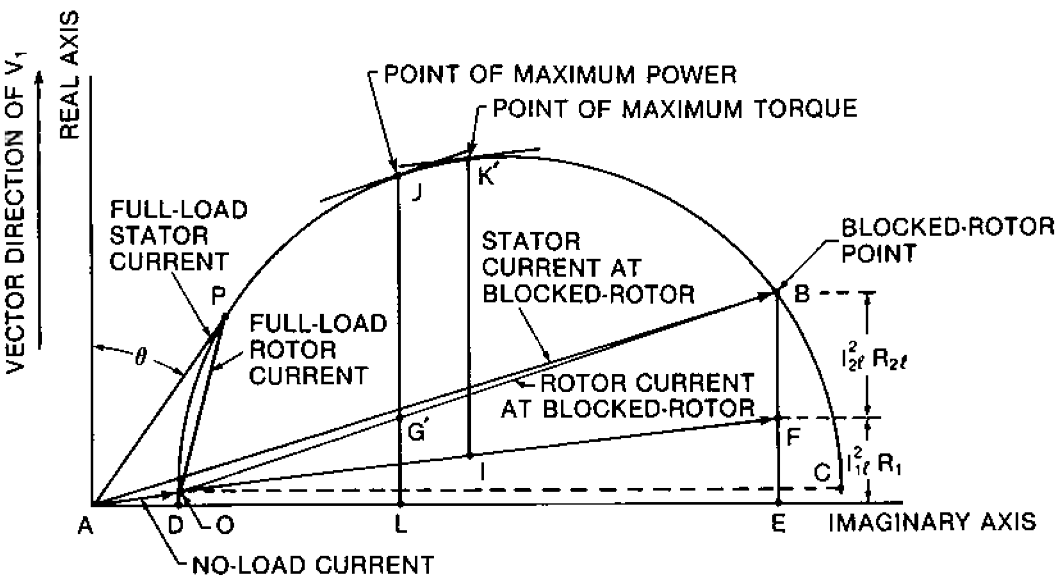
VECTOR DIRECTION OF V_1
REAL AXIS
POINT OF MAXIMUM POWER
POINT OF MAXIMUM TORQUE
J
K'
FULL-LOAD STATOR CURRENT
P
θ
FULL-LOAD ROTOR CURRENT
STATOR CURRENT AT BLOCKED-ROTOR
BLOCKED-ROTOR POINT
B
$I_{2\ell}^2 R_{2\ell}$
ROTOR CURRENT AT BLOCKED-ROTOR
G'
I
F
C
$I_{1\ell}^2 R_1$
A
D
O
L
E
IMAGINARY AXIS
NO-LOAD CURRENT

FIGURE 8.5 Conventional circle diagram showing maximum torque, maximum power, and maximum power factor.

are equal to watts/phase, and horizontal component of current, multiplied by stator phase voltage, are equal to reactive volt-amperes/phase. In general, any current component when multiplied by the phase voltage and by the cosine of its phase angle is equal to watts/phase, and when multiplied by the phase voltage and by the sine of its phase angle is equal to reactive volt-amperes/phase. When watts/phase or volt-amperes/phase are multiplied by the number of phases, the product is equal to machine watts or machine volt-amperes, of course.

It is necessary to determine point F so that the vertical distance EB may be divided into the rotor and the stator copper losses at blocked-rotor condition. To determine point F, calculate the stator winding copper loss at blocked-rotor conditions, using a value of stator resistance/phase determined by test, or a value supplied by the manufacturer, if that is available. Then the distance EF is determined as $I_{1\ell}^2(R_1/V_1)$. Point F is determined by laying off this distance from point E on vertical line EB.

8.6 STARTING TORQUE FROM THE CONVENTIONAL DIAGRAM

From eq. (5.80), the torque developed by the rotor is equal to

$$T = \frac{21.1}{n_s} I_2^2 \frac{R_2}{s} \quad \text{pound-feet} \tag{8.23}$$

or

$$T = \frac{7.04}{n_s}\left(3I_2^2\,\frac{R_2}{s}\right) \quad \text{pound-feet} \tag{8.24}$$

where the term $3I_2^2R_2/s$ is equal to the rotor slip loss. Point B, in Fig. 8.5, identifies the blocked-rotor operation point and the vertical current component BF is the in-phase component of blocked-rotor current attributable to rotor copper loss. If the current BF is multiplied by the stator phase voltage and by the number of phases, the resulting power expression is equal to the rotor I^2R loss for the rotor. Then

$$3V_1(BF) = 3I_{2\ell}^2R_{2\ell} \quad \text{watts} \tag{8.25}$$

which is the rotor slip loss at blocked-rotor conditions for $s = 1$. If the expression in eq. (8.25) is substituted into eq. (8.24), the result is the starting torque as determined from the circle diagram. Then

$$T_{st} = \frac{7.04}{n_s}\,3V_1(BF) \quad \text{pound-feet} \tag{8.26}$$

8.7 MAXIMUM TORQUE FROM THE CONVENTIONAL DIAGRAM

If the mechanical block is removed from the rotor and the rotor structure is allowed to accelerate, the variables in eq. (8.23) will change. The rotor phase current will decrease as the rotor-current vector rotates counterclockwise while following its locus. The rotor slip, in the denominator of eq. (8.23), will also decrease and this will occur in general, at a faster rate than the decrease of the I^2R term in the numerator of eq. (8.23), until point K' is reached on the current circle. At this point, the rotor slip is a maximum, and this point corresponds to the maximum torque produced by the rotor.

Point K' is determined by finding the maximum value of the in-phase component of the current vector IK', which, in turn, is determined by drawing a tangent to the circle, which is parallel to line OF. If IK' is multiplied by the stator phase voltage and by the number of phases, the resulting power is equal to the rotor slip loss at the operating point K', or

$$3V_1(IK') = 3I_2^2\,\frac{R}{s} \quad \text{watts} \tag{8.27}$$

Substituting the power expression in eq. (8.27) into eq. (8.24) gives the maximum torque as determined from the circle diagram, or

$$T_m = \frac{7.04}{n_s} 3V_1(IK') \quad \text{watts} \tag{8.28}$$

8.8 MAXIMUM POWER FROM THE CONVENTIONAL DIAGRAM

At blocked-rotor conditions, the current vector EB, in Fig. 8.5, is the energy component of phase current which sustains the power input to the motor. Since there is no power output at blocked-rotor conditions, vector EB also sustains all of the internal power losses. However, as the rotor accelerates and the rotor current operating point rotates counterclockwise along the circle, the vertical distance from OB to the point of intersection with the circle is the energy component of current which sustains power output for the phase. The length of this vertical line initially increases as the rotor accelerates and continues to increase until it reaches a maximum value at point H in Fig. 8.5. The point of maximum power is determined by drawing a line tangent to the circle which is parallel to line OB. Vector G'J is the energy component of phase current which produces this power output. If G'J is multiplied by the stator phase voltage and by the number of phases, the result is the maximum power output of the machine, or

$$P_m = 3V_1(G'J) \quad \text{watts} \tag{8.29}$$

8.9 MAXIMUM POWER FACTOR FROM THE CONVENTIONAL DIAGRAM

It is apparent by inspection of Fig. 8.5 that maximum power factor occurs when the vector AP, which represents the stator current, is tangent to the circle. The phase angle θ is a minimum, and $\cos\theta$ is a maximum, at this specific operating point. At any other operating point, corresponding to either an increase or decrease in load, the phase angle will increase and the power factor will decrease. The point of maximum power factor occurs reasonably close to the rated-load operating point for many, but not all, designs. It is further apparent by inspection of Fig. 8.5 that in the region of maximum power factor, the phase angle θ does not change rapidly as the operating load point is changed. Accordingly, this would indicate that the curve of power factor versus load is reasonably flat near its maximum, which it is for most designs.

Power factor, from a circuit point of view, is determined by the proportion of reactive volt-amperes to watts required by the parameters of the circuit. As the proportion of reactive volt-amperes increases, the power factor of the circuit decreases. Two design quantities that contribute to reactive volt-amperes in a polyphase induction motor are the magnetizing current and the leakage reactance. The vector AD, in Fig. 8.5, represents magnetizing current. It is apparent that increasing the length of the vector AD will move the circle more to the right, relative to the origin A. This, in turn, will cause the angle θ to increase and the power factor to decrease, for a given load point on the circle. The diameter of the circle is inversely proportional to the leakage reactance. Accordingly, if the leakage reactance is increased, the diameter of the circle is decreased. By inspection, it is apparent that this will result in an increase in the angle θ for a given load or fixed vertical distance to the operating point.

The observations above, although limited to power factor considerations in this case, are typical of the design and application relationships, which can be determined by inspection of the circle diagram. Thus the circle diagram is a useful tool for the engineer when it is interspersed with other available tools, such as the equivalent circuit, since it provides the ability to visualize immediately relationships not provided by other algorithms.

8.10 OPERATING-POINT PERFORMANCE FROM THE CONVENTIONAL DIAGRAM

In Fig. 8.6, the conventional circle diagram shown in Fig. 8.5 has been redrawn to eliminate some detail and to show additional construction lines which are useful for determining the operating performance of a polyphase induction motor. There are approximations involved in determining performance by use of the conventional circle diagram, as will become apparent in the following derivation of the method. However, it is possible to make adjustments to reduce the effect of some of these approximations, and such adjustments will be mentioned subsequently.

It has previously been noted that BE, multiplied by V_1 and by the number of phases, is equal to the sum of the stator and rotor copper losses in watts at blocked-rotor conditions, for which the rotor current (or current through the rotor and stator for the simplified equivalent circuit) is equal to OB. It would be intuitively expected that at a rotor current of OP corresponding to a normal operating point P in Fig. 8.6, the stator and rotor copper losses, in watts, would be equal to HM multiplied by V_1 and by the number of phases. This relationship will now be proven from geometric aspects of the circle diagram and related construction lines. However, this requires that the approximation be made that BE = BG, which is true to within an error of 3% or less for a typical design.

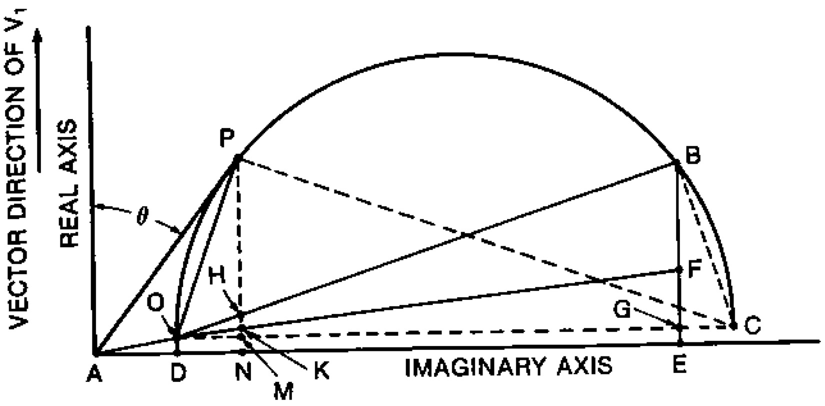

FIGURE 8.6 Conventional circle diagram for performance analysis.

Then the relationship to be derived, in geometric terms, is

$$\frac{HM}{BG} = \frac{(OP)^2}{(OB)^2} \quad \text{numeric} \tag{8.30}$$

Triangle OHM and triangle OBG are similar, since their respective sides are parallel. Then

$$\frac{HM}{BG} = \frac{OM}{OG} \quad \text{numeric} \tag{8.31}$$

Further, triangle OPM and triangle OPC are similar, since they both are right triangles with one contained within the other. Then the angle OPM is equal to the angle PCO, since they are corresponding angles of similar triangles. Accordingly,

$$\sin OPM = \sin PCO = \frac{OP}{OC} \quad \text{numeric} \tag{8.32}$$

From Fig. 8.6 and eq. (8.32),

$$OM = OP \sin OPM = OP \sin PCO = \frac{(OP)^2}{OC} \quad \text{amperes} \tag{8.33}$$

Also, from Fig. 8.6,

$$OG = OB \cos BOG \quad \text{amperes} \tag{8.34}$$

However, triangle OBG is similar to triangle OBC, since they are both right triangles and share another common angle. Accordingly,

$$\cos BOG = \cos COB \quad \text{numeric} \tag{8.35}$$

Substituting eq. (8.35) into eq. (8.34) yields

$$OG = OB \cos COB = OB \frac{OB}{OC} = \frac{(OB)^2}{OC} \quad \text{amperes} \tag{8.36}$$

Substituting eqs. (8.33) and (8.36) into eq. (8.31), we obtain

$$\frac{HM}{BG} = \frac{(OP)^2/OC}{(OB)^2/OC} \quad \text{numeric} \tag{8.37}$$

or

$$\frac{HM}{BG} = \frac{(OP)^2}{(OB)^2} \quad \text{numeric} \tag{8.38}$$

Equation (8.38) indicates that based on the conventional circle diagram, at any arbitrary operating point P, the vertical distance HM is proportional to the copper losses in the stator and rotor windings, just as the vertical distance BG is proportional to the copper losses at blocked rotor point B. As discussed earlier, the proportionality constant is $3V_1$ for a three-phase machine.

The distances BF and FG are respectively proportional to the rotor and to the stator I^2R losses at blocked-rotor conditions. Correspondingly, distances HK and KM are respectively proportional to the rotor and to the stator I^2R losses at the operating point P. For the distance HK to represent rotor I^2R loss, the conventional circle diagram procedure tacitly assumes that the ratio of ac to dc resistance of the rotor winding remains constant as the frequency of the rotor circuit decreases, which it does not, of course. An adjustment to compensate for this will be discussed subsequently. Also, the distance KM, which represents stator I^2R, is based on current OP, which does not include the magnetizing current as a component. Although consistent with the simplified equivalent circuit upon which the conventional circle diagram is predicated, lack of inclusion of the magnetizing current component in the stator copper losses as represented by distance KM will cause that distance to be somewhat in error. This error will vary from 2 or 3% for a four-pole machine to a significantly greater percentage for a slow-speed machine such as, for example, one wound for 20 poles, since the magnetizing current varies with the number of poles to be magnetized.

As discussed previously, the distance OD, when multiplied by the phase voltage and by the number of phases, is equal to the no-load losses (i.e., to the sum of core loss, friction and windage losses, and no-load stator copper loss). Since MN is equal to OD by construction, MN is also equal to the same losses, when multiplied by $3V_1$. The fact that the distance MN has a component proportional to no-load stator copper loss tends to compensate for the fact that the distance KM corresponds to the stator copper loss for the current OP, which does not contain a magnetizing current component.

Then the distance HN, multiplied by $3V_1$, is equal to all the machine losses considered by the conventional circle diagram, or

$$\sum L = 3V_1(HN) = 3I_1^2R_1 + 3I_2^2R_2 + CL + F\&W \quad \text{watts} \tag{8.39}$$

It is apparent that load loss is not included in the summation of losses shown in eq. (8.39) for the conventional circle diagram. It is not surprising that such should be the case because, historically, the concept of, and the need for, load loss developed after the circle diagram was put into use. Typically, load loss is equal to about 1% of the rating of the machine at full-load conditions. Again, an adjustment to compensate for this omission of the conventional circle diagram will be discussed subsequently.

Since vertical distances from the power line OB to the circle, when multiplied by $3V_1$, are equal to power output at the corresponding points on the circle, the output power at point P is

$$P_o = 3V_1(HP) \quad \text{watts} \tag{8.40}$$

The total electrical power input to the motor at point P is

$$P_i = 3V_1(NP) \quad \text{watts} \tag{8.41}$$

and the resulting efficiency is

$$\eta = \frac{P_o}{P_i} = \frac{HP}{NP} \quad \text{numeric} \tag{8.42}$$

The torque developed at this operating point is

$$T = \frac{60}{2\pi n_s} 3V_1(KP) \quad \text{newton-meters} \tag{8.43}$$

and in units of lb-ft, is equal to

$$T = \frac{7.04}{n_s} 3V_1(KP) \quad \text{pound-feet} \tag{8.44}$$

The power factor, for operating point P, is

$$PF = \cos\theta \quad \text{numeric} \tag{8.45}$$

where θ is the angle between the real axis and the current vector AP in Fig. 8.6.

All of the power transferred across the gap at point P is equal to the distance KP multiplied by $3V_1$, and the corresponding rotor winding I^2R loss is equal to the distance HK multiplied by $3V_1$. Since slip is equal to the ratio of rotor winding I^2R to the power transferred across the gap, the slip at operating point P is equal to

$$s = \frac{HK}{KP} \quad \text{numeric} \tag{8.46}$$

The starting torque and the maximum torque are, of course, unrelated to any particular steady-state operating point P and their values are determined by eqs. (8.26) and (8.28), respectively.

8.11 LIMITATIONS OF THE CONVENTIONAL DIAGRAM

The conventional circle diagram is limited by several approximations, some of which have been mentioned. It is in order to recapitulate these limitations in preparation for considering adjustments intended to improve this algorithm.

One of the early objections to the circle diagram was that it required graphic construction and that its accuracy was thereby limited. This objection was valid for the conditions that prevailed at an earlier date in the history of the induction motor. However, production of the diagram is within the graphic capability of many desk computers, which when aided by the computational capability of such computers, should tend to reduce this objection. It can be argued that use of the equivalent circuit will eliminate such concern, and this is a valid argument. However, the circle diagram does have the capability to provide considerable information on machine performance with a minimum of input data and to provide visualization of performance and how to change such performance for a given set of design parameters.

Basically, the circle diagram is a locus plot, on complex coordinates, of the current flow in the simplified equivalent circuit, and accordingly, it has essentially the same limitations as that circuit. The magnetizing reactance is assumed to be shunted across the stator supply bus, which is tantamount to assuming constant air-gap flux for the various points of operation. In the actual machine, the air-gap flux is affected by the voltage drop across the stator impedance. However, it should be noted that when the circle diagram is constructed from test data for the no-load point and for the blocked-rotor point, the resulting test data correspond to actual air-gap flux conditions that exist at these two test points.

Load loss is not considered in the conventional circle diagram, as is also true for both the simple and for the complete equivalent circuits. As noted above, the concept of load loss developed subsequent to the time that the circle diagram and the equivalent circuit were put into use. A method was provided, in Chapter 5 for considering load loss when using that circuit. A method will also be provided for considering this component of loss when using the circle diagram. Although the error introduced by ignoring load loss is of the order of magnitude of that inherent in graphical construction, it is still desirable to introduce an adjustment to the circle diagram to consider load loss. If the graphical construction and related calculations are done by a computer, it certainly is desirable to do so.

The diameter of the circle is equal to V_1/X_ℓ, where X_ℓ is the blocked-rotor value of leakage reactance, as determined by test. If test data are not available, the value of X_ℓ can be determined from design calculations or from estimating, but in any case, the blocked-rotor value of leakage reactance is used to establish the blocked-rotor point and hence the circle diameter. However, as mentioned previously, the value of blocked-rotor leakage reactance is less than that at running because of the effect of saturation and because of the effective reduction of rotor bar height due to nonuniform current distribution within the bar at line frequency. Accordingly, the diameter of the circle is greater at the blocked-rotor point, which is correct for that particular part of the circle. However, at other important operating points for which the current is lower and for which the leakage reactance is greater, the circle diameter should be less. Thus the actual locus of the current is more appropriately defined by a semiellipsoid than by a semicircle.

Another effect of the above-mentioned nonuniform current distribution in the rotor bar at line frequency is that the ratio of ac to dc rotor resistance is significantly greater than 1.0 at blocked-rotor conditions. As the rotor accelerates and the frequency of the rotor circuit decreases, this resistance ratio decreases and approaches 1.0 as a limit. Accordingly, the distance BF in Fig. 8.6, when multiplied by $3V_1$, is equal to the blocked-rotor copper loss in the rotor circuit. However, the distance HK, when multiplied by $3V_1$, represents a loss greater than the actual rotor copper loss at the operating point P, and the actual value of this loss may be computed as

$$(\text{rotor copper loss})_P = 3V_1(\text{HK})\,\frac{R_2}{R_{2\ell}} \quad \text{watts} \tag{8.47}$$

where as defined earlier, $R_{2\ell}$ is the resistance per phase of the rotor winding at blocked-rotor conditions.

8.12 CONCEPT OF THE ADJUSTED CIRCLE DIAGRAM

The adjusted circle diagram of the polyphase induction motor results from adjustments made to the conventional circle diagram in order to address the above-mentioned limitations of the latter diagram. Specifically, the adjusted circle diagram provides for changes to be made in the diameter to accommodate the change in leakage reactance; for a modification in the ratio of ac to dc rotor winding resistance, to correspond to the decrease in rotor circuit frequency; and for a procedure to consider load loss at load points. However, one additional item of data is required to construct the adjusted circle diagram, and that is the "running" value of leakage reactance. This information may be obtained from the manufacturer or it may be obtained locally by judicious interpretation of the blocked-rotor test data, as will be discussed subsequently.

The adjusted circle diagram is illustrated in Fig. 8.7. Point O is constructed from no-load test data, as discussed previously for the conventional diagram. Also, the arc BC of the larger circle, together with associated lines OB, OF, OG, BF, and FG are constructed from the blocked-rotor test data as discussed previously. Arc OK' of the smaller circuit is constructed by starting the arc at point O, with its diameter along line OG. The radius of the smaller circle is equal to $V_1/2X$, where X is the running value of leakage reactance. The arc for this circle need only be constructed from point O to point K', which represent the no-load operating point and the maximum-torque point, respectively. When the machine is operating at maximum torque, the current flowing through the windings has decreased to approximately 70% of that at locked rotor. At this lesser value of current, the effect of saturation of iron paths of leakage flux in reducing the leakage reactance is small to negligible and, accordingly, the running value of leakage flux is generally applicable at this point.

Only arc BC of the larger circle need be constructed. Slip is equal to 1.0 at point B and increases rapidly beyond this point as point S is approached. Thus point B is required for determining starting torque, and the arc BS is useful when the motor is used for reverse-current braking. The range from point B to point K' corresponds to the acceleration of the rotor from zero speed to the point of maximum torque. In general, this region is not suitable for prolonged operating points. The speed-torque curve of the motor has a flat to concave-upward characteristic in this region and the speed-torque curve of most driven loads would cross the motor torque curve at too small an angle to ensure speed stability. Also, for squirrel-cage motors, the magnitude of current flow is essentially equal to blocked-rotor current for most of the way from zero speed to the maximum torque point. Accordingly, the stator and rotor windings heating would be prohibitive for prolonged operation, aside from speed-torque stability considerations. Thus that portion of the current locus from point B to point K'is of no practical concern

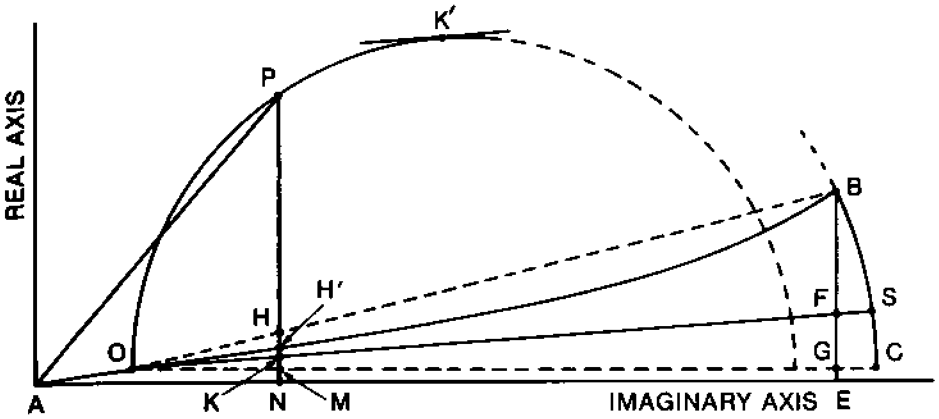

FIGURE 8.7 Adjusted circle diagram for performance analysis.

for continuous application of squirrel-cage motors which have fixed locations for the point of maximum torque.

The distance BF in Figs. 8.6 and 8.7, when multiplied by V_1, equals the rotor copper loss/phase at blocked rotor conditions. If the rotor resistance were constant at all rotor circuit frequencies, the distance HK in Fig. 8.6, when multiplied by V_1, would actually be equal to the rotor copper loss/phase at operating point P. However, as pointed out above, one of the limitations of the conventional circle diagram is that the rotor resistance decreases with decreasing frequency in the rotor circuit. As will be shown in Chapter 10, the ratio of ac to dc rotor resistance decreases in proportion to the square root of the rotor circuit frequency. A curve has been drawn between point O and point B, in Fig. 8.7, which shows this relationship and which should replace the straight line OB. It is apparent from an inspection of this curve that at the point of maximum torque, the rotor winding resistance will have approached its limiting dc value. Thus the distance H'K, and not HK, should represent the actual copper loss of operating point P.

As is also true for the other algorithms studied previously, the conventional circle diagram does not provide for direct evaluation of performance with load loss considered. Accordingly, additional steps must be taken with the circle diagram, as must also be taken for the equivalent circuit and for the vector diagram. Load loss can be determined by test, by calculation, or by comparison with data from a similar design. Thus it may be possible to obtain its value at rated load from the manufacturer. If its value is not known, a value of 1% of the machine's output rating may reasonably be used. In any case, more accurate performance results are possible if load loss is considered in the determination of such results. If the graphical and calculating capability of a computer is used, this increased accuracy is more probable than if manual techniques are used, of course. The procedure for evaluation of performance, with load loss considered, will become apparent when an actual example is subsequently used.

8.13 NUMERICAL EXAMPLE OF USE OF THE ADJUSTED DIAGRAM

The three-phase 60-Hz 4000-V four-pole 1000-hp squirrel-cage induction motor, the winding and other parameters for which are given in Table 5.1, will be used as a numerical example for calculating performance by use of the adjusted circle diagram. It will be assumed for this illustrative example that the winding parameters and loss data given in Table 5.1 is not known and that the data necessary to construct the circle diagram will be determined from test data. However, the same value of load loss as that given in the table will be used so that the results from the adjusted circle diagram are more directly comparable to those from the complete equivalent circuit.

8.14 DETERMINATION OF ADJUSTED-DIAGRAM CONSTRUCTION DATA FROM TEST DATA

As mentioned earlier, sufficient data can be obtained from a no-load test and a blocked-rotor test from which to construct the corresponding circle diagram for a given motor. The no-load test is conducted by applying rated voltage, at rated frequency and with a reasonable wave form, to the stator terminals and with no external mechanical load on the shaft. Let it be assumed that all of the conditions above have been met and that the motor has been allowed to operate until the power input has stabilized. Following that, let the stator current and power input be accurately measured, with the following results:

$$\text{no-load stator current} = I_n = 30.2 \quad \text{amperes/phase} \tag{8.48}$$

$$\text{no-load power losses} = P_n = 19,590 \quad \text{watts} \tag{8.49}$$

The no-load volt-ampere input to the machine is then equal to

$$(VA)_n = (3)(2309)(30.2) = 209,200 \quad \text{volt-amperes} \tag{8.50}$$

and the no-load power factor is equal to

$$(PF)_n = \frac{P_n}{(VA)_n} = \frac{19,590}{209,200} = 0.094 \quad \text{numeric} \tag{8.51}$$

The angle between the phase voltage applied to the stator and the resulting phase current is

$$\theta_n = \cos^{-1}(0.094) = -84.6 \quad \text{degrees} \tag{8.52}$$

Thus the no-load current vector can be described as

$$I_n = 30.2\underline{/-84.6^\circ} \quad \text{amperes/phase} \tag{8.53}$$

The magnetizing current is the larger of the two components forming this current, and it is essentially in quadrature with the applied voltage. The second, smaller component is in phase with the applied voltage and is the current that sustains core loss, friction and windage losses, and no-load I^2R loss.

The second of the two tests, the blocked-rotor test, is conducted by installing a mechanical block onto the rotor, such as a beam bolted to the coupling, and then applying a variable voltage, at rated frequency, to the stator terminals. The stator phase current and the power input to the machine is measured and recorded, for various voltage points. As indicated earlier, considerable care must be taken to prevent the windings from being subjected to excessive heating, due to the high magnitude of current at blocked-rotor conditions. To prevent excessive heating from occurring, the actual blocked rotor testing may be discontinued at a voltage value somewhat less than rated and the full-voltage values of phase current and power determined by a logical extension of the curves resulting from the test data taken up to that point.

Let it be assumed that the foregoing procedures and conditions for conducting a blocked-rotor test have been met and that the results for the 1000-hp numerical example are documented in Fig. 8.8. The rated-voltage values are

$$\text{blocked-rotor current} = I_\ell = 825 \quad \text{amperes/phase} \tag{8.54}$$

$$\text{blocked-rotor power} = P_\ell = 1404.8 \times 10^3 \quad \text{watts} \tag{8.55}$$

The blocked-rotor volt ampere input to the machine is equal to

$$(VA)_\ell = (3)(2309)(825) = 5714.8 \times 10^3 \quad \text{volts-amperes} \tag{8.56}$$

and the blocked-rotor power factor is equal to

$$(PF)_\ell = \frac{P_\ell}{(VA)_\ell} = \frac{1404.8 \times 10^3}{5714.8 \times 10^3} = 0.246 \quad \text{numeric} \tag{8.57}$$

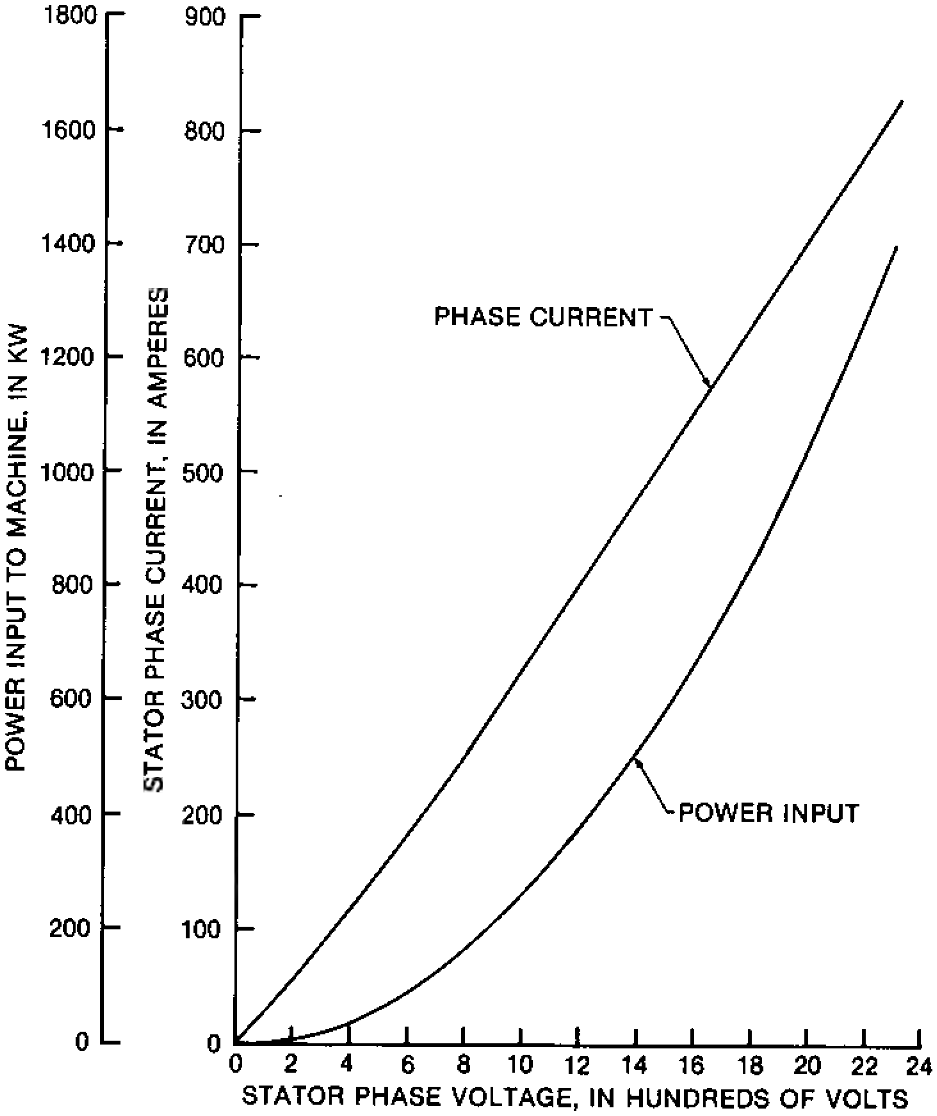

FIGURE 8.8 Blocked-rotor test data for the 1000-hp squirrel-cage induction motor example.

The phase angle between rated stator phase voltage and the resulting blocked-rotor phase current is

$$\theta_\ell = \cos^{-1}(0.246) = 75.8 \quad \text{degrees} \tag{8.58}$$

Accordingly, the blocked-rotor current vector determined from test can be described as

$$I_\ell = 825\underline{/-75.8^\circ} \quad \text{amperes/phase} \tag{8.59}$$

The additional items of information required to construct the adjusted circle diagram are the blocked-rotor leakage reactance X_ℓ and the running leakage reactance X. The blocked-rotor leakage reactance is determined by consideration of the driving-point impedance looking into the machine at the stator terminals under blocked-rotor conditions at rated voltage. At such conditions, saturation of the ferrous paths to leakage flux will be equal to that normal for the design at rated voltage. Then

$$Z_\ell = (R_{eq})_\ell + jX_\ell = [(R_{eq})_\ell^2 + X_\ell^2]^{1/2} \quad \text{ohms/phase} \tag{8.60}$$

Rearranging gives us

$$X_\ell = [(Z_\ell)^2 - (R_{eq})_\ell^2]^{1/2} \quad \text{ohms/phase} \tag{8.61}$$

But

$$(R_{eq})_\ell = \frac{P_\ell}{3I_\ell^2} \quad \text{ohms/phase} \tag{8.62}$$

and

$$Z_\ell = \frac{V_1}{I_\ell} \quad \text{ohms/phase} \tag{8.63}$$

Substituting eqs. (8.62) and (8.63) into eq. (8.61) yields

$$X_\ell = \left[\left(\frac{V_1}{I_\ell}\right)^2 - \left(\frac{P_\ell}{3I_\ell^2}\right)^2\right]^{1/2} \quad \text{ohms/phase} \tag{8.64}$$

which is the working equation for determining X_ℓ from test data.

The test value of I_ℓ is given in eq. (8.59) and the test value of P_ℓ is given in Fig. 8.8 for rated stator voltage of 2309 V per phase. Substituting these numerical values into eq. (8.64) and solving for X_ℓ yields

$$X_\ell = \left\{\left(\frac{2309}{825}\right)^2 - \left[\frac{1405 \times 10^3}{(3)(825)^2}\right]^2\right\}^{1/2} = 2.71 \quad \text{ohms/phase} \tag{8.65}$$

The running reactance can be determined in a similar manner, except at a lower voltage such that no significant saturation of the ferrous paths to leakage flux would exist. Then

$$X = \left\{ \left(\frac{V_1'}{I_\ell'} \right)^2 - \left[\frac{P_\ell'}{3(I_\ell')^2} \right]^2 \right\}^{1/2} \quad \text{ohms/phase} \tag{8.66}$$

where I_ℓ' and P_ℓ' are the stator phase current and the power input, respectively, at the reduced voltage, V_1'. Using a value of 400 V per phase for V_1' and using the values of I_ℓ' and P_ℓ' in Fig. 8.8 which correspond to this voltage, we obtain

$$X = \left\{ \left(\frac{400}{119} \right)^2 - \left[\frac{43{,}000}{(3)(119)^2} \right]^2 \right\}^{1/2} = 3.21 \quad \text{ohms/phase} \tag{8.67}$$

As noted earlier, the value of blocked-rotor reactance is less than that of running reactance (1) because of saturation of the ferrous paths to leakage reactance at high values of current and (2) because of the effective reduction in rotor-bar height and hence reduction in rotor-slot reactance with rated frequency in the rotor bar. The procedure above for determining running reactance from blocked-rotor test data at reduced voltage corrects for the effect of saturation. However, it does not correct for the reduction in effective rotor-bar height, since the blocked-rotor test resulted in rated frequency in the rotor winding at all voltages. Accordingly, this procedure must be considered an approximate one, in general. As will be shown in Chapter 9, the effective reduction in rotor-bar height at a given frequency varies with the actual bar height and with the square root of the bar conductivity. Thus deep rotor bars made of copper will exhibit a greater effect than less deep bars made of aluminum, brass, or bronze. For the 1000-hp numerical example being considered, the effect on the total running reactance is insignificant.

8.15 CONSTRUCTION OF THE ADJUSTED DIAGRAM

Having determined the no-load and the blocked-rotor currents in magnitude and in angle, and having determined the blocked-rotor and the running reactance, the adjusted circle diagram may be constructed. For this numerical example it is assumed that the necessary information is determined from testing. However, it is apparent that the same information might have been obtained from the manufacturer as design data.

An adjusted circle diagram has been constructed for the numerical example, using manual construction, with a scale of 1 in. to represent 50 A. Thus the base of the diagram has a spread of about 16 in. in the full-scale diagram. If a computer program is used to make and interpret the diagram, such an expanded scale is not required for accuracy, since the precise techniques of analytic geometry may be used. Figure 8.9 is a reduced-scale version of the full-scale diagram made for the numerical example.

To construct the diagram, point A is taken as the origin and point O is laid out from the tested value of no-load current, as $I_n = 30.2\underline{/-84.6^\circ}$ from eq. (8.53), using the real axis as angle reference. Point B is laid out from the torque value of blocked-rotor current, as $I_\ell = 825\underline{/-75.8^\circ}$ from eq. (8.59), again using the real axis as angle reference. Arc BC of the larger circle can then be determined by construction. The diameter of the smaller circle is equal to $V_1/2X$, where X is the total running reactance of the machine. From eq. (8.67) the value of X, as determined from test data, is 3.21 Ω/phase. Then the smaller radius is equal to 2309/(2)(3.21) = 360 A/phase. Arc OK' of the smaller circle is constructed by starting the arc at point O, with its diameter along line OC.

Having determined arc BC and arc OK' of the large circle and small circle, respectively, the necessary additional construction lines may be provided. Line BE, which is proportional to the sum of stator and rotor

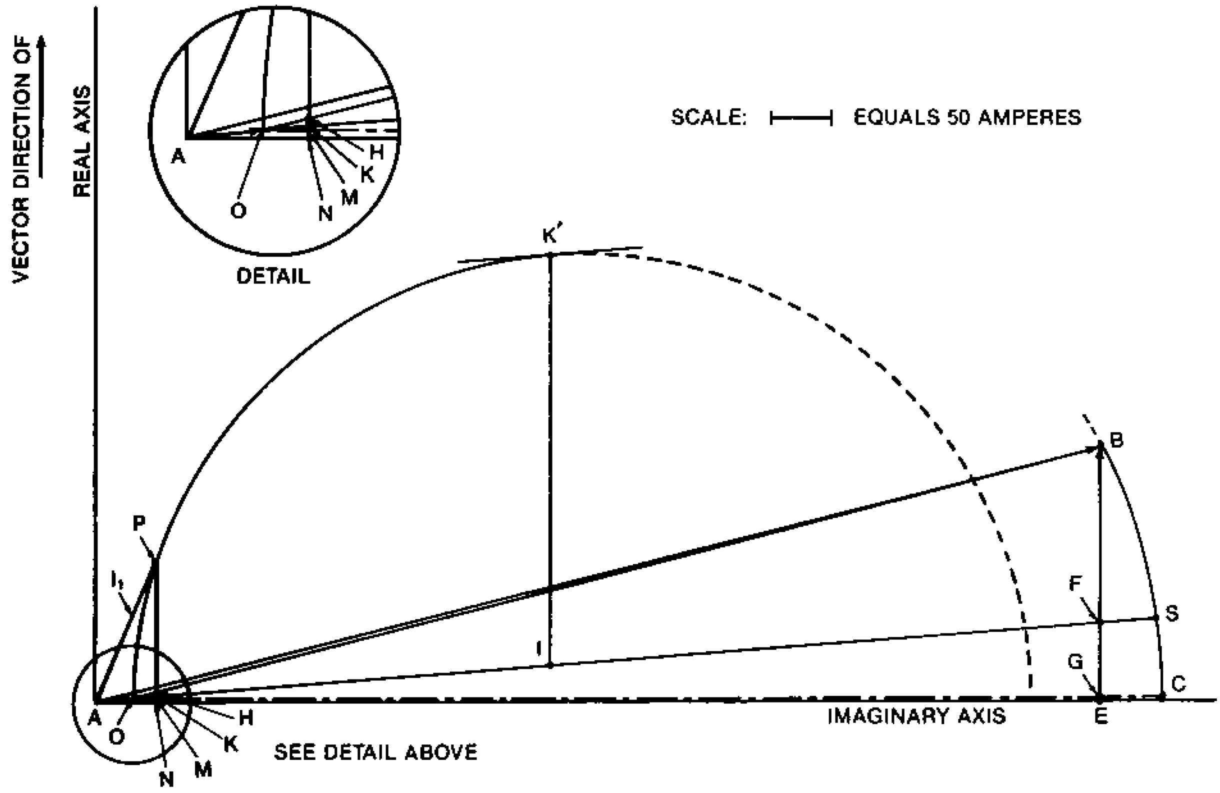

FIGURE 8.9 Adjusted circle diagram for the 1000-hp three-phase 60-Hz 4000-V squirrel-cage induction motor.

winding copper losses, at blocked-rotor condition, is drawn through point B to be perpendicular to line AE. Point G, which will be used subsequently for establishing similar triangles, denotes the intersection of line OC and line BE. Point F represents the demarcation between stator and rotor winding copper loss at blocked-rotor conditions. It is determined by calculating the stator copper loss component at blocked-rotor conditions as

$$P_{1\ell} = 3I_\ell^2 R_1 \quad \text{watts} \tag{8.68}$$

The value of I_ℓ, the stator current at full voltage, with the rotor blocked, will have been determined at test (see Fig. 8.8). The stator winding resistance/phase R_1 will have been determined by information supplied by the manufacturer or by having performed a simple measurement on the machine. Then, for the numerical example,

$$P_{1\ell} = (3)(825)^2(0.2145) = 438,000 \quad \text{watts} \tag{8.69}$$

The distance FE, in terms of amperes/phase, is equal to

$$FE = \frac{P_{\ell 1}}{3V_1} \quad \text{amperes/phase} \tag{8.70}$$

or, for this example,

$$FE = \frac{438,000}{(3)(2309)} = 63.2 \quad \text{amperes/phase} \tag{8.71}$$

The value of the line segment FE has dimensions of amperes in eq. (8.71). To convert it to a linear distance on the diagram, with a scale modulus of 50 A to 1 in., we use the formula

$$FE = \frac{63.2}{50} = 1.26 \quad \text{inches} \tag{8.72}$$

Since line segment BE is proportional to the sum of the rotor and stator copper losses at blocked-rotor conditions, the rotor copper loss is equal to

$$BF = BE - FE \quad \text{watts} \tag{8.73}$$

From eq. (8.55) or from Fig. 8.8, the tested value of power input to the machine at blocked-rotor conditions is

$$P_\ell = 1404.8 \times 10^3 \quad \text{watts} \tag{8.74}$$

Then, subtracting the stator copper loss, eq. (8.69), from the sum of the stator and rotor copper losses, eq. (8.74), the rotor copper loss is equal to

$$I_{2\ell}^2 R_{2\ell} = 1404.8 \times 10^3 - 438 \times 10^3 = 966.8 \times 10^3 \quad \text{watts} \tag{8.75}$$

To express the quantity above in terms of amperes on the diagram, we use the formula

$$BF = \frac{966.8 \times 10^3}{(3)\,(2309)} = 139.6 \quad \text{amperes/phase} \tag{8.76}$$

and to express amperes/phase as a distance on the diagram, we use

$$BF = \frac{139.6}{50} = 2.79 \quad \text{inches} \tag{8.77}$$

Having established point F on line BE, the line OF may now be drawn to show the division between rotor and stator copper losses for all values of current. Also, a line parallel to line OF, tangent to the smaller circle, may be drawn. The point of tangency of this line defines point K', which is required for determining maximum torque.

8.16 DETERMINATION OF MAXIMUM TORQUE AND STARTING TORQUE FROM THE ADJUSTED DIAGRAM

The maximum torque produced by the motor occurs when the loss in the rotor circuit is a maximum. As discussed earlier, this occurs when the vertical distance from line OF to point K' on the smaller circle, as represented by line IK', is a maximum. From eq. (8.28), maximum torque is equal to

$$T_m = \frac{7.04}{n_s} 3V_1 (IK') \quad \text{pound-feet} \tag{8.78}$$

The length of line IK', as measured on the full-scale diagram, is 6.5 in. This value must be multiplied by the scale modulus to give 6.5 × 50 = 325 A per phase. Then

$$T_m = \frac{7.04}{1800}(3)(2309)(325) = 8805 \quad \text{pound-feet} \tag{8.79}$$

Starting torque is proportional to the loss in the rotor circuit at blocked-rotor conditions. From eq. (8.26),

$$T_{st} = \frac{7.04}{n_s} 3V_1(BF) \quad \text{pound-feet} \tag{8.80}$$

The length of line BF, as determined by eq. (8.77), is 2.79 in. When this distance is multiplied by the scale modulus of the diagram, line BF represents 139.6 A. Then

$$T_{st} = \frac{7.04}{1800}(3)(2309)(139.6) = 3782 \quad \text{pound-feet} \tag{8.81}$$

8.17 DETERMINATION OF PERFORMANCE AT RATED LOAD FROM THE ADJUSTED DIAGRAM

Point P in Fig. 8.9 denotes the point of rated load on the diagram. Vertical line PN, when multiplied by the scale modulus and by $3V_1$, equals the total power input to the motor at rated load. Points H, K, and M are defined by the intersection of line PN with lines OB, OF, and OG, respectively. As shown previously, lines HK and KM are proportional to rotor and stator copper losses, respectively, for operating point P. However, even for the full-scale diagram, the lengths of these two line segments are too small to be read directly from the diagram with sufficient accuracy. Accordingly, the concept of proportionality of the corresponding sides of similar triangles should be used to determine the lengths of HK and KM. Thus

$$\frac{HM}{OM} = \frac{BG}{OG} \quad \text{numeric} \tag{8.82}$$

and with the previously mentioned approximation that BG = BE,

$$\frac{HM}{OM} = \frac{BE}{OE} \quad \text{numeric} \tag{8.83}$$

Then

$$HM = \frac{(BE)(OM)}{OE} \quad \text{inches} \tag{8.84}$$

From eqs. (8.72) and (8.77), BE = 1.26 + 2.79 = 4.05 inches. As measured from the full-scale diagram, OM = 0.366 in. and OG ≅ OE = 15.38 in. Substituting these values into eq. (8.84) yields

$$HM = \frac{(4.05)(0.366)}{15.38} = 0.0963 \quad \text{inches} \tag{8.85}$$

Also,

$$\frac{KM}{OM} = \frac{FG}{OE} = \frac{FE}{OE} \quad \text{numeric} \tag{8.86}$$

and

$$KM = \frac{(FE)(OM)}{OE} \quad \text{inches} \tag{8.87}$$

From eq. (8.72), FE = 1.26 in. Substituting this value and the other previously determined values into eq. (8.87) gives us

$$KM = \frac{(1.26)(0.366)}{15.38} = 0.030 \quad \text{inches} \tag{8.88}$$

Since KM is proportional to the stator copper losses, at load point P

$$3I_1^2R_1 = (3)(2309)(50)(0.030) = 10{,}391 \quad \text{watts} \tag{8.89}$$

Rotor copper losses, at load point P, are proportional to HK. Since

$$HM = HK + KM \quad \text{inches} \tag{8.90}$$

then

$$HK = HM - KM \quad \text{inches} \tag{8.91}$$

Substituting the values of HM and KM given in eqs. (8.85) and (8.88), respectively, into eq. (8.91) yields

$$HK = 0.0963 - 0.030 = 0.0663 \quad \text{inches} \tag{8.92}$$

Then the rotor copper loss, before adjusting for the effect of the decrease in R_2 due to the decrease in rotor-circuit frequency, is

$$(3I_2^2R_2)' = (3)(2309)(50)(0.0663) = 22{,}963 \quad \text{watts} \tag{8.93}$$

The value above was determined on the basis of similar triangles, which assumed that no decrease occurred in the value of R_2, as the frequency in the rotor circuit decreased from line frequency to 1 or 2 Hz/s. Then the actual rotor copper loss at load point P is

$$3I_2^2R_2 = \frac{R_2}{R_{2\ell}}(22{,}963) \quad \text{watts} \tag{8.94}$$

The ratio of $R_2/R_{2\ell}$ may be determined in any one of several different ways. It may be obtained from the manufacturer upon request. It may be determined locally by conducting a measurement of the rotor bar height and then utilizing quantitative information on the "deep bar" effect, given in Chap. 10. Also, an approximate value of the ratio at 60 Hz can be determined by empirical methods, such as the approximate relationship $R_{2\ell}/R_2 = 2.70h$, where h is the bar height in inches. This relationship applies to rectangular copper bars only. If the bar material is other than copper, this ratio should be multiplied by the square root of the ratio of the resistivity of the actual material to that of copper. If line frequency is other than 60 Hz, this ratio should also be multiplied by the square root of the ratio of that frequency to 60 Hz. Needless to say, if accurate results are desired, it is important that an accurate method be used, such as the one developed in a subsequent chapter. For purposes of the numerical example, it will be assumed that an accurate value of the ratio has been obtained. Then, substituting the value of the ratio $R_2/R_{2\ell}$ into eq. (8.94), we obtain

$$3I_2^2R_2 = \left(\frac{0.236}{0.490}\right)(22{,}963) = 11{,}059 \quad \text{watts} \tag{8.95}$$

Core loss, friction and windage losses, and no-load stator copper loss were determined by the no-load test. From eq. (8.49), the no-load power loss, at rated voltage, was determined to be

$$P_n = 19{,}590 \quad \text{watts} \tag{8.96}$$

To determine the core loss and friction and windage losses, the no-load stator copper loss must be subtracted from eq. (8.96). As discussed earlier, the no-load rotor copper loss is insignificant. From eq. (8.53), the measured no-load current was determined to be 30.2 A/phase. Then the no-load stator copper loss is

$$3I_n^2R_1 = (3)(30.2)^2(0.2145) = 587 \quad \text{watts} \tag{8.97}$$

Subtracting eq. (8.97) from eq. (8.94) to give core loss and friction and windage losses gives us

$$CL + F\&W = 19{,}590 - 587 = 19{,}003 \quad \text{watts} \tag{8.98}$$

The motor output at point P would be proportional to line PH if the value of the rotor winding resistance did not change from blocked-rotor conditions to normal operating conditions. However, since it changes from $R_{2\ell}$ to R_2 between these two operating points, it is necessary to add an additional component, equal to HK $(1 - R_2/R_{2\ell})$, to PH in order to determine power output. Then

$$P'_o = (3V_1)(50)\left[PH + HK\left(1 - \frac{R_2}{R_{2\ell}}\right)\right] \quad \text{watts} \tag{8.99}$$

Using a decimal measuring scale and a magnifying glass, the distance PH measured somewhere between 2.14 and 2.15 on the full-scale diagram. Substituting this value for PH, together with the value of HK given in eq. (8.92), into eq. (8.99) gives us

$$P'_o = (3)(2309)(50)\left[2.145 + (0.0633)\left(1 - \frac{0.236}{0.490}\right)\right] = 754{,}500 \quad \text{watts} \tag{8.100}$$

However, since load loss is not included in the various losses corresponding to distance HN, and since this component of loss does, in fact, exist, load loss must be subtracted from the power output. Accordingly,

$$P_o = P'_o - LL \quad \text{watts} \tag{8.101}$$

For the numerical example it will be assumed that the actual value of LL has been obtained from the manufacturer, as equal to 8000 W at rated load. Then

$$P_o = 754{,}500 - 8000 = 746{,}500 \quad \text{watts} \tag{8.102}$$

which is very close to rated power output of 746,000 W.

Efficiency is equal to

$$\eta = \frac{P_o}{P_o + \Sigma\ \text{losses}} \quad \text{numeric} \tag{8.103}$$

From eqs. (8.89), (8.95), (8.98) and a known value of LL = 8000 W, the losses at rated load may be calculated as

$$\Sigma \text{ losses} = 10{,}391 + 11{,}059 + 19{,}003 + 8000 = 48{,}453 \text{ watts} \qquad (8.104)$$

Then, from eq. (8.103), rated efficiency is equal to

$$\eta = \frac{746{,}500}{746{,}500 + 48{,}453} = 0.939 \quad \text{numeric} \qquad (8.105)$$

Power factor, at rated load, is equal to the ratio of input power to input volt-amperes, or

$$\mathrm{PF} = \frac{P_i}{(\mathrm{VA})_i} = \frac{P_o + \Sigma \text{ losses}}{3V_1I_1} \quad \text{numeric} \qquad (8.106)$$

The value of I_1 at rated load is proportional to the distance AP on the circle diagram, which measures 2.48 in. Accordingly,

$$I_1 = (2.48)(50) = 124 \quad \text{amperes/phase} \qquad (8.107)$$

Substituting the value of I_1 above, the value of P_o given in eq. (8.102), and the value of Σ losses given in eq. (8.104) into eq. (8.106), the rated power factor is equal to

$$\mathrm{PF} = \frac{746{,}500 + 48{,}453}{(3)(2309)(124)} = 0.925 \quad \text{numeric} \qquad (8.108)$$

Power factor can also be determined directly from the diagram as the cosine of the angle θ between the real axis and line AP, which is I_1. As measured by a protractor, $\theta = -22.5^\circ$. Then

$$\mathrm{PF} = \cos(-22.5^\circ) = 0.924 \quad \text{numeric} \qquad (8.109)$$

As discussed earlier, slip is equal to the rotor copper loss divided by the power transferred across the air gap. It has been traditional wisdom to determine slip from the conventional circle diagram as the ratio of line HK to line PK. However, this method contains some inaccuracies. The actual rotor copper loss is proportional to $(HK)(R_2/R_{2\ell})$ and the power transferred across the air gap should have a quantity proportional to $(HK)(1 - R_2/R_{2\ell})$ added to it. Also, the power transferred across the air gap contains two additional quantities, friction and windage losses and that portion of core loss which occurs on the rotor surface. Core loss and friction and windage losses as well as no-load copper losses are combined in, and are proportional to, line MN in both the conventional and the adjusted circle diagram. Thus the value of slip, as determined by the circle diagram, is normally too large.

TABLE 8.1 Comparison of Results of the Various Algorithms Used for Analyzing the Performance of the 1000-hp Three-Phase 60-Hz 4000-V Induction Motor Example

Symbol	Quantity	Units	Complete equivalent circuit results	Simplified equivalent circuit results, using V_1	Simplified equivalent circuit results, using V_1	Adjusted circle diagram results
P_o	Power output	hp	1000	1000	1000	1000
T_m	Maximum torque	lb-ft	8814	9089	8867	8805
T_{st}	Starting torque	lb-ft	3811	3879	3703	3782
PF	Power factor	per unit	0.923	0.922	0.923	0.925
η	Efficiency	per unit	0.941	0.942	0.941	0.939
I_2, I'	Rotor circuit	amperes/phase	115.9	113.3	116.2	115
I_1	Stator input current	amperes/phase	123.9	124	124	124
I_ℓ	Blocked-rotor current	amperes/phase	825	852	832	825

If the friction and windage losses are known, a reasonable value of slip may be determined as

$$s = \frac{I_2^2 R_2}{P_o + I_2^2 R_2 + F\&W} = \frac{(HK)(R_2/R_{2\ell})}{PH + HK(1 - R_2/R_{2\ell}) + (q)(MN)} \tag{8.110}$$

where q is the fractional part of MN, or of P_n, that is, friction and windage. However, slip, as calculated by eq. (8.110), will not be a precise value, although it will be a reasonable one.

8.18 COMPARISON OF PERFORMANCE AT RATED LOAD AS CALCULATED BY THE ADJUSTED DIAGRAM

The circle diagram completes the list of the various formal algorithms to be considered for analyzing the performance of the polyphase induction motor. The algorithms considered included the complete equivalent circuit; the simplified equivalent circuit, using V_1 as the driving voltage; the simplified equivalent circuit, using V_1' (V_1 adjusted for the stator impedance drop) as the driving voltage; the vector diagram; and the adjusted circle diagram. A comparison of the results of these algorithms, except for the vector diagram, is included in Table 8.1. The vector diagram is not included in Table 8.1 because it is not generally considered a free-standing and complete system for analysis of performance.

9

Stator Windings

9.1 Function and Importance of the Stator Winding 178

9.2 Stator Coils 179

  9.2.1 Types of coils 180
  9.2.2 Lap coils 180
  9.2.3 Wave coils 182
  9.2.4 Concentric coils 182
  9.2.5 Push-through coils 184
  9.2.6 Random coils and random-coil windings 185
  9.2.7 Formed coils and formed-coil windings 190
  9.2.8 Conductor material 194
  9.2.9 Turns, conductors, and strands 196

9.3 Eddy-Current Losses in the Copper Within the Slot 197

9.4 Additional Winding Losses Due to Circulating Currents in the Strands 205

9.5 Slot Factor 209

9.6 Numerical Example of Calculation of Eddy-Current Loss and Strand Loss in a Stator Winding 210

9.7 Induced Voltage in the Stator Coil 217

9.8 Coil-Pitch Factor 220

9.9 Use of the Coil-Pitch Factor in Controlling Harmonics 223

9.10 Distribution Factor 225

9.11 Use of the Distribution Factor in Controlling Harmonics 229

9.12 Voltage Induced in the Stator Phase Winding 231

9.13 Integral-Slot Windings 232

9.14 Fractional-Slot Windings 236

9.15 Generalized Rules for Determining Stator Winding Configurations 238

9.16 Unbalanced Windings 242

9.17 Stator Connection Diagrams 245

9.18 Magnetic Pull or Radial Decentering Force 246

9.19 Numerical Example of Calculation of Unbalanced Magnetic Pull 257

9.20 Temporary Operation with Damaged Stator Coils 259

9.1 FUNCTION AND IMPORTANCE OF THE STATOR WINDING

It is shown in Chapter 3 that three electromagnetic conditions are required to produce motor action. Those conditions are:

1. A rotating magnetic flux field across the air gap, produced by either the stator or the rotor, which links both the stator and rotor windings. For a polyphase induction motor, this rotating flux field is produced by the stator winding.
2. Axial current flow through conducting paths near the air-gap surface of the other member. For a polyphase induction motor, this axial current flow occurs in the rotor winding.
3. A component of the air-gap flux wave in time phase with a component of the axial current flow, if they are time-varying quantities. For a polyphase induction motor, these quantities have components in phase, the product of which is proportional to the rotor-circuit power factor.

The stator and the rotor windings, as well as the stator and the rotor cores, provide the basis for accomplishing the requirements listed above.

As discussed in Chapter 3, three individual stator windings separated by $2\pi/3$ electrical radians in space, each winding of which is excited by a separate voltage source that is displaced $2\pi/3$ electrical radians in time from each other one, will produce a magnetomotive-force wave which rotates around the air gap at an angular velocity of ω electrical radians/second. This magnetomotive-force wave produces a corresponding flux wave which also rotates around the air gap at the same angular velocity. The rotating flux wave induces a voltage in the axially located rotor bars, as well as in the stator conductors, the resulting voltage wave of which travels at an angular velocity of ω electrical radians/second when viewed from the stator.

The voltage induced in the rotor bars results in a corresponding current flow in the bars, the current wave of which, again, rotates around the air gap at an angular velocity of ω electrical radians/second as viewed from the stator. Since, as has been shown in Chapter 3, there will always be a component of the air-gap flux wave and a component of the rotor-current wave in time phase, a useful torque will be produced which will tend to cause the rotor structure to rotate, with the capability of driving a load.

From the discussion above it is apparent that the stator and rotor windings of an induction motor are central to producing the aforementioned three essential requirements for motor action. In an actual motor, these requirements are achieved by the appropriate configuration of the stator and rotor windings, as well as of the stator and rotor cores that carry the mutual flux. Although the stator and rotor windings are both considered basic to the concept and to the successful operation of a polyphase induction motor, an actual motor with a rotor consisting of only a solid steel rotor body, and without any specific rotor winding, can be designed to produce torque, even though the operating characteristics of such a machine are limited. In such a design, axial current flows in the high-resistance paths near the surface of the rotor, in response to the axial voltage induced along the surface region of the rotor by the rotating flux wave produced by the stator. On the other hand, an effective induction motor cannot be designed that will operate without a specific stator winding. Thus the stator winding is prime to the operation of a polyphase induction motor.

9.2 STATOR COILS

Stator coils are the basic elements of which the stator winding is comprised and, accordingly, it is appropriate that they should be the first topic to be considered in understanding the configuration of the stator winding. A coil consists of two active sides, with one or more insulated conductors in each side, which are embedded in stator slots and which, for a full-pitch coil, are π electrical radians or 180 electrical degrees apart. The active coil sides are connected by end loops, or end turns, on both ends of the coil, which are a continuation of the slot conductors and which form a series circuit around the two sides of the coil. If the air-gap flux density is equal to B webers/meter^2 at one coil side, it is equal to -B webers/meter^2 at the other coil side, since the coil sides span 180 electrical degrees for a full-pitch coil. Since the two coil sides are under the influence of flux of equal density but of opposite polarity, the voltages induced in the two coil sides will be of equal magnitude but in opposite directions. Accordingly, the two voltages will add algebraically around the coil loop. If the coil is not full pitch (i.e., if the two coil sides are less than 180 electrical degrees apart), the voltage induced in the two coil sides must be added vectorially and the total coil voltage will be slightly less than two times that induced in one of the two coil sides. It should be noted that in general it is desirable from an engineering standpoint for the coil span to be less than 180 electrical degrees, and that subject will be discussed subsequently in this chapter.

9.2.1 Types of Coils

As stated above, the active lengths of the various conductors of each coil side are connected to the corresponding conductors of the companion coil side, one coil throw away. This permits the voltages generated in the two coil sides to add, to give the voltage per turn. Then the turn voltages of all of the turns of a given coil will add to give the total voltage for that coil. In addition, a series path is provided for current to flow through all turns of the coil. The manner in which this is accomplished determines whether it is a lap, wave, or concentric coil.

9.2.2 Lap Coils

In Fig. 9.1, lap coils are shown being inserted into a partially wound stator. Each lap coil in the stator is identical to each other one. It is apparent from Fig. 9.1 that there are two coil sides in each slot and that for a given coil, one coil side is positioned in the bottom of a slot and the companion coil side is positioned in the top of a slot one coil throw away. Accordingly, such coils are two-layer coils, and there are as many individual coils as there are slots in the stator core.

The series turns of each coil terminate at the coil's two leads, shown in the figure. As discussed later in this chapter, several adjacent coils, equal to the number of slots per pole for each phase, are connected in series to form a coil group. For each such coil group, the "beginning" lead of the first coil constitutes a terminal lead for that particular group. The other lead, or the "end" lead, of the first coil is connected to the beginning lead of the second coil. The end lead of the second coil is connected to the beginning lead of the third coil, and so on. Finally, the end lead of the last coil of the group serves as the other terminal lead for that group of coils, and the group can then be connected in series or in parallel with similar groups of the same phase. The progression shown in Fig. 9.2 started with the left-hand lead of the first coil as the beginning lead. It is apparent that the right-hand lead of the first coil could have been chosen as the beginning and the progression would have been in the other direction. The various coil-to-coil lead connections within a group are made by brazing, soldering, or by mechanical crimping of ferrules into which the two leads have been inserted. The choice of the method used to make the lead connections is based on the mass and cross section of the copper of the lead conductors to be joined and not infrequently, on long-term reliability of the method, as determined by accelerated life testing.

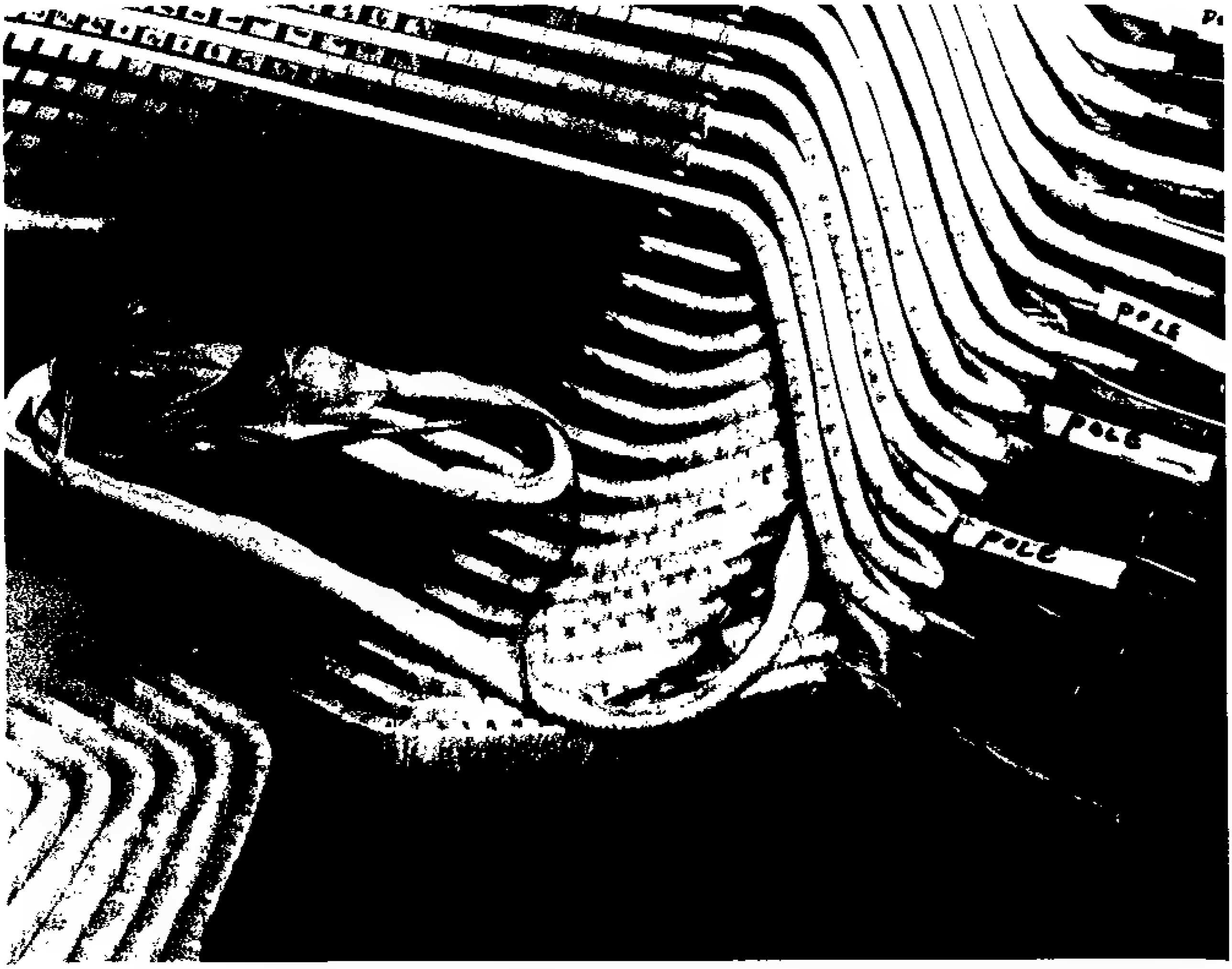
POLE
POLE
POLE

FIGURE 9.1 Lap-type formed coil being inserted into a stator core.

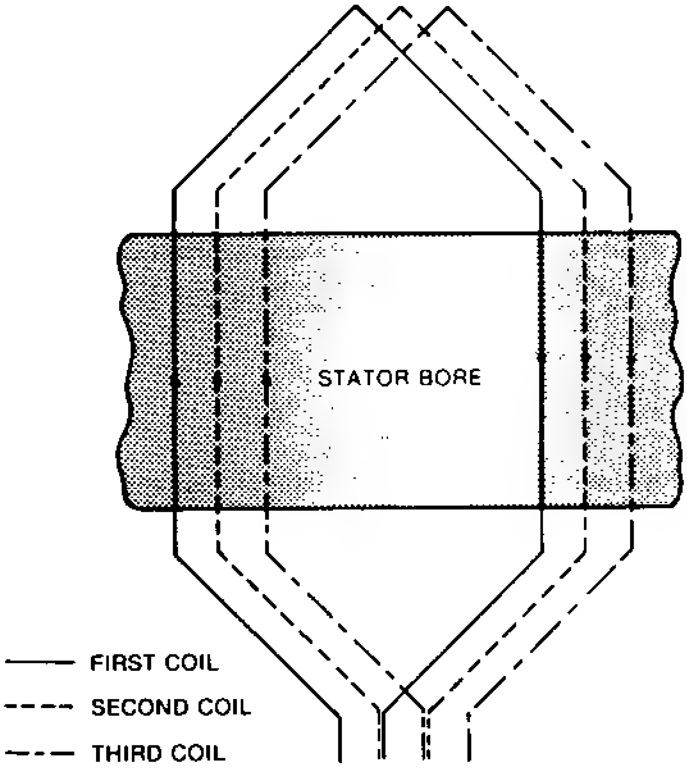
STATOR BORE
FIRST COIL
SECOND COIL
THIRD COIL

FIGURE 9.2 Schematic representation of a lap coil, showing one coil throw.

A winding made up from lap-type coils is called a lap winding. Essentially all polyphase induction motors manufactured in the United States use lap-wound stators. Lap windings are also used to a considerable extent in other parts of the world. Lap-type coils owe their popularity to the fact that the entire set of stator coils are identical, that they may be used for both full-pitch and fractional-pitch coil throws, and that such coils are amenable to a considerable degree of mechanization in their manufacture.

9.2.3 Wave Coils

Wave coils are schematically shown in Fig. 9.3. The two companion coil sides of a wave coil are connected on one end by end turns, in a manner similar to that used for lap coils. However, the end turns on the other end of the coil extend outward, instead of inward, and join corresponding end turns which extend outward from coils on each side, located one coil throw away. From an inspection of the figure it is apparent that the generated voltages in the four active coil sides which are connected in series will add and also that a series path is available for the flow of current through the two coils. There are two coil sides in each slot and, for a given coil, one coil side is positioned in the bottom of a slot and the companion coil side is positioned in the top of a slot one coil throw away. Thus the coils are two-layer coils. Windings made up from wave coils are called wave windings.

Wave windings are used extensively on the rotating armatures of direct-current machines. On such machines, each junction between coils on the connection end of the winding is connected to a commutator segment. For this reason, such a direct-current wave winding is called a closed winding. On the other hand, a polyphase induction motor has one or more continuous paths through each phase of the stator winding, and for wound-rotor machines, through each phase of the rotor winding. For this reason, such windings are called open windings.

Wave windings are more suited for few turns per coil and hence for lower voltages, in general. For this and other reasons, wave windings are very infrequently used for stators of polyphase induction motors. However, they are particularly suited for rotors of wound-rotor machines and are discussed in more detail in Chapter 10.

9.2.4 Concentric Coils

A third type of stator coil is the concentric coil, which is shown schematically in Fig. 9.4. In a concentric winding, the coils are connected in series to form a given group located concentrically relative to each other. The way in which the generated voltages in the various active coil sides add within a group and the way in which a series path is provided through the group for the flow of current are apparent from the figure. Obviously, all of the coils in a given stator cannot be identical in shape, and in general, there will be as many

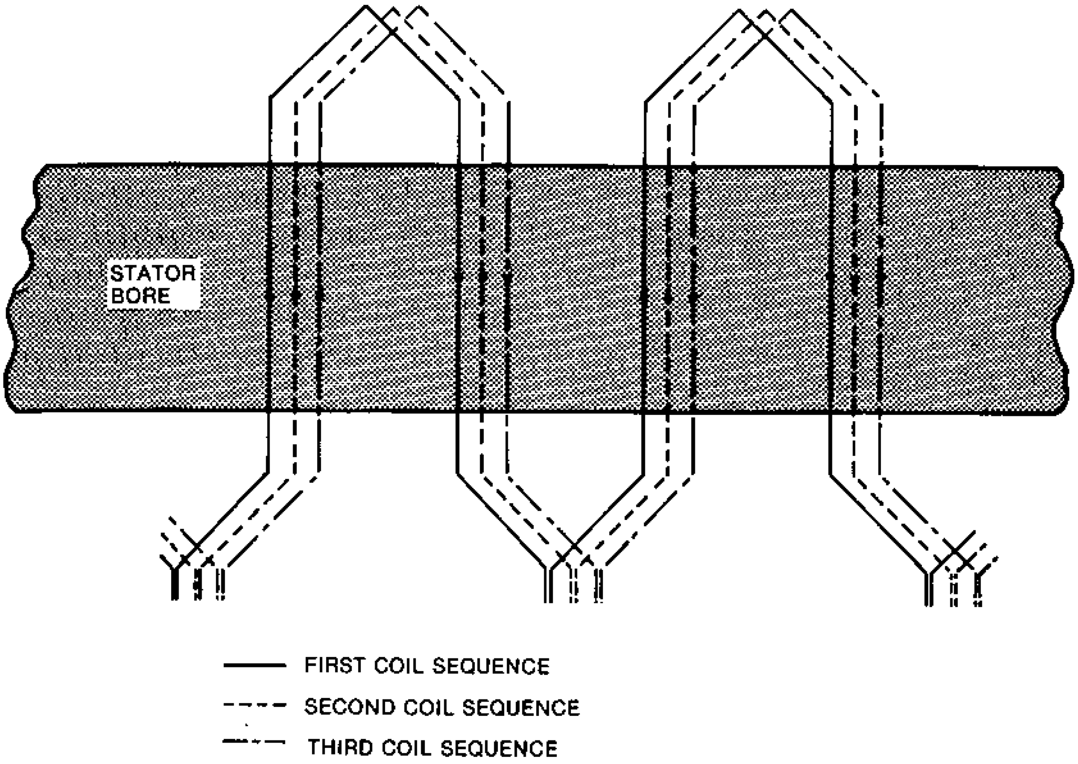
STATOR BORE
FIRST COIL SEQUENCE
SECOND COIL SEQUENCE
THIRD COIL SEQUENCE

FIGURE 9.3 Schematic representation of a wave coil, showing four coil throws.

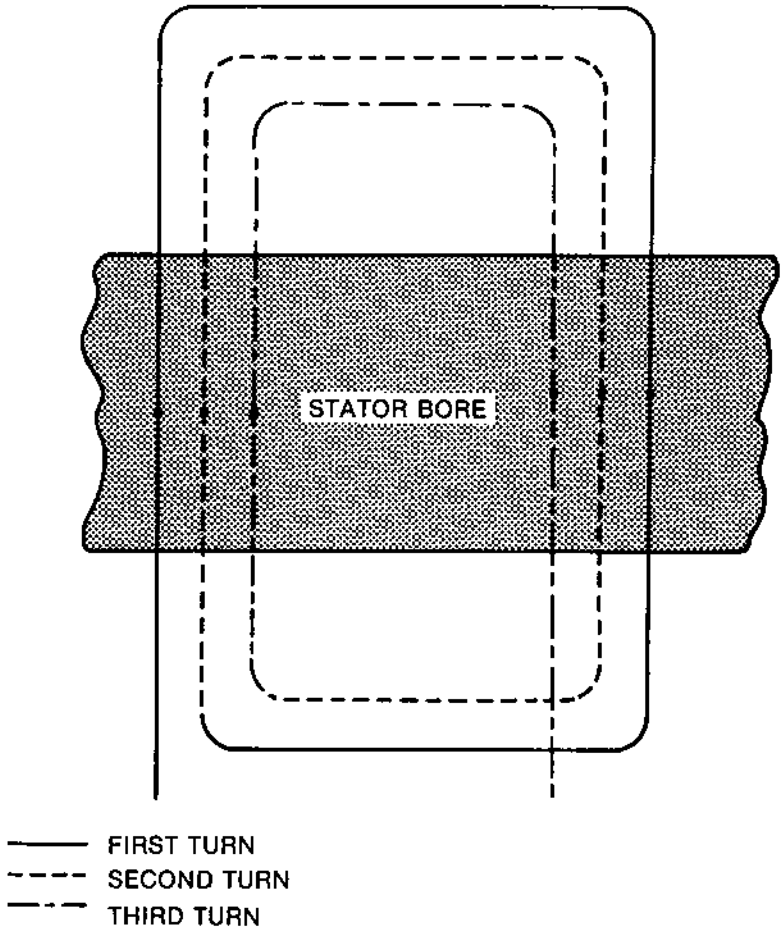
STATOR BORE
FIRST TURN
SECOND TURN
THIRD TURN

FIGURE 9.4 Schematic representation of a concentric coil, showing one coil throw.

different coil shapes as there are slots per pole per phase. The end-turn configuration does not lend itself to double-layer coils within each slot without significant additional bending and shaping of the end turns, and accordingly, concentric windings are usually single-layer windings. A winding built up from concentric coils will have the same magnetomotive-force waveform as that of a full-pitch double-layer lap or wave winding, for the same number of stator slots per pole per phase. The reason for this will become apparent when the winding distribution factor is considered.

Concentric stator windings are not used to any significant extent on polyphase induction motors manufactured in the United States, although such windings have been used to a limited extent on stators of large synchronous machines. However, concentric windings are frequently used on some types of single-phase motors.

9.2.5 Push-Through Coils

The last type of stator coil to be considered, the push-through coil, is shown in Fig. 9.5. This type of coil is not used in modern machines, but there are

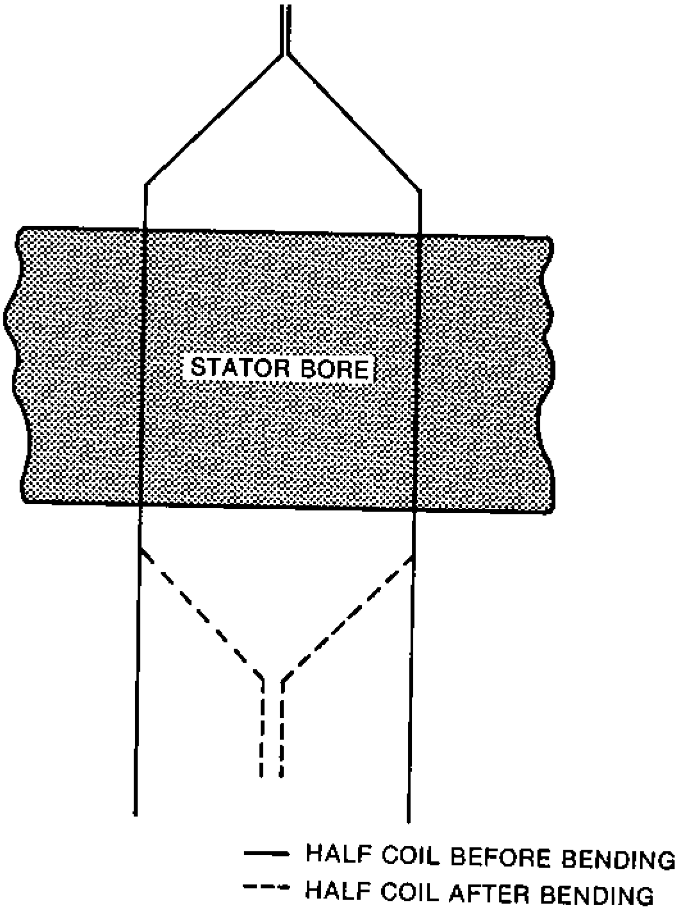

FIGURE 9.5 Schematic representation of a push-through coil, showing one coil throw.

some older machines still in service in which such coils will be found. The concept of push-through coils is apparent from the descriptive name and from an inspection of Fig. 9.5. The coils are manufactured as half coils, with the end turns formed on one end of the coil, and unformed, or left straight, on the other end. In winding the core, the straight portion is "pushed through" the slot and the end turn is then formed on the straight end by the winder, to resemble that on the opposite end. The companion coil half, which is a mirror image of the first half, is then pushed through the appropriate slot one coil throw away. The end turn of the second coil half is then hand formed by the winder to give a complete lap coil. Most windings using such coils are double-layer windings. For most push-through windings, the top of the core slot, adjacent to the air gap, is either closed or partially closed, to reduce electrical losses caused by harmonic fluxes resulting from permeance variation along the air gap associated with open slots.

9.2.6 Random Coils and Random-Coil Windings

Stator coils are also classified into random and formed types. This classification is based, in general, upon whether the top of the slots, into which the coils are inserted, are partially closed or are open, with random coils being used with partially closed slots. Typically, random coils are used on smaller machines, with lower power ratings and with stator voltage ratings of 600 V or less; whereas formed coils are used on larger machines, with larger power ratings and with voltage ratings in excess of 600 V. This dividing line is not a fixed one, however. Random-wound machines have been built with voltage ratings of 440 and 550 V, but with a power rating of several hundred horsepower. Also, random-wound machines have been built with a voltage rating of 2300 V and with a relatively low horsepower rating for that voltage.

Figure 9.6 shows the cross section of a partially closed stator slot, with two random-coil sides occupying the slot. As mentioned in Section 9.2.5, the use of partially closed stator slots tends to reduce the losses caused by harmonic fluxes resulting from permeance variations along the air gap associated with slot openings. Also, as will be seen later, the effective length of the air gap is decreased by the use of partially closed slots. This has the effect of requiring less magnetomotive force to produce the mutual flux, which tends to improve both efficiency and power factor. In addition, the cost of producing a set of random coils is less than that of an equivalent set of formed coils; and the cost of producing stator punchings with partially closed slots is essentially equal to that of producing stator punchings with open slots, using the same type of dies and presses. Accordingly, there are design reasons and economic motivations to use random stator coils and partially closed stator slots to the extent reasonably practical.

The end turns of random windings are not as amenable to receiving the bracing required to withstand electromagnetic forces as are the end turns of formed coils. Bracing requirements are a function of unsupported end-turn length and of the rating of the machine. Thus a point is reached, as the size of machines increase, at which it is desirable to make a transition from random to formed windings, because of bracing considerations. Also, although the insulation used on contemporary random windings is entirely adequate for lower stator voltages and lower power ratings, a point is again reached where because of scale considerations, a transition from random to formed windings should be made as voltage and power ratings increase. This transition is usually made at a stator voltage of 600 V and at a power rating of the machine normal to that stator voltage.

Random coils are made from copper wire of the desired diameter, covered with an insulating enamel or serving. This wire is wound under tension, around a rotating form with automatic equipment, which applies the desired number of turns per coil and which forms the resulting coil into a diamond shape of the appropriate dimensions. Two procedures are used for joining the series coils within a given group. One procedure is to produce the series coils in a connected gang with continuous wire of the appropriate length between the consecutive leads of the various coils within the group. The other procedure is to produce a number of identical coils, equal to the number of stator slots, with each coil having two leads of equal length. In both cases, the wires of the coil are fed into the stator slot one wire or so at a time, with one coil side being positioned in the top of a slot and with the

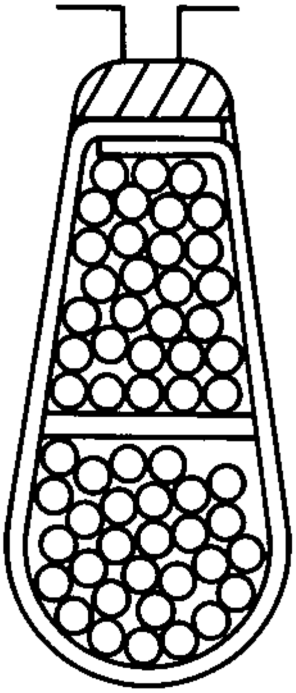

FIGURE 9.6 Cross-sectional view of two random-coil sides in a partially closed stator slot.

other coil side positioned in the bottom of a slot one coil throw away. For gang-connected random coils, the connection between the series coils in a group will have been made previously. For the individual random coils, it is necessary to connect the end lead of one coil to the beginning lead of the next coil in series, successively, until all the series coils in the group have been connected. Crimped ferrules are frequently used to make the coil-to-coil connections.

Prior to inserting the two coil sides of a random winding into the partially closed slots, a U-shaped insulating slot liner is placed in the slot to insulate the two coil sides from ground. After the bottom coil side is inserted into the slot, and prior to inserting the top side of another coil into the same slot, an insulating separator strip is placed over the bottom coil to separate and to insulate between the two coil sides. The slot liner and the separator strip are both shown in Fig. 9.6. As the stator core is being wound, insulating phase separators are placed between end turns of adjacent groups of coils. The phase separators can be seen between the 18 groups of coils in the completed wound-stator core shown in Fig. 9.7.

In order to wind the two coil sides from two different coils into one slot, the top coil sides of the first several coils, equal in number to that corresponding to about one coil throw, must be held upward temporarily until the stator winding is nearly completed and the last coils are inserted into the bottom of the corresponding slots. Then the top sides of the first several coils may be dropped into place to complete the winding. This procedure, which is called "making the jump," can be seen in Fig. 9.8, which shows the jump being made for a form-wound stator. The procedure is essentially the same for both random and formed coils. After the random coils are inserted into the slots and the slot wedges are driven into place, the various groups within each phase are connected together in the appropriate series, parallel, or series-parallel connection to give the desired turns in series, per phase. The three individual phase windings are then connected in wye or delta to give the completed three-phase winding. However, this is not always done internally, but is occasionally done external to the machine enclosure.

For the power ratings usually associated with random windings, it is occasionally the practice not to make the completed winding connection at this point. Instead, the ends of each phase are brought out by leads to permit what is called wye-delta starting. This is accomplished by starting and accelerating the machine to full speed with the stator phase windings connected in wye and then making a transition, by use of suitable contactors, to delta-connected phase windings for normal operation. This allows the motor to be started on a voltage that is $(1/1.732)(100) = 58\%$ of rated voltage, with approximately a 58% reduction of starting kVA requirement. Also, the ends of the parallel circuits of each phase are frequently brought out so that two circuits in each phase winding may be connected in parallel or in series. This allows

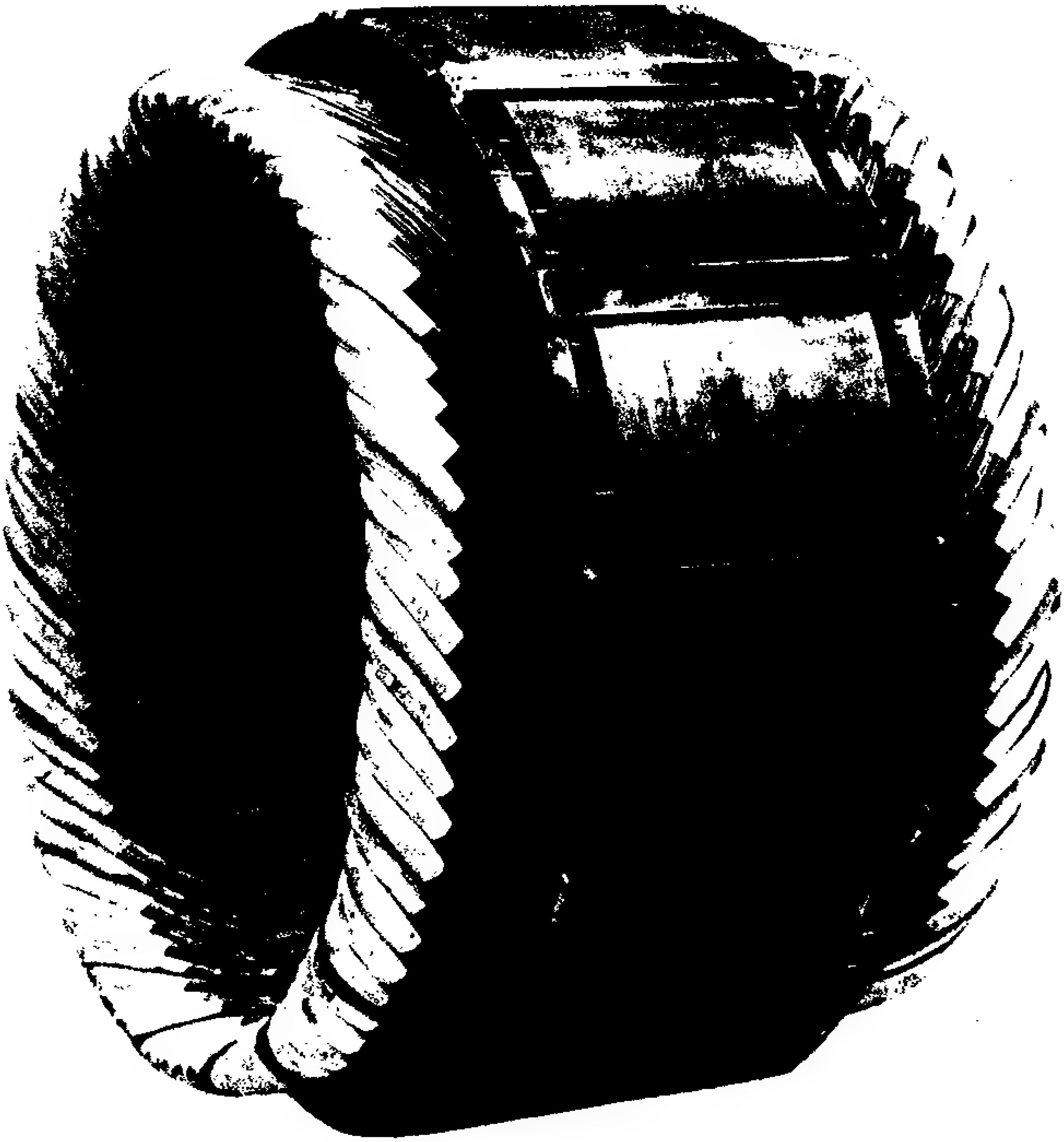

FIGURE 9.7 Random-wound stator core ready for immersion into a vacuum-pressure impregnation tank.

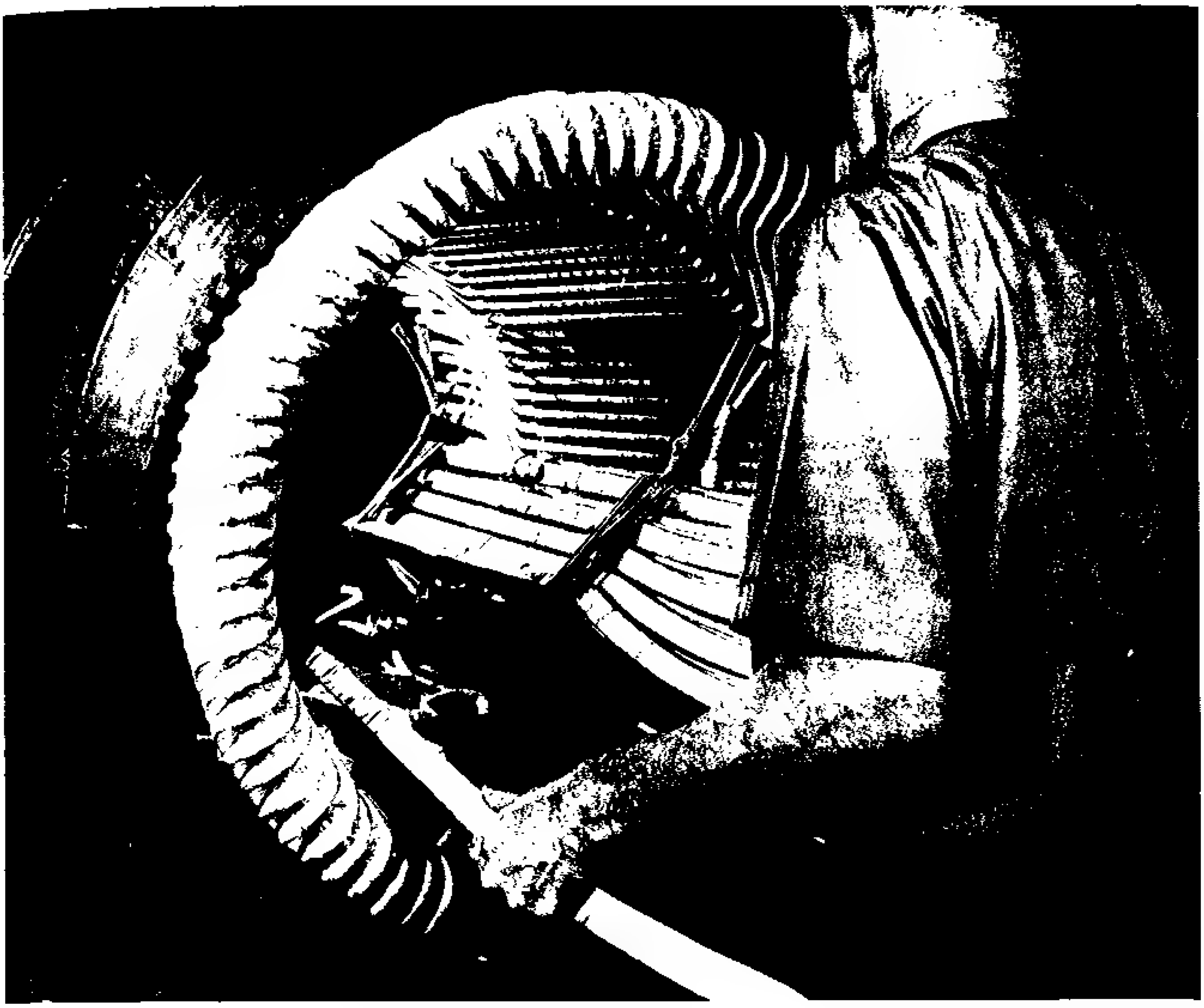

FIGURE 9.8 Form-wound stator core with the jump being made.

the machine to operate on either a 220- or a 440-V stator bus, for example. For such cases, instead of permanently making up the stator winding connections internally, sufficient leads are brought out for subsequent external connection into the various modes mentioned above.

After the stator core has been wound and the end turns braced, the wound core is then given an overall varnish treatment. There are two methods, in general, for applying the varnish treatment: the vacuum-pressure impregnation method and the conventional method. The vacuum-pressure impregnation (VPI) method, will be discussed in some detail in the next section, when formed coils and formed-coil windings are discussed, and the method is essentially identical for both random-coil and formed-coil windings. The conventional varnish treatment method, which has been the standard method, has been replaced by the VPI treatment method to a considerable extent, but not completely, for random-coil windings. The method consists of submerging the wound core, or the wound stator, into an open tank of varnish for several minutes. The workpiece is then withdrawn from the tank and allowed to drain until copious dripping has stopped. It is then placed inside an industrial oven and baked for a sufficient length of time and at a sufficient temperature to cure the varnish. Care is taken that the temperature is below that which would be injurious to the insulation. Frequently, several dip and bake cycles are applied to a new wound core or wound stator.

9.2.7 Formed Coils and Formed-Coil Windings

Formed coils are used with open stator slots. For such stator slots, the opening adjacent to the air gap has the same width as the rest of the slot, and the overall slot is rectangular in cross-sectional shape (see Fig. 9.9). Formed coils are used on machines with power and voltage ratings which are

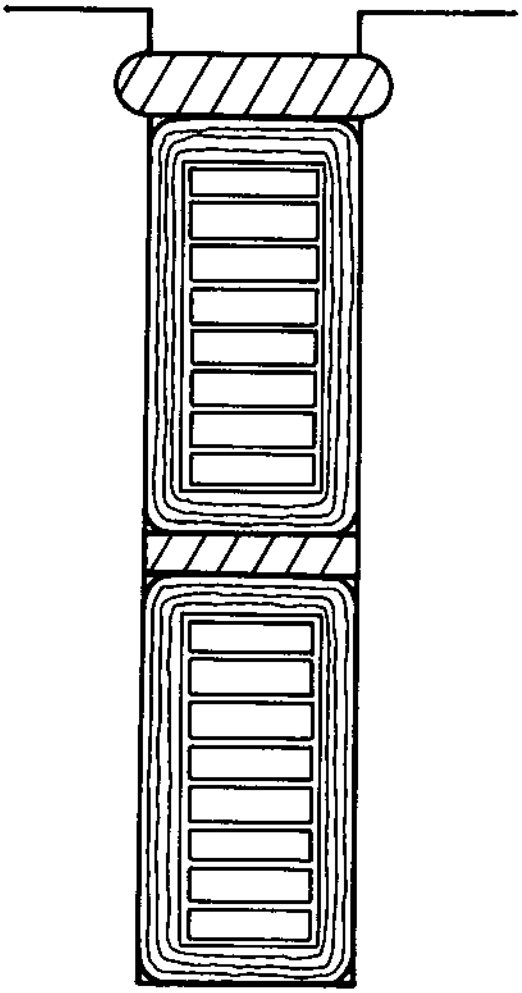

FIGURE 9.9 Cross-sectional view of two formed-coil sides in an open stator slot.

greater than that which is practical for random coils. As stated earlier, this transition occurs, in general, at a stator voltage of in excess of 600 V and at a power rating which is normal to that voltage. However, the transition point is not a fixed one, as noted in the preceding section.

The use of open slots tends to increase the losses caused by harmonic fluxes resulting from permeance variations along the air gap, which will tend to decrease efficiency. Also, use of open slots tends to increase the effective length of the air gap because flux paths across the air gap try to meet the stator gap surface at a 90-degree angle, including the upper portion of the open slot. This effect will be evaluated subsequently when Carter's coefficient is considered. It will be noted at this time, however, that an increase in effective air-gap length will tend to decrease the magnetizing reactance X_m, increase the magnetizing current I_m, and decrease the power factor. Fortunately, however, as can be predicted by dimensional analysis and as can be verified by the accumulated experience in industry, the efficiency and power factor of polyphase induction motors tend to increase as the physical dimensions of the machine increases. Thus any initial effect on efficiency and power factor that might be expected to occur from the transition from random to formed stator coils is of no practical consequence as the ratings progressively increase.

Figure 9.9 shows the cross section of an open stator slot with two formed-coil sides occupying the slot. Formed coils are made from rectangular copper wire that is covered with an insulating enamel or serving. The wire is successively wound around a pin located at each end of a bar of adjustable length, set at the proper distance between pins, which rotates on a shaft through its transverse axis. As the bar rotates on its axis and winds the coil, small platens or guards located on the sides of the pins cause each turn of rectangular wire to fall on top of the preceding one, in vertical alignment. After the correct number of turns have been wound onto the coil, an extended length of several inches of the first and last turns are left at one end of the coil and are "stubbed out" to provide coil leads. The coil, at this preliminary state of completion, is called a hairpin coil.

Various forming machines have been devised to receive the hairpin coil and to then reshape it into the form that is required, such that one coil side will fit into the bottom of a stator slot and the other coil side will fit into the top of another slot, one coil throw away. Coil-forming machines differ in detail and in degree of mechanical sophistication, but they have several general principles in common. The hairpin coil is placed into the forming machine, and jaws or pairs of plates then clamp the coil at various locations along its two sides and two ends. Controlled force is applied to the various clamp positions to cause movement of parts of the coil relative to each other, as follows:

1. Portions of the two coil sides, equal to a length slightly greater than the axial length of the stator core, are pulled apart, maintaining the two sides

parallel to each other and to the long axis of the coil. The amount of this lateral separation is about equal to one coil throw.

2. The two coil sides are given an angular displacement relative to each other. This corresponds to the angular displacement between the radial centerline of two stator slots, one coil throw apart.
3. The end turns receive a small radius, which causes a slight concavity on the end turns as seen from the stator bore.
4. The end turns will be given a small radially outward bend or "drop" to cause them to deflect radially outward relative to an imaginary extension of the cylinder of the stator bore.

After the foregoing forming operations have been performed, stator coils have the appearance of those shown in Figs. 9.1 and 9.8, except that the ground insulation has not yet been applied.

Ground insulation is used to isolate the phase voltage of the winding from the steel slot, which is usually at ground potential. Accordingly, each coil side must have ground insulation. Also, the end turns must be insulated to ground since they may come into contact with operating personnel. The slot portion and the end-turn portion of each coil receive about the same amount of ground insulation as a practical matter. The straight portion of each coil, which includes the slot length of the stator and an inch or so beyond the slot on each end, is insulated with ground insulation in the form of tape or in the form of a rectangular sheet called a "wrap," the length of which is equal to the full length of the straight portion. The amount of tape or wrap buildup that is required depends on the voltage classification of the stator winding. The two ends of the ground tape or ground wrap over the straight portion of the coil are scarfed, or tapered. Then, when ground tape is applied over the end turns, a more effective joint can be made, which will have adequate creepage and which will not have excessive buildup. After ground insulation has been applied to the straight portion of the coil, it is applied to the end turns by taping.

Typically, the ground insulation is either flake mica or reconstituted mica. The latter consists of particles of mica formed into a mat. For both types the mica is bonded to a pliable backing to form the tape or wrap. Tape is applied to the straight portion of the coil by hand or by machine and is applied to the end-turn portion by hand. The entire coil is then overtaped with a tape made from glass fiber or similar material, which will subsequently absorb varnish and which will act as an armor. For vacuum-pressure impregnated (VPI) windings, the stator coil is now ready to be wound into the stator core prior to varnish treatment. Many but not all original-equipment manufacturers use the VPI process for formed-coil stators. However, a considerable portion of coils for replacement windings are not of this type, and such non-VPI coils will receive a varnish treatment prior to being wound into the stator.

Formed coils are wound into the stator slot in a manner similar to that described previously for random coils, in general, except that the complete coil side is inserted into the slot for a formed coil, instead of one or two turns at a time being inserted into the slot as is done for a random coil. After the formed coils are wound into the stator, all connections have been made up, and the end turn bracing has been installed, the wound core is placed inside a pressure vessel and a vacuum is drawn. The vacuum is then held for a sufficient time to remove all air and moisture from the winding. Then a suitable varnish, such as an epoxy formulation, is forced into the pressure vessel and held at sufficient pressure, for sufficient time, to cause the varnish to impregnate the winding. Figure 9.10 shows a wound core positioned above the pressure vessel and about to be given a vacuum-pressure impregnation treatment. After removal from the pressure vessel, the wound core is placed in an industrial heating oven in order to cure the varnish.

The discussion above assumed that a prewound core, or an equivalent structural concept, was utilized to receive the stator coils. Such construction permits greater access to the stator core. This, in turn, allows the

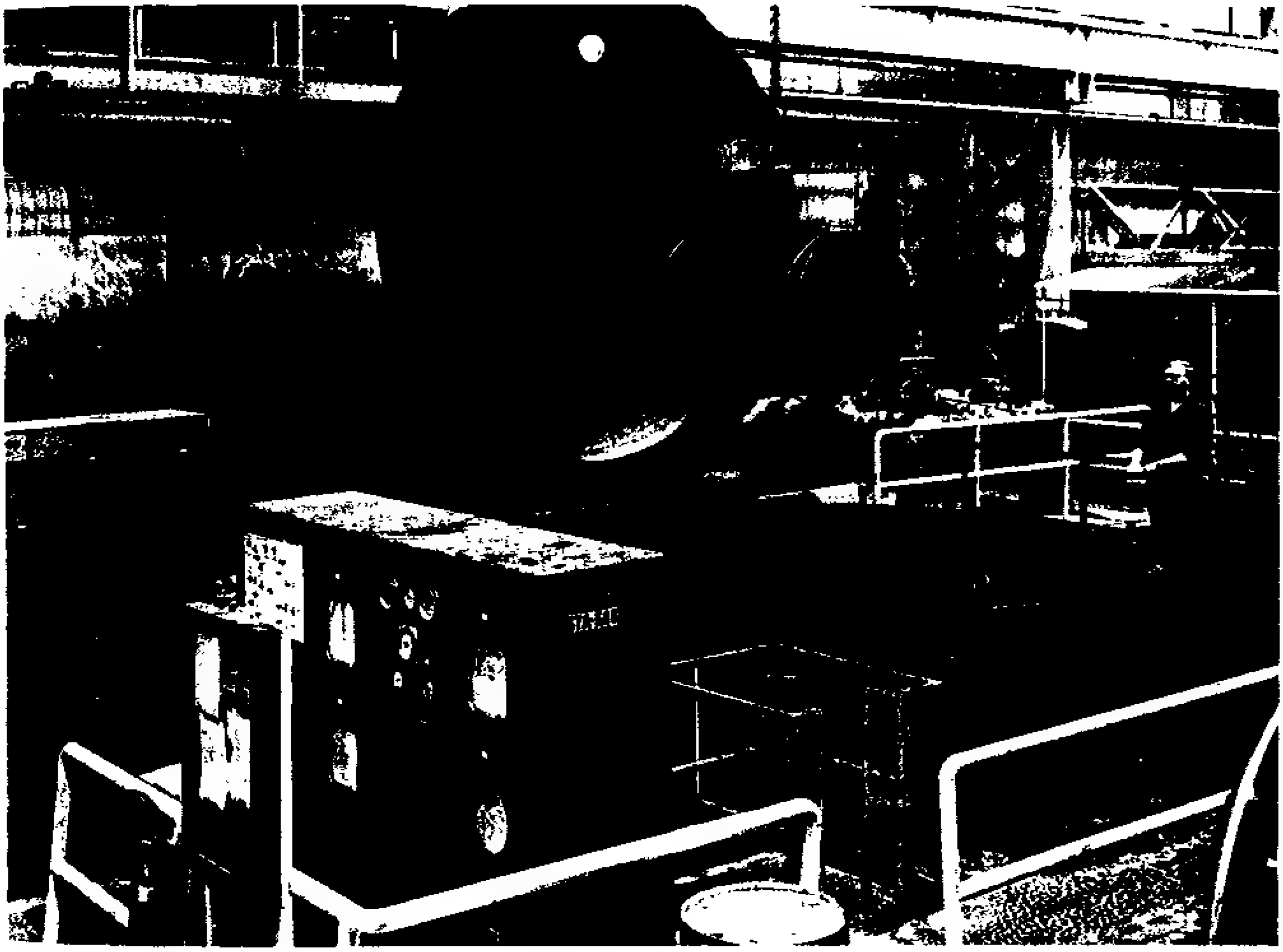

FIGURE 9.10 Wound-stator core about to be treated in a VPI facility.

core to be wound, wedged, connected, and braced at lower cost. It also takes less space in the varnish tank and in the oven. Moreover, use of prewound cores tends to shorten manufacturing cycles by permitting parallel manufacture of the motor frame and the prewound stator core along with the rotor. However, as the rating of machines increase, with a corresponding increase in physical size, a point is eventually reached at which the machines are too large for the prewound-core concept.

The size at which this occurs will, of course, vary from one manufacturer to another. For larger machines the stator punchings are stacked directly into the machined motor frame to produce the stator core, and the coils are wound directly into the stacked frame. For such construction the previous discussion is valid if it is remembered that the stator core is the stator core-in-frame and that the wound core is the wound frame.

9.2.8 Conductor Material

Electrical conductivity is obviously a very important physical property to consider in selecting a material for use as an electrical conductor, and it is essential for the material to have the greatest conductivity possible consistent with cost. The stator winding resistance loss is a significant component of the total losses of the machine and, accordingly, has a corresponding effect on efficiency. The power output of a given machine is limited by the temperature rise of the windings, and the stator I^2R loss is the largest contributor to the temperature rise of the stator winding. However, other physical properties, such as thermal conductivity, specific heat, and density, are also important, as will become apparent subsequently when such topics as motor heating and motor application are discussed. In addition, ductility is an important property for drawing the wire through dies for sizing as well as for forming the coil shape.

Of the materials that occur in nature, aluminum, copper, silver, and gold are the metallic elements that appear to have physical properties which would qualify them as good conductors. Because of the extremely small quantity of available gold, it may be disregarded for such an industrial use. Although silver is also reasonably scarce, its cost is approximately two orders of magnitude less than that of gold. Table 9.1 gives the abovementioned physical properties of aluminum, copper, and silver, except for ductility. All three of the metals have sufficient ductility to draw and to form adequately; beyond that, it is difficult to compare ductility in a simple but meaningful way. The cost of each metal is included with the physical properties in the table. The values are approximate because they will vary slightly, depending on purity, temperature, and so on. Also, the cost of the metals, in particular that of silver and copper, tends to fluctuate considerably. All values in the table are normalized as a percentage of the corresponding value of silver.

TABLE 9.1 Approximate Properties of Three Electrical Conducting Materials

	Metal (%)[a]		
Property	Aluminum	Copper	Silver
Electrical conductivity	57-60	94-97	100
Thermal conductivity	48	93	100
Specific heat (weight)[b]	383	165	100
Specific heat (volume)[c]	99	140	100
Density	26	85	100
Cost[d]	0.72	0.77	100

[a] All values are normalized on the corresponding value of silver.

[b] Specific heats are compared on the basis of energy/°C/unit weight.

[c] Specific heats are compared in the basis of energy/°C/unit volume.

[d] Costs are compared on the basis of equal weight.

The cost of silver is more than 100 times that of aluminum and of copper on the basis of equal weights. On the basis of equal volumes, the cost of silver is about 36 times that of aluminum and 110 times that of copper. Obviously, the cost of silver eliminates it from practical consideration for use in motor windings. If aluminum and copper are compared on the basis of weight, they are approximately equal in cost; if they are compared on the basis of volume, the cost of aluminum is one-third that of copper. Thus aluminum would appear to be a favorable choice. However, the conductivity of aluminum is approximately two-thirds of that of copper, so that it would be necessary to increase the cross-sectional area of the stator conductor and of the stator slot by an appropriate amount in order to maintain the same value of stator resistances and hence the same value of machine efficiency as that provided by copper. Because of ferromagnetic saturation, such a change would cause the stator-tooth flux density to be prohibitively high for the same amount of magnetic steel in the stator core. To compensate for this, it would be necessary to increase the amount of active material in the machine, by using a larger core diameter, a longer core length, or both. Increasing the physical size of the machine would, of course, adversely affect its cost. It is for such reasons as discussed above that copper has been selected as the choice of materials for stator conductors. It should be noted, however, that aluminum is a very commonly used material for squirrel-cage rotor windings, where other factors are present. This is discussed more fully in Chapter 10.

9.2.9 Turns, Conductors, and Strands

Each coil side, which occupies half of a slot, has a specific number of active conductors that are embedded in the slot of the magnetic core and are under the influence of the rotating flux wave. One turn of the complete coil consists of such a conductor in each of two companion coil sides, located one coil throw apart, and joined by extensions of the conductors through the end turns. Thus there are as many turns per coil as there are active conductors per coil side. The number of conductors per slot is equal to twice the number of conductors per coil side, or to twice the number of turns per coil. Then

$$N_c = \frac{Z_s}{2} \quad \text{numeric} \tag{9.1}$$

where N_c is the number of turns/coil and Z_s is the conductors/slot.

Accordingly, a given stator phase winding has twice as many series conductors per phase as series turns per phase. As will become apparent later in this chapter, as well as in Chapter 13, in which leakage reactance and magnetizing reactance are considered, the number of series turns per phase is an important quantity in determining machine performance.

Early in the process of designing a polyphase induction motor, the number of stator slots N_1 and the number of series turns per phase N_{st} will have been determined. These quantities then determine the number of conductors per slot Z_s that are required for the design. The net cross-sectional area within the slot available for the conductors is determined by subtracting the cross-sectional area of the wedge, ground insulation, and for random windings, separator strips between coil sides. Also, any other committed space within the slot, such as temperature-detector strips, must be subtracted from the slot space. The remaining cross-sectional area of the slot is available for the insulated conductors within that slot (see Figs. 9.6 and 9.9).

Since round wire is used for random windings, this area must be multiplied by a factor in the region of $\pi/4 = 0.785$, in order to give the solid cross-sectional area that can be occupied by the round insulated copper wire. This reduced net area divided by the conductors per slot Z_s gives the area available for each insulated random conductor. The resulting area per conductor will usually be larger than is desired, because of practical considerations of windability. Then several smaller wires in parallel, with a combined area equal to the available space, is used as one equivalent conductor. Since the several smaller wires are effectively short circuited at the ends of each coil, they act in parallel and have the same electromagnetic effect as an individual conductor, with a larger cross-sectional area for carrying current. Such a practice of winding a random-wound stator core with a certain number of strands of round wire in parallel to form a larger conductor is called winding with that number of "wires in hand."

A formed-coil winding utilizes rectangular conductors in a rectangular slot; accordingly, the net cross-sectional area available for each conductor is determined in terms of width and depth dimensions (see Fig. 9.9). The total ground insulation required in the width direction is subtracted from the slot width to give the width of the net conductor area. The slot wedge depth, the total ground insulation required in the depth direction, and any other depth space that is used for a desired purpose, such as for temperature detectors, are subtracted from the stator slot depth to give the total depth of the net space available for all conductors of the slot. This quantity, divided by the number of conductors per slot, gives the depth of the net conductor area. To reduce spurious eddy currents induced in the conductor due to the cross-slot leakage flux, the copper depth of each conductor should not exceed 0.20 in. and preferably, should be less. Since the depth space available for each conductor will generally exceed this amount and since the greater depth is required to limit the current density of the conductor, it is frequently necessary to use two or more strands in parallel for each conductor. Again, since the several strands that comprise such a conductor are effectively short circuited at the ends of each coil, the strands act in parallel and form one conductor.

For both random-coil and formed-coil windings, the net slot space that is available for conductors include the space to be used for the copper and the conductor insulation. Sufficient insulation is required between conductors to withstand the turn-to-turn voltage. This is usually accomplished by the use of enamel on round wire and by the use of enamel or serving on rectangular wire. Also, the strand wire is usually insulated to be adequate for the normal turn-to-turn voltage. In some large, formed-coil designs, the turn-to-turn voltage is considerable, and for such cases, additional insulation is added between the turns.

9.3 EDDY-CURRENT LOSSES IN THE COPPER WITHIN THE SLOT

As noted above, it is necessary to limit the thickness of conductors used in formed coils in order to limit the magnitude of spurious eddy-current losses produced in the slot portion of the coil caused by the cross-slot leakage flux. This is accomplished by using two or more insulated strands to form each turn if the thickness of the turn exceeds 0.150 to 0.200 in. The value of the actual I^2R loss of the stator winding with the spurious eddy-current losses considered can be significantly greater than that of the conventionally calculated I^2R loss, in which these additional losses are not considered if proper stranding practices are not used. These additional losses can produce greater heating of the slot portion of the stator winding and a lower true efficiency than anticipated, particularly in machines with ratings above 1500 hp.

The flow of current through the conductors within a stator slot produces a flux that encircles the conductors, called the stator-slot leakage flux. The leakage flux path is across the slot, from one side to the other, and then through the iron path around the slot provided by the adjacent teeth and the core yoke behind the slot. The reluctance of the iron path is negligible in comparison to that across the slot, so that the slot width and depth essentially determine the reluctance of the path to the flow of slot leakage flux. Figure 9.11 shows the distribution of the slot leakage flux density as a function of the slot depth.

The relationship between flux density B and the corresponding magnetic field strength that produces it is

$$B = \mu H \quad \text{webers/meter}^2 \tag{9.2}$$

where μ is the permeability in henrys/meter and H is the magnetic field strength in amperes/meter. The value of μ for the nonferrous material

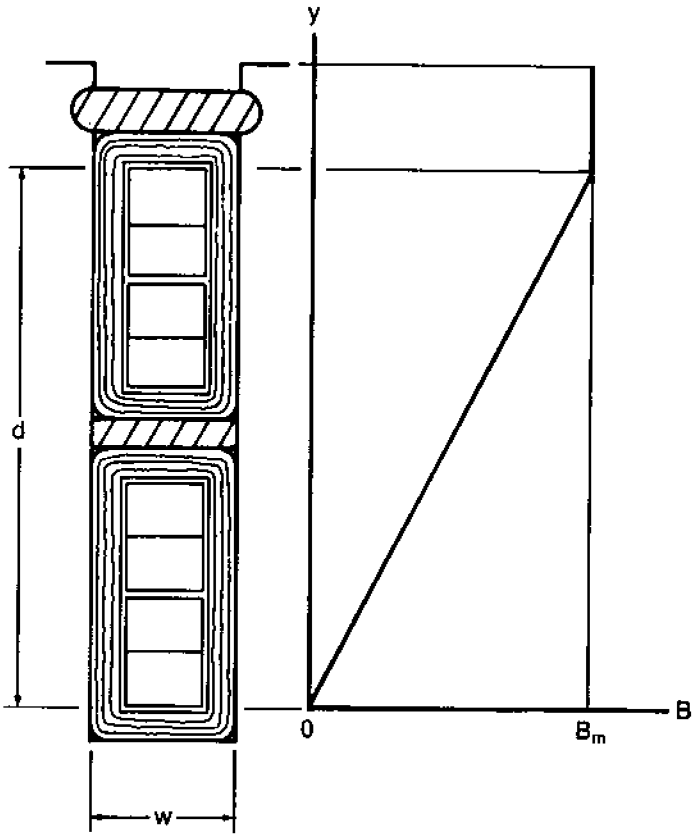

FIGURE 9.11 Cross-slot leakage flux density.

within the slot is $4\pi \times 10^{-7}$ H/m. The total value of H acting across the slot in Fig. 9.11 is

$$H = \frac{2K_sN_c \text{ (amperes/turn)}}{w} \quad \text{amperes/meter} \tag{9.3}$$

where K_s is the phase angle factor (dimensionless) and w is the slot width in meters. K_s is a factor that adjusts for any difference in phase angle between the currents in the two coil sides and which is a function of the coil pitch. This factor is considered in Chapter 13; for the present it is only necessary to know that the value of K_s is 1.0 for a full-pitch coil and somewhat less than 1.0 for a fractional-pitch coil. Substituting the values for μ and for H into eq. (9.2) gives us

$$B_m = \frac{8\pi K_sN_c \text{ (amperes/turn)}}{w \times 10^7} \quad \text{webers/meter}^2 \tag{9.4}$$

Equation (9.4) gives the maximum value of the cross-slot flux density B_m, which occurs at the top of the slot (see Fig. 9.11). At any vertical distance y along the slot, the value of B is

$$B = \frac{y}{d} B_m \quad \text{webers/meter}^2 \tag{9.5}$$

where d is the vertical distance from the bottom of the bottom coil to the top of the top coil, as shown in Fig. 9.11. By use of eqs. (9.4) and (9.5), the cross-slot leakage flux may be calculated at any point along the depth of the slot.

Equation (9.4) may be expressed with B in units of maxwells/in.^{2} and with w in units of inches by remembering that 10^8 maxwells equal 1 weber and that 39.37 inches equals 1 meter. Then

$$B_m = \frac{6.38K_sN_c \text{ (amperes/turn)}}{w} \quad \text{maxwells/inch}^2 \tag{9.6}$$

Equation (9.5) remains unchanged as long as consistent units are used for y, d, B_m, and B.

The coil configuration within the slot will now be analyzed to determine the additional losses due to eddy currents produced by leakage flux. Figure 9.12 shows an individual strand (or conductor, if there is only one strand/conductor), of unit length within the conductor.

In general, a quantity ϕ' of cross-slot leakage flux will induce a voltage v in a path within the strand which bounds that flux, and the value of the induced voltage is

$$v = -\frac{d\phi'}{dt} \quad \text{volts} \tag{9.7}$$

Since ϕ' is sustained by the stator current, which varies sinusoidally, the cross-slot leakage flux also varies sinusoidally. This flux may be expressed as

$$\phi' = \phi \sin \omega t \quad \text{webers} \tag{9.8}$$

Then the voltage induced within the conductor is

$$v = -\frac{d}{dt}(\phi \sin \omega t) = -\omega\phi \cos \omega t \quad \text{volts} \tag{9.9}$$

and the maximum value of v is

$$V_m = \omega\phi = 2\pi f\phi \quad \text{volts} \tag{9.10}$$

Consider the quantity of cross-slot leakage flux in Fig. 9.12 which flows through the area defined by the unit length of the strand and by a vertical distance equal to 2z, which is centered about the horizontal centerline of the strand. Then

$$\phi = 2zB \quad \text{webers} \tag{9.11}$$

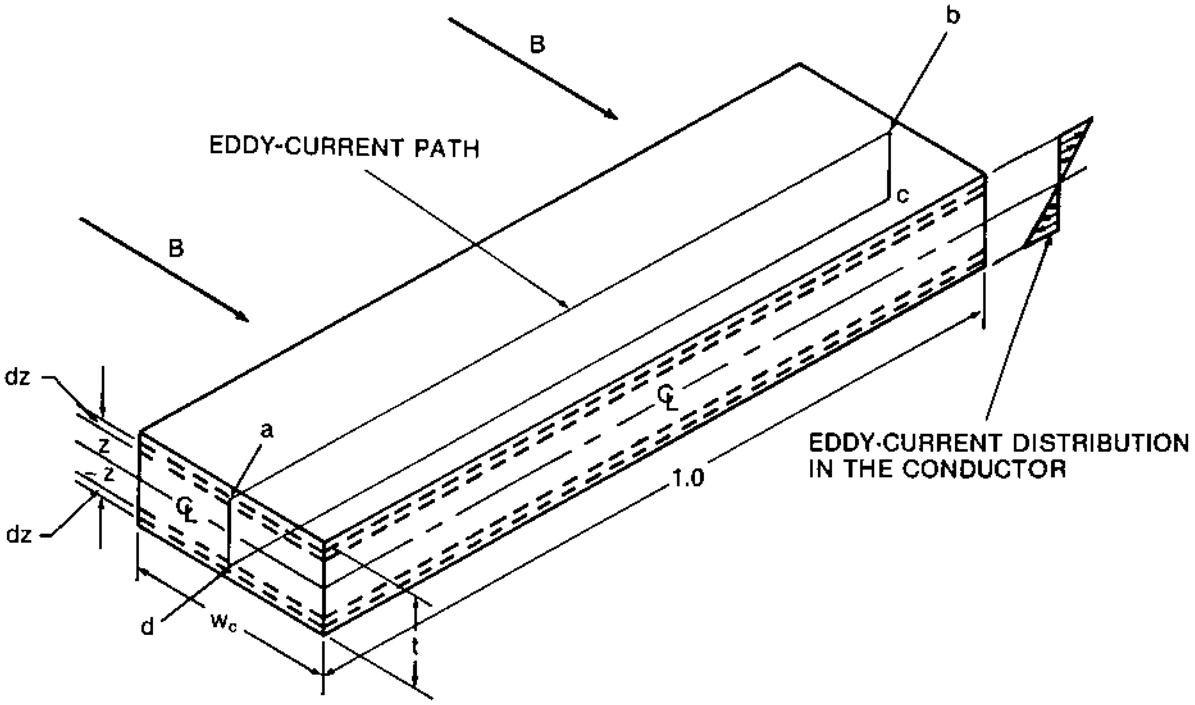

FIGURE 9.12 Stator coil strand, showing incremental eddy-current path.

Substituting eq. (9.11) into eq. (9.10) yields

$$V_m = (2\pi f)(2zB) = 4\pi fzB \quad \text{volts} \tag{9.12}$$

The maximum value of the current flowing in element dz in Fig. 9.12 is

$$I_m = \frac{V_m}{R} \quad \text{amperes} \tag{9.13}$$

and

$$R = \frac{\rho \ell_e}{A} \quad \text{ohms} \tag{9.14}$$

where

ρ = resistivity of copper, ohm-meters
ℓ_e = length of the elemental path, meters
A = cross-sectional area of the elemental path, meters^2

The length of the elemental path is

$$\ell_e = 2\ell + 4z \quad \text{meters} \tag{9.15}$$

However, since ℓ is, by definition, equal to unit length, 2ℓ is much greater than $4z$ and the length of the elemental path is essentially equal to $\ell_e = 2$. Also,

$$A = W_c\, dz \quad \text{meters}^2 \tag{9.16}$$

Then

$$R = \frac{2\rho}{W_c\, dz} \quad \text{ohms} \tag{9.17}$$

Substituting eq. (9.17) into eq. (9.13), the maximum value of the current in element dz in Fig. 9.12 is found to be

$$I_m = \frac{V_m W_c\, dz}{2\rho} \quad \text{amperes} \tag{9.18}$$

and the maximum value of the current density j_m in the element dz is

$$j_m = \frac{I_m}{A} = \frac{V_m}{2\rho} \quad \text{amperes/meter}^2 \tag{9.19}$$

Substituting the value of V_m from eq. (9.12) into eq. (9.19) and simplifying yields

$$j_m = \frac{2\pi f B z}{\rho} \quad \text{amperes/meter}^2 \tag{9.20}$$

The average loss density g in the element dz is

$$g = \frac{j_m^2 \rho}{2} \quad \text{watts/meter}^3 \tag{9.21}$$

Using the value of j_m from eq. (9.20) in eq. (9.21), we obtain

$$g = \frac{2\pi^2 f^2 B^2 z^2}{\rho} \quad \text{watts/meter}^3 \tag{9.22}$$

Equation (9.22) gives the average loss density g as a function of z for the element dz. The total loss in a unit length of the strand is equal to eq. (9.22) integrated over the thickness of the strand, with the integral multiplied by the strand width W_c:

$$L_c = W_c \int_{-t/2}^{t/2} \frac{2\pi^2 f^2 B^2 z^2}{\rho}\, dz = \left. \frac{2\pi^2 f^2 B^2 W_c z^3}{3\rho} \right|_{-t/2}^{t/2}$$

$$= \frac{\pi^2 f^2 B^2 W_c t^3}{6\rho} \quad \text{watts} \tag{9.23}$$

The volume of the unit length of strand in Fig. 9.12 is equal to

$$V_c = W_c t \quad \text{meters}^3 \tag{9.24}$$

Accordingly, at any point in the slot where the cross-slot leakage flux density is equal to B, the average loss density in the strand is equal to

$$D_c = \frac{L_c}{V_c} = \frac{(\pi f B t)^2}{6\rho} \quad \text{watts/meter}^3 \tag{9.25}$$

Equation (9.25) shows that the average loss density D_c in a stranded conductor varies as B^2. From eq. (9.5), B varies directly as the distance from the bottom of the bottom strand, or as y (see Fig. 9.11). Then

$$D_c = ky^2 \quad \text{watts/meter}^3 \tag{9.26}$$

where k is a constant. From this relationship, the average loss density in the top coil side, which occupies the top half of the slot, may be calculated by integrating eq. (9.26) from d/2 to d.

$$D_{tc} = \frac{k}{d/2} \int_{d/2}^{d} y^2 \, dy = \frac{2k}{d} \left. \frac{y^3}{3} \right|_{d/2}^{d}$$

$$= \frac{7}{12} kd^2 \quad \text{watts/meter}^3 \tag{9.27}$$

The average loss density in the top strand in the top coil side is equal to kd^2. Accordingly, the ratio of the average loss density in the top coil side to the average loss density in the top strand is

$$\frac{(7/12)kd^2}{kd^2} = \frac{7}{12} \quad \text{numeric} \tag{9.28}$$

Thus the average eddy loss density in the top coil side is equal to (7/12)(100) = 58.3% of that in the top strand of the slot.

The average loss density in the bottom coil side, which occupies the bottom half of the slot, is

$$D_{bc} = \frac{k}{d/2} \int_{0}^{d/2} y^2 \, dy = \frac{2k}{d} \left. \frac{y^3}{3} \right|_{0}^{d/2}$$

$$= \frac{kd^2}{12} \quad \text{watts/meter}^3 \tag{9.29}$$

The ratio of the average loss density in the bottom coil side to that in the top strand of the top coil is obtained by dividing eq. (9.29) by kd^2, or

$$\frac{(1/12)kd^2}{kd^2} = \frac{1}{12} \quad \text{numeric} \tag{9.30}$$

From eq. (9.30) the average eddy loss density in the bottom coil side is equal to (1/12)(100) = 8.3% of that in the copper in the top strand in the slot.

The average eddy loss density in both coil sides in the slot, in terms of that in the copper at the top of the slot, is equal to the average of that determined for the top coil side and for the bottom coil side, or to

$$\frac{7/12 + 1/12}{2} = \frac{1}{3} \quad \text{numeric} \tag{9.31}$$

The magnitude of eddy losses that occur in the slot portion of formed coils, due to trans-slot leakage flux, may be summarized as follows:

1. Average loss density in the top strand, at the top of the slot:

$$D_{ts} = \frac{(\pi f B_m t)^2}{6\rho} \quad \text{watts/meter}^3$$

2. Average loss density in the top coil side:

$$D_{tc} = \frac{(7/12)(\pi f B_m t)^2}{6\rho} \quad \text{watts/meter}^3$$

3. Average loss density in the bottom coil side:

$$D_{bc} = \frac{(1/12)(\pi f B_m t)^2}{6\rho} \quad \text{watts/meter}^3$$

4. Average loss density in both coil sides:

$$D_{av} = \frac{(1/3)(\pi f B_m t)^2}{6\rho} \quad \text{watts/meter}^3$$

where B_m is the leakage flux density in webers/meter^2 at the top of the slot. The value of B_m may be calculated from eq. (9.4).

Equation (9.25) may be expressed in units of watts/inch^3, with B in units of maxwells/inch^2, with t in units of inches and with ρ in units of ohm-inches, by remembering that there are 10^8 maxwells in 1 weber and that there are 39.37 inches in 1 meter. The average loss density in the top strand of the slot is then equal to

$$D_{ts} = \frac{(\pi f B_m t)^2}{6\rho \times 10^{16}} \quad \text{watts/inch}^3 \tag{9.32}$$

The average loss densities in the top coil side and in the bottom coil side, as well as the average for both coil sides when considered together, relative to that in the top strand remains 7/12, 1/12, and 1/3, respectively.

9.4 ADDITIONAL WINDING LOSSES DUE TO CIRCULATING CURRENTS IN THE STRANDS

Additional spurious losses occur in the winding due to circulating currents between the strands of a turn, which are short circuited at the ends of the coil. In Fig. 9.13a, strands 1a and 1b form the top turn of the top coil side in one slot. One coil throw away, the same two strands form the bottom turn of the companion coil side and the position of the two turns is reversed in the two slots. The cross-slot leakage flux density experienced by the two strands is different and, accordingly, the voltage induced in the two strands by that flux density will be different. Since the two strands that form a turn are short circuited at the ends of the coil, a circulating current will flow around the circuit consisting of the two strands and will produce additional losses within that circuit.

For the present it will be assumed that the vertical thickness of the strand insulation relative to the copper thickness is negligible. Then, by inspection of Fig. 9.13a, the average value of the alternating flux density at the junctions between strands, is equal to

$$B_{av} = \frac{B_m}{2}\left(\frac{1/4 + 3/4 + 1/4 + 3/4}{4}\right) = \frac{B_m}{4} \quad \text{webers/meter}^2 \tag{9.33}$$

The flux acting to induce strand-to-strand voltage, in unit length of the strand, is equal to

$$\phi = \frac{B_m}{4} t \quad \text{webers} \tag{9.34}$$

based on the assumption that $t = t_i$ in Fig. 9.13. The maximum value of the voltage generated in unit length of strand by the leakage flux ϕ is

$$V_m = 2\pi f \phi \quad \text{volts} \tag{9.35}$$

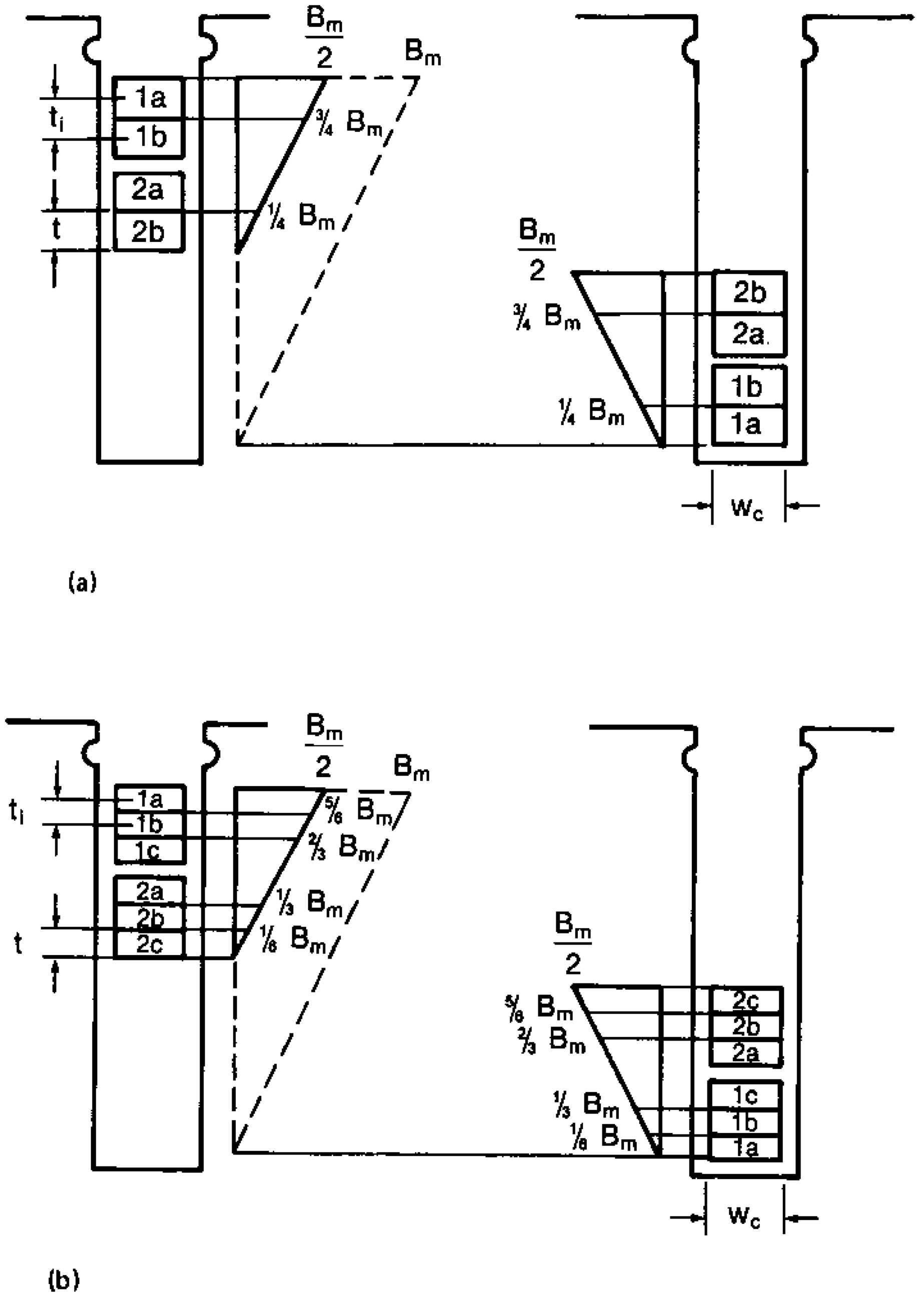
$\frac{B_m}{2}$
B_m
1a
1b
2a
2b
t_i
t
$\frac{3}{4} B_m$
$\frac{1}{4} B_m$
W_c
(a)
1c
2c
$\frac{5}{6} B_m$
$\frac{2}{3} B_m$
$\frac{1}{3} B_m$
$\frac{1}{6} B_m$
(b)

FIGURE 9.13 Cross-slot leakage flux density for companion coil sides located one coil throw apart: (a) two-turn coil with two horizontal strands/turn; (b) two-turn coil with three horizontal strands/turn.

Substituting eq. (9.34) into eq. (9.35) gives us

$$V_m = 2\pi f \frac{B_m}{4} t \quad \text{volts} \tag{9.36}$$

The maximum value of the circulating current is

$$I_m = \frac{V_m}{R} \quad \text{amperes} \tag{9.37}$$

where the resistance for unit length along the slot is

$$R = \frac{\rho \ell_s}{A} \quad \text{ohms} \tag{9.38}$$

Since current I_m in eq. (9.37) circulates around the loop of the complete diamond coil, the resistance of the copper in the end turns, as well as that of the slot portion, is acting to impede the flow of this current. Then, for unit length along the slot,

$$\ell_s = 2\left(\frac{\ell_t}{\ell_c}\right) \quad \text{meters} \tag{9.39}$$

where ℓ_c is the core length in meters and ℓ_t is the total length of one strand in one coil side, or one-half of the mean length of a coil turn, in meters. Although the analysis is based on a unit length of strand within the slot, the factor ℓ_t/ℓ_c adjusts for the additional resistance of the end-turn portion of the strand, referred to 1 unit of slot length.

The value of A in eq. (9.38) is

$$A = W_c t \quad \text{meters}^2 \tag{9.40}$$

Then the value of R is

$$R = \frac{2\rho}{W_c t} \frac{\ell_t}{\ell_c} \quad \text{ohms} \tag{9.41}$$

Substituting eqs. (9.36) and (9.41) into eq. (9.37), we obtain the maximum value of the circulating current:

$$I_m = \frac{\pi f(B_m/4)W_c t^2}{\rho} \frac{\ell_c}{\ell_t} \quad \text{amperes} \tag{9.42}$$

and the maximum value of the current density:

$$j_m = \frac{\pi f B_m t}{4\rho}\,\frac{\ell_c}{\ell_t} \quad \text{amperes/meter}^2 \tag{9.43}$$

The average loss density due to the circulating current in the strand is equal to

$$g = \frac{j_m^2 \rho}{2} \quad \text{watts/meter}^3 \tag{9.44}$$

or

$$g = \frac{\pi^2 f^2}{2\rho}\,\frac{B_m^2}{16}\,t^2\left(\frac{\ell_c}{\ell_t}\right)^2 \quad \text{watts/meter}^3 \tag{9.45}$$

It has been assumed that the strand insulation thickness was insignificant in comparison to the strand copper thickness. If the strand insulation thickness is sufficiently thick as to be considered, eq. (9.45) should be multiplied by $(t_i/t)^2$. By inspection of Fig. 9.13, it is apparent that with t_i being slightly greater than t, the value of B_{av} and of $B_m/4$ would change by the ratio t_i/t. Since B_m appears as a factor to the second power in eq. (9.45), B_m^2 should be multiplied by the factor $(t_i/t)^2$ in that equation. Accordingly,

$$g = \left(\frac{1}{2}\right)\left(\frac{1}{16}\right)\left(\frac{\ell_c}{\ell_t}\right)^2\left(\frac{t_i}{t}\right)^2 \frac{\pi^2 f^2 B_m^2 t^2}{\rho} \quad \text{watts/meter}^3 \tag{9.46}$$

Equation (9.46) can be written as

$$g = \frac{3}{16}\left(\frac{\ell_c t_i}{\ell_t t}\right)^2 \frac{(\pi f B_m t)^2}{6\rho} \quad \text{watts/meter}^3 \tag{9.47}$$

It was shown previously that the average loss density due to eddy current loss in the top strand at the top of the slot is equal to $(\pi f B_m t)^2/6\rho$ watts/meter^3. Thus the average loss density in a unit length of the slot due to currents circulating between strands is equal to $(3/16)(\ell_c/\ell_t)^2(t_i/t)^2$ or to $0.188(\ell_c/\ell_t)^2 \times (t_i/t)^2$ of the average loss density occurring in the top strand of the slot due to eddy-current loss.

The value of loss caused by circulating currents is based on a two-turn coil with two horizontal strands per turn, as shown in Fig. 9.13a. Figure 9.13b shows a two-turn coil with three horizontal strands/turn. If that configuration is analyzed in a similar way, the results are the same except that the factor 3/16 in eq. (9.47) is replaced by the factor 1/2.

9.5 SLOT FACTOR

The additional losses occurring within the slot portion of the stator winding from eddy currents within the strand copper and from circulating currents between strands was developed in Sections 9.3 and 9.4. These losses may be expressed in a more general and useful way. The combination of the two spurious losses above may be expressed as

$$D = \left[K_1 + K_2\left(\frac{\ell_c}{\ell_t}\,\frac{t_i}{t}\right)^2\right]\frac{(\pi f B_m t)^2}{6\rho} \quad \text{watts/meter}^3 \qquad (9.48)$$

where

K_1 = 0.333 when considering the average of the top and bottom coils
K_1 = 0.584 when considering the top coil only
K_1 = 0.083 when considering the bottom coil only
K_2 = 0.188 for two vertical strands/turn, two turns/coil
K_2 = 0.500 for three vertical strands/turn, two turns/coil

The foregoing values of K_2 are limited to the types of coils for which these values were determined: a two-turn coil with two strands per turn or a two-turn coil with three strands per turn. Both types of coils are frequently encountered in machine ratings associated with significant spurious losses in the stator slot.

To use eq. (9.48), the total volume of stator winding copper that is embedded within the slots is calculated and multiplied by eq. (9.48) to determine the additional losses caused by the cross-slot leakage flux. For smaller sizes of polyphase induction motors, this additional loss is normally too insignificant to consider from a practical standpoint. However, as the machine size increases, a point is eventually reached at which it could be significant. This point will vary depending on design practices of the particular manufacturer. It is reasonable that at ratings of 1500 to 2000 hp, the additional losses should at least be calculated to see if they are significant.

When using eq. (9.48), the value K_1 = 0.333 should be used when calculating stator I^2R losses for efficiency or power-factor considerations, since that value corresponds to the average loss throughout the slot. On the other hand, the value K_1 = 0.584 should be used when considering total loss density, as it relates to maximum coil temperature in the upper half of the stator slot and is frequently useful in calculating the coil hot-spot temperature. For this case the average loss density in the top coil, when multiplied by the copper volume of the top coil, embedded within the slot, gives the additional loss within the top coil.

Equations (9.47) and (9.48) may be expressed in units of watts/inch^3, with B_m in units of maxwells/inch^2, with t in units of inches and with ρ in units of ohm-inches by remembering that there are 10^8 maxwells in 1 weber and that there are 39.37 inches in 1 meter. Then eq. (9.47) may be written as

$$g = \frac{3}{16}\left(\frac{\ell_c t_i}{\ell_t t}\right)^2 \frac{(\pi f B_m t)^2}{6\rho \times 10^{16}} \quad \text{watts/inch}^3 \tag{9.49}$$

and eq. (9.48) may be written as

$$D = \left[K_1 + K_2\left(\frac{\ell_c t_i}{\ell_t t}\right)^2\right]\frac{(\pi f B_m t)^2}{6\rho \times 10^{16}} \quad \text{watts/inch}^3 \tag{9.50}$$

The numerical factors K_1 and K_2 remain unchanged, of course.

9.6 NUMERICAL EXAMPLE OF CALCULATION OF EDDY-CURRENT LOSS AND STRAND LOSS IN A STATOR WINDING

Determination of the additional losses in the stator winding due to cross-slot leakage flux will be illustrated using a numerical example. However, the 1000-hp induction motor used for previous numerical examples is too small in power rating for this effect to be significant, as the total of the additional losses occurring within the stator winding would not exceed a few percent of the normal stator I^2R losses, even if each stator conductor was not optimally divided into the proper number of strands. The probable variation between calculated and measured stator I^2R loss is usually in excess of 1% or so. Accordingly, a numerical example with a greater power rating will be used.

It is apparent from eq. (9.3) that the magnetic field strength acting to force leakage flux across the stator slot is proportional to the total amperes per slot, which is proportional to the power rating of the machine. From eq. (9.4) it is also apparent that the maximum value B_m of the alternating, cross-slot flux density is proportional to the cross-slot magnetic field strength, which varies with the power rating of the machine. Since the loss density of the spurious losses in the winding are proportional to B_m^2, a point is soon reached in the power rating of the machine at which the additional losses become significant if proper winding-design practices are not followed. To illustrate the calculation of these losses a 5000-hp polyphase induction motor will be used for the example, the stator-winding design of which is not fully optimized in order to emphasize these losses. For such a rating, the additional stator winding losses can be 10% or more of the normal stator I^2R loss if proper winding-design practices are not followed.

The numerical example will evaluate the eddy current and strand losses for a design with two turns/coil, or $N_c = 2$, and with the particular slot size shown in Fig. 9.14. As part of that evaluation, the additional losses from eddy currents and from circulating currents between strands will be determined for the two-turn coil for the following two cases of conductor stranding:

Case 1: Two-turn coil, two strands/turn
Case 2: Two-turn coil, three strands/turn

One strand/turn will not be evaluated for this design, as the additional losses would be prohibitive and the conductor thickness would be impractical.

The maximum value of the cross-slot leakage flux B_m will first be calculated since its magnitude is required to determine the additional copper losses. From eq. (9.6), when units of maxwells and inches are used, B_m is equal to

$$B_m = \frac{(6.38)K_s N_c \text{ (amperes/turn)}}{w} \quad \text{maxwells/inch}^2 \tag{9.51}$$

Since a two-turn coil design is being evaluated, $N_c = 2$ for both cases. The factor K_s, which adjusts for the phase angle between the current in the two coil sides in one slot, is equal to 0.917 for a coil throw equal to 88.9% of a pole pitch, which is the coil throw for the design being considered. The expected full-load current of the motor is 621 A per phase, and using a series phase winding connected in wye with the other two phase windings, the current through the turns of each coil is equal to 621 A. From an inspection of Fig. 9.14, the slot width w is equal to 0.600 in. Substituting the values above into eq. (9.51) yields

$$B_m = \frac{(6.38)(0.917)(2)(621)}{0.600} = 12.1 \times 10^3 \quad \text{maxwells/inch}^2 \tag{9.52}$$

If MKS units are being used, the working equation is then eq. (9.4).

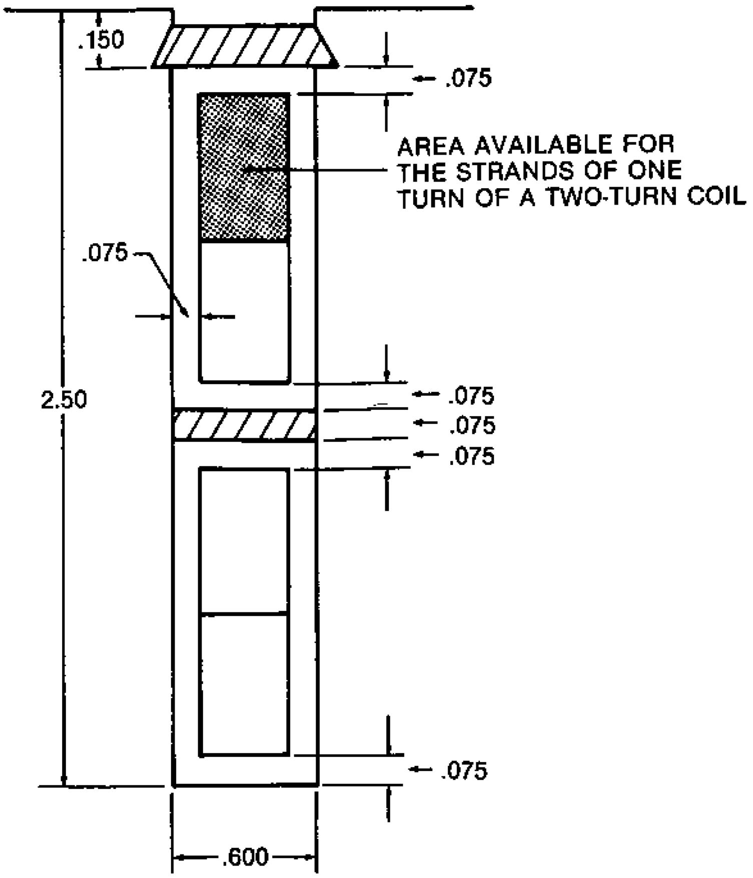
.150
.075
AREA AVAILABLE FOR THE STRANDS OF ONE TURN OF A TWO-TURN COIL
.075
2.50
.075
.075
.075
.075
.600

FIGURE 9.14 Stator-slot dimensions used in evaluating spurious slot losses at preliminary design stage.

$$B_m = \frac{8\pi K_s N_c \text{ (amperes/turn)}}{w \times 10^7} \quad \text{webers/meter}^2 \tag{9.53}$$

The width of the slot shown in Fig. 9.14 is equal to 1.52 cm (0.0152 m), and B_m is equal to

$$B_m = \frac{8\pi(0.917)(2)(621)}{(0.0152)(10^7)} = 0.1883 \quad \text{webers/meter}^2 \tag{9.54}$$

Next we check the value of B_m in eq. (9.54) against that in eq. (9.52):

$$B_m = \frac{(0.1883)(10^8)}{(39.37)^2} = 12.1 \times 10^3 \quad \text{maxwells/inch}^2 \tag{9.55}$$

which agrees with eq. (9.52).

Figure 9.14 shows the slot space available for one turn of the two-turn coil being evaluated. To determine the depthwise space available for the strands of one turn, a wedge-space allowance of 0.150 in., a midslot separator allowance of 0.075 in., and a total ground insulation allowance of 0.300 in. must be subtracted from the slot depth of 2.50 in., and the difference divided by (2 coil sides/slot)(2 turns/coil side) = 4 turns/slot. The depthwise space per turn is then equal to

$$\text{Depthwise space/turn} = \frac{2.50 - (0.150 + 0.075 + 0.300)}{4}$$

$$= 0.4938 \quad \text{inches} \tag{9.56}$$

Using an allowance of 0.015 in. for turn and/or strand insulation and selecting the next smaller available wire size, the copper thickness t of the strand and the depthwise distance t' between the horizontal centerlines of the strands for each of the two cases is as follows:

Case 1: $t = 0.230$ in. $t' = 0.245$ in.
Case 2: $t = 0.145$ in. $t' = 0.160$ in.

The copper width of the strand, for both cases, is equal to w, less the ground and the turn insulation allowance, or to 0.600 - (0.150 + 0.015) = 0.435 in.

From eq. (9.32), the average loss density in the top strand in the slot due to eddy-current losses is equal to

$$D_{ts} = \frac{(\pi f B_m t)^2}{6\rho \times 10^{16}} \quad \text{watts/inch}^3 \tag{9.57}$$

Using the value of B_m from eq. (9.52), the value of t from the tabulation above, and a value of resistivity for copper of $\rho = 0.890 \times 10^{-6}$ Ω-in. at 100°C, the average loss density in the top strand for case 1 is

$$D_{ts1} = \frac{[(\pi)(60)(12.1 \times 10^3)(0.230)]^2}{(6)(0.890)(10^{10})} = 5.15 \quad \text{watts/inch}^3 \tag{9.58}$$

Proceeding in a similar manner for case 2 and then tabulating the results for the two cases gives us:

Case 1: $D_{ts1} = 5.15$ W/in.^{3}
Case 2: $D_{ts2} = 2.05$ W/in.^{3}

From eq. (9.25), the average loss density in the top strand for a maximum value of cross-slot leakage flux density of B_m, with quantities expressed in MKS units, is

$$D_{ts} = \frac{(\pi f B t)^2}{6\rho} \quad \text{watts/meter}^3 \tag{9.59}$$

Using the value of B_m from eq. (9.54), the value of t from the tabulation, a value of resistivity for copper of $\rho = 2.26 \times 10^{-8}\ \Omega \cdot \text{m}$ at 100°C, and converting t from inches to meters, the loss density in the top strand for case 1 is

$$D_{ts1} = \frac{[\pi(60)(0.1883)(0.230)/39.37]^2}{(6)(2.26)(10^{-8})} = 317{,}000 \quad \text{watts/meter}^3 \tag{9.60}$$

To check eq. (9.60) against eq. (9.58), divide eq. (9.58), expressed in watts/meter^3, by $(39.37)^3$, the number of cubic inches in 1 cubic meter. Then

$$\frac{317{,}000}{(39.37)^3} = 5.19 \quad \text{watts/inch}^3 \tag{9.61}$$

Thus eqs. (9.57) and (9.59) give equivalent results when appropriate and consistent units are used with each equation.

To calculate the total losses in the winding resulting from cross-slot leakage flux, including the losses from circulating currents between the strands of a conductor, it is necessary to know the axial length ℓ_c of the stator core and the length ℓ_t of half of a coil turn. For the 5000-hp example, $\ell_c = 32$ in. and $\ell_t = 63$ in. From eq. (9.50), the average loss density in the slot portion of winding resulting from both eddy-current and strand loss is equal to

$$D' = \left[K_1 + K_2\left(\frac{\ell_c t_i}{\ell_t t_t}\right)^2\right] D_{ts} \quad \text{watts/inch}^3 \tag{9.62}$$

For case 1, $K_1 = 0.333$ for the average loss density for both coil sides embedded in the slot and $K_2 = 0.188$ for a two-turn coil with two strands/conductor. Then, using these values together with the value of D_{ts} for the top strand tabulated previously, the average loss density for the two coil sides embedded in the slot is equal to

$$D_1' = \left\{0.333 + 0.188\left[\frac{(0.230)(32)}{(0.245)(63)}\right]^2\right\}(5.15) = 1.94 \quad \text{watts/inch}^3 \tag{9.63}$$

and for case 2, remembering that $K_2 = 0.500$ for a two-turn coil with a three-strand conductor, we have

$$D_2' = \left\{0.333 + 0.500\left[\frac{(0.145)(32)}{(0.160)(63)}\right]^2\right\}(2.05) = 0.90 \quad \text{watts/inch}^3 \tag{9.64}$$

Tabulating the calculated values of D' for the two cases, we obtain

Case 1: $D_1' = 1.94$ W/in.^{3}
Case 2: $D_2' = 0.90$ W/in.^{3}

D' gives the average density of the spurious losses that occur in the top and bottom coil sides in the slot. The volume of the slot portion of the stator copper is equal to

$$V_s = N_1 A_s \ell_c \quad \text{inches}^3 \tag{9.65}$$

where N_1 is the number of stator slots and A_s is the cross-sectional area of copper in one slot in inches^2.

The machine used in the example has 72 stator slots. Also, A_s is calculated by multiplying the cross section of the bare-copper strand by the number of strands/slot. Then, for case 1,

$$V_{s1} = (72)(4)(2)(0.230)(0.435)(32) = 1844 \quad \text{inches}^3 \tag{9.66}$$

Performing similar calculations for case 2 and then tabulating the results for the two cases

Case 1: $V_{s1} = 1844$ in.^{3}
Case 2: $V_{s2} = 1744$ in.^{3}

The total spurious losses occurring in the copper embedded in the slot for the two cases is equal to

$$\Delta L = D'V_s \quad \text{watts} \tag{9.67}$$

and for case 1 specifically,

$$\Delta L_1 = D_1'V_{s1} \quad \text{watts} \tag{9.68}$$

Substituting the appropriate values from the preceding two tabulations into eq. (9.68) gives us

$$\Delta L_1 = (1.94)(1844) = 3577 \quad \text{watts} \tag{9.69}$$

Again, proceeding in a similar manner for case 2 and then tabulating the results for the two cases, we obtain:

Case 1: $\Delta L_1 = 3577$ W
Case 2: $\Delta L_2 = 1570$ W

To place the foregoing losses into perspective, the normal stator I^2R will be calculated for the stator winding corresponding to case 2. The resistance of the stator winding in ohms/phase is equal to

$$R_1 = \frac{\rho \ell}{A} \quad \text{ohms/phase} \tag{9.70}$$

where

ρ = resistivity of copper
ℓ = effective length of the stator phase winding
A = effective cross-sectional area of the phase winding

Equation (9.70) may be written as

$$R_1 = \frac{2\rho N_{st}\ell_t}{(N_c)(\text{area of one conductor})(\text{number of circuits})} \quad \text{ohms/phase} \tag{9.71}$$

where N_{st} is the number of series turns/phase, the number of circuits is the number of parallel circuits in the phase winding, and the other quantities are as defined earlier. For this example, $N_{st} = 48$ and the phase winding is a series circuit. Then

$$R_1 = \frac{(2)(0.89)(10^{-6})(48)(63)}{(3)(0.145)(0.435)(1)} = 0.0284 \quad \text{ohms/phase} \tag{9.72}$$

at 100°C. The normal full-load stator I^2R loss is then equal to

$$3I_1^2R_1 = (3)(621)^2(0.0284) = 32{,}857 \quad \text{watts} \tag{9.73}$$

The value of ΔL_1 and of ΔL_2, expressed as a percentage of normal stator copper loss, is as follows:

Case 1: $\frac{(3577)(100)}{32{,}857} = 10.9\%$

Case 2: $\frac{(1570)(100)}{32{,}857} = 4.8\%$

The eddy-current and strand losses for two strands/conductor in the tabulation above (i.e., for case 1) are too great to be acceptable; and these losses for case 2, although considerably less, are also significant. The design for this example was structured to ensure that the losses due to cross-slot leakage flux would be sufficient to illustrate the phenomenon, and the electrical design, intentionally, does not represent a fully optimized design for a 5000-hp induction motor. The design engineer would logically have selected two circuits/phase and a greater number of stator slots, such as 84 or 96. This would have the effect of reducing the magnetomotive force acting to force leakage flux across the stator slot, which would lower the spurious losses by the square of the per unit reduction. Also, the design engineer would have considered using a different number of turns/coil if that were necessary to achieve a physically realizable quantity for the series turns/phase, or N_{st}, to correspond to an increase in the number of stator slots. The concept of series turns/phase is considered in more detail later in this chapter when the voltage generated in the coil, in the group, and in the phase winding is investigated.

9.7 INDUCED VOLTAGE IN THE STATOR COIL

In the following discussion it will be assumed that the polyphase voltage, which is impressed across each of the stator phase windings, is balanced and that it has a sinusoidal wave shape. These assumptions are essentially correct for much of the voltage delivered by the electric-utility grid. However, they are not correct, in general, for the voltage output from such devices as rectifier-inverter systems, used to supply variable-frequency and variable-voltage power to synchronous and induction motors for variable-speed applications. Departure from a sinusoidal wave shape of the impressed voltage will result in time harmonics in the stator winding, and the effect of such harmonics for rectifier-inverter systems will be considered subsequently. Also, imbalance in voltage magnitude between phases of the impressed voltage will result in the flow of negative-sequence current in the motor windings. Such flow of negative-sequence current will result in additional spurious motor heating.

If the wave shape of the voltage impressed on the stator winding is sinusoidal and if there are sufficient slots/pole for each phase, the spatial distribution of the stator magnetomotive-force wave of each phase will approach, but will not exactly be, sinusoidal in shape. The deviation from a sine wave, which is usually not great, is due to the presence of space harmonics caused by the concentration of current within the stator coils, which give discrete steps along the air gap instead of a continuous distribution. For the present, however, it will be assumed that the magnetomotive-force wave has a sine-wave spatial distribution.

From eq. (3.11), the magnetomotive force produced by the three stator phase windings, each of which varies sinusoidally, combine to produce a rotating magnetomotive-force wave, with a magnetic field strength equal to

$$H_a = \frac{3H}{2} \sin(\omega t + \frac{\pi}{2} - \alpha) \quad \text{ampere-turns/meter} \tag{9.74}$$

relative to a fixed point on the stator, which is displaced α electrical degrees from the magnetic axis of the phase A winding. H is equal to the maximum field strength of each of the individual phase windings, in ampere-turns/meter. If the fixed reference point a is set for convenience, such that $\alpha = \pi/2$ electrical degrees, then eq. (9.74) may be written as

$$H_a = \frac{3H}{2} \sin \omega t \quad \text{ampere-turns/meter} \tag{9.75}$$

If the air gap is uniform in the radial dimension and if the preponderance of the magnetomotive force drop is across the air gap, with only a small percentage of the drop across the ferromagnetic portion of the magnetic circuit, the maximum value of the rotating air-gap flux-density wave B_m is nearly proportional to H_a. This is because of the fundamental relationship between flux density B and magnetic field strength H, that is,

$$B = \mu H \quad \text{webers/meter}^2 \tag{9.76}$$

The lack of exact proportionality between B_g and H_a is due to (1) the nonlinear magnetomotive-force drop of the flux paths in the steel stator and rotor cores, and to (2) the modulation from the slots of the otherwise uniform air-gap permeance. In addition, conditions 1 and 2 both contribute to total machine losses. Condition 1 contributes to saturation harmonics and condition 2 contributes to perturbations on the speed-torque curve and to zigzag leakage reactance, all of which is evaluated in appropriate chapters. However, conditions 1 and 2 normally have a minimal effect on the voltage that is induced in the stator coils by the air-gap flux density B_g, which will be assumed to vary sinusoidally.

From eqs. (9.75) and (9.76),

$$B_g = B_{gm} \sin \omega t \quad \text{webers/meter}^2 \tag{9.77}$$

where B_{gm} is the maximum value of B_g. The air-gap area/pole is equal to

$$A_p = \frac{\pi d \ell_c}{p} \quad \text{meters}^2 \tag{9.78}$$

where d is the stator bore diameter in meters, p is the number of poles, and ℓ_c is as defined previously. A_p is also equal to the air-gap area, which is bounded by a full-pitch coil. Then the flux/pole ϕ_p is equal to

$$\phi_p = \frac{2}{\pi} A_p B_{gm} \sin \omega t \quad \text{webers} \tag{9.79}$$

or to

$$\phi_p = \frac{2 d \ell_c}{p} B_{gm} \sin \omega t \quad \text{webers} \tag{9.80}$$

Equation (9.80) can be written as

$$\phi_p = \phi_{pm} \sin \omega t \quad \text{webers} \tag{9.81}$$

where ϕ_{pm} is the maximum value of the flux/pole and is equal to $2\,A_pB_{gm}/\pi$ webers.

Faraday's law, in the form given in eq. (2.12), relates the flux/pole and the instantaneous voltage induced in the coil which bounds that flux as

$$e_c = -N_c \frac{d\phi_p}{dt} \quad \text{volts} \tag{9.82}$$

where, as defined earlier in this chapter, N_c equals the number of turns/coil. Substituting eq. (9.81) into eq. (9.82) yields

$$e_c = -N_c \frac{d}{dt} (\phi_{pm} \sin \omega t) \quad \text{volts} \tag{9.83}$$

Equation (9.83) is expressed in instantaneous volts. To express the generated voltage in terms of rms, or effective, volts, we write

$$E_c = N_c \left[\frac{1}{\pi} \int_0^{\pi} \left(\frac{-d}{dt} \phi_{pm} \sin \omega t \right)^2 d\,\omega t \right]^{1/2} \quad \text{volts} \tag{9.84}$$

Performing the differentiation and multiplication inside the integral sign gives us

$$E_c = N_c\left[\frac{1}{\pi}\int_0^\pi (\phi_{pm}^2\ \omega^2 \cos^2 \omega t)\ d\,\omega t\right]^{1/2} \quad \text{volts} \tag{9.85}$$

Equation (9.85) may be written as

$$E_c = N_c\left(\frac{\phi_{pm}^2\omega^2}{\pi}\int_0^\pi \frac{1 + \cos 2\,\omega t}{2}\,d\,\omega t\right)^{1/2} \quad \text{volts} \tag{9.86}$$

which reduces to

$$E_c = N_c\left(\frac{\phi_{pm}^2\omega^2}{2}\right)^{1/2} = \frac{N_c\phi_{pm}\omega}{\sqrt{2}} \quad \text{volts} \tag{9.87}$$

Since $\omega = 2\pi f$, eq. (9.87) may be written as

$$E_c = \frac{2\pi}{\sqrt{2}}N_c\phi_{pm}f = 4.443N_c\phi_{pm}f \quad \text{volts} \tag{9.88}$$

The maximum value of flux/pole is in units of webers in eq. (9.88). If it is desired to use units of maxwells for ϕ_{pm}, the equation becomes

$$E_c = 4.443\left(\frac{N_c\phi_{pm}f}{10^8}\right) \quad \text{volts} \tag{9.89}$$

since there are 10^8 maxwells in 1 weber.

9.8 COIL-PITCH FACTOR

Equation (9.88) was derived for a full-pitch coil that spanned a full-pole pitch, or 180 electrical degrees. Essentially all stator windings are designed to have fractional-pitch coils, with a span of less than 180 electrical degrees, because this results in better designs, in general. The resulting machine will cost less overall, since the total amount of copper in the winding is reduced, even though the amount of steel in the magnetic core might be slightly increased. Also, the permeance to end-turn leakage reactance is reduced, resulting is less total leakage reactance for a given amount of mutual flux. Since output of an induction motor is limited by leakage reactance and by temperature rise, reduction of leakage reactance is frequently important when the design goal is to obtain more power output from a given amount of active material. In addition, judicious selection of the coil pitch is useful in controlling some of the space harmonics. However, use of a fractional-pitch coil will result in a slight reduction in the voltage generator in the coil. The ratio of the actual voltage induced in a coil to the voltage that would be induced in the same coil if it had a full span of 180 electrical degrees is called the coil pitch factor K_p.

The two sides of a given coil are in series and, accordingly, the voltage that is induced in the complete coil must equal the sum of the voltages existing in the two sides of that coil. If a given coil spans β electrical degrees, one coil side is β electrical degrees ahead of the other and the voltage vector of one coil side is displaced from that of the other coil side by β electrical degrees. See Fig. 9.15, in which E_{c1} represents the voltage existing in one coil side and E_{c2} represents that existing in the other coil side. One coil side is under the influence of a given pole and the companion coil side is under the influence of a pole of opposite polarity and, accordingly, the voltages existing in the two coil sides, at any instant of time, tend to be in opposite physical directions along the coil sides. However, the two voltages will add, since the two coil sides form a series circuit and since a progression around the series circuit will pass the two coil sides in opposite physical directions.

The vector resultant of E_{c1} and E_{c2} is determined by reversing the direction of one of the voltage vectors and then by adding this reversed vector to the other vector. In Fig. 9.15, vector E_{c2} is reversed to give $-E_{c2}$ and then added to vector E_{c1} to give the vector resultant E_{cr}. It is apparent from the figure that the vector resultant E_{cr} is equal to

$$E_{cr} = E_{c1} \cos\left(90 - \frac{\beta}{2}\right) + (-E_{c2}) \cos\left(90 - \frac{\beta}{2}\right) \quad \text{volts} \tag{9.90}$$

However, the magnitudes of the voltages of the two coil sides are equal, or

$$[E_{c1}] = [E_{c2}] = E \quad \text{volts} \tag{9.91}$$

so that

$$E_{cr} = 2E \cos\left(90 - \frac{\beta}{2}\right) = 2E \sin \frac{\beta}{2} \quad \text{volts} \tag{9.92}$$

If the coil had been a full-pitch coil, the corresponding vector resultant E'_{cr} would have been

$$E'_{cr} = 2E \quad \text{volts} \tag{9.93}$$

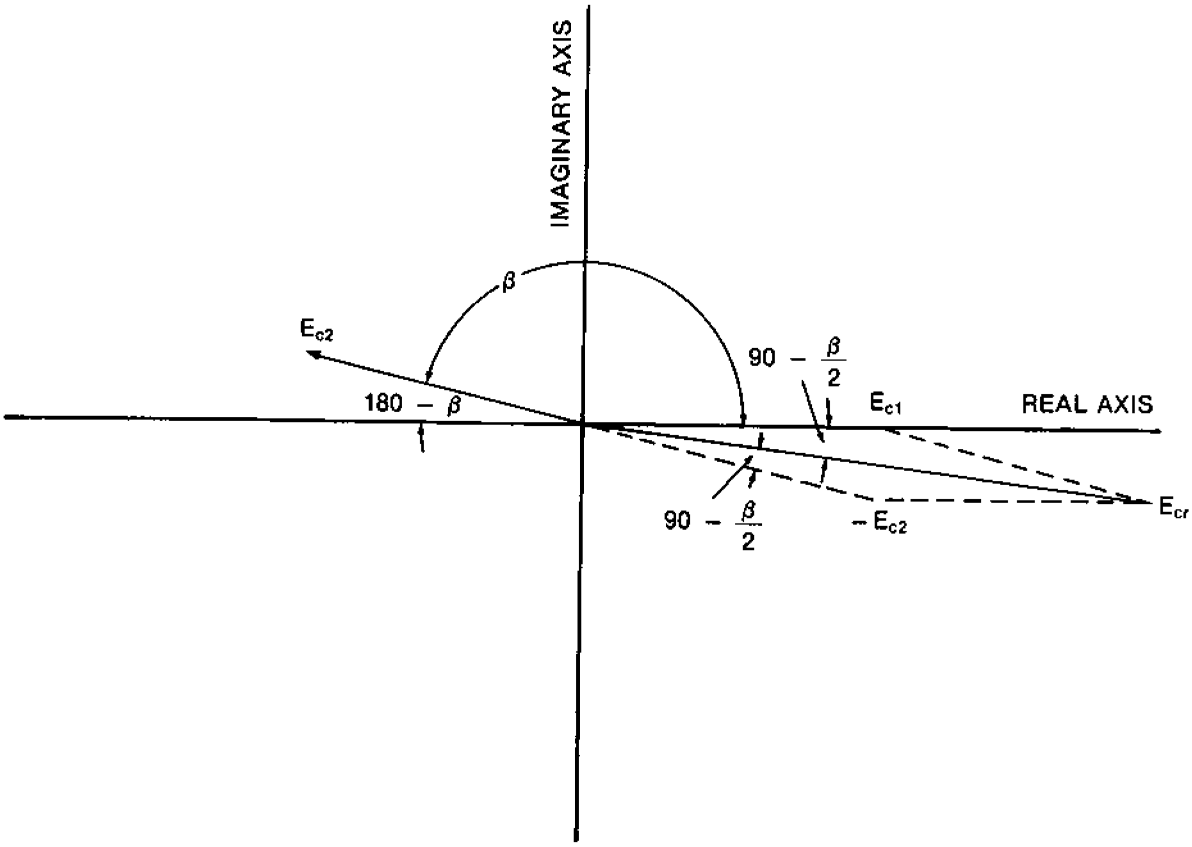

FIGURE 9.15 Resultant of the voltages in the two sides of a coil.

The pitch factor K_p is then equal to eq. (9.92) divided by eq. (9.93), or to

$$K_p = \frac{2E}{2E} \sin \frac{\beta}{2} = \sin \frac{\beta}{2} \quad \text{numeric} \tag{9.94}$$

For convenience, the term $\beta/2$ in eq. (9.94) is usually written as being equal to the per unit coil pitch, multiplied by 180/2 electrical degrees, or as

$$K_p = \sin\left[(\text{p.u. pitch})(90)\right] \quad \text{numeric} \tag{9.95}$$

The coil pitch factor can be calculated for any coil throw by using eq. (9.95). Assume that a four-pole stator has 84 slots and that the coil throw is 1 and 19. A coil throw of 1 and 19 corresponds to the coil spanning 18 slots. If the stator coil was a full-pitch one, the coil would span 84/4 = 21 slots. Then, from eq. (9.95), the coil pitch factor for the coil with a 1 and 19 throw is

$$K_p = \sin \frac{18}{21}(90) = 0.975 \quad \text{numeric} \tag{9.96}$$

The coil voltages given in eqs. (9.88) and (9.89) were derived on the basis of a full-throw, or full-pitch, coil. Accordingly, for these equations to be applicable to coils of any pitch, the right-hand side of the two equations must be multiplied by K_p. Then

$$E_c = 4.443 K_p N_c \phi_{pm} f \quad \text{volts} \tag{9.97}$$

when ϕ_{pm} is expressed in webers, and

$$E_c = 4.443 \left(\frac{K_p N_c \phi_{pm} f}{10^8} \right) \quad \text{volts} \tag{9.98}$$

when ϕ_{pm} is expressed in maxwells.

9.9 USE OF THE COIL-PITCH FACTOR IN CONTROLLING HARMONICS

The nth space harmonic of the air-gap flux wave will travel n wavelengths for each 360 electrical degrees of the fundamental scale, along the air gap. Thus for the nth space harmonic, the angular displacement between E_{c1} and E_{c2} in Fig. 9.15 is equal to $n\beta$ on the nth harmonic scale. Accordingly, eq. (9.92) is equal to

$$E_{crn} = 2E_n \sin\left(n \frac{\beta}{2}\right) \quad \text{volts} \tag{9.99}$$

and eq. (9.93) is equal to

$$E'_{crn} = 2E_n \quad \text{volts} \tag{9.100}$$

for the nth harmonic of induced voltage in the stator coil. The coil-pitch factor for any space harmonic n is equal to eq. (9.99) divided by eq. (9.100), or to

$$K_{pn} = \frac{2E_n}{2E_n} \sin\left(n \frac{\beta}{2}\right) = \sin\left(n \frac{\beta}{2}\right) \quad \text{numeric} \tag{9.101}$$

It will be noted now, and shown later, that even space harmonics do not exist in the rotating air-gap flux wave for a three-phase machine. Also, the third harmonic and all multiples of it do not exist in the line-to-line voltage of a three-phase machine. However, triplen space harmonics can exist, under certain conditions, in the voltage of the individual phases. The remaining harmonics in the spatial distribution of the rotating flux wave are those of odd order, except for the triplen order. Thus the fifth, seventh, eleventh, and so on, constitute the train of field harmonics present. Also, additional harmonics result from the presence of slot openings which interrupt the radial uniformity of the air-gap permeance. As will be seen later, the slot harmonics are of higher order, such as the seventeenth and nineteenth. However, unlike the space harmonics produced by the field, the slot harmonics are not affected by the pitch factor.

To understand how the coil pitch may be selected to reduce the magnitude of certain space harmonics in the rotating stator wave, consider a four-pole induction motor with 72 stator slots and with a coil throw of 1 to 16. Then there are 72/4 = 18 stator slots/pole and the stator coil spans 15 slots, with a per unit coil pitch of

$$\text{per unit coil pitch} = \frac{15}{18} = 0.833 \quad \text{numeric} \tag{9.102}$$

From eq. (9.101), the pitch factor for the fifth harmonic is

$$K_{p5} = \sin\left[(5)(0.833)(90)\right] = 0.256 \quad \text{numeric} \tag{9.103}$$

and the pitch factor for the seventh harmonic is

$$K_{p7} = \sin\left[(7)(0.833)(90)\right] = 0.262 \quad \text{numeric} \tag{9.104}$$

The maximum magnitudes of the fifth and seventh space harmonics, will not exceed 1/5 and 1/7, respectively, of that of the fundamental in the extreme case of a rectangular spatial distribution of the stator wave. Then, for the example above, the value of the fifth harmonic, in per unit of the fundamental, is reduced to less than

$$H_5 = \frac{1}{5}(0.256) = 0.051 \quad \text{numeric} \tag{9.105}$$

and the value of the seventh harmonic is reduced to less than

$$H_7 = \frac{1}{7}(0.262) = 0.037 \quad \text{numeric} \tag{9.106}$$

in per unit of the fundamental.

9.10 DISTRIBUTION FACTOR

As noted earlier, the stator winding is divided into groups of adjacent coils, which are connected in series, and the number of such coils within each group is equal to

$$\text{coils/group} = \frac{N_1}{pq} \quad \text{coils/pole/phase} \tag{9.107}$$

where, as defined earlier, p is equal to the number of poles and q is equal to the number of phases. All of the coils within a group are connected together to form a series path through the group. Accordingly, the voltages induced in the individual coils add to give the voltage induced in the group. However, the several coils that comprise the group are distributed over 360/(2)(3) = 60 electrical degrees for the usual case of 60-degree phase belts. Thus the voltages induced in the individual coils are not quite in phase and the vector sum of the individual coil voltages within the group is slightly less than the induced voltage within a given coil, multiplied by the number of coils in the group. This reduction in voltage is achieved by use of the distribution factor K_d in the equation for induced voltage within the group. Let N_g be equal to the number of coils/group. Then

$$N_g = \frac{N_1}{pq} \ \text{coils/group} \tag{9.108}$$

and let the angle between the voltages induced in adjacent coils, within one group, be α. Then, for the usual case of a group, or phase belt, which spans 60 electrical degrees,

$$\alpha = \frac{60}{N_g} \quad \text{electrical degrees/coil} \tag{9.109}$$

and for the less frequently encountered group, or phase belt, which spans 120 electrical degrees,

$$\alpha = \frac{120}{N_g} \quad \text{electrical degrees/coil} \tag{9.110}$$

Consider a three-phase four-pole machine that has 60 stator slots and, accordingly, 60 stator coils. Then, from eq. (9.108), the number of coils/group is equal to

$$N_g = \frac{60}{(4)(3)} = 5 \quad \text{coils/group} \tag{9.111}$$

The angle between coil voltages within the group, from eq. (9.109), is equal to

$$\alpha = \frac{60}{5} = 12 \quad \text{electrical degrees/coil} \tag{9.112}$$

for a 60-degree phase belt, which is normal for polyphase induction motors.

Figure 9.16a shows the individual coil voltages in magnitude and angle, which are superimposed on a coordinate system. The vector resultant of the individual voltage vectors is equal to

$$R = E_c(1 + 2\cos 12^\circ + 2\cos 24^\circ) = 4.7834E_c \quad \text{volts} \tag{9.113}$$

If the five individual coil voltages were located in one slot, the resultant would equal

$$R' = 5E_c \quad \text{volts} \tag{9.114}$$

The ratio of eq. (9.113) to eq. (9.114) is equal to the distribution factor K_d for this example, that is,

$$K_d = \frac{R}{R'} = \frac{4.7834E_c}{5E_c} = 0.957 \quad \text{numeric} \tag{9.115}$$

Thus the total voltage induced in this group, consisting of five adjacent coils connected in series, is 0.957 per unit of what it would be if the five coils were concentrated in one slot with the same angular location.

Figure 9.16b shows the individual coil voltages in their correct angular positions, arranged end to end, to equal the vector sum AB of the induced voltage across the N_g coils in series in the group. Point C is the center of an implied circle of which AB is a chord. Then the distribution factor K_d is equal to

$$K_d = \frac{\text{chord distance AB}}{N_g E_c} = \frac{AB}{N_g AD} \quad \text{numeric} \tag{9.116}$$

Since both the geometry and quantities in Fig. 9.16b can be treated in a general manner, as long as the product $N_g\alpha$ is equal to the number of degrees spanned by the phase belt, the figure will be used to derive the general form of K_d.

Construction line CF intersects angle α, to form two equal line segments, AF and FD. Similarly, construction line CH intersects angle $N_g\alpha$ to form the two equal line segments AH and HB. Then

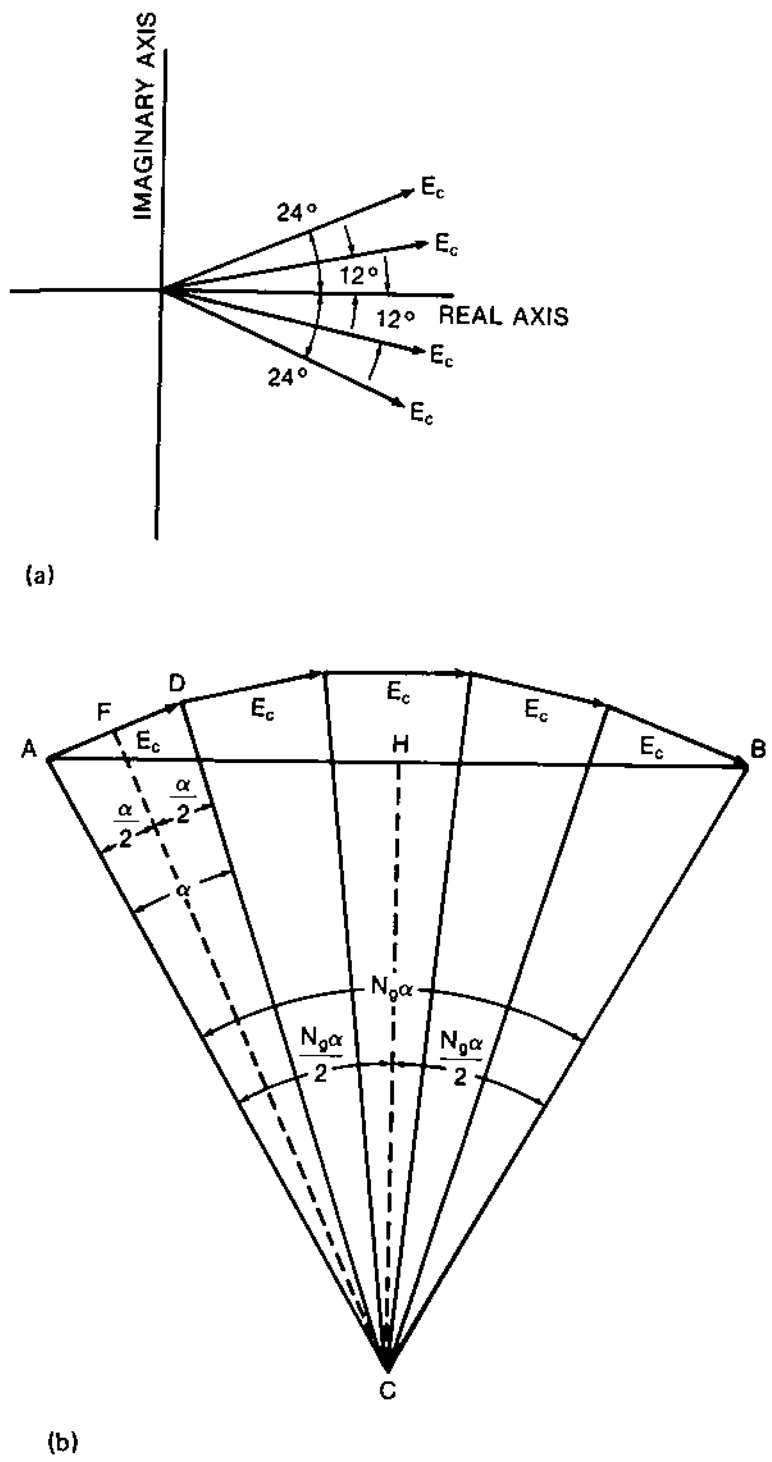
IMAGINARY AXIS
REAL AXIS
Ec
24°
12°
12°
24°
(a)
A
F
D
H
B
C
Ec
α/2
α
Ngα
Ngα/2
(b)

FIGURE 9.16 Induced coil voltages in a phase belt or group spanning 60 electrical degrees for a four-pole 60-slot stator: (a) superimposed coil-voltage vectors; (b) coil-voltage vectors distributed end to end.

$$\sin\frac{\alpha}{2} = \frac{AF}{AC} \quad \text{numeric} \tag{9.117}$$

and

$$AF = AC\sin\frac{\alpha}{2} \quad \text{volts} \tag{9.118}$$

Since

$$AD = AF + FD = 2AF \quad \text{volts} \tag{9.119}$$

then substituting eq. (9.118) into eq. (9.119) gives us

$$AD = E_c = 2(AC)\sin\frac{\alpha}{2} \quad \text{volts} \tag{9.120}$$

Also,

$$\sin\frac{N_g\alpha}{2} = \frac{AH}{AC} \quad \text{numeric} \tag{9.121}$$

and

$$AH = AC\sin\frac{N_g\alpha}{2} \quad \text{volts} \tag{9.122}$$

From Fig. 9.16b,

$$AB = AH + HB = 2AH \quad \text{volts} \tag{9.123}$$

Substituting eq. (9.122) into eq. (9.123) gives us

$$AB = 2(AC)\sin\left(\frac{N_g\alpha}{2}\right) \quad \text{volts} \tag{9.124}$$

Subsituting eqs. (9.120) and (9.124) into eq. (9.116) yields

$$K_d = \frac{2(AC)\sin(N_g\alpha/2)}{N_g(2)(AC)\sin(\alpha/2)} = \frac{\sin(N_g\alpha/2)}{N_g\sin(\alpha/2)} \quad \text{numeric} \tag{9.125}$$

This equation gives the distribution factor as a function of the quantities N_g and α, which are defined in eqs. (9.108), (9.109), and (9.110).

In eq. (9.115) it was determined that $K_d = 0.957$ for a stator with five coils/group and with an angle between slots equal to 12 electrical degrees. If similar calculations are performed for a corresponding stator with 60-degree phase belts, but (1) with six coils/group and 10 electrical degrees between slots and (2) with seven coils/group and 8.57 electrical degrees between slots, the resulting values of K_d are (1) 0.9561 and (2) 0.9558, respectively. As the value of N_g increases without limit, the number of individual coil voltage vectors also increase without limit. Simultaneously, the value of α and the length of the individual coil voltage vectors, or the magnitude of E_c, decrease and approach zero. Then, in the limit, K_d is equal to the ratio of the chord AB to the circular segment AB in Fig. 9.16.

For the usual case of a phase belt that spans 60 electrical degrees, or $\pi/3$ electrical radians, the limiting value of K_d is equal to

$$K_d = \frac{1}{\pi/3} = \frac{3}{\pi} = 0.9549 \quad \text{numeric} \tag{9.126}$$

and for a phase belt that spans 120 electrical degrees, or $2\pi/3$ electrical radians, the limiting value is equal to

$$K_d = \frac{\sqrt{3}}{2\pi/3} = 0.8270 \quad \text{numeric} \tag{9.127}$$

From eqs. (9.126) and (9.127), the ratio of the distribution factor for a stator with phase belts that span 60 electrical degrees to that for an otherwise identical stator, but with phase belts that span 120 electrical degrees, is equal to 0.9549/0.8270 = 1.155. This shows that a machine with 60-degree phase belts is capable of producing about 15% more induced voltage than an otherwise identical stator with 120-degree phase belts for the same mutual flux. Thus use of 60-degree phase belts permits more effective use of the winding.

9.11 USE OF THE DISTRIBUTION FACTOR IN CONTROLLING HARMONICS

As discussed in Section 9.9, the nth space harmonic of the air-gap flux wave will travel n wavelengths for each 360 electrical degrees of the fundamental scale. Accordingly, for the nth space harmonic, the angular displacement α between adjacent coils, or between adjacent slots, is equal to $n\alpha$ electrical degrees on the nth harmonic scale. Thus eq. (9.120) becomes

$$AD = 2(AC) \sin \frac{n\alpha}{2} \quad \text{volts} \tag{9.128}$$

and eq. (9.124) becomes

$$AB = 2(AC) \sin \frac{N_g n\alpha}{2} \quad \text{volts} \tag{9.129}$$

for the nth harmonic. Substituting eqs. (9.128) and (9.129) into eq. (9.116) gives us

$$K_{dn} = \frac{\sin (N_g n\alpha/2)}{N_g \sin (n\alpha/2)} \quad \text{numeric} \tag{9.130}$$

which gives the distribution factor for the nth harmonic.

Using the previous three stator windings with 60-degree phase belts (1) with five coils/group and 12 electrical degrees between slots, (2) with six coils/group and 10 electrical degrees between slots, and (3) with seven coils/group and 8.57 electrical degrees between slots, the distribution factor will be calculated for the fifth harmonic in each case. For case 1,

$$K_{d5} = \frac{\sin [(5)(5)(12)/2]}{5 \sin [(5)(12)/2]} = 0.200 \quad \text{numeric} \tag{9.131}$$

for case 2,

$$K_{d5} = \frac{\sin [(6)(5)(10)/2]}{6 \sin [(5)(10)/2]} = 0.197 \quad \text{numeric} \tag{9.132}$$

and similarly, for case 3,

$$K_{d5} = \frac{\sin [(7)(5)(8.57)/2]}{7 \sin [(5)(8.57)/2]} = 0.195 \quad \text{numeric} \tag{9.133}$$

If, on the other hand, there are only two coils per group, with 30 electrical degrees between adjacent coil sides, or slots, the value of K_{d5} is equal to

$$K_{d5} = \frac{\sin [(2)(5)(30)/2]}{2 \sin [(5)(30)/2]} = 0.259 \quad \text{numeric} \tag{9.134}$$

An inspection of the results in eqs. (9.131) through (9.134) shows that two coils/group, or six coils/pole, will provide a distribution factor of 0.259 for the fifth harmonic and that the rate at which K_{d5} decreases becomes smaller as the number of coils/group is increased further. The same pattern, in general, will be observed to hold for other space harmonics in the rotating wave. Thus it would appear that a reasonable wave shape is achieved by use of, say, four or five coils/group and that use of additional slots, or coils, does not result in further significant improvement. However, there are other reasons for using more slots, or coils, per group. Such reasons include the need to obtain a desirable ratio of stator slots to rotor slots in order to control load loss and the rotational component of core loss, to minimize perturbations on the speed-torque curve, to control electromagnetically induced noise, and to balance the electromagneto design in general. These design considerations are covered in the appropriate sections.

9.12 VOLTAGE INDUCED IN THE STATOR PHASE WINDING

Equations (9.97) and (9.98) both define the voltage induced in an individual stator coil with N_c turns and with a coil pitch that corresponds to the pitch factor K_p. The definition of induced voltage may now be expanded to include all the coils in the stator phase winding. Since the number of stator coils in the total three-phase winding is equal to the total number of slots in the stator core N_1, the total number of series coils/phase is equal to

$$N_q = \frac{N_1}{qC} \quad \text{series coils/phase} \tag{9.135}$$

where C is equal to the number of parallel circuits in each stator phase. The number of series turns/phase is equal to

$$N_{st} = N_q N_c = \frac{N_1 N_c}{qC} \quad \text{series turns/phase} \tag{9.136}$$

Accordingly, the voltage induced in the stator phase winding is equal to

$$E_1 = 4.443 K_p K_d N_{st} f \phi_{pm} \quad \text{volts/phase} \tag{9.137}$$

when ϕ_{pm} is expressed in webers, or to

$$E_1 = \frac{4.443 K_p K_d N_{st} f \phi_{pm}}{10^8} \quad \text{volts/phase} \tag{9.138}$$

when ϕ_{pm} is expressed in maxwells. Equations (9.137) and (9.138) give the functional relationship between the mutual flux/pole, induced voltage, stator frequency, and the stator winding configuration. This relationship is central to the electromagnetic operation of a polyphase induction motor.

TABLE 9.2 Magnitude of Induced Voltage Within the Stator Phase Winding

Component of winding	Value of induced voltage in the component[a] (V)
Phase	$E_1 = 4.443 K_p K_d N_{st} f \phi_{pm}$
Parallel circuit	$E_1' = [1] E_1$
Group	$E_g = \frac{C}{p} E_1$
Coil	$E_c = \frac{N_c}{N_{st} k_d} E_1$ $= \frac{qC}{N_1 K_d} E_1$

[a] ϕ_{pm} is expressed in webers. If it is expressed in maxwells, multiply ϕ_{pm} by 10^{-8}. The terms are defined in the text. For convenience, they are summarized here. C, number of parallel circuits in each stator phase; E_1, effective value of volts induced in the stator phase winding; E_1', effective value of volts induced in each parallel circuit = E_1; E_g, effective value of volts induced in each group of coils; E_c, effective value of volts induced in each coil; f, stator frequency, in hertz; k_p, stator coil-pitch factor; K_d, stator distribution factor; N_c, number of turns in each stator coil; N_{st}, number of turns in series in the phase winding; N_1, number of stator slots = number of stator coils; p, number of poles; q, number of phases; ϕ_{pm}, maximum value of mutual flux in webers.

The magnitude of induced voltage in various parts of the stator winding is given in Table 9.2.

9.13 INTEGRAL-SLOT WINDINGS

In an integral-slot winding, the number of coils connected in series to form each group is equal to an integer. Then

$$N_g = \frac{N_1}{pq} = \text{integer} \quad \text{coils/group} \tag{9.139}$$

A winding in which N_g is not an integer, such as $N_g = 15/2$, for example, is called a fractional-slot winding. Integral-slot windings provide more choices in connecting the groups together into parallel or series-parallel circuits to form the phase winding. From a design standpoint it is desirable to have several different choices for connecting the groups together, in order to arrive at the desired value of N_{st} for eq. (9.137). Integral-slot windings will be the first of the two types to be discussed.

Consider a four-pole stator winding with 48 stator slots. From eq. (9.139), the number of coils/group for this winding is equal to

$$N_g = \frac{48}{(4)(3)} = 4 \quad \text{coils/group} \tag{9.140}$$

In making up the groups, the winder will connect every four consecutive coils around the stator bore in series, which will result in a total of $N_1/N_g = 48/4 = 12$ such groups. This number of groups must be equally divided between the three phases, and this results in $12/3 = 4$ groups/phase. The physical locations of the four groups that comprise phase A are shown schematically in Fig. 9.17.

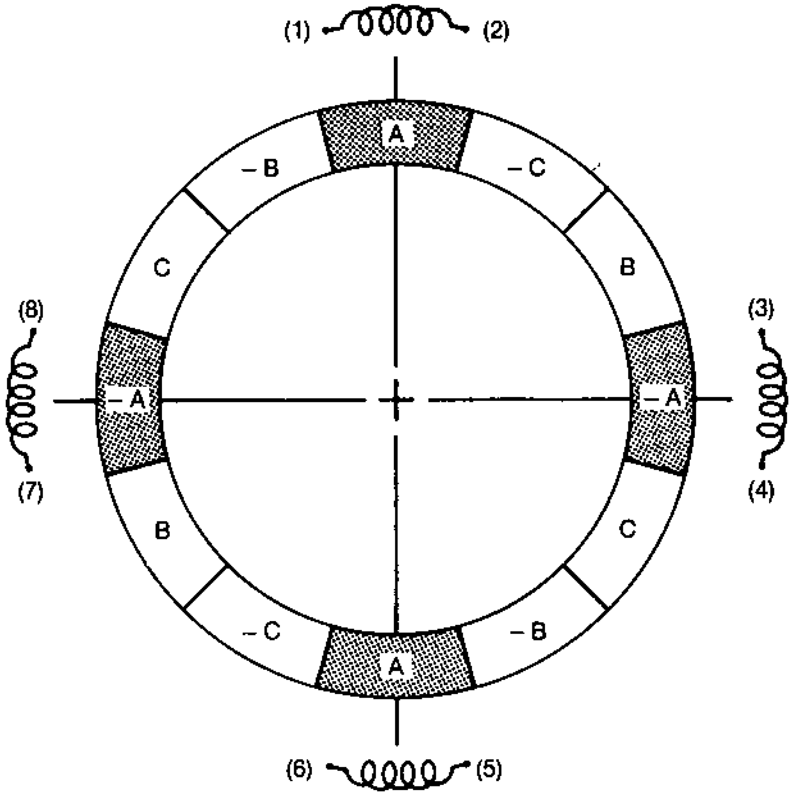

FIGURE 9.17 Physical locations of phase A coil groups of a four-pole 48-slot stator winding.

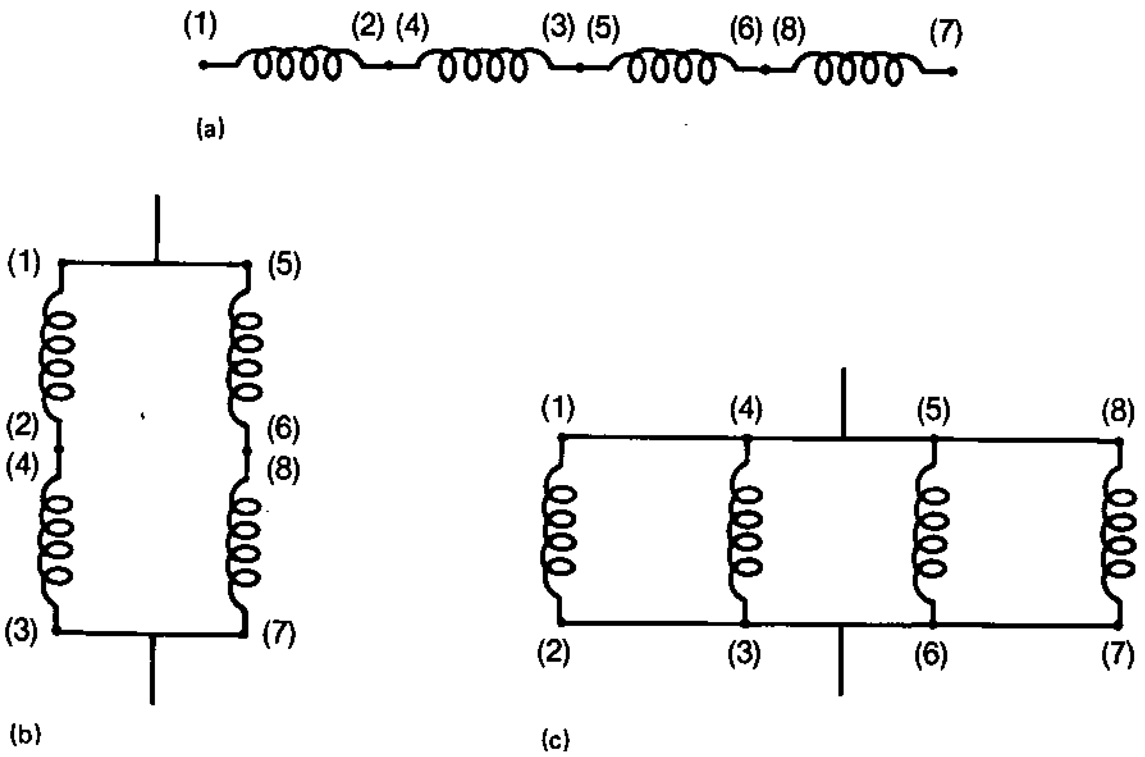

FIGURE 9.18 Possible modes for connecting the groups of a four-pole 48-slot stator phase winding: (a) series circuit; (b) two circuits in parallel; (c) four circuits in parallel.

The number of circuits in the phase winding must be divisible into the number of poles and, accordingly, it is possible to connect the four groups into any one of three different configurations to form the phase winding. The three possible configurations are:

1. Connect the four groups into one series circuit as shown in Fig. 9.18a, to give 16 coils in series in the phase winding.
2. Connect two circuits in parallel, with each circuit having two groups connected in series as shown in Fig. 9.18b, to give eight coils in series in the circuit.
3. Connect four circuits in parallel, with each circuit having one group as shown in Fig. 9.18c, to give four coils in series in the circuit.

If each coil has five turns, for example, the resulting value of series turns/phase N_{st} for the circuit shown in Fig. 9.18a can be calculated from eq. (9.136) as

$$N_{st} = \frac{N_1 N_c}{qC} = \frac{(48)(5)}{(3)(1)} = 80 \quad \text{series turns/phase} \tag{9.141}$$

Proceeding in a similar manner for the circuits shown in Fig. 9.18b and c and then tabulating the results for the three different possibilities:

1. For the phase winding in Fig. 9.18a, $N_{st} = 80$
2. For the phase winding in Fig. 9.18b, $N_{st} = 40$
3. For the phase winding in Fig. 9.18c, $N_{st} = 20$

The number of parallel circuits C in the phase winding must be either 4, 2, or 1 in order to have a balanced winding, with the same induced voltage and the same impedance drop in each circuit, for a given case. If none of the possibilities listed above provide the design engineer with an acceptable value of N_{st} for use in the fundamental design relationship between flux, voltage, and the winding configuration given in eq. (9.137), it will be necessary to change either the number of turns/coil N_c or the number of stator slots N_1. If the engineer decides on the latter option, the new choice for N_1 must be a multiple of $pq = (4)(3) = 12$, for the winding to be an integral-slot type. Thus the engineer could select 24, 36, 60, 72, and so on, in addition to 48. Obviously, a limitation in the number of permissible stator slots is a disadvantage of an integral-slot winding. On the other hand, this type of winding generally offers a greater choice in the number of permissible circuits C in parallel, as will become apparent when fractional-slot windings are considered, and this benefit tends to offset the above-mentioned limitation in the number of permissible stator slots.

The phase belts, or groups, for a given phase are located 180 electrical degrees apart, and accordingly, consecutive groups around the stator are under the influence of flux of different polarity at any given instant of time. Accordingly, when the four groups, identified as groups 1-2, 3-4, 5-6, and 7-8 in Fig. 9.17 are connected in series, in series-parallel, or in parallel, the polarity of each group must be considered. For example, in Fig. 9.18a, groups 3-4 and 7-8 must be reversed when connected with groups 1-2 and 5-6 so that the induced voltage will be in the same direction in all groups at any given instant of time. Such a reversal of alternate groups can be seen in the three different connections shown in Fig. 9.18.

Figure 9.18b shows two parallel circuits, each with two groups connected in series, to form the phase winding. In the figure, groups 1-2 and 4-3 are connected in series to form one circuit and groups 5-6 and 8-7 are connected in series to form the other circuit. This mode of connection of the groups to form the circuits in a multicircuit phase winding is called "adjacent poles in series," for the obvious reason that the groups which are connected in series are made up of adjacent pole groups of that phase. It would also have been possible to form one circuit by connecting groups 1-2 and 5-6 in series and to form the other circuit by connecting groups 8-7 and 4-3 in series. Then group ends 1 and 8 would be at a common potential at one end of the phase winding and group ends 6 and 3 would be at a common potential at the other end. This mode of connection of the groups to form parallel circuits is called "opposite poles in series," since such a circuit results from a series connection of pole groups which are physically located on opposite sides of the stator. The particular connection that is actually used for parallel-circuit phase windings in a given case is based on (1) the total length of connection cable required, (2) the mechanical uniformity of the connection "bundle" around the periphery of the connection end of the winding, and (3) the ability of the connection to permit the flow of equalizing currents which tend to reduce unbalanced magnetic force between the rotor and stator. The third item is considered later in the chapter.

In the discussion of integral-slot windings above, a four-pole stator with four groups/phase has been used to illustrate the various definitions and limitations involved in such a winding. It is apparent that the concept of an integral-slot winding can be extended to any number of poles and that the definitions and limitations can be generalized. First, however, the concept of a fractional-slot winding should be presented, so that the generalization can be extended to both types of windings.

9.14 FRACTIONAL-SLOT WINDINGS

In a fractional-slot winding, the number of coils connected in series to form each group is equal to a fraction instead of an integer. A fractional-slot winding will obviously permit a wider choice in selecting the number of stator slots N_1, which is frequently useful to the design engineer. However, the number of coils in all phase belts, or groups, are not equal and such nonuniformity between phase belts provides a source of additional reactance. Also, such nonuniformity can produce additional noise and core loss. These effects are more pronounced for machines with small air gaps. Further, as will soon be shown, the number of permissible parallel circuits within a given phase winding is, in general, limited. However, such windings have been successfully used by design engineers for many years and are frequently the proper choice for a given design.

The concept of fractional-slot windings is best understood by an example. Consider a four-pole stator winding with 54 stator slots. Then, from eq. (9.139), the number of coils/group for this winding is equal to

$$N_g = \frac{54}{(4)(3)} = \frac{9}{2} = 4\ 1/2 \quad \text{coils/group} \tag{9.142}$$

where, obviously, 4 1/2 coils/group is a mathematical, not a physically achievable, concept. It is appropriate to test this winding for feasibility using the three different circuit configurations that were found acceptable for the four-pole integral-slot winding considered previously. For the series circuit, the phase winding would consist of four groups connected in series, with each group having 4 1/2 coils on the average, or (4)(4 1/2) = 18 coils. This phase winding is acceptable. For the two-parallel configuration, the phase winding would consist of two circuits in parallel, each circuit of which would consist of two groups in series. Thus each circuit would have (2)(4 1/2) = 9 coils connected in series. Again, this circuit is acceptable. For the four-parallel configuration, the phase winding would consist of four circuits in parallel, with each circuit consisting of one group each, with 4 1/2 coils on the average. This proposed winding is not acceptable, for the following reasons. The winder, in making up the groups, will have connected consecutive coils into alternate groups of four and five coils each, completely around the stator. However, a four-parallel configuration, with two circuits of four coils each and two circuits with five coils each, will result in an unbalance in the induced voltages across the four parallel circuits, which will give rise to significant circulating currents between the four circuits. Also, there will be a difference in normal impedance drop across the four circuits. Accordingly, the proposed four-circuit phase winding is not acceptable in this case. Since the number of poles of a given phase winding must be divisible by the number of circuits in that winding, all four-pole windings have only three circuit possibilities, which are (1) a series circuit, (2) two circuits in parallel, and (3) four circuits in parallel. The series circuit and the two circuits in parallel have been found to be acceptable, whereas the four circuits in parallel has been found not to be acceptable. Thus the choices available to the design engineer are only the series and two-parallel configurations. The logic for the foregoing analysis of this fractional-slot winding is summarized in Table 9.3.

An additional example of a fractional-slot winding will be analyzed. Consider a 10-pole stator winding with 105 stator slots. The number of coils/group for this winding is equal to

$$N_g = \frac{105}{(10)(3)} = \frac{7}{2} = 3\ 1/2 \quad \text{coils/group} \tag{9.143}$$

Since the number of poles of a phase winding must be divisible by the number of circuits in that winding, the different circuit configurations to be evaluated

TABLE 9.3 Summary of Logic in Determining Permissible Circuits for a Four-Pole 54-Slot Stator

Phase winding	Group arrangement	Coils/circuit	Acceptable
Series circuit	Four groups in series	(4 1/2)(4) = 18	Yes
Two-parallel	Two groups in series/ circuit	(4 1/2)(2) = 9	Yes
Four-parallel	One group/circuit	(4 1/2)(1) = 4 1/2	No

TABLE 9.4 Summary of Logic in Determining Permissible Circuits for a 10-Pole 105-Slot Stator

Phase winding	Group arrangement	Coils/circuit	Acceptable
Series circuit	Ten groups in series	(3 1/2)(10) = 35	Yes
Two-parallel	Five groups in series/ circuit	(3 1/2)(5) = 17 1/2	No
Five-parallel	Two groups in series/ circuit	(3 1/2)(2) = 7	Yes
Ten-parallel	One group/circuit	(3 1/2)(1) = 3 1/2	No

are a series circuit, two circuits in parallel, five circuits in parallel, and 10 circuits in parallel. The logic for testing the acceptability of the four possibilities can be immediately formulated in the same manner as was done for the preceding example, and such a format is shown in Table 9.4. An examination of Table 9.4 shows that the stator phase winding can consist of either a series circuit of 35 coils or of five circuits in parallel, each circuit of which has seven coils in series. By comparison, a 10-pole integral-slot winding with, say, 120 stator slots would have an acceptable choice of all four of the circuit configurations.

9.15 GENERALIZED RULES FOR DETERMINING STATOR WINDING CONFIGURATIONS

Integral-slot windings are also called symmetrical windings, since all groups have the same number of coils in series, and fractional-slot windings are also called unsymmetrical windings, since all groups do not have the same number of coils in series. For both cases it is necessary that for parallel circuits, each circuit have the same number of coils in series. As was apparent from the previous examples, this requirement tends to limit the acceptable number of winding configurations for the fractional-slot, or unsymmetrical, winding. For integral-slot windings the number of circuits in parallel to be used in the phase winding must only be divisible into the number of poles. Since the number of coils/group is the same for all groups, each of the possible circuits will be balanced. However, selection of permissible circuit configurations for fractional-slot windings is more involved, as has been seen in the previous examples.

In general, for a fractional-slot winding, when the number of slots per pole per phase is reduced to a fraction with no common factors between the numerator and the denominator, the resulting fraction establishes the basis for determining the possible connections for designing a balanced winding. Let

$$N_g = \frac{N_1}{pq} = \frac{A}{B} \quad \text{slots/pole phase} \tag{9.144}$$

Restraints that this fraction imposes on the winding are

$$\frac{p}{B} = \text{maximum number of parallel circuits/phase} \tag{9.145}$$

Also,

$$\frac{p}{B} = \text{number of repeatable sections} \tag{9.146}$$

In addition,

$$\frac{B}{q} = \text{noninteger} \tag{9.147}$$

The restraints above will be applied to the examples discussed previously. First, consider the four-pole integral-slot winding with 48 stator slots. From eq. (9.140),

$$N_g = \frac{48}{(4)(3)} = \frac{4}{1} \quad \text{slots/pole phase} \tag{9.148}$$

Thus B = 1 and from eq. (9.145),

$$\frac{p}{B} = \frac{4}{1} = 4 = \text{maximum number of parallel circuits/phase} \tag{9.149}$$

From eq. (9.146),

$$\frac{p}{B} = \frac{4}{1} = 4 \text{ repeatable sections in the winding} \tag{9.150}$$

Also, from eq. (9.147),

$$\frac{B}{q} = \frac{1}{3} = \text{noninteger} \tag{9.151}$$

which is desirable. Then this winding will have balanced phases, will permit a maximum of four parallel circuits for the phase winding, and the grouping pattern repeats four times throughout the winding, which means that the grouping pattern is identical for each pole of the phase winding. These conclusions were also reached by the previous general analysis of the same winding.

Next, apply the restraints to the four-pole fractional-slot winding with 54 stator slots discussed previously:

$$N_g = \frac{54}{(4)(3)} = \frac{9}{2} \quad \text{slots/pole phase} \tag{9.152}$$

for which B = 2. From eq. (9.145),

$$\frac{p}{B} = \frac{4}{2} = 2 \text{ maximum number of parallel circuits/phase} \tag{9.153}$$

and from eq. (9.146),

$$\frac{p}{B} = \frac{4}{2} = 2 \text{ repeatable sections in the winding} \tag{9.154}$$

Also, from eq. (9.147),

$$\frac{B}{q} = \frac{2}{3} = \text{noninteger} \tag{9.155}$$

This winding, then, will have balanced phases, will permit a maximum of two parallel circuits for the phase winding, and the grouping pattern repeats two times throughout the winding. These conclusions correspond to those previously reached and tabulated in Table 9.3.

Again, applying the restraints to the last of the windings discussed previously, to the 10-pole fractional-slot winding with 105 stator slots:

$$N_g = \frac{105}{(10)(3)} = \frac{7}{2} \quad \text{slots/pole phase} \tag{9.156}$$

to determine that B = 2 for this example. From eq. (9.145),

$$\frac{p}{B} = \frac{10}{2} = 5 \text{ maximum number of parallel circuits/phase} \tag{9.157}$$

and from eq. (9.146),

$$\frac{p}{B} = \frac{10}{2} = 5 \text{ repeatable sections in the winding} \tag{9.158}$$

Also, from eq. (9.147),

$$\frac{B}{q} = \frac{2}{3} = \text{noninteger} \qquad (9.159)$$

Accordingly, this winding will have balanced phases, will permit a maximum of five parallel circuits for the phase winding, and the grouping pattern will repeat five times throughout the winding. A check of Table 9.4 will show that the conclusions above correspond to those reached previously and tabulated in that table.

The procedures above are applicable to both integral-slot and fractional-slot windings. An additional procedure is available which is only applicable to fractional-slot windings, for which a matrix is used to analyze the winding. The steps required to prepare such a matrix will be illustrated by using the 10-pole fractional-slot winding with 105 stator slots as an example. The steps are as follows:

1. Divide the number of stator slots N_1 by the number of poles p. From this fraction, establish another fraction of equal value, in which the numerator and denominator are integers and in which the numerator is the smallest integer that is divisible by the number of phases q. This new fraction is called the characteristic fraction. Performing this step for the example gives us

$$\frac{N_1}{p} = \frac{105}{10} = \frac{21}{2} \quad \text{slots/pole} \qquad (9.160)$$

2. Prepare a matrix with the number of horizontal divisions equal to the numerator of the characteristic fraction in eq. (9.160) and with the number of vertical divisions equal to p, the number of poles. See Fig. 9.19, where for the example, there are 21 horizontal divisions and 10 vertical divisions in the matrix.

3. For the usual case of a three-phase winding with 60-degree phase belts, divide the vertical divisions into three equal parts, labeled A, -C, and B, to correspond to the three adjacent phase belts, which span a total of 180 electrical degrees (see Fig. 9.19).

4. Starting at the first box, located in the upper, left-hand corner of the matrix, place a mark to indicate the presence of a coil. Then, continuing from left to right, horizontally, and from top to bottom, vertically, mark every kth box, where k is equal to the denominator of the characteristic fraction. For the example, k is equal to 2. For convenience in subsequent interpretation of the matrix, the mark can be an "a" for coils located in phase belt A, a "b" for coils located in phase belt B, and a "c" for coils located in phase belt -C, as has been done in Fig. 9.19.

p	A							−C							B						
1	a		a		a		a		c		c		c		b		b		b		b
2		a		a		a		c		c		c		c		b		b		b	
3	a		a		a		a		c		c		c		b		b		b		b
4		a		a		a		c		c		c		c		b		b		b	
5	a		a		a		a		c		c		c		b		b		b		b
6		a		a		a		c		c		c		c		b		b		b	
7	a		a		a		a		c		c		c		b		b		b		b
8		a		a		a		c		c		c		c		b		b		b	
9	a		a		a		a		c		c		c		b		b		b		b
10		a		a		a		c		c		c		c		b		b		b	

A	−C	B
4	3	4
3	4	3
4	3	4
3	4	3
4	3	4
3	4	3
4	3	4
3	4	3
4	3	4
3	4	3

FIGURE 9.19 Matrix for analyzing a 10-pole fractional-slot stator winding with 105 stator slots.

5. The following information can be determined from the matrix:

a. The number of coils/group and the location of each group, for the pq groups, or phase belts, throughout the winding
b. Starting from a given point in the winding, the consecutive coils to connect in series to make up the pq groups
c. The number of repeatable sections within the winding
d. The different phase-winding configurations possible, such as to have an equal number of coils in each circuit and to have the same number of coils in each phase

A grouping table can be formulated directly from the matrix, and such a table is shown in Fig. 9.19. It is also apparent from the figure that the grouping pattern repeats every two pole pitches, or 360 electrical degrees, and that there are five such repeatable sections in the winding. This permits five parallel circuits, as well as a series circuit, for the phase winding.

9.16 UNBALANCED WINDINGS

The fractional-slot windings which have been evaluated, up to now are unsymmetrical but are balanced; that is, they will not produce circulating currents between circuits or phases if the circuit configurations are selected in accordance with the criteria. It is now in order to apply the fractional-slot criteria to a winding that is both unsymmetrical and unbalanced and which, accordingly, should not be used, in general.

Consider a 12-pole fractional-slot winding with 150 stator slots. The number of slots per pole for each phase is equal to

$$\frac{N_1}{pq} = \frac{150}{(12)(3)} = \frac{25}{6} \quad \text{slots/pole phase} \tag{9.161}$$

and B is equal to 6. From eq. (9.145),

$$\frac{p}{B} = \frac{12}{6} = 2 = \text{maximum number of parallel circuits} \tag{9.162}$$

which shows that the maximum number of parallel circuits is equal to 2. However, from eq. (9.147),

$$\frac{B}{q} = \frac{6}{3} = 2 = \text{integer} \tag{9.163}$$

which immediately shows that such a proposed winding will not be balanced. This would normally be the end of the analysis, at which point the conclusion would have been reached that such a winding should not be considered. However, it is interesting to form the matrix discussed above, for whatever additional insight it might show.

Forming the characteristic fraction in accordance with eq. (9.160), we have

$$\frac{N_1}{p} = \frac{150}{12} = \frac{75}{6} \quad \text{slots/pole} \tag{9.164}$$

The corresponding winding matrix is shown in Fig. 9.20. It is apparent from the figure that the proposed winding is, indeed, unbalanced. The 12 groups in phase A have a total of 54 coils, whereas the 12 groups in each of the other two phases has a total of only 48 coils. The additional voltage generated in phase A and the additional impedance drop across that phase, in comparison to the other two phases of the stator winding, would result in an unacceptable level of imbalance between phases.

The amount of this imbalance can be significantly reduced by judicious grouping. If the two coils along the right-hand edge of phase A, marked by circles, are included with the -C phase belts, and if the two coils along the left-hand edge of phase A, also marked by circles, are included with the B phase belts, the phases will then have an equal number of coils. The corresponding grouping table is shown in Fig. 9.20. Each phase winding now has 50 coils and there are two repeatable sections in the winding, permitting either a series or a two-circuit phase winding. Although it is considerably improved with this grouping, the winding remains, fundamentally,

p	A																									−C																									B																									A	−C	B
1	a						a						a						a						ⓐ						b						b						b						b						c						c						c						c			4	5	4
2				a						a						a						a						b						b						b						b						c						c						c						c						4	4	4
3	a						a						a						a						a						b						b						b						b						c						c						c						c			5	4	4
4				a						a						a						a						b						b						b						b						c						c						c						c						4	4	5
5	ⓐ						a						a						a						a						b						b						b						b						c						c						c						c			4	4	4
6				a						a						a						a						b						b						b						b						c						c						c						c						4	4	4
7	a						a						a						a						ⓐ						b						b						b						b						c						c						c						c			4	5	4
8				a						a						a						a						b						b						b						b						c						c						c						c						4	4	4
9	a						a						a						a						a						b						b						b						b						c						c						c						c			5	4	4
10				a						a						a						a						b						b						b						b						c						c						c						c						4	4	5
11	ⓐ						a						a						a						a						b						b						b						b						c						c						c						c			4	4	4
12				a						a						a						a						b						b						b						b						c						c						c						c						4	4	4

FIGURE 9.20 Matrix for analyzing a 12-pole unbalanced stator winding with 150 stator slots.

an unbalanced winding, however. This is because of the cyclical shift of coils across the phases and because, as now grouped, the B and -C phase belts embrace slightly more than 60 electrical degrees.

In general, it is not recommended that unbalanced windings be used, even with the obvious improvement obtained from judicious grouping. However, economic and practical cases are occasionally encountered in field application of large motors for which such a practice might be considered and evaluated. Assume that the example just considered, with 150 stator slots, was a large mill motor that originally had a 10-pole winding with a synchronous speed of 720 rpm and that subsequently it was found desirable to decrease the speed by about 20%, because of application reasons at the mill. As originally built for 10-pole operation, the motor would have had an integral-slot balanced stator winding, whereas at 12-pole operating, it obviously would not. The chief engineer of the mill would not necessarily be expected to be knowledgeable about the feasibility of rewinding a given machine for a new speed. Accordingly, in such a case, the engineer should contact the original manufacturer of the motor, who would be in a position to evaluate the magnitude of imbalance and any significant change in losses, noise, and perturbations on the speed-torque curve. Because such proper evaluation requires considerable engineering time, the chief engineer of the mill should expect to be asked to pay for such services by the equipment manufacturer; such charges are entirely appropriate.

9.17 STATOR CONNECTION DIAGRAMS

The necessary information for connecting the winding after all coils have been inserted into the stator slots is contained in the stator connection diagram. The connection diagram will show the following information:

1. The specific adjacent coils to connect in series around the winding to make up the pq different groups.
2. The specific groups to connect in series, together with the polarity of the connection of each group, to form the individual circuits for each phase.
3. The specific ends of the specific parallel circuits to connect together to form the ends of each phase and to define that phase winding (if the phase winding is not a series circuit).
4. The specific ends of the three individual phase windings to connect together to form the neutral junction of the three-phase winding if the three-phase winding is wye-connected and if the three-phase connections are intended to be made internal to the machine.
5. The specific end-to-end connections of the three individual phase windings to form the delta if the three-phase winding is delta-connected and if the three-phase connections are intended to be made internal to the machine.

6. Identification of the connection leads of the three-phase winding (i.e., T_1, T_2, and T_3) to give the desired direction of rotation of the rotor when three-phase voltage is applied, the phase voltages of which reach their positive values in the same sequence.
7. Identification of the ends of phase windings for machines, the three-phase connections of which are made externally, for wye-delta reduced-voltage starting.
8. Identification of the ends of appropriate circuits of the various phase windings, the three-phase connections of which are made extenrally, for dual-voltage operation.

The format that is used to convey the foregoing set of information from the design engineer to the factory, as well as the colloquial name for the corresponding documents, vary from one manufacturer to another. It can range from schematically shown information contained on one drawing or computer printout sheet, to very pictorial and descriptive information requiring several drawings or computer printout sheets. In any case, it should contain the foregoing information in one form or another.

9.18 MAGNETIC PULL OR RADIAL DECENTERING FORCE

When the stator winding of a polyphase induction motor is excited, a tractive force or pull is exerted between the stator and rotor cores which is similar to that produced by an electromagnet on a steel workpiece. If the rotor is exactly centered relative to the stator bore, this force will be exerted in a radial direction and will be equal among the various poles of the stator. Accordingly, it is called the concentric magnetic force. If, however, the rotor is offset relative to the center of the stator bore such that the air gap is less at one point and greater at the diametrically opposite point, an imbalance will then exist in the radial magnetic forces around the air gap. In such a case, the point of minimum gap will experience a greater force than the diametrically opposite point of maximum gap, resulting in a force that tends to decenter the rotor further. Such a force is called an unbalanced magnetic pull or a radial-decentering force, and in some extreme cases, such as large, slow-speed machines, can result in the rotor surface making contact with the stator bore, or in "pullover."

As will be shown, the magnetic force exists by virtue of the energy stored in the magnetic field of the air gap and is proportional to the second power of the air-gap flux density and to the first power of the stator-bore area. Magnetic pull is of most concern in large, slow-speed machines, which have relatively smaller radial air gaps and for which the structural flexibility relative to the magnitude of the force is greater. Fortunately, the magnitude of magnetic pull can be limited by the design of the stator winding

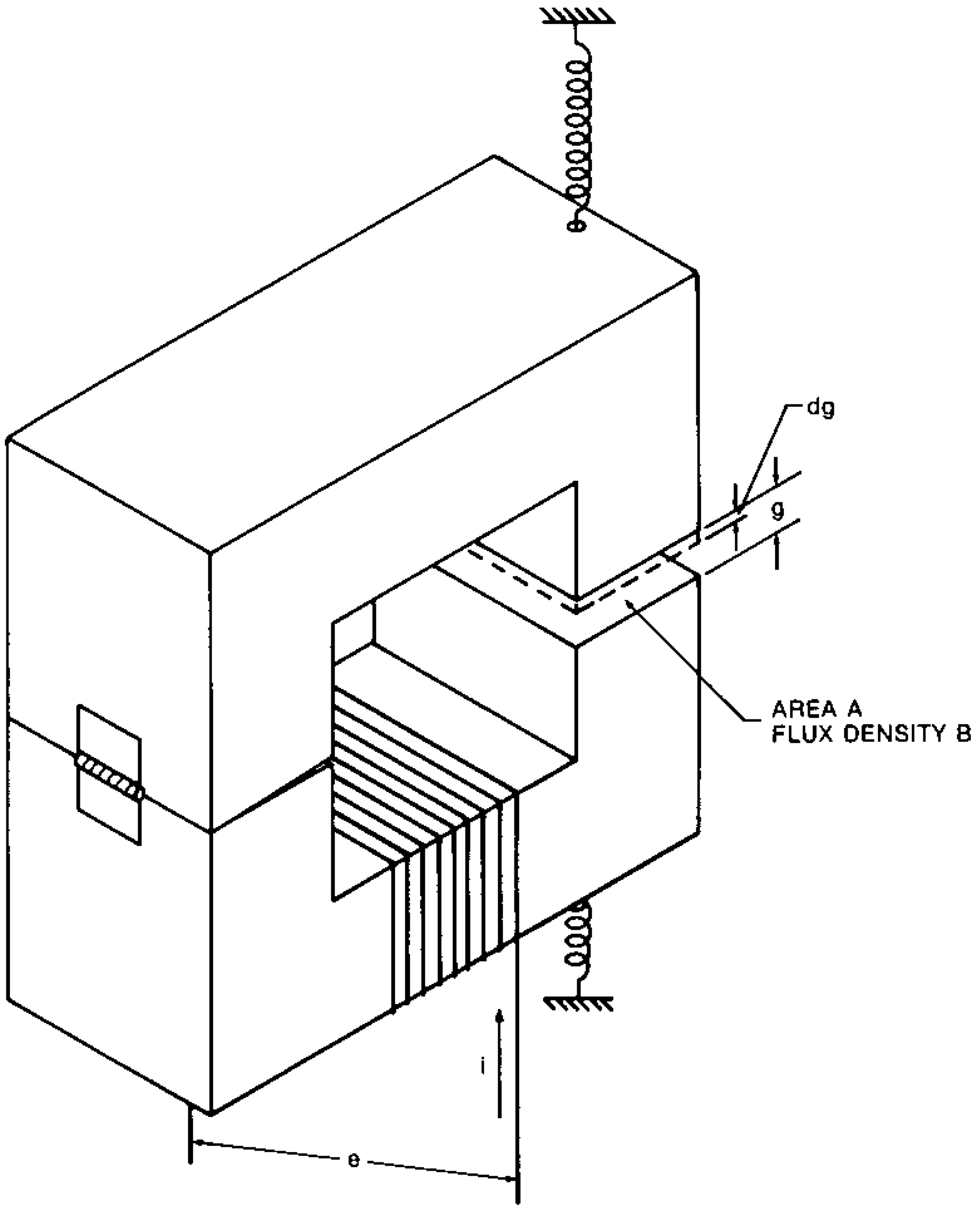

FIGURE 9.21 Model for analysis of stored energy in a magnetic field.

configuration, and for larger, low-speed machines, it is important that this be considered in the design of the stator winding. Limitation of magnetic pull by design of the stator winding will be discussed subsequently in this section. First, however, the fundamental equation for the tractive force of an electromagnet will be determined.

Consider the electromagnetic model shown in Fig. 9.21. Assume that the exciting coil is so designed that any leakage flux is trivial compared to the flux ϕ in the ferromagnetic yoke and air gap. Also, assume that the geometry of the yoke and the length g of the air gap is such that essentially all of the magnetomotive force drop is across the air gap and that the drop along the yoke can be ignored. Let the two springs that separate the two parts of the yoke be continuously adjusted in some manner, such as to maintain the length of the air gap at a value of g during any change in the magnitude of the current.

Then let a voltage e be impressed across the inductive circuit in Fig. 9.21, which causes a current i to flow through the coil. A voltage e_i will be induced in the coil, which is equal to

$$e_i = L \frac{di}{dt} \quad \text{volts} \tag{9.165}$$

and which will be in such a direction as to oppose the impressed voltage. The impressed voltage e must also provide a component equal to the potential drop across the resistance of the circuit. Thus the impressed voltage is equal to

$$e = -e_i + iR \quad \text{volts} \tag{9.166}$$

or

$$e = -L \frac{di}{dt} + iR \quad \text{volts} \tag{9.167}$$

where L is the inductance of the coil in henrys. If both sides of eq. (9.167) are multiplied by i dt, the result is the differential equation for circuit energy, or

$$ei\,dt = i^2R\,dt + Li \frac{di}{dt}\,dt \quad \text{joules} \tag{9.168}$$

The energy received from the supply bus during the time T that the current is increasing from zero to I is equal to

$$J = \int_0^T i^2R\,dt + \int_0^I Li\,di \quad \text{joules} \tag{9.169}$$

The first integral in eq. (9.169) is equal to the heat energy dissipated in the resistance of the circuit in time T. The second integral is equal to the energy stored in the magnetic field during the same time period, or to

$$J_s = \int_0^I Li\,di = \frac{1}{2}LI^2 \quad \text{joules} \tag{9.170}$$

The inductance L of the coil is equal to

$$L = \frac{N\phi}{I} \quad \text{henrys} \tag{9.171}$$

where N is the number of turns of the coil and where ϕ is the flux flowing in the magnetic yoke and air gap, sustained by the current I. Substituting eq. (9.171) into eq. (9.170) gives us

$$J_s = \frac{1}{2}\left(\frac{N\phi}{I}\right) I^2 = \frac{1}{2}(NI)\phi \quad \text{joules} \tag{9.172}$$

But ϕ can be replaced by BA, where B is the average flux density in the air gap in webers/meter^2 and where A is the cross-sectional area of the flux path in meters^2. Also, the magnetomotive force NI can be replaced by Hg, where H is the magnetic field strength in ampere-turns/meter and g is the radial length of the air gap in meters, since it has been assumed that any magnetomotive force drop across the ferromagnetic portion of the magnetic circuit is negligible in comparison to that across the air gap. Then, making the foregoing substitutions in eq. (9.172), we have

$$J_s = \frac{1}{2}(Hg)(BA) \quad \text{joules} \tag{9.173}$$

Since

$$B = \mu H \quad \text{webers/meter}^2 \tag{9.174}$$

then

$$H = \frac{B}{\mu} \quad \text{amperes/meter} \tag{9.175}$$

Substituting eq. (9.175) and the value of permeability of air, or $\mu = 4\pi \times 10^{-7}$ H/m, into eq. (9.173) yields

$$J_s = \frac{1}{2}\left(\frac{Bg10^7}{4\pi}\right)(BA) = \frac{10^7}{8\pi} AgB^2 \quad \text{joules} \tag{9.176}$$

which gives the stored energy in the air gap in terms of the flux density B and of the air-gap volume Ag.

If the air-gap length g in Fig. 9.21 is allowed to decrease by the increment dg, the corresponding decrease in the stored energy in the air gap is equal to

$$dJ_s = \frac{10^7}{8\pi} AB^2 \, dg \quad \text{joules} \tag{9.177}$$

or

$$\frac{dJ_s}{dg} = \frac{10^7}{8\pi} AB^2 \quad \text{newtons} \tag{9.178}$$

But since

$$F = \frac{dJ}{dg} \quad \text{newtons} \tag{9.179}$$

then, in the limit, the force in the direction of the incremental motion dg is equal to

$$F = \frac{10^7}{8\pi} AB^2 \quad \text{newtons} \tag{9.180}$$

Equation (9.180) is the fundamental equation of tractive force for an electromagnet, with A and B expressed in MKS units of meters^2 and of webers/meter^2, respectively. This equation may be expressed in terms of pounds, inches^2, and maxwells/inch^2 by remembering that 1 weber = 10^8 maxwells, that 1 meter^2 = $(39.37)^2$ inches^2, and that 1 newton = 1/4.448 pounds. Then

$$F = \frac{10^7 (39.37)^2}{(8\pi)(10^{16})(4.448)} AB^2 = \frac{AB^2}{72 \times 10^6} \quad \text{pounds} \tag{9.181}$$

Equations (9.180) and (9.181) are used to calculate the balanced radial force between the stator bore surface and the rotor surface, which is called the concentric force. Since this force is balanced around the rotor, it does not cause the rotor to decenter radially. However, the equation for magnetic pull, which is derived below, which contains eq. (9.180) as a factor, will tend to cause the rotor to decenter radially.

In the typical case in practice, there will be a radial offset in the position of the rotor structure relative to the geometric center of the stator bore. The force of gravity will tend to cause the rotor to be in the lowest vertical position that the bearing clearances permit. The shaft will experience some static deflection in a vertical direction at the axial center of mass of the rotor structure due to the force of gravity. Also, for either belt or chain drives, there will be a lateral force imposed on the end of the

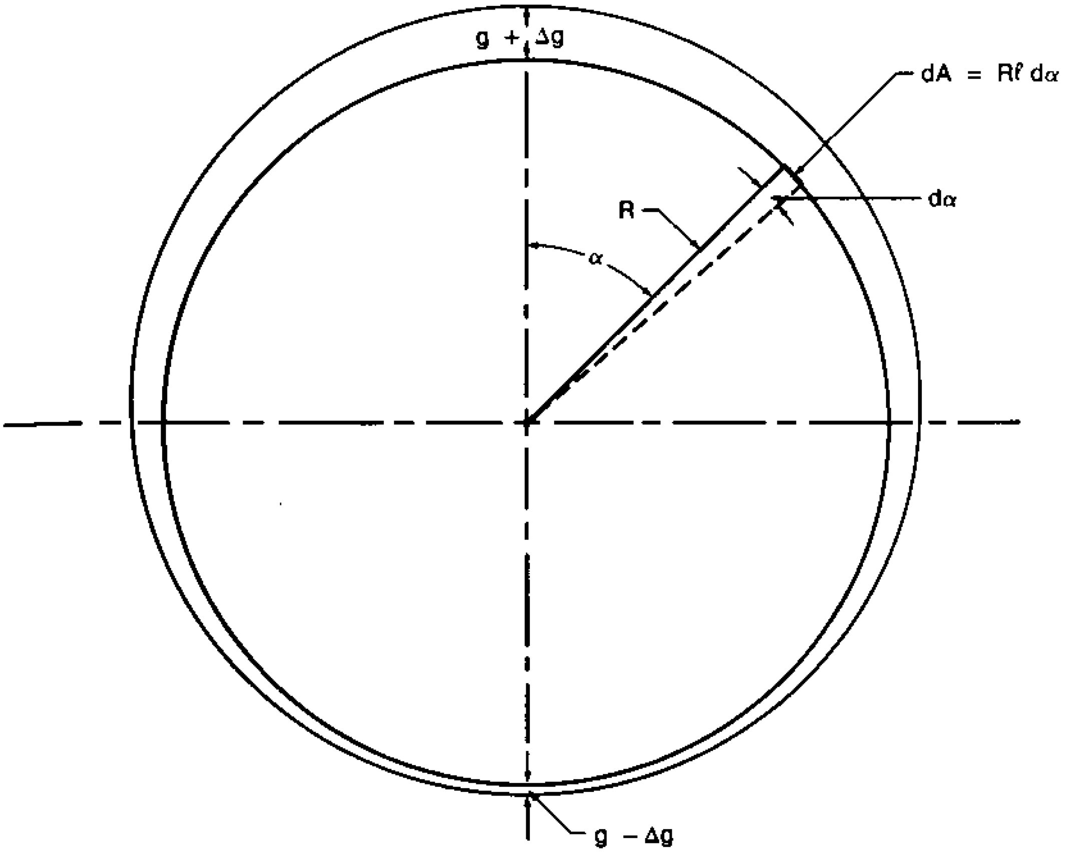

FIGURE 9.22 Offset rotor in a stator, with definition of increments for use in analyzing offset magnetic pull.

shaft extension, which will be superimposed on the other forces. Thus some amount of offset of the rotor within the stator bore is normal and the magnetic pull resulting from this offset must be considered in the design of a polyphase induction motor. The equation for unbalanced magnetic pull will now be determined.

Let an induction motor rotor with a normal radial air gap of g meters be offset in a vertically downward direction relative to the stator bore by Δg meters, as shown in Fig. 9.22. The radial eccentricity of the air gap at any point is then equal to $\Delta g \cos \alpha$, where α is the angle in radians, as measured from the top of the air gap in a clockwise direction, as shown in Fig. 9.22. Accordingly, the radial air gap at any point a is equal to

$$g_a = g + \Delta g \cos \alpha \quad \text{meters} \tag{9.182}$$

Then the radial air gap g_t at the top and the radial air gap g_b at the bottom of the bore are, respectively, equal to

$$g_t = g + \Delta g \quad \text{meters} \tag{9.183}$$

$$g_b = g - \Delta g \quad \text{meters} \tag{9.184}$$

The flux density will be increased in the region of minimum gap and decreased in the region of maximum gap because of the difference in reluctance of the air gaps at the two locations. The flux associated with one pole, at any instant of time, can return through the contiguous halves of the adjacent pole areas such that there can be differentials in flux density, per 180 electrical degrees of span, around the circumferential bore. If the magnetomotive force drop across the ferromagnetic part of the flux paths is small in comparison to that across the air-gap part, which it normally is, the relationship between air-gap flux density and radial air-gap length at any point a is very closely equal to

$$\frac{B_a}{B} = \frac{g}{g + \Delta g \cos \alpha} \quad \text{numeric} \tag{9.185}$$

so that

$$B_a = B \frac{g}{g + \Delta g \cos \alpha} = B \frac{1}{1 + \Delta g/g \cos \alpha} \quad \text{webers/meter}^2 \tag{9.186}$$

For an incremental angle $d\alpha$, the corresponding incremental area on the surface of the rotor is equal to

$$dA = \ell R \, d\alpha \quad \text{meters}^2 \tag{9.187}$$

where ℓ is the axial length and R is the radius of the rotor in meters. From eq. (9.180), the incremental force on the rotor associated with the incremental area dA and flux density B_a is

$$dF = \frac{10^7}{8\pi} B_a^2 \ell R \, d\alpha \quad \text{newtons} \tag{9.188}$$

The vertical component of dF along the axis of displacement is

$$dF_v = \frac{10^7}{8\pi} B_a^2 \ell R \cos \alpha \, d\alpha \quad \text{newtons} \tag{9.189}$$

with the understanding that an upward force is positive and a downward force is negative, because of the polar coordinate convention adopted in Fig. 9.22. Substituting the value of the flux density B_a given in eq. (9.186) for any general point a into eq. (9.189) yields

$$dF_v = \frac{10^7}{8\pi} \frac{B^2 \ell R \cos\alpha \, d\alpha}{(1 + \Delta g/g \cos\alpha)^2} \quad \text{newtons} \tag{9.190}$$

Expanding the denominator of eq. (9.190) gives us

$$dF_v = \frac{10^7}{8\pi} \frac{B^2 \ell R \cos\alpha \, d\alpha}{1 + 2\,\Delta g/g \cos\alpha + (\Delta g/g \cos\alpha)^2} \quad \text{newtons} \tag{9.191}$$

Discarding the term $[(\Delta g/g)\cos\alpha]^2$ in the denominator since it is negligible in comparison to $(1 + 2\,\Delta g/g \cos\alpha)$, we obtain

$$dF_v = \frac{10^7}{8\pi} \frac{B^2 \ell R \cos\alpha \, d\alpha}{1 + 2\,\Delta g/g \cos\alpha} \quad \text{newtons} \tag{9.192}$$

Multiplying numerator and denominator by the expression $[1 - 2\,\Delta g/g)\cos\alpha]$

$$dF_v = \frac{10^7}{8\pi} \frac{B^2 \ell R[1 - (2\,\Delta g/g)\cos\alpha]\cos\alpha \, d\alpha}{1 - (2\,\Delta g/g \cos\alpha)^2} \quad \text{newtons} \tag{9.193}$$

Again discarding the term $[2\,(\Delta g/g)\cos\alpha]^2$ in the denominator since it is negligible in comparison to 1, we have

$$dF_v = \frac{10^7}{8\pi} B^2 \ell R \left(1 - \frac{2\,\Delta g}{g}\cos\alpha\right)\cos\alpha \, d\alpha \quad \text{newtons} \tag{9.194}$$

Integrating eq. (9.194) from $\alpha = \pi/2$ to $\alpha = \pi$ and multiplying by 2 to determine the vertical component of force exerted on the bottom half of the rotor gives us

$$F_{vb} = \frac{10^7}{8\pi} 2B^2 \ell R \int_{\pi/2}^{\pi} \left(1 - \frac{2\,\Delta g}{g}\cos\alpha\right)\cos\alpha \, d\alpha \quad \text{newtons} \tag{9.195}$$

which may be written as

$$F_{vb} = \frac{10^7}{8\pi} 2B^2 \ell R \left(\int_{\pi/2}^{\pi} \cos\alpha \, d\alpha - \int_{\pi/2}^{\pi} \frac{2\,\Delta g}{g}\cos^2\alpha \, d\alpha\right) \quad \text{newtons} \tag{9.196}$$

and

$$F_{vb} = \frac{10^7}{8\pi} 2B^2 \ell R \left(-1 - \frac{2\,\Delta g}{g}\,\frac{\pi}{4}\right) \quad \text{newtons} \tag{9.197}$$

which is the vertical component of force exerted on the bottom half of the rotor by the air-gap flux. Integrating eq. (9.194) from $\alpha = 0$ to $\alpha = \pi/2$ and multiplying by 2 to determine the vertical component of force exerted on the top half of the rotor, we obtain

$$F_{vt} = \frac{10^7}{8\pi} 2B^2 \ell R \int_0^{\pi/2} \left(1 - \frac{2\,\Delta g}{g} \cos\alpha\right) \cos\alpha \, d\alpha \quad \text{newtons} \tag{9.198}$$

and

$$F_{vt} = \frac{10^7}{8\pi} 2B^2 \ell R \left(1 - \frac{2\,\Delta g}{g}\,\frac{\pi}{4}\right) \quad \text{newtons} \tag{9.199}$$

Adding eqs. (9.197) and eq. (9.199) to determine the magnitude and direction of the net force on the rotor along the vertical axis gives us

$$F_v = -\frac{10^7}{8\pi} B^2 2\pi R \ell \,\frac{\Delta g}{g} \quad \text{newtons} \tag{9.200}$$

or

$$F_v = -\frac{10^7}{8\pi} B^2 A_c \,\frac{\Delta g}{g} \quad \text{newtons} \tag{9.201}$$

where $A_c = 2\pi R\ell$ is equal to the area of the rotor cylinder. The negative sign of eq. (9.200) indicates that the net vertical component of unbalanced magnetic pull is exerted in a downward direction, as anticipated, and may be discarded. The term $\Delta g/g$ is the per unit displacement of the rotor relative to the normal radial gap and B is the average gap density.

Equation (9.201) has been derived in terms of the MKS system of units. If B is in units of maxwells/inch^2, Δg and g are in units of inches, and A_c is in units of inches^2, the equation is

$$F_v = -\frac{B^2 A_c}{(10^6)(72)}\,\frac{\Delta g}{g} \quad \text{pounds} \tag{9.202}$$

The stator winding configuration has a significant effect on unbalanced magnetic pull, which is not shown by eq. (9.201) or (9.202). As discussed above, an offset in the rotor position causes a difference in the average air-gap flux density. Accordingly, the voltages induced in the coils located in areas of high flux density will be greater than in coils located in areas of low flux density. This, in turn, will cause currents to flow such as to oppose the cause, or to tend to equalize the flux densities in the air gap. The greater the number of parallel circuits/phase, the greater is the ability of the stator winding to be effective in equalizing any differentials in the air-gap flux density. Both analysis and testing show that unbalanced magnetic pull is approximately, but not exactly, inversely proportional to the number of parallel circuits in the stator phase winding. Thus an n-circuit winding will have approximately 1/n of the unbalanced magnetic pull for a given per unit offset as that of an otherwise identical case, except for the case of a series stator winding. The exception to this generalization is that of two-circuit windings, for which the test results are inconsistent to some extent. One explanation for this is that the physical orientation of the winding, relative to the offset, affects the ability of the two-circuit winding to equalize differences in air-gap flux densities. Then, to make them applicable to windings in general, eqs. (9.201) and (9.202) should be divided by C, the number of parallel circuits in the stator winding, with the understanding that for a two-circuit winding, C should be set at C = 1, as for a series circuit. Then

$$F = \frac{10^7}{8\pi} \frac{B^2 A_c}{C} \frac{\Delta g}{g} \quad \text{newtons} \tag{9.203}$$

for MKS units, and

$$F = \frac{B^2 A_c}{(10^6)(72)} \frac{\Delta g}{g} \quad \text{pounds} \tag{9.204}$$

when inches, pounds, and maxwells are used as units. The negative signs have been discarded in eqs. (9.203) and (9.204), with the understanding that unbalanced magnetic force is an average force on the rotor in the direction of the offset.

The ability of parallel circuits to reduce the magnitude of magnetic pull is further enhanced by the use of equalizer connections. Corresponding points in parallel circuits will all be at essentially identical potentials if the average air-gap flux density is the same around the air gap. Then an electrical cable connecting such points should not experience any current flow under conditions of a rotor located concentric to the stator bore. If, however, the rotor is offset such that there is a difference in flux density in different locations, the voltage induced in coils located in the region of greater flux density will be greater than that in coils located in the region of less flux density. The presence of cable between corresponding points in parallel circuits, such as the midpoints, will allow equalizing currents to flow which, as discussed above for parallel circuits, tend to equalize any difference in flux density around the air gap. The use of equalizer connections permits equalizing current to flow between more points of what should be equal potential, thereby increasing the amount of equalization possible compared to that of parallel circuits alone.

There are several additional items that tend to make the magnitude of magnetic pull slightly less than that calculated by the equations above. In the derivation of unbalanced magnetic pull, it was assumed that the magnetomotive force drop across the flux path in the magnetic steel of the stator and rotor cores was negligible in relation to that across the air gap (i.e., that there was no saturation). The effect of saturation is to reduce magnetic pull slightly. Also, current flow in the rotor bars of a squirrel-cage rotor tends to reduce magnetic pull somewhat, although the winding of a wound-rotor motor has less effect in such a reduction. In addition, leakage permeance paths between the rotor and stator, such as through the shaft, end shields, or bearing brackets, bearings and frame, allow alternate paths for flux between the rotor and stator. To the extent that such paths exist, they tend to slightly lower magnetic pull. This effect is most pronounced for two-pole machines, for which the flux/pole is the greatest. For two-pole machines, leakage permeance can make a difference in the force of several percentage points. For machines with a greater number of poles, the effect is negligible. Finally, the way in which the groups are connected in series to form a circuit appears to have some effect on the amount of magnetic pull produced by a given machine. Intuitively, it would seem that windings with "opposite poles in series" should result in the optimum connection, since the same current is forced to flow through diametrically opposite portions of the stator winding. However, testing and field experience does not consistently support this conclusion. Other factors, such as physical symmetry of the windings and connection leads, also appear to have some effect.

Although specific practices may differ among engineers, a prevalent practice is to use eqs. (9.203) and (9.204) as given, or in slightly modified forms, to calculate unbalanced magnetic pull and in the design of the stator winding, to avoid series circuits, to use as many parallel circuits as is consistent with cost and other design considerations, and for two-circuit and three-circuit windings, consider the use of equalizer connections when calculations indicate that not using them would result in too high a value of magnetic pull. Also, to counter the effect of unbalanced magnetic pull, as well as for justifiable mechanical reasons, the shaft, frame, end shields or bearing brackets, bearings, rotor spider, and rotor core should be designed to be sufficiently stiff.

Before leaving the subject of magnetic pull, it will be noted that the subject is more complicated than just the consideration of the average force in the direction of the offset. Machines are also subject to two times line frequency forces, due to a rotor offset. This is a force component in addition to the usual force of two times line frequency, in a mode for which the number of nodes is twice the number of poles. Equalizer connections will tend to reduce this force, as well as the average force associated with an offset rotor. Also, under certain conditions, a torque can be produced which attempts to cause the rotor to whirl with the point of minimum gap rotating at synchronous speed. The electromagnetic fundamentals associated with forces of two times line frequency will be more easily understood after the stator magnetomotive-force wave is considered.

9.19 NUMERICAL EXAMPLE OF CALCULATION OF UNBALANCED MAGNETIC PULL

Calculation of unbalanced magnetic pull will be illustrated with a numerical example. Assume that the design engineer is considering various alternatives at the electromagnetic design stage of a 1000-hp three-phase 60-H 4000-V squirrel-cage induction motor. Among the electromagnetic alternatives being considered are the following two:

Parameter	Design X	Design Y	Units
Stator bore, d	20	20	inches
Core length, ℓ	15	16	inches
Air-gap length, g	0.080	0.075	inches
Maximum air-gap flux density, B_{gm}	40,000	39,000	maxwells/inch^2
Number of stator circuits/phase, C	2	3	numeric

The design engineer is interested in knowing, among other characteristics, the unbalanced magnetic pull for each design alternative.

The rotor surface area A for design X is equal to

$$A = \pi[(d - 2g)]\ell = \pi[(20 - 0.16)][(15)] = 934.9 \quad \text{inches}^2 \tag{9.205}$$

The air-gap flux density for design X is given in the tabulation as B_{gm} = 40,000 M/in^2. This is the maximum value of air-gap flux density, whereas the average value is used in calculating unbalanced magnetic pull. Since the ratio of the average to the maximum value of a sine wave is $2/\pi$, the average value of air-gap flux density for design X is

$$B_g = \frac{2}{\pi}(40,000) = 25,500 \quad \text{maxwells/inch}^2 \tag{9.206}$$

The equation for calculating unbalanced magnetic pull, using units of inches, maxwells/inch^2, and pounds, is

$$F = \frac{B^2 A}{(10^6)(72)(C)} \frac{a}{g} \quad \text{pounds} \tag{9.207}$$

Using an offset of the rotor of 10% (i.e., a/g = 0.10) and substituting the values above for design X into eq. (9.207), but remembering that for series and two-parallel circuits the number of stator circuits/phase C should be set at 1, we have

$$F = \frac{(25,500)^2(934.9)(0.10)}{(10^6)(72)(1)} = 844.3 \quad \text{pounds} \tag{9.208}$$

Repeating the procedure above for design Y gives us

$$F = \frac{(24,200)^2(997.8)(0.10)}{(10^6)(72)(3)} = 270.5 \quad \text{pounds} \tag{9.209}$$

If the parameters are converted to MKS units, the corresponding values for design X are:

stator bore, d $= \dfrac{20}{39.37} = 0.508$ m

core length, ℓ $= \dfrac{15}{39.37} = 0.381$ m

average air-gap flux density, B_g $= \dfrac{2}{\pi}(40,000)(39.37)^2\left(\dfrac{1}{10^8}\right)$

$= 0.395$ W/m^2

air-gap length, g $= \dfrac{0.08}{39.37} = 0.002$ m

In MKS units, the rotor surface A is equal to

$$A = \pi[(d - 2g)]\ell = \pi[(0.508 - 0.004)][0.381] = 0.603 \quad \text{meters}^2 \tag{9.210}$$

The equation for unbalanced magnetic pull, using MKS units, is

$$F = \frac{10^7 B^2 A}{8\pi C}\,\frac{a}{g} \quad \text{newtons} \tag{9.211}$$

Substituting the values above into eq. (9.211), the unbalanced magnetic pull for a 10% rotor offset for design X is equal to

$$F = \frac{(10^7)(0.395)^2(0.603)(0.10)}{(8\pi)(1)} = 3743 \quad \text{newtons} \tag{9.212}$$

Since there are 4.448 newtons in 1 pound of force,

$$F = \frac{3743}{4.448} = 842 \quad \text{pounds} \tag{9.213}$$

which corresponds to eq. (9.208).

9.20 TEMPORARY OPERATION WITH DAMAGED STATOR COILS

Induction motors of various sizes are used on applications for which it is critical that the driven equipment not be shut down for a prolonged period. Power station auxiliaries and key drive motors in continuous-process plants, are typical of such applications. In some cases a backup motor is already in place and can immediately be put into service after a given motor fails; frequently, this is done automatically by the plant's control system. In other cases, at least for some standard ratings, spare motors are available at the site, and in a relatively short time, a replacement motor can be put into service following a motor failure, with small loss in production at the plant. However, there are a large number of critical drive motors for which backup has not been provided. Accordingly, the chief engineer of the plant will be motivated to make a temporary repair in order to protect plant production, in case of failure of such a motor. The following discussion addresses this situation.

Historically, the component of an industrial induction motor most likely to fail is the winding or the bearings. If a bearing should fail, it would normally be expected that the plant would have spare bearings in storage, or that a bearing could be obtained quickly from local sources. In either case, the time required to replace a failed bearing should not be great. If, on the other hand, one or more stator coils should fail, removal of the old coils and replacement with new ones would require considerable time and loss of plant production. If there are only one or so failed coils per circuit, one action frequently considered is to electrically disconnect the failed coils, leaving the leads of the failed coil open circuited, and then to reconnect the disturbed group by "jumpering" around the failed coil. If it is feasible, such a practice would permit the plant to continue production while replacement coils were being made by the manufacturer. This practice is referred to as "cutting out" coils.

The action described above is fraught with considerable risk and should not be undertaken without sufficient study by a person competent to make such a study. The act of electrically removing a coil from a group and from a circuit results in an electrical imbalance between circuits and is somewhat similar to the serious case of an unbalanced winding. Since the induced voltage as well as the impedance will be different between the affected circuit and the circuits in parallel with it, circulating current will flow between the circuits. Also, circulating current will flow between the phases in the typical case of coil removal. The circulating currents will result in greater stator heating for the same power output, or in less power output for the same heating.

The amount of circulating current that results from the electrical removal of a stator coil is roughly proportional to the square of the reciprocal of the number of coils in series in the original circuit. Thus, if one coil is electrically removed from a stator winding with eight original coils in series in the circuit in one motor, and if one coil is similarly removed from a stator winding with 12 original coils in series in the circuit in another motor, the first motor will, roughly, have $(12/8)^2 = 2.25$, say 2 to 2 1/2, times as much per unit circulating current as the second motor. This, of course, will result in considerably more stator winding heating for the first motor, with the need to reduce the shaft output significantly while operating with a "cutout" coil.

The chief engineer of a plant in which such an action is being considered should make certain that a person competent to do so has (1) fully identified the extent of the winding failure, (2) has adequate information about the normal configuration of the winding, and (3) has had sufficient time to study the facts before being required to make a recommendation. The recommendation should then include a statement that the motor can, or cannot, be operated with the failed coils "cut out" of the winding and if the decision is yes, at what reduced shaft power, without a rate of deterioration of the remainder of the stator winding from excess heating, which is unacceptable to the plant. Large electric utilities and major industrial companies will probably have people in their organizations who are competent to make such decisions and will probably also have policies and procedures concerning such actions. Smaller organizations, which would not be expected to have the specific competence to undertake the above, should not hesitate to find that competence outside their own organizations. The best source of such knowledge is probably the original manufacturer of the motor. If the motor manufacturer is contacted, they should be given the model and serial numbers of the machine and information about the failed winding in sufficient detail that the number of coils to be cut out and their locations within the winding are clear and exact. It is probable that an engineer from the manufacturer's organization will desire to visit the site in order to determine personally all the information that will be required, and that should be encouraged by the owner of the failed motor.

10

Rotor Windings

10.1 Function and Importance of the Rotor Winding 264

10.2 General Types of Rotor Windings 265

10.3 Squirrel-Cage Rotor Windings 266

- 10.3.1 Cast-aluminum rotor winding construction 266
- 10.3.2 Fabricated rotor winding construction 269
- 10.3.3 Stresses in squirrel-cage rotor windings 273
- 10.3.4 Types of squirrel-cage rotor bars 276
- 10.3.5 Deep-bar effect 278
- 10.3.6 Utilization of the deep-bar effect 289
- 10.3.7 Numerical example of use of deep-bar effect 292
- 10.3.8 Concept of the multiple-cage rotor winding 295
- 10.3.9 Use of a lattice network in analyzing the multiple-cage rotor winding 298
- 10.3.10 Numerical example of the use of a lattice network for a rectangular bar 305
- 10.3.11 Numerical example of the use of a lattice network for a multiple-cage bar 309
- 10.3.12 Rotor skew 312
- 10.3.13 Numerical example of calculating skew factor 315
- 10.3.14 Calculation of the phase resistance of a squirrel-cage rotor winding 316
- 10.3.15 Numerical example of calculating phase resistance of a squirrel-cage rotor winding 320
- 10.3.16 Transient temperature rise of the rotor winding during changes in speed 322
- 10.3.17 Numerical example of transient temperature rise of the rotor winding during acceleration 328

10.4 Wound-Rotor Windings 330

10.4.1 Effect of centrifugal force on rotor-coil design and selection 330
10.4.2 Types of wave windings 331
10.4.3 Wound-rotor slots and the corresponding coil configurations 333
10.4.4 Modified-wave winding 336
10.4.5 Wound-rotor distribution factor and pitch factor 341
10.4.6 Phase voltage of the wound-rotor winding 342
10.4.7 Rotor phase current, rotor phase resistance, and rotor I^2R loss 344
10.4.8 Relationship between collector-ring voltage and current 345
10.4.9 Collectors and brushes 347
10.4.10 Brush friction loss and brush electrical loss 349
10.4.11 Numerical example of calculating brush friction and electrical losses 352
10.4.12 Banding of rotor end turns 353

10.1 FUNCTION AND IMPORTANCE OF THE ROTOR WINDING

In previous chapters it has been shown that the air-gap flux wave, rotating at synchronous speed, successively induces a voltage in each of the axially located rotor bars, or coil sides, which form the rotor winding. The resulting voltage wave of the rotor winding rotates at an angular velocity of ω radians/second as seen from a point on the stator. This rotating voltage wave, in turn, successively causes a current to flow in each of the rotor bars, or coil sides, producing a rotor winding current wave which also rotates at an angular velocity of ω radians/second as seen from a point on the stator. The current wave lags the induced voltage wave, in time, by θ_2 electrical radians, which is equal to the power-factor angle of the rotor phase winding.

As shown previously, the rotor phase current reacts on the air-gap flux to produce a torque, the magnitude of which is proportional to the air-gap flux, to the rotor phase current, and to the sine of the angle γ between them, or

$$T = 3\phi \times I_2 = 3\phi I_2 \sin \gamma \quad \text{newton-meters} \qquad (10.1)$$

for a three-phase machine, where $\phi \times I_2$ is the vector cross product of the two quantities. As shown in Chapter 7, eq. (10.1) reduces to

$$T = 3\phi I_2 \cos \theta_2 \quad \text{newton-meters} \tag{10.2}$$

where, as stated above, θ_2 is the power factor of the rotor phase winding. The physical relationship between angle γ and angle θ_2 is shown in Fig. 7.2. The torque produced by the rotor phase current reacting on the air-gap flux accelerates the rotational inertia of the rotor structure and of the connected load to full speed and then drives the connected load at full speed. Thus the rotor phase current, in cooperation with the air-gap flux wave produced by the stator winding develops the accelerating and the load torque for which the machine is designed. The rotor winding, then, in coordination with the stator winding and with the stator and rotor cores, which carry the mutual flux, completes the transformation of electrical energy into mechanical energy in rotational form at the drive shaft.

10.2 GENERAL TYPES OF ROTOR WINDINGS

The two types of polyphase induction motor rotor windings in general use are the squirrel-cage type and the phase-wound type. Although these two types of rotor windings differ considerably in detail, both perform the same fundamental functions, as delineated in the preceding paragraph. Phase-wound rotor windings, which are usually called wound-rotor windings, are made up of individual coils in a manner similar to, but not identical with, the stator windings discussed in Chapter 9. The three individual phase windings are usually connected in wye, although some have been connected in delta, to form the three-phase rotor winding. Leads from the terminals of the rotor winding are "brought out" for external connection by means of collector rings, or slip rings, which rotate with the winding, and which mate with brushes, which are stationary. This permits variable resistance to be inserted externally into the rotor winding, for increasing the starting torque, for reducing the starting current, and for controlling the operating speed, as discussed previously.

Squirrel-cage rotor windings consist of axial uninsulated bars, which are short circuited at each end of the rotor core by circumferential end rings. This configuration of conducting material allows axial rotor currents to flow, the flow pattern of which generally mimics that of the companion stator winding as discussed previously. Such windings are formed by casting using the rotor core as a partial mold, and by fabrication, in which the axial bars are brazed or welded to the circumferential end rings. Cast rotor windings are made of aluminum or aluminum alloys. Fabricated rotor windings are made of copper or copper alloys, and of aluminum or aluminum alloys.

Phase-wound rotor windings and squirrel-cage rotor windings are both discussed later in this chapter. The majority of polyphase induction motors manufactured and placed in service are squirrel-cage motors.

However, there are also a considerable number of wound-rotor motors in service. Some of the largest ratings of induction motors are those of wound-rotor motors. Such machines would have a prohibitive effect on the local electric utility systems during startup if the starting kVA were not reduced by the use of external resistance in the motor circuit during the starting period.

10.3 SQUIRREL-CAGE ROTOR WINDINGS

10.3.1 Cast-Aluminum Rotor Winding Construction

A cast-aluminum rotor winding consists of a set of uninsulated aluminum rotor bars which are short-circuited at each end by circumferential aluminum end rings. The two end rings, the inboard sides of which seat against the ends of the rotor core, perform the dual function of completing the electrical circuit of the rotor winding and of assisting in mechanically retaining the rotor punchings in an axial direction. The casting is produced by utilizing the stacked rotor core as a partial mold to form the rotor bars and by using additional circumferential molds, located on each end of the core, to form the two end rings. Figure 10.1 shows a simplified, sectional view of such a mold arrangement, as viewed through a plane that has been passed through a diameter of the core and end-ring mold.

The melting point of aluminum is about 660°C, or 1220°F. The melting point of steel depends on the amount of carbon, silicon, and other elements present, but it is in the vicinity of 1370°C, or 2500°F. Accordingly, it is possible to utilize the stacked rotor core as part of the mold, for containment of the molten aluminum, and to produce cast-aluminum rotors without injury to the steel of which the core is made.

The electrical resistivity of aluminum is about $3.7 \times 10^{-8}\ \Omega \cdot \mathrm{m}$ at operating temperature. The electrical resistivity of steel can vary from 20×10^{-8} to $160 \times 10^{-8}\ \Omega \cdot \mathrm{m}$ at operating temperature, depending on the elements in addition to iron that are present. Thus the electrical resistivity of the steel core would be at least one order of magnitude greater than that of the aluminum rotor bars, even if the core is made of solid steel. However, the rotor core is a laminated structure, made of a stack of punchings, each of which is from about 0.50 mm (0.019 in.) to about 0.60 mm (0.024 in.) thick. There will be several hundred such laminations in one core length. The surface of the laminations may have received any one of several kinds of treatment, which will have increased the electrical resistivity across the laminations. The net effect of all of the above is that the electrical resistivity across the laminations of the rotor core is at least two orders of magnitude greater than along the rotor bar, located in the slot. Conversely stated, the electrical conductivity along the aluminum rotor bar in the slot is at least two orders of magnitude greater than that across the rotor laminations outside the slot. Accordingly, the axial rotor current flow in

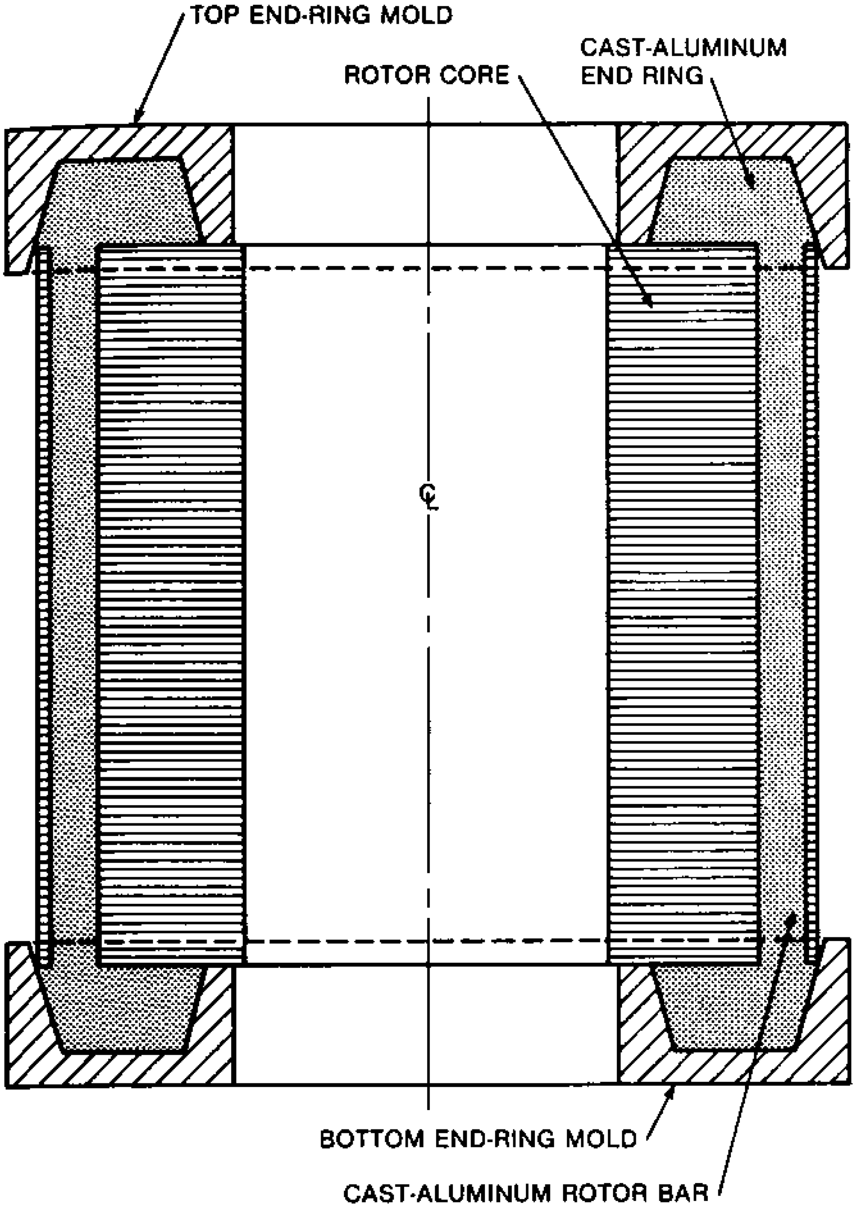
TOP END-RING MOLD
ROTOR CORE
CAST-ALUMINUM END RING
℄
BOTTOM END-RING MOLD
CAST-ALUMINUM ROTOR BAR

FIGURE 10.1 Simplified cross-sectional view of rotor core and end-ring molds used for producing a cast-aluminum rotor winding.

response to the induced rotor voltage will be properly channeled within the bar and a cast-aluminum squirrel-cage rotor winding will operate satisfactorily without ground insulation.

Cast-aluminum rotor slots may be closed at the top or they may be semiclosed, with the width of the opening at the air gap considerably less than that of the rest of the slot. For semiclosed slots, a temporary dam must be positioned over the slot opening for all slots and for the full length of the rotor core, prior to casting the rotor. This may be done in various ways, such as by the use of slightly tapered temporary inserts or by placing a specially designed temporary band around the periphery of the rotor core.

Also, as the size and rating of the motor increase, a point is reached where it is desirable to use radial air ducts in the rotor and stator cores to improve heat dissipation. For some manufacturers this point is reached within the range of ratings for which cast-aluminum rotor winding construction is used. For such cases, additional steps must be taken to confine the molten aluminum as it passes the intersections of the slot channel and the radial air ducts. A variety of ways, with different degrees of cost, simplicity, ease of use, and so on, have been used by the various manufacturers to accomplish this. They generally fall into three categories: (1) permanent circumferential slot channels across the ducts, which are made from steel or other metal with a high melting point relative to aluminum; (2) sacrificial circumferential channels, which are made from a brittle metal alloy or ceramic which is easily shattered and removed after casting; and (3) removable and reusable circumferential channels, which are made from a metal with a high melting point relative to aluminum.

Casting of the rotor winding is normally done with the rotor core in vertical orientation, as shown in Fig. 10.1. The molten aluminum may be poured, using gravity feed, or it may be injected into the mold under pressure. A system of risers may be employed to vent captured gases within the mold cavity, as well as to provide a reservoir feed for preventing shrinkage of the poured aluminum just prior to solidification. Also, the casting may be done with the core and end-ring molds rotating, in order to utilize the effect of centrifugal force in distributing the molten metal, or it may be done statically. Factors that influence the choice of the casting process are the cross-sectional area of the slot, the cross-sectional area of the end ring, the length of the core, the total volume of the aluminum winding, the temperature of the steel core just prior to pouring the molten aluminum, past practices that have proven successful, and the total cost of the process. Figure 10.2 shows a cast-aluminum squirrel-cage rotor winding after the steel punchings of the core have been removed. Fan blades and rotor-balancing studs may also be cast as an integral part of the end rings by providing corresponding configurations in the pattern from which the end-ring mold is made. A completed squirrel-cage rotor with a cast-aluminum winding is shown in Fig. 10.3.

The simplicity and reliability of cast-aluminum rotor windings make such windings a very desirable design choice for use in squirrel-cage machines. Accordingly, essentially all squirrel-cage polyphase induction motors, through about 500 hp at 1800 rpm, utilize cast-aluminum rotor windings. In addition, some manufacturers have successfully used such rotor windings in larger ratings. However, as the machine size increases, such parameters as (1) the volume of the mold cavity, which must be filled with molten aluminum, (2) the volume of steel rotor core, which acts as a heat sink, and (3) the length of the passages through which the molten aluminum must flow all increase. The net result is that because of scale effects associated with increasing size, a point is reached at which a

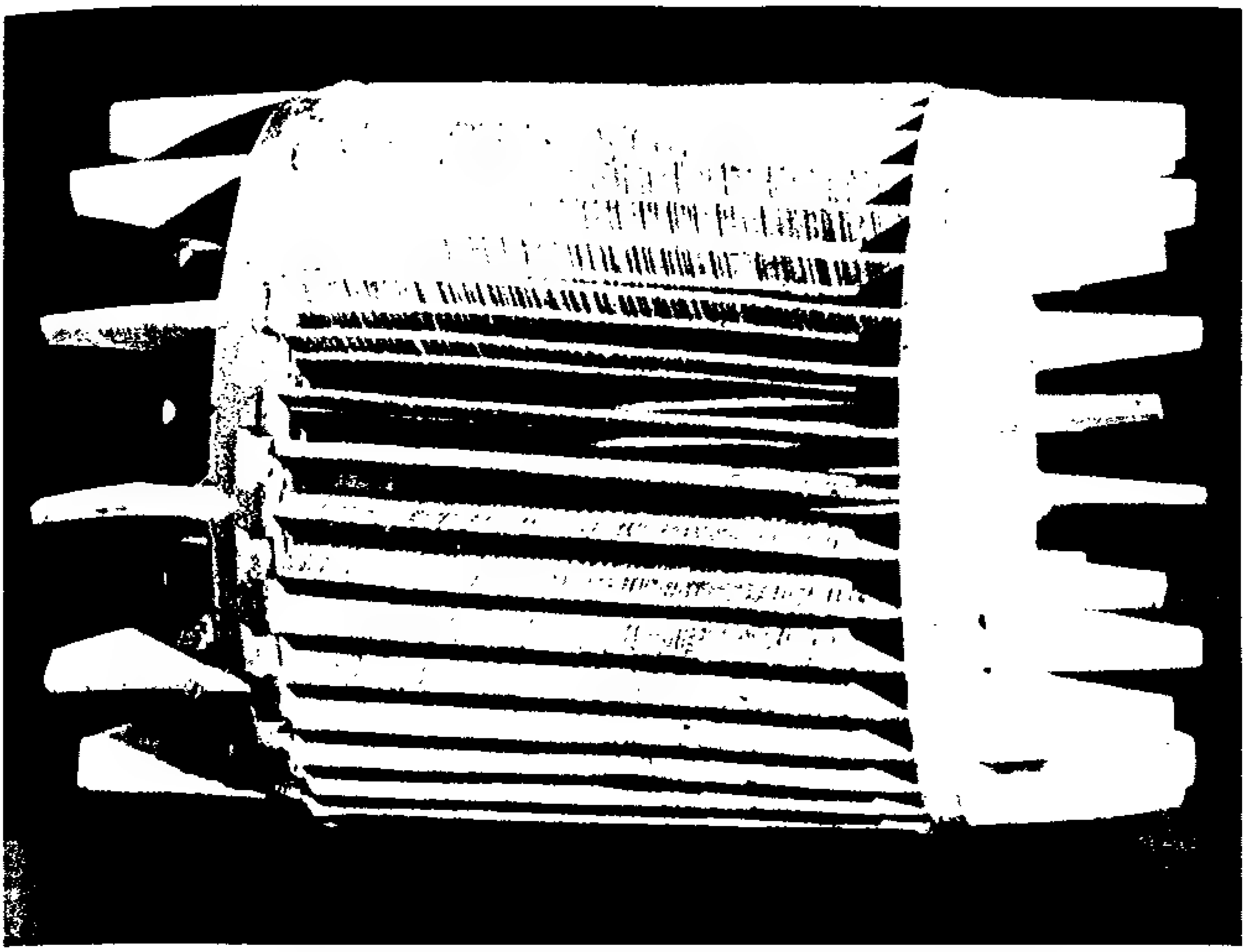

FIGURE 10.2 Cast-aluminum rotor winding after the steel rotor punchings have been removed.

transition is made from cast aluminum to fabricated rotor windings. Although as stated above, it varies from one manufacturer to another, the transition point typically is in excess of a rating of 500 hp at 1800 rpm.

10.3.2 Fabricated Rotor Winding Construction

In form and function a fabricated squirrel-cage rotor winding is generally similar to a cast squirrel-cage rotor winding except that it is a fabrication instead of a casting. Also, unlike some cast windings, which have fan blades integrally cast with the end rings, the fan blades of fabricated rotors are separately mounted and are not part of the end-ring structure. The rotor bars and end rings are made of copper and copper alloys, and of aluminum and aluminum alloys. The bars are driven into one end of the slot channels of the rotor core, the slots of which may be closed or semiclosed at the air-gap surface of the rotor. End rings are formed by circumferentially rolling

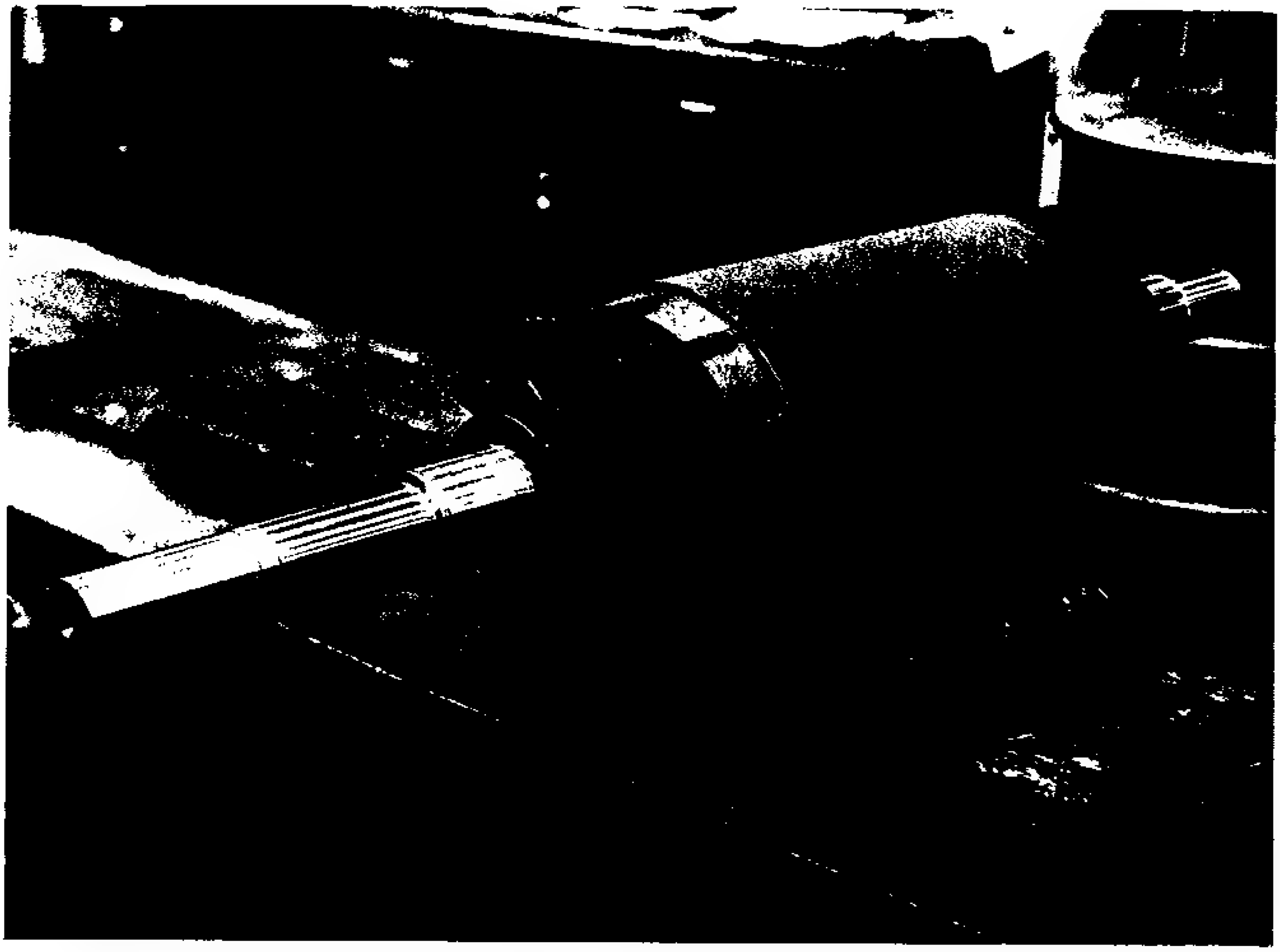

FIGURE 10.3 Completed squirrel-cage rotor with a cast-aluminum winding.

rectangular metal stock, or by metal casting, as a separate operation, prior to assembly.

The end ring is positioned against the corresponding rotor bars in various ways in preparation for metal joining. The end ring may or may not have axial grooves milled into the outside diameter (OD) to receive the bars. Figure 10.4 shows an end view and a lateral view of four typical practices for fitting the end ring against the corresponding rotor bars. Figure 10.4a shows a basic joint in which the mechanical joint and the electrical conducting surface are located at the bottom edge of the rotor bar and the mating part of the OD of the end ring, on which it seats. This joint is used primarily with copper or copper alloy bars and end rings, for which the metal joint is made by brazing. Figure 10.4b shows a refinement of this practice, in which the rotor bars are located in axial grooves that have been machined into the top portion of the end ring. The electrical conducting surface is located around the three sides of the bar, which are in contact with the ring. Again, this practice is used primarily with copper or copper alloy bars and end rings, and the metal joint is made by brazing.

Figure 10.4c shows a practice in which the end ring has both axial grooves in the top portion and a circumferential step in the upper, outboard corner. The void associated with this step provides a circumferential cavity for receiving a metal deposit in an automated metal-joining procedure such as tungsten-inert gas welding, for use with aluminum or aluminum alloy. Electrical conduction is from the end of the bar to the bottom of the

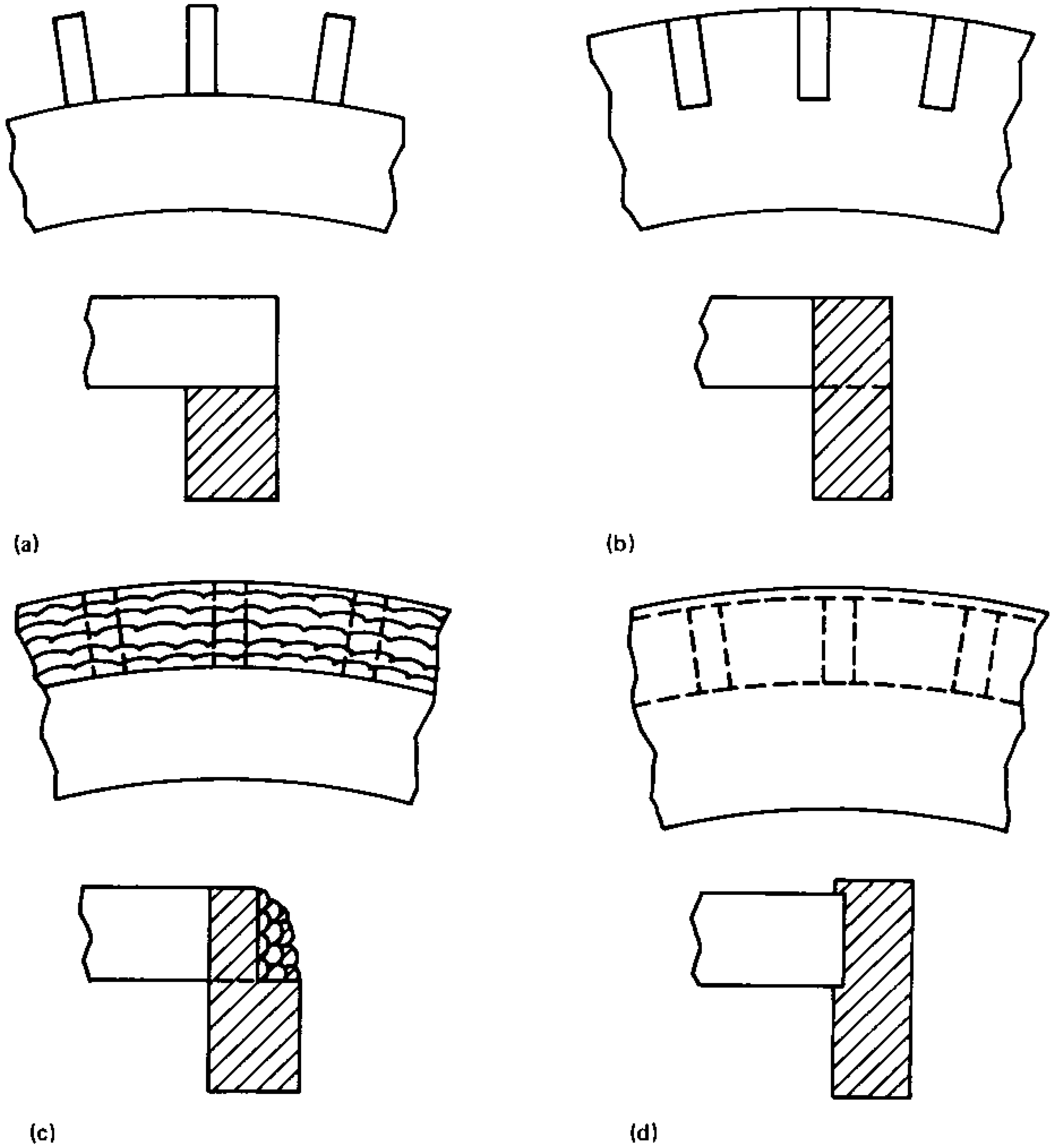

FIGURE 10.4 Various ways of joining rotor bars to end rings for fabricated rotors: (a) basic joint; (b) joint with recessed purchase; (c) joint with recessed purchase and preparation for welding; (d) joint with circumferential preparation on side of end ring.

circumferential step in the end ring, through the deposited metal. The end ring may be produced by rolling of rectangular metal stock to form the ring, followed by machining. However, it may be preferable to produce it as a separate casting, depending on the size of the ring and the amount of production. For this type of construction, the inboard side of the end ring can be positioned against the outboard end of the rotor core, to serve a second function of helping to retain the rotor punchings in an axial direction. Figure 10.5 shows a rotor for which such construction has been used to produce the squirrel-cage winding. The circumferentially deposited metal on the outboard end of the end ring, resulting from the welding process, is apparent from the axial view of the rotor. Figure 10.6 shows a similar rotor, complete with fans, ready to be installed into a machine.

Figure 10.4d shows a practice in which a circumferential groove has been prepared on the inboard side of the end ring. This groove has the proper radial depth to receive, and to seat, the ends of the rotor bars. It serves the two functions of mechanically locating the end ring relative to the bars, and of serving as a preparation for brazing the two parts together. If the

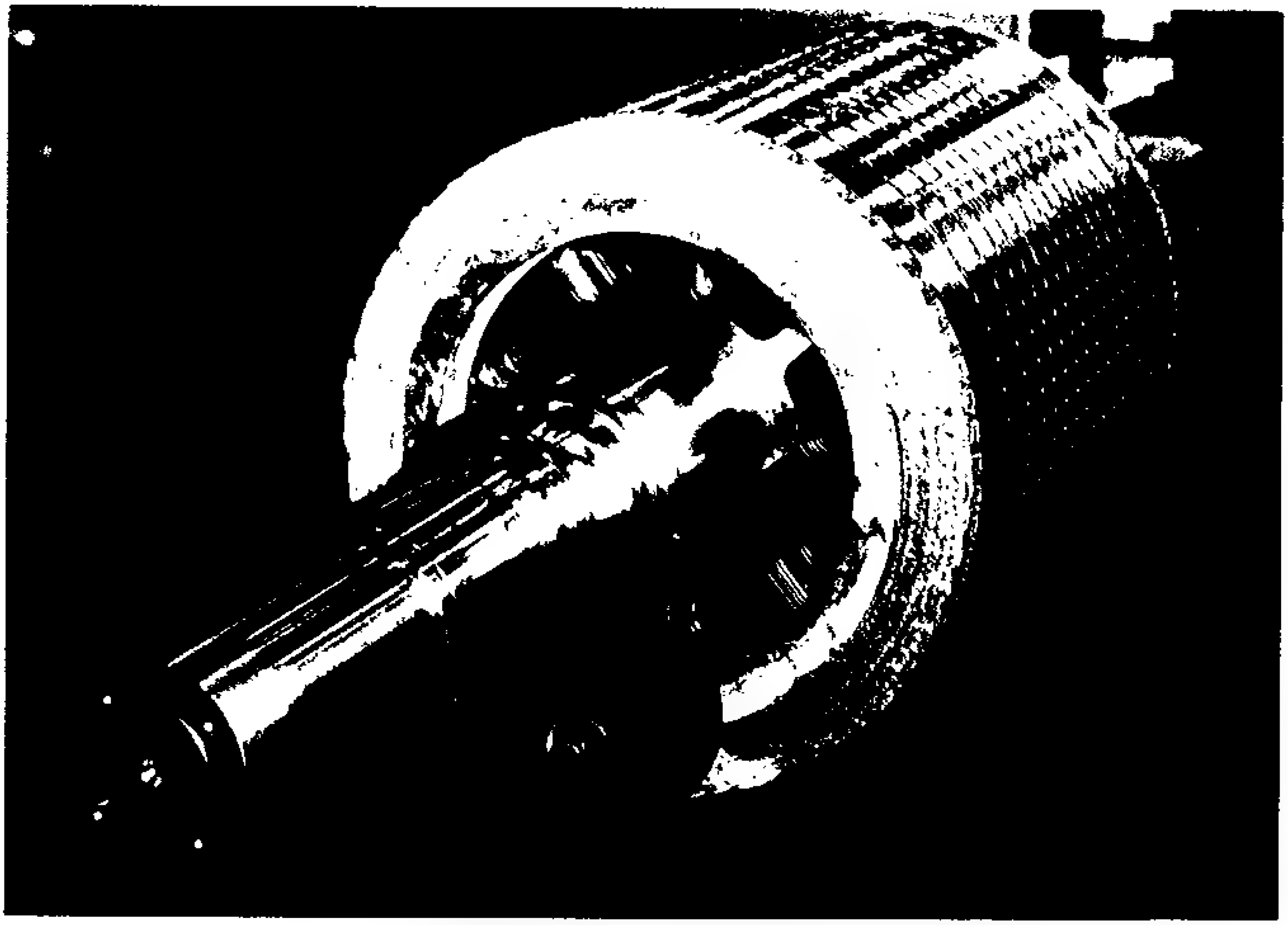

FIGURE 10.5 Squirrel-cage rotor with a fabricated-aluminum winding immediately after welding of the cage.

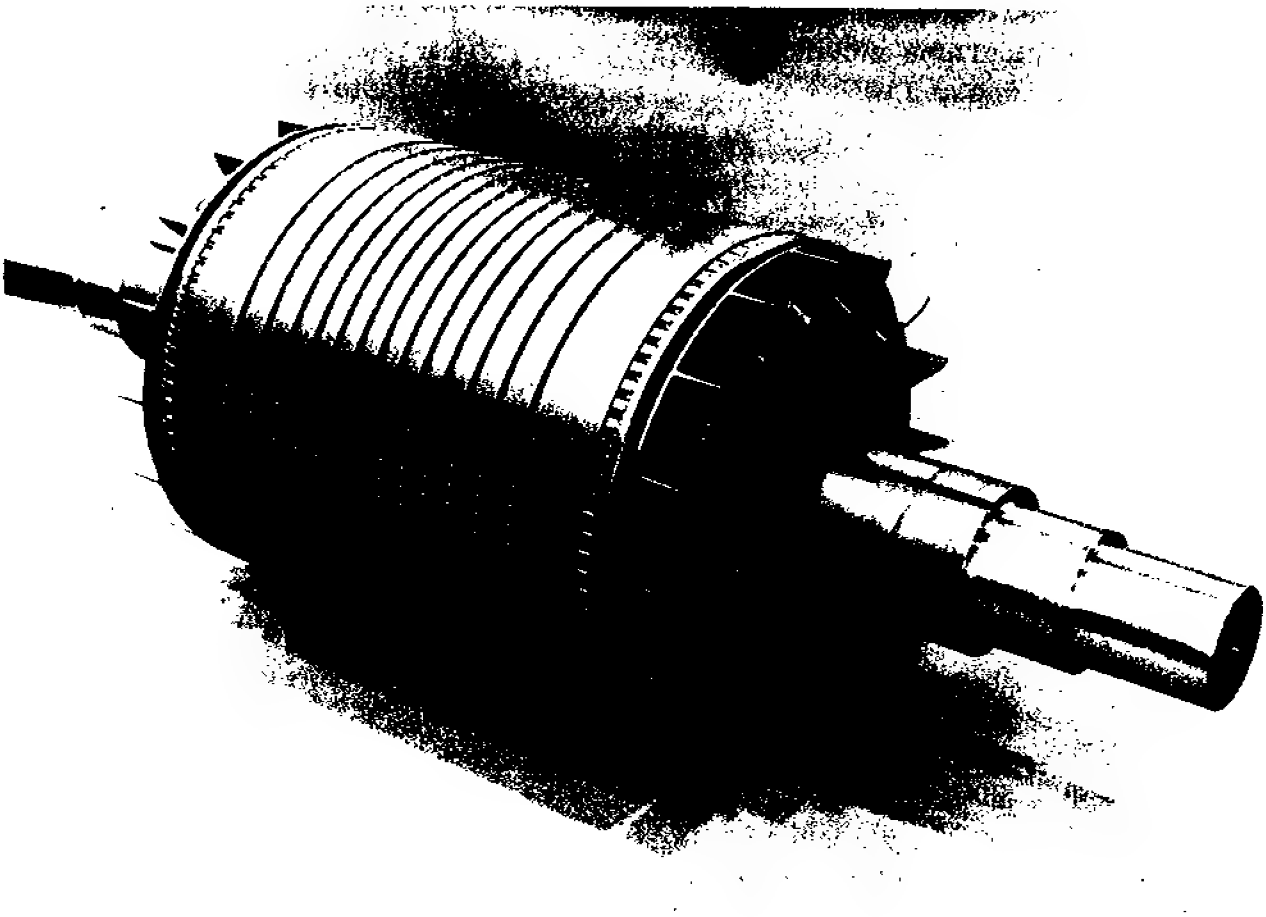

FIGURE 10.6 Completed squirrel-cage rotor with a fabricated winding.

rotor is oriented with its axis in a vertical position, the circumferential groove can act as a retaining basin for molten brazing material, with the opportunity for some degree of process automation. After one end is brazed, the rotor can be rotated end for end, and the opposite end can then be brazed. This construction is more adaptable to rotor windings made of copper and copper alloy than to those made of aluminum and aluminum alloy.

10.3.3 Stresses in Squirrel-Cage Rotor Windings

The rotor winding is subjected to both mechanical and thermal stresses and the design of the winding must be adequate to withstand such stresses. The mechanical stresses result from centrifugal force due to the rotation of the rotor. The thermal stresses result primarily from transient differences in temperature between the circular end ring and the circular rotor punchings, caused by acceleration, plugging, reversal, and so on, of the rotor. The mechanical and thermal stresses are considered in more detail in a subsequent chapter. Here they are considered only to the extent of discussing the parameters that affect their magnitudes.

From Newtonian mechanics, the centrifugal force exerted on a body of mass m kilograms moving in a curved path with a tangential velocity of v meters/second and with a radius of curvature of R meters at the point in the curved path being considered is equal to

$$F = m\frac{v^2}{R} \quad \text{newtons} \tag{10.3}$$

Since the rotor winding rotates in a circular path, at a constant speed of n rpm, the tangential velocity v of a point on the winding is equal to

$$V = \frac{2\pi Rn}{60} \quad \text{meters/second} \tag{10.4}$$

where R is the radius of gyration of that point. Substituting eq. (10.4) into eq. (10.3) to express centrifugal force F in terms of the speed of rotation gives us

$$F = \frac{m}{R}\left(\frac{2\pi Rn}{60}\right)^2 = \left(\frac{2\pi}{60}\right)^2 mRn^2 \quad \text{newtons} \tag{10.5}$$

Equation (10.5) may be expressed in the FPS system of units by remembering that for m, 1 kilogram = 0.4536 pound, that 1 meter = 39.37 inches, and that for F, 1 newton = 1/4.448 pound. Then

$$F = \left(\frac{2\pi}{60}\right)^2\left(\frac{0.4536}{39.37}\right)\left(\frac{1}{4.448}\right)WR(\text{rpm})^2$$

$$= 28.4WR\left(\frac{\text{rpm}}{1000}\right)^2 \quad \text{pounds} \tag{10.6}$$

where W is the weight in pounds and R is the radius of gyration in inches.

To appreciate the effect of dimensions, or scale, on the mechanical stresses within the parts of a rotor, consider the following. The normal volume and weight of a motor component tend to increase by a power of from 2 to 3 of the linear dimensions, depending on the part, for a line of reasonably homogeneous polyphase induction motors. Let a certain rotor part near the OD of the rotor weigh 5 lb for a rotor with a rotor diameter of 10 in. Then, for another machine, with a rotor diameter of 20 in., the corresponding rotor part could be expected to weight about $(5)(20/10)^{2.5} =$ 28.3 lb. Assuming that both motors operate at 1785 rpm and utilizing eq. (10.6), the centrifugal force associated with the 5-lb part for the rotor with a 10-in. diameter is

$$F = (28.4)(5)\left(\frac{10}{2}\right)\left(\frac{1785}{1000}\right)^2 = 2262 \quad \text{pounds} \tag{10.7}$$

For the corresponding 28.3-lb part for the motor with a 20-in. diameter, the centrifugal force is

$$F = (28.4)(28.3)\left(\frac{20}{2}\right)\left(\frac{1785}{1000}\right)^2 = 25,608 \quad \text{pounds} \tag{10.8}$$

Comparisons of eqs. (10.7) and (10.8) show that the centrifugal force associated with a given rotor part, for a homologous line of induction motors, increases by about a factor of 10 for a linear dimensional increase of 2 in the product line. This would suggest, and experience has verified, that as the rating increases, mechanical stress considerations become an increasingly important part of the design of the rotor structure, including the rotor winding. For the polyphase induction motor ratings in the standard NEMA motor frames, the mechanical stress level in the rotor winding, although considered, is not a determining factor in the configuration of the winding. However, at a rating of 1000 hp at 1800 rpm, mechanical stresses in the rotor body and winding must be considered, and at a rating of a few thousand horsepower they become one of the significant factors in the mechanical design and configuration of the total rotor, including the winding.

Thermal stresses in the rotor winding result from the high rate at which energy is dissipated in the rotor winding, which occurs concurrent with, and as a result of, a change in speed of the rotating structure. As will be shown subsequently in this chapter, a quantity of energy which is approximately equal to the kinetic energy stored in the rotational inertia of the motor rotor and connected load is dissipated in the rotor winding during the time that the machine is accelerating.

The opportunity for transfer of such energy from the rotor winding into adjacent parts and into the ambient during the short time involved is limited. Accordingly, 90% or more of it acts on the rotor winding to produce a thermal transient. As discussed later, the magnitude of that thermal transient is a function of the rotational inertia of the rotating parts, of the weight of the rotor winding, and of the specific heat of the rotor winding material. The relationship between a transient temperature rise of the rotor winding and the resulting thermal stresses in parts of that rotor winding will be discussed in a cursory manner at this time to show the basis of that relationship.

If a squirrel-cage winding experiences an increase in temperature of $\Delta T\,^\circ C$, in a relatively short time, it can reasonably be expected that the rotor core temperature will be relatively unaffected for the first few seconds, at least. Then the increase in the winding temperature of ΔT will cause the rotor bars to try to increase in axial length and the end rings to try to increase in circumference relative to their previous dimensions and relative to the unaffected rotor core. A temporary increase of small magnitude in the axial length of the rotor winding would not be expected to be significant, and experience indicates that such is the case. This is because the rotor winding will tend to increase in length symmetrically about the axial centerline, with essentially equal increases at each end and without undesirable consequences. On the other hand, a temporary increase in the circumference of the end ring will (1) tend to produce a corresponding compressive stress in the end ring if it is restrained and is not allowed to expand, and/or (2) tend to produce stress in the rotor bars to which it is fastened, to the extent that it does expand.

Concerning the first effect, the squirrel-cage winding experiences a centrifugal force that varies as the second power of rotor speed, concurrent with, and independent of, the thermal transient [see eq. (10.5)]. Thus both centrifugal force and thermal growth try to expand the circumference of the end ring. The actual amount of end-ring expansion that occurs depends on the behavior of the elastic system consisting of the end ring, rotor-bar extensions, and the retaining ring, if any, which may be used over the end ring. The fundamental difference between centrifugal force and thermal growth is that centrifugal force is an external force that acts on the end ring, whereas thermal growth is an internal state of the material for which it is normal for the end ring to have a greater circumference, because of an increase in temperature. Concerning the second effect, listed in the preceding paragraph, if the inboard side of the end ring is flush with the end of the rotor core, typical of a cast-aluminum rotor winding, expansion of the end ring will cause a shear stress in the rotor bars at the end of the core. If, however, the end ring joins the rotor bars some distance outboard from the end of the core, as it usually does for large motors, expansion of the end ring will cause a bending stress in the rotor bars, at about the point where they emerge from the end of the rotor core.

Thus stress within the various parts of a squirrel-cage rotor winding is a normal condition that results from operation of the machine. The configuration of the winding, including the cross-sectional area and the shape of the rotor bars, the cross-sectional area of the end rings, and the length of the bar extensions, must be such as to limit the stresses to acceptable values for the materials being used. As the tangential velocity of the rotor increases, a point is reached for which it is necessary to use steel retaining rings over the end rings in order to limit the stresses in the aluminum or copper winding.

10.3.4 Types of Squirrel-Cage Rotor Bars

A wide variety of cross-sectional shapes are used for cast-aluminum rotor bars, and there are several reasons why this occurs. It requires no more production time or cost to punch a complicated slot shape into rotor lamination blanks than a less complicated one, using an automatic punch-press line.

Since for cast-aluminum rotors, the rotor bar is formed by casting molten aluminum, or aluminum alloy, into the rotor-slot channels in the rotor core, the production time and cost are essentially unchanged by the cross-sectional shape of this channel, within reasonable limits. On the other hand, specific design requirements of rotor-bar resistance and of rotor-slot leakage reactance, during the acceleration period, can be achieved by logical design of the cross-sectional shape of the bar and slot, as will be shown later in this chapter. Based on the above, there is considerable motivation for the manufacturer to design the cross-sectional shape of the rotor bar, such as to optimize performance results. By and large, this has been done in the industry. Thus there are a large number of rotor-bar shapes which are extant throughout the industrial art, many of which have acquired whimsical and nostalgic names, such as "flowerpots," "doghouses," and "barbells."

The variety of cross-sectional shapes, which are used for fabricated-rotor bars, are considerably more limited than for cast-aluminum rotor bars and, again, there are good reasons for this. As the ratings and frame sizes of polyphase induction motors increase, the radial depth of the rotor bar correspondingly increases. As will be subsequently shown, the deep-bar effect increases with the radial dimension of the rotor bar. This effect produces a rotor-bar resistance which is greatest at blocked-rotor conditions and which decreases as the rotor-circuit frequency decreases. Because of the greater radial depth of the bar of fabricated winding and of the correspondingly greater degree of deep-bar effect, a special shape is frequently not required. Also, the production time and cost required to achieve a specific cross-sectional shape, other than a rectangle, are considerably more for a fabricated-rotor winding, compared to a cast-aluminum rotor winding. In addition, the end region of the rotor bar must fit against the end ring, as well as be joined to that part by some metal-joining process appropriate to the material used. Consideration of the metal-joining process and of the necessary preparation of the bar and end ring for the joint tend to discourage, or to eliminate, some cross-sectional shapes.

For fabricated-rotor windings, made of aluminum or aluminum alloy, it is possible to extrude a cross-sectional shape of bar which is tapered and in some cases, which has a step, or offset. Obviously, however, the freedom of design choice is not as broad as for a bar of a cast-aluminum rotor winding. For fabricated rotor windings made of copper or copper alloy, a rectangular bar shape is generally used for the rotor bar. By machining rectangular bar stock, inverted-T shapes and tapered shapes can be produced and used, if necessary, but with an increase in production time and in cost. From the above it is apparent that for fabricated rotors, the choice of cross-sectional shapes is more limited than for cast-aluminum rotors. However, as noted above, this does not place a significant limitation on the optimization of starting performance and on full-speed performance, because of benefit of the deep-bar effect.

10.3.5 Deep-Bar Effect

Consider a circular conductor which is carrying alternating current, as shown in Fig. 10.7a. The current sustains a circumferential magnetic field around the conductor, which causes circumferential leakage flux to link the conductor about its center. Then a circular element of area at the center of the conductor will see a greater amount of leakage flux than a corresponding circular element near the OD of the conductor. Let the widths of the two circular elements be sized such as to have equal dc resistances. Since the leakage flux linking the inner element is greater than that linking the outer one, its reactance will be correspondingly greater. Accordingly, since the two elements are in parallel and since the impedance of the outer element is less, more current will flow in the outer element than in the inner one. If the conductor is assumed to consist of a very large number of such concentric elements in parallel, it is apparent that the current distribution will be nonuniform and will tend to crowd toward the OD of the conductor. Thus the full cross section of the conductor will not be as completely utilized with ac as with dc current. This produces an effective ac resistance which increases with frequency, and which is known as skin effect.

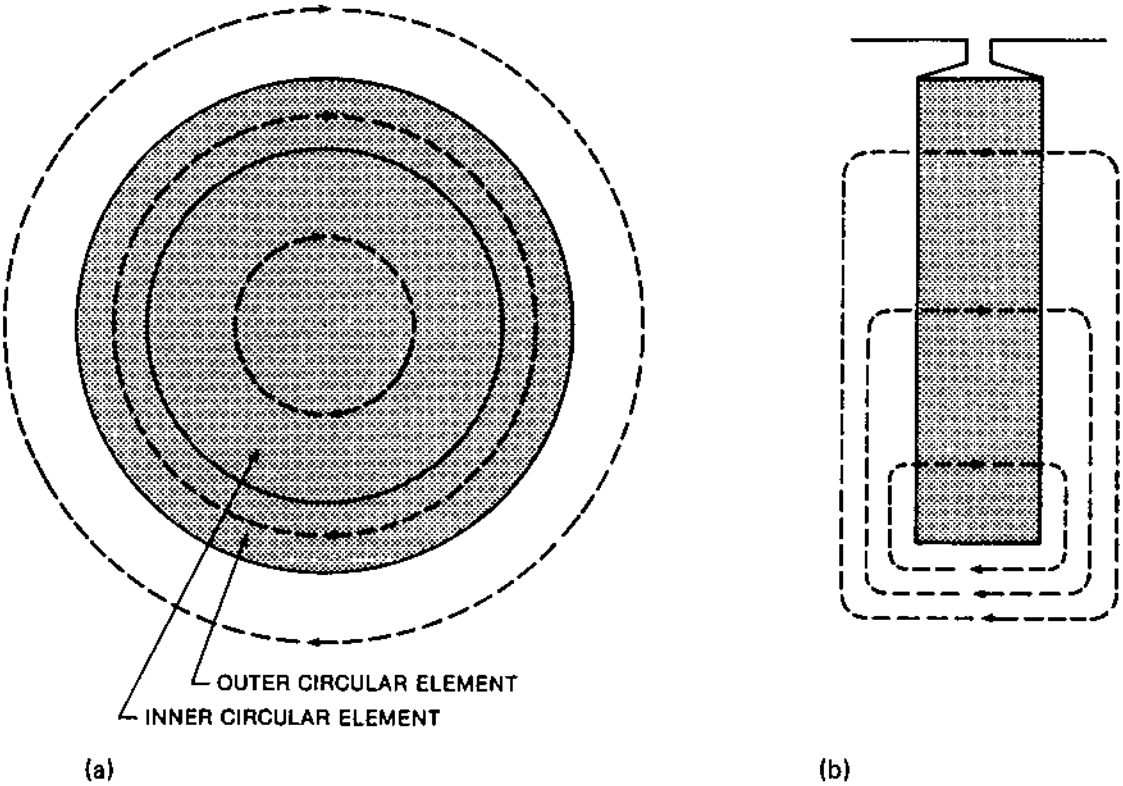

FIGURE 10.7 Cross-sectional views of a circular conductor and of a rotor bar, showing similarities between skin effect and deep-bar effect: (a) skin effect of a circular conductor in air; (b) deep-bar effect of a rotor bar in a rotor core.

The deep-bar effect of the rotor bars of a squirrel-cage induction motor is essentially the same phenomenon as skin effect. Consider Fig. 10.7b, which shows the cross-slot leakage flux path of a rotor bar. If the permeance of the steel rotor core is large in comparison to that of the nonmagnetic materials in the slot, which it is, all of the leakage flux will cross the slot, passing through the bar, and will return through the adjacent teeth and the yoke section under the slot. Thus rectangular elements, which cross the slot and which are distributed along the height of the slot, replace the concentric elements which cross the radius of the previously discussed circular conductor. As would be expected, the circuit results are similar, with the current being crowded to the top of the bar and with the effective bar resistance increasing as a function of the rotor-circuit frequency. The functional relationship between rotor-bar resistance and rotor-circuit frequency for deep bars will now be determined.

The deep-bar effect can be analyzed by use of Maxwell's field equations or by use of circuit theory. The following analysis makes use of the circuit-theory approach, since the rotor winding is usually regarded as a circuit element. Figure 10.8 shows a rotor bar positioned in the slot, somewhat representative of a fabricated-rotor bar. The bar width w_b must be slightly less than the rotor-slot width w, such that the bar can be driven into the slot without significant upsetting of the rotor laminations. Let $k = w_b/w$, so that

$$kw = w_b \quad \text{meters} \tag{10.9}$$

The dc resistance of unit length of the bar, that is, the resistance of unit length of the bar, with no skin effect, is

$$R_{dc} = \frac{\rho \ell}{A} = \frac{\rho \ell}{kwd} \quad \text{ohms/meter} \tag{10.10}$$

which is the base resistance to which the ac resistance, including that due to skin effect, will eventually be compared. Current flow in the bar will produce cross-slot leakage flux, as shown in Fig. 10.7b. At any point in the slot

$$B = \mu H = \frac{4\pi}{10^7} H \quad \text{webers/meter}^2 \tag{10.11}$$

where

B = cross-slot leakage flux density, webers/meter^2
μ = permeability of the nonmagnetic material within the slot, henrys/meter
H = magnetic field strength, amperes/meter

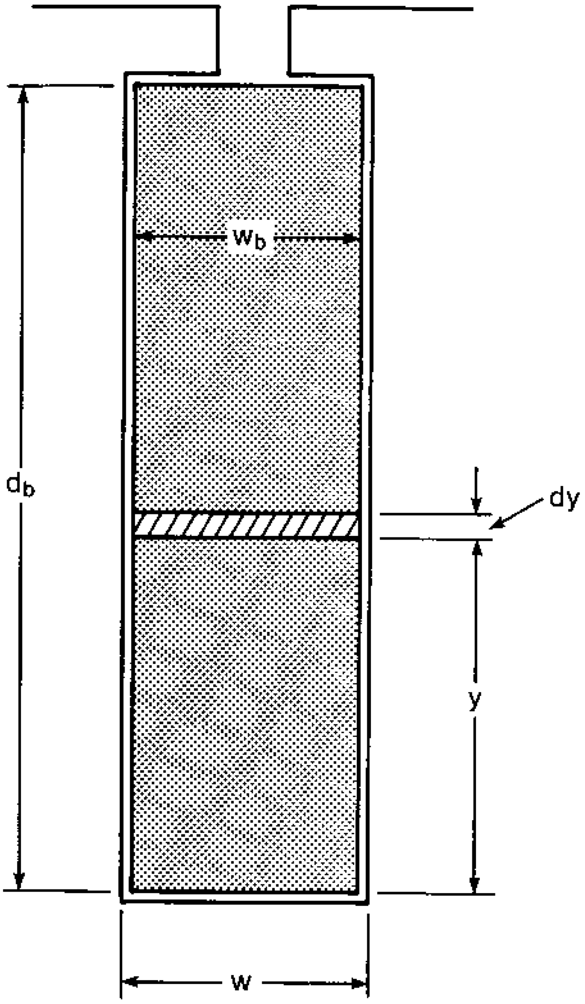

FIGURE 10.8 Cross-sectional view of a rotor bar in its slot, with definition of terms used in the derivation of deep-bar effect.

The flux density B is, in general, equal to

$$B = \frac{4\pi}{10^7 w}\int kwj_b\, dy = \frac{4\pi k}{10^7}\int j_b\, dy \quad \text{webers/meter}^2 \tag{10.12}$$

where j_b is the current density in the bar. At some point y, the flux density is equal to

$$B = \frac{4\pi k}{10^7}\int_0^y j_b\, dy \quad \text{webers/meter}^2 \tag{10.13}$$

The total leakage flux is, in general, equal to

$$\phi = \int B\,dy \quad \text{webers} \tag{10.14}$$

and at some point y, the leakage flux linking the bar area beneath that point is equal to

$$\phi = \int_{y}^{d_b} B\,dy \quad \text{webers} \tag{10.15}$$

The voltage induced by the alternating cross-slot leakage flux ϕ is, in general, equal to

$$e = -\frac{d\phi}{dt} = -\frac{d}{dt}\left(\int B\,dy\right) \quad \text{volts} \tag{10.16}$$

and for some point y is equal to

$$e = -\frac{d}{dt}\left(\int_{y}^{d_b} B\,dy\right) \quad \text{volts} \tag{10.17}$$

But ϕ is in phase with the rotor-bar current I_b, which produces it, and varies sinusoidally at the same frequency as the rotor current. Then, in general,

$$e = -\omega(1/\underline{90^\circ}) \int B\,dy = -2\pi fj \int_{y}^{d_b} B\,dy \quad \text{volts} \tag{10.18}$$

The factor $1/\underline{90^\circ}$, which is equal to the complex operator j, causes the induced voltage to lag the flux by $\pi/2$ electrical radians, or 90 electrical degrees, which it should. The current density in the bar is

$$j_b = -\frac{e}{\rho} \quad \text{amperes/meter}^2 \tag{10.19}$$

The negative sign in eq. (10.19) is required, because the polarity of the voltage should be that of a driving-point voltage (i.e., the externally impressed voltage, minus the induced voltage). Then, in general, the current density is equal to

$$j_b = \frac{j2\pi f}{\rho} \int B\, dy \quad \text{amperes/meter}^2 \tag{10.20}$$

and at some point y it is equal to

$$j_b = \frac{j2\pi f}{\rho} \int_y^{d_b} B\, dy \quad \text{amperes/meter}^2 \tag{10.21}$$

The rate of change of j_b along y is obtained by differentiating eq. (10.20) with respect to y, or

$$\frac{dj_b}{dy} = \frac{j2\pi f B}{\rho} \quad \text{amperes/meter}^3 \tag{10.22}$$

Substituting eq. (10.12) into eq. (10.22) yields

$$\frac{dj_b}{dy} = \frac{j8\pi^2 kf}{\rho \times 10^7} \int j_b\, dy \quad \text{amperes/meter}^3 \tag{10.23}$$

Differentiating eq. (10.23) with respect to y gives us

$$\frac{d^2 j_b}{dy^2} = \frac{j8\pi^2 kf}{\rho \times 10^7} j_b \quad \text{amperes/meter}^4 \tag{10.24}$$

To simplify eq. (10.24), let

$$\gamma = \sqrt{\frac{j8\pi^2 kf}{\rho \times 10^7}} \quad \text{1/meters} \tag{10.25}$$

Then eq. (10.24) may be written as

$$\frac{d^2 j_b}{dy^2} = \gamma^2 j_b \quad \text{amperes/meter}^4 \tag{10.26}$$

which gives the fundamental relationship in differential form between j_b and y. The fundamental relationship between B and y is also required. The rate of change of B, along y, is obtained by differentiating eq. (10.12) with respect to y, or

$$\frac{dB}{dy} = \frac{4\pi k}{10^7} j_b \quad \text{webers/meter}^3 \qquad (10.27)$$

Substituting eq. (10.20) into eq. (10.27) yields

$$\frac{dB}{dy} = \frac{j8\pi^2 kf}{\rho \times 10^7} \int B\, dy \quad \text{webers/meter}^3 \qquad (10.28)$$

Differentiating eq. (10.28) with respect to y gives us

$$\frac{d^2 B}{dy^2} = \frac{j8\pi^2 kf}{\rho \times 10^7} B = \gamma^2 B \quad \text{webers/meter}^4 \qquad (10.29)$$

which is the required fundamental relationship in differential form between B and y.

Equation (10.29) is a second-order linear differential equation with constant coefficients, which can be solved by use of the differential operator D. Equation (10.29) can be rewritten as

$$(D^2 - \gamma^2)B = (D + \gamma)(D - \gamma) = 0 \quad \text{webers/meter}^4 \qquad (10.30)$$

and the solution is

$$B = a\epsilon^{\gamma y} + b\epsilon^{-\gamma y} \quad \text{webers/meter}^2 \qquad (10.31)$$

The coefficient γ of the variable y in the two exponents may be written as

$$\gamma = \sqrt{2j}\sqrt{\frac{4\pi^2 kf}{\rho \times 10^7}} = (1 + j)\delta \quad 1/\text{meters} \qquad (10.32)$$

where

$$\delta = \sqrt{\frac{4\pi^2 kf}{\rho \times 10^7}} \quad 1/\text{meters} \qquad (10.33)$$

Then eq. (10.31) may be rewritten as

$$B = a\epsilon^{(1+j)\delta y} + b\epsilon^{-(1+j)\delta y} \quad \text{webers/meter}^2 \tag{10.34}$$

which may be expressed in terms of hyperbolic functions as

$$\begin{aligned} B &= a\{\cosh[(1 + j)\delta y] + \sinh[(1 + j)\delta y]\} \\ &\quad + b\{\cosh[(1 + j)\delta y] - \sinh[1 + j)\delta y]\} \quad \text{webers/meter}^2 \end{aligned} \tag{10.35}$$

This equation can be simplified by combining like terms, to be

$$B = M \cosh[(1 + j)\delta y] + N \sinh[(1 + j)\delta y] \quad \text{webers/meter}^2 \tag{10.36}$$

where M and N are constants.

Equation (10.26) can be solved in an analogous manner, to give

$$j_b = S \cosh[(1 + j)\delta y] + T \sinh[(1 + j)\delta y] \quad \text{amperes/meter}^2 \tag{10.37}$$

where S and T are constants. The constants of integration in eqs. (10.36) and (10.37) are determined from the actual physical conditions that exist in the machine. At the bottom of the rotor bar, where $y = 0$, the cross-slot flux density B is equal to zero. For this to be true, the constant M must equal zero in eq. (10.36), since $\cosh 0 = 1$ and $\sinh 0 = 0$. Also, at the top of the rotor bar, where $y = d_b$, the cross-slot flux density B is equal to $4\pi I_b/10^7 w$, where I_b is the bar current, in amperes. Then the value of the constant N is equal to

$$N = \frac{4\pi I_b}{10^7 w \sinh[(1 + j)\delta d_b]} \quad \text{webers/meter}^2 \tag{10.38}$$

and eq. (10.36) then becomes

$$B = \frac{4\pi I_b}{10^7 w} \frac{\sinh[(1 + j)\delta y]}{\sinh[(1 + j)\delta d_b]} \quad \text{webers/meter}^2 \tag{10.39}$$

From inspection of eq. (10.22) it is apparent that dj_b/dy is equal to zero when the cross-slot leakage flux B is equal to zero, and accordingly, this relationship will be used to evaluate the constants of integration for eq. (10.37). Differentiating eq. (10.37) with respect to y and equating to the expression on the right-hand side of eq. (10.22), we obtain

$$\frac{dj_b}{dy} = S(1 + j)\delta \sinh[(1 + j)\delta y] + T(1 + j)\delta \cosh[(1 + j)\delta y]$$
$$= \frac{j2\pi fB}{\rho} \quad \text{amperes/meter}^3 \tag{10.40}$$

Then, at the bottom of the rotor bar, where $y = 0$ and where $B = 0$,

$$S(0) + T(1 + j)\delta = 0 \quad \text{amperes/meter}^3 \tag{10.41}$$

For eq. (10.41) to hold, T must equal zero. Then eq. (10.37) becomes

$$j_b = S \cosh[(1 + j)\delta y] \quad \text{amperes/meter}^2 \tag{10.42}$$

To evaluate the constant S, differentiate eq. (10.42) with respect to y and equate to the expression on the right-hand side of eq. (10.22).

$$\frac{dj_b}{dy} = S(1 + j)\delta \sinh[(1 + j)\delta y] = \frac{j2\pi fB}{\rho} \quad \text{amperes/meter}^3 \tag{10.43}$$

At the top of the rotor bar, $y = d_b$ and $B = 4\pi I_b/(10^7 w)$. Then

$$S(1+j)\delta \sinh[(1+j)\delta d_b] = \frac{j2\pi f}{\rho} \frac{4\pi I_b}{10^7 w} = \frac{j8\pi^2 f I_b}{10^7 \rho w} \quad \text{amperes/meter}^3 \tag{10.44}$$

and

$$S = \frac{j8\pi^2 f I_b}{10^7 \rho w} \frac{1}{(1 + j)\delta \sinh[(1 + j)\delta d_b]} \quad \text{amperes/meter}^2 \tag{10.45}$$

Rearranging eq. (10.45), remembering that $2j = (1 + j)^2$ and multiplying numerator and denominator by k gives us

$$S = 2j \frac{4\pi^2 f I_b k}{10^7 \rho w k} \frac{1}{(1 + j)\delta \sinh[(1 + j)\delta d_b]}$$
$$= \frac{(1 + j)^2 \delta^2 I_b}{wk(1 + j)\delta \sinh[(1 + j)\delta d_b]} \quad \text{amperes/meter}^2 \tag{10.46}$$

or

$$S = \frac{(1 + j)\,\delta I_b}{wk \sinh[(1 + j)\,\delta\, d_b]} \quad \text{amperes/meter}^2 \tag{10.47}$$

Substituting eq. (10.47) into eq. (10.42)

$$j_b = \frac{(1 + j)\delta I_b}{wk} \, \frac{\cosh[(1 + j)\delta y]}{\sinh[(1 + j)\delta\, d_b]} \quad \text{amperes/meter}^2 \tag{10.48}$$

Equation (10.48) gives the eddy-current density that exists in the rotor bar as a function of radial position in the bar and is the solution to the differential equation given in eq. (10.26). Equation (10.39) gives the cross-slot leakage flux density again, as a function of radial position in the rotor bar, and is the solution to the differential equation given in eq. (10.29). The eddy-current flow in the bar, of course, results from the cross-slot leakage flux and is in opposition to that flux.

The in-phase component of the impedance drop, for unit length along the axial dimension of the rotor bar, and at some point y in the radial dimension of the bar, is

$$V_r = j_b \rho \quad \text{volts} \tag{10.49}$$

for unit length of the bar. Substituting eq. (10.48) into eq. (10.49) yields

$$V_r = \frac{(1 + j)\delta I_b \rho}{wk} \, \frac{\cosh[(1 + j)\delta y]}{\sinh[(1 + j)\delta\, d_b]} \quad \text{volts} \tag{10.50}$$

The corresponding reactive component of the impedance drop is

$$V_x = j2\pi f \phi \quad \text{volts} \tag{10.51}$$

for unit length of the bar.

The flux that crosses the slot and, accordingly, links all bar currents below some point y, in the radial dimension of the bar, is given in eq. (10.15) as

$$\phi = \int_y^{d_b} B\, dy \quad \text{webers} \tag{10.52}$$

Substituting eq. (10.39) into eq. (10.52) and performing the indicated integration gives us

$$\phi = \frac{4\pi I_b}{10^7 w} \int_y^{d_b} \frac{\sinh[(1+j)\delta y]}{\sinh[(1+j)\delta d_b]}\, dy$$

$$= \frac{4\pi I_b}{10^7 w} \frac{\cosh[(1+j)\delta d_b] - \cosh[(1+j)\delta y]}{(1+j)\delta \sinh[(1+j)\delta d_b]} \quad \text{webers} \qquad (10.53)$$

Then the complete impedance drop for unit length along the axial dimension of the bar at some point y in the bar cross section is

$$V = V_r + V_x = V_r + j2\pi f\phi \quad \text{volts} \qquad (10.54)$$

and substituting eqs. (10.50) and (10.53) into eq. (10.54) yields

$$V = \frac{(1+j)\delta I_b \rho}{wk} \frac{\cosh[(1+j)\delta y]}{\sinh[(1+j)\delta d_b]}$$

$$+ (j2\pi f) \frac{4\pi I_b}{10^7 w} \frac{\cosh[(1+j)\delta d_b] - \cosh[(1+j)\delta y]}{(1+j)\delta \sinh[(1+j)\delta d_b]} \quad \text{volts} \qquad (10.55)$$

Multiplying the numerator and denominator of the second term of eq. (10.55) by ρk and rearranging the equation, we obtain

$$V = (1+j)\delta \frac{I_b \rho}{wk} \frac{\cosh[(1+j)\delta y]}{\sinh[(1+j)\delta d_b]}$$

$$+ 2j \frac{4\pi^2 kf}{10^7 \rho} \frac{I_b \rho}{wk} \frac{\cosh[(1+j)\delta d_b] - \cosh[(1+j)\delta y]}{(1+j)\delta \sinh[(1+j)\delta d_b]} \quad \text{volts} \qquad (10.56)$$

Remembering that $\sqrt{2j} = 1 + j$ and remembering the definition of δ in eq. (10.33) gives us

$$V = (1+j)\delta \frac{I_b \rho}{wk} \frac{\cosh[(1+j)\delta y]}{\sinh[(1+j)\delta d_b]}$$

$$+ (1+j)^2 \delta^2 \frac{I_b \rho}{wk} \frac{\cosh[(1+j)\delta d_b] - \cosh[(1+j)\delta y]}{(1+j)\delta \sinh[(1+j)\delta d_b]} \quad \text{volts} \qquad (10.57)$$

Multiplying the numerator and denominator of both terms of eq. (10.57) by d_b, we have

$$V = (1 + j)\delta \frac{I_b \rho}{wkd_b} \frac{d_b \cosh[(1 + j)\delta y]}{\sinh[(1 + j)\delta d_b]}$$

$$+ (1+j)^2 \delta^2 \frac{I_b \rho}{wkd_b} \frac{d_b\{\cosh[(1+j)\delta d_b] - \cosh[(1+j)\delta y]\}}{(1 + j)\delta \sinh[(1 + j)\delta d_b]} \quad \text{volts} \tag{10.58}$$

The low-frequency, or dc, ohmic resistance of unit length of the bar is equal to

$$R_{dc} = \frac{\rho}{wkd_b} \quad \text{ohms} \tag{10.59}$$

Substituting eq. (10.59) into eq. (10.58) and then simplifying the expression yields

$$V = I_b R_{dc} \frac{(1 + j)\delta d_b \cosh[(1 + j)\delta d_b]}{\sinh[(1 + j)\delta d_b]} \quad \text{volts} \tag{10.60}$$

By using hyperbolic and circular trigonometry and then collecting real and imaginary terms, eq. (10.60) reduces to

$$V = I_b R_{dc} \delta d_b \frac{\cosh \delta d_b \sinh \delta d_b + \cos \delta d_b \sin \delta d_b}{\sinh^2 \delta d_b \cos^2 \delta d_b + \cosh^2 \delta d_b \sin^2 \delta d_b}$$

$$+ jI_b R_{dc} \delta d_b \frac{\cosh \delta d_b \sinh \delta d_b - \cos \delta d_b \sin \delta d_b}{\sinh^2 \delta d_b \cos^2 \delta d_b + \cosh^2 \delta db \sin^2 \delta d_b} \quad \text{volts} \tag{10.61}$$

Further simplifying, by using the double-angle formulae for both the hyperbolic and trigonometric functions, gives us

$$V = I_b R_{dc} \delta d_b \frac{\sinh 2\delta d_b + \sin 2\delta d_b}{\cosh 2\delta d_b - \cos 2\delta d_b}$$

$$+ jI_b R_{dc} \delta d_b \frac{\sinh 2\delta d_b - \sin 2\delta d_b}{\cosh 2\delta d_b - \cos 2\delta d_b} \quad \text{volts} \tag{10.62}$$

which is the desired expression for the deep-bar effect, which relates rotor-bar impedance to the variable δ.

The first term of the equation gives the ac resistance of the bar and the second term gives the leakage reactance of the bar, for $\ell_b = 1.0$, both expressed as the dc resistance of the bar multiplied by a function of δd_b. Since δ has units of 1/meters and d_b has units of meters, the product δd_b is dimensionless and, accordingly, dimensions of inches may be used, as long as dimensions of ohm inches are used for ρ, in determining δ. The trigonometric-hyperbolic function in eq. (10.62) rapidly approaches unity as the variable δd_b increases. Hence at values of δd_b in excess of 1.5, the equation may be simplified to

$$V = I_b R_{dc} \delta d_b + j I_b R_{dc} \delta d_b \qquad \text{for } \delta d_b > 1.5 \qquad \text{volts} \tag{10.63}$$

It is apparent from eq. (10.63) that in the region of δd_b encountered at blocked-rotor conditions, the ohmic values of the ac resistance of the bar and of the leakage reactance of the bar are equal.

10.3.6 Utilization of the Deep-Bar Effect

The rotor-circuit frequency is a maximum at blocked-rotor condition and decreases as the rotor accelerates and approaches full speed, at which point the rotor-circuit frequency is of the order of 1 to 2 Hz. Current crowding, at blocked-rotor conditions, tends to crowd the current to the top of the rotor bar, and such crowding reduces the effective depth of the bar. This reduction in effective rotor-bar depth has two consequences: (1) that the ac, or effective, bar resistance tends to increase, and (2) that the bar portion of the slot leakage reactance, referred to the stator, tends to decrease and to approach equality with the effective bar resistance.

A curve of the ratio of ac to dc rotor-bar resistance as a function of the dimensionless variable δd_b is given in Fig. 10.9. From eq. (10.62) the ac or effective resistance of unit length of the bar is equal to

$$R_{ac} = R_{dc} \delta d_b \frac{\sinh 2\delta d_b + \sin 2\delta d_b}{\cosh 2\delta d_b - \cos 2\delta d_b} \qquad \text{ohms} \tag{10.64}$$

Accordingly, the ratio R_{ac}/R_{dc} is equal to

$$\frac{R_{ac}}{R_{dc}} = \delta d_b \frac{\sinh 2\delta d_b + \sin 2\delta d_b}{\cosh 2\delta d_b - \cos 2\delta d_b} \qquad \text{numeric} \tag{10.65}$$

As stated above, the product δd_b is dimensionless, provided that consistent units are used for the rotor-bar resistivity ρ, which is one of the

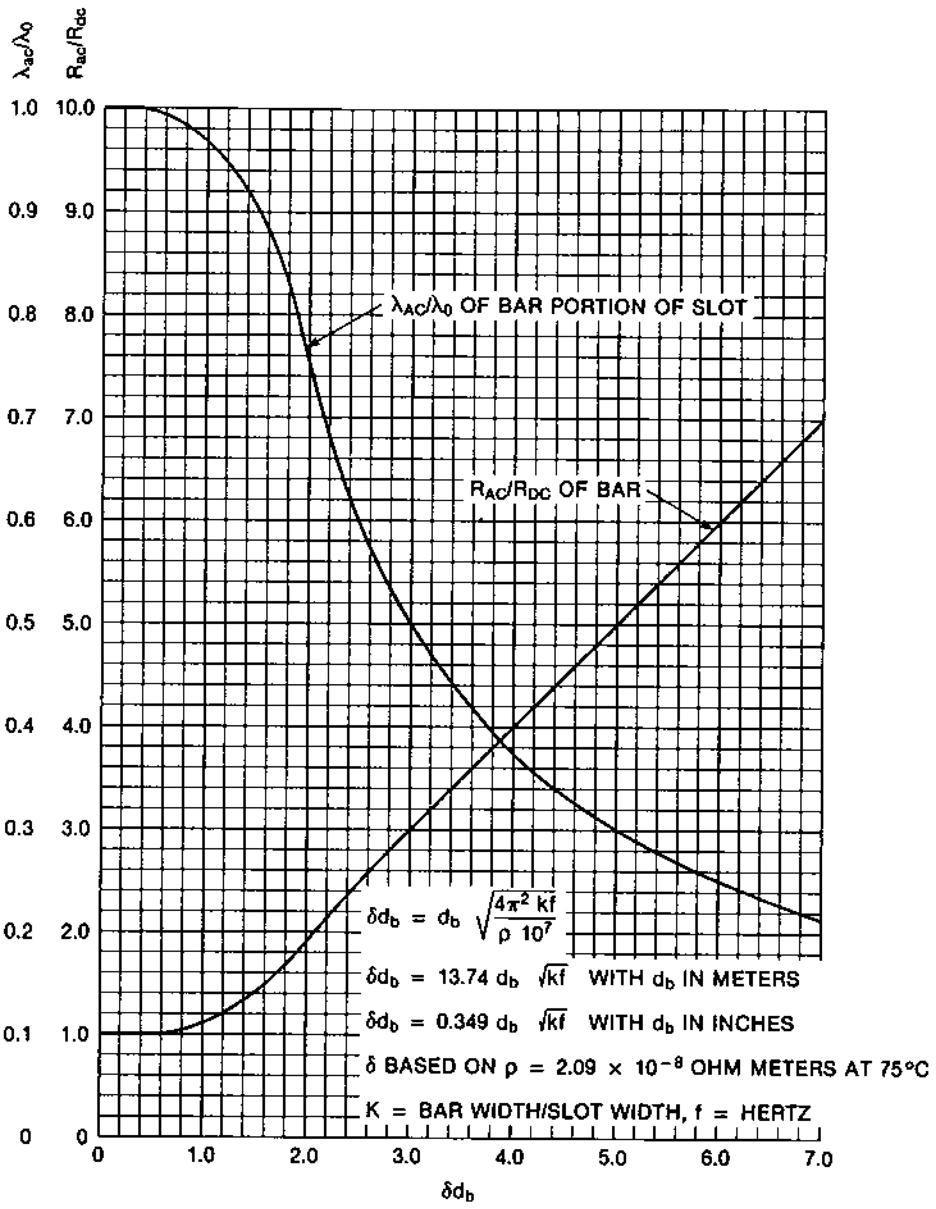

FIGURE 10.9 Curve of R_{ac}/R_{dc} and curve of λ_{ac}/λ_0 versus δd_b for a rectangular bar.

factors in δ. However, since δ is inversely proportional to $\sqrt{\rho}$, as shown in eq. (10.33), the numerical magnitude of δ will depend on the metal of which the rotor bar is made and on the assumed temperature of the bar at startup. Use of a metal that has a greater resistivity than copper, such as brass or aluminum, will give a numerical value of δ which is less than that for copper and, accordingly, will give a lower value of R_{dc}/R_{ac} for the bars of that rotor winding. Also, if the assumed temperature of the rotor bars, in a given case, is less than that for which the curve is constructed, the resulting value of δ will be greater and the corresponding value of R_{ac}/R_{dc} will also be proportionally greater.

A curve of the ratio of ac rotor-bar reactance (i.e., reactance at blocked-rotor conditions) to that at full-speed conditions is also given in Fig. 10.9. From eq. (10.63) the reactive component of the rotor-bar voltage drop, along the bar, for values of δd_b of 1.5 or more, is equal to

$$V_r = jI_b R_{dc} \delta d_b \quad \text{for } \delta d_b > 1.5 \quad \text{volts} \tag{10.66}$$

The value of eq. (10.66) is not changed if the numerator and denominator are multiplied by δd_b. Then for δd_b greater than 1.5,

$$V_r = \frac{jI_b R_{dc} \delta^2 d_b^2}{\delta d_b} \quad \text{volts} \tag{10.67}$$

Substituting the expression for δ from eq. (10.33) for the δ in the numerator of eq. (10.67) and rearranging the equation gives us

$$V_r = j2\pi f I_b \frac{2\pi}{10^7} \frac{d_b}{w} \frac{1}{\delta d_b} \quad \text{volts} \tag{10.68}$$

Multiplying the numerator and denominator of eq. (10.68) by 3 and by 2 yields

$$V_r = j2\pi f I_b \frac{4\pi}{10^7} \frac{d_b}{3w} \frac{3}{2\delta d_b} \quad \text{volts} \tag{10.69}$$

If units of inches are used instead of meters for the slot geometry, and units of maxwells are used instead of webers for the cross-slot leakage flux, eq. (10.69) becomes

$$V_r = j2\pi f I_b (3.19) \frac{d_b}{3w} \frac{3}{2\delta d_b} \quad \text{volts} \tag{10.70}$$

It will be shown in Chapter 13 that the permeance for that portion of the rotor slot which is occupied by the bar in Fig. 10.8 is equal to $d_b/3w$. Then eqs. (10.69) and (10.70) may be written as

$$V_r = j\omega I_b \text{ (permeability of slot contents)}$$
$$\times \text{ (permeance factor of slot) } \frac{3}{2\delta d_b} \quad \text{volts} \tag{10.71}$$

or

$$V_r = jI_b X_0 \frac{3}{2\delta d_b} \quad \text{volts} \tag{10.72}$$

where X_0 is the bar portion of the rotor-slot leakage reactance in the region of full speed. However, eq. (10.66), from which eq. (10.72) is derived, is the reactive component of voltage drop, along the bar, and may be written as

$$V_r = jI_b X_{ac} \quad \text{volts} \tag{10.73}$$

where X_{ac} is the leakage reactance of the bar portion of the slot reactance, at blocked-rotor conditions. Equating eqs. (10.72) and (10.73) and solving for the ratio X_{ac}/X_0 yields

$$\frac{X_{ac}}{X_0} = \frac{3}{2\delta d_b} \quad \text{numeric} \tag{10.74}$$

Equation (10.74) may be written as

$$\frac{X_{ac}}{X_0}\,\delta d_b = \frac{3}{2} \quad \text{for } \delta d_b > 1.5 \quad \text{numeric} \tag{10.75}$$

Equation (10.75) shows a hyperbolic relationship between the variable X_{ac}/X_0 and δd_b for values of δd_b greater than 1.5. Very low values of δd_b and the corresponding values of X_{ac}/X_0 are of no practical value, normally. For very low values of δd_b, the relationship departs from a hyperbola and the variable X_{ac}/X_0 approaches unity, as a limit, as δd_b approaches zero. This can be shown by expanding eq. (10.65) into a complex series and then repeating some of the previous operations. In the curve in Fig. 10.9 the variable X_{ac}/X_0 is replaced with λ_{ac}/λ_0, in terms of the corresponding ratio of the permeance of the bar portion of the rotor slot. This is done so as to be consistent with the terminology that is used in Chapter 13.

10.3.7 Numerical Example of Use of Deep-Bar Effect

Use of the deep-bar effect will be illustrated with a practical design evaluation being made by a design engineer. The engineer is evaluating the use of two different bar materials and bar sizes for a fabricated-rotor design, as follows:

Case 1:

Bar material	Aluminum
Bar size	0.300 in. wide, 2.00 in. deep
Slot width	0.315 in.

Case 2:

Bar material	Copper
Bar size	0.250 in. wide, 1.50 in. deep
Slot width	0.265 in.

Concerning decision-making background information, assume that the design engineer's company has received an order for a large number of duplicate squirrel-cage induction motors. The company has manufacturing facilities for producing both copper- and aluminum-fabricated rotor windings. The production time and cost of producing each type of windings is sufficiently close that for this order, it is not a significant factor in making the decision.

The design engineer is interested in the ratio of starting torque to starting current, since the specifications for the order being considered include stringent requirements for both performance items. Accordingly, as an initial evaluation, the engineer wanted to compare the product of $(R_{ac}/R_{dc})(\lambda_{ac}/\lambda_0)$ for the two cases. Obviously, the ratio R_{ac}/R_{dc} is proportional to the starting torque, other factors being equal. Also, the greater the ratio λ_{ac}/λ_0, the less will the deep-bar effect reduce the starting current, other factors being equal.

The parameters for using the curve in Fig. 10.9 are given below.

Case 1:

$$d_b = 2.00 \text{ in.}$$

$$k = \frac{w_b}{w} = \frac{0.300}{0.315} = 0.952$$

$$\rho = 3.47 \times 10^{-8}\ \Omega \cdot \text{m at } 75^\circ\text{C}$$

$$f = 60 \text{ Hz}$$

Case 2:

$$d_b = 1.50 \text{ in.}$$

$$k = \frac{0.250}{0.265} = 0.943$$

$\rho = 2.09 \times 10^{-8}\ \Omega\cdot\text{m}$

$f = 60\ \text{Hz}$

The curves were drawn on the basis of $\rho = 2.09 \times 10^{-8}\ \Omega\cdot\text{m}$ at 75 C. Then, in determining δd_b for use with the curve, it is necessary to multiply by the square root of the ratio 2.09/3.47 for the aluminum bar used in case 1. The values of δd_b for the two cases are as follows:

Case 1:

$$\delta d_b = 0.349 d_b \sqrt{kf}\sqrt{\frac{2.09}{3.47}} = (0.349)(2.0)\sqrt{(0.952)(60)}\sqrt{\frac{2.09}{3.47}}$$

$$= 4.09$$

$$\frac{R_{ac}}{R_{dc}} = 4.09$$

$$\frac{\lambda_{ac}}{\lambda_0} = 0.366$$

$$\frac{R_{ac}}{R_{dc}}\,\frac{\lambda_{ac}}{\lambda_0} = (4.09)(0.366) = 1.50$$

Case 2:

$$\delta d_b = 0.349 d_b \sqrt{kf} = (0.349)(1.50)\sqrt{(0.943)(60)} = 3.94$$

$$\frac{R_{ac}}{R_{dc}} = 3.94$$

$$\frac{\lambda_{ac}}{\lambda_0} = 0.379$$

$$\frac{R_{ac}}{R_{dc}}\,\frac{\lambda_{ac}}{\lambda_0} = (3.94)(0.379) = 1.50$$

The design engineer correctly concluded that the product $(R_{ac}/R_{dc}) \times (\lambda_{ac}/\lambda_0)$ would equal 1.5 for all consistent cases, and that other criteria for evaluating cases 1 and 2 should be selected, such as physical strength and specific heat of the two materials or the cross-sectional bar areas required to maintain the desired value of full-speed R_2, and the effect of such areas on the flux densities in the rotor teeth and yoke, for example.

10.3.8 Concept of the Multiple-Cage Rotor Winding

The deep-bar effect, operating on rectangular bars, is not effective in increasing the ratio R_{ac}/R_{dc} of the rotor winding for bar depths less than about 1.25 cm or about 0.5 in. Even at a bar depth of 2.5 cm, or about 1.0 in., this ratio, for the slot portion of the bar, is only 2.7 for a rectangular copper bar and even less for a rectangular aluminum bar. When the resistance of the end-ring portion of the rotor winding is also considered, the ratio of R_{ac}/R_{dc} of the entire rotor winding, with 1.0-in.-deep rectangular bars, is probably in the region of 2.5 for a copper bar 1 in. deep. For many applications it is necessary to have a starting torque of 200% or more of the full-speed torque rating of the machine. For such applications which fall into the lower power ratings, such as the standard NEMA ratings, it is necessary to use a rotor-winding design that will produce a greater ratio of R_{ac}/R_{dc}. This is achieved, in effect, by use of two or more rotor cages in parallel, and the resulting rotor winding is called a multiple-cage winding.

Figure 10.10 shows the cross section of a double-cage rotor winding and the cross-slot leakage flux which links the two bars. At blocked-rotor conditions, when the rotor-circuit frequency is equal to line frequency, the slot leakage flux linking the bottom bar B, and the resulting leakage reactance exhibited by that bar at line frequency, will force most of the total rotor-bar current into the top bar (T). The top bar has been designed to have greater resistance than the bottom bar (B) and with the bottom bar being ineffective in carrying current at blocked-rotor conditions, this will result in a greater rotor I^2R loss under these conditions. Since, as shown earlier, torque is proportional to rotor I^2R loss, the double-cage rotor winding will result in considerably more starting torque than, say, a rotor winding with rectangular bars of the same bar depth.

As the rotor accelerates and increases in speed, the frequency of the rotor circuit decreases in inverse proportion to the rotor speed. As the rotor-circuit frequency decreases, the rotor-circuit leakage reactance also decreases, as viewed from the rotor, which permits increasingly more uniform current density between the top and bottom bars. Finally, at full speed, the magnitude of the rotor leakage reactance becomes an insignificant part of the rotor circuit impedance. The total rotor bar current then divides between the two rotor bars essentially in inverse proportion to their respective dc resistances, which gives an overall value of rotor resistance which is compatible with a reasonable value of full-speed efficiency. Accordingly, an appropriately designed double-cage rotor winding permits a high value of starting torque and a reasonable value of full-speed efficiency for polyphase induction motors of small to moderate power ratings (i.e., through about 250 hp).

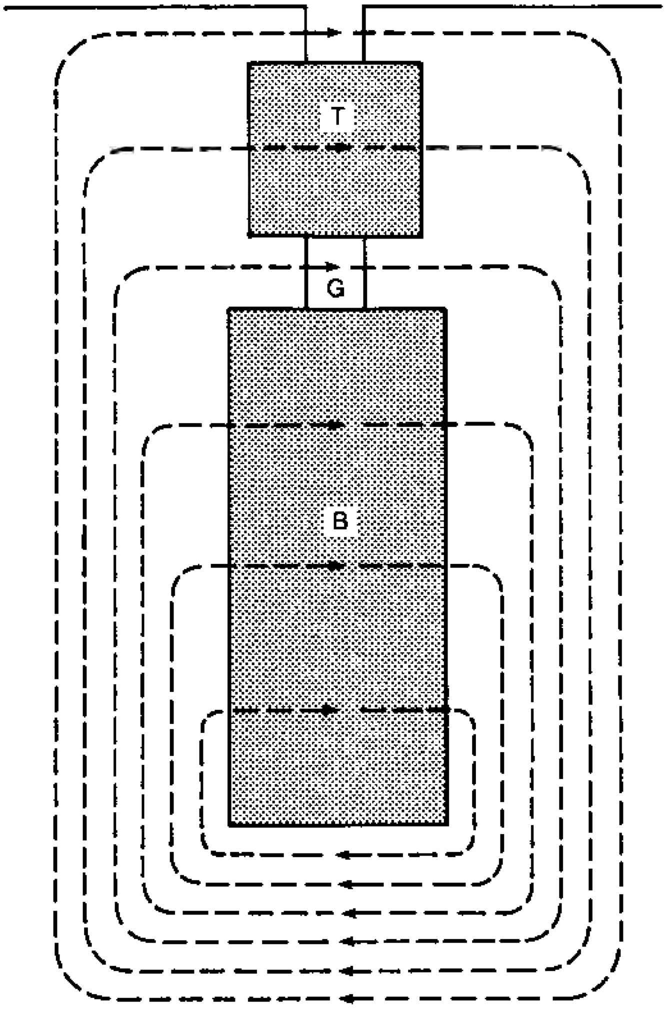

FIGURE 10.10 Conceptual view of slot leakage flux in a multiple-cage rotor winding.

In practice, the geometry of the leakage flux slot G, between the top and bottom bars, is one set of parameters that can be varied to obtain a desired design goal. Also, the dimensions of the top and bottom bars are two other sets of parameters that affect the starting torque, full-load efficiency, and to some extent, the maximum torque. Since most of the motor ratings that utilize multiple-cage rotor windings are in the rating span for which cast aluminum is suitable and generally used, the top and bottom bars are made of cast aluminum, and the cavity associated with the leakage-flux gap G between the two bars is also filled with cast aluminum. Thus the cross-sectional view of the rotor winding shown in Fig. 10.10 can be regarded as that of a triple-cage winding.

At the design stage, care must be taken that the width of the gap G is sufficient that the steel in the adjacent tooth region does not saturate. Such saturation would cause the width of the gap effectively to be greater than the value assumed for the calculation of the ac resistance and leakage reactance of the rotor winding at blocked-rotor conditions. This would, of course, result in a discrepancy between the calculated and tested values of blocked-rotor current. This can be prevented by an appropriate calculation based on the anticipated current in the bottom bar at blocked-rotor conditions, and on the magnitude of cross-slot leakage flux which will cause saturation of the steel that is adjacent to the leakage flux gap G. The leakage flux density across G is equal to

$$B_G = \frac{4\pi}{10^7} \frac{I_{B\ell}}{W_G} \quad \text{webers/meter}^2 \tag{10.76}$$

where $I_{B\ell}$ is the estimated current in the bottom bar blocked-rotor conditions and W_G is the width of the slot at G. Saturation of the steel, which is normally used in rotor laminations of small to medium-sized motors, can be assumed to be well under way at a flux density of 1.6 to 1.7 W/m^2. Using a value of 1.65 W/m^2 as indicative of impending saturation, substituting that value into eq. (10.76) and solving for W_G yields

$$W_G = \frac{7.62}{10^5} I_{B\ell} \quad \text{cm} \tag{10.77}$$

If W_G is expressed in inches, eq. (10.77) then becomes

$$W_G = \frac{3}{10^5} I_{B\ell} \quad \text{inch} \tag{10.78}$$

Then, to prevent saturation of the adjacent tooth steel and, inadvertently, the effective widening of W_G, the design value of W_G should be equal to, or greater than, that indicated in eq. (10.77) or (10.78).

Another precaution that must be taken at the design stage for multiple-cage rotor windings is to provide sufficient volume of the top bar to prevent that bar from attaining too great a temperature rise during acceleration, or from any other rapid change in rotor speed, such as reverse-voltage braking, plugging, and so on. As mentioned previously, and as discussed subsequently in this chapter, the great rate at which energy is dissipated in the rotor winding during a rapid change in rotor speed, such as during acceleration, causes a transient temperature rise of the rotor winding because the rate of production of heat energy greatly exceeds the rate at which it can be removed by conduction or convection. Because the multiple-cage effect causes most of the rotor current to flow through the top bar when the rotor-circuit frequency is a significant fraction of line frequency, most of the energy dissipation will occur in that bar during periods of high slip operation. Also, the top bar is mechanically isolated, to some extent, from the more massive lower bar. During the relatively short period of acceleration or other rapid change in rotor speed, there will be no opportunity for the heat energy in the top bar to be removed by conduction to the lower bar and adjacent core teeth or by convection to the cooling air. Thus it is important that the volume of the top bar be sufficient to absorb most of the energy produced in the top bar, without exceeding a transient temperature that is noninjurious to the bar material during a rapid change in speed, such as during acceleration.

10.3.9 Use of a Lattice Network in Analyzing the Multiple-Cage Rotor Winding

At full-speed operation when the rotor-circuit frequency is low, the top and bottom bars in Fig. 10.10 are effectively in parallel. Under such conditions, the two bar currents essentially divide in inverse proportion to their dc resistance, with nearly uniform current density across each bar. However, when the rotor-circuit frequency is relatively great, such as during starting, two discrete impedance branches in parallel do not correctly portray the physical conditions that exist in the rotor winding. For a typical small to medium-sized polyphase motor, which would probably be using a multiple-cage rotor winding, the bottom bar, and usually the top bar, are sufficiently deep as to experience deep-bar effect with nonuniform current density existing in each of the bars. Also, the mutual reactance between the top and bottom bars under such conditions is more complicated than it would be if

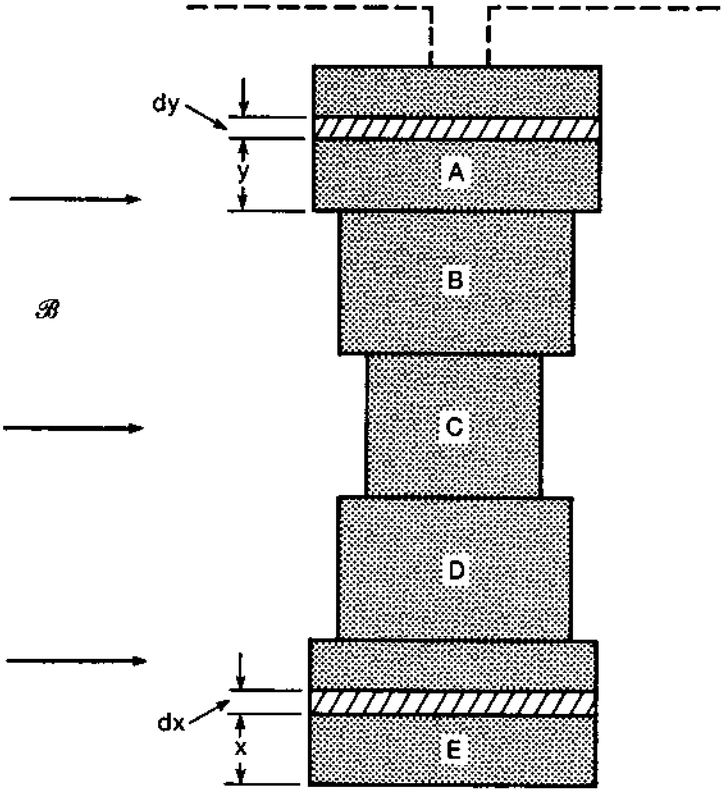

FIGURE 10.11 Conceptual view of slot leakage flux in a multiple-cage rotor winding.

the current density was uniform in each bar. For such reasons, a lattice network is useful in analyzing a multiple-cage rotor winding when the rotor-circuit frequency is in the region of line frequency.

For the lattice-network concept, the entire rotor-bar depth is divided into incremental layers and the incremental thickness is chosen such that the deep-bar effect is insignificant for each increment. The choice of an incremental thickness of 0.10 in. (about 0.25 cm) will essentially eliminate any deep-bar effect, as can be determined by examining Fig. 10.9. The various incremental layers are assumed to operate as conventional parallel circuits, with self- and mutual reactances between layers, which can be calculated in a conventional manner. The lattice-network method may be regarded as a finite-element approach to the calculation of the ac resistance and reactance of the rotor bar.

Reactance of polyphase induction motors, including stator leakage, rotor leakage, and magnetizing reactance, will be considered in detail in a subsequent chapter. At this time, it is only necessary to understand the source of the equations for self and mutual reactance of the elemental layers of the rotor bar, used in the lattice network. Figure 10.11 shows five arbitrary layers, A through E, of a rotor bar. Each layer is assumed to be sufficiently small in the vertical dimension as to have negligible deep-bar effect.

Consider unit length of layer or increment E. The flux density at point x in that increment is equal to

$$B_x = \mu H_x = \frac{4\pi}{10^7} H_x \quad \text{webers/meter}^2 \tag{10.79}$$

If a total of 1 A flows in increment E, the current at point x is x/d_E amperes. Then the flux density at that point is

$$B_x = \frac{4\pi}{10^7 W_E} \frac{x}{d_E} \quad \text{webers/meter}^2 \tag{10.80}$$

The flux within the element dx, for unit length of the rotor bar, is

$$B_x \, dx = \frac{4\pi}{10^7 W_E} \frac{x}{d_E} \, dx \quad \text{webers} \tag{10.81}$$

This flux links x/d_E of the increment E. Then the linkage of E, due to the flux within itself, is

$$\psi_E = \frac{4\pi}{10^7 W_E} \int_0^{d_E} \left(\frac{x}{d_E}\right)^2 dx = \frac{4\pi}{10^7} \frac{d_E}{3W_E} \quad \text{webers} \tag{10.82}$$

The flux density above E due to current in increment E is uniform within each increment above it, and the flux linkage that it produces above itself for unit length of bar is

$$\psi'_E = \frac{4\pi}{10^7}\left(\frac{d_D}{W_D} + \frac{d_C}{W_C} + \frac{d_B}{W_B} + \frac{d_A}{W_A}\right) \quad \text{webers} \tag{10.83}$$

Since the expressions in both eqs. (10.82) and (10.83) resulted from 1 A flowing in element E, the total self-inductance of increment E due to its own flux is then

$$L_E = \frac{4\pi}{10^7}\left(\frac{d_E}{3W_E} + \frac{d_D}{W_D} + \frac{d_C}{W_C} + \frac{d_B}{W_B} + \frac{d_A}{W_A}\right) \quad \text{henrys} \tag{10.84}$$

where the subscripts of d and W refer to the dimensions of the corresponding increments. Proceeding in a similar manner, the total self-inductance of increment D due to its own flux is equal to

$$L_D = \frac{4\pi}{10^7}\left(\frac{d_D}{3W_D} + \frac{d_C}{W_C} + \frac{d_B}{W_B} + \frac{d_A}{W_A}\right) \quad \text{henrys} \tag{10.85}$$

The total self-inductance of increment C due to its own flux is equal to

$$L_C = \frac{4\pi}{10^7}\left(\frac{d_C}{3W_C} + \frac{d_B}{W_B} + \frac{d_A}{W_A}\right) \quad \text{henrys} \tag{10.86}$$

The total self-inductance of increment B due to its own flux is equal to

$$L_B = \frac{4\pi}{10^7}\left(\frac{d_B}{3W_C} + \frac{d_A}{W_A}\right) \quad \text{henrys} \tag{10.87}$$

and finally, the total self-inductance of increment A due to its own flux is equal to

$$L_A = \frac{4\pi}{10^7}\,\frac{d_A}{3W_A} \quad \text{henrys} \tag{10.88}$$

To determine the mutual inductance between increments B and increment A in Fig. 10.11, consider unit length of increments A and B. The flux density at point y in increment A due to the flow of 1 A of current in increment B is

$$B_y = \mu H_B = \frac{4\pi}{10^7 W_A} \quad \text{webers/meter}^2 \tag{10.89}$$

The flux within the element dy for unit length of the rotor bar is

$$B_y\, dy = \frac{4\pi}{10^7 W_A}\, dy \quad \text{webers} \tag{10.90}$$

This flux links y/d_A of increment A. Accordingly, the mutual flux linkage of increment A due to flux in that increment, which is produced by current flowing in increment B, is

$$\psi_{AB} = \frac{4\pi}{10^7 W_A} \int_0^{d_A} \frac{y}{d_A}\, dy = \frac{4\pi}{10^7} \frac{d_A}{2W_A} \quad \text{webers} \tag{10.91}$$

and since the linkage above results from 1 A, the mutual inductance is

$$M_{BA} = M_{AB} = \frac{4\pi}{10^7} \frac{d_A}{2W_A} \quad \text{henrys} \tag{10.92}$$

The mutual inductance of increment C with increment B is determined in a similar manner, but it must be remembered that the uniform flux through increment A due to 1 A in increment C links both increments. Then

$$M_{CB} = \frac{4\pi}{10^7}\left(\frac{d_B}{2W_B} + \frac{d_A}{W_A}\right) \quad \text{henrys} \tag{10.93}$$

Using analogous reasoning gives us

$$M_{DC} = \frac{4\pi}{10^7}\left(\frac{d_C}{2W_C} + \frac{d_B}{W_B} + \frac{d_A}{W_A}\right) \quad \text{henrys} \tag{10.94}$$

and

$$M_{ED} = \frac{4\pi}{10^7}\left(\frac{d_D}{2W_D} + \frac{d_C}{W_C} + \frac{d_B}{W_B} + \frac{d_A}{W_A}\right) \quad \text{henrys} \qquad (10.95)$$

The set of inductances in eqs. (10.84) through (10.88) which we will call set I, represents the total self-inductance due to its own flux for each of the five increments considered. The set of inductances in eqs. (10.92) through (10.95), which we call set II, represents the mutual inductance of a given increment with the increment immediately above it. If an equation in set II is subtracted from the equation for the corresponding increment in set I, a value of inductance is obtained for the increment concerned which, for purposes of constructing the lattice network, will be called the self-inductance of that increment (as opposed to total self-inductance). This resulting set is called set III. The self-inductance of a given increment n is then

$$\begin{aligned}(\text{self-inductance})_n &= (\text{total self-inductance})_n \\ &\quad - (\text{mutual inductance})_{n,n-1} \quad \text{henrys} \qquad (10.96)\end{aligned}$$

or in terms of the set designations given above,

$$(\text{set III})_n = (\text{set I})_n - (\text{set II})_{n,n-1} \quad \text{henrys} \qquad (10.97)$$

Proceeding to carry out the operation indicated in eqs. (10.96) and (10.97) to establish set III gives us

$$L_A - 0 = \frac{4\pi}{10^7}\frac{d_A}{3W_A} \quad \text{henrys} \qquad (10.98)$$

since increment A is the top increment of the bar, with no other increment above it with which to have a mutual effect. Multiplying eq. (10.98) by 2πf to obtain reactances instead of inductances, we obtain

$$X_a = \frac{8\pi^2 f}{10^7}\frac{d_A}{3W_A} \quad \text{ohms} \qquad (10.99)$$

For increment B,

$$X_b = 2\pi f(L_B - M_{BA}) \quad \text{ohms} \qquad (10.100)$$

and after substituting the values of L_B and M_{BA} into eq. (10.100), from sets I and II, respectively,

$$X_b = \frac{8\pi^2 f}{10^7}\left(\frac{d_B}{3W_B} + \frac{d_A}{W_A} - \frac{d_A}{2W_A}\right) = \frac{8\pi^2 f}{10^7}\left(\frac{d_B}{3W_B} + \frac{d_A}{2W_A}\right) \quad \text{ohms} \tag{10.101}$$

Proceeding in a similar manner to complete set III, we have

$$X_c = \frac{8\pi^2 f}{10^7}\left(\frac{d_C}{3W_C} + \frac{d_B}{2W_B}\right) \quad \text{ohms} \tag{10.102}$$

and

$$X_d = \frac{8\pi^2 f}{10^7}\left(\frac{d_D}{3W_D} + \frac{d_C}{2W_C}\right) \quad \text{ohms} \tag{10.103}$$

and finally,

$$X_e = \frac{8\pi^2 f}{10^7}\left(\frac{d_E}{3W_E} + \frac{d_D}{2W_D}\right) \quad \text{ohms} \tag{10.104}$$

The following definitions will be established, the numerical values of which are easily determined from the dimensions of the various increments.

$$X_A = k\,\frac{d_A}{3W_A} \quad \text{ohms} \tag{10.105}$$

$$X_B = k\,\frac{d_B}{3W_B} \quad \text{ohms} \tag{10.106}$$

$$X_C = k\,\frac{d_C}{3W_C} \quad \text{ohms} \tag{10.107}$$

$$X_D = k\,\frac{d_D}{3W_D} \quad \text{ohms} \tag{10.108}$$

$$X_E = k\,\frac{d_E}{3W_E} \quad \text{ohms} \tag{10.109}$$

where $k = 8\pi^2 f/10^7$. Using the definitions above, set III then transforms to

$$X_a = X_A \quad \text{ohms} \tag{10.110}$$

$$X_b = X_B + \frac{3}{2}X_A \quad \text{ohms} \tag{10.111}$$

$$X_c = X_C + \frac{3}{2}X_B \quad \text{ohms} \tag{10.112}$$

$$X_d = X_D + \frac{3}{2}X_C \quad \text{ohms} \tag{10.113}$$

$$X_e = X_E + \frac{3}{2}X_D \quad \text{ohms} \tag{10.114}$$

By using the definitions in eqs. (10.105) through (10.109) and, also, multiplying by the factor $2\pi f$, the mutual inductances in set II transform to the following reactances:

$$X_{BA} = \frac{3}{2}X_A \quad \text{ohms} \tag{10.115}$$

$$X_{CB} = \frac{3}{2}X_B + 3X_A \quad \text{ohms} \tag{10.116}$$

$$X_{DC} = \frac{3}{2}X_C + 3X_B + 3X_A \quad \text{ohms} \tag{10.117}$$

$$X_{ED} = \frac{3}{2}X_D + 3X_C + 3X_B + 3X_A \quad \text{ohms} \tag{10.118}$$

Figure 10.12 is a lattice network that represents the reactances in set II [eqs. (10.115) through (10.118)] and in set III [eqs. (10.110) through (10.114)]. It is the equivalent circuit for a five-increment rotor bar with a generalized shape. If it is desired to use more increments, the network in Fig. 10.12 may be symmetrically extended. Since the network is general, it may be used for rotor bars of any shape, such as inverted-T bars, inwardly tapered bars, outwardly tapered bars, and multiple-cage bars. It should be kept in mind that the equivalent circuit represents only the reactances due to leakage flux through the bar. The leakage reactance, due to flux across the steel lip or overhang of the tooth above the bar, must be added to that of the equivalent circuit to represent the leakage reactance of the entire slot. This is considered in Chapter 13. The resistances R_A through R_E are the dc resistances for unit length of each increment and are determined by the cross-sectional area and by the resistivity of the increment. The rotor bar should be divided into sufficient increments that there

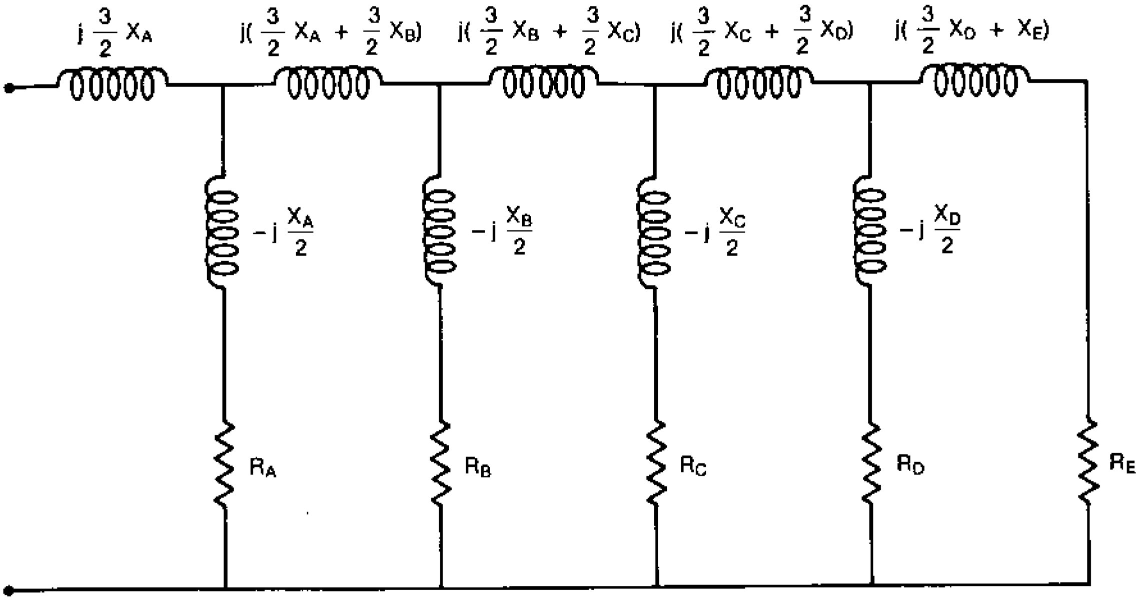
$j\frac{3}{2}X_A$
$j(\frac{3}{2}X_A + \frac{3}{2}X_B)$
$j(\frac{3}{2}X_B + \frac{3}{2}X_C)$
$j(\frac{3}{2}X_C + \frac{3}{2}X_D)$
$j(\frac{3}{2}X_D + X_E)$
$-j\frac{X_A}{2}$
$-j\frac{X_B}{2}$
$-j\frac{X_C}{2}$
$-j\frac{X_D}{2}$
R_A
R_B
R_C
R_D
R_E

FIGURE 10.12 Lattice network for representing a rotor bar divided into five increments.

is no significant amount of deep-bar effect in a given increment. Inspection of the curves in Fig. 10.9 indicate that an incremental thickness of about 0.25 cm (about 0.10 in.) is adequate to remove the deep-bar effect.

Two numerical examples of the use of a lattice network will be given. The first example will be for a rectangular rotor bar, the results of which may be compared directly with results from the curves in Fig. 10.9. The second example will be for a multiple-cage rotor bar of the same depth and dc resistance as the rectangular bar used in the first example. This will show the benefit of the multiple-cage effect, in comparison to the deep-bar effect, in increasing the ratio R_{ac}/R_{dc} for rotor bars of comparable size.

10.3.10 Numerical Example of the Use of a Lattice Network for a Rectangular Bar

The rotor-bar cross section shown in Fig. 10.13a is used for this numerical example. The aluminum bar is divided into six increments, each of 0.20 in. thickness. In practice, this would be too great an incremental thickness to use if the computation was to be done by digital means. However, use of six increments will illustrate the method adequately and will, at the same time, show the anticipated small but real effect on the ratio λ_{ac}/λ_0 of not using sufficiently small increments. Dimensions in inches are being used for the slot cross section in the example. For those who prefer to work in the metric system, use of a bar depth of 3 cm and a bar width of 1.08 cm, with 0.50-cm increments, will give essentially the same results. For purposes of calculating the resistance and the leakage reactance of each increment, the length of the bar is assumed to be 1 m (39.37 in.). Any bar length could have been used, of course, as long as the equations used were consistent with that length.

The rotor-bar material is aluminum, with a resistivity of 1.36 × 10^{-6} Ω-in. Then the resistance of R_A and of each other increment is equal to

$$R_A = \frac{\rho \ell}{A} = \frac{(1.36 \times 10^{-6})(39.37)}{(0.425)(0.20)} = 0.6299 \times 10^{-3} \quad \text{ohms} \qquad (10.119)$$

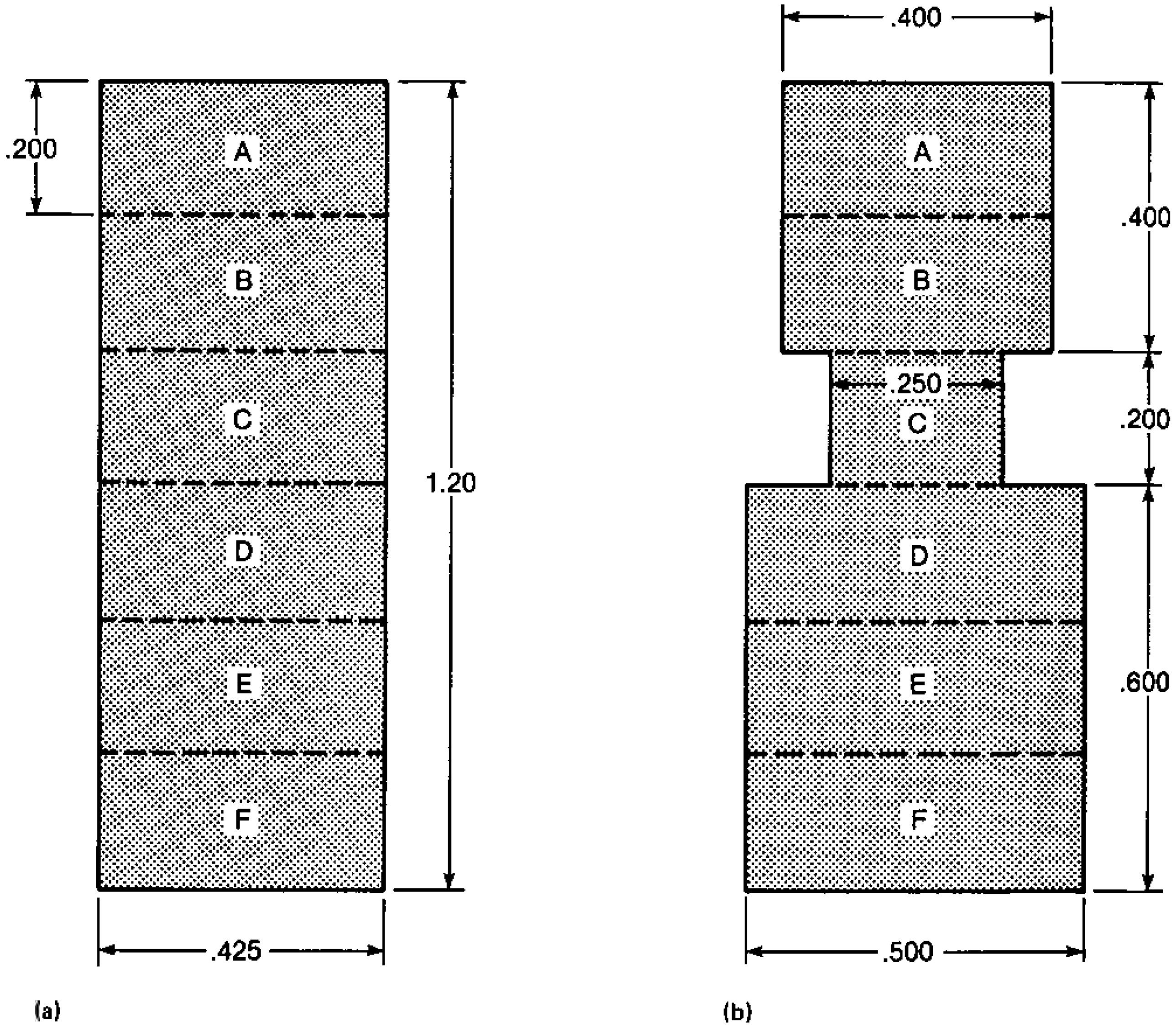

FIGURE 10.13 Rotor bar cross sections used for two numerical examples: (a) rectangular rotor bar; (b) triple-cage rotor bar.

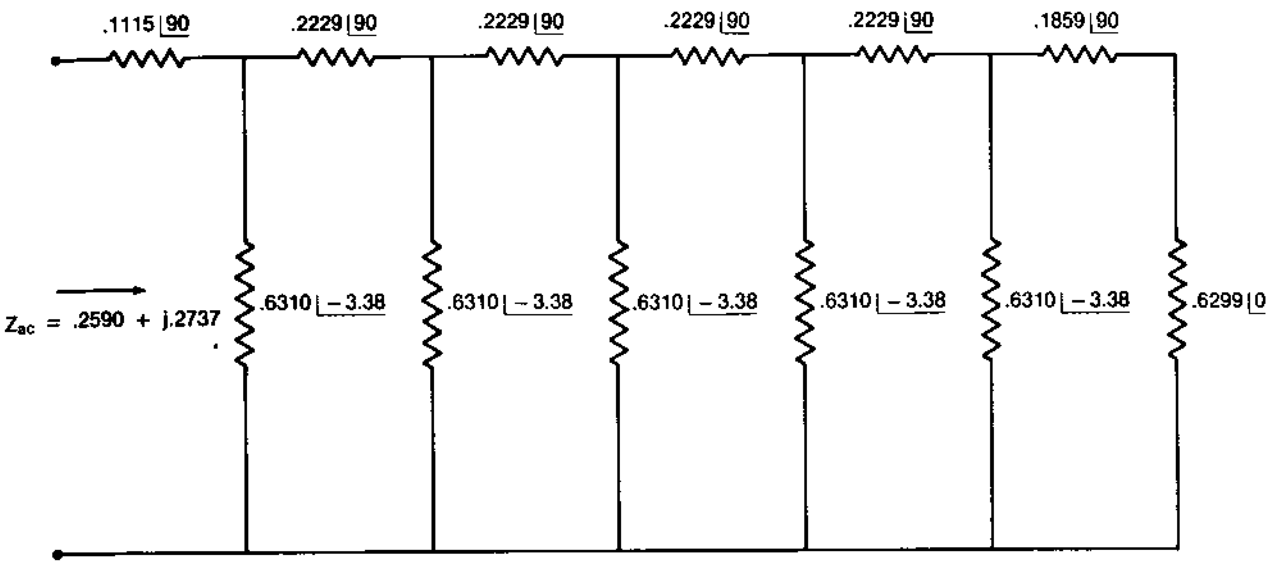

FIGURE 10.14 Lattice network used for calculating the deep-bar effect of a rectangular rotor bar.

The reactance defined in eq. (10.105) and the corresponding reactance of all other elements is equal to

$$X_A = \frac{8\pi^2 f}{10^7}\,\frac{d_A}{3W_A} = \frac{8\pi^2(60)}{10^7}\left[\frac{0.20}{(3)(0.425)}\right] = 0.07431 \times 10^{-3} \quad \text{ohms} \tag{10.120}$$

For convenience, the resistance and reactance values can be normalized by multiplying each of them by 10^3, and subsequently, after the calculations have been performed, the results should be multiplied by 10^{-3}. Then, using the foregoing values of R and X, normalized, and applying them to the network in Fig. 10.12, the network in Fig. 10.14 results.

The network in Fig. 10.14 can be reduced by digital methods or can be reduced by conventional circuit analysis, such as by paralleling the two right-hand branches and then paralleling the result with the next branch to the left, and so on. The resulting ac impedance, looking into the network, as physically seen from the top of the bar, is

$$Z_{ac} = 0.2590 + j0.2737 \times 10^{-3} \quad \text{ohms} \tag{10.121}$$

and the ac resistance of the bar is

$$R_{ac} = 0.2590 \times 10^{-3} \quad \text{ohms} \tag{10.122}$$

The dc resistance of the bar is

$$R_{dc} = \frac{\rho \ell}{A} = \frac{(1.36 \times 10^{-6})(39.37)}{(0.425)(1.20)} = 0.105 \times 10^{-3} \quad \text{ohms} \tag{10.123}$$

The ratio of ac-to-dc resistance for the bar, as determined by the lattice network, is

$$\frac{R_{ac}}{R_{dc}} = \frac{0.2590}{0.1050} = 2.47 \quad \text{numeric} \tag{10.124}$$

From Fig. 10.9, the quantity δd_b is equal to

$$\delta d_b = 0.349 d_b \sqrt{Kf} \quad \text{numeric} \tag{10.125}$$

for copper and with d_b in inches. The resistivity of the bar is 1.65 that of copper, so that for this numerical example,

$$\delta d_b = (0.349)(1.2) \sqrt{\frac{(1)(60)}{1.65}} = 2.53 \quad \text{numeric} \tag{10.126}$$

From the curve in Fig. 10.9,

$$\frac{R_{ac}}{R_{dc}} = 2.50 \quad \text{numeric} \tag{10.127}$$

The value calculated from the lattice network is in close agreement with that determined from the curve. The permeance due to leakage flux through the bar, with uniform current density throughout the bar such as that at full rotor speed, is

$$\lambda = \frac{d_b}{3W_b} = \frac{1.20}{(3)(0.425)} = 0.941 \quad \text{numeric} \tag{10.128}$$

The inductance of the bar for 39.37 in. of bar length is equal to

$$L = \frac{4\pi}{10^7} \lambda = \frac{4\pi}{10^7} (0.941) = 1.182 \times 10^{-6} \quad \text{henrys} \tag{10.129}$$

and the leakage reactance of the bar for 39.37 in. of bar length and referred to stator frequency is

$$X_0 = 2\pi fL = (2\pi)(60)(1.182 \times 10^{-6}) = 0.4456 \times 10^{-3} \quad \text{ohms} \tag{10.130}$$

Then

$$\frac{X_{ac}}{X_0} = \frac{\lambda_{ac}}{\lambda_0} = \frac{0.2737 \times 10^{-3}}{0.4456 \times 10^{-3}} = 0.614 \quad \text{numeric} \tag{10.131}$$

From the curve in Fig. 10.9,

$$\frac{\lambda_{ac}}{\lambda_0} = 0.595 \quad \text{numeric} \tag{10.132}$$

The value of R_{ac}/R_{dc} as determined by the lattice network is within about 1% of that determined by the curve of the deep-bar effect, whereas the value of λ_{ac}/λ_0 as determined by the lattice network is within about 3% of that determined by the curve. The correlations above should not be surprising. The value of δd_b for the 0.20-in.-deep increment used in the example is equal to 0.42. An examination of the curve in Fig. 10.9 shows that this value of δd_b would not cause any deep-bar effect on the resistance of the increment but that it would cause some, although slight, effect on the bar leakage reactance. But, again, for very accurate results, the incremental thickness should be in the region of 0.10 in. (0.25 cm).

10.3.11 Numerical Example of the Use of a Lattice Network for a Multiple-Cage Bar

The rotor-bar cross section shown in Fig. 10.13b is used for the multiple-cage rotor bar example. The bar is made of aluminum and is divided into six increments, each equal to 0.20 in. However, since it is a multiple-cage bar, the increments are not all of equal width. As for the previous example, a bar length of 1 m (39.37 in.) is assumed.

The resistances of the various increments are as follows:

$$R_A = R_B = \frac{\rho \ell}{A} = \frac{(1.36 \times 10^{-6})(39.37)}{(0.40)(0.20)} = 0.6693 \times 10^{-3} \quad \text{ohms} \tag{10.133}$$

$$R_C = \frac{(1.36 \times 10^{-6})(39.37)}{(0.25)(0.20)} = 1.0709 \times 10^{-3} \quad \text{ohms} \tag{10.134}$$

$$R_D = R_E = R_F = \frac{(1.36 \times 10^{-6})(39.37)}{(0.50)(0.20)} = 0.5354 \times 10^{-3} \quad \text{ohms} \tag{10.135}$$

The reactances defined in eqs. (10.105) through (10.109) extended to cover X_F are equal to

$$X_A = X_B = \frac{8\pi^2 f}{10^7} \frac{d_A}{3W_A} = \frac{8\pi^2(60)}{10^7} \frac{0.20}{(3)(0.40)} = 0.07896 \times 10^{-3} \quad \text{ohms} \tag{10.136}$$

$$X_C = \frac{8\pi^2(60)}{10^7} \frac{0.20}{(3)(0.25)} = 0.1263 \times 10^{-3} \quad \text{ohms} \tag{10.137}$$

$$X_D = X_E = X_F = \frac{8\pi^2(60)}{10^7} \frac{0.20}{(3)(0.50)} = 0.06317 \times 10^{-3} \quad \text{ohms} \tag{10.138}$$

Normalizing the resistances and reactances by multiplying by 10^3 and then applying them to the network in Fig. 10.12 gives the result shown in Fig. 10.15. Again, this network can be reduced by digital methods or by conventional methods.

The resulting ac impedance looking into the network in Fig. 10.15, as seen from the top of the bar, is equal to

$$Z_{ac} = (0.3025 + j0.2830) \times 10^{-3} \quad \text{ohms} \tag{10.139}$$

and the ac resistance of the bar is

$$R_{ac} = 0.3025 \times 10^{-3} \quad \text{ohms} \tag{10.140}$$

The dc resistance of the bar is

$$R_{dc} = \frac{\rho \ell}{A} = \frac{(1.36 \times 10^{-6})(39.37)}{0.510} = 0.105 \times 10^{-3} \quad \text{ohms} \tag{10.141}$$

and the ratio of starting resistance to running resistance of the bar is

$$\frac{R_{ac}}{R_{dc}} = \frac{0.3025}{0.1050} = 2.88 \quad \text{numeric} \tag{10.142}$$

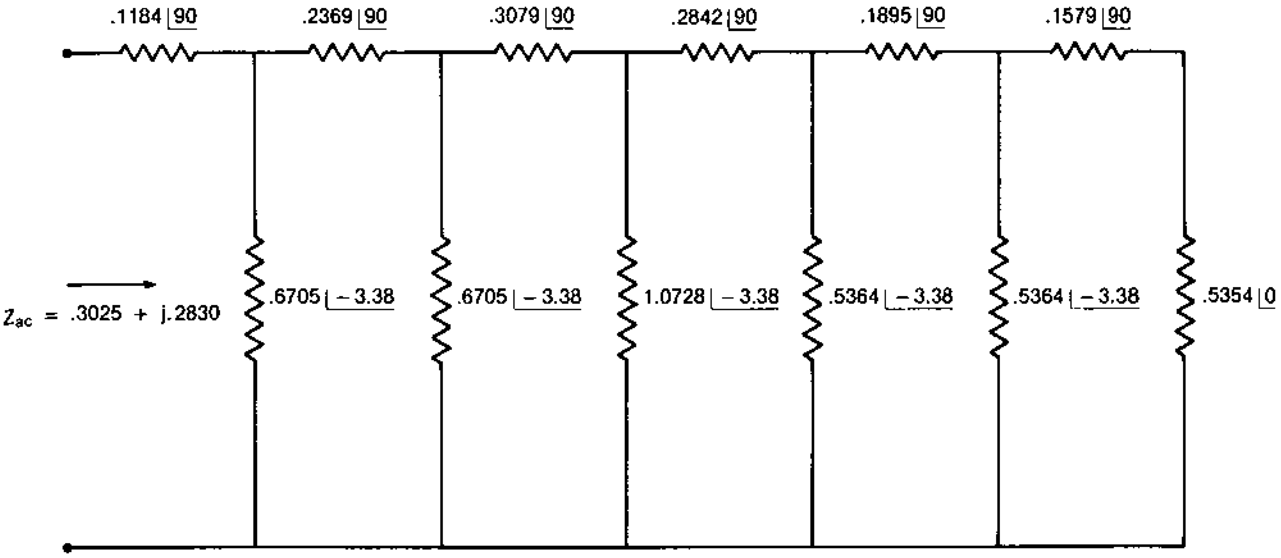

FIGURE 10.15 Lattice network used for calculating the ratios R_{ac}/R_{dc} and X_{ac}/X_0 of a multiple-cage rotor bar.

The ac reactance of the bar (i.e., the reactance exhibited by the bar with line frequency in the rotor circuit) at blocked-rotor conditions is

$$X_{ac} = 0.2830 \times 10^{-3} \quad \text{ohms} \tag{10.143}$$

Under full-speed conditions, the frequency of the rotor circuit is very low and the rotor-bar current through the three parts of the bar tends to divide in inverse proportion to the dc resistance of the parts. The behavior of a multiple-bar motor is discussed in Section 13.10. Using equations developed in Chapter 13, the "running" value of leakage reactance of the rotor bar X_0 referred to stator frequency is

$$X_0 = 0.7343 \times 10^{-3} \quad \text{ohms} \tag{10.144}$$

Then the ratio X_{ac}/X_0 for the bar portion of the rotor slot leakage reactance is equal to

$$\frac{X_{ac}}{X_0} = \frac{0.2830}{0.7343} = 0.385 \quad \text{numeric} \tag{10.145}$$

A comparison of the resistance and reactance ratios of the multiple-cage bar above with the rectangular bar of equal depth and cross section considered previously shows that the multiple-cage bar exhibits a greater ratio R_{ac}/R_{dc}

and a lower ratio of blocked-rotor reactance to running reactance. As noted earlier, the greater ratio R_{ac}/R_{dc} of the multiple-cage bar compared to that of a rectangular bar of the same depth and of the same dc resistance, explains why the multiple-cage bar is frequently applied to small and medium-sized polyphase induction motors.

10.3.12 Rotor Skew

Stator slots cause harmonics in the stator-winding magnetomotive-force wave, due to currents being concentrated in discrete slots and cause harmonics in the rotating flux wave, due to variations in the air-gap permeance caused by the slot openings. Such harmonics can cause perturbations on the speed-torque curve, additional noise, additional losses, and so on. Unlike space harmonics, stator slot harmonics are not affected by the pitch factor or the distribution factor of the stator winding. However, if the slots of either the stator core or the rotor core are skewed, such as to have a slight displacement from a true axial line along the core, some of the problems caused by slot harmonics will be reduced. It is easier, in practice, to skew the rotor core and winding than to skew the stator core and winding. Accordingly, in small to medium-sized polyphase induction motors, where skewing is used to some extent, it is normal practice to skew the rotor core.

In theory, if the slots in the rotor core are skewed 2π electrical radians on the harmonic scale of a given slot harmonic produced by the stator winding, the voltage induced in the rotor bar for that harmonic should cancel along the length of the bar, and no net harmonic voltage should result. Then since the net induced voltage for that harmonic is zero, no harmonic bar current should flow, with no harmonic torque, no additional losses, and so on, being produced. This theoretical expectation is partially, but not totally, realized, however. The rotor bars are short circuited by the steel rotor core to a random and not fully predictable extent, which can provide a path for harmonic current to flow between points on the rotor with a potential difference in harmonic voltage. Nevertheless, rotor skewing is a useful and frequently used practice for small to medium-sized polyphase induction motors and is beneficial for many applications.

Although rotor skewing will reduce some of the undesirable effects caused by stator slot harmonics, it will effectively increase the leakage reactance of the machine to some extent. This can be understood intuitively by considering the effect of skew on the induced voltage along the bar. As the rotating air-gap flux wave passes a given bar, the peak of the fundamental component of that wave will see sections along a given bar at successively later times. This has the effect, as seen by the rotor, of either (1) slightly reducing the magnitude of the fundamental of the induced voltage wave or of (2) causing the magnitude of the fundamental component of the rotating air-gap flux wave to appear smaller (i.e., for the ratio of mutual flux to total flux to be reduced) as seen by the rotor. Since the induced

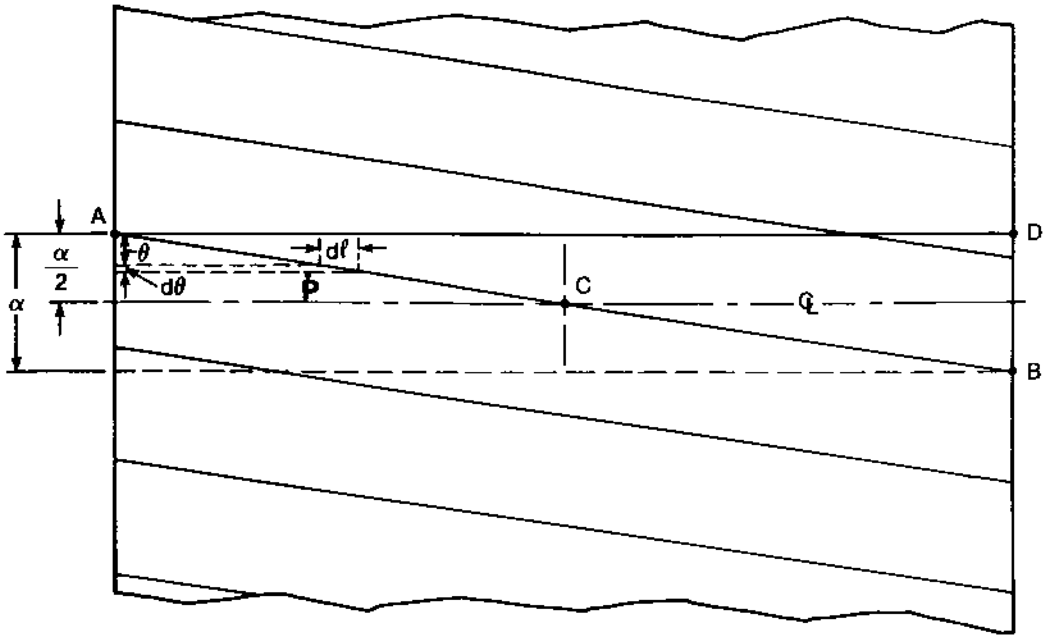

FIGURE 10.16 Relationships used to derive the skew factor for a squirrel-cage rotor with skewed slots.

voltage in a given stator coil side is unaffected by rotor skew, the circuit effect of rotor skew is usually handled by an increase in leakage reactance. The quantitative effect of skew is given by the skew factor, which will now be derived.

Figure 10.16 shows a portion of the air-gap surface of a squirrel-cage rotor with skewed bars, in which the amount of skew has been exaggerated to illustrate relationships more easily. The slanted line AB represents the rotor bar under consideration, and point C represents the axial centerline of the bar. For purposes of this analysis, the amount of skew of a rotor bar is defined in terms of the angular advance, in electrical radians or electrical degrees, of one end of the bar relative to the other end. Thus in Fig. 10.16, point B is advanced α electrical radians ahead of point A. The midpoint of the bar, or point C, is advanced $\alpha/2$ electrical radians ahead of point A. In practice, the amount of rotor skew is often specified in centimeters, or inches, of advance.

The voltage that is induced by the fundamental component of the rotating air-gap flux wave in successive elements along the rotor bar is shifted in time phase with respect to each preceding increment. It is this progressive shift in time phase of the induced voltage along the length of a skewed bar which causes a reduction in the net induced voltage. Point P on bar AB is advanced by θ electrical radians ahead of point A. Let E_b be the voltage induced in the full length of a rotor bar without skew, such as from point A to point D. Then the incremental voltage dE induced in an elemental length $d\ell$ of the bar, corresponding to an incremental angle $d\theta$, is

$$dE = \frac{E_b \, d\theta}{\alpha} \quad \text{volts} \tag{10.146}$$

and assuming that the air-gap flux wave is rotating in the positive direction of θ, the incremental voltage dE will have a phase angle θ with respect to point A (see Fig. 10.16). To calculate the total net voltage along the skewed bar, it is convenient to project it onto the horizontal line, running through point C at the center of the bar, which is displaced $\alpha/2$ radians from point A, the angular reference point. Then the projection of the incremental voltage dE onto the horizontal line is

$$dE = \frac{E_b}{\alpha} \cos\left(\theta - \frac{\alpha}{2}\right) d\theta \quad \text{volts} \tag{10.147}$$

and the net voltage in the bar from point A to point B is determined by summing eq. (10.147) from $\theta = 0$ to $\theta = \alpha/2$ and then multiplying by 2. Thus

$$E = 2\int_0^{\alpha/2} \frac{E_b}{\alpha} \cos\left(\theta - \frac{\alpha}{2}\right) d\theta$$

$$= \frac{2E_b}{\alpha} \int_0^{\alpha/2} \left(\cos\theta \cos\frac{\alpha}{2} + \sin\theta \sin\frac{\alpha}{2}\right) d\theta \quad \text{volts} \tag{10.148}$$

or

$$E = \frac{2E_b}{\alpha} \sin\frac{\alpha}{2} \quad \text{volts} \tag{10.149}$$

Since the voltage induced in a bar without skew, i.e., bar AD, is equal to E_b volts, the skew has reduced the voltage in bar AB by the ratio E/E_b or by

$$K_s = \frac{\sin(\alpha/2)}{\alpha/2} \quad \text{numeric} \tag{10.150}$$

where K_s is the skew factor for the fundamental. Equation (10.150) may be generalized to cover any harmonic, as done in Chapter 9 for the pitch factor and the distribution factor. The skew factor for any harmonic of order n is equal to

$$K_{sn} = \frac{\sin(n\alpha/2)}{n\alpha/2} \quad \text{numeric} \tag{10.151}$$

As mentioned earlier, one effect of skew is to increase the ratio of leakage flux to mutual flux, and the manner in which this effect is calculated is considered in Chapter 13.

10.3.13 Numerical Example of Calculating Skew Factor

Assume that a design engineer is finalizing the design of an eight-pole polyphase induction motor, the rotor diameter of which is 53 cm (about 21 in.). The engineer has decided to use 72 stator slots, which will produce slot harmonics of seventeenth and nineteenth order in the rotating air-gap wave, as discussed in Chapter 12. Since the design engineer is concerned about the spurious effects that such harmonics can cause, the engineer is now determining what amount of rotor skew to use to control their effect on the speed-torque curve. Specifically, the engineer is determining the effect on the seventeenth and nineteenth harmonics of a rotor-bar skew equal to 2.5 cm (about 1 in.) on the rotor periphery.

The circumference of the rotor, (53)π cm along the rotor OD, corresponds to 2π mechanical radians. This peripheral distance, divided by the number of pairs of poles, corresponds to 2π electrical radians. Accordingly, (53)(π)/4 = 41.63 cm (about 16.4 in.) represents 2π electrical radians, for purposes of calculating α, the angle of skew. Then the skew in electrical radians, which corresponds to 1.0 in. along the rotor periphery, is

$$\alpha = \left(\frac{2.5}{41.63}\right)(2\pi) = 0.377 \quad \text{radians} \tag{10.152}$$

Substituting eq. (10.152) into eq. (10.151), the skew factor for the seventeenth harmonic is equal to

$$K_{s17} = \frac{\sin[(17)(0.377)/2]}{(17)(0.377)/2} = 0.0196 \quad \text{numeric} \tag{10.153}$$

and for the nineteenth harmonic is equal to

$$K_{s19} = \frac{\sin[(19)(0.377)/2]}{(19)(0.377)/2} = 0.119 \quad \text{numeric} \tag{10.154}$$

The design engineer concluded that for the design under consideration, an angle of skew of $\alpha = 0.377$ electrical radian greatly reduces the effect of the seventeenth slot harmonic and significantly reduces the effect of the nineteenth slot harmonic as viewed from the rotor winding circuit.

10.3.14 Calculation of the Phase Resistance of a Squirrel-Cage Rotor Winding

Considered in the aggregate, a squirrel-cage winding consists of a number of axial rotor bars arranged around the periphery of the magnetic core of the rotor which are short circuited at each end by circumferential end rings (see Fig. 10.2). There is no insulation between individual bars, except for that provided by the relatively greater resistivity of the steel core compared to that of the bars. However, the rotor-bar currents of a squirrel-cage winding flow in bands that tend to mimic the flow of stator phase current, such as to form apparent phases within the rotor winding. Thus it is possible to calculate the phase resistance of a squirrel-cage rotor winding.

As discussed previously, the rotating air-gap flux wave produced by the stator induces a rotating voltage wave in the rotor bars, and this rotating voltage wave, in turn, causes a rotating rotor-bar current wave to flow in the cage winding. This rotor-bar current, together with corresponding pairs of rotor bars, which form equivalent rotor turns, produces a magnetomotive force in the rotor winding which reacts against an equal and opposite magnetomotive force in the stator winding. The relative angular positions of the currents that correspond to these magnetomotive forces, as viewed from the stator, can be seen in the vector diagram shown in Fig. 7.2. It can be seen that for the rotor phase current I_2, there is an equal and opposite component of stator current, which is designated $-I_2$ on the vector diagram. This stator current component is equal in magnitude to the rotor current I_2, which has been referred to the stator side by being multiplied by $1/a$, the reciprocal of the turns ratio. It can also be seen in Fig. 7.2 that the in-phase voltage drop caused by I_2 flowing in the rotor phase is equal to I_2R_2/s. The equation for calculating R_2 will now be determined.

Let I_b be the effective rotor-bar current, and for purposes of simplicity, let I_{12} be the corresponding component of stator current, which is designated as $-I_2$ in the vector diagram in Fig. 7.2. Then the relationship between total rotor ampere-turns and total counteracting stator ampere-turns is

$$I_b \frac{N_2}{2} = I_{12} q N_{st} K_{p1} K_{d1} \quad \text{ampere-turns} \tag{10.155}$$

where N_2 is the number of rotor slots and the other quantities are as defined previously. (See the list of definitions in Table 9.2, for example.)

$$I_b = \frac{2qI_{12}N_{st}K_{p1}K_{d1}}{N_2} = \frac{Z_1 I_{12} K_{p1} K_{d1}}{N_2} \quad \text{amperes} \tag{10.156}$$

where $Z_1 = 2qN_{st}$, the total conductors in series in the stator winding.

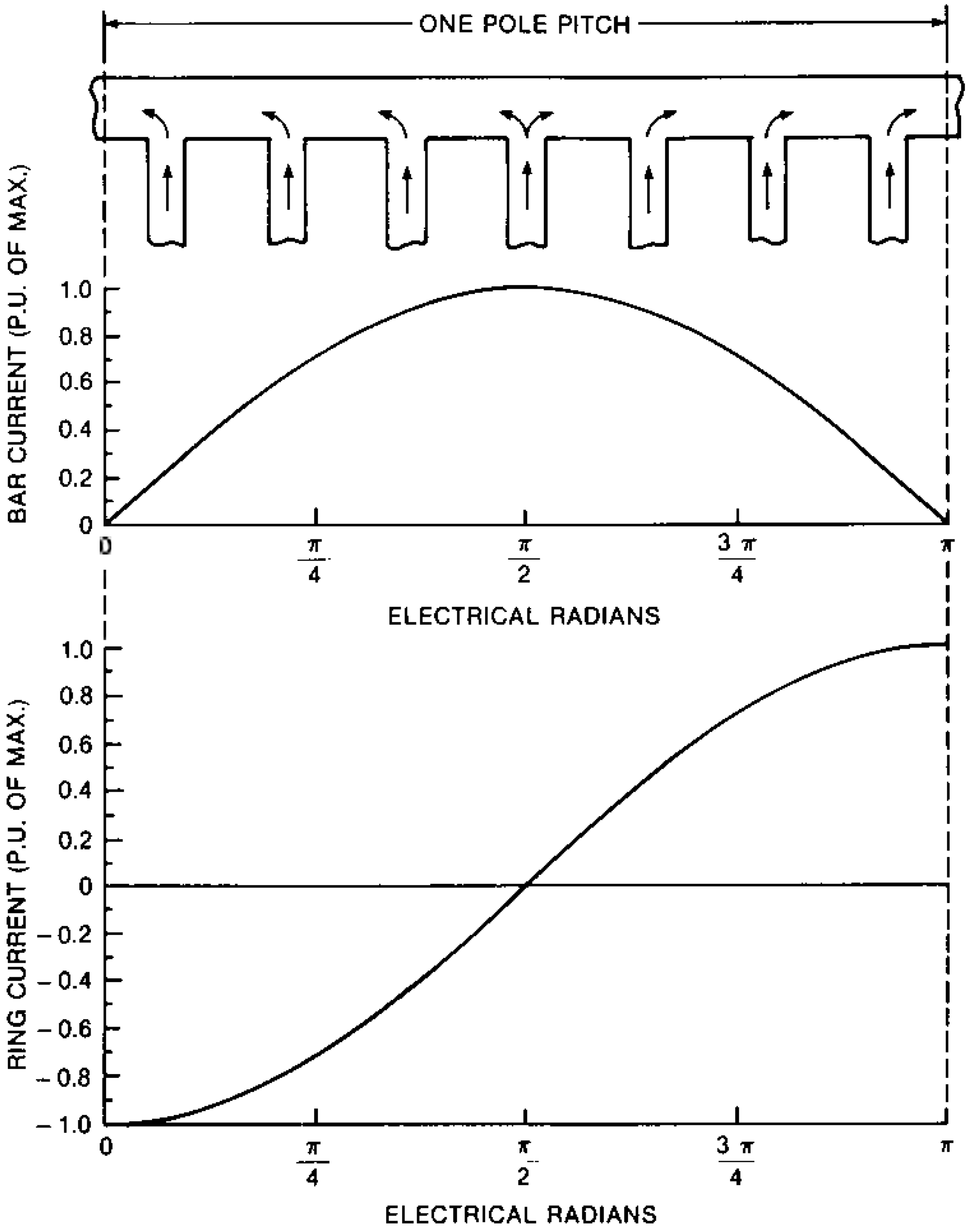

FIGURE 10.17 Relationship between rotor-bar current and end-ring current.

The current in the end ring is equal to the sum of the rotor bar current along one-half of a pole pitch (see Fig. 10.17). If the bar currents were all at their maximum values at the same time, the maximum ring current would be equal to

$$I'_{rm} = \frac{\sqrt{2}\, I_b N_2}{2p} \quad \text{amperes} \qquad (10.157)$$

in each ring. However, the current distribution in the rotor bars along the pole pitch is sinusoidal and the average value is equal to $2/\pi$ of the maximum value. Then the maximum current in each end ring is equal to

$$I_{rm} = \frac{\sqrt{2}\, I_b N_2}{2p} \frac{2}{\pi} = \frac{\sqrt{2}\, N_2 I_b}{p\pi} \quad \text{amperes} \tag{10.158}$$

and the effective current in each ring is equal to

$$I_r = \frac{\sqrt{2}\, N_2 I_b}{p\pi}\left(\frac{1}{\sqrt{2}}\right) = \frac{N_2}{p\pi} I_b \quad \text{amperes} \tag{10.159}$$

Substituting eq. (10.156) into eq. (10.159) and simplifying yields

$$I_r = \frac{Z_1 I_{12} K_{p1} K_{d1}}{p\pi} \quad \text{amperes} \tag{10.160}$$

The total loss in all N_2 bars is equal to

$$W_b = I_b^2 R_b N_2 = I_b^2 \frac{\rho \ell_b}{A_b} \quad \text{watts} \tag{10.161}$$

where

ℓ_b = bar length, meters
A_b = cross-sectional area of the bar, meters^2
ρ = resistivity of the bar material, ohm-meters

Substituting eq. (10.156) into eq. (10.161) yields

$$W_b = \left(\frac{Z_1 I_{12} K_{p1} K_{d1}}{N_2}\right)^2 \frac{\rho \ell_b N_2}{A_b}$$

$$= \frac{I_{12}^2 Z_1^2 K_{p1}^2 K_{d1}^2}{N_2} \frac{\rho \ell_b}{A_b} \quad \text{watts} \tag{10.162}$$

The total loss in the two end rings is equal to

$$W_r = 2 I_r^2 R_r = 2 I_r^2 \frac{\rho \pi D_r}{A_r} \quad \text{watts} \tag{10.163}$$

where

D_r = mean diameter of the end ring, meters
A_r = cross-sectional area of one end ring, meters^2
ρ = resistivity of the end-ring material, ohm-meters

Substituting eq. (10.160) into eq. (10.163) gives us

$$W_r = 2\left(\frac{Z_1 I_{12} K_{p1} K_{d1}}{p\pi}\right)^2 \frac{\rho\pi D_r}{A_r}$$

$$= \frac{2Z_1^2 I_{12}^2 K_{p1}^2 K_{d1}^2 \rho D_r}{p^2 \pi A_r} \quad \text{watts} \tag{10.164}$$

The I^2R loss per phase is equal to the sum of eqs. (10.162) and (10.164), divided by the number of phases q, or

$$I_2^2 R_2 = \frac{I_{12}^2 Z_1^2 K_{p1}^2 K_{d1}^2}{q}\left(\frac{\ell_b}{N_2 A_b} + \frac{2D_r}{p^2 \pi A_r}\right)\rho \quad \text{watts/phase} \tag{10.165}$$

Thus the phase resistance of the cage winding of the rotor, referred to the stator is equal to

$$R_2 = \frac{Z_1^2 K_{p1}^2 K_{d1}^2 \rho}{q}\left(\frac{\ell_b}{N_2 A_b} + \frac{2D_r}{p^2 \pi A_r}\right) \quad \text{ohms/phase} \tag{10.166}$$

and since $Z_1 = 2qN_{st}$, where N_{st} are the stator winding series turns/phase,

$$R_2 = 4qN_{st}^2 K_{p1}^2 K_{d1}^2 \rho\left(\frac{\ell_b}{N_2 A_b} + \frac{2D_r}{p^2 \pi A_r}\right) \quad \text{ohms/phase} \tag{10.167}$$

Equation (10.167) has been derived with bar and end-ring dimensions assumed to be in units of meters and with the resistivity of the cage material assumed to be in units of ohm-meters. However, if cage dimensions are in units of inches and resistivity is in units of ohm-inches, eq. (10.167) may be used without change. This is because the dimensional units cancel in the equation, leaving only ohms, such that any consistent set of units may be used.

If the rotor bars are skewed, the skew factor K_s should be included as a factor in eq. (10.167). However, the magnitude of K_s is small for typical amounts of skew. The skew factor in the example in Section 10.3.13 is $K_s = \sin(0.377/2)/(0.377/2) = 0.994$. Accordingly, this factor is, not infrequently, ignored when calculating the resistance of skewed rotors, the amount of skew of which is within typical limits. Also, in the derivation of eq. (10.167), it was assumed that the current in the end ring had a sinusoidal distribution, as shown in Fig. 10.17. If the number of rotor bars per pair of poles (i.e., $2N_2/p$) is a small number, the end-ring current departs from a sinusoidal distribution, which affects the end-ring component of resistance. Even for slow-speed machines with a large number of poles, for which the number of rotor slots increase at a lower rate than the number of poles, it is usually not a significant problem. This is because, as is apparent from eq. (10.167), the end-ring component of total rotor phase resistance decreases as the square of the number of poles, making that component a progressively smaller component of total rotor resistance, as the number of poles increase. Thus this effect is also insignificant for the typical design, and is usually ignored.

The rotor bar is surrounded on three sides, as well as on part of the top, by the steel rotor core. Since steel has very great permeance to the flow of slot leakage flux compared to air, such proximity of steel greatly increases slot leakage flux, which, in turn, affects the amount of ac-to-dc resistance exhibited by the bar. On the other hand, the end ring is surrounded by air on at least three and, frequently, on four sides, such that the permeance of the end-ring path to leakage flux is considerably less per ampere than that of the bar. Although the end ring does exhibit some increase in resistance at line frequency, it is usually not sufficient as to affect the ratio of R_{ac}/R_{dc} of the rotor phase significantly. Thus it is usually ignored, which is a conservative design practice, as far as it affects the calculated value, compared to the tested value, of starting torque.

10.3.15 Numerical Example of Calculating Phase Resistance of a Squirrel-Cage Rotor Winding

The parameters necessary for calculating the rotor phase resistance of a given squirrel-cage induction motor are as tabulated in Table 10.1. The number of series turns/phase N_{st} is equal to

$$\text{series turns/phase} = \frac{(\text{turns/coil})(\text{total number of slots})}{(\text{number of phases})(\text{number of circuits})} \quad \text{numeric} \tag{10.168}$$

TABLE 10.1 Tabulation of Pertinent Parameters for Calculating the Phase Resistance of the Squirrel-Cage Rotor Winding, Used as a Numerical Example

Parameter	Symbol	Value	Unit
Number of poles	p	4	numeric
Number of phases	q	3	numeric
Line frequency	f	60	hertz
Number of stator slots	N_1	84	numeric
Number of rotor slots	N_2	107	numeric
Length of rotor bar	ℓ_b	63.5	centimeters
Depth of rotor bar	d_b	2.5	centimeters
Cross-sectional area of rotor bar	A_b	1.62	centimeters^2
Mean diameter of end ring	D_r	44	centimeters
Cross-sectional area of end ring	A_r	25	centimeters^2
Resistivity of rotor winding	ρ_2	3.45×10^{-8}	ohm-meters
Number of stator turns/coil	N_c	7	numeric
Number of stator circuits	C_1	2	numeric
Stator pitch factor	K_{p1}	0.989	numeric
Stator distribution factor	K_{d1}	0.955	numeric
Rotational inertia of motor	$(WK^2)_m$	32.7	kilogram-meters^2
Rotational inertia of external load	$(WK^2)_L$	143	kilogram-meters^2

Substituting the corresponding stator quantities from Table 10.1 into eq. (10.168) gives us

$$N_{st} = \frac{(7)(84)}{(3)(2)} = 98 \quad \text{numeric} \qquad (10.168a)$$

Then, substituting the value of N_{st} from eq. (10.168a) and the value of the other required parameters from Table 10.1, into eq. (10.167) yields

$$R_2 = \left[(4)(3)(98)^2(0.989)^2(0.955)^2\left(\frac{3.45}{10^8}\right)\right]\left[\frac{0.635}{(107)(0.000162)} + \frac{(2)(0.44)}{(4)^2\pi(0.0025)}\right]$$

$$= 0.155 \quad \text{ohms/phase} \tag{10.169}$$

The value of R_2 determined above is the dc value, which exists when the rotor-circuit frequency is relatively low. To determine the ac value of R_2 or the blocked-rotor value $R_{2\ell}$, the quantity δd_b must first be found. From Fig. 10.9,

$$\delta d_b = 13.74 d_b \sqrt{kf} \quad \text{numeric} \tag{10.170}$$

when d_b is expressed in meters. For this example the value of k, the ratio of bar width to slot width, will be assumed to be close to 1.0. Then for the bar depth given in Table 10.1,

$$\delta d_b = (13.74)(0.025)\sqrt{60} = 2.66 \quad \text{numeric} \tag{10.171}$$

and from Fig. 10.9, the corresponding value of R_{ac}/R_{dc} for the bar is 2.63. Then eq. (10.169) becomes

$$R_{2\ell} = [0.003547][(36.6)(2.63) + 7.0] = 0.366 \quad \text{ohms/phase} \tag{10.172}$$

and the ratio of blocked-rotor resistance to running resistance of the rotor phase winding is

$$\frac{R_{2\ell}}{R_2} = \frac{0.366}{0.155} = 2.36 \quad \text{numeric} \tag{10.173}$$

10.3.16 Transient Temperature Rise of the Rotor Winding During Changes in Speed

A change in speed of the rotor of an induction motor, produced by its own electromagnetic means, results from either an accelerating torque or a decelerating torque which is developed by that motor. Thus to increase the speed of the rotor from a standstill condition to full speed requires that the rotor develop an accelerating torque. Similarly, to decrease the speed of the rotor by means of electrical braking, such as by applying reverse-sequence voltage to the stator winding, requires that the rotor develop a decelerating torque. It was shown previously that the torque developed by the rotor is proportional to the slip losses within the rotor circuit. Equation (5.78), for example, states that

$$T = \frac{60}{2\pi}\frac{1}{n_s}3I_2^2R_2 = \frac{90}{\pi}\frac{1}{n_s}I_2^2R_2 \quad \text{newton-meters} \tag{10.174}$$

Thus it could be expected that changes in rotor speed would result in the dissipation of considerable heat energy within the rotor winding, as indeed, it does. For a wound-rotor motor, most of this energy is dissipated in the external resistor outside the machine. For a squirrel-cage motor, however, the energy is dissipated within the volume of the rotor cage, and since this occurs in a relatively short period of time, it can result in a short-time, or transient, temperature rise of the rotor winding if the rotational inertia of the rotor and connected load is sufficient. A procedure for determining the rotor-bar and end-ring temperature rise, associated with a change in rotor speed, will now be developed for squirrel-cage motors.

Equation (10.174) can be written as

$$P_m = \omega_s T_m \quad \text{watts} \tag{10.175}$$

where

P_m = power which is electromagnetically delivered to the rotor
T_m = resulting total torque which is developed by the motor, including the relatively small amount required to overcome rotor friction and windage
ω_s = synchronous speed, or angular velocity, of the rotor structure, radians/second

During the change in speed, the power loss in the rotor winding is equal to the power P_m delivered to the rotor, less the power P_a required to accelerate the rotational inertia of the rotating system, and less any power P_L that might be delivered to the connected load, or

$$P = P_m - P_a - P_L \quad \text{watts} \tag{10.176}$$

The power required to accelerate, or to decelerate, the rotational inertia is equal to

$$P_a = \omega T_a \quad \text{watts} \tag{10.177}$$

and any power delivered to the connected load is equal to

$$P_L = \omega T_L \quad \text{watts} \tag{10.178}$$

where ω is the angular velocity of the rotor structure in radians/second. Substituting eqs. (10.175), (10.177), and (10.178) into eq. (10.176) gives us

$$P = \omega_s T_m - \omega T_a - \omega T_L \quad \text{watts} \tag{10.179}$$

The torque T_m developed by the motor is equal to the torque required to accelerate, or decelerate, the rotational inertia, plus any friction torque delivered to the connected load, or

$$T_m = T_a + T_L \quad \text{newton-meters} \tag{10.180}$$

Then eq. (10.179) may be written as

$$P = T_m(\omega_s - \omega) \quad \text{watts} \tag{10.181}$$

The energy dissipated in the rotor winding during the time required to change rotor speed is

$$\mathcal{E} = \int_{t_1}^{t_2} P\,dt \quad \text{joules} \tag{10.182}$$

or, substituting eq. (10.181) into eq. (10.182),

$$\mathcal{E} = \int_{\omega_1}^{\omega_2} T_m(\omega_s - \omega)\,dt \quad \text{joules} \tag{10.183}$$

where ω_1 and ω_2 correspond to the angular velocity of the rotor at times t_1 and t_2, respectively. The torque required to accelerate an inertia equal to I, in kilogram-meters^2, is

$$T_m - T_L = I\alpha = I\,\frac{d\omega}{dt} \quad \text{newton-meters} \tag{10.184}$$

Solving for dt yields

$$dt = \frac{I}{T_m - T_L}\,d\omega \quad \text{seconds} \tag{10.185}$$

Substituting eq. (10.185) into eq. (10.183) gives us

$$\mathcal{E} = \int_{\omega_1}^{\omega_2} I\left(\frac{T_m}{T_m - T_L}\right)(\omega_s - \omega)\, d\omega \quad \text{joules} \tag{10.186}$$

However, it is more convenient to evaluate the integral above if the variable is rotor slip instead of rotor angular velocity. The slip s at an angular velocity ω of the rotor structure for a motor with a synchronous angular velocity of ω_s of

$$s = \frac{\omega_s - \omega}{\omega_s} \quad \text{numeric} \tag{10.187}$$

Rearranging eq. (10.187), we obtain

$$\omega_s - \omega = (\omega_s)\, s \quad \text{radians/second} \tag{10.188}$$

and differentiating yields

$$-d\omega = \omega_s\, ds \quad \text{radians/second} \tag{10.189}$$

Substituting eqs. (10.188) and (10.189) into eq. (10.186) gives us

$$\mathcal{E} = -I\omega_s^2 \int_{s_1}^{s_2} \frac{T_m}{T_m - T_L}\, s\, ds \quad \text{joules} \tag{10.190}$$

where s_1 and s_2 are the values of slip that correspond to the rotor-structure angular velocities of ω_1 and ω_2, respectively. For the frequently encountered case of starting a squirrel-cage motor from standstill and allowing the rotor and connected load to accelerate to full speed, and for which there is negligible load torque T_L required by the driven equipment during acceleration, eq. (10.190) is equal to

$$\mathcal{E} = \frac{1}{2} I\omega_s^2 \quad \text{joules} \tag{10.191}$$

The expression on the right-hand side of eq. (10.191) will be recognized as being equal to the kinetic energy stored in a rotational mass I, the angular velocity of which is ω_s radians/second. Thus, for this very typical case, the heat energy dissipated within the rotor winding, during the acceleration period, is equal to the kinetic energy stored in the rotating mass, at full speed.

The derivations of the integral given in eq. (10.190) and of the specific solution given in eq. (10.191) were based on the use of the MKS system of units. These equations may be converted to use the FPS system of units by remembering that there are 3.281 feet in 1 meter, 2.205 pounds mass in 1 kilogram, and 0.7375 foot-pound in 1 joule. Also, use of rotor speed in rpm instead of in radians/second may be achieved by remembering that $\omega = 2\pi(\text{rpm})/60$. Then

$$\mathcal{E} = \frac{0.231(\text{WK}^2)(\text{rpm})^2}{10^3} \quad \text{joules} \tag{10.192}$$

where WK^2 is expressed in units of pound-feet^2.

During the relatively short time required for a change in rotor speed, the amount of heat energy transferred from a squirrel-cage winding is small to negligible. On the assumption of no heat lost during a change in speed, the transient temperature rise of the rotor bars and end rings can be determined by dividing the heat energy $\mathcal{E}$ produced in the rotor winding by the specific heat and by the weight of the winding. However, for practical reasons, it is more convenient to divide $\mathcal{E}$ by the winding volume and by the specific heat in corresponding terms of volume instead of weight. Further, by easily made and entirely adequate approximations, the temperature rise of the rotor bars and of the end rings can be determined separately. Then

$$\Delta T_b = \frac{(R_b/R_t)\mathcal{E}}{C_v V_b} \quad {}^\circ\text{C} \tag{10.193}$$

and

$$\Delta T_r = \frac{(R_r/R_t)\mathcal{E}}{C_v V_r} \quad {}^\circ\text{C} \tag{10.194}$$

where

R_b/R_t = ratio of bar resistance to total rotor winding resistance
R_r/R_t = ratio of the total end-ring resistance to total rotor winding resistance
V_b = total volume of the rotor bars, centimeters^3 or inches^3

TABLE 10.2 Tabulation of Specific Heat Values in Volumetric Units for Use in Calculating Rotor-Bar and End-Ring Transient Temperature Rise

Material	C_v	
	joules/(in.^{3}·°C)	joules/(cm^3·°C)
Aluminum[a]	37-40	2.26-2.44
Copper	57.4	3.50
Brass	53.0	3.23

[a] The value will vary slightly depending on other component materials added to aluminum to control resistivity and on the amount of porosity of the casting.

V_r = total volume of the end rings, centimeters^3 or inches^3
C_v = specific heat of the bar and the end-ring material, joules/(inch^3·°C) or joules/(cm^3·°C)

Typical values of C_v for copper, aluminum, and brass are given in Table 10.2.

The quantities R_b/R_t and R_r/R_t are determined from the rotor-winding resistance calculation. R_b is defined as the average of the ac and dc resistance of the bars, or

$$R_b = \frac{R_{bac} + R_{bdc}}{2} = \frac{k}{2}\left[\left(\frac{R_{ac}}{R_{dc}} + 1\right)\frac{\ell_b}{N_2 A_b}\right] \quad \text{ohms/phase} \qquad (10.195)$$

where k is a constant [see eq. (10.166)] and R_{ac}/R_{dc} is the ratio of ac-to-dc resistance of the bar resulting from the deep-bar effect or multiple-cage effect. R_r is defined as

$$R_r = k\frac{2D_r}{p^2 \pi A_r} \quad \text{ohms/phase} \qquad (10.196)$$

and R_t is defined, in terms of the total phase resistance, as

$$R_t = \frac{R_2 + R_{2\ell}}{2} = \frac{k}{2}\left[\left(\frac{\ell_b}{N_2 A_b} + \frac{2D_r}{p^2 \pi A_r}\right) + \left(\frac{R_{ac}}{R_{dc}}\frac{\ell_b}{N_2 A_b} + \frac{2D_r}{p^2 \pi A_r}\right)\right]$$

$$\text{ohms/phase} \qquad (10.197)$$

Using the three definitions above, the quantities R_b/R_t and R_r/R_t in eqs. (10.193) and (10.194), respectively, are equal to

$$\frac{R_b}{R_t} = \frac{R_{bac} + R_{bdc}}{R_2 + R_{2\ell}} \quad \text{numeric} \tag{10.198}$$

and

$$\frac{R_r}{R_t} = \frac{2R_r}{R_2 + R_{2\ell}} \quad \text{numeric} \tag{10.199}$$

In actual practice, R_b/R_t and R_r/R_t are determined by use of the appropriate factors determined previously from the rotor-winding resistance calculation, as will become apparent in the following numerical example.

10.3.17 Numerical Example of Transient Temperature Rise of the Rotor Winding During Acceleration

The motor, the parameters of which are given in Table 10.1, will be used as a numerical example for calculating the transient rotor-winding temperature rise resulting from the motor accelerating its own rotor inertia, and that of the connected load, to full speed. It will be assumed that the load torque required by the connected load is negligible during the acceleration period.

From eq. (10.191), the energy dissipated in the rotor winding during the acceleration period is

$$\mathcal{E} = \frac{1}{2} I\omega_s^2 \quad \text{joules} \tag{10.200}$$

The inertia to be accelerated is equal to 32.7 $\text{kg}\cdot\text{m}^2$ for the rotor and 143 $\text{kg}\cdot\text{m}^2$ for the external load, or a total of 175.7 $\text{kg}\cdot\text{m}^2$. Since the stator winding is wound for four poles, it has a synchronous speed of 1800 rpm. This speed, in radians/second, is

$$\omega_s = \frac{2\pi(\text{rpm})}{60} = \frac{2\pi(1800)}{60} = 188.5 \quad \text{radians/second} \tag{10.201}$$

Substituting the values above into eq. (10.200), we obtain

$$\mathcal{E} = \frac{(175.7)(188.5)^2}{2} = 3.122 \times 10^6 \quad \text{joules} \tag{10.202}$$

Using eq. (10.195) and referring to the previous calculation of rotor resistance made for the same motor in Section 10.3.15, we find

$$R_b = \frac{k}{2}\left[\left(\frac{R_{ac}}{R_{dc}} + 1\right)\frac{\ell_b}{N_2 A_b}\right] = \frac{k}{2}\left[(3.63)(36.6)\right] = 66.5k \quad \text{ohms/phase} \tag{10.203}$$

and using eq. (10.196), we have

$$R_r = k\frac{2D_r}{p^2 \pi A_r} = k\frac{(2)(0.44)}{(4)^2(\pi)(0.0025)} = 7k \quad \text{ohms/phase} \tag{10.204}$$

and using eq. (10.197), we obtain

$$R_t = \frac{k}{2}\left\{(36.6 + 7) + \left[(2.63)(36.6) + 7\right]\right\} = 73.5k \quad \text{ohms/phase} \tag{10.205}$$

Then

$$\frac{R_b}{R_t} = \frac{66.5}{73.5} = 0.905 \quad \text{numeric} \tag{10.206}$$

$$\frac{R_r}{R_t} = \frac{7}{73.5} = 0.095 \quad \text{numeric} \tag{10.207}$$

The total volume of the bars is equal to

$$V_b = N_2 A_b \ell_b = (107)(1.62)(63.5) = 11{,}007 \quad \text{centimeters}^3 \tag{10.208}$$

and the total volume of the two end rings is equal to

$$V_r = 2\pi D_r A_r = (2\pi)(44)(25) = 6911 \quad \text{centimeters}^3 \tag{10.209}$$

From eq. (10.193), the transient temperature rise of the rotor bars is

$$\Delta T_b = \frac{(R_b/R_t)\mathcal{E}}{C_v V_b} \quad {}^\circ\text{C} \tag{10.210}$$

Substituting the values of R_b/R_t, $\mathcal{E}$, and V_b given in equations (10.206), (10.202), and (10.208), respectively, and the value of C_v from Table 10.2 into eq. (10.210) gives us

$$\Delta T_b = \frac{(0.905)(3.122 \times 10^6)}{(2.35)(11,007)} = 109 \quad {}^\circ C \tag{10.211}$$

From eq. (10.194), the transient temperature rise of the rotor end rings is

$$\Delta T_r = \frac{(R_r/R_t)\mathcal{E}}{C_v V_r} \quad {}^\circ C \tag{10.212}$$

and substituting the values of R_r/R_t, $\mathcal{E}$, and V_r given in equations (10.207), (10.202), and (10.209), respectively, and the value of C_v from Table 10.2 into eq. (10.212), we obtain

$$\Delta T_r = \frac{(0.095)(3.122 \times 10^6)}{(2.35)(6911)} = 18.3 \quad {}^\circ C \tag{10.213}$$

It is frequently, but not always, a specification requirement that a squirrel-cage motor be capable of accelerating the combined inertia of the motor rotor and that of the connected load (or of a specific amount of external inertia) to full speed twice in succession, with no rest period between the successive starts. Then, assuming that little or no heat energy was transferred from the rotor winding during the two successive starts and the intervening coast down, such a starting cycle requirement for the example above would result in the rotor bars reaching a transient temperature rise of approximately 200°C and the end rings reaching a corresponding temperature rise of approximately 35°C, both values being generally acceptable.

10.4 WOUND-ROTOR WINDINGS

10.4.1 Effect of Centrifugal Force on Rotor-Coil Design and Selection

Lap-type coils similar to those used for stator windings can be used for wound-rotor windings. In fact, in some small to medium-sized ratings, such coils have been used to some extent for this purpose. However, the wave-type coil is more suited to the overall requirements of windings for wound-rotor machines. In eqs. (10.5) and (10.6) it is shown that the centrifugal force exerted on a rotating part is proportional to the mass of the part, to the distance from the shaft centerline to the centroid of the part, and to the second power of the speed of rotation. Thus the amount of centrifugal force exerted on the rotor winding becomes an increasingly important factor as the machine size increases. Since only a very minor portion of the small induction motors now being manufactured are of the wound-rotor type, centrifugal force on the rotor winding is an important design consideration on essentially all wound-rotor motors that are built, which are essentially all in the larger ratings.

For lap-type windings, for which the adjacent coils of a given phase within a given pole span are connected together to form a group, the various groups must be connected to the other groups of that phase, in the required series-parallel combination, to form each of the phase windings. Thus a considerable amount of insulated copper cable or strap must be used for these interconnections to form each of the individual phase windings. Use of wave-type coils, on the other hand, will reduce the additional insulated copper cable or strap that must be used to form the individual phase windings (see Fig. 9.3.). Because the end extensions of the coils span outward, on the connection end to form a continuous wave around the periphery of the rotor, there is no need for cross connections for interconnecting coil groups which are distributed around the entire rotor OD. Thus considerably less insulated copper cable or strap is used, and that which is required is more symmetrically located around the OD of the rotor. This produces a rotor structure, the weight of which is more symmetrically distributed, and which can be more easily braced against centrifugal force, more easily balanced, and more easily kept in balance over the life of the motor.

10.4.2 Types of Wave Windings

As a wave winding progresses around the periphery of the rotor, the axial or conductor portion of the winding passes through each successive pole area in opposite directions and thus the voltage induced in each successive conductor will add in the progression. After the first such circular progression has been completed and at the start of the second progression, the starting point will be at a slot adjacent to the starting slot for the first progression. If the second starting slot is adjacent but just short of the first starting slot, it is called a retrogressive wave winding. If it is adjacent but just beyond the first starting slot, it is called a progressive wave winding.

A wave winding is further classified as being a true or a modified wave winding. For a true-wave winding, the combination of the number of rotor slots to the number of poles is such that all coils have the same throw, whereas for a modified-wave winding, there will be one location for each phase, where the throw is shortened by one slot for each progression around the rotor periphery, as will be shown later. All of the individual coils are identical in a given set of modified-wave coils, and the shorter coil throw at the one location is achieved by bending the coil end a small additional amount to cause the straight portion to fall into the desired slot. A typical example will illustrate these two different types of wave windings.

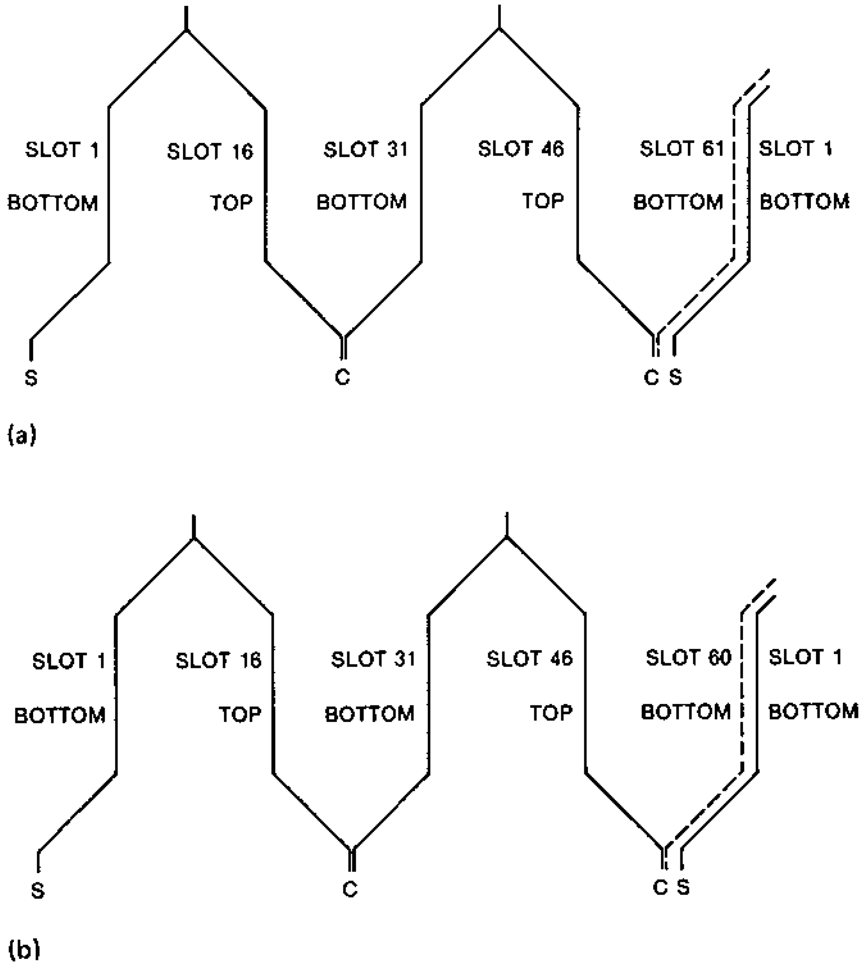
SLOT 1
BOTTOM
SLOT 16
TOP
SLOT 31
BOTTOM
SLOT 46
TOP
SLOT 61
BOTTOM
SLOT 1
BOTTOM
S
C
C S
(a)
SLOT 1
BOTTOM
SLOT 16
TOP
SLOT 31
BOTTOM
SLOT 46
TOP
SLOT 60
BOTTOM
SLOT 1
BOTTOM
S
C
C S
(b)

FIGURE 10.18 Schematic diagram which shows the difference between a true-wave and a modified-wave winding: (a) one progression of a retrogressive, true-wave winding for a four-pole rotor with 61 slots; (b) one progression of a retrogressive modified-wave winding for a four-pole rotor with 60 slots.

Figure 10.18a shows one progression around the rotor for a true-wave winding. The four-pole rotor has 61 slots, such that there are 61/4 = 15 1/2 slots/pole. One coil side of the first coil is positioned in the bottom of slot 1 and the other coil side is positioned in the top of slot 16. The first coil then joins the second coil at the connection end of the rotor, at the first point C, at the bottom of the figure. One coil side of the second coil is positioned in the bottom of slot 31 and the other in the top of slot 46. At this point, the four conductors, provided by the two coils, have spanned four poles of air-gap flux. The second coil then joins the third coil at the connection end, at the second point C; the first side of the third coil is positioned in the bottom of slot 61; and so on. The conductor at the bottom of slot 61, which is adjacent to slot 1, is the first conductor of the second progression around the rotor. The last conductor of the first progression falls one slot short of the first conductor of the second progression, and hence the winding is retrogressive. Further, the span between each coil side and the successive coil side is identical, which is characteristic of a true wave winding.

Figure 10.18b shows one corresponding progression around the rotor for a modified-wave winding. For this case the four-pole rotor has only 60 slots, which is one less than for the preceding case. Thus there are 60/4 = 15 slots/pole. The first progression around the periphery of the rotor is generally similar to that for the preceding case, with one significant exception. One coil side of the first coil is positioned in the bottom of slot 1 and the other coil side is positioned in the top of slot 16. The first coil then joins the second coil at the connection end of the rotor at the first point C. One coil side of the second coil is positioned in the bottom of slot 31 and the other in the top of slot 46. Again, at this point, the two coils have spanned four poles of air-gap flux. The second coil then joins the third coil at the connection end, at the second point C, and the first side of the third coil is positioned in the bottom of slot 60. The coil throws from slot 1 to slot 16, from slot 16 to slot 31, and from slot 31 to slot 46 are all uniform and are equal to a span of 15 slots. However, to insert the first side of the third coil into slot 60, the third coil must be slightly forced to the left one slot pitch, in order for the conductor to fall into slot 60 instead of into slot 1. Thus the coil throw from slot 46 to slot 60 is intentionally reduced to a span of 14 slots. The intentional shortening of this span will occur at this location for a total of five such progressions around the periphery of the rotor, at which time one-half of one phase, or one-sixth of the total winding will have been completed. This winding is also a retrogressive winding, but it is a modified-wave winding rather than a true-wave winding.

The apparent mechanical symmetry of the true-wave winding, such as that shown in Fig. 10.18a, is misleading and may give rise to a false sense of confidence in this type of winding. Use of true-wave windings leads to problems in electrical balance between sections of the winding such that it is difficult to parallel sections without producing circulating currents. For the example shown in Fig. 10.18a, the number of slots per pole per phase is equal to $N_2/pq = 61/(4 \times 3) = 61/12$. This fraction has no common denominators between the numerator and the denominator, so that the value of B, as defined in Section 9.15, is $B = 12$. Since 12 is divisible by 3, the number of phases, the general winding criteria would indicate that the resulting three-phase winding will not be balanced. Thus, for the above and other reasons, true-wave windings are seldom used on wave-wound rotors of induction motors, whereas the modified-wave type has been the standard winding.

10.4.3 Wound-Rotor Slots and the Corresponding Coil Configurations

For essentially all wound-rotor designs, the number of rotor slots is chosen such that (1) the number of rotor slots N_2 is a multiple of the product of the number of phases p and the number of poles q, that is

$$\frac{N_2}{pq} = \text{integer} \quad \text{numeric} \tag{10.214a}$$

or (2) the number of rotor slots is a multiple of the product of the number of phases and the number of pairs of poles,

$$\frac{2N_2}{pq} = \text{integer} \quad \text{numeric} \tag{10.214b}$$

The first case, or the criterion given in eq. (10.214a), will give equal coil grouping, which, as shown for stator windings in Chapter 9, will maximize the maximum permissible number of parallel circuits possible. The second case, or the criterion given in eq. (10.214b), will give unequal coil grouping, which will limit the maximum permissible number of parallel circuits possible.

Double-layer coils with two coil sides per slot are used almost exclusively in the United States for wound-rotor windings. As is true for stator windings, this gives a total number of coils that is equal to the number of slots. The need to withstand centrifugal force places a significant constraint on the design of the slot and on the choice of the conductor. The slot opening must be sufficiently wide to permit passage of one conductor, but it must be sufficiently narrow to limit the span of the slot wedge and to provide an adequate purchase for securing the wedge. The smallest power ratings of wound-rotor motors use insulated round wire with several "wires in hand" to form a conductor, similar to that discussed for random stator windings in Chapter 9. For such designs, the winding is similar to that used for insulated strap designs, such as that shown in Fig. 10.18. The several wires in hand, which form one conductor, start at point S in the figure and are positioned in slots 1 and 16, for example. Depending on the total number of turns desired for the phase winding, the random conductor is then (1) repeated through slots 1 and 16, to give more than one turn, or it is (2) immediately routed into slots 31 and 46, as would be done for a strap conductor. If more than one turn is wound in slots 1 and 16, as in choice 1 above, the conductor is then routed into slots 31 and 46 to form a wave progression, where again, the desired number of turns will be wound before proceeding with the wave progression. When inserting the several wires in hand into the slot, they may be fed into the slot one or two at a time, which permits having a small slot opening. Use of random rotor windings is restricted to the lower power ratings, and since very few wound-rotor units are now produced in such ratings, this type of winding and slot is not often encountered in new machines.

Most wound-rotor motors, of medium to large power rating, use four straps per slot, as shown in Fig. 10.19. In part (a) of the figure, the slot opening is sufficiently wide to permit just one insulated strap to pass. This reduces the opening at the air gap to half of the total slot opening. Thus the unsupported wedge span is reduced to one-half and the bending moment on the wedge is reduced to one-fourth of that of a fully open slot. The slot opening in part (a) is offset to one side of the slot, whereas the slot opening in part (b) is centered about the radial centerline of the slot.

The design in Fig. 10.19b permits a more symmetrical cross-sectional wedge shape and a more uniform purchase for the wedge. Both slots are adequate, however, if the radial thickness and the material of the wedge are properly selected. Some winders believe that the offset wedge opening allows for easier positioning of the four insulated straps into location after insertion, but this is probably a personal preference. The pair of straps

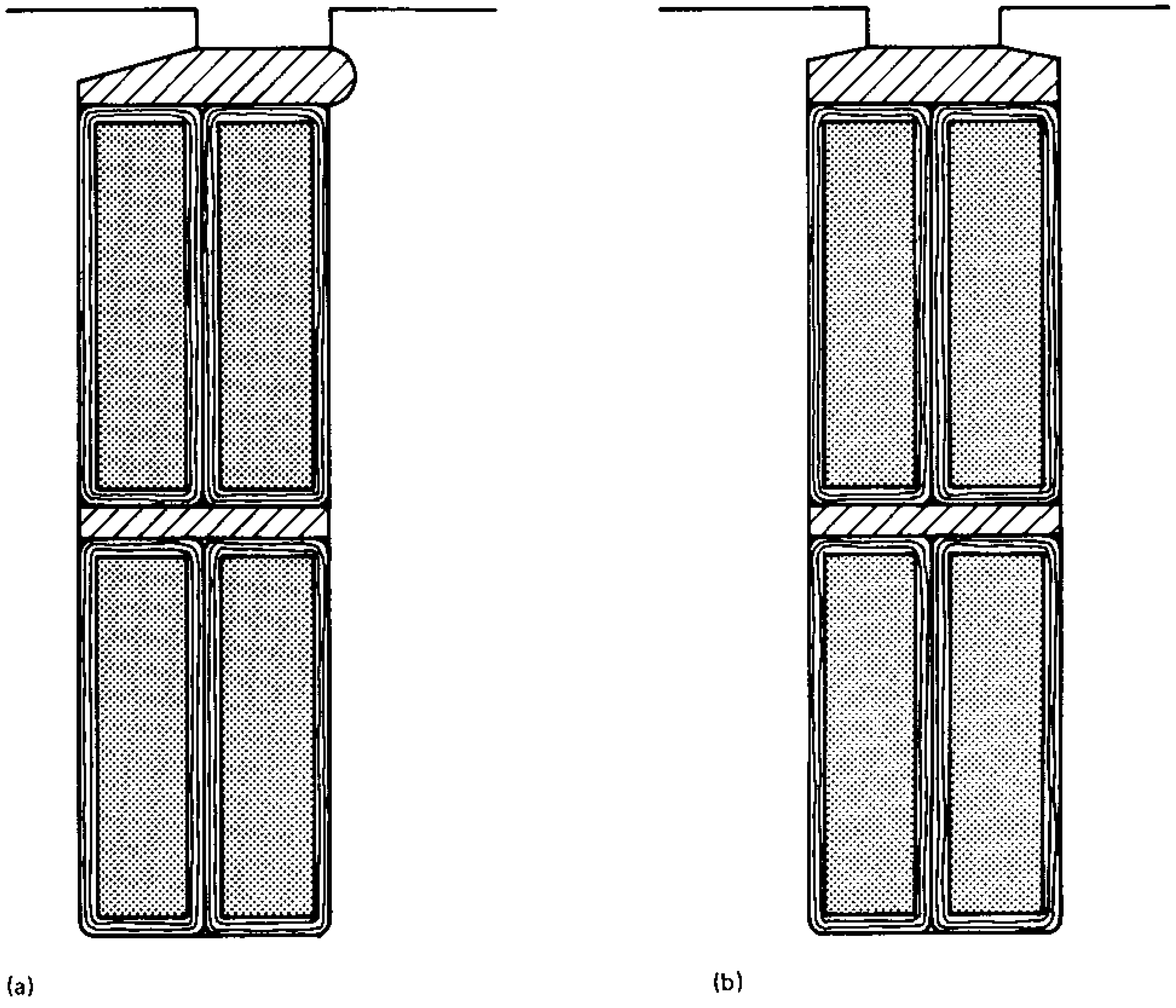

FIGURE 10.19 Types of wound-rotor slots: (a) offset opening and four straps/slot; (b) centered opening and four straps/slot.

located in the top or in the bottom of the slot in Fig. 10.19 constitute one coil side in the winding progression described previously. One complete wave-type coil will span from point S to point C in Fig. 10.18 and will consist of two insulated straps that nest together to form a complete coil. The two straps are brazed together at the two ends, where the ground insulation has been omitted intentionally. Connections between successive coils, identified by C's in Fig. 10.18, is accomplished by placing "clips" (special connection ferrules) over the adjacent ends of the two consecutive coils and then brazing them together.

Two additional configurations of wave-type coils are occasionally encountered. One of them is what might be considered a transition from the use of round wire, of random coils, to the use of insulated copper strap, just described. For this configuration, the two insulated straps in the top or bottom of the slot are replaced with a larger number, such as four, of smaller insulated rectangular copper sections. During winding, the copper sections are individually fed through the slot opening and then manipulated into place. The bundle of four or more insulated copper straps are, in some designs, circumferentially wrapped with tape in the end-turn region, beyond the slot region, to hold them in place until circumferential banding can be applied to the entire set of end turns.

The second additional configuration of wave-type coil has one insulated copper strap in each coil side, instead of the usual two. It has the advantage of being more easily secured and braced, in the end-turn region, but it cannot be inserted into the slot from the slot opening and yet have an effective wedge design. This requires that the coil side be inserted from the end of the slot, as for a "push-through" stator coil (see Fig. 9.5). After the coil side has been inserted into the slot, through the end of the slot, the extended, straight end must be formed, by the winder, at the winding workstation. However, it is bent outwardly to form a wave progression, instead of inwardly to form a diamond, as shown in Fig. 9.5. This kind of coil design offers a limited design choice of rotor voltage, requires considerable hand labor, and is susceptible to the whims of individual operator variations in forming the end turns on the connection end, compared to those produced by a forming machine. Wound-rotor induction motors with this configuration of rotor coils will be encountered in the field, but relatively infrequently.

10.4.4 Modified-Wave Winding

As discussed in Section 10.4.2, the modified-wave coil is the basic coil used for wound rotors. This is because it results in a winding that is electrically balanced, because fewer cross connections are required and the cross connections that are required are more symmetrically distributed around the periphery of the rotor. Rotor windings made up from modified-wave coils are called modified-wave windings. The rotor winding can be a two-phase, three-phase, or four-phase winding, and it will produce a net torque when operating with a three-phase stator. However, the rotor must be wound for the same number of poles as the stator, in order for the induced voltages and the resulting rotor currents not to cancel and thus to produce a net torque. A three-phase rotor winding is the most economical and practical, as it requires only three collector rings, yet effectively utilizes the rotor periphery, whereas both two-phase and four-phase rotors require four collector rings. Since successive coil sides of wave coils alternately occupy the top and bottom positions of slots, wave coils are usually inserted into the rotor core before the connections are made, as is done for lap coils. However, special cases or circumstances may arise with wave windings where this is not completely possible.

In accordance with eqs. (10.214a) and (10.214b), the number of rotor slots N_2 is a multiple of the number of poles p and the number of phases q and is an even number. To prevent having the last coil side fall into the same slot as the starting coil side for a given progression around the rotor periphery, the winder is instructed to deliberately reduce the throw of the last span by one slot. As discussed earlier, this is what distinguishes the modified-wave winding from the true-wave winding. To provide further understanding of the modified-wave winding, the four-pole 60-slot example mentioned in Section 10.4.2 will be more completely analyzed and discussed. This particular slot-to-pole combination has been used to some extent for medium-sized four-pole wound-rotor motors, it exhibits the various design aspects of a modified wave winding, and it has sufficiently few poles to be a suitable pedagogic example without being tedious.

Figure 10.20 shows a layout of the first section of one phase of the winding. To begin connecting the various wave coils to form the first phase, the winder selects a slot that has the proper orientation relative to the rotor structure, such as the collector terminals. The phase winding starts at point S_1, the first coil side of the first coil passes through the bottom of slot 1, and the second side of this coil passes through the top of slot 16. The end of the first coil then connects to the beginning of the second coil, at point C_1. The first coil side of the second coil passes through the bottom of slot 31 and the second side of this coil passes through the top of slot 46. The end of the second coil terminates at point C_2, where it connects to the beginning of the third coil. Up to this point, the three coil throws have spanned 15 slots (i.e., 1 to 16, 16 to 31, and 31 to 46). The first coil side of the third coil must now pass through the bottom of slot 60, to span 14 instead of 15 slots, in order to have a retorgressive modified-wave winding for the first section. The four remaining progressions are completed around the rotor periphery in a homologous manner, in accordance with Fig. 10.20. This forms the first section of the phase winding, which consists of a series circuit from point S_1 to point F_1. Within this series circuit, coil sides alternately run from front to back, and from back to front and are under the influence of flux of alternate polarity. Thus the voltages induced in the coil sides will add, and a series path is provided for rotor current to flow, which can react with the air-gap flux to produce torque.

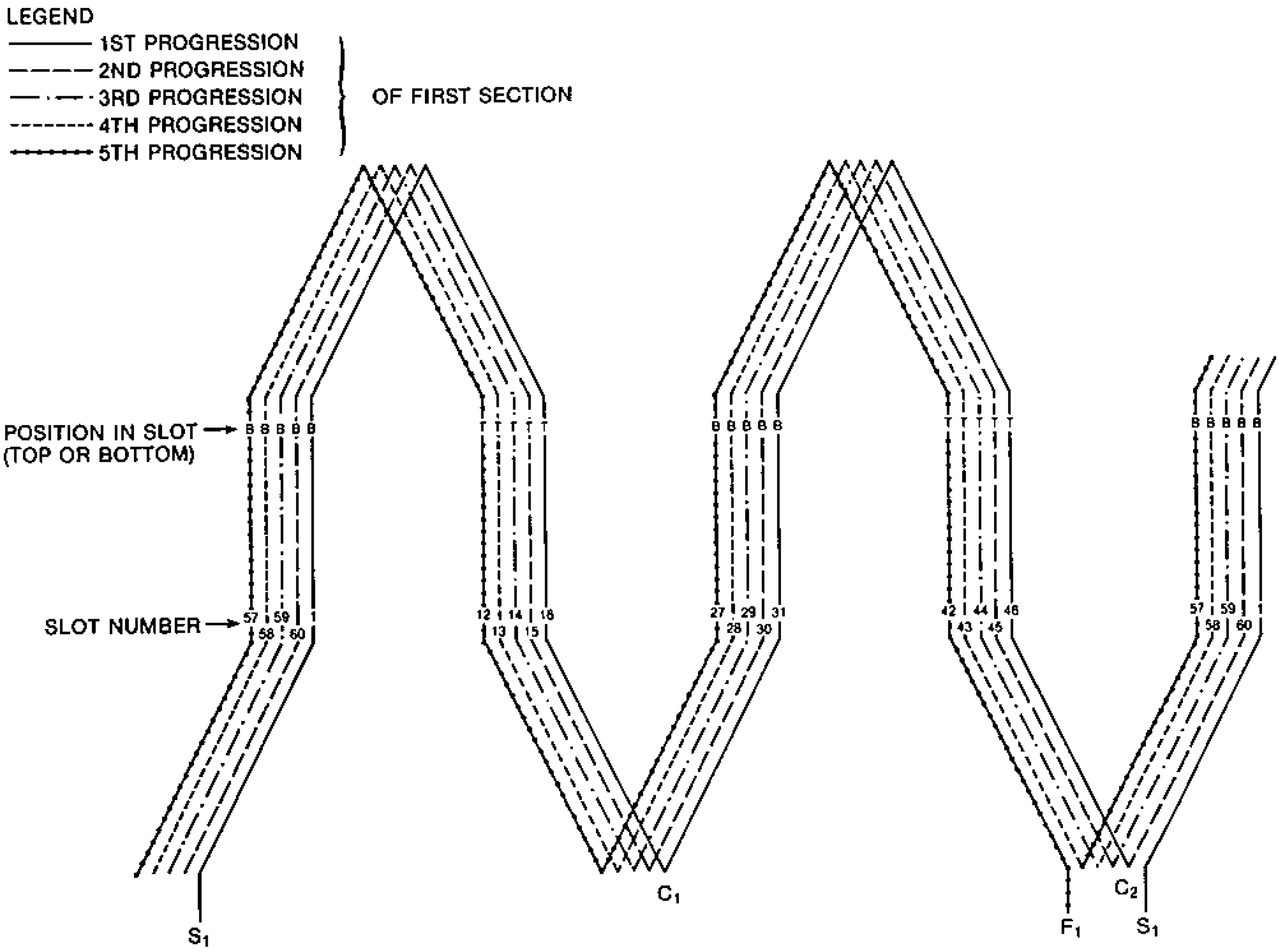
LEGEND
1ST PROGRESSION
2ND PROGRESSION
3RD PROGRESSION
4TH PROGRESSION
5TH PROGRESSION
OF FIRST SECTION
POSITION IN SLOT
(TOP OR BOTTOM)
SLOT NUMBER
B B B B B
T T T T T
57 58 59 60 1
12 13 14 15 16
27 28 29 30 31
42 43 44 45 46
S1
C1
F1
C2
S1

FIGURE 10.20 Layout of first section of one phase of a four-pole 60-slot modified-wave winding.

From the above and from an inspection of Fig. 10.20 it is apparent that the first section of coils for the phase just considered occupies only one-half of the cross-sectional space (i.e., the bottom half or the top half) of the slots concerned. Thus it would appear that in making up the connections for the second section of the same phase, the new section should "double back" and occupy the remaining half of the same slots. This would then give a second series circuit with the same phase relationship between voltages induced in the coil sides as for the first circuit or section. Accordingly, the two sections could then be connected in parallel or in series to form the phase winding. The second section of the phase winding is, in fact, made up as just discussed, as can be seen in the winding layout shown in Fig. 10.21.

The second section starts at point S_2, the first coil side of the first coil passes through the top of slot 27, and the second side of the same coil passes through the bottom of slot 12. The end of the first coil is then connected to the beginning of the second coil, at point C_3. The first coil side

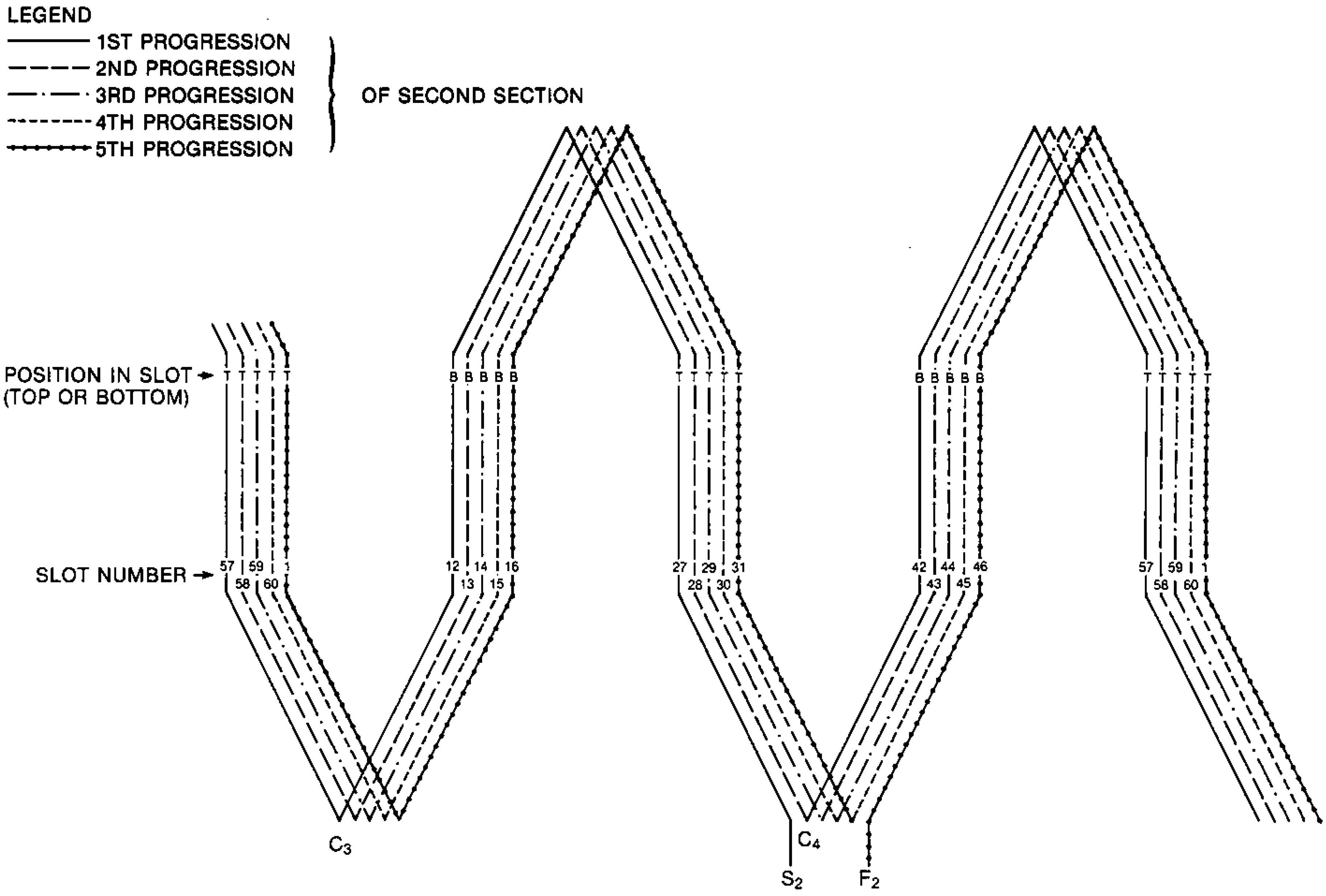
LEGEND
1ST PROGRESSION
2ND PROGRESSION
3RD PROGRESSION
4TH PROGRESSION
5TH PROGRESSION
OF SECOND SECTION
POSITION IN SLOT
(TOP OR BOTTOM)
SLOT NUMBER
T T T T T
57 58 59 60 1
B B B B B
12 13 14 15 16
T T T T T
27 28 29 30 31
B B B B B
42 43 44 45 46
T T T T T
57 58 59 60 1
C_3
C_4
S_2
F_2

FIGURE 10.21 Layout of second section of one phase of a four-pole 60-slot modified-wave winding.

of the second coil passes through the top of slot 57 and the second coil side of this coil passes through the bottom of slot 42. The second coil terminates at point C_4, where it connects to the third coil. Up to this point the three coil throws have spanned 15 slots (i.e., 27 to 12, 12 to 57, and 57 to 42). Now, however, the first coil side of the third coil must pass through the top of slot 28, to span 14 instead of 15 slots, in order to have a retrogressive modified-wave winding for this section. The four remaining progressions of the second section are completed around the rotor periphery in a similar manner, in accordance with Fig. 10.21, and these five progressions form the second section of the phase winding. The second section forms a series circuit that has been routed through the same slots as the series circuit that formed the first section. Thus, as stated earlier, the two sections can be connected in series or in parallel to produce the complete phase winding. In forming the phase winding, 20 slots, or one-third of the total rotor slots, have been used. The other two phase windings are formed in a similar manner, to give three individual phase windings, the magnetic axis of which are displaced $2\pi/3$ electrical radians, or 120 electrical degrees, apart. The three individual phases can be connected in wye or in delta, to form the complete three-phase winding for the rotor. Cables, or insulated copper straps, are used to connect the ends of the three-phase winding to three collector rings.

The choice of a wye or a delta connection is based on a design balance and on coordination with the external resistor and its associated control. A wye connection will reduce the current through the brushes and collector rings by $1/\sqrt{3}$ and will increase the maximum collector-ring voltage by $\sqrt{3}$ compared to a delta connection for the same power rating of the motor. The converse is, of course, true for a delta connection compared to a wye connection. As the collector ring current increases, the total cross-sectional area of brushes also increases. This, in effect, requires more brushes and more mechanical rigging to hold the brushes in place. Also, more brushes, in sliding contact with the collector rings, and more current flow through the brushes and collector rings, gives rise to more friction loss and more electrical loss in the collector and brush system.

On the other hand, a 73% greater maximum operating voltage in the rotor circuit caused by use of a wye connection could require using rotor-winding ground insulation and collector insulation of the next greater voltage class, with the resulting reduction in active copper space in the rotor slot and an increase in cost. Also, there is a reluctance on the part of some design engineers to use delta-connected stator or rotor windings because of the additional heating from ferromagnetically produced third-harmonic currents, which result in no torque at the shaft. Thus the choice between a wye or delta connection for the rotor winding is ultimately a design decision.

10.4.5 Wound-Rotor Distribution Factor and Pitch Factor

The distribution factor is determined in essentially the same manner for a modified-wave winding as for a lap winding. The number of progressions around the rotor periphery per section for each phase of the wave winding, corresponds to the number of coils per group of the lap winding. From eq. (9.125) the distribution factor of a winding is equal to

$$K_d = \frac{\sin(N_g \alpha/2)}{N_g \sin(\alpha/2)} \quad \text{numeric} \tag{10.215}$$

For the four-pole 60-slot rotor winding just considered,

$$N_g = \frac{N_2}{pq} = \frac{60}{(4)(3)} = 5 \quad \text{numeric} \tag{10.216}$$

and α, the electrical angle between slots, is equal to

$$\alpha = \frac{60}{N_g} = \frac{60}{5} = 12 \quad \text{electrical degrees} \tag{10.217}$$

Then, substituting eqs. (10.216) and (10.217) into eq. (10.215), we obtain

$$K_d = \frac{\sin[(5)(12)/2]}{5\sin(12/2)} = 0.957 \quad \text{numeric} \tag{10.218}$$

which is the same value as the distribution factor for a three-phase lap winding with five coils/group.

It is usually economical, and technically desirable, to use a coil pitch of less than unity for stator windings. However, this is not necessarily true for rotor windings. The stator winding produces the rotating magnetomotive force wave, which, in turn, produces the rotating air-gap flux wave. A stator coil pitch of 85% will result in a reduction of air-gap flux of less than 3%. For most designs, this represents a favorable economic trade-off between the stator winding cost and the magnetic core cost. Also, the space harmonics of the stator magnetomotive force wave can be controlled effectively by a judicious choice of the stator coil pitch. Thus there are important design reasons for using less than 100% pitch for the stator winding.

On the other hand, it is not usually economical or desirable, from a design standpoint, to use less than a full coil pitch for the rotor winding. The function of the rotor is to produce torque, from the interaction of rotor current and air-gap flux, in a limited space. A rotor-coil pitch of less than unity would tend to reduce the voltage induced in the rotor coil sides, which, in turn, would tend to cause less rotor current to flow, at a given slip. This would, of course, be counterproductive to the effective production of torque in the limited space near the periphery of the rotor. Also, the rotor contains all of the stator harmonics, in addition to the rotor incidental harmonics, which depend on the stator harmonics and which are discussed in Chapter 12. Thus control of most rotor harmonics depends on the control of stator harmonics. About the only exception to this is the control of slot harmonics by the use of appropriate skew, which is usually not used on wound-rotor motors. Thus there is small motivation for the design engineer to desire to reduce the coil throw to less than full, for a rotor winding.

As is apparent for the four-pole 60-slot example, after a complete progression around the periphery of the rotor, the next coil side is placed in a slot adjacent to the starting slot. This, of course, places a limitation on the choice of throw between the individual coil sides, in general, but there is some limited opportunity to use a reduced throw between coil sides if that should be desired. The throw between adjacent coil sides, as determined by the connection between coil sides on the front and on the rear of the winding, can be varied from full throw. However, the sum of the front and rear throws for a given coil, in terms of slots, must equal the number of slots past which the coil would progress if all coil throws were maximum. Thus, for the first progression of the example in Fig. 10.20, one coil side must be in slot 1, one coil side must be in slot 31, and the second progression must start in slot 60. This would give some limited opportunity for changing the position of such coil sides as that in slot 16. However, since there is usually no good technical reason for changing from the use of maximum pitch, it is normal to use maximum pitch.

It will be noted that in spanning the four poles in Fig. 10.20, the individual coil-side throws are $16 - 1 = 15$, $31 - 16 = 15$, $46 - 31 = 15$, and $60 - 46 = 14$, in terms of rotor slots. The number of slots per pole is equal to $N_2/p = 60/4 = 15$. Thus three of the throws are full and one throw is $14/15 = 0.933$ throw, for one complete progression around the rotor periphery. On the basis of a simple arithmetic average, the pitch factor for the progression would be equal to $[\sin(0.933)(90) + 3]/4 = 0.9986$. Since this number, as well as other corresponding numbers for modified-wave windings, is so close to 1.0, it is usual to consider that such a winding, connected for maximum pitch, has a value of K_p equal to 1.0.

10.4.6 Phase Voltage of the Wound-Rotor Winding

As discussed earlier, the rotating air-gap flux wave induces the voltages E_1 and E_2 in the stator and in the rotor phase windings. The induced rotor voltage E_2 is the driving voltage in the rotor circuit. If the collector rings of a wound-rotor motor are short circuited, or if the rotor phase circuit is otherwise closed through an external resistance, this voltage will force rotor phase current to flow. This current will, in turn, interact with the air-gap flux to produce motor torque.

In eqs. (4.34) and (4.35) it was shown that the voltages induced in the stator and rotor phase windings are related by the turns ratio, or

$$E_1 = aE_2 \quad \text{volts/phase} \tag{10.219}$$

This equation can be written as

$$E_2 = \frac{1}{a} E_1 = \frac{N_{st2}K_{p2}K_{d2}}{N_{st1}K_{p1}K_{d1}} E_1 \quad \text{volts/phase} \tag{10.220}$$

The quantity E_2 is an important quantity that is used frequently in the design and application of wound-rotor induction motors. Its value can be determined from the calculated value of E_1, using the relationship above, if that value is known. To determine E_1, assume that the rotor circuit is open circuited, that is, that the slip rings are not short circuited or connected to any external impedance, and that the rotor is blocked, or at zero speed. Under these conditions the stator current is equal to

$$I_{10} = \frac{V_1}{R_1 + j(X_1 + X_m)} \quad \text{amperes/phase} \tag{10.221}$$

Then E_1 is equal to the impedance drop caused by this current flowing through the magnetizing reactance, X_m, or

$$E_1 = jI_{10}X_m \quad \text{volts/phase} \tag{10.222}$$

Since E_1 and E_2 are equal, when referred to the stator side, E_2 is determined by referring the foregoing value to the rotor side, in accordance with eq. (10.220). Equation (10.220) gives E_2 in terms of volts/phase. For a delta-connected rotor winding, the volts between collector rings will equal the phase volts. For a wye-connected rotor winding, however, the phase value must be multiplied by $\sqrt{3}$ in order to equal the voltage across collector rings. A numerical example of the calculation above is given in Section 4.7.1 The value of E_2 can also be determined by testing at blocked rotor with the rotor circuit open.

10.4.7 Rotor Phase Current, Rotor Phase Resistance, and Rotor I^2R Loss

The total ampere-turns produced by the rotor winding is equal to the total counteracting ampere-turns produced by the stator winding, or

$$I_2 N_{st2} K_{p2} K_{d2} = I_{12} N_{st1} K_{p1} K_{d1} \quad \text{amperes-turns} \tag{10.223}$$

where I_{12} is the component of stator current designated as $-I_2$ in the vector diagram in Fig. 7.2, which counteracts the rotor current, where the subscripts 1 and 2 denote stator and rotor quantities, respectively, and where the other quantities are as defined previously. Solving eq. (10.223) for the rotor phase current yields

$$I_2 = \frac{N_{st1} K_{p1} K_{d1}}{N_{st2} K_{p1} K_{d1}} I_{12} = aI_{12} \quad \text{amperes/phase} \tag{10.224}$$

where a is, of course, the effective turns ratio for the machine. The rotor phase current I_2 can be determined, in magnitude and angle, by solving one of the several algorithms presented previously, such as the equivalent circuit. If the algorithm is solved with all quantities referred to the stator side, as is the custom, the magnitude of I_2 should then be transferred back to the rotor side by multiplying it by the effective turns ratio if the value of the actual amperes that flow in the rotor phase is desired. If only the approximate magnitude of I_2 is desired, it may be determined by calculating I_{12} as

$$I_{12} \cong \frac{746 \text{ hp} + \text{F\&W}}{\sqrt{3}\ V_1} \quad \text{amperes/phase} \tag{10.225}$$

and then substituting eq. (10.225) into eq. (10.224).

The resistance of the rotor phase winding is equal to

$$R_2 = \frac{\rho \ell_2}{A_2} \quad \text{ohms/phase} \tag{10.226}$$

where

ρ = resistivity of copper
ℓ_2 = effective length of the rotor phase winding
A_2 = effective cross-sectional area of the phase winding

Equation (10.226) may be written as

$$R_2 = \frac{2\rho N_{st2}\ell_{t2}}{(N_{c2})(\text{area of one conductor})(C_2)} \quad \text{ohms/phase} \tag{10.227}$$

where

N_{st2} = number of turns, in series, in the phase winding
ℓ_{t2} = length of one conductor or of one-half of one turn, of the rotor coil
N_{c2} = number of turns in the rotor coil, which is usually only one or two
C_2 = number of parallel circuits in the rotor phase winding

and where the "area of one conductor" is the cross-sectional area of one turn of the rotor coil. The I^2R loss in the rotor winding is then equal to

$$\text{rotor copper loss} = 3I_2^2R_2 \quad \text{watts} \tag{10.228}$$

10.4.8 Relationship Between Collector-Ring Voltage and Current

Writing Kirchhoff's voltage equation around the rotor circuit as

$$sE_2 = I_2(R_2 + jsX_2) \quad \text{volts/phase} \tag{10.229}$$

or

$$E_2 = I_2\left(\frac{R_2}{s} + jX_2\right) \quad \text{volts/phase} \tag{10.230}$$

then multiplying eq. (10.230) by I_2, we obtain

$$E_2I_2 = I_2^2\frac{R_2}{s} + jI_2^2X_2 \quad \text{volt-amperes/phase} \tag{10.231}$$

Equation (10.231) was written with E_2 and I_2 as quantities associated with the phase winding. If volt-amperes for the entire rotor is desired, the equation must be multiplied by 3, or

$$3E_2I_2 = 3I_2^2\frac{R_2}{s} + j3I_2^2X_2 \quad \text{volt-amperes} \tag{10.232}$$

This equation can be written in descriptive terms as

$$\text{total rotor VA} = \text{power transferred across air gap} + j(\text{total rotor VAR}) \quad \text{volt-amperes} \tag{10.233}$$

If the power factor of the rotor circuit was equal to unity, if there were no electrical losses in the rotor, and if the friction and windage were zero, eq. (10.232) could be written as

$$3E_2I_2 = 746 \text{ hp} \quad \text{watts} \tag{10.234}$$

However, the rotor circuit power factor is not quite equal to unity, and there are electrical losses in the rotor, including rotor copper losses, a component of core loss which occurs near the surface of the rotor, and the losses associated with the voltage drop between the brushes and the collector rings. Also, the rotor experiences a windage loss, from rotating in air, and a friction loss, from action of the bearings and the brushes. The total effect of these items, although variable from design to design, is reasonably constant as a small percentage of the power output across a range of power ratings. Thus it is reasonable to use a factor to cover the combined effect of the items. One such factor, frequently used for medium-power ratings, is 1.045. Then

$$3E_2I_2 = (746)(1.045)\text{hp} \quad \text{watts} \tag{10.235}$$

Also, if E_2 and I_2 are to be treated as values at the collector rings, the left-hand side of eq. (10.235) should be multiplied by $1/\sqrt{3}$; then

$$E_rI_r = \frac{(746)(1.045)}{\sqrt{3}} \text{ hp} = 450 \text{ hp} \quad \text{watts} \tag{10.236}$$

where E_r is the voltage between collector rings, at blocked-rotor conditions, with the rotor circuit open, and I_r is the current that flows through the collector rings at rated horsepower. The equation above shows a hyperbolic relationship between E_r and I_r for a given power output rating.

The exact value of E_r and I_r can both be calculated precisely by use of the equivalent circuit or by other means as soon as sufficient machine parameters have been determined. However, eq. (10.236) has at least two useful purposes. It provides the design engineer with a large number of corresponding pairs of rotor circuit characteristics, very early in the design process. This offers the engineer the opportunity, for example, to select the number of rotor turns in series N_{st2} about as soon as the physical dimensions of the rotor have been established. Also, it provides the control

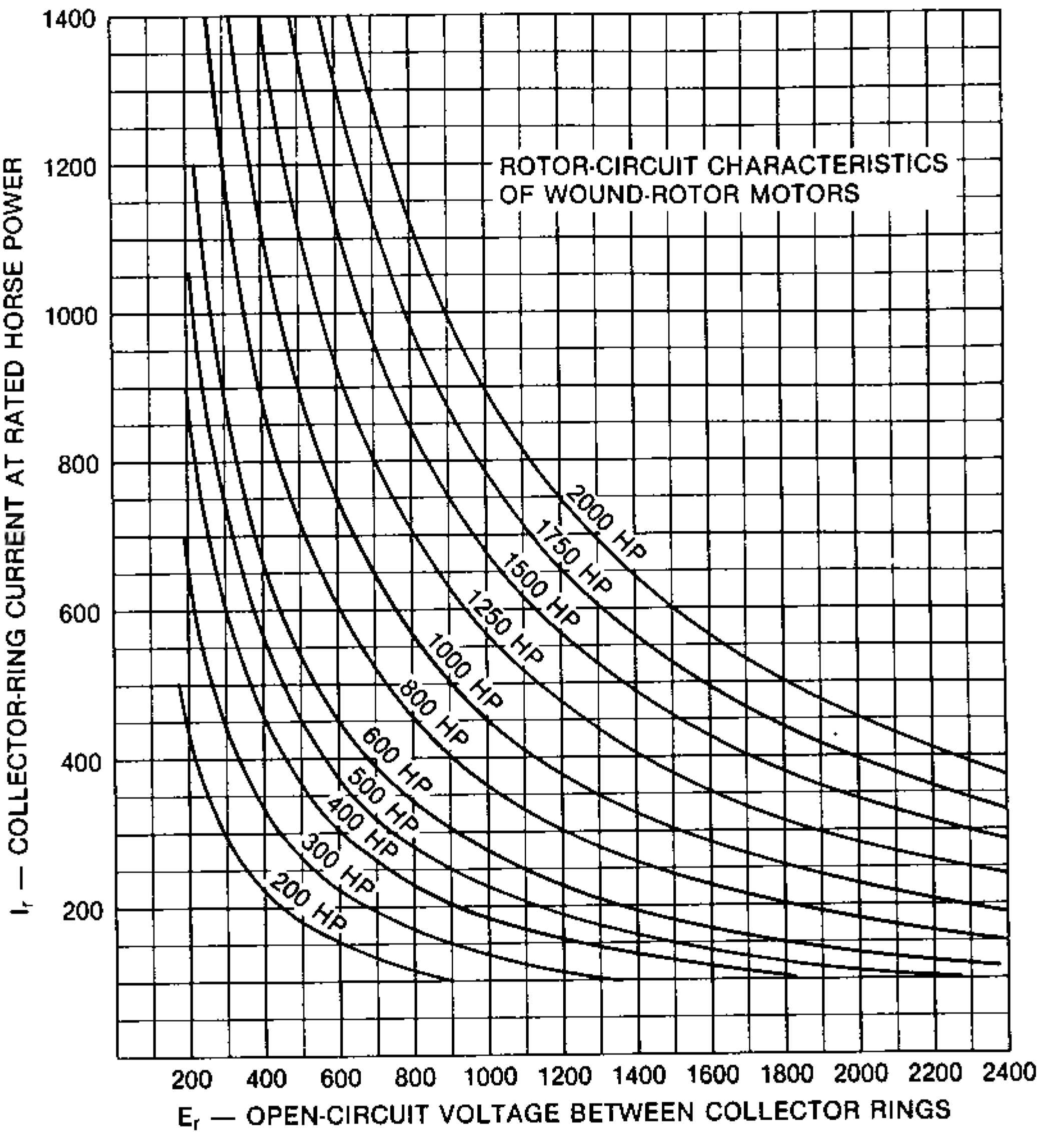

FIGURE 10.22 Rotor-circuit characteristics of wound-rotor induction motors.

engineer with realistic choices of E_r versus I_r early in the design process so that the control manufacturer and the motor manufacturer can coordinate on a timely basis—to the benefit of both. Figure 10.22 gives corresponding values of E_r and I_r for wound-rotor motors of medium power ratings, in accordance with eq. (10.236).

10.4.9 Collectors and Brushes

External connection to the internal wound-rotor circuit is accomplished by use of three rotating collector rings and three corresponding sets of stationary mating brushes. The ends of the three-phase winding (i.e., the outer ends of the wye or the corners of the delta) are connected to the three collector rings. Three sets of stationary brushes individually mate with the three collector rings, to provide static line-to-line connections, outside the machine, to a three-phase variable resistor. As discussed earlier, the capability to vary the resistive component of rotor impedance with an external resistor permits us to achieve several application goals, including the following:

1. Limiting the current and kVA demand on the local power system, while starting a large induction motor
2. Accelerating driven equipment with a very high value of rotational inertia to full speed without overheating the motor rotor
3. Causing the motor to develop maximum torque at any speed or, by stepping, at all speeds, during acceleration
4. Providing a high starting torque while retaining a low rotor I^2R loss at full-speed operation
5. Providing infinite speed control but at the expense of considerable loss in efficiency at lower speeds

Also, having the capability to make external connections to the rotor circuit of a wound-rotor motor permits that motor to be used, in combination with other machines, to accomplish additional design goals. These include frequency changing and speed control, with utilization of the accompanying slip loss. These topics will be discussed subsequently, when applications are considered.

The collector assembly is located on the connection end of the rotor and consists of three rings, a collector bushing, insulation between the rings and the bushing, and three insulated leads, one from each ring to the end of the collector. The collector rings used on wound-rotor motors are usually made of brass or bronze, although steel rings have been used. The ODs of the rings are turned to a smooth finish and then polished. The collector bushing consists of a steel cylinder the ID and OD of which are turned to the desired dimensions. The ID of the bushing has a close fit with the corresponding OD of the shaft fit and the two members may or may not be keyed together, depending on the bushing-to-shaft fit. Ground insulation is circumferentially placed over the bushing and the three collector rings are then located over the insulation. Installation of the rings is usually accomplished by heating the rings to increase their IDs sufficiently to permit them to be seated over the insulation, and then allowing them to cool, which provides a shrink fit with the collector body. Insulated conductor studs or straps are individually connected to each collector ring and then routed to the inboard side of the collector, under the inner rings, for connection to the winding. The electrical parts of the collector must be insulated from ground and the three individual rings must be adequately insulated from each other to withstand maximum line-to-line rotor voltage. For applications, for which reverse-sequence stator voltage is occasionally applied, such as for "plugging," the ring-to-ring insulation must be suitable for two times maximum line-to-line rotor voltage. Because the rings have a potential difference between them as well as to ground, accumulated carbon dust, oil, or moisture can cause collector-insulation failure. Adequacy of insulation is an important factor in the design of collectors and, accordingly, the subject of collectors is discussed further in Chapter 11.

The several brushes associated with one collector ring are distributed around a portion of the ring periphery and are held in place by the brush holders. The brush holders are usually made of brass or bronze and are, in effect, boxes into which the brushes fit, with a clearance such that the brushes are permitted to move radially but not in any other direction. The end of the box, next to the ring, is set to have a radial clearance of about 5 mm (3/16 in.) with the OD of the ring. Each brush is held against the ring by means of a spring on the outer end of each brush. The brush pressure will vary depending on the composition of the brush, and the recommended pressure should be obtained from the brush manufacturer. Typically, it is in the range 15 to 20 kP (2 to 3 psi). Brush leads or "pigtails," fastened to the individual carbon brushes by rivets, are connected in parallel to the brush terminal for each ring to form each of the three external connections of the rotor winding. The three sets of brushes, brush holders, springs, terminals, and so on, form one assembly, called the brush rigging.

The rate at which carbon brushes wear, as measured in units of, say, millimeters of radial brush reduction per 1000 hours of operation, is greatly affected by two environmental factors: dryness (i.e, lack of moisture) and temperature. Tests show that the rate of brush wear has essentially an exponential relationship with air dryness, in the range of very dry to moderately dry air, with increasing air dryness measured by decreasing dew point or by decreasing relative humidity. The relative humidity of the air in which the brushes operate should be equal to 30 to 35%, to prevent excessive brush wear. Tests also show that the rate of brush wear has essentially an exponential relationship with brush temperature. The total temperature of the brush (i.e., the ambient temperature in the region of the brush plus the temperature rise of the brush above ambient) should be kept well below 100°C. For most types of carbon brushes, a total temperature of not more than 70 to 80°C is compatible with a reasonable rate of brush wear. Brush wear rate is also increased by brush vibration and by various chemical contaminants in the cooling air.

10.4.10 Brush Friction Loss and Brush Electrical Loss

Offhand, it would not be expected that the surface of a polished collector ring, rubbing against a carbon brush, with a moderate pressure between them, would produce a significant amount of friction loss. The coefficient of friction between a collector ring and a brush varies from 0.07 to 0.32, depending on the brush used, and a coefficient of friction of 0.20 is not unusual.

This, together with the total cross-sectional area of brushes used with collector rings, can result in sufficient loss as to be significant.

The coefficient of friction between two sliding members is defined as

$$\mu = \frac{F}{N} \quad \text{numeric} \tag{10.237}$$

where

μ = coefficient of friction, dimensionless
F = retarding force along the plane of sliding, newtons
N = compressive force between the two members, newtons

For the configuration consisting of several brushes located around the periphery of three collector rings, the retarding force is equal to

$$F = \mu N = \mu P_b A_b N_b \quad \text{newtons} \tag{10.238}$$

where

P_b = brush pressure, pascals
A_b = cross-sectional area of one brush, meters^2
N_b = total number of brushes in contact with all rings, dimensionless

The work done, or the energy loss, due to the retarding force, is equal to the force, multiplied by the distance described by a point on the rotating collector, or

$$W_f = Fs = \mu P_b A_b N_b s \quad \text{newton-meters} \tag{10.239}$$

where

W_f = work done, newton-meters
s = distance traveled by a point on the collector, meters

The power loss is equal to the work done in unit time, or

$$P_f = \frac{W_f}{t} = \mu P_b A_b N_b 2\pi R_r \left(\frac{\text{rpm}}{60}\right) \quad \text{watts} \tag{10.240}$$

where R_r is the radial distance from the center of the shaft to the OD of the collector ring. Then the frictional power loss in the collector is

$$P_f = 0.105 \mu P_b A_b N_b R_r (\text{rpm}) \quad \text{watts} \tag{10.241}$$

The equation for P_f can be expressed in units of inches, pounds, and seconds by remembering that 1 watt is equal to 1 newton-meter per second, that 4.448 newtons of force equal 1 pound of force and that 1 meter equals 39.37 inches. Then

$$P_f = (0.105)\left(\frac{4.448}{39.37}\right)\mu P_b' A_b' N_b R_r' \text{ (rpm)}$$
$$= 0.012\mu P_b' A_b' N_b R_r' \text{ (rpm)} \quad \text{watts} \tag{10.242}$$

where

P_b' = brush pressure, pounds/inch^2
A_b' = cross-sectional area of one brush, inches^2
R_r' = radius of collector, inches

There is an additional loss associated with brushes and collector rings, called the electrical loss, which is caused by the contact voltage drop from the brush to the ring. It is equal to

$$P_e = N_b V_b I_b \quad \text{watts} \tag{10.243}$$

where V_b is the contact voltage drop between brush and collector in volts and I_b is the current through one brush in amperes.

The value of the coefficient of friction depends on the composition of the brush and on the condition of the collector-ring surface. As mentioned earlier, μ varies widely from one brush type to another, with a typical value being about 0.20. The brush pressure is originally determined by the motor manufacturer whose recommendations should generally be followed. Typical brush pressure is in the range 14 to 21 kP (2 to 3 psi). The value of the contact voltage drop is also a function of the composition of the brush and of the condition of the collector-ring surface. It varies from about 0.40 V to well over 1.0 V. If the customer needs the value, it should be obtained from the manufacturer.

A film over the collector-ring surface is normal and is essential to good brush and collector-ring operation over a long period. The film will automatically form on the contact surface of the collector after a period of operation if the surface of the ring is clean and is well polished at startup and if environmental conditions are reasonable. Certain environmental conditions in addition to atmospheric temperature and dryness, mentioned earlier, can affect brush and collector wear and operation. Sulfur dioxide or hydrogen sulfide contamination in the cooling air that passes over the collector will produce adverse results. Also, chlorine or gases from chlorine compounds can produce undesirable effects. All of the considerations noted above notwithstanding, if reasonable precautions are taken and if normal maintenance is conducted periodically, brushes and collector rings used on wound-rotor motors, can be expected to give excellent service.

10.4.11 Numerical Example of Calculating Brush Friction and Electrical Losses

An industrial plant has an eight-pole 2000-hp induction motor, which is one of the prime drive motors of the plant. The normal shaft load for this motor is about 80% of the motor's nameplate rating. To keep the kVA demand factor for the plant within economical limits during starting, the motor is a wound-rotor instead of a squirrel-cage type. The chief engineer is interested in determining the friction and the electrical losses produced by the brushes and collector. The ambient temperature, in the vicinity of the motor, is over 50°C and the engineer is evaluating whether an auxiliary stream of cooling air should be directed over the collector to reduce the temperature of the brushes and hence the rate of brush wear. As part of this evaluation, it is necessary to know the total watts of loss produced by the brushes and collector.

The chief engineer has determined the following information from the motor manufacturer or from local sources:

$\mu = 0.14$ numeric
$A_b' = 1.0$ in.^{2}
$P_b' = 2.2$ psi
$N_b = 36$
$R_r' = 5$ in.
$V_b = 0.47$ V
$E_r = 1250$ open-circuit voltage, between rings, at standstill

The engineer is aware of the relationships given in eqs. (10.236), (10.242), and (10.243), and the calculations proceed as follows. The normal shaft power of the motor is

$$\text{hp} = (0.80)(2000) = 1600 \quad \text{horsepower} \tag{10.244}$$

The current through each collector ring I_r can then be calculated from eq. (10.236) as

$$E_r I_r = 450\ \text{hp} \quad \text{watts} \tag{10.245}$$

and

$$I_r = \frac{450\ \text{hp}}{E_r} = \frac{(450)(1600)}{1250} = 576 \quad \text{amperes/ring} \tag{10.246}$$

The power loss due to brush friction can be calculated from eq. (10.242) as

$$P_f = 0.012\mu P'_b A'_b N_b R'_r \text{ (rpm)}$$

$$= (0.012)(0.14)(2.2)(36)(5)(900) = 599 \quad \text{watts} \qquad (10.247)$$

and the power loss due to contact voltage drop can be calculated from eq. (10.243) as

$$P_e = N_b V_b I_b \quad \text{watts} \qquad (10.248)$$

$$= (36)(0.47)\left(\frac{576}{12}\right) = 812 \quad \text{watts} \qquad (10.249)$$

Then the total power loss produced by the brushes and collector is

$$P_t = P_f + P_e = 599 + 812 = 1411 \quad \text{watts} \qquad (10.250)$$

10.4.12 Banding of Rotor End Turns

A significant portion of the total rotor winding is, necessarily, located outside the slots of the rotor core and must therefore be braced against centrifugal force. Most of the weight of the rotor end turns is due to copper, which has a density greater than that of steel. Also, the circumferential bundle of end turns is located at essentially the maximum radius of the rotor. Thus from eq. (10.5) or (10.6) it is apparent that the centrifugal force exerted on the rotor end turns increases with their mass and density and with their mean radius. As the size of the machine increases, centrifugal force on the end turns can become very great, and thus it is necessary to retain them against centrifugal force.

Retaining is accomplished, in practice, by circumferential banding. An appropriate high-strength banding material such as monofilament glass tape is circumferentially wrapped around the end turns under tension. The banding material is saturated with an insulating resin, such as an epoxy or a polyester formulation, prior to banding. The resin is then cured, after banding, by applying heat, at a specified temperature and for a specified time, to produce an effective retaining band. Before the banding is applied, an insulating strip with good resistance to "cut through" is wrapped around the periphery of the end turns, to serve as a base to receive the banding tape. It is usual to support the underside or the ID of the coil extensions for some range of ratings, or where the flexibility of the coil extensions is such that they would experience too great an amount of inward deflection when applying the banding under tension. Figure 10.23 shows a large wound-rotor assembly with banded end turns.

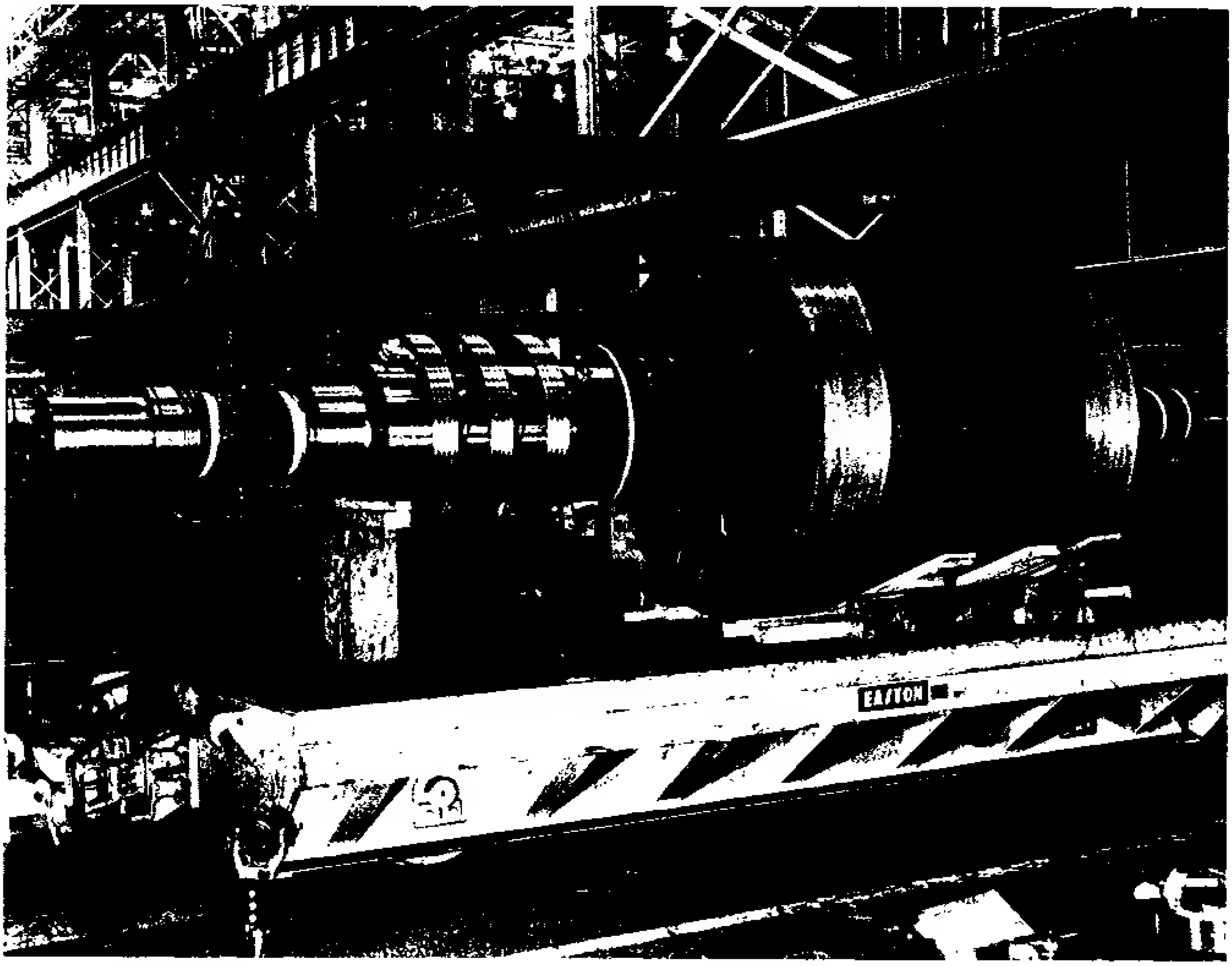

FIGURE 10.23 Large wound rotor, showing banding of end turns.

After a machine has been in service for some time, it may be required to repair a rotor coil that has been damaged mechanically or in some other way. If it is necessary to remove the banding to service the coil, which it probably will be, considerable caution should be observed and a conservative program should be followed. The combined effect of continuous centrifugal force, continuous operating temperature of the winding and the proximity of the aforementioned epoxy or polyester resin, as well as of other insulating varnishes, will tend to cause adhesion between the banding and the coil extensions. Thus, when the banding is removed, cracks and tears may be produced in the ground insulation of the coil extension. Such defects can vary from those which are not perceptible, to larger ones, which are apparent. In any case, it can be reasonably assumed that a visual check is not adequate. Also, an overpotential test for, say, 1 minute, or even 5 minutes, will not necessarily reveal all defects and certainly does not duplicate operating service. It is for such reasons that a conservative program should be followed if the banding should be removed on a wound rotor that has been in operation. Because of the inability to make certain that all of the possible defects have been noticed and of the inability to reasonably duplicate long-range operating conditions, some organizations recommend a policy of replacing the winding before rebanding if the banding is removed. Removing the old ground insulation from, and reinsulating, the original copper is tantamount to new coils in this case. Although such a policy may appear stringent, it is probably the most economical in the long run for an important drive motor.

11

Dielectrics and Insulation

11.1 Function, Scope, and Importance of Insulation 358

11.2 Relative Aspect of Insulators and Conductors 360

11.3 Methodology Used in Understanding and in Applying Insulation 361

11.4 Electrostatic Background of Dielectrics 362

11.5 Capacitors and Capacitance 365

11.6 Physical Behavior of Dielectric Materials 371

- 11.6.1 Polarization 372
- 11.6.2 Absorption 376
- 11.6.3 Dielectric Conduction 379
- 11.6.4 Dielectric Loss 380
- 11.6.5 Dielectric Breakdown 383

11.7 Factors Affecting Insulation Strength 388

- 11.7.1 Temperature 388
- 11.7.2 Time 389
- 11.7.3 Frequency 389
- 11.7.4 Additional Voltage Characteristics 390
- 11.7.5 Material Thickness 391
- 11.7.6 Mechanical Factors 393
- 11.7.7 Contaminants 394

11.8 Corona 396

11.9 Capacitance to Ground 398

11.10 Charging Current and Charging Volt-Amperes for High-Potential Testing 401

11.11 Numerical Example of Calculation of Phase-Winding Capacitance to Ground, Charging Current, and Charging Volt-Amperes 402

11.12 Winding Surges 405

11.13 Temperature Classes of Insulation 419

11.14 Insulation Resistance Testing 420

11.15 Creepage, Tracking, and Arc Resistance 424

11.16 Application of Insulation to Windings 424

11.1 FUNCTION, SCOPE, AND IMPORTANCE OF INSULATION

The function of a motor is to convert electrical power, received from the stator bus, to mechanical power, delivered at the motor shaft. To accomplish this, as discussed previously, magnetic flux must flow in the magnetic circuit, consisting of the stator core, rotor core, and air gap, and current must flow in the stator winding and in the rotor winding. Stator current is produced by the bus voltage, which is applied across the stator phase windings, and rotor current is produced by the induced voltage, which appears across the rotor phase windings. The primary purpose of stator insulation, then, is to withstand phase-to-phase and phase-to-ground voltage and thus to channel the phase currents into the desired paths. Insulation serves a similar function, of course, in phase-wound rotors, the phase leads of which must be brought outside the motor for external connection to stationary devices. Insulation is also required to withstand voltages associated with the following machine subassemblies:

1. Collectors
2. Brush rigging
3. Winding connections
4. Winding leads
5. Ancillary equipment, such as space heaters, temperature probes, and so on
6. Stator cores and, in some cases, rotor cores
7. Bearings

The need for insulation is apparent for the first five items above, but such need may not be apparent for the last two items. Accordingly, that need will now be given in summary form. As will be discussed subsequently, the stator and rotor cores are constructed by stacking together steel punchings, whose individual thicknesses can vary from 0.35 mm (0.014 in.)

to 0.65 mm (0.026 in.), to obtain the desired core length. The alternating flux tends to induce a voltage, in an axial direction, in the stator and rotor cores, just as it does in the stator and rotor windings. Again, as will be discussed subsequently, core loss is a function of the individual punching thickness and of the frequency of flux change. Then, to keep stator core loss within acceptable limits, it is necessary for the individual punchings to be insulated from each other by use of an insulating layer, such as enamel or oxide coating. Even though the total insulation thickness between laminations is only of the order of 0.013 mm (0.0005 in.), it can account for 3% or more of the solid length of the stator core. Since the normal rate of flux change in the rotor core is typically 1 Hz or less for a squirrel-cage induction motor, it is not necessary for insulation to be applied to individual rotor punchings, except in special cases. However, wound-rotor induction motors can operate for prolonged periods at any subsynchronous speed, with a corresponding increase in the rate of flux change in the rotor core. Accordingly, the individual rotor punchings should be insulated for all wound-rotor motors, and such is normal practice.

Current flow through bearings due to spurious voltages has several causes. One significant cause that is frequently encountered is magnetic dissymmetry due to the use of segmented stator punchings. For machines of intermediate and larger power rating, the individual punchings are produced as segments and several such segments are required to form one circle of punchings. This is done to reduce the scrap resulting from the punch-press operation and thus to reduce the cost of producing the punchings. Such a practice, however, results in several joints around the periphery of the stator core, at the locations at which the various segments join each other to form the circle. Depending on the ratio of poles to joints, as will be discussed later, this practice can result in a dissymmetry in magnetic reluctance along the two half-circles of the core, at some instants of time, as the stator magnetomotive force wave rotates around the core. If the impressed magnetomotive force is balanced, it will tend to sum to zero, around the circle. The net result of unbalanced reluctance and balanced, impressed magnetomotive force around the circle is a residual magnetomotive force, usually of low magnitude, which varies with time. This varying residual magnetomotive force in the stator core can act as the exciting primary of a crude transformer, the secondary of which consists of the shaft, bearings, bearing brackets, and frame. Thus a voltage can be induced in this elementary secondary, which can cause a current to flow. For small to medium-sized power ratings, the impedance to this current flow is reasonably great, relative to the induced voltage, with an insignificant amount of resulting current flow. However, for larger machines, for certain combinations of stator-punching joints to poles, it is necessary to apply an insulating barrier between the bearing and the bearing seat, sufficient to withstand the voltage encountered and thus to interrupt current flow through the bearing assembly. If the current flow is not interrupted, in such cases, bearing damage can occur, which will probably result in bearing failure.

From all of the above, it is apparent that insulation plays a significant role in several different motor subassemblies, all of which are essential to proper operation of the motor. However, of the several previously listed subassemblies that require insulation, the design and application of a suitable insulation system for the stator winding and for the wound-rotor winding require the greatest amount of engineering and laboratory work and have the greatest effect on the service record of the machine. This is because the stator and rotor windings are prime components of the machine and because the insulation associated with them must withstand severe duty on a continuous basis. For example, the insulation between the copper conductor and the steel slot of the stator must continuously withstand a voltage of from a few hundred volts for the smallest machines to well over 10,000 V for the largest machines. In addition, surges, which can result from such causes as lightning and switching, occasionally travel into the stator winding and produce short-time voltages with crest values of from a few times to many times the normal voltage across the insulation. In addition to withstanding both normal and abnormal voltages, stator and wound-rotor insulation must resist electromagnetic forces, conduct the heat energy resulting from winding I^2Rt losses, and cope with a generally unfavorable environment which can, and occasionally does, contain conducting contaminants, acids, caustics, moisture, and high ambient temperature.

To underscore the above statistically, winding insulation failure is the greatest single cause of motor outages throughout the United States and probably throughout the world. The specific causes of failure span a wide range, including initial defects in material and workmanship, use of motors for applications for which their particular insulation systems were not designed or intended, abuse of motors at the site, surges, excess heating, improper maintenance, inadvertent mechanical damage, and so on. Nevertheless, an up-to-date insulation system for a motor, which is properly applied and properly maintained and which has adequate protection from voltage surges, can be expected to provide 20 or more years of service on the average.

11.2 RELATIVE ASPECT OF INSULATORS AND CONDUCTORS

The ability of a material to insulate is a relative term, since an insulator will conduct, to some small extent, and since any given conductor is not a perfect one, even though perfection in conduction has been approached in cryogenic experiments. The ability of an element or compound to conduct, or conversely, to insulate, is ultimately based on the fact that all matter is structured from electrical particles and that for some materials, electrons are held in greater restraint than for other materials. If an electric field is impressed across a given material, that material is considered to be a conductor or an insulator depending on whether a relatively great number, or relatively few, electrons are displaced, as measured by the flow of electric charge per unit of time or by current. Thus the ratio of applied potential to resulting current, or resistance, is one important measure of an insulator.

The transition from a good conductor to a good insulator spans many orders of magnitude, such that the definition of a conductor or of an insulator is expressed in terms of relative magnitudes. Within the family of metals, at room temperature, mercury has a resistivity of $96 \times 10^{-8}\ \Omega \cdot \mathrm{m}$, whereas silver has a resistivity of $1.59 \times 10^{-8}\ \Omega \cdot \mathrm{m}$. Thus the ratio of resistivity of these two conductors is equal to 0.60×10^2, a value that approaches two orders of magnitude. Hard rubber, a material used in laboratories to isolate and to hold electric charges, has a resistivity of about $1 \times 10^{16}\ \Omega \cdot \mathrm{m}$. Molded mica, an insulating material that is frequently used in rotating machine windings, has a resistivity of about $1 \times 10^{13}\ \Omega \cdot \mathrm{m}$. The ratio of resistivity of these two insulators is equal to 10^3, or three orders of magnitude. On the other hand, the ratio of resistivity of hard rubber, a highly insulative material, to silver, a highly conductive material, is equal to 10^{24}. Because of the foregoing considerations, materials are classified into the three classes—conductors, semiconductors, and insulators—based on the resistivity they exhibit. For any such classification, the boundaries between classes will be arbitrary to some extent. One classification is as follows:

Class	Resistivity ($\Omega \cdot \mathrm{m}$)
Conductor	Less than 10^{-5}
Semiconductor	Between 10^{-5} and 10^{8}
Insulator	Greater than 10^{8}

11.3 METHODOLOGY USED IN UNDERSTANDING AND IN APPLYING INSULATION

One of the earliest contributions to the accumulated knowledge of insulation was made by Siemens in 1864, when he determined that an alternating voltage when applied to a capacitor resulted in a loss in the dielectric of the capacitor. Since then, various scientists and engineers, including Maxwell, Hopkinson, Pellat, von Schweidler, Wagner, Whitehead, Miner, and others, have contributed to the present state of theoretical knowledge of insulation and dielectrics.

In parallel with this, many engineers, chemists, and other technical people have conducted an enormous amount of test work to determine the effect of voltage, time, electrode shape, temperature, humidity, contaminants, and so on, on the voltage-breakdown strength and on the longtime endurance of various insulations. Such test work has had at least two categories of benefit to the industrial art. The first category of benefits is that the insulation that is used on present-day motor windings has become increasingly more predictable and reliable. The second category of benefits is that techniques and procedures for testing and evaluating insulation have greatly improved. Some of the improvements in test procedures have been incorporated into standards accepted throughout the country, such that test results can now be presented and compared, on a meaningful basis, across a broad technical community.

The present approach, in general, is to benefit from the accumulated knowledge of the past and to combine the theoretical approach and the experimental approach. Thus theoretical expectations can be correlated with test results and test results can be evaluated against a theoretical background. When any promising, new insulation component or system becomes a candidate to replace an existing one, it can be subjected to a series of credible acceptance tests prior to being put into service and thus greatly enhance reliability.

11.4 ELECTROSTATIC BACKGROUND OF DIELECTRICS

Since insulation is used to withstand voltage and since a voltage, or a potential difference, implies the presence of an electric field, it is apparent that insulation must function in the presence of an electric field. Thus it is in order to summarize some of the pertinent physical relationships that exist in electric fields which are fundamental to dielectric phenomenon.

Quantitative knowledge of electric fields essentially started with the epochal experiments conducted by Coulomb in 1784 and 1785. The conclusions from his experiments are summarized in the well-known physical law that bears his name. If two charges q_1 and q_2 of the same polarity are separated by a distance of d meters, a repulsive force of F newtons will be exerted on each charge, and that force is equal to

$$F = \frac{q_1 q_2}{4\pi\epsilon d^2} \quad \text{newtons} \tag{11.1}$$

where ϵ is the permittivity of the medium between the two charges. The permittivity of free space ϵ_0 in the MKS system of units, is equal to

$$\epsilon_0 = \frac{1}{36\pi} \times 10^{-9} \quad \text{farads/meter} \tag{11.2}$$

It is interesting to note in passing that the permittivity and permeability of free space have the following relationship to the speed of wave propagation of an electromagnetic field in free space:

$$v = \frac{1}{\sqrt{\mu_0 \epsilon_0}} = \frac{1}{\sqrt{(4\pi \times 10^{-7})[1/(36\pi) \times 10^{-9}]}} = 3 \times 10^8 \text{ meters/second} \qquad (11.3)$$

Equation (11.1) can be written as

$$F = \frac{q_1 q_2}{4\pi K \epsilon_0 d^2} \text{ newtons} \qquad (11.4)$$

where K is the ratio of the permittivity of a given medium to that of free space, or

$$K = \frac{\epsilon}{\epsilon_0} \text{ numeric} \qquad (11.5)$$

and is called the dielectric constant of the dielectric medium.

The electric field intensity or the field strength can be determined from eq. (11.1). Let q_1 equal a unit charge and let a second charge $q = q_2$ be placed at a distance x meters from the unit charge. Then the mechanical force exerted on the unit charge in this electric field is

$$E = \frac{q}{4\pi \epsilon x^2} \text{ newtons} \qquad (11.6)$$

For the present E will be regarded as a mechanical force vector, exerted on a unit charge located in an electric field. Subsequently, however, it will become apparent that it is also the gradient of that electric field and is a measure of the field strength.

Since a charge in an electric field experiences a force, it would appear that such a field has the capability to do work on the charge. The ability of a field to do work is considered to be the field's potential and, in this case, the electric field's potential. Assume that a unit charge is, somehow, located at an infinite distance from a second charge q. Since the unit charge is at an infinite distance from charge q, there will be no force of repulsion between them. However, let the unit charge be moved toward point p, which is x meters from charge q. The work done on the unit charge and the energy stored in the unit charge due to the electric field is then

$$V = -\int_{\infty}^{x} E \, dx \text{ joules/coulomb} \qquad (11.7)$$

or, from eq. (11.6),

$$V = -\int_{\infty}^{x} \frac{q}{4\pi\epsilon x^2}\, dx = \frac{q}{4\pi\epsilon x} \quad \text{joules/coulomb} \tag{11.8}$$

However, units of joules/coulomb correspond to units of volts in the MKS unit system, so that eqs. (11.7) and (11.8) can also be expressed in the more familiar units of volts. Thus the electric potential, or the voltage at point p in the field, is equal to

$$V = \frac{q}{4\pi\epsilon x} \quad \text{volts} \tag{11.9}$$

If eq. (11.7) is differentiated with respect to distance x, the derivative is equal to eq. (11.6), or

$$\frac{dV}{dx} = -\frac{d}{dx}\left(\int_{\infty}^{x} E\, dx\right) = -E \quad \text{volts/meter} \tag{11.10}$$

Thus, E in eqs. (11.6) and (11.10), is the gradient, expressed in volts/meter, of the potential field V expressed in volts. The concept of gradient is used in insulation work to indicate the degree to which a piece of insulation is being stressed in an electric field (i.e., the voltage gradient across it) in such units as volts/mil or in volts/millimeter.

In the rationalized MKS system of units, the quantity of electric flux ψ that emanates from a charge of q coulombs is

$$\psi = q \quad \text{coulombs} \tag{11.11}$$

The electric flux density D at a distance of x meters from the charge is

$$D = \frac{\psi}{A} = \frac{q}{A} = \frac{q}{4\pi x^2} \quad \text{coulombs/meter}^2 \tag{11.12}$$

Solving for q in eqs. (11.6) and (11.12), equating the two resulting expressions, and solving for D yields

$$D = \epsilon E \quad \text{coulombs/meter}^2 \tag{11.13}$$

which gives the value of electric flux density D in terms of electric field strength E and in terms of the permittivity ϵ of the material in which the field is acting. Equation (11.13) can also be written in terms of the dielectric constant K of the material and the permittivity of free space ϵ_0, as

$$D = K\epsilon_0 E \quad \text{coulombs/meter}^2 \tag{11.14}$$

Gauss's theorem applied to a region in an electric field states that the flux leaving that region is equal to the enclosed charge. To show this, assume that a charge q is located at some point p and that at a distance of a meters from p, the electric flux density is D coulombs/meter^2. Then the total electric flux is

$$\psi = \int_s D\,ds \quad \text{coulombs} \tag{11.15}$$

Substituting eq. (11.12) into eq. (11.15) gives us

$$\psi = \int_s \frac{q}{4\pi a^2}\,ds \quad \text{coulombs} \tag{11.16}$$

However, the magnitude of the charge q and the distance a are assumed to be constant, so that eq. (11.16) may be written as

$$\psi = \frac{q}{4\pi a^2}\int_s ds \quad \text{coulombs} \tag{11.17}$$

But the surface integral is equal to $4\pi a^2$ when evaluated at the distance a from the charge q. Then

$$\psi = \frac{q}{4\pi a^2}\,4\pi a^2 = q \quad \text{coulombs} \tag{11.18}$$

which, not surprisingly, is consistent with the amount of flux emanating from a charge, as required by the rationalized MKS system of units.

11.5 CAPACITORS AND CAPACITANCE

As stated earlier, the primary function of motor insulation is to withstand voltage. Thus, for the application of ground insulation to stator coils, for example, the insulation serves as a voltage barrier that separates two metallic surfaces formed by the copper conductor and the steel slot. This is equivalent to an extended capacitor, with the ground insulation serving as the dielectric medium of that capacitor. Accordingly, the concept of capacitance is fundamental to dielectric behavior and it is appropriate to summarize the performance and characteristics of capacitors and capacitance.

Capacitance is the capability of a capacitor to hold an electric charge. The ratio of the charge q on the plates of the capacitor, to the voltage V that produced it is the capacitance C of the capacitor. This definition results directly in the well-known equation

$$C = \frac{q}{V} \quad \text{farads} \tag{11.19}$$

The capacitance of a capacitor, or condenser, depends on its geometry and on the dielectric constant K of the dielectric material between its plates. The capacitance for two important geometric configurations (i.e., parallel plates and concentric plates) will now be determined.

A parallel-plate capacitor is shown in Fig. 11.1a. Two parallel plates, each with an area of A meters^2, are separated by a distance of d meters. A homogeneous insulating material with a dielectric constant of K is located between the two plates. When a potential difference of V volts is impressed across the plates, a charge of q coulombs appears on each plate. From Gauss's theorem, eq. (11.18), the electric flux leaving one plate and entering the other, is equal to the charge, or

$$\psi = q \quad \text{coulombs} \tag{11.20}$$

The electric flux density in the homogeneous insulating material between the two plates, is

$$D = \frac{\psi}{A} = \frac{q}{A} \quad \text{coulombs/meter}^2 \tag{11.21}$$

From eq. (11.13),

$$D = \epsilon E \quad \text{coulombs/meter}^2 \tag{11.22}$$

Substituting eq. (11.22) into eq. (11.21) and solving for the electric field strength E, we have

$$E = \frac{q}{\epsilon A} \quad \text{volts/meter} \tag{11.23}$$

From eq. (11.10),

$$V = -\int E \, dx \quad \text{volts} \tag{11.24}$$

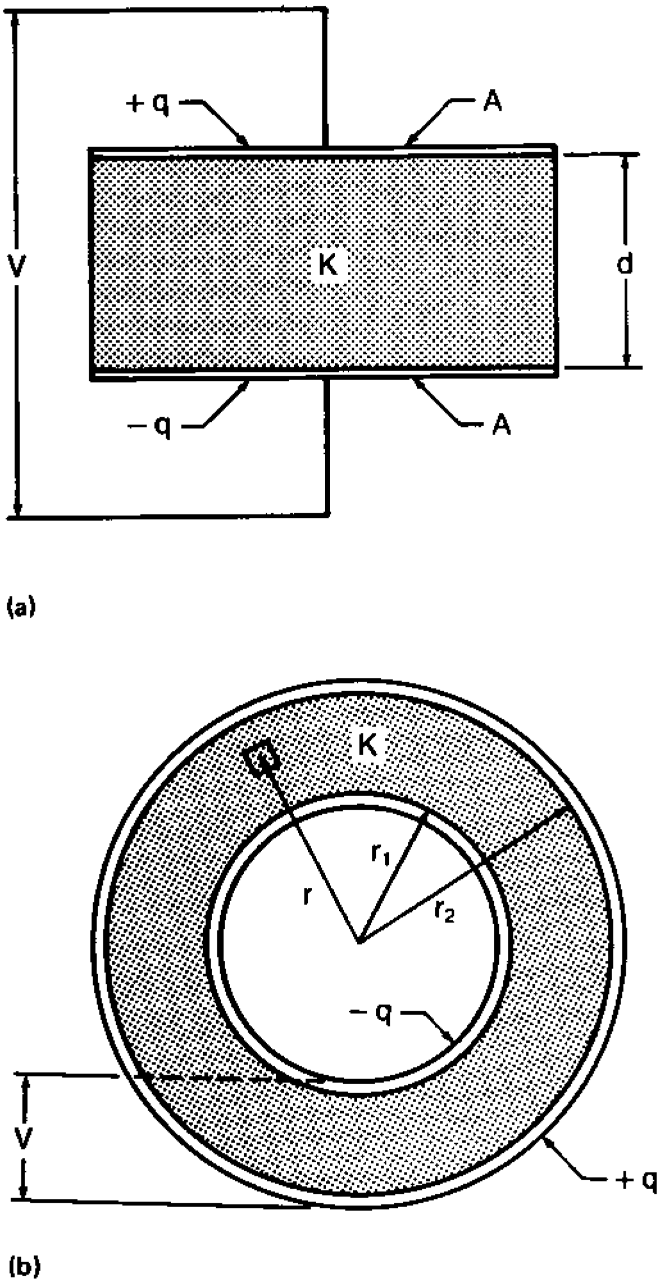

FIGURE 11.1 Definitions of quantities used for deriving equations for the capacitance of two geometric configurations: (a) parallel-plate capacitor; (b) concentric-plate capacitor.

Substituting eq. (11.23) into eq. (11.24) and performing the integration gives us

$$V = -\int_0^d \frac{q\,dx}{\epsilon A} = \frac{qd}{\epsilon A} = \frac{qd}{k\epsilon_0 A} \quad \text{volts} \tag{11.25}$$

From eq. (11.19) the capacitance C of a capacitor is defined as

$$C = \frac{q}{V} \quad \text{farads} \tag{11.26}$$

Then, substituting eq. (11.25) into eq. (11.26) yields

$$C = \frac{K\epsilon_0 A}{d} \quad \text{farads} \tag{11.27}$$

Since $\epsilon_0 = 1/(36\pi) \times 10^{-9}$ F/m, eq. (11.27) can be written as

$$C = \frac{KA \times 10^{-9}}{36\pi d} \quad \text{farads} \tag{11.28}$$

which is the equation for the capacitance of a parallel-plate capacitor, with a homogeneous dielectric medium between plates such as that shown in Fig. 11.1a.

A concentric-plate capacitor is shown in Fig. 11.1b. The inner and the outer plates of this capacitor are r_1 and r_2 meters, respectively, from the center, and the annular space between the two plates is filled with a homogeneous dielectric material with a permittivity of ϵ. The length of the capacitor is L meters. Again, the electric flux ψ, flowing from one plate to the other, is equal to q coulombs, so that the flux density is equal to

$$D = \frac{q}{A} \quad \text{coulombs/meter}^2 \tag{11.29}$$

and the electric field strength is equal to

$$E = \frac{q}{\epsilon A} = \frac{q}{\epsilon 2\pi r L} \quad \text{volts/meter} \tag{11.30}$$

where r is the radius to a point in the dielectric medium located r meters from the center. Again, from eq. (11.10),

$$V = -\int E\,dx = -\int E\,dr \quad \text{volts} \tag{11.31}$$

Substituting eq. (11.30) into eq. (11.31) and performing the integration gives us

$$V = -\int_{r_1}^{r_2} \frac{q\,dr}{\epsilon 2\pi r L} = \frac{q}{2\pi\epsilon L} \ln \frac{r_2}{r_1} \quad \text{volts} \tag{11.32}$$

Substituting eq. (11.32) into eq. (11.19) to determine the capacitance, we obtain

$$C = \frac{q}{V} = \frac{2\pi\epsilon L}{\ln(r_2/r_1)} \quad \text{farads} \tag{11.33}$$

Since $\epsilon = K\epsilon_0$,

$$C = \frac{2\pi KL \times 10^{-9}}{36\pi \ln(r_2/r_1)} = \frac{KL \times 10^{-9}}{18 \ln(r_2/r_1)} \tag{11.34}$$

which is the equation for the capacitance of a concentric-plate capacitor with a homogeneous dielectric material between plates, such as that shown in Fig. 11.1b. The energy stored in an electric field associated with a charged capacitor is evident when a charged capacitor is short circuited. Consider some instant of time during the period when a capacitor is being charged. At that instant, let the charge on the plates of the capacitor be q coulombs and let the resulting difference in potential between the plates be v volts. From eq. (11.19), v is equal to

$$v = \frac{q}{C} \quad \text{volts} \tag{11.35}$$

This difference in potential, which is actually potential energy per unit charge, multiplied by the differential charge dq, is equal to the corresponding increase in differential energy dj that the capacitor receives from the addition of charge dq. Summing all such differential charges, from 0 to the final charge Q, gives the final value of energy stored in the electric field of the charged capacitor, or

$$J = \int_0^Q \frac{q}{C}\,dq = \frac{1}{2}\frac{Q^2}{C} = \frac{1}{2} CV^2 \quad \text{joules} \tag{11.36}$$

As might be expected, this relationship has a symmetrical correspondence to the relationship which gives the energy stored in a magnetic field associated with an inductance L. In eq. (9.170) it was shown that the energy stored in a magnetic field is

$$J = \frac{1}{2} LI^2 \quad \text{joules} \tag{11.37}$$

where I is the final value of the current that sustains the magnetic field.

From eqs. (11.28) and (11.34) it is apparent that the capacitance C of a capacitor varies directly with the dielectric constant K of the dielectric material located between the plates. Thus for two capacitors with identical geometrics but different dielectric materials, the ratio of dielectric constants of the two materials is equal to the ratio of the corresponding capacitances, or

$$\frac{K_1}{K_2} = \frac{C_1}{C_2} \quad \text{numeric} \tag{11.38}$$

The dielectric constant of air is very nearly equal to 1.0 (actually 1.00059, at 1 atmosphere of pressure). Then if the capacitance C_x of a capacitor is measured with a dielectric material x between the plates, and if the capacitance C_a of the same capacitor is measured again with only air between the plates, the dielectric constant K_x of the material is equal to

$$K_x = \frac{C_x}{C_a} \quad \text{numeric} \tag{11.39}$$

Equation (11.39) offers a simple method to determine the dielectric constant of insulating materials using a parallel-plate capacitor.

In insulation systems such as the ground insulation of a coil, the ground wall frequently consists of two or more different insulation materials. Since their dielectric constants will differ, in general, such a composite insulation is equivalent to a capacitor with two or more dielectric materials in series between the plates. Consider Fig. 11.2, which gives a schematic representation of such a capacitor, with the dielectric consisting of materials a and b. From eq. (11.26) the voltage across material a is

$$V_a = \frac{q}{C_a} \quad \text{volts} \tag{11.40}$$

and the voltage across material b is

$$V_b = \frac{q}{C_b} \quad \text{volts} \tag{11.41}$$

Solving eqs. (11.40) and (11.41) for q, equating the two equations, and rearranging, we obtain

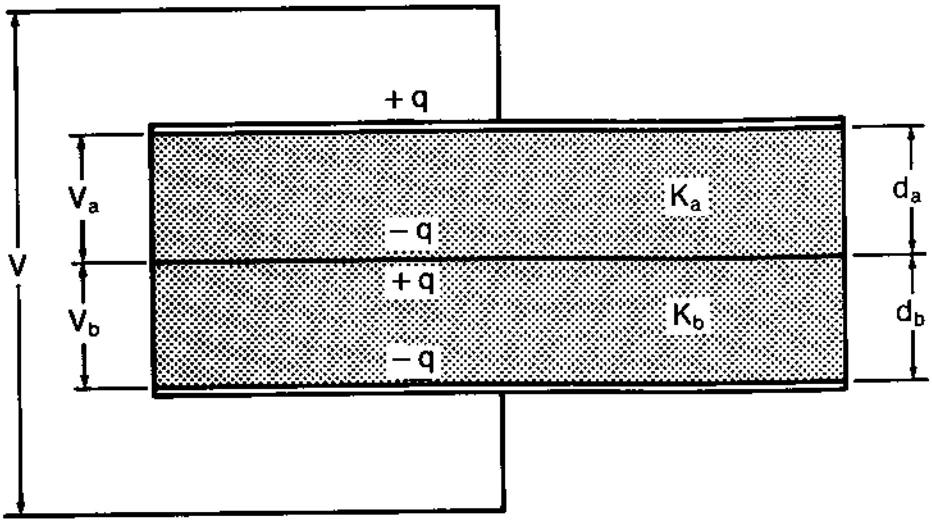

FIGURE 11.2 Dielectric materials in series in a capacitor.

$$\frac{V_a}{V_b} = \frac{C_b}{C_a} \quad \text{numeric} \tag{11.42}$$

Thus the voltages across the two dielectrics or insulating materials divide in inverse proportion to the dielectric constants. Obviously, the voltage gradients of the two materials also divide in inverse proportion to the dielectric constants. Thus

$$\frac{V_a/d_a}{V_b/d_b} = \frac{g_a}{g_b} = \frac{K_b}{K_a} \quad \text{numeric} \tag{11.43}$$

Then the insulating material with the lower dielectric constant must withstand the greater voltage gradient. As discussed subsequently, this is an important consideration in insulation systems and is responsible for the breakdown of air in insulation voids, which gives rise to bulk corona.

As will become apparent subsequently, the "dielectric constant" is not a constant from a strict standpoint. It is affected, in varying amounts, by frequency, temperature, voltage, and humidity. Past studies of scientists and engineers, seeking explanations for the variation of K with frequency and other variables, have contributed to a greater understanding of dielectric behavior.

11.6 PHYSICAL BEHAVIOR OF DIELECTRIC MATERIALS

Most dielectric materials tend, in various degrees, to exhibit certain physical behavior in common. For example, the dielectric constant K of most dielectric materials decreases with an increase in frequency of the electric field. This characteristic was initially called anomalous dispersion because it was considered to be an anomaly by some of the early investigators. However, subsequent pursuit of a suitable explanation has resulted in a better understanding of this, as well as of other aspects of dielectric behavior.

The physical characteristics of dielectric materials may be classified in general into five basic categories of physical phenomena: (1) polarization, (2) absorption, (3) dielectric conduction, (4) dielectric loss, and (5) dielectrical breakdown. The first category to be considered is polarization.

11.6.1 Polarization

A dielectric material is said to be polarized when the centroid of the positive charges does not coincide with the centroid of the negative charges within some given piece or volume of that material (i.e., when the two charge centroids are separated by a distance). Some dielectric materials become polarized only when an electric field is impressed across them, whereas others are polarized without the need for such a field. Polarization can be more easily understood and discussed in terms of electric dipoles. A dipole is a mathematical formulation of the physical concept described above. Dielectric materials have, to various degrees, the ability to form dipoles at the electronic, atomic, molecular, and higher structural levels, such that they can exhibit electric-charge polarity. This ability has a profound effect on the behavior and performance of such materials, under the influence of electric fields, and it provides an important basis for understanding the behavior of insulation in withstanding a voltage that is impressed across it.

Consider Fig. 11.3a, which is a schematic representation of an electric dipole. From eq. (11.9), the electric potential at point P in the field due to the negative charge -q is

$$V_{p1} = \frac{-q}{4\pi\epsilon X_1} \quad \text{volts} \tag{11.44}$$

and the electric potential at point P due to the positive charge +q is

$$V_{p2} = \frac{q}{4\pi\epsilon X_2} \quad \text{volts} \tag{11.45}$$

The net potential due to the presence of both charges is

$$V_p = \frac{q}{4\pi\epsilon}\left(\frac{1}{X_2} - \frac{1}{X_1}\right) = \frac{q(X_1 - X_2)}{4\pi\epsilon X_1 X_2} \quad \text{volts} \tag{11.46}$$

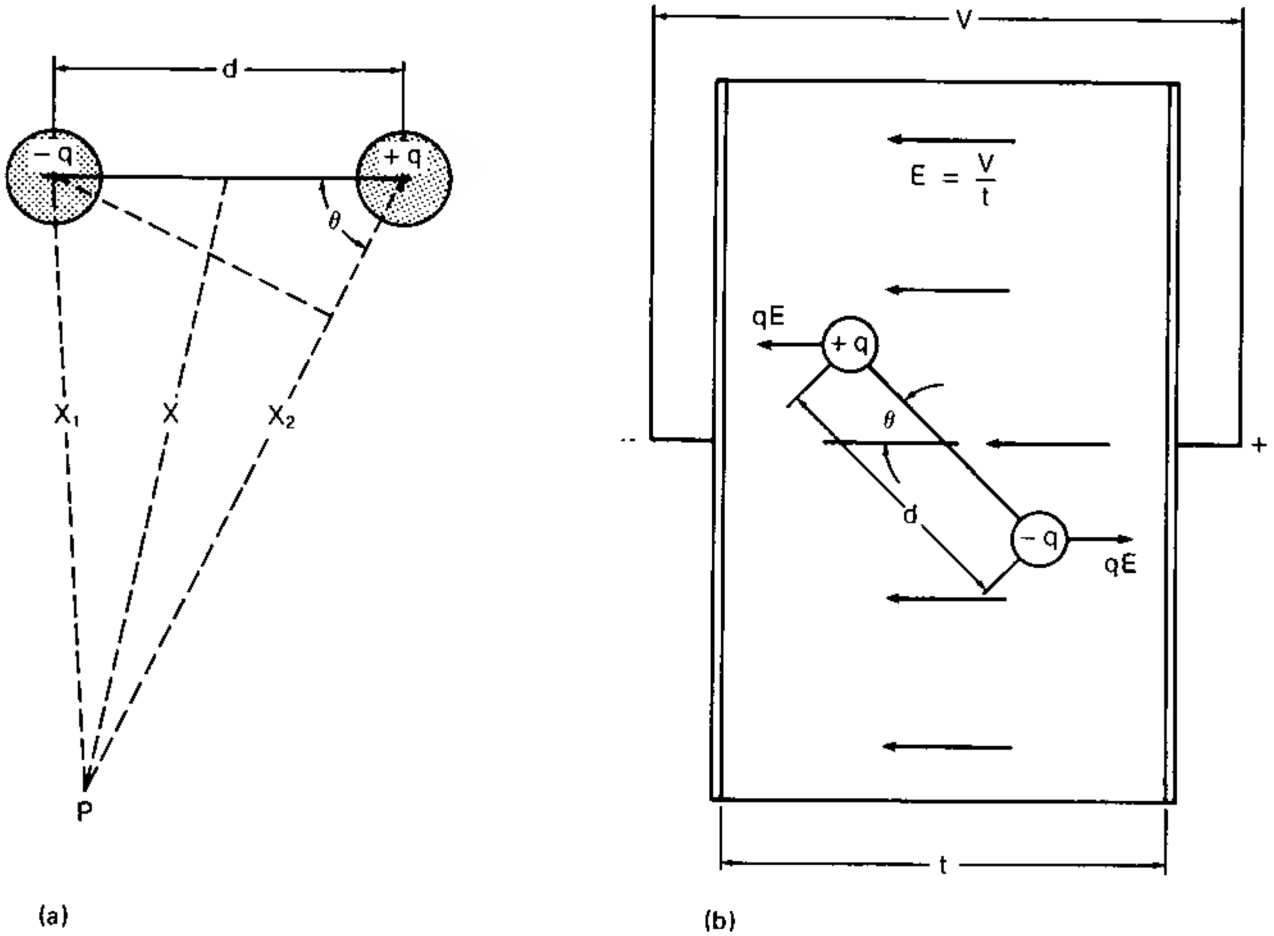

FIGURE 11.3 Electric dipoles in dielectric materials: (a) schematic representation of an electric dipole; (b) dipole alignment in an electric field.

For atomic, molecular, and even larger structural dipoles, the distance d is very small relative to the distance X and, accordingly, the three distances X, X_1, and X_2 may be regarded as equal and the expression $X_1 - X_2$ may be regarded as equal to d cos θ. Then eq. (11.46) may be written as

$$V_p = \frac{qd \cos \theta}{4\pi \epsilon X^2} \quad \text{volts} \tag{11.47}$$

which is the electric potential at point P due to the dipole.

The quantity qd is numerically equal to the dipole moment. It may also be considered a vector, in which case the vector direction is from the negative to the positive charge. It is obvious that the unit coulomb-meters is huge compared to the electric charge and distance associated with atoms, molecules, and so on. Accordingly, another unit has been adopted for the dipole moment qd, which is the debye. One debye is equal to $1/3 \times 10^{-29}$ C.m. Unfortunately, the debye unit is not a member of the MKS system of units. It is, however, an appropriate unit for use by those physicists and chemists who do fundamental work in the field of dielectrics.

Figure 11.3b shows a piece of dielectric material across which a potential difference of V volts is impressed and in which a macroscopic dipole is schematically shown. The voltage applied across a thickness of t meters results in an average electric field strength of $E = V/t$ volts/meter in the dielectric. This field strength is, in effect, a force per unit charge. Thus the charge +q at one end of the dipole under the influence of the electric field E produces a mechanical force of qE newtons directed toward the negative plate or electrode. Similarly, an equal force is produced at the other end of the dipole, due to the charge -q, which is directed toward the positive plate or electrode. The two equal but oppositely directed forces, separated by a distance d, constitute a couple that is equal to $qE \sin \theta$ newton-meters. Thus, when an electric field is impressed across a dielectric material that contains dipole formations or which can develop such formations under the influence of the field, the dipoles are subjected to a torque that tends to produce alignment with the direction of the electric field. In summary, then, dipoles tend to align themselves with the electric field direction when subjected to such a field. If, however, the electric field is an alternating one, each dipole must attempt to reverse its charge orientation at a time rate proportional to the frequency of the field, and this accounts for a dielectric phenomenon of considerable importance.

Electronic polarization results from displacement of the centroid of the negative charge of the orbital electrons with respect to the centroid of the positive charge of the nucleus of a given atom. Elements with orbital electrons that are less tightly bound, such as hydrogen, are more easily polarized than are others which are more tightly bound. The time required for the dipoles associated with electronic polarization to form in an electric field is very short. Accordingly, for frequencies in the power, audio, and radio range, the dipoles can form, reverse, and re-form at a time rate that is proportional to the frequency of the impressed field. However, at frequencies corresponding to some point in the visible-light frequency, the dipole reorientation cannot occur in the time associated with one alternation of the frequency. At this point, electronic polarization tends to be incomplate, or to break down, and the dielectric material then tends to exhibit a decrease in its dielectric constant K with an increase in frequency.

Atomic polarization results from displacement of the centroid of atoms in a molecule or molecular lattice or from displacement of the centroid of ions in a crystal. Since the mass of the particle associated with atomic polarization is greater than that associated with electronic polarization, the time required for dipole reversal is correspondingly greater. Accordingly, atomic polarization tends to break down at frequencies corresponding to some point in or near the infrared frequencies. The dielectric material then tends to show a decrease in its dielectric constant K with an increase in frequency.

For both electronic and atomic polarization, the corresponding dipoles are produced by action of an applied electric field and the dipoles cease to exist when the field is discontinued. However, certain molecules have a permanent or built-in dipole moment because of a structural dissymmetry in the arrangement of the ions that form the molecule. Water, for example, has a dielectric constant in the region 78 to 81. This is because the water molecule H_2O is arranged with one oxygen ion at a given point, with the two hydrogen ions positioned obliquely to the left and obliquely to the right, respectively, which is an unsymmetrical arrangement. If the water molecule had a symmetrical arrangement, such as H–O–H, it would exhibit a much lower value of dielectric constant.

Dipole polarization results from the interaction of an electric field with molecules that have a permanent dipole moment due to structural dissymmetries. For this type of polarization, the dielectric constant K tends to decrease with an increase in frequency within the power and audio range. Debye made a comprehensive study of this type of polarization and in doing so, significantly increased the state of knowledge of dielectric behavior. One of the benefits of Debye's work is the prediction of a decrease in K with an increase in temperature for many dielectric materials.

Interface polarization occurs in heterogeneous materials, and results from accumulation of charges at the various interfaces between components if the components differ in dielectric constant and in conductivity. Practical insulation materials have components for which the dielectric constant and conductivity differ, so that the conditions for this type of polarization are normally present. For interface polarization, the dielectric constant tends to decrease with an increase in frequency within the power and audio frequencies.

In summary, each of the four different types of polarization can affect the dielectric constant of a dielectric material, depending on the specific material and on the region of the frequency spectrum being considered. Figure 11.4 shows the variation of the dielectric constant with frequency for a hypothetical material. At low frequencies, all four types of polarization occur and thus contribute to the value of the dielectric constant. However, as the frequency of the impressed electric field is increased, the various types of polarization cease to occur, in succession, because of the inability of the associated dipoles to form, reverse, and re-form in the decreasing time interval associated with one cycle of the frequency. Figure 11.4 is, of course, illustrative of a hypothetical dielectric material, and practical insulations differ considerably from one material to another in the contribution to the dielectric constant of each type of polarization. Although not shown in Fig. 11.4, each decrease in dielectric constant is accompanied by an increase in ac conductivity of the dielectric material. Also, it should be noted in passing that the dielectric constant K is related to the index of

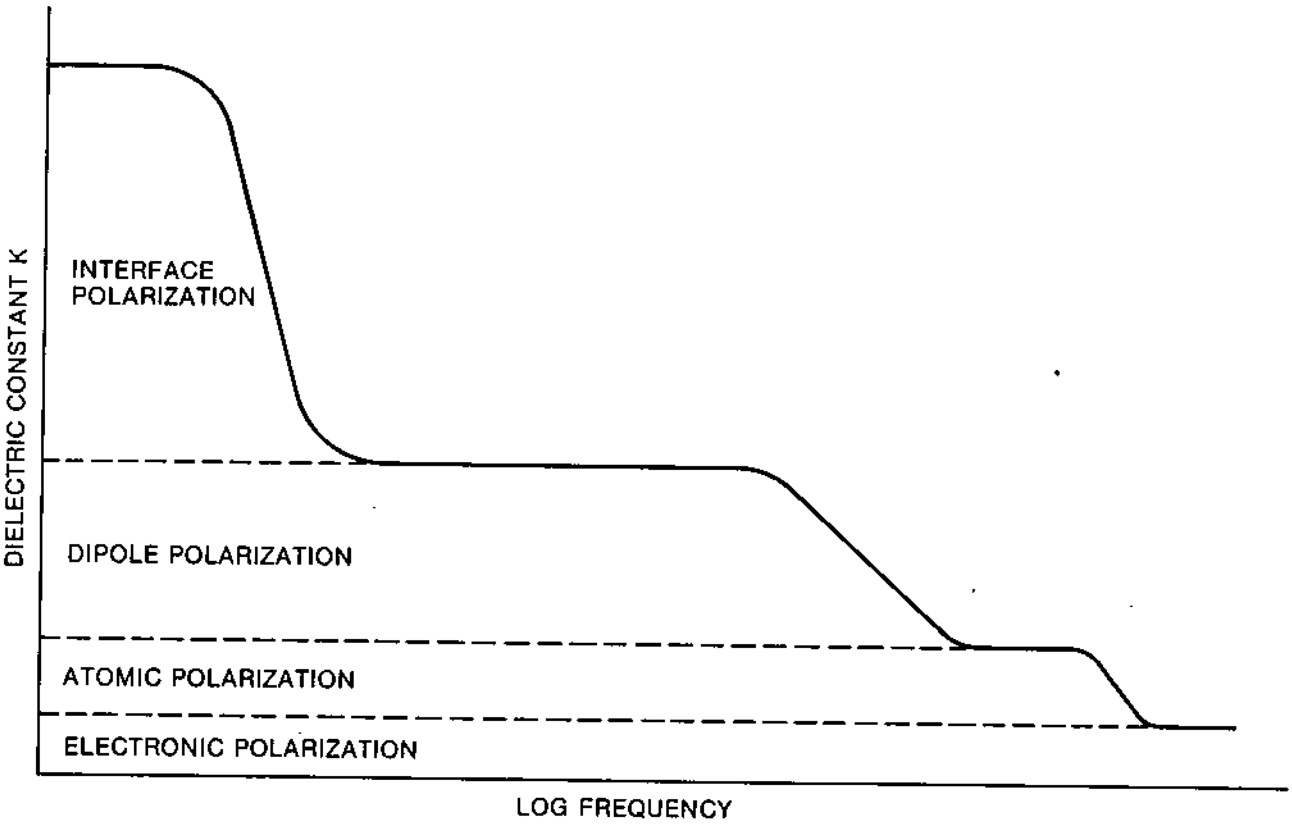

FIGURE 11.4 Polarization regions for a hypothetical dielectric material.

refraction n within the optic range of frequencies. Maxwell and Debye have shown this relationship to be $K = n^2$.

The dielectric constant of some common materials is given in Table 11.1. These values are to be regarded as typical and not exact, as there are small variations from one published value to another for a given material. Also, the overall dielectric constant of composite insulating materials, such as mica tape and wrap, will depend on the binder and backing used and to some extent on the fabrication process used by a given manufacturer.

11.6.2 Absorption

The phenomenon of absorption can be demonstrated by use of a capacitor model. Let a capacitor with a capacitance of C_0 farads be enclosed in a suitable containment chamber, and let electrical leads from the plates be brought out from the chamber by means of seals in the chamber walls. Then by use of a high-performance vacuum pump, let the chamber be evacuated until it approaches a perfect vacuum. At this point the condition between the condenser plates approaches that of a perfect dielectric and the corresponding dielectric constant is very, very close to unity. Under these conditions, let a direct voltage of V volts be placed between the capacitor plates. An initial charging current will result as electrical charges rush to charge the plates, and as soon as the plates are charged, the charging current will become equal to zero. From eq. (11.36) the energy stored in the capacitor is equal to $(1/2)CV^2$ joules. If the charged capacitor plates are short circuited (i.e., if the capacitor is discharged), a discharge current will flow in the opposite direction until the accumulated charges are removed from the plates. The discharge current will continue to flow until all of the energy stored in the charged capacitor [i.e., $(1/2)CV^2$ joules] is dissipated in the circuit as i^2Rt. Such a cycle can be considered the behavior of an essentially perfect dielectric during charge and discharge.

The behavior of a practical dielectric, on the other hand, is more complicated. For this case, let the containment chamber be opened and let a practical dielectric with a dielectric constant of K be placed between

TABLE 11.1 Tabulation of the Approximate Dielectric Constant for Some Common Materials

Material	Dielectric constant K at power frequency[a]
Air[b]	1.0006
Hydrogen[b]	1.0003
Water[c]	81
Mica	5-6
Mica tape or wrap	3-4.5
Fiber[d]	2
Vinyl	4
Asphalt	2.7
Paraffin	2.1
Porcelain	7.0
Silica	3.8
Transformer oil[c]	2.13
Wood, dry and untreated	2.5-6.8
Wood, impregnated with oil	2.5-5.0

[a] Dimensionless.

[b] At 1 atm of pressure.

[c] At room temperature.

[d] Various paper-type fibers.

the plates of the same capacitor. From eq. (11.39), the capacitor now has a capacitance of $C_p = KC_0$ farads. Let a direct voltage of V volts again be impressed across the capacitor plates. As for the previous case, a charging current will flow, but an additional component of current, called conduction current, will also flow. A practical dielectric material has a definite, although normally low value of conductivity, whereas the conductivity of vacuum is zero. The charging component of current will continue to flow until the capacitor plates are fully charged, with a charge value equal to C_pV coulombs, at which time it will cease. However, the conduction component of current will continue to flow as long as the voltage V is impressed across capacitor plates, because of the inherent conductivity of the dielectric material located between the plates. When the voltage V is removed, the conduction component of current immediately ceases. During discharge of the capacitor, the conduction component of current is not present and only the discharge component exists. The discharge component will continue to flow until the stored energy, $(1/2)C_pV^2$ joules, is dissipated as i^2Rt. Thus for a practical dielectric material, the difference between the capacitor current during charging and discharging is equal to the conduction current for that particular material.

There are many practical dielectric materials which show a third component of current, called absorption current. For such materials, following application of voltage, the initial value of charging current decreases as the capacitor plates are charged. However, the rate at which the current flow approaches zero tends to be lower, or the charging process tends to take more time, than would intuitively be expected. Similarly, when the capacitor is discharged, the discharge current tends to require longer to approach and reach zero than would intuitively be expected. This "delaying" phenomenon is exhibited physically in still another manner. Assume that a capacitor with such a dielectric is being discharged by short circuiting the two plates with a conductor. Let the short-circuiting conductor be open circuited as the discharge current is approaching zero. If the capacitor is again short circuited, discharge current will again flow and will be greater in value than it is just preceding the opening of the discharging circuit. This new current will also tend to decrease and to approach zero. Such a rejuvenation of a capacitor can usually be achieved some number of times for a dielectric that exhibits this property. This phenomenon is called absorption. Most dielectric materials are affected by absorption, although other materials, primarily gases, are not as affected. Absorption has not been explained in fundamental terms to the benefit of all research people who have worked on or seriously considered the subject. Such people as Maxwell, Wagner, von Schweidler, Hopkinson, Anderson, Keane, Joffe, Pellat, Whitehead, and Miner have all thought about the subject and some have contributed theoretical explanations. Many of the theories consider changes in conductivity, structure, polarization, and electron motion. Others believe that it is an anomaly which has not yet been fully explained. In any case, absorption appears to have an implicit relationship with dielectric resistivity or, conversely stated, with dielectric conductivity.

The insulation resistance value determined during a 1-minute test period is essentially a measurement of absorption current. The true leakage current across the insulation, upon which true insulation resistance is dependent, is a relatively small part of the total current flow during the first minute of testing of the insulation resistance of a rotating machine winding. This subject is considered to a greater extent later in this chapter.

11.6.3 Dielectric Conduction

As stated in Section 11.2, materials are broadly classified into conductors, semiconductors, and insulators, depending on their respective resistivities. One such classification, for example, defines insulators, or dielectrics, as materials that have volume resistivities of $10^8\ \Omega \cdot \mathrm{m}$ or greater. Prima facie, this value of resistivity would appear sufficiently large as to cause the conduction of current through insulation to be negligible and thus of no practical consequence. However, it was noted in Section 11.6.2 that a conduction component of current does indeed flow. It must be remembered that in the practical application of insulation to rotating machines, large cross sections and small thicknesses of the insulating material are involved, which tend to lower the overall resistance and to increase the overall conductance. Consider a 1000 to 1250-hp 4000-V polyphase induction motor. The cross-sectional area of the stator-slot portion alone of the stator-winding insulation is typically about 7 m^2 (10,800 $\mathrm{in.}^2$). The wall thickness of the ground insulation, next to the iron core, is typically about 1.91 mm (0.075 in.). Then, by a simple application of Ohm's law, the conduction current that flows across the insulation wall is

$$I = \frac{V}{R} = \frac{(2309)(7)}{(0.00191)(10^8)} = 0.085 \quad \text{amperes} \tag{11.48}$$

Thus the volumetric conduction current through the slot portion of the stator ground insulation for insulation with a resistivity of $10^8\ \Omega \cdot \mathrm{m}$ is approximately 10^2 mA for a machine of this size. New ground insulation would be expected to have a volume resistivity in excess of $10^8\ \Omega \cdot \mathrm{m}$. However, after having been in service for a reasonable period of time, and after having been exposed to various contaminants and environmental conditions, including moisture, the bulk resistivity of motor winding insulation could approach a value of 10^8 or $10^9\ \Omega \cdot \mathrm{m}$.

Two types of dielectric resistance exist: volume resistance and surface resistance. Volume resistance is resistance that impedes the flow of conduction current through a dielectric, such as from one plate to the other in a charged capacitor or from the copper conductor to the steel core in an excited stator winding. Volume resistance is useful, together with other dielectric information, in determining the suitability of a given winding for field service. It is also useful, for quality-control purposes, in the production of insulating tapes and wraps and as one of the checks of a completed winding. The value of the measured resistance will vary considerably depending on the temperature of the dielectric and the presence of moisture or other impurities within the dielectric.

Surface resistance is resistance that impedes the flow of creeping or tracking current on the surface of a dielectric, usually due to the presence of contaminants on the insulation surface. It is useful in such insulation applications as porcelain insulators, lightning arrestors, wound-rotor collectors, and so on. Also, as will be seen subsequently, it is important in controlling surface corona of high-voltage stator windings.

Both volume insulation resistance and surface insulation resistance are expressed in units of 10^6 ohms, or megohms. This unit is used so that it will not be necessary to use a large number in order to express the value of the insulation resistance of, say, a stator winding. Procedures for determining the insulation resistance of machine windings are given later in the chapter.

11.6.4 Dielectric Loss

In 1864, Siemens observed that when an alternating voltage is impressed across a dielectric material, internal losses are produced that result in some heating of the material. As has been determined in subsequent years, such dielectric losses result from the flow of absorption current and conduction current. Of the two components of ac loss, absorption loss is the greater.

Figure 11.5 shows the vector diagram of a dielectric material with an ac voltage V impressed across it. In this figure the scale of the real, or x, axis has been intentionally exaggerated to delineate more clearly the various losses and the associated angles. OD is the actual charging current that sustains the charging volt-amperes if the dielectric was a perfect one with no absorption effect. However, as noted earlier, actual dielectrics exhibit considerable absorption effect, and thus OC is the actual charging current, or the component of current across the dielectric which leads the impressed voltage by $\pi/2$ electrical radians. Then DC is the component of charging current associated with absorption.

CB is the in-phase current that sustains the dielectric loss associated with absorption, and DB is the total absorption current. Accordingly, OB is the dielectric current if there is no conduction. However, essentially all dielectrics except gases exhibit conduction, and current BA is the in-phase current that sustains the conduction losses. The vector sum of the total quadrature current OC and of the total in-phase current CA is equal to OA,

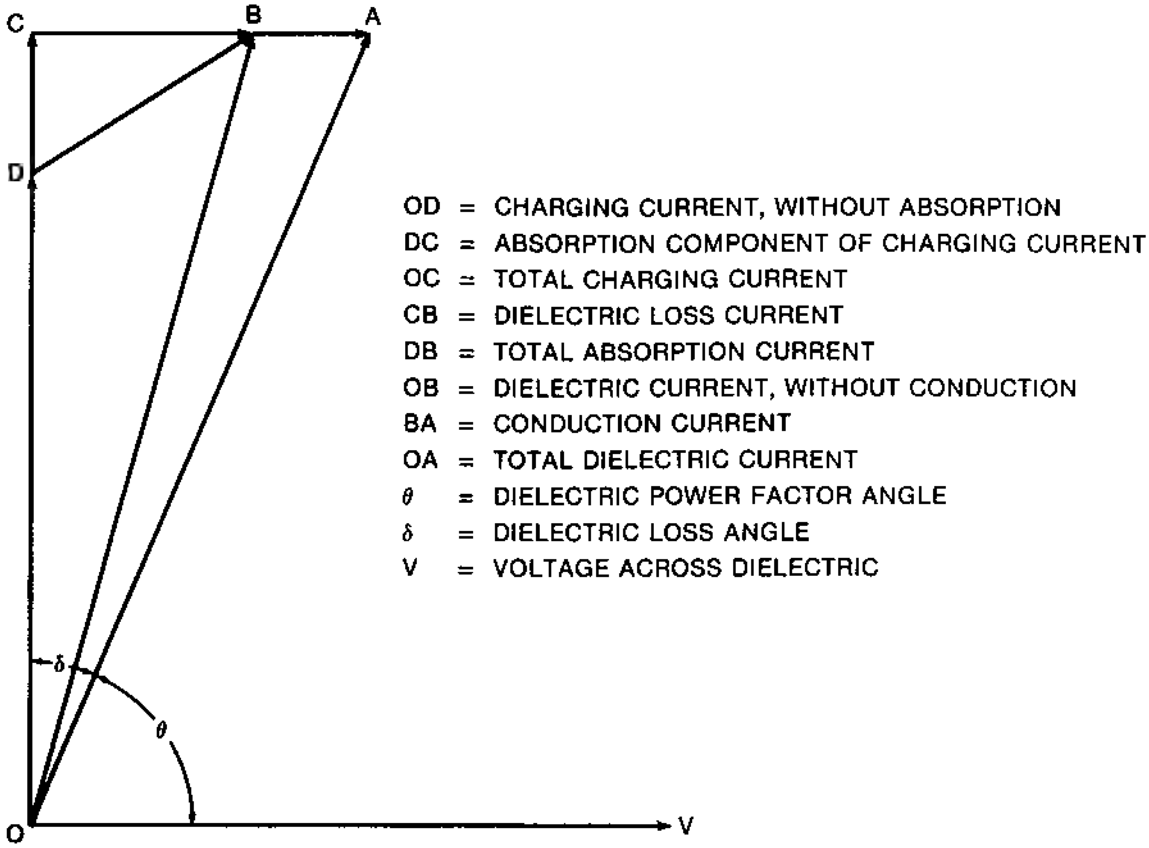
C
B
A
D
O
V
δ
θ
OD = CHARGING CURRENT, WITHOUT ABSORPTION
DC = ABSORPTION COMPONENT OF CHARGING CURRENT
OC = TOTAL CHARGING CURRENT
CB = DIELECTRIC LOSS CURRENT
DB = TOTAL ABSORPTION CURRENT
OB = DIELECTRIC CURRENT, WITHOUT CONDUCTION
BA = CONDUCTION CURRENT
OA = TOTAL DIELECTRIC CURRENT
θ = DIELECTRIC POWER FACTOR ANGLE
δ = DIELECTRIC LOSS ANGLE
V = VOLTAGE ACROSS DIELECTRIC

FIGURE 11.5 Vector diagram of voltage, currents, and angles associated with a dielectric material.

which is the total dielectric current considering both absorption and conduction. Since the total dielectric current OA leads the impressed voltage V by the angle θ, the power factor of the dielectric is

$$(PF)_d = \cos\theta \quad \text{numeric} \tag{11.49}$$

The angle δ is called the defect angle of the dielectric. Then the power factor can also be written as

$$(PF)_d = \sin\delta \quad \text{numeric} \tag{11.50}$$

since $\theta + \delta = \pi/2$ radians. The loss in watts within the dielectric with an alternating voltage V at a fixed frequency f impressed across it is

$$P_d = V(OA)\cos\theta = V(OA)\sin\delta \quad \text{watts} \tag{11.51}$$

From inspection of the vector diagram in Fig. 11.5, we find that

$$OA = \frac{OC}{\cos \delta} \quad \text{amperes} \tag{11.52}$$

But OC is the capacitive current component, which leads V by $\pi/2$ radians. Then

$$OC = \frac{V}{X_d} = 2\pi f C_d V \quad \text{amperes} \tag{11.53}$$

Substituting eq. (11.53) into eq. (11.52) yields

$$OA = \frac{2\pi f C_d V}{\cos \delta} \quad \text{amperes} \tag{11.54}$$

Then, substituting eq. (11.54) into eq. (11.51), we obtain

$$P_d = 2\pi f C_d V^2 \frac{\sin \delta}{\cos \delta} = 2\pi f C_d V^2 \tan \delta \quad \text{watts} \tag{11.55}$$

From eq. (11.39), C_d is equal to

$$C_d = K_d C_a \quad \text{farads} \tag{11.56}$$

where K_d is the dielectric constant of the dielectric material and C_a is the capacitance of the same capacitor with air between the plates. Substituting eq. (11.56) into eq. (11.55) gives us

$$P_d = 2\pi f K_d C_a V^2 \tan \delta = kV^2 f K_d \tan \delta \quad \text{watts} \tag{11.57}$$

where k is a constant. Thus when an alternating voltage, at a fixed frequency is impressed across a dielectric, the resulting dielectric losses are proportional to the frequency, to the second power of the impressed voltage, to the dielectric constant, and to the tangent of the defect angle. In eq. (11.57) the factors f and V^2 are dependent on the external voltage that is impressed across the dielectric. On the other hand, the factor $K_d \tan \delta$ is dependent on the dielectric material. Thus $K_d \tan \delta$ can be used as an index of the dielectric loss of dielectric material. This index of dielectric loss of a dielectric material is called the loss factor, or

$$\text{loss factor} = K \tan \delta \quad \text{numeric} \tag{11.58}$$

The dissipation factor of a dielectric material is defined as

$$\text{dissipation factor} = \tan \delta \quad \text{numeric} \tag{11.59}$$

and, accordingly,

$$\text{loss factor} = (K)(\text{dissipation factor}) \quad \text{numeric} \tag{11.60}$$

Even though a high value of dielectric constant K is desirable for some applications, the product K tan δ must be kept sufficiently low as to maintain the dielectric losses within limits that are acceptable.

11.6.5 Dielectric Breakdown

The electrical breakdown strength of dielectric materials is considered here from two points of view. First, we regard it as a dielectric phenomenon and as part of dielectric behavior. Then we regard it as a prime subject in evaluating and applying insulating materials to motor windings and consider the important factors that affect it. The first point of view is discussed in this section, and the second, in Section 11.7.

As the electric field strength across a dielectric material is increased (i.e., as the voltage gradient is increased), a point is eventually reached at which there is a rapid increase in conduction current, which becomes an avalanche if the impressed voltage is not immediately removed. At this point the material appears to have been transformed from an insulator to a semiconductor, the dielectric strength of the material has been reached, and dielectric breakdown is impending. The mechanism of dielectric breakdown is different for the three different phases of matter. The gaseous dielectric is the first to be considered.

The breakdown of a gas due to an electric field is understood theoretically to a greater extent than that of liquid or solid dielectrics. Maxwell, Townsend, Loeb, Schumann, Thomson, Paschen, Slepian, Cobine, and others have contributed to our present understanding of the subject. The molecules of a gas such as air or hydrogen are relatively far apart compared to the molecules of matter in the liquid or solid phase, allowing a relatively large mean free path for free electrons. Also, a gaseous dielectric subjected to an electric field exhibits little or no conduction current or absorption current between electrodes below the voltage breakdown gradient, which simplifies the breakdown mechanism.

The electric field will influence free electrons within the gas, causing them to accelerate. The velocity and associated energy of the moving electrons depend on the electric field strength, or gradient. If the kinetic energy associated with the moving electron is sufficiently great, electrons will strike electrically neutral gas atoms or molecules and will dislodge charged particles. These particles, in turn, possess kinetic energy and will have the opportunity of striking and affecting additional neutral atoms and molecules. If the electric field intensity is increased, a critical gradient is eventually reached at which an avalanche current occurs and the gas breaks down dielectrically. This value of field intensity E_s is the sparking gradient, and the product of E_s and the distance between plates or electrodes δ is equal to the sparking potential, or

$$V_s = E_s\delta \quad \text{volts} \tag{11.61}$$

In 1889, Paschen experimentally determined that the sparking potential of a gas is a function f_1 of only the product $p\delta$, or pressure times gap length, at a given temperature. This has come to be known as Pachen's law, which is functionally stated, for a constant temperature, as

$$V_s = f_1(p\delta)_T \quad \text{volts} \tag{11.62}$$

If the effect of temperature on the sparking potential is to be considered in the functional relationship, the density d should be used instead of the pressure p. Then for a constant pressure, Paschen's law is functionally stated as

$$V_s = f_2(d\delta)_p \quad \text{volts} \tag{11.63}$$

This is because the number of collisions that an electron makes in crossing a gap from one electrode to another with a constant field is proportional to the density d and the length of the path or gap δ.

The breakdown potentials of air and of other common gases are published in various texts, articles, and other references. Such data are usually given in the form of a curve, with V_s plotted versus $p\delta$ or $d\delta$ for various conditions of temperature, for various shapes of electrodes, and using various units. Figure 11.6 shows Paschen's relationship for air and hydrogen between parallel plates with p in mmHg and with δ in millimeters of gap length. As will subsequently become apparent, the sparking potential of air is important in determining the threshold value of corona in motor windings.

The breakdown of a liquid dielectric due to an electric field is not as theoretically straightforward as is that for a gas. Efforts have been made to consider liquids as greatly compressed gases and to apply Paschen's law. However, actual values of breakdown voltage obtained by testing liquid dielectrics do not compare favorably with the values obtained by attempting to apply Paschen's law for gases in the pressure or density ranges required for liquids.

For some dielectrics a small amount of contamination will greatly reduce the dielectric strength. This is true of hydrocarbons, for which oxygen, water, and so on, significantly affect the dielectric strength. For

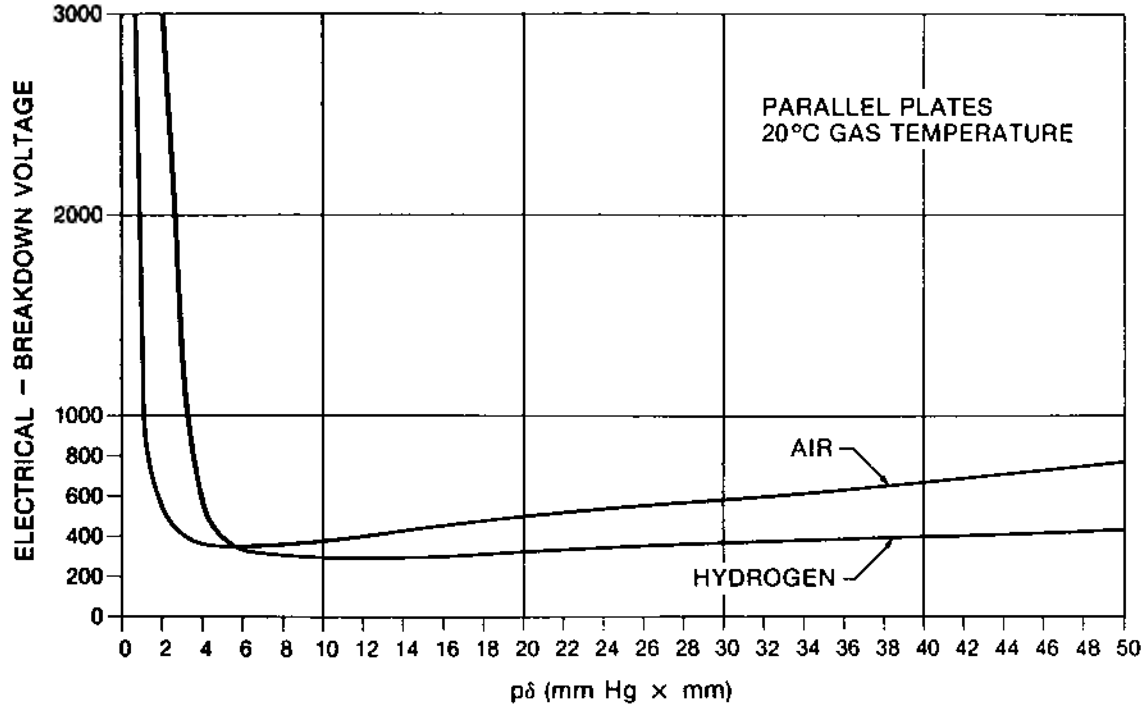

FIGURE 11.6 Breakdown voltage for air and hydrogen, with parallel plates or electrodes.

some liquids the application of an electric field results in partial dissociation with ion formation. The movement of ions through the liquid can result in the production of additional ions. Also, some dissociation of the liquid can result in the production of additional compounds not present in the pure liquid before it was stressed by an electric field. This effect is seen, in some cases, in the insulating oil used in transformers and in the oil used in oil-filled cables. In most cases, the dielectric strength of liquids must be determined by testing.

This is also true for solid dielectrics. If the electric field impressed across a solid piece of insulation is increased, a voltage gradient is eventually reached at which there is a sudden and significant increase in what has been the conduction and/or absorption current. The result is that the piece of insulation fails; that is, it is punctured or charred in some portion of its cross-sectional area. Such an insulation failure is clearly a manifestation of a progressive instability mechanism which has become critically unstable or which has "run away." The sudden avalanche of current indicates that there is a sudden movement of electrons and that the previous restraints on charge movement has decreased below a critical value. Various theories have been developed to explain this, and they may generally be classified as ionic, thermal, and disruptive mechanisms.

The ionic theory of solid-dielectric breakdown assumes what is essentially an electrolytic model. Free ions present in the solid move in proportion to the strength of the impressed electric field. For a fixed dielectric thickness, the ion movement would appear to be proportional to the voltage across that thickness and would appear to follow Ohm's law until a critical voltage gradient is reached. At some critical ion density corresponding to the critical gradient for the material, the ionic movement approaches an avalanche, which results in dielectric failure. One explanation of the critical gradient is based on the concept of ionic equilibrium. The rate of ionic formation by electrons leaving molecules, and the rate of ionic neutralization by electrons joining molecules, are in equilibrium. However, as the electric field intensity approaches the critical gradient for that material, the ions approach a velocity which tends to destroy that equilibrium condition, resulting in an avalanche.

The thermal theory of solid-dielectric breakdown assumes a thermal model dependent on electrical resistance. It considers the rate at which the resulting losses are removed and the effect of any resulting localized increase in temperature on the resistance, which is locally exhibited by the material. The theory further assumes that all dielectric materials are somewhat heterogeneous, which they are. It follows that within the volume of the dielectric material, some small volumes, layers, or filaments of the material will have lower resistance than others. Then if an electric field is impressed across the material, nonuniform current distribution will result. The regions of lower resistance will conduct more current than will the other regions, and more heat energy will be developed in these regions. If the rate at which heat can be removed by thermal conduction is at least equal to the rate at which heat is being produced, the dielectric continues to function as an insulator. If, on the other hand, the rate of heat production exceeds the rate of heat removal, the vulnerable regions of low resistivity become increasingly hot locally. This may tend to reduce further the resistance of these local regions, since many dielectric materials have negative coefficients of resistance. Then according to the thermal theory, the process is continuous and at some critical gradient results in local thermal instability and dielectric failure. This model requires that the resistance of the vulnerable regions of the material exhibit an appropriate functional relationship with temperature. One such function, offered by Wagner, is

$$R = R_0\left(\frac{k}{k + T}\right)^{\alpha} \quad \text{ohms} \tag{11.64}$$

where k is a constant, T is temperature on some scale, and $\alpha \geqq 1.0$. The thermal model above assumes the presence of a weak region within the dielectric material. There are other thermal models that do not make this particular assumption, but they require other assumptions.

The disruptive theory of solid-dielectric breakdown is based on the concept that such a breakdown results from failure of molecular and other bonds within the structure of the material. This theory suggests a parallel mechanism between mechanical failure from a mechanical force, and

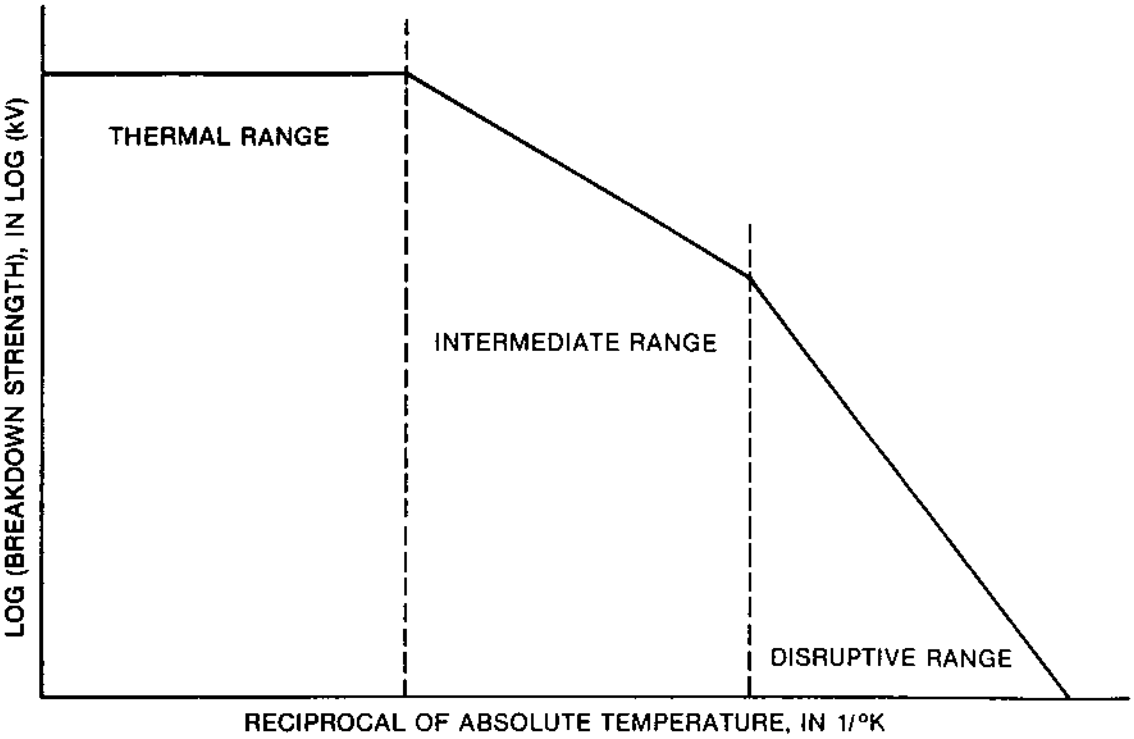

FIGURE 11.7 Curve of log electrical-breakdown strength versus reciprocal of absolute temperature for a hypothetical dielectric.

electrical failure from an electric field. There is some evidence of such a parallel relationship. It is known, for example, that repeated voltage surges which are significant but which are not sufficient to cause electrical failure initially, will eventually lower the breakdown strength of insulation. This effect of repeated electrical stressing appears similar to the reduction of mechanical strength from repeated application of mechanical stress (i.e., from fatigue). It also appears that there is an interaction between mechanical and electrical stress within a given material. The electrical breakdown strength of a solid dielectric is significantly reduced when a mechanical stress, which approaches its mechanical limit, is applied to the sample. Further, cracks and other mechanical defects in dielectric materials with crystalline structures will adversely affect the insulating ability of such materials.

There are practical indications that the ionic, thermal, and disruptive mechanisms of failure operate in combination in electrical breakdown. If the logarithm of electrical breakdown strength is plotted against the reciprocal of absolute temperature, as shown in Fig. 11.7, the resulting curve tends to be linear or to have a constant slope throughout a region, with up to as many as three such regions for the full range of the variable 1/T. A reasonable inference is that a specific failure mechanism is dominant in each region. Moon and Norcross presented this very interesting observation to the American Institute of Electrical Engineers (now the Institute of Electrical and Electronics Engineers) in 1930.

11.7 FACTORS AFFECTING INSULATION STRENGTH

Insulation strength is obviously of prime importance in evaluating and applying insulation to motor windings. Various factors affect the electrical strength, and determine the useful life, of insulation components and insulation systems. Among these are temperature, time, frequency, voltage (including gradient, wave shape, repeated overstressing, etc.), thickness, mechanical stress, and contamination. These factors are considered below.

11.7.1 Temperature

An increase in insulation temperature can, and not infrequently does, result from causes external to the insulation. The stator winding I^2Rt losses of a motor must be conducted through the ground wall of the insulation and then be carried away by convection of the cooling air. If the rate of production of I^2Rt heat energy is too great relative to the ability of the conduction-convection path to transfer heat energy, the thermal drop from the copper to the ambient air will be greater than desired. Also, if the temperature of the ambient air is too great, the insulation temperature will also be greater than desired. An increase in insulation temperature can also result from dielectric losses that occur within the insulation itself, as discussed previously. However, an increase in temperature from whatever source has a generally unfavorable effect on insulation, including a decrease in insulation resistance, a decrease in electrical breakdown strength, and an increase in dielectric loss. As discussed in Section 11.6.5, as many as three different electrical-breakdown mechanisms (i.e., ionic, thermal, and disruptive) can occur as the temperature is increased.

The length of time in which voltage is applied has an influence on the electrical strength of insulation at increased temperatures. The short-time electrical strength to voltage does not appear to be influenced to any significant degree by the temperature of the insulation, as long as the temperature is not sufficiently great as to destroy the integrity of the sample. However, the long-time electrical strength of insulation is adversely affected by the simultaneous application of voltage and elevated temperature to the material.

A temporary, short-run exception to the above generally adverse effect on insulation of an increase in temperature is that of curing the resins which are a normal part of the insulation system of a winding. The winding is treated with a resin and then cured by heating within an industrial oven, as discussed in Chapter 9. This heating tends to drive off any gaseous compounds and to "cure" the resin compounds. Without this manufacturing operation, the insulation system would not be adequate and such an operation can be considered a one-time event in which increased temperature benefits, rather than adversely affects, an insulation system.

Various insulating materials exhibit different degrees of imperviousness to temperature. Some fibrous materials, such as paper and cloth, are not suitable for very high temperatures. Materials such as mica and certain synthetic resins, on the other hand, are suitable for continuous operation at 155°C or more. Accordingly, an insulation system is designed and proven, by evaluation tests, to be suitable for continuous operation at a given operating temperature. The electrical industry has established a set of continuous operating temperatures, which are incorporated into industry standards in the United States and other parts of the world. Three such standard operating temperatures, which include most present-day designs, are 130, 155, and 180°C, or in terms of alternative nomenclature, class B, class F, and class H. This subject is discussed in greater detail in Section 11.13.

11.7.2 Time

The length of time that a voltage is applied to insulation significantly affects the electrical breakdown strength of that insulation. Essentially all insulating materials can withstand a greater voltage for a short time than for a longer time. A voltage-time curve for a given material can be constructed from test data. This is done by applying an increasingly greater voltage across each successive sample from a lot of several samples. Then by observing the length of time that each sample will withstand its particular voltage, and by plotting the corresponding values of voltage and time, such a curve can be constructed. As a matter of technique, of course, it is desirable to use several samples at each voltage and to maintain a fixed temperature. The result will give a curve in which the failure voltage decreases as the time increases and which tends to approach an asymptotic value of voltage, corresponding to failure at an infinite time.

If the logarithm of time to failure is plotted against the reciprocal of the aging temperature, in kelvin^{-1}, the result should give a straight line, with one or more slopes, throughout the span of the reciprocal of temperature. Such a plot is called an Arrhenius plot. One inference from the plot is that a single failure mechanism tends to dominate through a region of a given slope. Miner has suggested that short-time failure is due almost entirely to the aforementioned disruptive mechanism, and that long-time failure is more complicated and involves the ionic and thermal mechanisms. Also, if the electrical gradient across the insulation is sufficiently great, corona will tend to cause the insulation samples to deteriorate. Corona is discussed in Section 11.8.

11.7.3 Frequency

Electrical strength of insulation generally decreases with increasing frequency such that at radio frequencies it is only 10 to 20% of that at 60 Hz. However, up to 100 Hz, this change is insignificant for most insulation materials and is generally ignored.

It is reasonable that electric strength of insulation should decrease with increased frequency. To the extent that dielectric loss is constant for one cycle, such loss is proportional to frequency. As noted when the three dielectric-breakdown mechanisms were considered, internal heating as well as external heating can contribute to dielectric loss and hence to a general reduction in electrical strength.

11.7.4 Additional Voltage Characteristics

Since the electrical strength of an insulating material is equal to that magnitude of voltage which causes electrical breakdown under the fixed conditions of the test, it is apparent that the voltage magnitude is a very significant characteristic of applied voltage. Also, as just discussed, the time interval during which the voltage is applied is very significant and the frequency of the voltage starts to become significant at some point beyond the power range of the spectrum. However, there are additional characteristics of the applied voltage that should be mentioned.

In general, most insulation materials can withstand a greater direct or dc voltage than an alternating or ac voltage. Typically, the breakdown strength for dc voltage is about 60% greater than for ac voltage for the same material. Also, the rate of rise to crest, or the steepness of the leading edge, of a voltage wave has a great influence on the ability of insulation to withstand such a voltage. For example, composite insulation, typical of a stator coil, will exhibit from two to three times the magnitude of breakdown-voltage strength for a voltage surge with a steep wavefront as for a 60-Hz voltage. A "1 1/2 × 40" voltage surge is frequently used for testing and comparison purposes. Such a wave reaches its crest value in 1 1/2 μs and then decreases to half of its crest value 40 μs later.

It has been observed that if insulation fails due to a voltage with a steep wavefront, such as the above-mentioned 1 1/2 × 40 wave shape, the instant of failure will occur at some point after the wave crest has been reached and when the actual voltage has decreased. This effect is called "time lag." To explain the effect further, a hypothetical example will be used. Assume that an insulation sample is subjected to a 1 1/2 × 40 surge and that it fails 25 μs after being subjected to an 80-kV crest value. Then assume that a second, identical insulation sample is subjected to a surge of the same shape and with a 90-kV crest value, which fails 12 μs after the crest. By continuing this procedure using identical insulation samples and successively increasing the crest value of the surge, a time-lag curve can be constructed for the particular insulation being tested. If corresponding time-lag curves are determined for several insulating materials or composite insulation systems of interest, the results can be compared as one step in insulation coordination. Thus for several interconnected items of equipment, it can be determined which item of equipment will provably have an insulation failure first when the interconnected system is subjected to a voltage surge such as might occur from switching or from an inadequately attenuated lightning stroke.

It was mentioned in Section 11.6.5 that there is evidence of a parallel between mechanical-strength fatigue, from repeated application of mechanical stress, and electrical-strength fatigue, from repeated application of electrical stress. Experience indicates that a phenomenon such as insulation fatigue does, indeed, exist. Let a motor winding, for example, be repeatedly subjected to voltage surges the crest value and rate of rise of which is not sufficient to fail the insulation initially. If the surges are repeated a sufficient number of times, an insulation failure will occur and the motor will be put out of service. In general, as the voltage crest and/or the rate of rise of the voltage to crest is increased, the number of surge occurrences that are required to cause failure is decreased. This subject is considered further in Section 11.12.

11.7.5 Material Thickness

Although an insulation sample 2 cm thick will withstand a greater voltage than an otherwise identical sample 1 cm thick, it will not withstand twice the voltage of the thinner sample. Testing shows that in general, the electrical strength per unit thickness decreases as the sample thickness is increased. Thus an air gap of 0.0025 cm (about 0.001 in.) will withstand up to about 450 V. This represents an electrical field intensity or gradient of 180 V per 10^{-3} cm (about 450 V/mil) across the insulation. An air gap of 0.025 cm (about 0.010 in.) will withstand up to about 1600 V. For this thickness the gradient is 64 V per 10^{-3} cm (about 160 V/mil). Thus for a one-decade increase in thickness, the electrical-breakdown strength of air expressed as an electrical-strength gradient has decreased by a factor of more than 2.8. In general, the electrical strength of solid insulating materials expressed as a gradient also tends to decrease with an increase in thickness. Some materials, however, such as glass, tend to exhibit an approximate proportionality between breakdown voltage and thickness, at least within certain ranges of thickness.

As stated earlier, all the I^2Rt heat energy produced by the stator winding must travel through the insulation ground wall by thermal conduction. Thus the greater the thickness of this ground wall, the greater the temperature drop from the copper to the outside of the stator-coil insulation. To limit the operating temperature of the stator-winding copper and hence the hot-spot temperature of the stator insulation for a given temperature class, the permissible stator current density must also be limited. This has the effect of increasing the amount of copper and, to some extent, the amount of magnetic core material required for a given rating. Also, as noted above, the per unit electrical strength of insulation used for motor windings tends to decrease as the thickness is increased. Thus there are good engineering as well as economic reasons for limiting the insulation thickness of the stator winding. Accordingly, the ground-wall thickness is selected so as generally to minimize the thickness of the wall, but to have a thickness that will

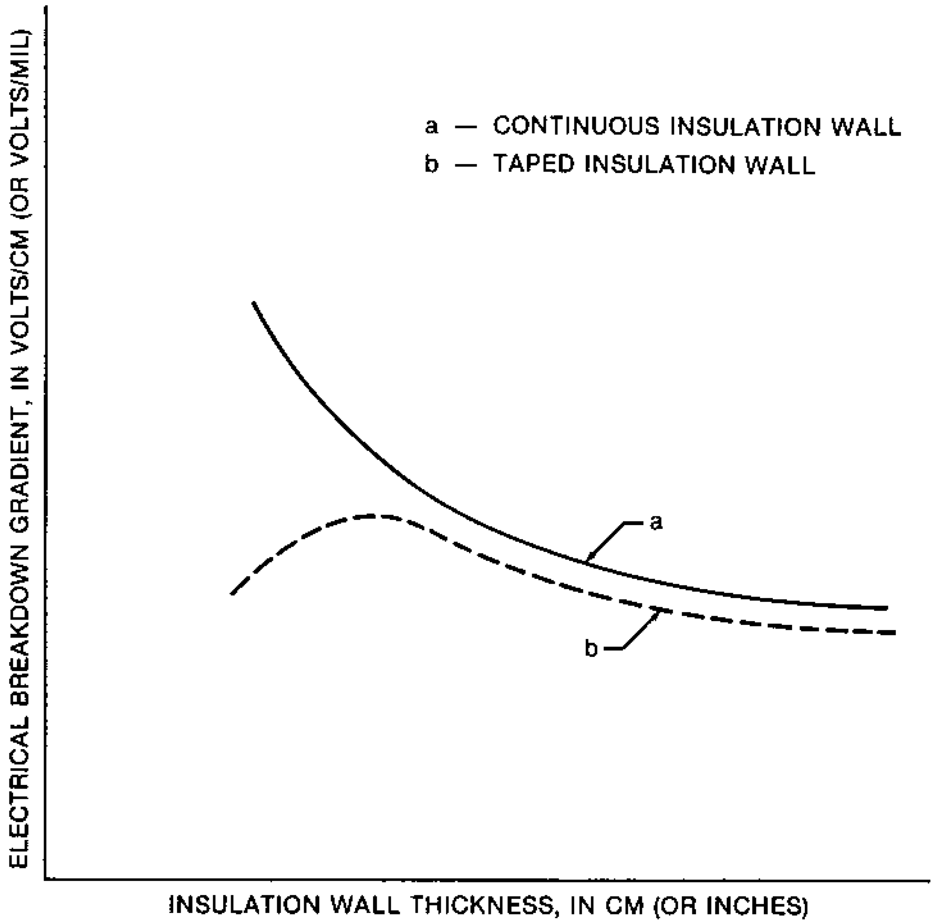

FIGURE 11.8 Electrical strength versus insulation wall thickness for hypothetical wrap and tape materials.

handle the voltage class. One consideration in determining the thickness of the ground wall for a given voltage class is to control internal corona (Section 11.8.).

Curve a of Fig. 11.8 shows electrical strength expressed as a gradient versus insulation-wall thickness for continuous materials such as those typically used for ground insulation. For composite wrap-type ground insulation, for example, the overall electrical strength expressed as an electrical-strength gradient decreases with increasing thickness, just as it does for the insulation components that form the system. Composite tape-type ground insulation, on the other hand, has a somewhat different characteristic of electrical-strength gradient versus thickness. Tape is applied circumferentially around the coil side, and the tape edges are either butt lapped or overlapped, such as half-lapped. For dielectric-strength reasons, the choice is usually to overlap the tape. If the tape is butt lapped, the line of the joints should coincide with the centerline of the previous course of tape, so as to maximize the amount of prime insulating material, instead of air or resin, throughout the insulation wall. Tape-type insulation is not as consistent as wrap-type insulation; this is true in particular for the first or second courses of tape. Accordingly, a tape-type insulation structure will exhibit a characteristic of electrical-strength gradient versus thickness similar to that shown in curve b of Fig. 11.8.

11.7.6 Mechanical Factors

It was noted earlier that if certain dielectric materials were mechanically stressed to a significant extent, the electrical strength of these materials would be adversely affected. This has been determined to be true in particular for dielectric materials that have a crystalline structure. Composite insulation systems used for insulating motor windings are typically made from components such as both flake and reconstituted mica tape or wrap, glass tape, various curing resins, and solid synthetic materials. These materials do not appear to be crystalline to any extent and thus the above-mentioned interaction between mechanical stress and electrical-breakdown stress does not exist to any degree in insulation systems for motor windings. However, certain mechanical factors do directly affect the service life of motor insulation.

As discussed earlier, squirrel-cage induction motors, which are started at full voltage and braked by application of reverse-sequence stator voltage, experience a stator current which is about 6 to 6.5 times that at rated-current full-speed conditions. The electromagnetic forces exerted on the stator-winding end turns associated with the flow of stator current are 35 to 40 times greater than at rated-current full-speed conditions, since such forces are proportional to the second power of the stator current. Thus if the end turns are inadequately braced, considerable flexure of the end turns occurs each time that the machine is started and each time that the voltage sequence is reversed in braking. Depending on the bracing design and on the amound of end-turn flexure permitted, a sufficient number of starts or reversals will cause insulation damage and in some cases, failure. However, since about the mid-1960s, most induction motors, in sizes for which end-turn flexure is significant, have been manufactured using bracing designs which greatly limit the amount of flexure possible. This improvement has resulted in a significant decrease in winding failures due to end-turn flexure.

Each coil side, located in its slot in the stator core, experiences the flow of an alternating current during operation, which causes the coil structure, including its insulation, to be subjected to alternating electromagnetic forces. The insulation system is capable of withstanding dynamical forces of the magnitude normally encountered, provided that the coils are tightly wedged. However, if the two coil sides are free to move within the slot, the dynamic forces will cause motion of the two coil sides, with eventual mechanical deterioration. It is for this reason that the coil sides must be tightly wedged within the slot. If the total conductor-copper thickness and vertical insulation buildup is such that they sum to less than the slot depth beneath the wedge, it is normal practice to use "filler strips" made from insulating material to fill the vertical void. It is also good practice to check the stator coils for tightness within the slots during periods of preventive maintenance of the motor. If the coil sides appear loose and if the design is such that the wedges can be removed without damage to the coils, a filler strip of the proper thickness should be located above the top coil and under the wedge, and then new wedges inserted.

The coefficients of thermal expansion of the various components of an insulation system are, as might be expected, not identical to each other. Also, the average coefficient of expansion of the insulation system is different from that of the copper conductor or the steel core. Thus, for long stator coils, the effect of differential thermal expansion can be significant. The layered structure of the prime insulation materials, such as mica tape, mica wrap, or glass tape, together with the flexibility of most of the resins used, tends to absorb the differential expansion to a reasonable extent. However, it is necessary to consider differential thermal expansion when designing and verifying a new insulation system, particularly for large machines.

11.7.7 Contaminants

Insulation systems are fabricated from components, some of which are organic and some of which are inorganic in chemical structure. Thus they are potentially susceptible to a wide range of chemical contaminants, ranging from acids to bases. Accordingly, it is important that adequate steps be taken early in the application stage to ensure that a clean supply of ventilating air is available for cooling the motor. This can be accomplished by proper choice of the motor enclosure or by installing a separate supply of clear air. However, for most motor applications, the two most prevalent contaminants, as well as the ones that cause the most problems, are water and conducting materials.

Water vapor is a component of air and, accordingly, is an ever-present part of the environment. Moisture, in the amount usually found in air, constitutes no problem to the insulation of an operating motor winding which is heated from its own I^2R losses. Water should not, of course, be able to enter the various motor-enclosure openings or to be drawn into the ventilating openings, due to the movement of the ventilating air. However, when a motor winding is not excited, care should be taken to keep the temperature of the insulation a few degrees above ambient temperature so that moisture will not collect on the surfaces of the insulation or, for old insulation, will not invade the insulation through any openings, such as between tape laps, etc. For mediums-sized and larger motors, this is usually done by space heaters installed inside the motor frame, which are excited when voltage is removed from the stator winding. It can also be done by applying a low voltage across the winding—sufficient to raise the winding temperature about 5°C but not sufficient to cause any rotation of the rotor.

Water on or within the insulation can have two adverse effects. It can, in some cases, cause dry contaminants, which might be on the surface of, or within, the insulation, to become more conductive. Also, it can significantly reduce the insulation resistance of the winding. Although insulation resistance is not directly related to the electrical-breakdown strength of insulation, there is an implicit relationship, such that a winding with a low insulation resistance is at increased risk of failure. The ratio of the insulation resistance, following a 10-minute test to that following a 1-minute test is called the polarization index. This ratio is a better indicator of the suitability of a winding for service than is a given value of insulation resistance alone. In general, a winding should not be considered suitable for service unless its polarization index is equal to 2.0 or more. This subject is discussed further in Section 11.14.

Conducting materials of various kinds are very prevalent in many of the environments in which induction motors are applied. Metal particles, in the form of chips, mill scale, and so on, can result from manufacturing processes being done in the general area. They can also result from repair work that was done in the area which required the sawing, drilling or other operations on metals, such as steel, copper, brass, or aluminum. If such metal residue is inadequately removed from the local area, such as being dispersed by an air-pressure hose instead of being collected by a vacuum cleaner, it will remain in the environment and can be drawn into the motor enclosure by high-velocity cooling air. Once inside the machine, some metal particles will lodge in the insulation wall, on the end turns, or in air ducts. Ferromagnetic material such as steel particles will be attracted by the rotating electromagnetic field and, again, caused to lodge into the insulation wall. At best, metal particles embedded within an insulation wall will degrade the insulation, by replacing dielectric material with highly conductive material. Also, there is some probability that a particle of metal could invade the winding sufficiently to make contact between two points separated by a potential difference, such as between a conductor and a stator-core tooth or between two conductors.

Carbon dust is an additional undesirable conducting contaminant for motor windings. It can result from a manufacturing process such as occurs in some parts of the rubber industry, for example. Also, it can be produced within a wound-rotor motor, due to wear of the carbon brushes on the collector rings, if the brush grade is improper for the current density, if the air is too dry in the vicinity of the collector, if the ambient temperature is too great, if the tangential speed of the rings is too great, or if the contact surface of the rings is not sufficiently smooth. In general, it is smaller in particle size than metal residue and can penetrate many windings. Also, in some older collector designs, which have axial, leading-edge voids between rings, sufficient carbon dust can collect as to cause significant tracking, with eventual flashover.

11.8 CORONA

Corona is a problem at the voltages for which formed coils are used for the stator winding and is not a problem at the voltages for which random coils are used. Corona results from the electrical breakdown of the gas within voids inside solid insulation, as well as on the surface of the insulation. In the case of motors, the gas that breaks down is usually air. Corona that occurs in voids within the insulation is called bulk, or volume, corona; that which occurs on the surface is called surface corona. For the insulation systems used on motor windings, such breakdown of air does not result in immediate failure of the insulation. However, it does have a long-time effect on insulation life, affecting some insulation materials more than others, and is a consideration in determining the working voltage gradient for insulation systems and in the selection of the prime insulating material for stator windings. The breakdown of air by an electric field results in the formation of ozone and nitrous oxide. Long-time exposure to corona activity will cause insulation deterioration, but some insulating materials, such as mica, are much less affected by corona action than are other materials.

The presence of corona-producing voids within the insulation wall can be controlled by use of coil-fabricating techniques, which cause the circumferential wraps and tapes to be compressed into a more compact mass. Also, the use of vacuum-pressure impregnation (VPI) techniques, as discussed in Section 9.2.6, is useful in reducing such voids. If the coil does not fit tightly into the slot, the corresponding gap can contain air which will break down electrically and cause slot corona. Again, this can be controlled by use of VPI techniques, in which a separate prewound core is wound, vacuum-pressure impregnated with resin, cured in an industrial oven, and then installed into the motor frame, as discussed in Section 9.2.7. For machines that are too large for VPI treatment, or for which such treatment has not been chosen, the outer surface of the coil for a length slightly greater than the slot length can be treated with a conducting paint. Thus those areas of the coil side that do not make contact with the side of the slot will be electrically in contact with the stator core and with ground potential.

The end turns, which extend beyond the two ends of the stator core, present a somewhat different configuration for corona than does the slot portion of the coil. The surface of the coil at the point where it emerges from the slot is at ground potential. The electrical gradient along the surface of the end turns is significant even for some distance toward the end of the coil. For high-voltage stators, this gradient can result in the electrical breakdown of air and hence in surface corona. However, by applying paint of the proper resistivity over a portion of the insulation surface of the end turns, a more favorable distribution of the voltage can be achieved and surface corona reduced or eliminated.

The cause of electrical breakdown of air which results in motor insulation can be understood in terms of the sparking potential of air and in terms of a capacitor model of insulation. Paschen's law, illustrated in Fig. 11.6, shows that for a given value of pressure p and for a fixed condition of the electrode geometry, the sparking voltage of air varies with the gap distance δ of the air void. Air voids within the insulation, as well as between the insulation surface and the steel slot side, are of random and nonuniform length, in the direction of the voltage gradient. Also, the geometry of the "electrodes" or equivalent capacitor plates varies widely. Thus electrode geometry is also random within the insulation. Accordingly, it is not appropriate to apply the data in Fig. 11.6 directly to the simplified two-capacitor model of the actual insulation. However, test data have been determined on the electrical breakdown of air voids in actual insulation. Such data, which have been collected in various forms for well over 50 years, would indicate that air breaks down at a gradient of 3.30 to 3.50 effective volts per 10^{-6} m, or about 85 to 90 effective volts/mil.

The dielectric constant K_a of air is equal to 1.0 and the dielectric constant of composite insulation K_i is equal to 3.0 or more. It was shown previously that for two capacitors connected in series, the ratio of electrical gradients is inversely proportional to the ratio of the dielectric constants. Thus, from eq. (11.43),

$$\frac{g_i}{g_a} = \frac{K_a}{K_i} \quad \text{numeric} \tag{11.65}$$

Solving for the electrical gradient of the insulation g_i, we have

$$g_i = g_a \frac{K_a}{K_i} \quad \text{volts/meter} \tag{11.66}$$

Using an average value of $g_a = 3.40$ V per 10^{-6} m for the breakdown of air and values of $K_a = 1.0$ and $K_i = 3.0$ for the dielectric constants of air and for composite insulation, respectively, in eq. (11.66),

$$g_i = (340)(1/3) = 1.13 \quad \text{volts}/10^{-6}\ \text{meter} \tag{11.67}$$

or, in terms of volts/mil,

$$g_i = \frac{(1.13)(10^3)}{39.37} = 28.7 \quad \text{volts/mil} \tag{11.68}$$

Thus corona could be expected to be present in higher-voltage insulation systems which are electrically stressed, with gradients in the region of 1.13 V per 10^{-6} m, or 28 V/mil.

11.9 CAPACITANCE TO GROUND

The stator-winding insulation is adjacent to the conductor copper on one side and to the slot wall of the stator core on the other side. The surface areas of contact on both sides are considerable relative to the scale of the motor. This configuration, then, constitutes an extended capacitor, with one plate at winding potential, with the other plate at ground potential, and with the insulation serving as the dielectric medium. The resulting capacitance of this extended capacitor is called the capacitance to ground of the stator winding.

There is a reactive or charging kVA associated with the winding capacitance to ground. Thus when conducting tests on the insulation of large motors located at remote sites, it is necessary to compute an approximate value of the charging kVA, so that an adequately sized transformer can be made available for the testing. For large generators, knowledge of the winding capacitance to ground is occasionally useful for establishing proper grounding and for calculating system-recovery voltage.

Capacitance to ground is calculated by use of a parallel-plate capacitor model, since such a model corresponds to the actual physical configuration to a reasonable extent. In eq. (11.28), the capacitance for such a capacitor was shown to be

$$C = \frac{KA \times 10^{-9}}{36\pi d} = \frac{KA \times 10^{-9}}{36\pi t_i} \quad \text{farads/winding} \tag{11.69}$$

In this case, K, A, and t_i correspond to the following machine quantities:

K = average dielectric constant of the insulation, from the copper conductor to the steel wall of the slot; typically between 3.0 and 4.0, dimensionless

A = entire area of the winding that is in contact with the steel slots, meters^2

t_i = insulation thickness, from the copper conductor to the steel wall of the slot, meters

To determine the area A of the plates of the capacitor model for formed-coil windings, the appropriate peripheries of the winding copper and of the steel slot will first be determined and their values then averaged to obtain the average effective periphery. This effective periphery will then be multiplied by a corresponding effective slot length and by the number of slots, to give the area of the plates. The periphery around the three pertinent sides of the copper conductors which is common to both the copper and the insulation is equal to

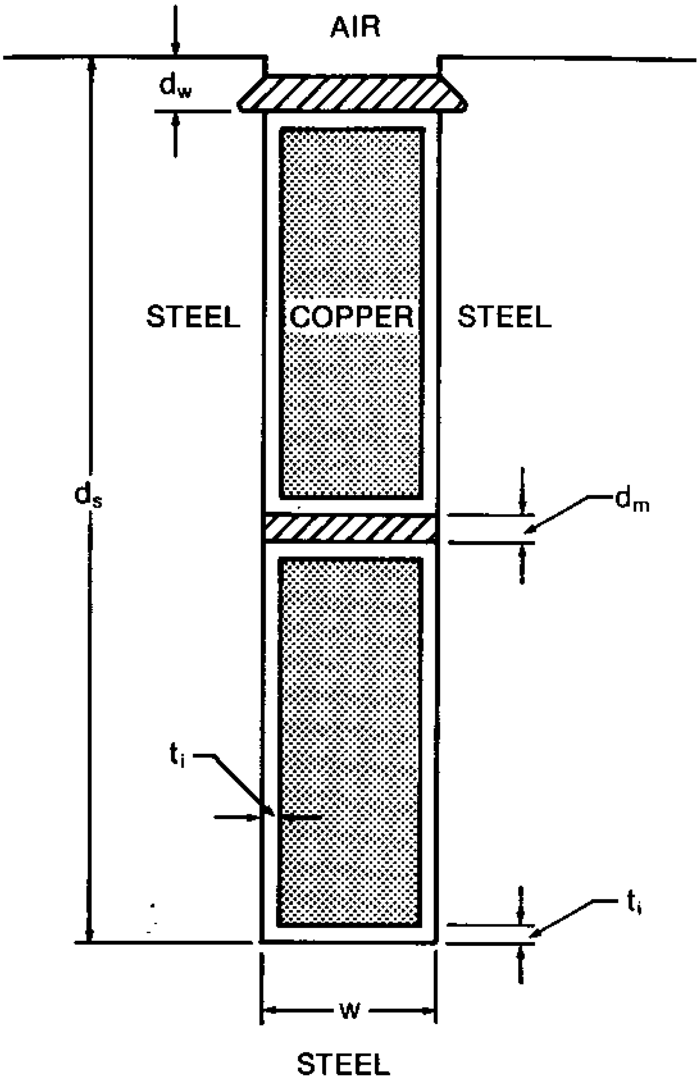

FIGURE 11.9 Stator-slot geometry used for calculating winding capacitance to ground.

$$P_{cu} = 2(d_s - d_w - d_m - 4t_i) + w - 2t_i \quad \text{meters} \tag{11.70}$$

where the quantities are as defined in Fig. 11.9. The periphery around the three sides of the steel slot which is common to both the steel and the insulation is equal to

$$P_s = 2(d_s - d_w) + w \quad \text{meters} \tag{11.71}$$

The average effective periphery is

$$P = \frac{P_{cu} + P_s}{2} = 2d_s - 2d_w - d_m - 5t_i + w \quad \text{meters} \tag{11.72}$$

The effective slot length is equal to the gross length of core ℓ_c in meters, less the total axial length of the radial ventilating ducts, if any, in the core. Then

$$\ell_e = \ell_c - N_d w_d \quad \text{meters} \tag{11.73}$$

where N_d is the number of radial ventilating ducts and w_d is the width of each radial ventilating duct in meters. The area A of the plates is then equal to

$$A = N_1 P \ell_e = N_1(2d_s - 2d_w - d_m - 5t_i + w)(\ell_c - N_d w_d) \quad \text{meters}^2 \tag{11.74}$$

where N_1 is the number of stator slots. The winding capacitance to ground is determined by calculating the plate area A, by use of eqs. (11.72), (11.73), and (11.74). Then, using this value of A together with the proper value for t_i and K, the winding capacitance to ground is calculated by use of eq. (11.69). This value of capacitance as calculated by eq. (11.69) is for the entire three-phase winding. If two of the phases are grounded and the capacitance to ground of the remaining phase determined, experience indicates that it is about 40% instead of 33% of the three-phase capacitance. Then

$$C_p = 0.4C \quad \text{farads/phase} \tag{11.75}$$

where C_p is the capacitance of the phase winding and C is the capacitance of the entire three-phase winding.

The equation for the effective perimeter P in eq. (11.72) is based on a formed-coil winding, since the need for calculating the capacitance to ground is much greater for the larger ratings, which use formed coils. If it is desired to calculate the capacitance to ground for a random winding, the value of P is calculated in a slightly different and somewhat simpler manner. Refer to the cross-sectioned sketch of a random coil and slot, which is shown in Fig. 9.6. The value of P is calculated as the perimeter of the slot-liner insulation, less the width of the bottom of the slot wedge. The remainder of the calculation in determining the winding capacitance is performed in the same manner as for a formed-coil winding.

The equation for calculating the entire winding capacitance to ground, eq. (11.69), was derived in terms of the MKS system of units. That equation can be changed to accept dimensions in inches by remembering that there are 39.37 inches in 1.0 meter. Accordingly,

$$C = \frac{KA \times 10^{-9}}{36\pi t_i} \frac{1}{39.37} = 0.225 \frac{KA}{t_i} \times 10^{-12} \quad \text{farads/winding} \tag{11.76}$$

where t_i is in inches and A is in inches^2.

11.10 CHARGING CURRENT AND CHARGING VOLT-AMPERES FOR HIGH-POTENTIAL TESTING

The windings of rotating electrical machinery built in the United States are given a high-potential test equal to 2 × (rated voltage) + 1000 V to ground from a 60-Hz source prior to shipment. The winding must successfully withstand such a high potential for 1 minute to complete the test successfully. At various stages of manufacture, the winding receives a considerably greater test voltage to ground, with the value above being the final and confirming test prior to shipment. Because of the aforementioned distributed winding capacitance to ground, there is an associated charging current and charging volt-amperes which determines the size of the step-up transformer required for conducting the test. In conducting the test, the ground insulation of each phase is normally tested separately, with both ends of the other two phases connected to ground. Machines which are subsequently rewound are also given such a test. In addition, machines in service may from time to time be given a somewhat reduced high-potential test to determine that the insulation is adequate. Thus high-potential tests are very useful.

If there was no other component of current than that which sustains the reactive volt-amperes, the charging current would be equal to the test voltage V_t, divided by the impedance, which would be essentially all capacitive reactance X_{ct}, or

$$I = \frac{jV_t}{X_{ct}} = -j2\pi fC_pV_t \quad \text{amperes/phase} \tag{11.77}$$

or, in terms of magnitude only,

$$I = 2\pi fC_pV_t \quad \text{amperes/phase} \tag{11.78}$$

However, as discussed earlier in this chapter, a component of current that sustains dielectric loss and a component of conduction current is also present (refer to Fig. 11.5). It is impractical to attempt to calculate the foregoing two components of test current, considering the variations in insulation, the inexactness of the parameters involved, and so on. However, these components can be included for typical insulation in the total dielectric current, or "charging current," by use of an empirical factor k_i, which varies with the ratio of test voltage to rated voltage. Such values of k_i are tabulated in Table 11.2. Then the current flow associated with applying a high-potential test to one phase of a winding and which has come to be called the charging current throughout industry is equal to

$$I_{ch} = 2\pi fk_iC_pV_t \quad \text{amperes/phase} \tag{11.79}$$

The value of I_{ch} is not a very large quantity when expressed in amperes. When expressed in milliamperes, it is equal to

TABLE 11.2 Tabulation of Empirical Factor Used in Calculating Charging Current for High-Potential Testing

Test voltage/rated voltage	Value of k_i
1.00	1.00
1.25	1.03
1.50	1.05
1.75	1.10
2.00	1.15
2.25	1.20
2.50	1.25

$$I_{ch} = 2\pi f k_i C_p V_t \times 10^3 \quad \text{milliamperes/phase} \tag{11.80}$$

The associated volt-amperes is equal to

$$(VA)_{ch} = V_t I_{ch} \quad \text{volt-amperes/phase} \tag{11.81}$$

when I_{ch} is expressed in amperes.

11.11 NUMERICAL EXAMPLE OF CALCULATION OF PHASE-WINDING CAPACITANCE TO GROUND, CHARGING CURRENT, AND CHARGING VOLT-AMPERES

Calculation of the capacitance to ground, the charging current, and the charging volt-amperes will be illustrated by using the stator-slot dimensions shown in Fig. 9.14. Since the dimensions shown in Fig. 9.14 are in inches, the calculation of the phase-winding capacitance to ground will use inches instead of metric units. Further, it will be assumed that the number of stator slots N_1, the gross length of the stator core ℓ_c, the number of radial air ducts N_d, and the axial dimensions of each stator duct W_d are as follows:

$N_1 = 84$

$\ell_c = 38$ in.

$N_d = 19$

$w_d = 0.250$ in.

The remainder of the required parameters are available from an inspection of Fig. 9.14. The average, effective periphery of the slot insulation is given in eq. (11.72), which is applicable to inch units as well as to metric units. Then

$$P = 2d_s - 2d_w - d_m - 5t_m + w \quad \text{inches} \tag{11.82}$$

Substituting the appropriate dimensions from Fig. 9.14 into eq. (11.82) yields

$$P = (2)(2.50) - (2)(0.150) - (0.075) - (5)(0.075) + 0.600 = 4.85 \quad \text{inches} \tag{11.83}$$

To obtain the effective slot length, the total radial air duct space must be subtracted, because of the absence of the stator-core steel within the duct space. The effective slot length as given in eq. (11.73) is also applicable to inch units as well as to metric units. Then

$$\ell_e = \ell_c - N_d w_d \quad \text{inches} \tag{11.84}$$

Selecting the corresponding dimensions from the tabulation above and substituting them into eq. (11.84), we have

$$\ell_e = 38 - (19)(0.25) = 33.25 \quad \text{inches} \tag{11.85}$$

Similarly, eq. (11.74) is applicable for calculating the plate area in units of inches^2 as well as in meters^2. Then

$$A = N_1 P \ell_e \quad \text{inches}^2 \tag{11.86}$$

Substituting the appropriate values into eq. (11.86) gives us

$$A = (84)(4.85)(33.25) = 13{,}546 \quad \text{inches}^2 \tag{11.87}$$

The winding capacitance to ground C, using dimensional units in inches, is shown in eq. (11.76) to be

$$C = 0.225 \frac{KA}{t_i} \times 10^{-12} \quad \text{farads/winding} \tag{11.88}$$

It will be assumed that the stator winding insulation is primarily mica, with a dielectric constant K equal to 4.0. Then, substituting K, A, and t_i into eq. (11.88) yields

$$C = \frac{(0.225)(4)(13,564)}{0.075} \times 10^{-12} = 0.162 \times 10^{-6} \quad \text{farads/winding} \tag{11.89}$$

The value above is the capacitance to ground of the entire stator winding. A high-potential test is usually accomplished by testing one phase at a time with voltage applied from copper to ground, with both ends of the other two phases connected to ground. The phase-winding capacitance to ground, in terms of the total winding capacitance to ground, is given in eq. (11.75) as

$$C_p = 0.4C \quad \text{farads/phase} \tag{11.90}$$

or, for this example,

$$C_p = (0.4)(0.162 \times 10^{-6}) = 0.065 \times 10^{-6} \quad \text{farads/phase} \tag{11.91}$$

which is the calculated phase-winding capacitance to ground.

Since the subject winding has a voltage rating of 4000 V, the final high-potential test is conducted at (2)(4000) + 1000 = 9000 V to ground at 60 Hz for 1 minute. From eq. (11.80), the charging current in milliamperes is equal to

$$I_{ch} = 2\pi f k_i C_p V_t \times 10^3 \quad \text{milliamperes/phase} \tag{11.92}$$

From Table 11.2, $k_i = 1.2$ for a value of $V_t/V_s = 9000/4000 = 2.25$. Substituting this value together with the other pertinent values into eq. (11.92), we obtain

$$I_{ch} = (2)(\pi)(60)(1.2)(0.065 \times 10^{-6})(9000)(10^3) = 265 \quad \text{milliamperes/phase} \tag{11.93}$$

or 0.265 A per phase. From eq. (11.81), the corresponding charging volt-amperes is equal to

$$(VA)_{ch} = V_t I_{ch} \quad \text{volt-amperes/phase} \tag{11.94}$$

Substituting the value of the test voltage V_t and the charging current I_{ch} into eq. (11.94) yields

$$(VA)_{ch} = (9000)(0.265) = 2385 \quad \text{volt-amperes/phase} \tag{11.95}$$

Thus a step-up transformer of about 2.5 kVA is required for the high-potential test when testing one phase at a time.

11.12 WINDING SURGES

As mentioned earlier, voltage surges with steep wavefronts are produced by lightning strokes on transmission and distribution lines, on exposed components in substations, and on other exposed electrical system components. They are also produced by switching, by intermittent short circuits, and depending on the electrical system involved, by other sources. The ability of a given insulation system to withstand short-time overvoltages is significantly greater than its ability to withstand a long-time overvoltage. However, repeated overvoltages, even of short duration, will have a cumulative effect in weakening insulation and can ultimately result in failure.

The stator windings of motors may be connected to distribution lines of the same nominal voltage, or the motors may be located near substations, at which the voltage has been reduced to utilization level by transformation. In either case, however, the motor windings are subjected to whatever voltage surges might exist in the voltage supply. As detection and measuring equipment have improved over the years, it has become apparent that a greater number of surges occur than previously thought and that surges can have steeper wavefronts than previously thought.

The subject of surges is a complicated one and the various approaches used in analyzing surges are not necessarily identical. Complete books have been devoted to the subject of voltage surges in electrical equipment. The subject is a concentrated and highly specialized field of electrical engineering. However, because of the significance of the subject, particularly as it applies to insulation life, there is a need for many engineers to have some knowledge of the basic relationships between distributed inductance, distributed capacitance, surge impedance, and so on, of windings, all of which are important in the basic understanding of voltage surges and in protecting against them. Thus it is appropriate that the subject be included as one of the topics in understanding induction-motor behavior. The treatment of the subject must, of necessity, be cursory and have, as its goal, only the basic understanding of the subject.

The stator winding is an iterative structure, that is, there is a recurrence of similar elements along its length. Such recurring elements can be based on (1) inductors (i.e., half-turns), (2) turns, (3) coils, or (4) groups of coils. The inductors, or half-turns, and the complete turns have series impedance along their lengths. They have distributed capacitance and distributed conductance to ground for that portion of their length within the core. In addition, there is inductor-to-inductor or turn-to-turn capacitance for their full respective lengths. The coils, considered as the base, have series impedances along their full lengths and have distributed capacitance and distributed conductance to ground for that portion of their length within the core. Further, there is some mutual reactance between coils. Although groups do constitute recurring entities in a winding, they are limited in quantity, as there are only p groups in a phase winding. A two-pole phase winding, for example, has only two groups per phase. The base that recurs in the greatest quantity, within a winding, is the inductor or half-turn.

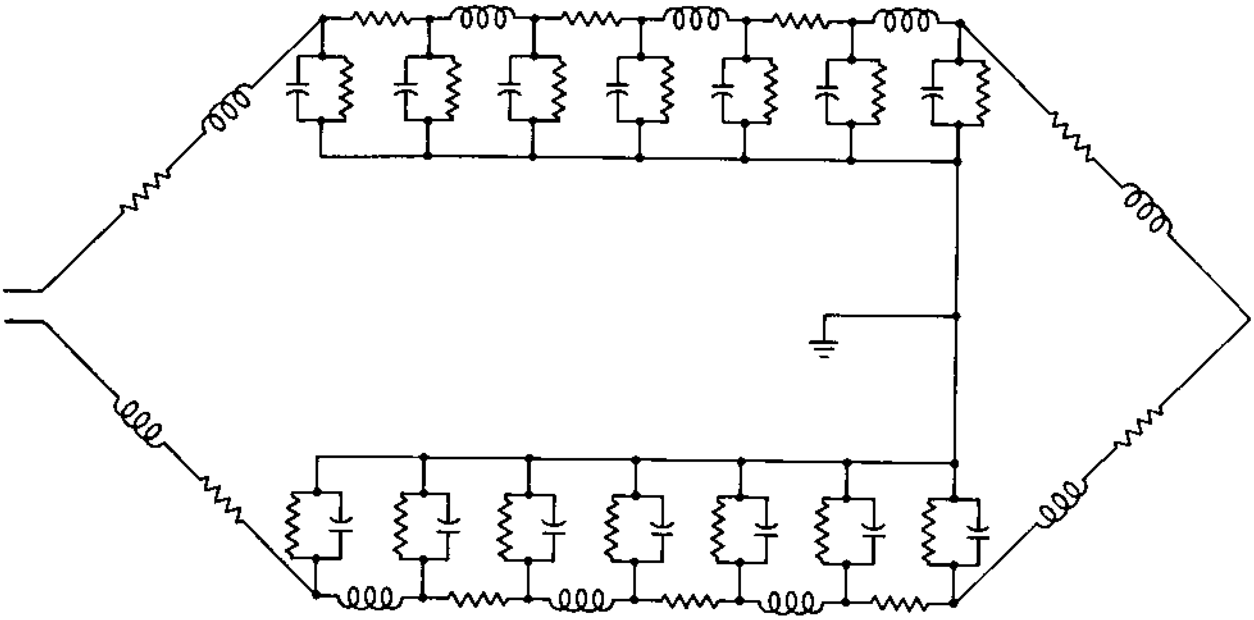

FIGURE 11.10 Schematic representation of a stator coil as the physical base for iterative structures.

However, for a cursory analysis of surge phenomenon, the effort is simplified if the coil is used as the physical base. This choice neglects the effect of turn-to-turn capacitance in the initial analysis, but that effect will be considered subsequently. Figure 11.10 shows a physical model that represents such a base.

In Fig. 11.10, the series impedance consists of the coil resistance, which is distributed along some length of the coil, and of coil reactance, which is also distributed along some length of the coil. However, the reactance distribution per unit of coil length is different between the slot portion and the end-turn portion of the coil, because of the difference in general configuration of the two portions and because the slot portion is embedded within the steel slot. The shunt impedance to ground consists of the distributed coil capacitance to ground and of the distributed resistance to ground through the ground insulation. The shunt impedance to ground is shown as distributed along the slot portion of the coil only, because the coil is embedded within the steel core for only that portion of the coil. Actually, for larger machines, both circumferential and radial bracing structures, frequently made of metal and at ground potential, are positioned around the OD of the end turns. Thus, for such designs, there is some admittance to ground for the end-turn portion of the coil. However, this is a small percentage of that for the slot portion and can be ignored. Also, for the high-frequency harmonics, associated with the steep wavefront of a surge, there is an implied resistance, due to eddy-current loss in the core, which is in parallel with the series reactance. This is not considered in the physical model, shown in Fig. 11.10, but the effect of such eddy-current losses will subsequently be considered.

The network shown in Fig. 11.10 is linear and free of internal voltages. Accordingly, in common with this type of network, it can be represented by an equivalent-T network, at least at a given frequency. Further, since it is bilateral, the resulting network will be symmetrical so that the series impedance can be split between the two sides. At this point it is not claimed that the network is valid over a range of frequencies and that important characteristic will be addressed subsequently. Then the network shown in Fig. 11.11 between terminals 1 and 2 and terminals 3 and 4, with lumped parameters, represents some length ℓ along the coil.

Let the variable impedance Z_L be placed across the output terminals 3 and 4 of the equivalent-T network. If this variable impedance is set at $Z_L = 0$, the network output is short circuited. Then, by inspection of Fig. 11.11, the input impedance Z_{in} is equal to

$$Z_{in} = Z_{sc} = \frac{Z_A}{2} + \frac{Z_A Z_B}{Z_A + 2Z_B} \quad \text{ohms} \tag{11.96}$$

If the external impedance is disconnected for the moment, then $Z_L = \infty$ and the network output is open circuited. Then, by inspection of Fig. 11.11, Z_{in} is equal to

$$Z_{in} = Z_{oc} = \frac{Z_A}{2} + Z_B \quad \text{ohms} \tag{11.97}$$

If a succession of identical T-section networks, such as shown in Fig. 11.11, are connected in series, that is, with terminals 1 and 2 of each successive one connected to terminals 3 and 4 of the previous one, the input

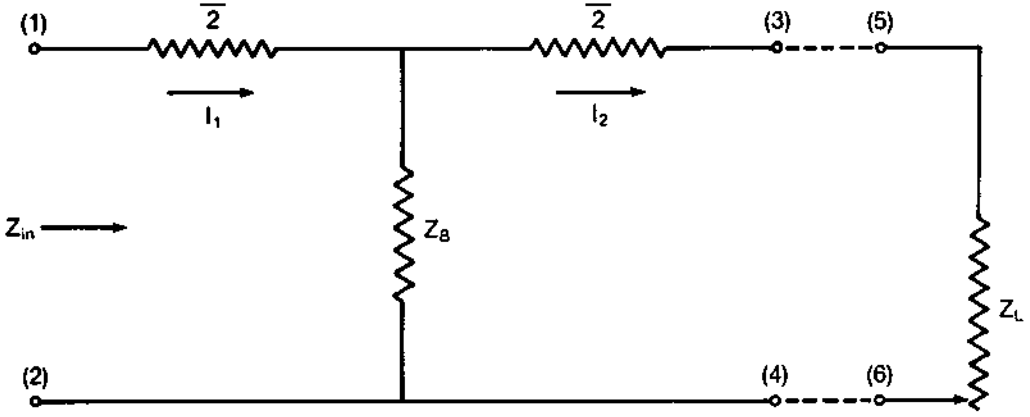

FIGURE 11.11 Equivalent-T network of the network in Fig. 11.10 with impedance Z_L added.

impedance Z_{in} of the first section will, of course, change. As the number of such sections are added, the value of Z_{in} will increase and approach a finite and limiting asymptotical value Z_0. This asymptote is the value that would ultimately be reached if sections were added without limit. It is apparent that after a large number of sections have been added, one section could be added or removed without the value of Z_0 being apparently affected. Accordingly, if one T section is connected to an impedance equal to Z_0 (i.e., if $Z_L = Z_0$ in Fig. 11.11), the input impedance Z_{in} would also equal Z_0. Z_0 is alternatively called the iterative impedance, the characteristic impedance, or the surge impedance.

Let Z_R in Fig. 11.11 be set at $Z_R = Z_0$. Then, from the above, Z_{in} is also equal to Z_0 under these conditions. From an inspection of Fig. 11.11,

$$Z_{in} = Z_0 = \frac{Z_A}{2} + \frac{Z_B(Z_A/2 + Z_0)}{Z_A/2 + Z_B + Z_0} \quad \text{ohms} \tag{11.98}$$

Solving for Z_0 yields

$$Z_0^2 = \frac{Z_A^2}{4} + Z_A Z_B \quad \text{ohms}^2 \tag{11.99}$$

and

$$Z_0 = \sqrt{\frac{Z_A^2}{4} + Z_A Z_B} \quad \text{ohms} \tag{11.100}$$

Multiplying Z_{sc} in eq. (11.96) by Z_{oc} in eq. (11.97) gives us

$$Z_{sc} Z_{oc} = \left(\frac{Z_A}{2} + \frac{Z_A Z_B}{Z_A + 2Z_B}\right)\left(\frac{Z_A}{2} + Z_B\right) \quad \text{ohms}^2 \tag{11.101}$$

which simplifies to

$$Z_{sc} Z_{oc} = \frac{Z_A^2}{4} + Z_A Z_B \quad \text{ohms}^2 \tag{11.102}$$

However, from eq. (11.100),

$$Z_0^2 = \frac{Z_A^2}{4} + Z_A Z_B \quad \text{ohms}^2 \tag{11.103}$$

Substituting eq. (11.103) into eq. (11.102), we have

$$Z_0^2 = Z_{sc} Z_{oc} \quad \text{ohms}^2 \tag{11.104}$$

or

$$Z_0 = \sqrt{Z_{sc} Z_{oc}} = \sqrt{\frac{Z_A^2}{4} + Z_A Z_B} \quad \text{ohms} \tag{11.105}$$

Thus the surge impedance of a large number of iterative impedance and admittance elements which are connected in series can be related to impedance tests made on one of the elements. A phase winding is not necessarily equivalent to that of a long telephone line, for example, in the number of respective impedance elements in series. However, as an electrical structure that is built up from repetitive lengths ℓ, within the winding, its impedance, consisting of both series impedance and shunt impedance (or admittance to ground), tends to approach a limiting value. Thus the concept of surge impedance is useful, although not perfect, in visualizing the behavior of a stator winding subjected to an incoming surge.

The rate of propagation of a surge through a phase winding can be understood in terms of the propagation constant of an element of an iterative structure. Again, let $Z_L = Z_0$ in Fig. 11.11. Then, from an inspection of the figure, the ratio of the current input at terminals 1 and 2 to the current output at terminals 3 and 4 is equal to

$$\frac{I_1}{I_2} = \frac{Z_A/2 + Z_B + Z_0}{Z_B} = 1 + \frac{Z_A}{2Z_B} + \frac{Z_0}{Z_B} \quad \text{numeric} \tag{11.106}$$

Expressing the ratio I_1/I_2 as an exponential function of ϵ, the base of the natural logarithm, we have

$$\frac{I_1}{I_2} = \epsilon^{\gamma} = 1 + \frac{Z_A}{2Z_B} + \frac{Z_0}{Z_B} \quad \text{numeric} \tag{11.107}$$

where γ is a complex quantity called the propagation constant. Breaking γ into its real and imaginary parts, we have

$$\gamma = \alpha + j\beta \quad \text{radians/meter} \tag{11.108}$$

For n such iterative elements in series, the propagation constant is equal to

$$n\gamma = n\alpha + jn\beta \quad \text{radians/meter} \tag{11.109}$$

From eq. (11.107), the output current and voltage will both have a phase shift relative to the input current and voltage. This phase shift will be cumulative and for n elements in series, it will be equal to $n\beta$. Then, along the n-element length, the current will have a sinusoidal distribution and the distance between two corresponding points, such as between two adjacent maximum values on this "wave," will equal one "wavelength." If $N_{w\ell}$ is the number of elements per wavelength, then

$$N_{w\ell}\beta = 2\pi \quad \text{radians} \tag{11.110}$$

$$N_{w\ell} = \frac{2\pi}{\beta} \quad \text{numeric} \tag{11.111}$$

Since the wave propagates at a velocity of one wavelength per cycle, the velocity of the wave is

$$V = N_{w\ell}f = \frac{2\pi f}{\beta} = \frac{\omega}{\beta} \quad \text{meters/second} \tag{11.112}$$

The equivalent-T network, used to represent an iterative element within the stator-phase winding, was constructed from lumped parameters Z_A and Z_B for some winding length ℓ. As such, the T network is valid at only a single frequency, and eqs. (11.105) and (11.112), which were derived from it, are also valid at only the same frequency, in general. To approach an equivalency to the phase winding, subjected to a surge, it is necessary to break the coils (or winding) into small lengths, with inductance, capacitance, and resistance, which will hold for a wide range of frequencies. Pursuant to this, let $\Delta\ell$ be a small but representative distance along the coil. Let Z be the series coil impedance per unit length of the phase winding, and let Y be the admittance to ground of the coil per unit length of the winding. Then

$$Z_A = Z\,\Delta\ell \quad \text{ohms} \tag{11.113}$$

and

$$Z_B = \frac{1}{Y\,\Delta\ell} \quad \text{ohms} \tag{11.114}$$

The surge impedance, as derived in eq. (11.105), is equal to

$$Z_0 = \sqrt{\frac{Z_A^2}{4} + Z_A Z_B} \quad \text{ohms} \tag{11.115}$$

Substituting eq. (11.113) and eq. (11.114) into eq. (11.115) yields

$$Z_0 = \sqrt{\frac{(Z\,\Delta\ell)^2}{4} + \frac{Z}{Y}} \quad \text{ohms} \tag{11.116}$$

The surge impedance, for a winding with distributed series impedance and with distributed admittance to ground, is equal to the limit of eq. (11.116) as $\Delta\ell$ approaches zero. Then

$$Z_0 = \lim_{\Delta\ell \to 0} \sqrt{\frac{(Z\,\Delta\ell)^2}{4} + \frac{Z}{Y}} = \sqrt{\frac{Z}{Y}} \quad \text{ohms} \tag{11.117}$$

Since the series resistance is small, in comparison to the series reactance, the magnitude of Z is determined primarily by the series reactance ωL. Similarly, the conductance to ground is small compared to the capacitive susceptance to ground. Accordingly, the magnitude of Y is determined primarily by the capacitive susceptance ωC. Then eq. (11.117) can be written as

$$Z_0 = \sqrt{\frac{Z}{Y}} = \sqrt{\frac{L}{C}} \quad \text{ohms} \tag{11.118}$$

which is independent of frequency.

It is desirable to obtain an expression for the velocity of propagation of a surge as given in eq. (11.112), in a form which is also independent of frequency. From eq. (11.107),

$$\epsilon^{\gamma} = 1 + \frac{Z_A}{2Z_B} + \frac{Z_0}{Z_B} \quad \text{numeric} \tag{11.119}$$

but from eq. (11.105),

$$Z_0 = \sqrt{Z_A Z_B + \left(\frac{Z_A}{2}\right)^2} \quad \text{ohms} \tag{11.120}$$

Substituting eq. (11.120) into eq. (11.119) gives us

$$\epsilon^{\gamma} = 1 + \frac{Z_A}{2Z_B} + \sqrt{\frac{Z_A}{Z_B} + \left(\frac{Z_A}{2Z_B}\right)^2} \quad \text{numeric} \tag{11.121}$$

The third term of eq. (11.121) can be expanded by the binomial expansion. For n = 1/2, this expansion is

$$(a+b)^{1/2} = a^{1/2} + \frac{a^{-1/2}b}{2} - \frac{a^{-3/2}b^2}{8} + \cdots \quad \text{numeric} \qquad (11.122)$$

Substituting the third term of eq. (11.121) into eq. (11.122), to obtain its binomial expansion, we have

$$\sqrt{\frac{Z_A}{Z_B} + \left(\frac{Z_A}{2Z_B}\right)^2} = \left(\frac{Z_A}{Z_B}\right)^{1/2} + 1/2\left(\frac{Z_A}{Z_B}\right)^{-1/2}\left(\frac{Z_A}{2Z_B}\right)^2 + \cdots \quad \text{numeric} \qquad (11.123)$$

Then, rewriting eq. (11.121), with the third term expanded in accordance with eq. (11.123), yields

$$\epsilon^{\gamma} = 1 + \frac{Z_A}{2Z_B} + \left(\frac{Z_A}{Z_B}\right)^{1/2} + 1/2\left(\frac{Z_A}{Z_B}\right)^{-1/2}\left(\frac{Z_A}{2Z_B}\right)^2 + \cdots \quad \text{numeric} \qquad (11.124)$$

Simplifying eq. (11.124) gives us

$$\epsilon^{\gamma} = 1 + \frac{Z_A}{2Z_B} + \left(\frac{Z_A}{Z_B}\right)^{1/2} + \frac{1}{8}\left(\frac{Z_A}{Z_B}\right)^{3/2} + \cdots \quad \text{numeric} \qquad (11.125)$$

Again, using the concept of having a small length $\Delta\ell$ be a small representative length along the phase winding, and substituting the resulting equivalents of Z_A and Z_B from eqs. (11.113) and (11.114), respectively, into eq. (11.125), we obtain

$$\epsilon^{\gamma} = 1 + \frac{1}{2}ZY(\Delta\ell)^2 + (ZY)^{1/2}\,\Delta\ell + \frac{1}{8}(ZY)^{3/2}(\Delta\ell)^3 + \cdots \quad \text{numeric} \qquad (11.126)$$

Rearranging eq. (11.126) in terms of increasing powers of ZY gives us

$$\epsilon^{\gamma} = 1 + (ZY)^{1/2}\,\Delta\ell + \frac{1}{2}(ZY)(\Delta\ell)^2 + \frac{1}{8}(ZY)^{3/2}(\Delta\ell)^3 + \cdots \quad \text{numeric} \qquad (11.127)$$

The classical expansion of ϵ^{γ} into an exponential series is

$$\epsilon^{\gamma} = 1 + \gamma + \frac{\gamma^2}{2!} + \frac{\gamma^3}{3!} + \cdots \quad \text{numeric} \tag{11.128}$$

It should be noted that the nth term of eq. (11.127) contains $(\Delta\ell)^{n-1}$, which rapidly converges the series, and the series is essentially equal to its first three terms. Equations (11.127) and (11.128) are the same series and, accordingly, corresponding terms of the two series are equal to each other. Then, equating the second term of eq. (11.127) to the corresponding term of eq. (11.128), we have

$$\gamma = \sqrt{ZY}\ \Delta\ell \quad \text{radians/meter} \tag{11.129}$$

where γ is the propagation constant for a length $\Delta\ell$. For unit length, $\ell = 1$, and the propagation constant is

$$\gamma = (\sqrt{ZY}\ \Delta\ell)\frac{1}{\Delta\ell} = \sqrt{ZY} \quad \text{radians/meter} \tag{11.130}$$

Again, since the series resistance is small compared to the series reactance, Z is essentially equal to ωL, and since the conductance to ground is small compared to the capacitive susceptance to ground, Y is essentially equal to ωC. Substituting these values into eq. (11.130) for Z and Y yields

$$\gamma = \omega\sqrt{LC} \quad \text{radians/meter} \tag{11.131}$$

Since from eq. (11.108), $\gamma = \alpha + j\beta$, eq. (11.131) can be written as

$$\alpha + j\beta = \omega\sqrt{LC} \quad \text{radians/meter} \tag{11.132}$$

The term α is the attenuation factor and the term β is the wavelength factor. Since series resistance and conductance to ground are not being considered, α can be neglected and only the magnitude of β used. Then

$$\beta = \omega\sqrt{LC} \quad \text{radians/meter} \tag{11.133}$$

From eq. (11.112), the velocity of propagation of the surge is

$$V = \frac{\omega}{\beta} \quad \text{meters/second} \tag{11.134}$$

Substituting eq. (11.133) into eq. (11.134) gives us

$$V = \frac{1}{\sqrt{LC}} \quad \text{meters/second} \tag{11.135}$$

which is the velocity of propagation of surge through a motor winding.

To summarize, the impedance exhibited by a winding to an incoming surge is approximately equal to $Z_0 = \sqrt{L/C}$ ohms and the velocity of propagation of that surge through the winding is approximately equal to $V = \sqrt{1/LC}$ meters/second. L is the distributed series inductance per unit length of the winding, and C is the distributed capacitance to ground per unit length of the winding. The values of C and L are different between the slot portion and the end-turn portion of the phase winding. The capacitance to ground and the leakage reactance is much greater for the slot portion, because of the close proximity of the slot steel. Accordingly, the velocity of propagation of the surge through this portion of the winding is considerably less. In many cases, it is an order of magnitude less than that through the end-turn portion. A typical velocity through the slot portion is 15 to 20 m/μs and a typical velocity through the end-turn portion is 150 to 200 m/μs.

The values of C and L to use in determining surge impedance Z_0 are the weighted average of that for the slot portion and for the end-turn portion per unit length of the phase winding. The value of the surge impedance of a motor winding, as seen between one stator-phase terminal and ground, is typically between 600 and 900 Ω. On the other hand, the value of the surge impedance for the electrical system, which connects to the motor, is usually less. Distribution power cables have typical values of Z_0 between 35 and 60 Ω and overhead distribution lines have typical values between 350 and 450 Ω.

When a surge enters a phase winding, it propagates along the conductor, decreasing its velocity in the slot portion, and increasing its velocity in the end-turn portion of the winding. The time required for the wave to propagate to the neutral end of the phase winding varies from 100 μs to a fraction of that time. If the neutral is ungrounded, the wave is reflected back toward the terminal end of the phase, at double peak value and at the same velocity. At the terminal end, part of the reflected wave continues out onto the line, and part is reflected from the terminals toward the neutral again, but with a change in sign. This process continues until the surge has dissipated. Such dissipation results from the successive loss of part of the wave each time it returns to the terminal end of the winding and from losses associated with the aforementioned eddy currents within the magnetic core. The steep front, as well as other parts of the wave, when analyzed by Fourier analysis, is equivalent to a band of high-frequency oscillations, and these oscillations cause eddy-current losses in the steel core. It should be recognized that the foregoing discussion of reflections that occur within a phase winding with an ungrounded neutral is somewhat idealized. Depending on the equivalent impedance of the ungrounded neutral, as seen by a surge that is traveling toward it, the reflections can be somewhat distorted.

If the neutral end of the phase is grounded, the behavior of the surge is essentially the same, except that the reflections which occur at the neutral end of the winding reverse their signs and do not double in peak value. If, however, the neutral is grounded through a resistance which is equal to the surge impedance of the winding, there is no reflection of the original wave at the neutral. However, there are good operating and relaying reasons for not having a motor grounded through several hundred ohms of resistance. Prevention of peak-voltage multiplication, due to surge reflections, can also be achieved by use of line-to-ground capacitance at the motor terminals. A value of shunt capacitance of 0.5 μF per phase will prevent significant reflections from occurring. As will be discussed subsequently, such capacitance to ground at the motor terminals will also prevent excessive turn-to-turn voltage, which is one of the major concerns of exposure to surges.

The ability of shunt capacitance to reduce surge-voltage buildup can be understood by the concept of superposition. A rectangular wave shape (i.e., a wave with a very steep front) will produce the maximum effect of voltage buildup in an ungrounded winding. Capacitance to ground has the effect of reducing the rate of rise of the front of the wave. A wave that has such a wavefront can be considered the equivalent of a positive rectangular component and a negative, sloped component, the two components of which add at all instants of time to give the wave with the reduced rate of rise. The positive rectangular component will produce a double-peak value at the neutral, because of reflection. The negative sloped component will also produce a double-peak value, because of reflection at the neutral, but it will be negative. The two components add to give the voltage produced by the actual sloped wave, which is certainly less than that produced by the rectangular wave alone.

Ground insulation is damaged if the peak voltage to ground of a surge exceeds the surge or short-time electrical strength of the insulation. It may also be damaged from frequent peak voltages to ground which do not exceed the short-time strength of the insulation but which are significant. This corresponds to the "electrical fatigue" effect of a dielectric material, which was discussed earlier in the chapter. The peak value of the voltage to ground, which appears across ground insulation, can be limited by use of shunt capacitors, provided that they are located solidly at the motor terminals, which they certainly should be. It can also be limited by the condition of grounding at the neutral of the winding, as discussed earlier.

Turn insulation is damaged if the peak turn-to-turn voltage in any coil resulting from a surge exceeds the short-time electrical strength of the insulation between adjacent copper turns. Again, it is also damaged from frequent peak turn-to-turn voltages which do not exceed the short-time strength of the turn insulation. Maximum turn-to-turn surge voltage usually occurs in the terminal coil of the phase winding. Although it could conceivably occur at the neutral of an unprotected motor due to reflections, experience does not indicate that this is very probable. The vulnerability of unprotected turn insulation on the terminal coil can be understood in terms of distributed capacitance between turns. The terminal coil is the first one to experience the surge wave, and thus the distributed turn-to-turn capacitance of that coil tends to absorb the voltage of the surge and to distribute it more or less uniformly between the turns of that coil. The resulting turn-to-turn voltage can be significant if the peak voltage of the surge is sufficiently great.

The way in which shunt capacitance to ground, applied at the winding terminals, can reduce the peak turn-to-turn voltage due to a surge traveling through the terminal coil, can be illustrated by Fig. 11.12. As discussed earlier, such capacitance to ground can reduce the time rate of rise to crest of the traveling surge. Figure 11.12a represents a surge with a high rate of rise traveling through part of the phase winding. For this surge, the time required for the front of the wave to rise from zero to crest is about equal to the time required for the crest of the wave to travel from a point on the first turn to a corresponding point on the second turn. Thus essentially all of the crest value of the voltage V_S appears across the turn insulation between the two turns. Figure 11.12b represents an identical set of conditions, except that shunt capacitance to ground at the terminal end of the phase has decreased the time rate of rise to crest to about half of that shown in part (a) of the figure. In part (b), the crest voltage V_S of the surge is equal in magnitude to that in part (a). However, because of the reduced slope of the wavefront for the surge in part (b), it requires twice as long for the wavefront to travel from zero value to its full crest value. Accordingly, the same value of peak voltage is distributed across two turns instead of one, and the resulting turn-to-turn voltage is about half of that for the wavefront shown in part (a).

To protect turn insulation adequately from surges, a capacitance of 0.2 μF per phase from the motor terminals to ground is required. As mentioned earlier, a capacitance from the motor terminals to ground of 0.5 μF per phase is required to prevent a buildup of phase-winding voltage from reflections if the neutral is ungrounded. Since there are good application reasons for not grounding the neutrals of stator windings in many cases, a capacitance of 0.5 μF per phase should, in general, be applied in order to have general protection from surges. In applying capacitors for surge protection, a package of capacitors and lightning arrestors are applied together. The cost of such a protective package is a small percentage of the total cost of a typical medium or large motor installation.

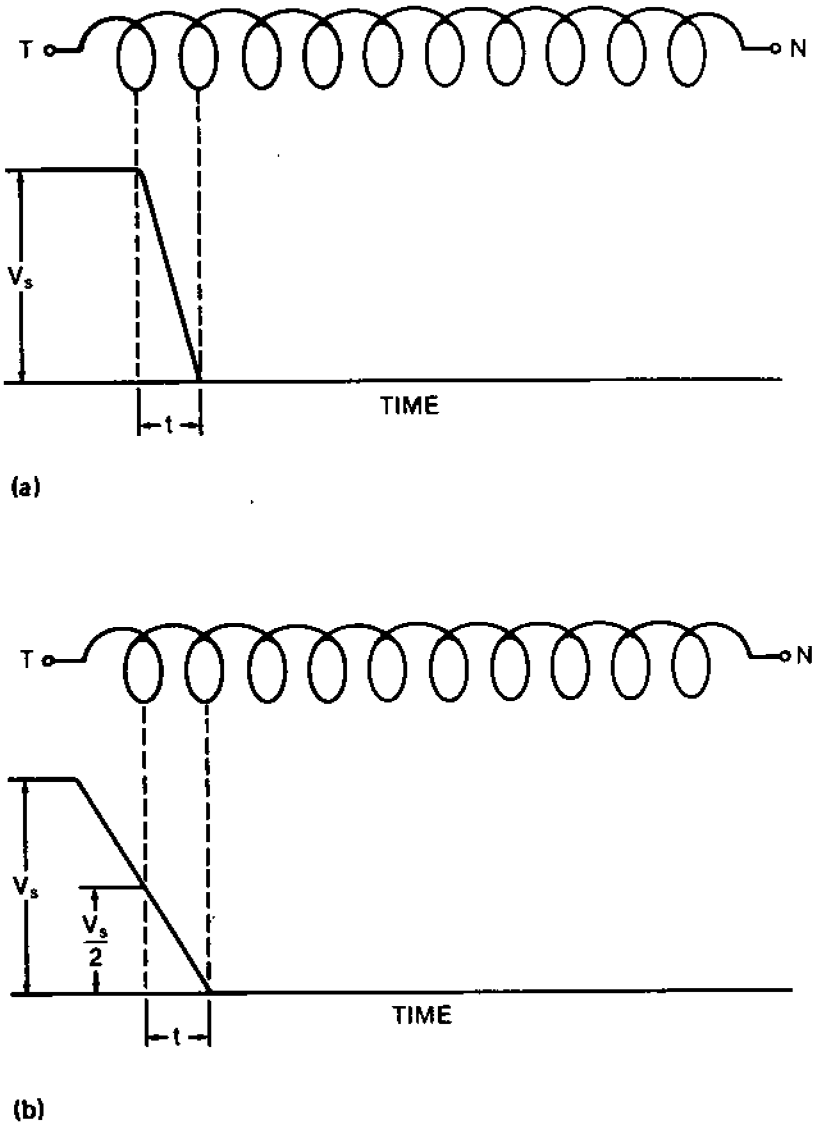

FIGURE 11.12 Diagrammatic representation of turn-to-turn voltage as affected by the steepness of the surge wavefront: (a) surge with a steep wavefront; (b) surge with a medium wavefront.

When installing such a protective package, it is important that it be located solidly at the motor terminals if full protective benefit of the protective equipment is to be realized. If it is more remotely located, the additional circuit inductance from the point of location to the motor terminals can significantly reduce the overvoltage protection provided to the motor windings. Shunt-capacitor ratings are shown in Table 11.3 and station-type lightning arrestor ratings are shown in Table 11.4.

TABLE 11.3 Shunt-Capacitor Ratings for Use in Overvoltage Protection of Motor Windings

Motor bus voltage rating (line-to-line rms kV)	Capacitor voltage rating (line-to-line rms kV)	Capacitor capacitance rating (μF/phase)
2.4	2.4	0.50
4.16	4.16	0.50
4.8	4.8	0.50
6.9	6.9	0.50
11.5	11.5	0.25[a]
13.8	13.8	0.25[a]

[a] Use 0.25 μF per phase if the motor has no direct connection to exposed overhead lines and when connection to transmission lines is not through wye-wye transformers or autotransformers. If such connections exist, use 0.50 μF per phase.

TABLE 11.4 Station-Type Lightning Arrestor Ratings for Use in Overvoltage Protection of Motor Windings

Motor bus voltage rating (line-to-line rms kV)	Station-type arrestor rating (nameplate rms kV)
2.4	3.0
4.16	4.5
4.8	6.0
6.9	7.5
11.5	12.0
13.8	15.0

11.13 TEMPERATURE CLASSES OF INSULATION

The active parts of a motor, such as the windings and the magnetic core, operate at a temperature above ambient temperature, because of the losses that are produced within these parts. Temperature rise and leakage reactance constitute the two limitations to power output of a motor of a given frame size. Early in the history of the design and manufacture of rotating electrical machines, it became apparent that there was a need for some standard for temperature classification of insulation. In the United States the basic concept of insulation classification was first offered by Steinmetz and Lamme in 1912 or 1913. Because of the professional stature of these two giants in the electrical industry, the concept they presented was well received and accepted. In 1920, the International Electrotechnical Commission issued Standard No. 34, which offered classification of insulating materials by chemical composition. In 1925, this Commission reissued Standard No. 34, with material classifications of O, A, B, and C, which allowed maximum operating temperatures of 90, 105, and 130°C, respectively, for the first three classes. No temperature limit was specified for class C insulation.

The American Institute of Electrical Engineers (now the Institute of Electrical and Electronics Engineers) became involved in classifying insulation at about the beginning of this century. From that early work, an important document, entitled AIEE No. 1, was produced and issued in 1925. After subsequent changes, this document eventually became AIEE Standard No. 1, General Principles for Temperature Limits in the Rating of Electrical Equipment, issued in 1957. It included the above-mentioned O, A, and B classifications, with maximum operating temperatures of 90, 105, and 130°C, respectively, as well as the C classification, with a maximum operating temperature of "over 220°C." It included the additional classifications

TABLE 11.5 Temperature Classification of Electrical Insulation

Temperature range (°C)	Preferred temperature index (°C)	Alternative nomenclature[a]
90–104	90	O
105–129	105	A
130–154	130	B
155–179	155	F
180–199	180	H
200–219	200	–
220 and above	—	C

[a] The alternative nomenclature for a given temperature class corresponds to the preferred temperature index for the same temperature class.

of F and H, with maximum operating temperatures of 155 and 180°C, respectively. The present equivalent of this document, issued in 1969, contains a range of temperatures for each temperature class, with a preferred temperature index for each class. The temperature range and preferred temperature index, together with the previously used alternative nomenclature, is given in Table 11.5.

11.14 INSULATION RESISTANCE TESTING

Insulation resistance of a stator winding, or of the winding of a wound rotor, is simply the ratio of dc voltage applied across the insulation to the resulting dc current through the insulation. However, there are some number of factors that affect the results of the test and some number of procedures to follow in conducting the testing. Also, it is important that the measured results be interpreted properly, in accordance with dielectric behavior. The measurement of insulation resistance is normally an easily performed dielectric test. Properly interpreted, it can be a very useful tool in determining the present condition of a motor winding. The factors that affect the results, the procedures for conducting the test, and the interpretation of the test results are considered in this section.

If a voltage is applied between the copper and the steel core, it represents a capacitor for which the copper represents one plate, the steel slots represent the other plate, and the insulation is the dielectric medium.

Accordingly, it will tend to behave as a distributed capacitor. As discussed earlier in this chapter, the dc current flowing through the insulation will consist of three components. One component is the charging current, the magnitude of which is significant only until the capacitor plates are charged, after which it becomes essentially zero. This current will have become insignificant by the time the first readings are taken. The second component is the absorption current, the magnitude of which is also initially significant. The absorption current decreases with time and tends to approach a low value. The absorption current is the primary component of current during the first several minutes of testing. The third component of current is the conduction current through the insulation wall, and any surface-creepage current, such as could occur on the collector surface of a wound rotor. The conduction current is the predominating component of current, after the first few minutes, by which time the absorption current will have decreased to a low value.

After the dc test voltage has been removed from across the insulation and an appropriate discharge circuit has been established for current flow, the discharge current will consist of two components. One component is the reverse of the charging current and is the manifestation of electrical charges flowing from the equivalent capacitor plates. The time required for this to occur depends on the resistance of the discharge circuit, but it is a very short time. The second component of discharge current is the absorption current, which requires a considerably greater length of time to reach zero. The third component of current, which was present when voltage was applied across the insulation (i.e., conduction current) ceases to exist when the voltage is removed, of course.

During a test, the insulation resistance of a winding will tend to increase with time until a reasonably constant value is reached. Insulation that has absorbed moisture or other contaminants, such as conducting dirt, will reach an essentially constant value in 2 to 3 minutes. On the other hand, insulation that is relatively new and which is dry will require a time measured in hours instead of minutes to reach a constant value. If insulation resistance is plotted against time on log-log paper, the slope of the essentially linear plot, up to the point of attaining a constant value, is an indicator of the quality of the insulation. The slope is greater for a winding with insulation in good condition than for a winding with insulation in poor condition.

An important quantity that is very useful in determining the condition of insulation is the polarization index. It is defined as the ratio of the insulation-resistance reading after 10 minutes of testing to that after 1 minute of testing, and its value is related to the above-mentioned plot of log (insulation resistance) versus log (time). The polarization index of a motor winding being tested should equal 2.0 or more before the machine is again placed in service. If it is lower than that value, the probability is great that the insulation has absorbed considerable moisture and/or that its surface, and possibly its volume, contains conducting or semiconducting contamination.

The insulation resistance of a winding is affected by various factors, among which are (1) moisture, (2) surface contamination, (3) test voltage level, (4) time, and (5) temperature. Moisture is generally detrimental to insulation, and moisture, whether on the surface of or inside the winding, will result in lower insulation resistance readings. For a machine in operation, the I^2R losses will generally maintain the insulation in a dry condition. There are a few exceptions to this, of course, such as using an inappropriate enclosure for the application, the rupture of one or more tubes in the heat exchanges of an enclosed, water-cooled machine, and so on. However, if a machine is out of operation, even for a short time, moisture will condense on the winding if the temperature of the insulation is not kept a few degrees above that of the ambient air. As stated earlier, this can be accomplished by use of space heaters or by applying a very reduced voltage across the winding terminals. If a winding shows a low value of insulation resistance, it should be dried out and the test repeated to determine if the problem is due to moisture.

Surface contamination can also significantly reduce the insulation resistance of a winding. The type of dirt typically found in the vicinity of an industrial-motor site may or may not be conductive. However, the presence of moisture usually causes the combination to be conductive. On older insulation, dirt and moisture can penetrate the insulation, such as between layers of tape. As mentioned earlier, wound-rotor brushes, under certain conditions, can produce carbon dust, which is both penetrative and conductive. If it is apparent that the winding is contaminated, it should be cleaned and the insulation resistance then tested or retested. Obviously, the cause of the contamination should be corrected, if that is possible.

When performing an insulation resistance test, applications of dc voltage to a winding will electrically stress the winding to some extent. Accordingly, the test voltage should be appropriate for the insulation class. Typically, the applied dc voltage is from 500 to 5000 V and should be less than the voltage rating of the winding (except for a 440-V winding, for which a test voltage of 500 V is frequently used). Insulation that is dry and in good condition should not show any great difference in insulation resistance, for different values of voltage used for the test, although it may slightly decrease with increasing voltage. However, a significant decrease in insulation resistance with increasing voltage is indicative of moisture, dirt, damaged insulation, or some combination of those factors.

As mentioned above, insulation resistance tends to increase with the length of the test, and this resistance-time effect is used to define and to determine the polarization index. Also, insulation resistance varies with the temperature of the winding. Most insulation materials show a decrease in insulation resistance with an increase in the temperature of the insulation. Frequently, insulation resistance values are used to compare with previously measured values, and thus to track the winding condition over a number of years. For such a comparison to be valid, though, all values must be referred to a common temperature base, such as a 40°C base. This can be done by measuring the insulation resistance at several different temperatures, but with all of them above the dew point. If insulation resistance is then plotted on a log scale and temperature is plotted on a uniform scale, the resulting plot should be reasonably close to a straight line. From this plot, the insulation resistance that corresponds to a selected temperature base, such as 40°C, can be determined. This base value can then be recorded for future comparison purposes. If, for some reason, it is not possible to measure the insulation resistance at several temperatures, an alternative method is available, but it is not as accurate as the method described above. This alternative method is given in IEEE Standard 43-1974, Recommended Practice for Testing Insulation Resistance of Rotating Machinery. The insulation resistance R_t of the winding is determined at some temperature t. Then a correction factor K_t is read from a correction curve, which is provided in Fig. 1 of Standard 43-1974. The insulation resistance R_c corrected to 40°C is then approximately

$$R_c = K_t R_t \quad \text{megohms} \tag{11.136}$$

It is desirable to measure the insulation resistance of one phase at a time. By so doing, the resulting values of the three different phases can be compared. Also, the testing of individual phases gives an indication of the condition of the phase-to-phase insulation, since the other phases would be grounded. To perform an insulation resistance test on one phase, the neutral end of the phase winding is opened and is isolated from ground and from any other circuit. It is preferable that the two ends of the phase being tested be connected together, to reduce surges, in case of an insulation failure during a test. To obtain a true indication of the insulation resistance of the winding alone, the terminal end of the phase should be disconnected from the power cables that connect the winding to the bus, circuit breaker, or motor starter. Also, auxiliary equipment, such as shunt capacitors and lightning arrestors, should be isolated from the phase winding. As stated above, the other two phases should be grounded at each end of the two windings.

The insulation resistance between the copper and the core, which is at ground potential, can be determined by several methods. A frequently used method is that of using self-contained equipment which has a hand-driven or power-driven dc generator and an ohmmeter. This method has the advantage that instantaneous corresponding values of voltage and milliamperes are used automatically to produce the ohmic value. Similar self-contained equipment is available that utilizes a rectifier instead of a generator to develop the dc test voltage. Also, traditional methods of measuring resistance may be used, such as the bridge-circuit method and the voltmeter-microammeter method. Caution must be used to protect personnel from direct voltage, of course, for those methods that use such voltage. After the testing is completed, the winding should be grounded to remove the charge completely. The duration of the grounding should be equal to not less than four times the charge time.

It is local practice, in some cases, to test the insulation resistance of the entire winding instead of individual phases. This will save time and effort. However, such a practice does not permit comparisons of insulation resistance between the different phases or of tracking individual phases over a period of time. Regardless of whether the individual phases are tested or the complete winding is tested, the minimum acceptable value of insulation resistance should be obtained from the manufacturer for the specific motor under consideration. Such information is usually contained in the instruction manual.

11.15 CREEPAGE, TRACKING, AND ARC RESISTANCE

A track is localized damage or deterioration on the surface of insulation which has resulted from the flow of charges. Such damage usually occurs as the result of an arc. Tracking is the process that results in the production of a track. In the process of tracking, the arc produces sufficient energy on the insulation surface as to cause thermal damage, which results in the track. As the length of the track is increased, the voltage gradient, at the end of the track, also increases. At some point, the track will have spanned a sufficient distance that the voltage gradient will reach a critical value and the track will then rapidly progress the remaining distance between the points of potential difference. Creepage is related to the tracking phenomenon and is an increase in surface leakage current along an insulation surface between points with a difference in potential. As the creepage increases, the flashover-voltage strength along the surface of the insulation is decreased and the probability of a flashover is increased.

Creepage current and tracking usually result from the accumulation of contamination and moisture on the surface of the insulation. As noted earlier, much of the contamination prevalent at motor sites is semiconductive or conductive and in the presence of moisture becomes even more conductive. If the surface resistance due to contamination or other causes reaches a value of $10^7\ \Omega$ per square unit of surface, tracking can occur on that surface. This, in turn, can lead to arcing. The practical problems of creepage and tracking on the end turns of high-voltage stator windings and in collectors, together with actions to be taken to prevent such an effect, were discussed previously.

11.16 APPLICATION OF INSULATION TO WINDINGS

The practical application of insulation to random stator windings was discussed in Section 9.2.6. The practical application of insulation to formed-coil stator windings, the engineering and manufacturing approach to which is somewhat different from that for random stator windings, was discussed in Section 9.2.7. Also, the practical application of insulation to coils for wound rotors was discussed in Section 10.4.3. In general, class B or class F insulation is used for most applications, while class H insulation is used for certain special applications. Thus the hottest portions of the insulation will be operating at temperatures of from 130°C for class B to 180°C for class H.

Mica tape and wrap backed with a glass or fiber matrix are used for the prime ground insulation for most formed-coil windings. Mica is also used for the prime ground insulation for some random windings, but synthetic materials are also used. Turn insulation consists primarily of synthetic films for random windings, and of synthetic films, glass, or other serving, or a combination, for formed-coil windings. The windings in both cases are treated with high-temperature synthetic resins such as epoxy or polyester formulations. Many, although not all, wound stator cores, are vacuum-pressure impregnated with resin to prevent internal voids. This practice has many benefits, such as helping to control internal corona.

The various motor manufacturers tend to centralize the development and application of insulation to the product line. Thus a suitable insulation system is developed using specialized expertise, and then proven by test. From that point on, it is an established system and is generally applied to the product line on a consistent basis. For most organizations, changes in the standard system are permitted only with the approval of the engineering manager in charge of a product line, and then, only for good reason. Such centralized control tends to provide customers with a specific level of insulation-design quality, based on an insulation system that has been prequalified by testing.

12

Magnetomotive Forces Acting Across the Air Gap

12.1 Introduction 428

12.2 Magnetomotive Force Produced by One Stator Coil 429

12.3 Magnetomotive Force Produced by a Pair of Coil Groups of Opposite Polarity 434

12.4 Magnetomotive Force Produced by One Phase 436

12.5 Magnetomotive Force Produced by the Complete Stator Winding 438

12.6 Example of the Graphical Construction of the Magnetomotive-Force Wave Produced by a Three-Phase Stator Winding 441

12.7 The Equivalent Circuit with the Space Harmonics Considered 445

12.8 Magnetizing Current 446

12.9 Various Types of Harmonics Present in the Air Gap 449

- 12.9.1 Stator-space harmonics 449
- 12.9.2 Stator-slot harmonics 450
- 12.9.3 Rotor-slot harmonics 451
- 12.9.4 Harmonics in the air-gap permeance 451
- 12.9.5 Rotor harmonics 453

12.10 Perturbations on the Speed-Torque Curve 453

- 12.10.1 Asynchronous crawling 454
- 12.10.2 Synchronous locking 458
- 12.10.3 Synchronous crawling 462

12.11 Electromagnetically Induced Noise and Vibration 466
  12.11.1 Magnetic-force waves 467
  12.11.2 Mechanical compliance of various motor parts 469
  12.11.3 Selection of the number of stator and rotor slots to avoid magnetic noise and vibration 472
  12.11.4 Frequency of the force wave 475
  12.11.5 Numerical example of rotor-slot selection 476
12.12 Additional Effects of Harmonics 477

12.1 INTRODUCTION

As shown in Chapter 3, a balanced three-phase voltage applied to the terminals of a three-phase stator winding will result in a rotating magnetic field that travels around the air gap at synchronous speed. If the field strength of, say, phase A is equal to H cos ωt ampere-turns/meter, and that of phases B and C are equal in magnitude but successively displaced $(2/3)\pi$ electrical radians in time, the resulting rotating magnetic field is a sinusoidal function of $\alpha - \omega t$, with a maximum field strength of (3/2)H ampere-turns/meter. This field strength is a vector quantity, which is the gradient in the direction of H (i.e., across the air gap) of the magnetomotive force F produced by current flowing in the three-phase winding. The magnetomotive force, in turn, will cause a magnetic flux, $\Phi = F/R$, to flow across the air gap and through the magnetic core, as indicated in Figs. 3.1 and 3.3, where R is the reluctance of the magnetic path.

In deriving the relationship above in Chapter 3, it was assumed that the spatial distribution of the stator magnetomotive force wave was sinusoidal for each of the phase windings, which resulted in a sinusoidal, rotating three-phase magnetomotive force wave. It was also assumed that the air-gap permeance was uniform, which resulted in a sinusoidal, rotating magnetic flux wave. Accordingly, analysis of the performance of polyphase induction motors up to this point has been based on such an assumed sinusoidal distribution of magnetomotive force and flux. However, the stator magnetomotive force wave does not have an exact sinusoidal spatial distribution and the air-gap permeance is not exactly uniform, because current is concentrated in discrete slots instead of being distributed uniformly along the air gap. Up to this point, the analysis of performance has considered only the fundamental component of the magnetomotive force wave and of the mutual flux wave. The effect of harmonics has been tacitly ignored, except for occasional comments that this subject would be considered subsequently. The presence of harmonics in the air-gap magnetomotive force wave has detrimental effects on the performance of polyphase induction motors, including (1) perturbations on the speed-torque curve, (2) noise, (3) vibration, (4) additional losses, and (5) voltage ripples, which are reflected back into the stator supply voltage. In this chapter the various air-gap harmonics are identified and the significant effects produced by the presence of such harmonics are considered.

12.2 MAGNETOMOTIVE FORCE PRODUCED BY ONE STATOR COIL

Consider a single full-pitch stator coil through which a current of I' amperes is flowing. For the moment it will be assumed that the magnitude of I' is fixed in time (i.e., that it is unidirectional). Such a coil is shown in Fig. 12.1a. In this figure the two sides of the coil, located π electrical radians apart, along the stator bore produce a rectangular magnetomotive force wave. The first coil side of a second coil, located π electrical radians farther along the stator bore, is also shown to complete the wave shape for a span of 2π electrical radians. If the coil consists of N_c series turns, the magnetomotive force F is equal to $N_c I'$ ampere-turns for the span, zero to π electrical radians, and the wave has a rectangular wave shape. The magnetomotive force is equal to $-N_c I'$ for the span, π to 2π electrical radians, as is apparent from Fig. 12.1.

The wave shape shown in Fig. 12.1 is a single-valued function, is defined at all points, has a finite number of discontinuities, and has a finite number of maxima and minima. Thus it can be expressed by means of the classical Fourier series as

$$F = \frac{A_0}{2} + A_1 \cos \alpha + A_2 \cos 2\alpha + A_3 \cos 3\alpha + \cdots$$
$$+ B_1 \sin \alpha + B_2 \sin 2\alpha + B_3 \sin 3\alpha + \cdots \quad \text{ampere-turns/coil} \tag{12.1}$$

for which

$$A_0 = \frac{1}{\pi} \int_0^{2\pi} F \, d\alpha \quad \text{ampere-turns/coil} \tag{12.2}$$

and

$$A_n = \frac{1}{\pi} \int_0^{2\pi} F \cos n\alpha \, d\alpha \quad \text{ampere-turns/coil} \tag{12.3}$$

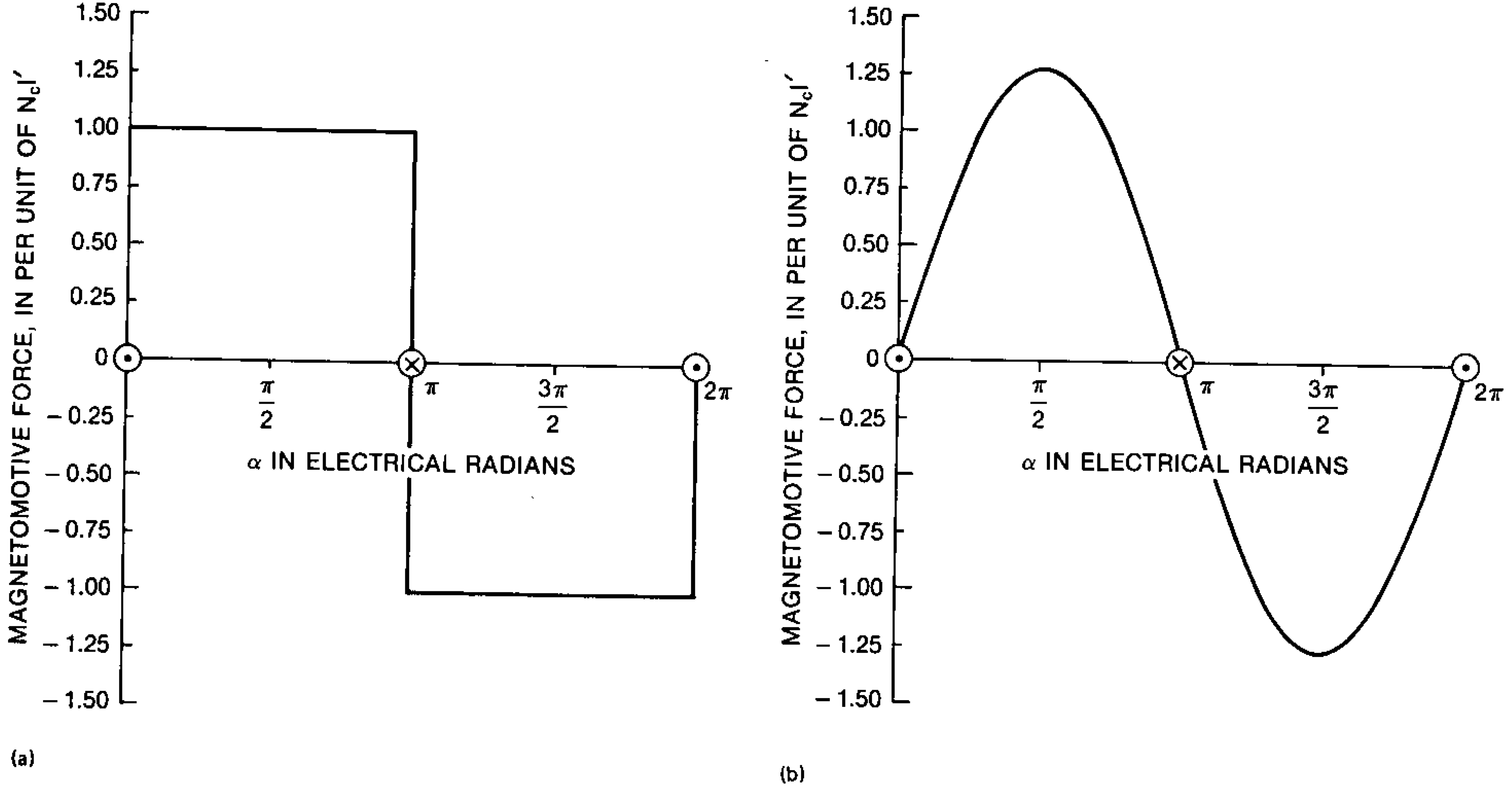

FIGURE 12.1 Magnetomotive-force wave produced by a full-pitch coil: (a) actual wave; (b) fundamental component of wave.

and

$$B_n = \frac{1}{\pi}\int_0^{2\pi} F \sin n\alpha \, d\alpha \quad \text{ampere-turns/coil} \tag{12.4}$$

where n is the order of the harmonic. Since from inspection of Fig. 12.1 the wave is symmetrical about the α axis, the value of A_0 is zero. Evaluating A_n from eq. (12.3), we have

$$A_n = \frac{1}{\pi}\left(\int_0^{\pi} N_c I' \cos n\alpha \, d\alpha - \int_{\pi}^{2\pi} N_c I' \cos n\alpha \, d\alpha\right) = 0$$

$$\text{ampere-turns/coil} \tag{12.5}$$

Evaluating B_n from eq. (12.4) gives us

$$\begin{aligned} B_n &= \frac{1}{\pi}\left(\int_0^{\pi} N_c I' \sin n\alpha \, d\alpha - \int_{\pi}^{2\pi} N_c I' \sin n\alpha \, d\alpha\right) \\ &= \frac{4N_c I'}{\pi} \frac{1}{n} \sin (n\alpha) \quad \text{ampere-turns/coil} \end{aligned} \tag{12.6}$$

Thus the single-coil magnetomotive force wave shown in Fig. 12.1 can be expressed by the Fourier series

$$F = \frac{4N_c I'}{\pi} (\sin \alpha + 1/2 \sin 2\alpha + 1/3 \sin 3\alpha + \cdots) \quad \text{ampere-turns/coil} \tag{12.7}$$

From the first term of eq. (12.7), the fundamental of the rectangular wave produced by the coil and shown in Fig. 12.1b has a maximum value equal to $4N_c I'/\pi$. Since the average value of a sine wave is equal to $2/\pi$ of the maximum value, the average value of the fundamental $F_{1\text{-av}}$ shown in Fig. 12.1b is equal to

$$F_{1\text{-av}} = \frac{2}{\pi} \frac{4N_c I'}{\pi} = \frac{8N_c I'}{\pi} \quad \text{ampere-turns/coil} \tag{12.8}$$

The average value of the rectangular wave shown in Fig. 12.1 is equal to

$$F = N_c I' \quad \text{ampere-turns/coil} \tag{12.9}$$

For a fixed amount of reluctance, the amount of flux across the air gap for a span of $\alpha = \pi$ electrical radians along the stator bore is proportional to the magnetomotive force acting across the gap. Then the ratio of eq. (12.8) to eq. (12.9) gives the ratio of the fundamental flux to the total flux produced by one coil, or

$$\frac{F_{1-av}}{F} = \frac{8N_c I'/\pi^2}{N_c I'} = \frac{8}{\pi^2} = 0.8106 \quad \text{numeric} \qquad (12.10)$$

Since the fundamental is the useful component of air-gap flux, eq. (12.10) can be considered one measure of the effectiveness of the mutual flux produced by a single full-pitch coil.

The wave shape shown in Fig. 12.1 and the Fourier series in eq. (12.7), which represents it, are for a full-pitch stator coil, whereas most stator coils are designed to have a fractional pitch. Equation (12.7) can be extended to include fractional-pitch coils by multiplying each term on the right-hand side of the equation by the appropriate pitch factor K_{pn}, as defined in eq. (9.101). This can be understood by viewing the induction of a voltage within a coil, due to a change in the flux through the coil, as another aspect of essentially the same phenomenon as that of the production of a magnetomotive force and the resulting production of a flux by a current (or moving electrical charge) flowing in the coil. The two actions can be viewed as essentially inverse effects of the interactions of a magnetic field through a coil and the electric field along the perimeter of that coil. In Sections 9.7 and 9.8 it was shown that the voltage induced in a fractional-pitch coil is equal to that induced in a similar full-pitch coil, multiplied by the pitch factor. Correspondingly, the magnetomotive force produced by a fractional-pitch coil is equal to that produced by the same coil if it were full pitch, but multiplied by the pitch factor K_{pn}. Then eq. (12.7) can be written for the general case of a coil of any per unit coil pitch p as

$$F = \frac{4N_c I'}{\pi} (K_p \sin \alpha + 1/2\, K_{p2} \sin 2\alpha$$
$$+ 1/3\, K_{p3} \sin 3\alpha + \cdots) \quad \text{ampere-turns/coil} \qquad (12.11)$$

It was initially assumed that the current I' flowing in the coil was fixed in time, or that it was unidirectional. Now, let the current vary sinusoidally with time, as

$$i = \sqrt{2}\, I \cos \omega t \quad \text{amperes/coil} \qquad (12.12)$$

where I is the effective value of the current in the coil. Then eq. (12.11) becomes

$$\text{MMF} = \frac{4N_c\sqrt{2}\,I}{\pi}(\cos\omega t)(K_p \sin\alpha + 1/2\,K_{p2}\sin 2\alpha + 1/3\,K_{p3}\sin 3\alpha + \cdots) \quad \text{ampere-turns/coil} \tag{12.13}$$

where MMF is the instantaneous value of the field produced by the coil. From an inspection of eq. (12.13) it is apparent that the fundamental and each harmonic of the magnetomotive-force wave pulsate sinusoidally with time and at the same frequency. However, such a pulsating field can be resolved into two fields, constant and equal in magnitude, which rotate in opposite directions, as will be discussed subsequently.

The fundamental of the field wave in eq. (12.13) is equal to

$$(\text{MMF})_1 = \frac{4N_c\sqrt{2}\,IK_p}{\pi}(\sin\alpha)(\cos\omega t) \quad \text{ampere-turns/coil} \tag{12.14}$$

However, since

$$(\sin\alpha)(\cos\omega t) = 1/2\sin(\alpha - \omega t) + 1/2\sin(\alpha + \omega t) \quad \text{numeric} \tag{12.15}$$

eq. (12.14) can be written as

$$(\text{MMF})_1 = \frac{2N_c\sqrt{2}\,IK_p}{\pi}\left[\sin(\alpha - \omega t) + \sin(\alpha + \omega t)\right] \quad \text{ampere-turns/coil} \tag{12.16}$$

In a corresponding manner, the nth harmonic can be written as

$$(\text{MMF})_n = \frac{2N_c\sqrt{2}\,I}{\pi}\left[\frac{K_{np}}{n}\sin(n\alpha - \omega t) + \frac{K_{np}}{n}\sin(n\alpha + \omega t)\right] \quad \text{ampere-turns/coil} \tag{12.17}$$

Consider the fundamental component given in eq. (12.16). The first term of eq. (12.16) corresponds to a traveling wave which travels at synchronous speed in the positive direction of rotation, and the second term corresponds to another traveling wave which travels at synchronous speed in the opposite direction of rotation. Thus if α is set equal to $\omega t + \pi/2$ such that the point α rotates around the positive direction of the air gap at synchronous speed, the first trigonometric term in eq. (12.16) becomes sin ($\pi/2$). Accordingly, the field is constant in magnitude as it rotates around the stator bore in the positive direction at an angular velocity of ω electrical radians/second. At the same time, the second trigonometric term in eq. (12.16) becomes $\sin(\pi/2 + 2\omega t)$, and the point α, which is rotating in the positive direction at synchronous speed, sees the second field rotating in the opposite direction at an angular velocity of twice synchronous speed. Then this second field is rotating at synchronous speed in the negative direction of rotation. Incidentally, the only reason for setting α equal to $\omega t + \pi/2$ instead of simply ωt was the pedagogical one of having the value of the traveling wave be other than zero at $\omega t = 0$, and no generality is lost by selection of this particular convention.

Consider the nth harmonic of the magnetomotive-force wave, as given in eq. (12.17). From the above it is apparent that similar logic can be applied successively to each harmonic, such as the nth harmonic, to reveal two traveling waves, equal in magnitude, which travel in opposite directions at synchronous speed on the nth harmonic scale. The nth harmonic will have n times the number of poles on the harmonic scale as does the fundamental on the fundamental scale. In both cases, the two component waves will travel two pole pitches, or 2π electrical radians, on their respective scales for each cycle. Thus the nth harmonic will actually travel at 1/nth the velocity of the fundamental. The complete magnetomotive-force wave, produced by a single coil with N_c turns and with a per unit pitch of p, is

$$\begin{aligned}(\text{MMF})_c = {} & \frac{2N_c\sqrt{2}\,I}{\pi}\left[K_p \sin(\alpha - \omega t) + 1/2\, K_{p2} \sin(2\alpha - \omega t)\right.\\ & \left. + 1/3\, K_{p3} \sin(3\alpha - \omega t) + \cdots\right]\\ & + \frac{2N_c\sqrt{2}\,I}{\pi}\left[K_p \sin(\alpha + \omega t) + 1/2\, K_{p2} \sin(2\alpha + \omega t)\right.\\ & \left. + 1/3\, K_{p3} \sin(3\alpha + \omega t) + \cdots\right] \quad \text{ampere-turns/coil} \qquad (12.18)\end{aligned}$$

12.3 MAGNETOMOTIVE FORCE PRODUCED BY A PAIR OF COIL GROUPS OF OPPOSITE POLARITY

As defined in Chapter 9, a group of stator coils consists of several adjacent coils connected in series and equal in number to the complete set of stator coils divided by the number of poles p and phases q. Thus a group represents several adjacent coils that produce identical magnetomotive forces, the centerlines of which are separated by an angular distance equal to that which separates adjacent slots. Accordingly, the total magnetomotive force produced by one coil group is equal to that given in eq. (12.18), multiplied by the number of coils per group N_g and with each harmonic component, such as the nth, multiplied by the distribution factor for that harmonic, such as K_{dn}. The general form of the distribution factor, which is applicable to all harmonics as well as to the fundamental, is defined in eq. (9.130). Then the total magnetomotive force produced by one group of stator coils is equal to

$$
\begin{aligned}
(\mathrm{MMF})_g = {} & \frac{2N_cN_g\sqrt{2}\,I}{\pi}\Big[K_pK_d\sin(\alpha-\omega t)+\frac{1}{2}K_{p2}K_{d2}\sin(2\alpha-\omega t) \\
& +\frac{1}{3}K_{p3}K_{d3}\sin(3\alpha-\omega t)+\cdots\Big] \\
& +\frac{2N_cN_g\sqrt{2}\,I}{\pi}\Big[K_p'K_d\sin(\alpha+\omega t)+\frac{1}{2}K_{p2}K_{d2}\sin(2\alpha+\omega t) \\
& +\frac{1}{3}K_{p3}K_{d3}\sin(3\alpha+\omega t)+\cdots\Big] \quad \text{ampere-turns/group}
\end{aligned}
\tag{12.19}
$$

In Chapter 9 it was shown that for the normal case of groups that encompass $\pi/3$ electrical radians, or 60 electrical degrees, there will be one group per pole pitch for each phase. The polarity of the current in adjacent groups of the same phase winding will be π radians out of time phase, since they have corresponding positions in adjacent poles which have opposite magnetic polarities. In the general case, this will be true for any two coil groups within the same phase which have positions around the stator that differ by an odd multiple of π electrical radians. This can be seen by an inspection of Fig. 9.17. Accordingly, if eq. (12.19) represents, say, the "A" phase group, corresponding to terminals (1) and (2) at the top of Fig. 9.17, the adjacent "-A" phase group, corresponding to terminals (3) and (4) at the right-hand side of the figure, is equal to the negative of eq. (12.19), but with the position angle α advanced to $\alpha + \pi$ electrical radians. Such a pair of coil groups combine to produce the mutual flux per pole. However, the sum of the magnetomotive force produced by the groups must be divided by 2, and the result has units of magnetomotive force per group. This is because the mutual flux per pole is common to the two poles. This can be seen from an inspection of the prototype magnetic circuit shown in Fig. 3.3.

Adding the nth harmonics of the pair of groups discussed above, we have

$$
\begin{aligned}
(\mathrm{MMF})_g = {} & \frac{N_cN_g\sqrt{2}\,I}{\pi}\,\frac{K_{pn}K_{dn}}{n}\big[\sin(n\alpha-\omega t)+\sin(n\alpha+\omega t)\big] \\
& -\frac{N_cN_g\sqrt{2}\,I}{\pi}\,\frac{K_{pn}K_{dn}}{n}\big\{\sin[n(\alpha+\pi)-\omega t] \\
& +\sin[n(\alpha+\pi)+\omega t]\big\} \quad \text{ampere-turns/group}
\end{aligned}
\tag{12.20}
$$

Since $\sin(\theta + \phi) = \sin(n\theta + \phi)$ for all even values of n, the two terms in eq. (12.20) cancel for all even harmonics. Also, since $\sin(\theta + \phi) = -\sin(n\theta + \phi)$ for all odd values of n, the two terms in the equation add for all odd harmonics, including the fundamental components. Then the magnetomotive force per group, produced by two cooperating groups of coils electrically connected and carrying the same current, is

$$\begin{aligned}(\text{MMF})_{2g} = {} & \frac{2N_c N_g \sqrt{2}\, I}{\pi}\Big[K_p K_d \sin(\alpha - \omega t) + \frac{1}{3}K_{p3}K_{d3}\sin(3\alpha - \omega t) \\ & + \frac{1}{5}K_{p5}K_{d5}\sin(5\alpha - \omega t) + \cdots\Big] \\ & + \frac{2N_c N_g \sqrt{2}\, I}{\pi}\Big[K_p K_d \sin(\alpha + \omega t) + \frac{1}{3}K_{p3}K_{d3}\sin(3\alpha + \omega t) \\ & + \frac{1}{5}K_{p5}K_{d5}\sin(5\alpha + \omega t) + \cdots\Big] \quad \text{ampere-turns/group}\end{aligned} \tag{12.21}$$

12.4 MAGNETOMOTIVE FORCE PRODUCED BY ONE PHASE

For a two-pole winding there are two groups of coils for each of the phase windings, which cooperate, as shown in eq. (12.21), to provide that phase's contribution to producing the rotating air-gap flux wave. Since only one pair of poles are required to form the flux wave around the gap, all of the phase winding is utilized uniformly. For a four-pole winding there are four groups of coils for any given phase, so that two pairs of cooperating groups provide that phase's contribution to producing the rotating air-gap flux wave. Since two pairs of poles are required to form the flux wave around the gap, again, all of the phase winding is utilized uniformly; and so on, for windings of any number of pairs of poles. Thus the machine is magnetized by uniform use of all the groups of each phase winding for the complete periphery of the stator bore.

In eq. (9.137) the voltage induced in a phase winding was shown to be

$$E_1 = 4.443 K_p K_d N_{st} f \phi_{pm} \quad \text{volts/phase} \tag{12.22}$$

Solving for ϕ_{pm}, the maximum value of the flux per pole, gives us

$$\phi_{pm} = \frac{E_1}{4.443 K_p K_d N_{st} f} \quad \text{webers} \tag{12.23}$$

where N_{st} is the number of series turns per phase. To obtain the desired value of ϕ_{pm}, the various groups of stator coils in each phase are connected in one of the possible series, parallel, or series-parallel combinations, as discussed in Sections 9.13 and 9.14 and as shown in Fig. 9.18, to give the proper value of N_{st}. From the design engineer's point of view, the desired values of ϕ_{pm} is a function of the required machine characteristics, the frame size, and the number of poles, and to obtain this value of ϕ_{pm}, the necessary value of N_{st} is obtained by the proper selection of the number of stator slots N_1, the number of turns/coil N_c, and the number of parallel circuits C in each phase. Since flux is proportional to the magnetomotive force that produces it, the required magnetomotive force is also obtained by the proper selection of the same parameters.

The magnetomotive force produced by one phase of the stator winding can be obtained in terms of N_{st}. Although eq. (12.21) gives the magnetomotive force per group produced by two cooperating groups of coils, that equation can be transformed to the magnetomotive force produced by a phase winding in terms of phase parameters. Consider the common factor $2N_cN_g\sqrt{2}\,I/\pi$ in eq. (12.21). Since

$$N_{st} = \frac{N_1 N_c}{qC} \quad \text{series turns/phase} \tag{12.24}$$

then

$$N_c = \frac{N_{st} qC}{N_1} \quad \text{turns/coil} \tag{12.25}$$

Also,

$$N_g = \frac{N_1}{pq} \quad \text{coils/group} \tag{12.26}$$

Substituting eqs. (12.25) and (12.26) into the above-mentioned common factor in eq. (12.21) and simplifying yields

$$\frac{2N_c N_g \sqrt{2}\ I}{\pi} = \frac{2N_{st} C\sqrt{2}\ I}{\pi p} \quad \text{ampere-turns/group} \tag{12.27}$$

The current I in eq. (12.27) is the effective value of the current flowing through the coils in each group. If there are C parallel circuits in each phase, the phase current I_1 is then equal to

$$I_1 = CI \quad \text{ampere/phase} \tag{12.28}$$

Accordingly, eq. (12.27) can be written as

$$\frac{2N_{st}C\sqrt{2}\,I}{\pi p} = \frac{2N_{st}\sqrt{2}\,I_1}{\pi p} \quad \text{ampere-turns/phase} \tag{12.29}$$

and the complete expression for the air-gap magnetomotive force wave, produced by one phase of the stator, is

$$\begin{aligned}(\text{MMF})_{ph} = \frac{2N_{st}\sqrt{2}\,I_1}{\pi p} \Big[&K_pK_d \sin(\alpha - \omega t) + \frac{1}{3}K_{p3}K_{d3}\sin(3\alpha - \omega t) \\ &+ \frac{1}{5}K_{p5}K_{d5}\sin(5\alpha - \omega t) + \cdots \\ &+ K_pK_d\sin(\alpha + \omega t) + \frac{1}{3}K_{p3}K_{d3}\sin(3\alpha + \omega t) \\ &+ \frac{1}{5}K_{p5}K_{d5}\sin(5\alpha + \omega t) + \cdots\Big] \quad \text{ampere-turns/phase}\end{aligned} \tag{12.30}$$

12.5 MAGNETOMOTIVE FORCE PRODUCED BY THE COMPLETE STATOR WINDING

The magnetomotive-force expression in eq. (12.30) is for one phase, and for a three-phase stator, there are three similar magnetomotive forces, produced by the three phases, which are separated in angular position by $2\pi/3$ electrical radians, or 120 electrical degrees. If the impressed stator voltage is from a balanced three-phase source, each phase voltage and each phase current will successively lag the preceding one in time by a similar angle. The resulting three-phase magnetomotive force is equal to the sum of the magnetomotive forces produced by the three individual phases, with appropriate consideration for the difference in angular position and time phase between the phases.

The phase value of the magnetomotive force given in eq. (12.30) is composed of a series of odd harmonics. The expression for the nth harmonic can be written as

$$(\text{MMF})'_{ph} = \frac{2N_{st}\sqrt{2}\,I_1}{\pi p} K_{pn}K_{dn}\frac{1}{n}\left[\sin(n\alpha - \omega t) + \sin(n\alpha + \omega t)\right]$$

$$\text{ampere-turns/phase/harmonic} \tag{12.31}$$

Considering only the trigonometric terms for the moment, and adding the nth harmonics produced by the three different phases, we obtain

$$\begin{aligned}\Sigma_n &= \sin(n\alpha - \omega t) + \sin(n\alpha + \omega t) + \sin[n(\alpha - 120) - (\omega t - 120)] \\ &\quad + \sin[n(\alpha - 120) + (\omega t - 120)] + \sin[n(\alpha - 240) - (\omega t - 240)] \\ &\quad + \sin[n(\alpha - 240) + (\omega t - 240)] \quad \text{numeric} \qquad (12.32)\end{aligned}$$

By use of the relationship $\sin(\theta \pm \phi) = \sin\theta\cos\phi \pm \cos\theta\sin\phi$, eq. (12.32) can be reduced to

$$\begin{aligned}\Sigma_n &= \sin(n\alpha - \omega t) + \sin(n\alpha + \omega t) + 2\sin[n(\alpha - 120)]\cos(\omega t - 120) \\ &\quad + 2\sin[n(\alpha - 240)]\cos(\omega t - 240) \quad \text{numeric} \qquad (12.33)\end{aligned}$$

and by use of the relationship $\sin\theta\cos\phi = 1/2\sin(\theta + \phi) + 1/2\sin(\theta - \phi)$, eq. (12.33) can be reduced to

$$\begin{aligned}\Sigma_n &= \sin(n\alpha - \omega t) + \sin[n\alpha - \omega t - (n-1)(120)] \\ &\quad + \sin[n\alpha - \omega t - (n-1)(240)] \\ &\quad + \sin(n\alpha + \omega t) + \sin[n\alpha + \omega t - (n+1)(120)] \\ &\quad + \sin[n\alpha + \omega t - (n+1)(240)] \quad \text{numeric} \qquad (12.34)\end{aligned}$$

Evaluating eq. (12.34) for n = 1, or for the fundamental, and simplifying the resulting expression yields

$$\begin{aligned}\Sigma_1 &= 3\sin(\alpha - \omega t) + \sin(\alpha + \omega t) + \sin(\alpha + \omega t - 120) \\ &\quad + \sin(\alpha + \omega t - 240) = 3\sin(\alpha - \omega t) \quad \text{numeric} \qquad (12.35)\end{aligned}$$

Thus the backward-rotating fields of the three different phases cancel and the forward-rotating fields add. Evaluating eq. (12.34) for n = 3, and reducing any resulting numerical angles which are in excess of 360 electrical degrees to their basic angular equivalents, we obtain

$$\begin{aligned}\Sigma_3 &= \sin(3\alpha - \omega t) + \sin(3\alpha - \omega t - 240) + \sin(3\alpha - \omega t - 120) \\ &\quad + \sin(3\alpha + \omega t) + \sin(3\alpha + \omega t - 120) + \sin(3\alpha + \omega t - 240) = 0 \\ &\qquad \text{numeric} \qquad (12.36)\end{aligned}$$

From eq. (12.36) it is apparent that both the backward- and the forward-rotating fields of the third harmonic are equal to zero. All of the triplen harmonics of higher order (i.e., the ninth, fifteenth, etc.) are also equal to zero, as would be expected and as can be verified by use of eq. (12.34). Evaluating eq. (12.34) for n = 5, and simplifying the resulting numerical angles, gives us

$$\begin{aligned}\Sigma_5 &= \sin(5\alpha - \omega t) + \sin(5\alpha - \omega t - 120) + \sin(5\alpha - \omega t - 240)\\ &\quad + \sin(5\alpha + \omega t) + \sin(5\alpha + \omega t - 0) + \sin(5\alpha + \omega t - 0)\\ &= 3 \sin(5\alpha + \omega t) \quad \text{numeric} \end{aligned} \tag{12.37}$$

Then, for the fifth harmonic, the forward-rotating fields of the three different phases cancel and the backward-rotating fields add. Evaluating eq. (12.34) for n = 7 and again simplifying the resulting numerical angles, we obtain

$$\begin{aligned}\Sigma_7 &= \sin(7\alpha - \omega t) + \sin(7\alpha - \omega t - 0) + \sin(7\alpha - \omega t - 0)\\ &\quad + \sin(7\alpha + \omega t) + \sin(7\alpha + \omega t - 240) + \sin(7\alpha + \omega t - 120)\\ &= 3 \sin(7\alpha - \omega t) \quad \text{numeric} \end{aligned} \tag{12.38}$$

Accordingly, for the seventh harmonic, the backward-rotating fields of the three different phases cancel and the forward-rotating fields add; and so on for the eleventh, thirteenth, seventeenth, and so on, harmonics. If the process above is repeated for the higher harmonics, it will be found that the harmonics (with the triplen harmonics eliminated) are alternately forward rotating and backward rotating. Then the fundamental as well as the seventh, thirteenth, and nineteenth harmonics are forward-rotating fields, and the fifth, eleventh, and seventeenth harmonics are backward-rotating fields.

The complete expression for the magnetomotive-force wave produced by a three-phase stator is then

$$\begin{aligned}(\mathrm{MMF})_{3\phi} &= \frac{6N_{st}\sqrt{2}\, I_1}{\pi p}\Big[K_pK_d \sin(\alpha - \omega t) + \frac{1}{5}K_{p5}K_{d5} \sin(5\alpha + \omega t)\\ &\quad + \frac{1}{7}K_{p7}K_{d7} \sin(7\alpha - \omega t)\\ &\quad + \frac{1}{11}K_{p11}K_{d11} \sin(11\alpha + \omega t) + \frac{1}{13}K_{p13}K_{d13} \sin(13\alpha - \omega t)\\ &\quad + \frac{1}{17}K_{p17}K_{d17} \sin(17\alpha + \omega t) + \cdots\Big]\\ &\qquad \text{ampere-turns/winding} \end{aligned} \tag{12.39}$$

Although the harmonic train extends indefinitely, the 17th or the 19th harmonic is about as high an order as is normally required, for the various considerations which require the use of such harmonics. The coefficient of eq. (12.39) is written in various alternate forms in the technical literature, such as

$$\frac{6N_{st}\sqrt{2}\,I_1}{\pi p} = \left(\frac{3}{2}\right)\frac{4}{\pi}\,\frac{N_{st}}{p}\,(\sqrt{2}\,I_1) = (0.90)\,\frac{3N_{st}}{p}\,I_1 \quad \text{ampere-turns/winding} \qquad (12.40)$$

Further, it can be shown that, in general, the polyphase magnetomotive force coefficient is equal to $0.90qN_{st}I_1/p$ ampere-turns/winding for a q-phase stator winding.

12.6 EXAMPLE OF THE GRAPHICAL CONSTRUCTION OF THE MAGNETOMOTIVE-FORCE WAVE PRODUCED BY A THREE-PHASE STATOR WINDING

From an inspection of eq. (12.39) it is apparent that the three-phase magnetomotive force is equal to the sum of the fundamental and the various harmonics shown in that equation for all values of ωt. However, each harmonic will travel along the air gap at a different speed from that of the fundamental and from that of each other harmonic. Thus the wave shape of the magnetomotive force produced by the three-phase winding will change continuously as a function of time. This can be illustrated by laying out the magnetomotive-force wave of each phase at a specific instant of time for a given stator winding, and then adding the three magnetomotive forces for 2π electrical radians along the air gap. The result is the wave shape of the rotating three-phase magnetomotive-force wave at that instant of time. If the procedure above is repeated for another instant of time, the resulting three-phase wave shape will, in general, be somewhat different from that of the first wave.

This has been done in Figs. 12.2 and 12.3 for a four-pole induction motor with 60 stator slots and with a full-pitch stator winding. The stator winding for this example has $N_1/pq = 60/(4 \times 3) = 5$ coils in each group. The layout of the magnetomotive forces is done only for the first two pole pitches around the periphery of the stator bore, since the second two poles pitches will repeat the pattern of the first two. The scale of the ordinate (i.e., the magnetomotive force scale) is in per unit of the maximum height of the individual phase wave.

First, consider Fig. 12.2. The wave shapes in this figure correspond to the instant when the current in phase A and the corresponding magnetomotive force of phase A are at their maximum values. At this time the currents in phases B and C, and their respective magnetomotive forces, are at -0.50 of their maximum values. The current in phase A flowing through the coils of group A will cause a progressive increase in magnetomotive force, from one slot to another, at this particular time. Also, the current in phase A flowing through the coils of group -A will cause a progressive decrease in magnetomotive force, from one slot to another, at the same

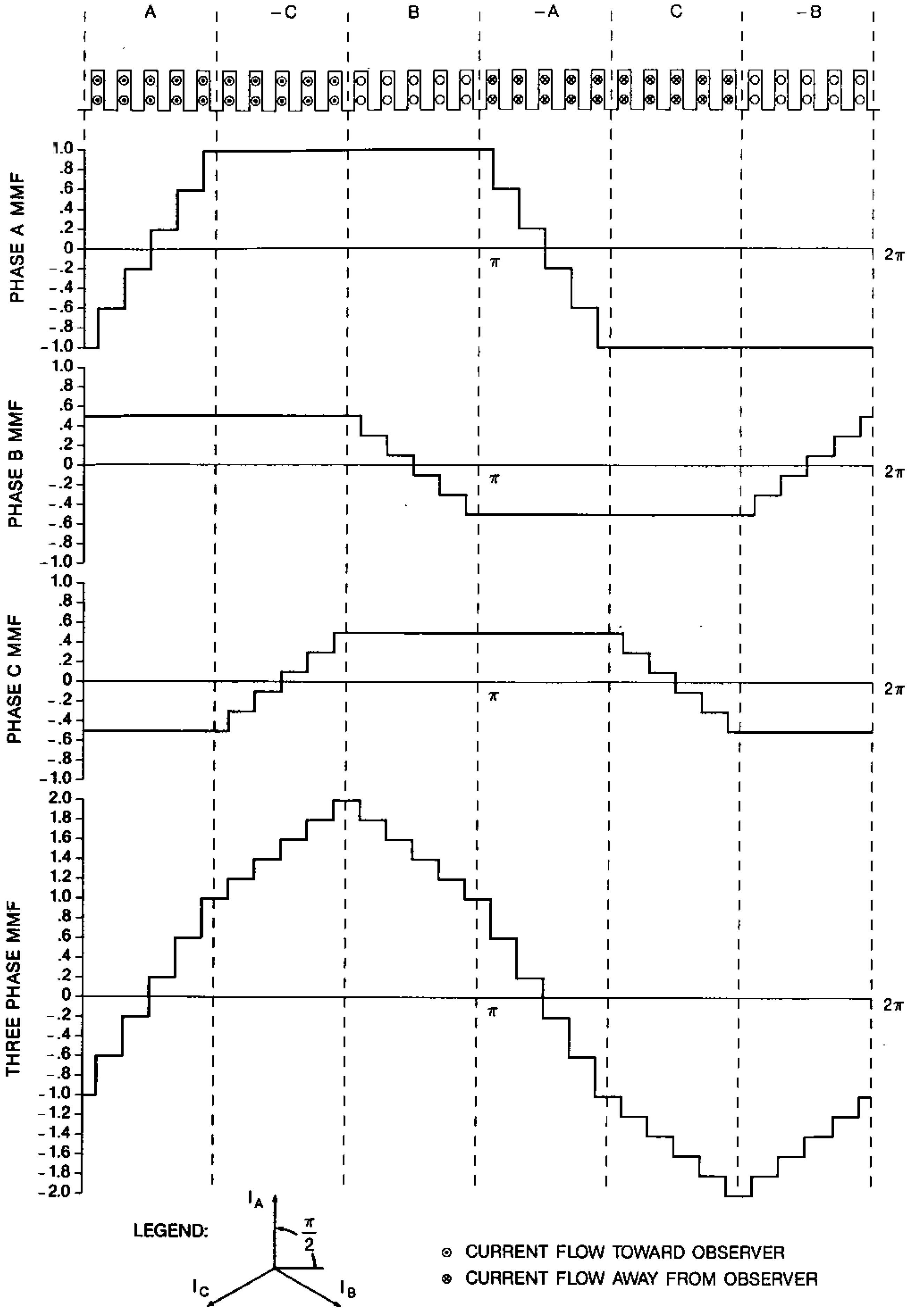

FIGURE 12.2 Magnetomotive-force wave shape for a three-phase full-pitch stator winding with 60 slots at the times when phase A current is at maximum value.

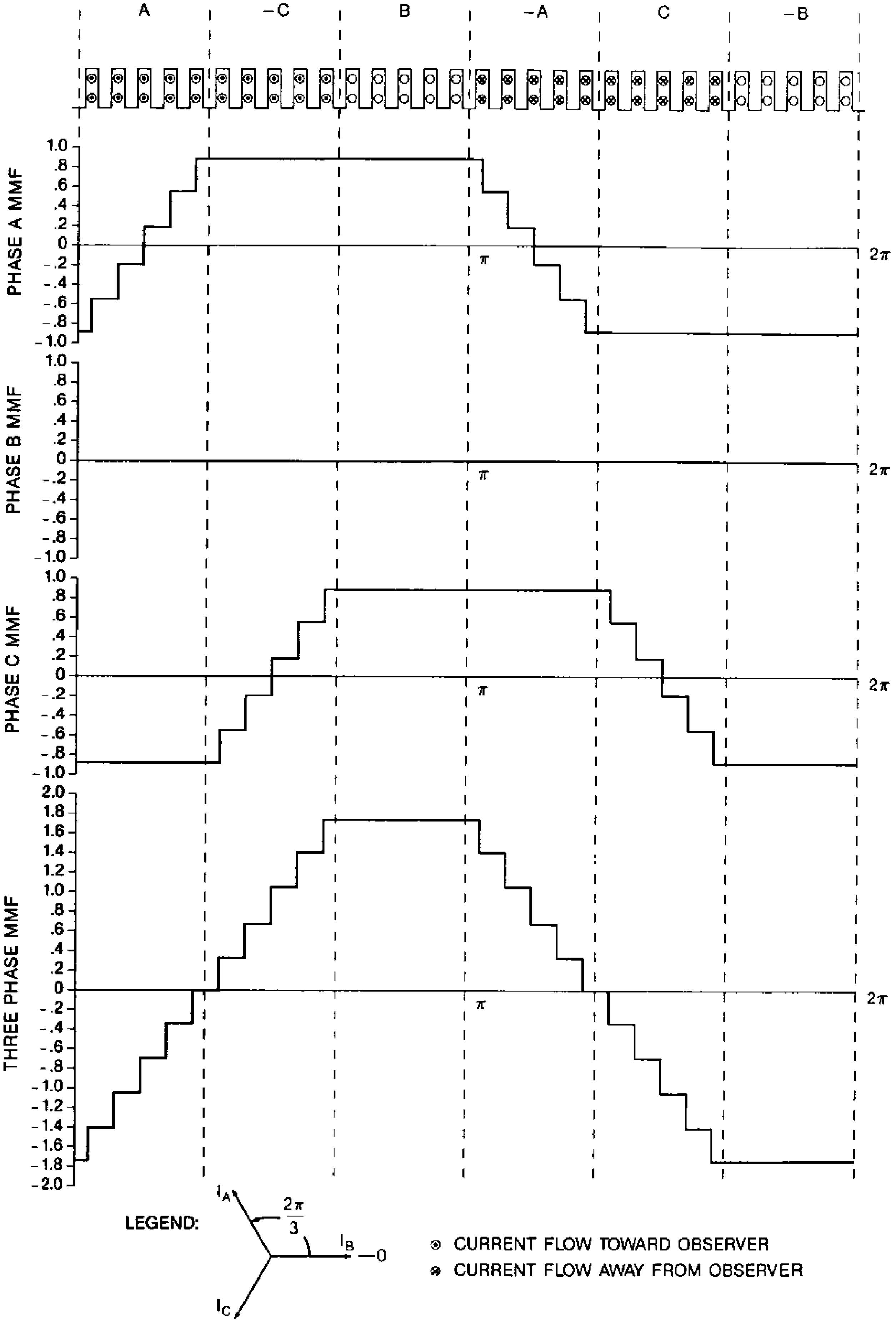

FIGURE 12.3 Magnetomotive-force wave shape for a three-phase full-pitch stator winding with 60 slots at a time 30 electrical degrees later than that of Fig. 12.2.

instant. This results in the magnetomotive-force wave shape for phase A, as shown in the figure. From the point of view discussed in Section 12.3, coil groups A and -A can be considered as two cooperating phase groups which, cooperatively, produce the magnetomotive force attributable to phase A along two pole pitches.

Since the current in phase B is negative at this time, it will cause a progressive decrease in magnetomotive force, from one slot to another as it flows through the coils of group B, and will cause a progressive increase in magnetomotive force from one slot to another as it flows through the coils of group -B. This, then, results in the magnetomotive force wave shape for phase B, at this instant of time, as shown in Fig. 12.2. However, the current in phase C, which is also negative, will cause a progressive increase in magnetomotive force from one slot to another as it flows through the coils of group -C, and will cause a progressive decrease in magnetomotive force from one slot to another as it flows through the coils of group C. Again, this results in the magnetomotive-force wave of phase C, as shown in the figure, for this instant of time.

In Fig. 12.3 the magnetomotive forces are laid out for the same stator winding, but for an instant of time corresponding to $\omega t = \pi/6$ electrical radians, or 30 electrical degrees, later. At this time, the phase currents are $I_A = \sqrt{3}/2$, $I_B = 0$, and $I_C = -\sqrt{3}/2$. If the corresponding magnetomotive force is laid out for each individual phase and then the individual phase values added for various points along the stator bore to give the three-phase magnetomotive-force wave, the wave shape shown in Fig. 12.3 will result.

Since the six coil groups occupy the same physical positions along the two pole pitches for both figures, the difference in appearance of the wave shapes is due only to the difference in the values of the phase currents for the two cases. However, even though the coil groups, and therefore the magnetomotive force of each phase, remain fixed in space, the resulting three-phase magnetomotive-force wave does progress in space as a function of time. By inspection of the two figures it is apparent that the center of the three-phase wave has progressed $\pi/6$ electrical radians, or 30 electrical degrees, in the positive direction, from Figs. 12.2 and 12.3. That amount of angular progression of the three-phase rotating wave is exactly equal to the angular progression of the angle ωt of the current and hence of the applied voltage. Expressed in other terms, the three-phase magnetomotive-force wave rotates in synchronism with the impressed voltage, requiring one cycle for each pair of poles. Figures 12.2 and 12.3 represent the two limits in wave shape of the three-phase wave, and each wave shape repeats every $\pi/3$ electrical radians. The wave shape at all other instants of time is somewhere between these two limits.

As mentioned earlier, a full-pitch winding was intentionally assumed for this example. Such a winding will have the maximum amplitudes of the various odd harmonics present, since none of these harmonics will have been decreased by their respective pitch factors, as discussed in Section 9.9. In actual practice, the design engineer would have selected a coil throw of 1-13 to 1-15, instead of a full-coil throw of 1-16, to limit some of the adverse effects of space harmonics.

12.7 THE EQUIVALENT CIRCUIT WITH THE SPACE HARMONICS CONSIDERED

The complete equivalent circuit of the polyphase induction motor shown in Fig. 5.4, and the analysis of this circuit as discussed in Chapter 5, are based on utilizing only the fundamental component of the air-gap magnetomotive force wave and hence only the fundamental component of the air-gap flux wave. For most designs and in most applications, this is sufficiently accurate for performance calculation, as the wave shape of the stator wave can be made to approach that of a sine wave to an acceptable extent. This is done by using a sufficiently large number of coils or slots per phase group and by judicious choice of the coil pitch, as discussed in Chapter 9. However, it should be kept in mind that the various space harmonics and the fundamental are superposed and that each separate harmonic can act independently and can interact with any other one.

It is occasionally a useful concept to visualize the electromagnetic behavior of the various space harmonics as being similar to the behavior of separate motors, with a common stator winding and a common shaft, but with magnetizing reactances and secondary impedances corresponding respectively to the air-gap flux wave of each specific harmonic. The complete equivalent circuit of such a conceptual motor, as suggested by Alger and others, is shown in Fig. 12.4. Viewing the various space harmonics from the point of view above is useful, for example, in evaluating the effect of the various harmonic torques on the fundamental speed-torque curve.

In this circuit the phase quantities V_1, R_1, X_1, R_2, X_2, and X_m are identical to those used with the standard equivalent circuit, such as that shown in Fig. 5.4. The magnetizing reactance of each of the harmonics, such as X_{m-5}, is based on the component of air-gap flux of that particular harmonic. The rotor parameters R_{2-n} and X_{2-n} are based on the impedance of the actual rotor winding, but to the flow of current that has the number of poles corresponding to the harmonic being considered. It will be noted that the slip function of R_{2-n} for each harmonic is set up for the rotor slip for that particular harmonic, and is dependent on the order of the harmonic and on whether the harmonic field is forward rotating or backward rotating. Thus the nth slip-function term is $R_{2-n}/[1 - n(1 - s)]$ if it is a forward-rotating field, and $R_{2-n}/[1 + n(1 - s)]$ if it is a backward-rotating field.

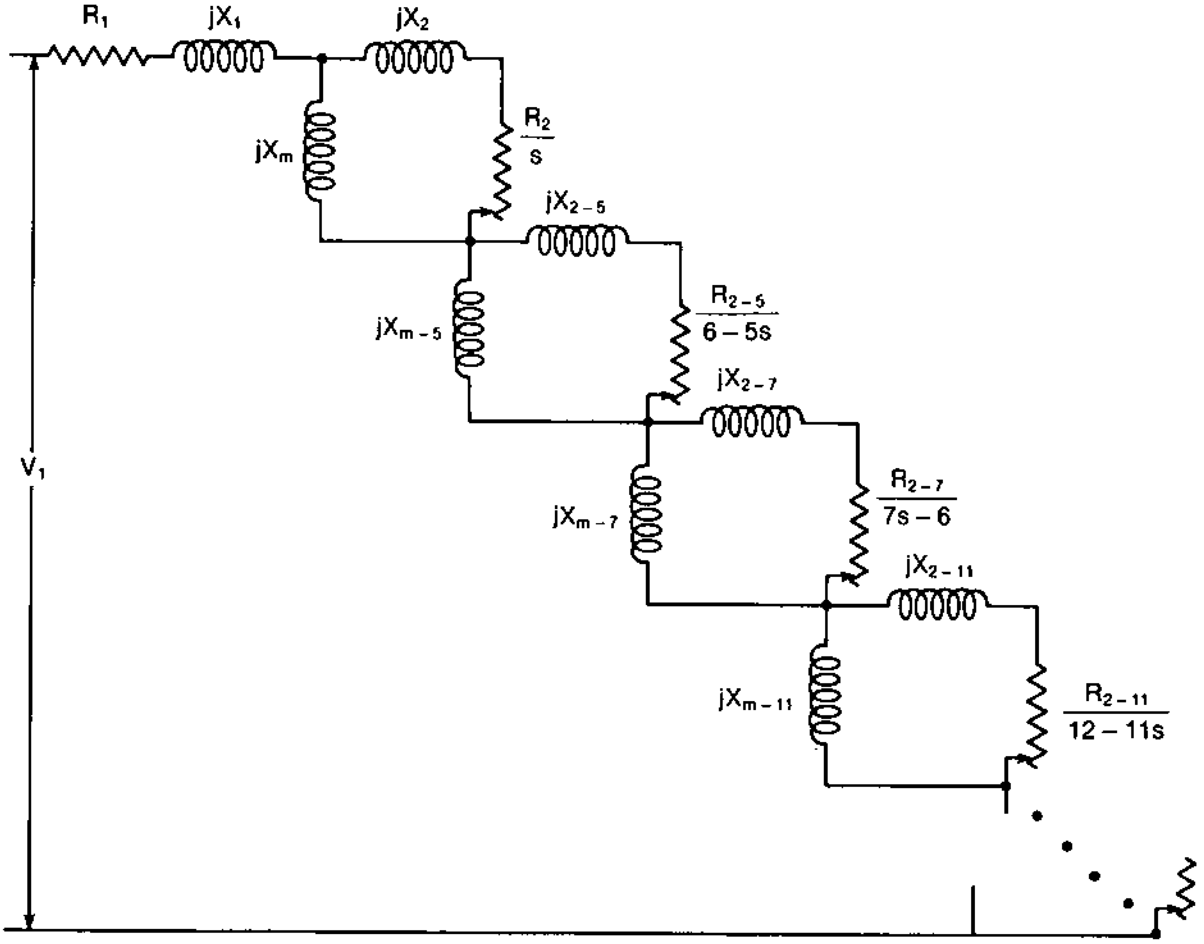

FIGURE 12.4 Polyphase induction motor equivalent circuit, considering the magnetomotive-force space harmonics.

12.8 MAGNETIZING CURRENT

The normal notation of phase current I_1 was used in the derivation of the magnetomotive-force wave in order to distinguish the magnitude of total phase current from the magnitude of current flowing in phase groups of the parallel circuits within the phase winding. That purpose having now been achieved, it is appropriate to replace it with the normal notation for magnetizing current per phase I_m, since this current is the phase value of the current, which together with the series turns per phase N_{st}, sustains the rotating magnetomotive-force wave, which magnetizes the machine. Then eq. (12.39) should be written as

$$(\text{MMF})_{3\phi} = \frac{6N_{st}\sqrt{2}\,I_m}{\pi p}\Big[K_pK_d\sin(\alpha - \omega t) + \frac{1}{5}K_{p5}K_{d5}\sin(5\alpha + \omega t) + \frac{1}{7}K_{p7}K_{d7}\sin(7\alpha - \omega t) + \frac{1}{11}K_{p11}K_{d11}\sin(11\alpha + \omega t)\cdots\Big] \quad \text{ampere-turns} \qquad (12.41)$$

The maximum value of the fundamental of the rotating three-phase magnetomotive-force wave, from eq. (12.41), is

$$(\text{MMF})_m = \frac{6N_{st}\sqrt{2}\,I_mK_pK_d}{\pi p} \quad \text{ampere-turns} \qquad (12.42)$$

The quantity $(\text{MMF})_m$ can also be expressed in terms of the maximum value of the rotating air-gap flux wave B_m, of the effective length of the radial air gap g', and of the maximum value of the magnetic field intensity across the air gap. The maximum value of the magnetic field intensity across the air gap is equal to

$$H_m = \frac{(\text{MMF})_m}{g'} \quad \text{ampere-turns/meter} \qquad (12.43)$$

The relationship between B_m and H_m is

$$B_m = \mu H_m = \frac{4\pi}{10^7}H_m \quad \text{webers/meter}^2 \qquad (12.44)$$

Substituting eq. (12.43) into eq. (12.44) yields

$$B_m = \frac{4\pi(\text{MMF})_m}{10^7 g'} \quad \text{webers/meter}^2 \qquad (12.45)$$

Solving eq. (12.45) for $(\text{MMF})_m$ gives us

$$(\text{MMF})_m = \frac{B_m g' 10^7}{4\pi} \quad \text{ampere-turns} \qquad (12.46)$$

Equating eqs. (12.42) and (12.46), solving for I_m, and simplifying gives us

$$I_m = \frac{296 \times 10^3 B_m p g'}{N_{st} K_p K_d} \quad \text{amperes/phase} \tag{12.47}$$

The effective increase in the length of the air gap due to the effect of the slot openings and of the radial ventilating duct openings in causing air-gap flux fringing is discussed in Chapter 14. It will suffice to say at this point that this phenomenon of the air-gap flux field is handled by calculating a "fringing factor" K_f. The effective air gap g' is equal to the actual gap g, multiplied by the fringing factor K_f, or

$$g' = K_f g \quad \text{meters} \tag{12.48}$$

Then eq. (12.47) can be written as

$$I_m = \frac{296 \times 10^3 B_m p K_f g}{N_{st} K_p K_d} \quad \text{amperes/phase} \tag{12.49}$$

In deriving eq. (12.49), it has tacitly been assumed that all the magnetomotive force is consumed in forcing the mutual flux across the air gap and that none is consumed in the core. Although the reluctance of air is orders of magnitude greater than that of the steel core, there is considerable magnetomotive-force drop along the flux path in the core due to the length of this path in comparison to that of the air gap. It will vary in typical machines from only a few percent to as much as 20% of the total magnetomotive force, depending on such factors as the number of poles, types of steel, desired power factor, and so on. The concept of saturation of ferromagnetic materials and calculation of the magnetomotive-force drop in flux paths in steel is discussed in Chapter 14. For eq. (12.49), saturation is handled by calculating a saturation factor K_s, which is defined as

$$K_s = \frac{\begin{matrix}\text{(magnetomotive force drop} \\ \text{across air)}\end{matrix} + \begin{matrix}\text{(magnetomotive force drop} \\ \text{across steel core)}\end{matrix}}{\text{magnetomotive force drop across air}} \quad \text{numeric} \tag{12.50}$$

Equation (12.49) should then be written as

$$I_m = \frac{296 \times 10^3 B_m p K_f K_s g}{N_{st} K_p K_d} \quad \text{amperes/phase} \tag{12.51}$$

Equation (12.51) can be modified to use units of maxwells/inch^2 for B_m and units of inches for g, by remembering that there are 10^8 maxwells in 1 weber and that there are 39.37 inches in 1 meter. Then

$$I_m = \frac{0.116 B_m p K_f K_s g}{N_{st} K_p K_d} \quad \text{amperes/phase} \tag{12.52}$$

12.9 VARIOUS TYPES OF HARMONICS PRESENT IN THE AIR GAP

Before considering the various effects that the several types of air-gap harmonics produce, it is in order to identify the harmonics by type. Up to this point, only the stator space harmonics have been evaluated. Although this type of harmonic is very important, there are other types of harmonics in the air gap, including (1) stator-slot harmonics, (2) rotor-slot harmonics, (3) the harmonics that result from variations in permeance around the air gap, which are called permeance harmonic fields, and (4) other rotor harmonics, including the rotor incidental harmonics. Various interactions between combinations of the aforementioned harmonics produce the harmonic effects, mostly undesirable, which will be considered subsequently.

12.9.1 Stator-Space Harmonics

The set of harmonics present in the three-phase magnetomotive-force wave and shown in eq. (12.39) are called the stator space harmonics or stator field harmonics. When they act together and include the fundamental, the resulting magnetomotive-force wave shape resembles that of the specific example shown in Figs. 12.2 and 12.3. Their combined electrical and mechanical effects on the behavior of a polyphase motor can be visualized as constituting a corresponding set of motors of small power rating mounted on a common shaft and electrically connected in series with the fundamental motor. The induction-motor equivalent circuit can be extended to include this concept, as shown in Fig. 12.4.

Equation (12.39) shows the complete, rotating, three-phase magnetomotive-force wave produced by a three-phase stator, expressed as a series of harmonics. Considering the fundamental component as a harmonic of order one, the series consists of odd terms only, with the triplen terms missing. Beginning with the fundamental term, the harmonic terms are alternately forward rotating and backward rotating. It is normal practice to designate the forward-rotating terms as (+) harmonics, or as (F), and the backward-rotating terms as (-), or as (B), harmonics. Then the orders of the actual space harmonics of the stator are -5, 7, -11, 13, -17, 19, and so on; expressed otherwise, they are 5B, 7F, 11B, 13F, 17B, 19F, and so on, where F is understood to mean forward rotating and B is understood to mean backward rotating. The maximum value of a given order of harmonic, such as the nth, is equal to (1/n)th of $6N_{st}\sqrt{2}\ I_1/(\pi p)_1$ multiplied by the pitch factor and by the distribution factor for that harmonic. As noted earlier, judicious choice of the stator pitch offers an opportunity to control the magnitude of an undesirable harmonic. Since the fifth order and the seventh order have the greatest magnitudes, the pitch factor is generally chosen to minimize their effects, with the selection of a pitch of from 80 to 90%. This choice of pitch will reduce the fundamental induced voltage by less than 5%.

Stator space harmonics are also called stator field harmonics, since they constitute the harmonics of the stator magnetomotive-force field wave. Each space harmonic, or field harmonic, of order n has a corresponding number of poles, which is equal to

$$N_{pn} = np \quad \text{poles} \tag{12.53}$$

where p is the number of motor poles. This relationship is apparent from the fact that the nth harmonic must experience n complete cycles, along the air gap, for one cycle experienced by the fundamental wave along 2π electrical radians on the fundamental scale.

Although relatively few two-phase induction motors are now produced, it is appropriate to note the harmonics present in the stator magnetomotive-force wave of such machines. They are -3, +5, -7, +9, -11, +13, -15, +17, and so on. Since the triplen harmonics do not cancel in a two-phase stator, they must appear in the rotating air-gap magnetomotive force and flux wave. The space harmonics of two-phase stators arise from the same cause as for three-phase stators, which is the channeling of stator current into coils connected in series within stator phase groups.

The preceding analysis of the magnetomotive-force wave has been based on an integral-slot stator winding (i.e., a winding for which N_1/pq is equal to an integer). As mentioned earlier, a fractional-slot winding (i.e., a winding for which N_1/pq is not an integer) will produce space subharmonics. The primary effects of subharmonics are (1) a slight increase in reactance and (2) a slight increase in losses, and usually such subharmonic effects are not very significant.

12.9.2 Stator-Slot Harmonics

The concentration of stator current into discrete slots causes the abrupt change in magnetomotive force from one slot to another along a phase group, which is apparent in Figs. 10.2 and 10.3. Such discrete steps, instead of a gradual increase or decrease in magnetomotive force of the fundamental, produce a stationary wave of $2N_1/p$ poles. This stationary wave interacts with the rotating fundamental of p poles to give the rotating stator-slot harmonic wave of $2N_1 \pm p$ poles and with a harmonic order of $2N_1/p \pm 1$. It can interact with any space harmonic, in addition to the fundamental, to give additional rotating stator-slot harmonic waves. For the space harmonic of order n, the resulting stator-slot harmonic will have a number of poles equal to

$$(N_{s1})_n = 2N_1 \pm np \quad \text{poles} \tag{12.54}$$

and with a harmonic order of

$$(n_{s1})_n = \frac{2N_1}{p} \pm n \quad \text{numeric} \tag{12.55}$$

The orders of the slot harmonics are generally not as important as are the number of poles. This will become apparent subsequently, when the effect of slot harmonics on the speed-torque curve is considered. As mentioned previously, unlike the stator space harmonics, the stator-slot harmonics are not directly affected by the stator-pitch factor.

12.9.3 Rotor-Slot Harmonics

Also, the concentration of rotor current into discrete slots causes abrupt changes in the rotor magnetomotive force from one rotor slot to another. Again, this causes a standing wave of $2N_2/p$ poles. In a manner analogous to that for the stator, this stationary rotor wave interacts with the rotating fundamental wave of p poles to give the rotating rotor-slot harmonic wave of $2N_2 \pm p$ poles and with a harmonic order of $2N_2/p \pm 1$. It can interact with any space harmonic in addition to the fundamental, to give additional rotating rotor-slot harmonic waves. In general, for the nth-order space harmonic, the resulting rotor-slot harmonic will have a number of poles equal to

$$(N_{s2})_n = 2N_2 \pm np \quad \text{poles} \tag{12.56}$$

with harmonic orders of

$$(n_{s2})_n = \frac{2N_2}{p} \pm n \quad \text{numeric} \tag{12.57}$$

Like the stator-slot harmonics, the rotor-slot harmonics are not directly affected by the stator-pitch factor. However, they are affected by the rotor-skew factor, as defined in eq. (10.151).

12.9.4 Harmonics in the Air-Gap Permeance

The permeance of the air gap is a function of the radial length of the air gap. However, both the stator- and rotor-slot openings produce cyclical variations in the radial air-gap length as a function of distance around the periphery of the gap. Such cyclical variations can be expressed in terms of trigonometric functions, for both the stator and the rotor, which modulate the average radial length and hence the permeability of the average air gap.

Let β be the angle in mechanical radians of a point somewhere along the stator bore and let $\beta = 0$ at the centerline of a given stator slot. If the variation in permeance produced by the stator slots is approximated as a sinusoidal variation, the cyclical function that gives this variation, in per unit, caused by the stator can be approximated as $1 + (P_1/P_{av}) \sin N_1\beta$, where P_1 is half of the total change in air-gap permeance due to the stator, and P_{av} is the average value of the air-gap permeance. Also, the cyclical function, which gives the variation in per unit caused by the rotor, can be approximated as $1 + (P_2/P_{av}) \sin N_2(\beta - n_r t)]$, where P_2 is half of the total change in permeance due to the rotor, n_r is rotor speed in mechanical radians, and t is time measured in seconds.

The combined effect on the air-gap permeance of the rotor and the stator slot openings is equal to the product of the two functions above, multiplied by the average permeance. Then

$$P = P_{av}\left(1 + \frac{P_1}{P_{av}} \sin N_1\beta\right)\left\{1 + \frac{P_2}{P_{av}} \sin[N_2(\beta - n_r t)]\right\} \quad \text{webers/ampere} \tag{12.58}$$

Performing the multiplication indicated in eq. (12.58) gives us

$$\begin{aligned} P = {} & P_{av} + P_2 \sin[N_2(\beta - n_r t)] + P_1 \sin N_1\beta \\ & + \frac{P_1P_2}{P_{av}} \sin[N_2(\beta - n_r t)] \sin N_1\beta \quad \text{webers/ampere} \end{aligned} \tag{12.59}$$

Since $\sin\theta \sin\phi = 1/2 \cos(\theta - \phi) - 1/2 \cos(\theta + \phi)$,

$$\begin{aligned} P = {} & P_{av} + P_2 \sin[N_2(\beta - n_r t)] + P_1 \sin(N_1\beta) \\ & + \frac{P_1P_2}{2P_{av}} \{\cos[(N_2 - N_1)\beta - N_2 n_r t] \\ & - \cos[(N_2 + N_1)\beta - N_2 n_r t]\} \quad \text{webers/ampere} \end{aligned} \tag{12.60}$$

which is the air-gap permeance of a three-phase induction motor.

The term P_{av} is the average permeance of the air gap. When P_{av} is multiplied by the rotating fundamental of the stator magnetomotive-force wave, the result is the rotating fundamental component of the air-gap flux, with units of webers. The term $P_2 \sin[N_2(\beta - n_r t)]$ corresponds to the variations in permeance caused by the rotor slots, and the term $P_1 \sin N_1\beta$ corresponds to the variations in permeance caused by the stator slots. The term

$$(P_1P_2/2P_{av}) \cos[(N_2 - N_1)\beta - N_2n_rt]$$

corresponds to a rotating field with $2(N_2 - N_1)$ poles, and as will be subsequently apparent, can contribute to synchronous locking and crawling. The term

$$(P_1P_2/2P_{av}) \cos[(N_2 + N_1)\beta - N_2\,n_rt]$$

corresponds to a rotating field with $2(N_1 + N_2)$ poles. This term contributes much less to synchronous locking and crawling torques, because of its greater number of poles.

12.9.5 Rotor Harmonics

The rotor winding of a squirrel-cage rotor will produce a fundamental current wave and hence a fundamental magnetomotive-force wave. This current results from the voltage induced in the rotor bars by the fundamental of the rotating stator flux waves. The rotor winding of a wound-rotor motor will produce space harmonics in addition to the fundamental, since the rotor current is channeled through phase belts. As noted earlier, for both types of rotor windings, rotor-slot harmonics will exist because of concentration of current into rotor slots.

The associated rotating flux waves of all the magnetomotive-force harmonics present in the stator, in addition to the stator fundamental field, will induce corresponding voltages in the rotor winding. These harmonic rotor voltages will cause harmonic currents of the same order to flow in the rotor winding. Thus the rotor will, in general, contain all harmonics that are present in the stator. In addition, a set of incidental rotor harmonics will be set up, due to the interaction of rotor-slot harmonics with the various orders of stator harmonics present in the rotor. Fortunately, many of the rotor harmonics are of too high an order to be significant.

12.10 PERTURBATIONS ON THE SPEED-TORQUE CURVE

Early in the history of induction motors it became apparent that irregularities occurred occasionally in the lower portion of the speed-torque curve, which deviated considerably from that predicted by calculation. In some cases, dips would occur in the speed-torque curve such that the torque produced by the motor was less than the torque required by the driven load, causing the motor to "hang up." In other cases, the motor would tend to run at a low speed, or to lock at standstill, as if it had synchronized at such a speed. As might be expected, such unpredictable and at that time perplexing behavior had the effect of stimulating considerable interest and study among engineers in both the United States and Europe. During the next several decades a considerable number of significant technical papers were published by Arnold, la Cour, Fraenchel, Dreese, Stiel, Graham, Kron, Weber, Lee, Trickey, Moller, Richter, and others. This period of study and publication resulted in understanding the background causes of speed-torque perturbations. In general, such perturbations are classified, in terms of the undesirable effects on the speed-torque, as (1) asynchronous crawling torques, (2) synchronous crawling torques, and (3) synchronous locking torques. The first results from superposing a low-order space harmonic or slot harmonic on the fundamental, and the last two result from interactions of the space harmonics and the slot harmonics. The tendency for these effects to occur can be controlled or eliminated by taking appropriate steps at the design stage, including proper choice of stator and rotor slots for a given number of poles, rotor-bar skewing, and judicious choice of stator-coil throw. Since it can be assumed that the motor manufacturers are familiar with the design steps that should be taken to control such undesirable speed-torque effects, it is not very probable that such effects will occur on new machines. However, not infrequently, the stators of older machines are subsequently reconnected, or even rewound, for a different speed and hence for a different number of poles. For all such cases, the possibility of undesirable speed-torque effects, and as discussed subsequently, the possibility of additional noise, should be investigated.

The undesirable speed-torque effects of asynchronous crawling torques, synchronous crawling torques, and synchronous locking torques will be considered sufficiently to gain general understanding. For a deep understanding of the subject, the reader is referred to the publications on this subject included in the list at the end of the book.

12.10.1 Asynchronous Crawling

As discussed earlier, each stator space harmonic of order n represents a rotating magnetomotive-force wave with np poles. This rotating magnetomotive-force wave, acting on the average air-gap permeance, produces a rotating air-gap flux wave of the same number of poles. This rotating air-gap flux wave induces voltages in the various rotor bars, which, in turn, produces a corresponding rotating rotor-current wave. The angular velocity of the harmonic rotor-current wave, as viewed from the stator, is equal to that of the harmonic air-gap flux wave, and since both waves have the same number of poles, they can interact to produce a torque. As shown in eq. (7.40), the fundamental torque is equal to the vector cross product of the air-gap

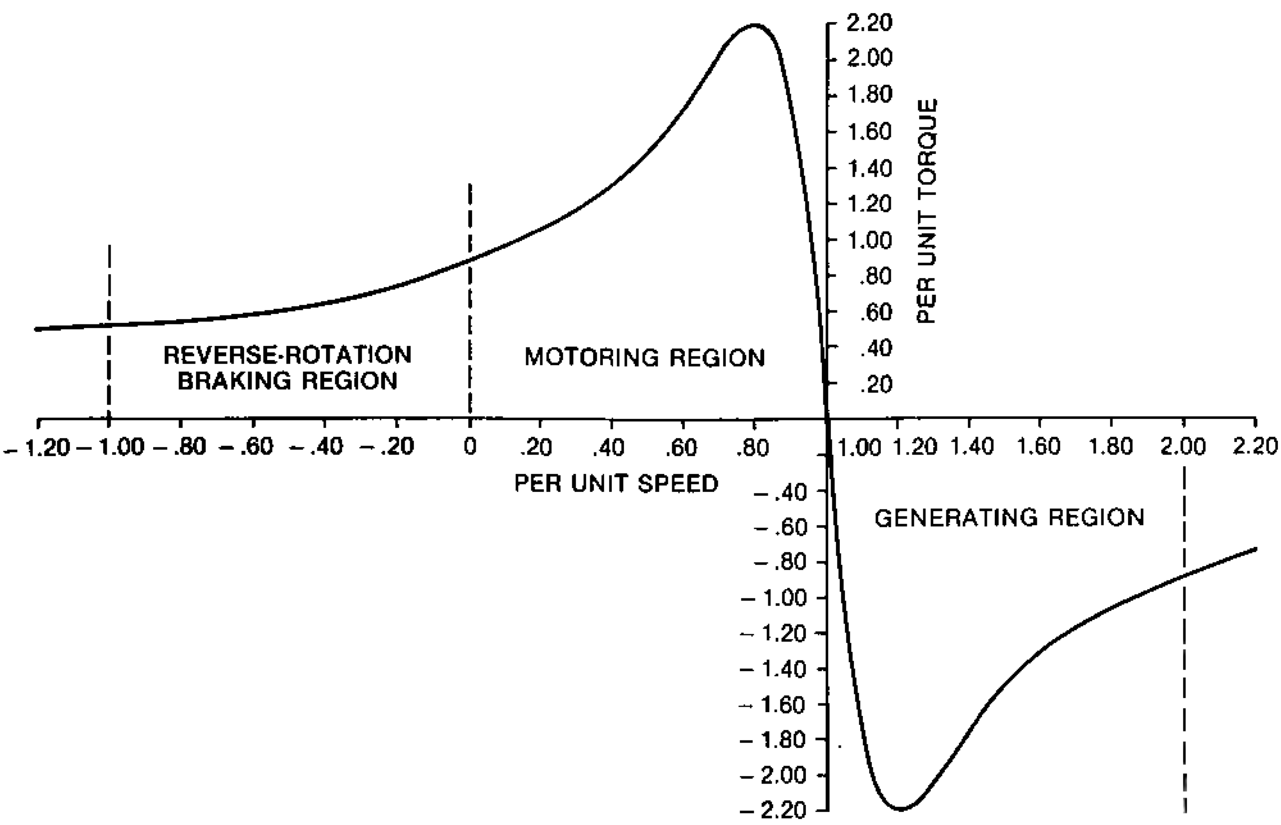

FIGURE 12.5 Extended speed-torque curve produced by the fundamental, showing the various regions of operation.

flux and the rotor current, or to $T = \phi_m \times I_2$ newton-meters, and for the nth space harmonic, $T_n = \phi_{mn} \times I_{2n}$, where in this case it is understood that the subscript n refers to harmonic values of ϕ_m and I_2. Before discussing how the various harmonic torques cause speed-torque problems, when they are superposed over the fundamental torque, it is necessary to understand the directional sense and shape of any speed-torque relationship, fundamental or harmonic, relative to the several regions of operation of the extended speed-torque curve.

Figure 12.5 shows the speed-torque curve produced by the fundamental air-gap flux and rotor-current waves for a rotor-speed range of from -1.0 to +2.0 per unit of synchronous speed N_s. Such an extended speed-torque curve can be constructed by using eq. (5.87), for example, and by then calculating corresponding points of speed and torque for a range of per unit slip of from +2.0 to -1.0.

The region of fundamental motor speed from 0 to 1.0 per unit of N_s, with a corresponding slip of from 1.0 to 0 per unit, represents the motoring region of the speed-torque curve which is the normal mode of operation. Within this region of operation, the motor rotor will produce a motoring torque in the positive direction of rotation. If, however, the motor rotor is driven against the positive direction of rotation, with positive-sequence voltage still applied to the stator terminals, the rotor is then rotating in a direction opposite to the direction of the three-phase field. The motion of the rotor bars relative to the rotating flux field continues to be in the same direction as before. However, since the resulting torque tends to cause rotation in the positive direction, with positive-sequence voltage still applied to the stator winding, this torque opposes the negative direction of rotation of the rotor. This mode of operation represents the reverse-rotation braking region of the speed-torque curve. Whereas the electrical power supplied to the stator winding is equal to the sum of the motoring power and the machine losses for motor action, it is equal to the sum of the braking power and the machine losses for braking action at a constant reverse speed. If, however, the rotor and connected load either increases or decreases in speed, this equality is no longer true, since the kinetic energy of the rotating system is changing.

A third mode of operation of a polyphase induction motor is generating in the generating region of the speed-torque curve. If the motor is allowed to accelerate to full speed in the motoring mode, it will reach a constant speed that is just below synchronous speed. If, somehow, the motor is driven through synchronous speed at this point, with positive-sequence voltage still applied to the stator winding, the torque produced by the motor will approach zero as the rotor approaches synchronous speed. At exact synchronous speed, there is no relative motion between the rotor bars and the rotating stator-flux wave and hence no torque is produced by the rotor. As the rotor speed is increased above synchronous speed, with positive-sequence voltage continuing to be supplied to the stator winding, the motion of the rotor bars changes relative to the rotating flux field, with a consequent change in the direction of the rotor-bar currents. The machine is now generating, that is, it is delivering an in-phase component of current and volt-amperes to the line, but it continues to draw magnetizing current and magnetizing volt-amperes from the line, to sustain the rotating flux field in the air gap. The mechanical power being delivered to the rotor shaft by whatever prime mover that is driving the rotor is equal to the sum of the electrical power delivered to the line and the machine losses.

With the foregoing background as to the directional sense and shape of speed-torque relationships within the extended speed-torque curve of the fundamental, it will now become apparent how the stator-space harmonics as well as the slot harmonics cause asynchronous crawling. All of the space harmonics present in the three-phase magnetomotive force wave will produce corresponding torques, with the forward-rotating harmonics producing torques that tend to cause rotation in the forward direction and with the backward-rotating harmonics producing torques that tend to cause rotation in the backward direction. Also, the forward-rotating slot harmonics, such as that with $2N_1 + p$ poles, will produce torques that tend to cause rotation in the forward direction, and the backward-rotating slot harmonics, such as that with $2N - p$ poles, will produce torques that tend to cause rotation in the

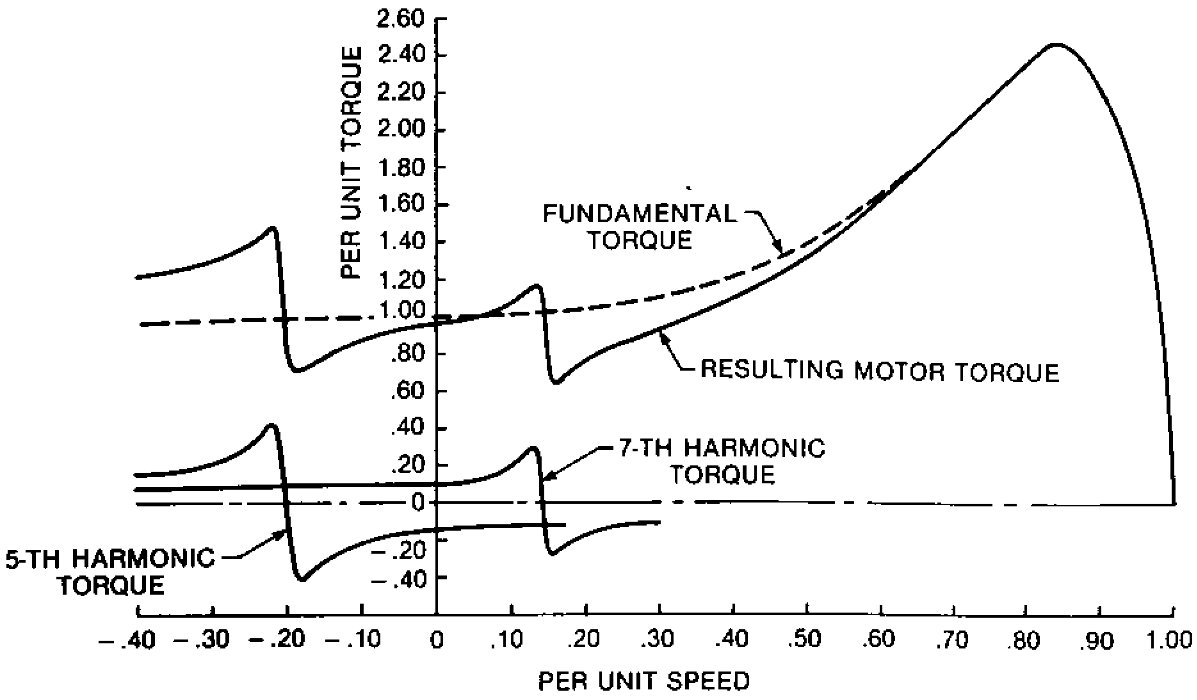

FIGURE 12.6 Speed-torque curve produced by the fundamental, fifth harmonic, and seventh harmonic space waves, showing the perturbations produced by the harmonics.

backward direction. Each forward torque and each backward torque will reach its respective synchronous speed at (1/n)th of fundamental synchronous speed, where n is the order of the particular harmonic. For the forward-rotating harmonics this will occur in the forward direction of rotation or in the motoring region of Fig. 12.5, and for the backward-rotating harmonics, this will occur in the reverse direction of rotation or in the reverse-rotation braking region of Fig. 12.5.

In Fig. 12.6, the torques produced by the fifth and seventh space harmonics are superposed on the fundamental torque to show the resulting irregularities on the fundamental speed-torque curve. The forward-rotating seventh harmonic produces a motoring torque in the speed range from zero speed to its synchronous speed, at $1/7 = 0.143$ per unit speed on the fundamental speed scale. Above this point the rotor speed of the motor is greater than synchronous speed of the seventh harmonic and it operates in its generating region. Thus it tends to reduce slightly the torque produced by the fundamental and tries to return an equivalent amount of electrical power to the stator bus. During a driven reverse rotation of the motor rotor, the seventh space harmonic produces a reverse-rotation braking torque which adds directly to that produced by the fundamental.

The forward direction of the motor rotor is opposite to the direction of rotation of the backward-rotating fifth harmonic. Then, as far as the fifth harmonic is concerned, the rotor is being driven in that harmonic's reverse direction. Accordingly, it produces a reverse-rotation braking torque for forward rotation of the motor rotor. On the other hand, when the motor rotor is actually driven in a reverse direction, that direction corresponds to the forward direction of the fifth harmonic, and the fifth harmonic torque is in its motoring region from zero speed to its synchronous speed, which occurs at $1/5 = 0.20$ per unit speed in the reverse direction. Within this speed range, this harmonic produces a torque that tends to produce rotation in this direction. At reverse-rotor speeds in excess of 0.20 per unit, the fifth harmonic is in its generating region, which tends to take power from the rotating system and to return it to the stator bus.

The effects of the torques produced by the forward-rotating seventh harmonic and by the backward-rotating fifth harmonic are shown in Fig. 12.6. It is apparent from an inspection of this figure that a "dip" in motor accelerating torque has occurred at a rotor speed slightly greater than synchronous speed for the seventh harmonic. Normally, the magnitude of the seventh harmonic is not sufficiently great for the resulting dip in motor torque to be a problem. However, if the stator winding has an adverse coil pitch and if the torque requirement of the connected load is significant during acceleration, it is then possible to have a very small amount of net accelerating torque in this region of the motor speed-torque region. Then the motor will accelerate very slowly through such a region, or will "crawl." In severe cases, the net accelerating torque will be extremely small or even less than the torque required by the load. In such a case, the motor will "hang up" and not accelerate to full speed. This, of course, is a serious problem, because the stator current is six to seven times rated current during acceleration, with rated voltage applied to the stator winding. This amount of current results in heat production in the stator winding at a rate of from 35 to 50 times that at rated stator current.

It is also apparent by inspection of Fig. 12.6 that a dip has occurred in the reverse-rotation braking region of the motor speed-torque curve due to the fifth harmonic torque. The significance of this effect is that the motor will not develop as great an amount of reverse-rotation braking torque in the vicinity of 0.20 per unit reverse speed as it otherwise would have developed.

Only the effects of the fifth and seventh space harmonics have been shown in Fig. 12.6. Of course, all the other space harmonics, and all slot harmonics, have a corresponding effect in producing asynchronous crawling, to the extent of their actual magnitudes in a given machine.

12.10.2 Synchronous Locking

In Section 12.9.2 it was shown that the variation in magnetomotive force caused by the stator-slot steps interacts with the fundamental and harmonics of the rotating magnetomotive-force space wave of the stator to produce stator-slot harmonics. From eq. (12.54) the number of poles of the stator-slot harmonic caused by interaction of the nth space harmonic with the aforementioned steps in the MMF wave, associated with N_1 stator-slot steps, is

$$(N_{s1})_n = 2N_1 \pm np \quad \text{poles} \tag{12.61}$$

where p is equal to the number of poles of the motor. It was shown in Section 12.9.3 that in a similar manner, the variation in magnetomotive force caused by the rotor-slot steps interacts with the fundamental and harmonics of the rotating magnetomotive-force space wave of the stator to produce rotor-slot harmonics. Similarly, the number of poles of the rotor-slot harmonic caused by interaction of the nth space harmonic with the magnetomotive-force wave, associated with N_2 rotor-slot steps, as given by eq. (12.56), is

$$(N_{s2})_n = 2N_2 \pm np \quad \text{poles} \tag{12.62}$$

If the fundamental and the harmonics through the nineteenth harmonic are considered, there are 14 stator-slot harmonics and 14 rotor-slot harmonics. Synchronous locking will tend to occur if the number of poles $(N_{s1})_n$ of a stator-slot harmonic is equal to the number of poles of a rotor-slot harmonic $(N_{s2})_n$ and if these two harmonic fields rotate in the same direction, thereby providing the requirements for sunchronizing the two fields. Thus at the design stage, steps should be taken to prevent this from occurring.

The stator-slot harmonic and rotor-slot harmonic poles are determined by the number of stator slots N_1 and by the number of rotor slots N_2. The stator space harmonics result from stator current flow being confined to phase groups, which, in turn, depend on the number of poles p and the number of phases q for which the stator is wound. Thus it should be expected intuitively that there is a relationship among N_1, N_2, p, and q which would predict when synchronous locking is imminent. Such a relationship, or rule, for symmetrical windings, is

$$N_2 - N_1 = kpq \quad \text{numeric} \tag{12.63}$$

where k is an integer, for which k = 1 is the most significant case. The rule, given in eq. (12.63), is tantamount to requiring that the quantity $(N_2 - N_1)$ be equal to a multiple of the number of phase groups in the stator winding, since the total numbers of such phase groups is equal to pq. Although this relationship could have been derived in a heuristic manner from consideration of the fourth term of eq. (12.60), it is more direct at this point to establish its applicability by intuitively expecting that such a rule should exist and then to establish that expectation by numerical verification. Accordingly, the accuracy and applicability of this rule in predicting synchronous locking will be illustrated by a numerical example.

Consider a six-pole, three-phase induction motor with 54 stator slots and with 72 rotor slots. Then, applying the rule above, for $N_2 = 72$, $N_1 = 54$, $p = 6$, and $q = 3$,

$$N_2 - N_1 = (54 - 72) = k(6)(3) = -18 \quad \text{numeric} \tag{12.64}$$

Obviously, $k = -1$ and this choice of rotor slots relative to the number of stator slots will cause synchronous locking to occur. To show the actual basis for locking, in this case, the stator-slot harmonic poles and the rotor-slot harmonic poles, through the nineteenth stator space harmonic, will be calculated, tabulated, and compared. The number of poles of the stator-slot harmonics resulting from the stator-slot current steps interacting with the fundamental of the stator magnetomotive-force wave is

$$(N_{s1}) = 2N_1 \pm p = (2)(54) \pm 6 = 114,\ 102 \quad \text{poles} \tag{12.65}$$

The slot harmonic corresponding to $2N_1 + p$ is a forward-rotating field. Thus it will always rotate in the same direction as the associated stator space harmonic (or fundamental, in this case). If the slot harmonic corresponding to $2N_1 - p$ has a positive value of poles, it rotates in a direction opposite to the direction of the associated space harmonic. If the slot harmonic corresponding to $2N_1 - p$ has a negative value of poles, both of the slot harmonics rotate in the same direction as that of the associated space harmonic. Thus for the two slot harmonics given in eq. (12.65), the one with 114 poles rotates in a forward direction and the one with 102 poles rotates in a backward direction. A simple notation that shows both the number of poles and the direction of rotation of the harmonic for this case is 114F, 102B.

Similarly, the number of rotor-slot harmonic poles resulting from the rotor-slot current steps interacting with the stator magnetomotive-force fundamental is

$$(N_{s2})_1 = 2N_2 \pm p = (2)(72) \pm 6 = 150,\ 138 \quad \text{poles} \tag{12.66}$$

Since both values of poles are positive, the rotor-slot harmonic with 150 poles rotates in the same direction as the fundamental space wave, which is forward, and the rotor-slot harmonic with 138 poles rotates in the opposite direction, which is backward. In terms of the above-mentioned notation, the two rotor-slot harmonic poles can be designated as 150F, 138B.

The number of poles of the stator-slot harmonics resulting from the stator-slot current steps interacting with the fifth harmonic of the stator magnetomotive-force wave is

TABLE 12.1 Tabulation of Stator-Slot Harmonic Poles and Rotor-Slot Harmonic Poles for a Six-Pole Three-Phase Induction Motor with 54 Stator Slots and 72 Rotor Slots, Used as a Numerical Example of Synchronous Locking

Stator-space harmonic poles	Stator-slot harmonic poles		Rotor-slot harmonic poles	
1F	114F	102B	150F	138B
5B	138B	78F	174B	114F
7F	150F	66B	186F	102B
11B	174B	42F	210B	78F
13F	186F	30B	222F	66B
17B	210B	6F	246B	42F
19F	222F	6F	258F	30B

$$(N_{s1})_5 = 2N_1 \pm np = (2)(54) \pm (5)(6) = 138,\ 78 \quad \text{poles} \tag{12.67}$$

Both values of poles in eq. (12.67) are positive and the fifth space harmonic is a backward-rotating wave. Then the slot harmonic with 138 poles is also backward rotating and the slot harmonic with 78 poles rotates in an opposite direction (i.e., it is forward rotating). Thus they can be designated as 138B, 78F.

Also, the number of rotor-slot harmonic poles resulting from the rotor-slot current steps interacting with the fifth harmonic of the stator magnetomotive-force wave is

$$(N_{s2})_5 = 2N_2 \pm np = (2)(72) \pm (5)(6) = 174,\ 114 \quad \text{poles} \tag{12.68}$$

Again, since both values of poles in eq. (12.68) are positive and the fifth space harmonic is a backward-rotating wave, the two rotor-slot harmonic poles above may be designated as 174B, 114F.

Proceeding in a similar manner, all of the stator-slot harmonic poles and all of the rotor-slot harmonic poles have been calculated for this example, through the nineteenth space harmonic, and the results tabulated in Table 12.1. A comparison of the stator-slot harmonics with the rotor-slot harmonics shows 12 different sets of harmonic poles, each set of which is common, in number of poles and in direction of rotation between the rotor and the stator. Of these 12 sets, six rotate in the forward direction and six rotate in the reverse direction. Thus this machine will tend to lock at standstill, as predicted by eq. (12.64), and accordingly, the number of rotor slots is not a proper choice.

12.10.3 Synchronous Crawling

It was just shown that synchronous locking will occur (1) if the number of stator-slot harmonic poles, and (2) if the directions of rotation of corresponding rotor and stator harmonic fields are the same. As noted above, this will provide the conditions for the various pairs of harmonic fields to operate in synchronism in the vicinity of zero speed. On the other hand, synchronous crawling will occur (1) if the number of stator-slot harmonic poles equals the number of rotor-slot harmonic poles, and (2) if the directions of rotation of corresponding rotor and stator harmonic fields are opposite each other. The relationship or rule that predicts this condition for symmetrical stator windings is

$$N_2 - N_1 = kp \quad \text{numeric} \tag{12.69}$$

where k is an integer, for which $k = 1$ and $k = 2$ are significant cases.

For the condition of synchronous crawling, a rotor-slot harmonic field and a stator-slot harmonic field with an equal number of poles rotate in opposite directions around the air gap at an angular velocity corresponding to that number of harmonic poles. The two rotating harmonic fields will try to lock into synchronism as they pass one another. This attempt to lock will generally affect the normal acceleration of the motor due to the fundamental torque at the point where it occurs. Thus the motor is said to "crawl" at this point on the speed-torque curve. The rotor speed at which synchronous crawling occurs is

$$(\text{rpm})_{sc} = \frac{p}{N_2} N_s \quad \text{revolutions/minute} \tag{12.70}$$

where N_s is the synchronous speed of the fundamental wave. The direction of crawling is forward if the direction of rotation of the stator-slot harmonic is forward, and it is backward if the direction of rotation of the stator-slot harmonic is backward.

The concept of synchronous crawling will be illustrated by a numerical example. Consider the six-pole three-phase motor with 54 stator slots which was used for the preceding example, but with 66 rotor slots. Then $N_2 = 66$, $N_1 = 54$, $p = 6$, and $q = 3$. Applying the rule, given in eq. (12.69), we obtain

$$N_2 - N_1 = 66 - 54 = 6k = 12 \quad \text{numeric} \tag{12.71}$$

TABLE 12.2 Tabulation of Stator-Slot Harmonic Poles and Rotor-Slot Harmonic Poles for a Six-Pole Three-Phase Induction Motor with 54 Stator Slots and 66 Rotor Slots, Used as a Numerical Example of Synchronous Crawling

Stator-space harmonic poles	Stator-slot harmonic poles		Rotor-slot harmonic poles	
1F	114F	102B	138F	126B
5B	138B	78F	162B	102F
7F	150F	66B	174F	90B
11B	174B	42B	198B	66F
13F	186F	30B	210F	54B
17B	210B	6F	234B	30F
19F	222F	6F	246F	18B

Then k = 2, which is a low integer, and synchronous crawling should be expected. This can be verified by calculating the stator-slot harmonic poles and the rotor-slot harmonic poles produced by each of the stator-space harmonics in accordance with the procedure given earlier, tabulating the results, and then comparing their values and their directions.

Table 12.2 shows the number of poles and the directions of the stator-slot harmonic and the rotor-slot harmonics for this example through the nineteenth space harmonic of the stator. A comparison of the stator-slot harmonics with the rotor-slot harmonics shows six different sets of harmonic poles, each of which is common in number of poles and opposite in direction of rotation. In all cases, the concerned stator-slot harmonic field rotates in the reverse direction. Thus the motor will tend to crawl in the reverse direction. From eq. (12.70), the speed at which crawling will occur is

$$(\text{rpm})_{sc} = \frac{p}{N_2} N_s = \left(\frac{6}{66}\right)(1200) = 109 \quad \text{revolutions/minute} \qquad (12.72)$$

Another numerical example will be used to illustrate synchronous crawling further. The same motor will be used but with the number of rotor slots changed to 42. Then, for this example, $N_2 = 42$, $N_1 = 54$, $p = 6$, and $q = 3$. Applying the rule given in eq. (12.69) gives us

$$N_2 - N_1 = 42 - 54 = 6k = -12 \quad \text{numeric} \qquad (12.73)$$

TABLE 12.3 Tabulation of Stator-Slot Harmonic Poles and Rotor-Slot Harmonic Poles for a Six-Pole Three-Phase Induction Motor with 54 Stator Slots and 42 Rotor Slots, Used as a Numerical Example of Synchronous Crawling

Stator-space harmonic poles	Stator-slot harmonic poles		Rotor-slot harmonic poles	
1F	114F	102B	90F	78B
5B	138B	78F	114B	54F
7F	150F	66B	126F	42B
11B	174B	42F	150B	18F
13F	186F	30B	162F	6B
17B	210B	6F	186B	18B
19F	222F	6F	198F	30F

For this example, $k = -2$, which is a low integer, indicating that synchronous crawling should occur. Again, the stator-slot harmonic poles and the rotor-slot harmonic poles produced by each of the stator-space harmonics have been calculated and tabulated in Table 12.3. An inspection of the tabulation shows seven different sets of harmonic poles, each set of which is common in number of poles and opposite in direction of rotation. This will tend to cause the motor to crawl, and since the direction of the concerned stator-slot harmonic-field rotation is in the forward direction in all cases, the direction of crawl will also be in the forward direction. The speed at which crawling will occur, from eq. (12.70), is

$$(\text{rpm})_{sc} = \frac{p}{N_2} N_s = \left(\frac{6}{42}\right)(1200) = 171 \quad \text{revolutions/minute} \qquad (12.74)$$

For both of the preceding two numerical examples, the choice of rotor slots relative to the number of stator slots was improper and synchronous crawling occurred. The crawling resulted from stator-slot harmonic fields trying to synchronize with rotor-slot harmonic fields, with the same number of poles, rotating in the opposite direction to the stator harmonics. In one case, the concerned stator-slot harmonics rotated in the backward direction, which determined that the crawling was in the backward direction.

In the other case, the concerned stator-slot harmonics rotated in the forward direction, and accordingly, the crawling was in the forward direction.

A fourth numerical example will be given, for which synchronous crawling, as well as synchronous locking, should not occur. Again, the same motor will be used except that 64 stator slots will be chosen. Then, for this example, $N_2 = 64$, $N_1 = 54$, $p = 6$, and $q = 3$. Applying the rule from eq. (12.69) to determine if synchronous crawling should be expected to occur yields

$$N_2 - N_1 = 64 - 54 = 6k = 10 \quad \text{numeric} \tag{12.75}$$

Since $k = 10/6$, and since this is not an integer, synchronous crawling will not occur. Also, applying the rule from eq. (12.64) to determine if synchronous locking should be expected to occur, we have

$$N_2 - N_1 = 64 - 54 = 18k = 10 \quad \text{numeric} \tag{12.76}$$

This results in $k = 10/18 = 5/9$, which is also not an integer, and accordingly, synchronous locking will not occur. The stator-slot harmonic poles and the rotor-slot harmonic poles have been calculated for this example and tabulated in Table 12.4. It is apparent from an inspection of Table 12.4 that

TABLE 12.4 Tabulation of Stator-Slot Harmonic Poles and Rotor-Slot Harmonic Poles for a Six-Pole Three-Phase Induction Motor with 54 Stator Slots and 64 Rotor Slots, Used as a Numerical Example of a Machine Without Synchronous Locking and Synchronous Crawling

Stator-space harmonic poles	Stator-slot harmonic poles		Rotor-slot harmonic poles	
1F	114F	102B	134F	122B
5B	138B	78F	158B	98F
7F	150F	66B	170F	86B
11B	174B	42F	194B	62F
13F	186F	30B	206F	50B
17B	210B	6F	230B	26F
19F	222F	6F	242F	14B

none of the stator-slot harmonics have a number of poles common with that of the rotor-slot harmonics. Thus this choice of rotor slots is proper, at least from the standpoint of avoiding synchronous locking torques and synchronous crawling torques.

12.11 ELECTROMAGNETICALLY INDUCED NOISE AND VIBRATION

There are two primary sources of noise in polyphase induction motors: magnetically induced noise, called "magnetic noise," and noise induced by flow of air, called "windage noise." Generally, windage noise has a reasonably uniform distribution of intensity across the audio spectrum, and in such cases it is due predominantly to air turbulence. Occasionally, however, the pulsing of cooling air into a cavity or an air duct can produce the effect of a crude pipe organ, which gives a high intensity of noise at that particular auditory frequency. This will occur when air is pulsed at a constant frequency, which is approximately equal to the resonant "pipe-organ" frequency of the cavity or duct, the length of which corresponds to a quarter wavelength for a closed-end cavity and to a half wavelength for an open-ended duct. For such cases, the windage noise spectrum will have a high intensity in the region of the resonant frequency of the inadvertent pipe-organ cavity. The noise source considered in this chapter, however, is that caused by magnetic sources. The magnetic-noise content can be determined relative to the total noise content by recording the audio spectrum at full speed, with the stator winding excited, and then removing excitation from the stator winding and repeating the measurement.

The fundamental induction-motor torque as well as the parasitic torques discussed in various sections up to this point, result from one rotating harmonic wave interacting with another one to produce tangential force. This tangential force, multiplied by the radius of the rotor, gives the resulting torque which acts on the rotor. Rotating harmonic waves interacting with one another can also produce radial forces between the rotor and the stator. These radial forces rotate around the air gap at a fixed speed. Thus from a fixed point in space, such as a point on the stator core, the magnitude of the force will vary sinusoidally with time. Thus it can act as an exciting force on the stator core and frame as well as on the rotor core and structure, to produce cyclical compliance of segments, or all, of the stator and the rotor. A circumferential length of the stator core, for example, can act as a length of beam, supported at each end, with a thickness equal to the effective radial thickness of the stator yoke. If any radial force being produced has a frequency as seen by the beam that is approximately equal to the natural frequency of this beam, vibration or noise, or both, will result. As will be seen, the smaller the number of poles of the force wave, the greater is the chance of producing magnetic noise. Thus the key to avoiding unacceptable magnetic noise is to use a combination of stator slots and rotor slots which result in a large number of poles for the various force waves that are produced.

12.11.1 Magnetic-Force Waves

If the fundamental of the rotating magnetomotive-force field and each of the various rotating harmonic magnetomotive-force fields present in the air gap are multiplied by the permeance wave, given in eq. (12.60), the result is the rotating fundamental flux wave and a train of rotating, harmonic flux waves. The fundamental flux wave, of course, reacts with the fundamental component of rotor current to produce the fundamental torque. If the magnitude ϕ_n of each harmonic flux wave expressed in webers is divided by its respective area per pole in meters^2, the result is another train of rotating harmonic flux-density waves, the magnitude of any one of which is B_n, with units of webers/meters^2. The jth harmonic can be expressed in general terms as

$$B = B_j \sin(\omega_j t - K_j x) \quad \text{webers/meters}^2 \tag{12.77}$$

where

ω_j = angular velocity of the wave
K_j = constant
t = time variable, seconds
x = space variable, along the air gap, meters

It was shown in eq. (9.180) that the radial magnetic force between the rotor and the stator is equal to

$$F = \frac{10^7}{4\pi} AB^2 \quad \text{newtons} \tag{12.78}$$

where A is the cross-sectional area of the flux path in meters^2 and B is the air-gap flux density in webers/meters^2. Thus, to transform a rotating harmonic flux-density wave into a corresponding rotating radial magnetic-force wave, the flux-density wave must be raised to the second power. The various harmonic flux-density waves rotate at different angular velocities, with some traveling in the forward direction and some traveling in the reverse direction. Accordingly, the air-gap flux and air-gap flux density at a fixed point on the stator bore will contain a sampling of the various harmonic components present in the air gap. Considering two components at a time, this provides a large number of combinations of flux and flux density which can be multiplied together to produce the B^2 term. The possible combinations are: (1) the squaring of a single stator wave, (2) the squaring of a single rotor wave, (3) the product of two different stator waves, (4) the product of two different rotor waves, and (5) the product of a stator wave and a rotor wave. Then, in general, a rotating magnetic-force wave results from multiplying a rotating flux-density wave such as that shown in eq. (12.77), of harmonic order j, by a second rotating flux-density wave of harmonic order k, giving

$$F_{jk} = \frac{10^7}{4\pi} A_{jk}[B_j \sin(\omega_j t - K_j x)][B_k \sin(\omega_k t - K_k x)] \quad \text{newtons} \qquad (12.79)$$

Since $\sin\theta \sin\phi = 1/2 \cos(\theta - \phi) - 1/2 \cos(\theta + \phi)$, eq. (12.79) may be written as

$$\begin{aligned} F_{jk} &= \frac{C_{jh} B_j B_k}{2} \cos[(\omega_j - \omega_k)t - (K_j - K_k)x] \\ &\quad - \frac{C_{jk} B_j B_k}{2} \cos[(\omega_j + \omega_k)t - (K_j + K_k)x] \quad \text{newtons} \qquad (12.80) \end{aligned}$$

where $C_{jk} = A_{jk}\, 10^7/4\pi$.

Equation (12.80) gives the radial magnetic-force wave expressed in general terms. Various conclusions, of considerable significance, may be drawn from this equation, including the following:

1. For the more usual case of two different harmonic orders interacting (i.e., for $j \neq k$):

a. The radial magnetic-force wave consists of two separate waves.
b. One force wave has an angular velocity equal to the difference between the angular velocities of the two parent harmonic flux waves and a number of poles equal to the difference between the number of poles of the two parent waves.
c. The other force wave has an angular velocity equal to the sum of the angular velocities of the two parent harmonic flux waves and a number of poles equal to the sum of the number of poles of the two parent harmonics.

2. For the case of harmonics of equal orders and equal numbers of poles interacting (i.e., for the case of $j = k$):

a. The first term of eq. (12.80) is fixed in space (i.e., the wave has zero force poles and it does not rotate).
b. The second term of eq. (12.80) is a force wave that has twice the number of poles and twice the angular velocity of either of the parent harmonics.

3. As shown in eq. (12.80), the angular velocity and the number of poles of a given radial magnetic-force wave is also equal to the sum and the difference of the corresponding quantities of the two harmonic magnetomotive-force waves that produced the two harmonic flux waves, shown in eq. (12.79). This is, of course, because the angular velocity and the number of poles of a harmonic flux wave have a one-to-one correspondence to the corresponding quantities of the harmonic magnetomotive-force wave which produced that flux wave. Thus the number of poles of the stator-slot harmonics and of the rotor-slot harmonics present in the air gap can be utilized directly in determining the number of poles of the radial force waves.

As will become apparent, the avoidance of undesirable magnetic noise, and in some cases, significant vibration, consists of applying the conclusions above, in a practical way, to eliminate stator and rotor harmonics and, in particular, slot harmonics, which produce radial magnetic-force waves with a few number of force poles.

12.11.2 Mechanical Compliance of Various Motor Parts

A radial magnetic force wave, with its line of action radially across the air gap, will exert a mechanical force on the stator-bore area and on the rotor-surface area adjacent to the air gap. This force can be regarded as having a sinusoidal distribution along the air gap, with a given number of poles, and the resulting wave shape rotates around the air gap at a specific angular velocity. The number of poles of the force wave determines the span over which the force associated with one force-pole pitch acts and the angular velocity of the force wave determines the exciting frequency of the force in producing noise and vibration.

To limit core loss, the stator core is built up of thin circumferential laminations. The individual laminations are usually complete circles for small motors, and are usually segments of circles for larger motors. The stack of laminations is held in compression by various mechanical means, such as axial keying, and the outer diameter of the punchings seat against several axial "ribs" of the frame or core superstructure. Although the core is sufficiently stiff as to be entirely functional, in essentially all cases it is certainly less stiff than the same dimensional form made of solid steel. Also, the rotor core is built up of laminations. Single-segment rotor laminations are now generally used for most machines, except for the largest ratings. Such circular punchings are either (1) heated and pressed over the rotor spider or shaft to give an interference fit at normal operating temperature, or they are (2) "cold" pressed over the spider or shaft. In both cases, they are pressed in an axial direction and keyed to keep the stack under compression. If the rotor laminations are stacked directly on the shaft, the inner diameter of the rotor core will be completely seated against solid metal. If the laminations are stacked on an intervening structure called a rotor spider, the inner diameter of the rotor core will be seated against the axial ribs of the spider. In either case, the mechanical support on the inside

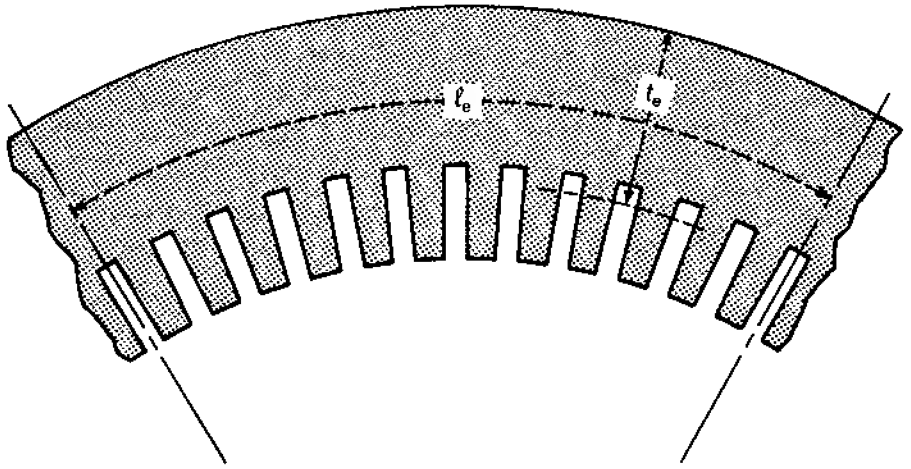

FIGURE 12.7 Section of stator core, showing rudimentary beam which is subjected to cyclical deflection from rotating force waves in the air gap.

diameter of the rotor core occurs at a considerably smaller diameter than the corresponding mechanical support of the stator core on its outside diameter. Also, the mean diameter of the stator core is considerably greater than that of the rotor core, and this provides a longer segmental distance for a force wave, with a given number of poles to act upon it, than for the rotor core. For all of the foregoing reasons, the stator core is more compliant to radial force waves than is the rotor, with one exception, which will be discussed subsequently.

At a given instant of time, one force pole of the rotating force wave will give a sinusoidal force distribution along a circumferential length of the core, equal in length to the mean circumference of the core, divided by the number of poles of the force wave. At that instant of time, the core sector, defined by this circumferential span, can be considered as a rudimentary beam, such as that shown in Fig. 12.7. In this figure the effective length of the beam ℓ_e is equal to one pole span of the force wave, and the force loading of the beam has a sinusoidal distribution, as stated above. The condition of the beam endings will be somewhere between "built-in" endings to fully pivoted endings, based on the number of lamination segments per circle, the circumferential length of a lamination segment relative to ℓ_e, retained stacking pressure between laminations, surface friction of the laminations, and so on. In any case, the deflection of the beam in bending is approximately proportional to the third power of ℓ_e, in accordance with flexural beam theory. Thus it is apparent that as ℓ_e decreases, corresponding to an increase in the number of poles of the force wave acting on a given core, the radial deflection of that core decreases at a rapid rate. Accordingly, in general, only radial force waves with a low number of poles are effective in producing significant magnetic noise or vibration. The radial dimension t_e of the punching, corresponding to its effective radial thickness as a beam, also significantly affects the core deflection. In general, the ratio t_e/ℓ_e decreases as the synchronous speed of the machine decreases or as the number of motor poles increases. Thus a force wave with, say, four force poles will generally cause a greater amount of deflection for a slow-speed motor than for a higher-speed motor for a given amount of radial force.

A radial force wave with two force poles presents an interesting case. For this case, the radial forces are unbalanced, whereas they are balanced for all force waves with force poles in excess of two. Force waves with two force poles produce two general effects. The first effect is that since the magnetic forces are not balanced, an unbalanced radial force rotates rapidly around the air gap. If the transverse resonant frequency of the rotor structure and shaft, considered as a beam between the bearing supports, is near the frequency of the unbalanced magnetic force (i.e., $\omega/2\pi$ of the rotating force wave), considerable noise and vibration will occur. The second effect is that with only two force poles, the circumferential span of the stator punching, corresponding to the effective length ℓ_e of the equivalent beam, is very long. Thus the radial deflection of the stator core could be very significant, with a high probability of unacceptable noise and vibration levels.

The combinations of air-gap harmonic waves that can interact to produce force waves with two force poles is somewhat limited. Two stator waves cannot cooperate to produce such a wave for a typical stator winding with phase groups of $\pi/3$ electrical radians, ot 60 electrical degrees, because the required harmonics cannot coexist with such a winding. For the same reason, two rotor harmonics of a wound-rotor winding cannot cooperate to produce a force wave with two force poles. However, a squirrel-cage rotor with an odd number of rotor slots N_2 will usually result in such a force wave, for the following reason. As discussed in Chapter 9, it is desirable to have an even number of stator slots N_1, so that the stator winding will be the more desirable integral-slot type. If a given stator slot is aligned with a given rotor slot, then the stator slot, which is diametrically opposite, will be in alignment with a rotor tooth if N_1 is even and N_2 is odd. Thus for an odd value of N_2, one end of a rotor diameter will see a minimum value, and the opposite end of the same diameter will see a maximum value of air-gap permeance. The overall effect is that a force wave with two force poles will result. Accordingly, odd values of N_2 should be avoided. However, force waves with two force poles can also result from cooperation between a stator harmonic and a rotor harmonic in some cases.

All force waves with a number of force poles greater than two are balanced waves. A force wave with zero force poles is also balanced and, as noted earlier, occurs when parent harmonic order j equals parent harmonic order k, that is, when $j = k$, in the first term of eq. (12.80). Since this produces zero force poles, the wave is fixed in space and does not rotate. The pulsating force has a radial line of action about a wave centerline which is circular. Thus the core vibrates radially inward and radially outward, as a whole, about a circular centerline and with uniform distribution of the force along the circle. Force waves with zero force poles are produced only by the cooperation of a stator harmonic and a rotor harmonic with the sane number of harmonic poles.

Force waves that produce four force poles will cause four points of maximum force, as the wave rotates, with the forces being alternately inward directed and outward directed, along radial lines. Thus such a wave will tend to distort the core into a rotating ellipse. Since a core is compliable to this mode of force application, considerable radial core deflection and noise can result. Thus this force wave should be avoided, if possible. A force wave with four force poles, in common with all force waves with force poles in excess of two, can be produced (1) by two stator harmonics (2) by two rotor harmonics, (3) by a stator harmonic cooperating with a rotor harmonic, (4) by a single stator harmonic, and (5) by a single rotor harmonic. Thus there is significant opportunity for the production of higher-order force waves, those with more than two force poles. Fortunately, the effectiveness of a given force wave in producing noise and vibration decreases rapidly as the number of force poles increases.

12.11.3 Selection of the Number of Stator and Rotor Slots to Avoid Magnetic Noise and Vibration

It should now be apparent that the various rotating harmonic flux waves which are present in the air gap can interact in various ways to produce rotating magnetic-force waves and hence to produce possible objectional magnetic noise. Prime among such rotating harmonics are the stator-slot harmonics and the rotor-slot harmonics. The force waves have force poles that are equal to the sums and the difference of the two parent harmonics that produce them, and the force waves, with few force poles, tend to produce the most undesirable noise effect. Then, in the case of slot harmonics, which can act as potential parents to producing troublesome force waves, it is important to avoid differences between N_1 and N_2 which result in force waves with few force poles. As discussed in Chapter 9, there are some number of significant constraints placed on the selection of the number of stator slots N_1. Thus the selection of a favorable quantity $(N_1 - N_2)$ generally consists of selecting the quantity N_1 and then selecting the quantity N_2, such as to reduce the probability of undesirable noise and, at the same time, not enhance any other problem.

A given stator-slot harmonic and a given rotor-slot harmonic can cooperate to produce two force waves with force poles equal to the sum and the difference of the poles of the two harmonics. In considering magnetic noise produced by slot harmonics, as stated above, only the differences are significant. From eqs. (12.54) and (12.56), the difference in numbers of poles between a stator-slot harmonic and a rotor-slot harmonic is

$$(N_{s1})_n - (N_{s2})_n = 2N_1 \pm np - 2N_2 \pm np \quad \text{force poles} \qquad (12.81)$$

Considering both parent slot harmonics to be associated with the fundamental space harmonic [i.e., $n = 1$ in eq. (12.81)] and also considering for the moment that $N_1 > N_2$, eq. (12.81) can be written as

$$\begin{aligned}(2N_1 \pm p) - (2N_2 \pm p) &= 2N_1 - 2N_2\\ &= 2N_1 - 2N_2 + 2p \qquad \text{force poles}\\ &= 2N_1 - 2N_2 - 2p\end{aligned} \tag{12.82}$$

If, on the other hand, $N_2 > N_1$, eq. (12.82) can be written as

$$\begin{aligned}(2N_1 \pm p) - (2N_1 \pm p) &= 2N_2 - 2N_1\\ &= 2N_2 - 2N_1 + 2p \qquad \text{force poles}\\ &= 2N_2 - 2N_1 - 2p\end{aligned} \tag{12.83}$$

Also, considering the slot harmonic associated with the fundamental to be one parent, considering the slot harmonic associated with the fifth space harmonic to be the other parent, and considering $N_1 > N_2$, eq. (12.81) becomes

$$\begin{aligned}(2N_1 \pm 5p) - (2N_2 \pm p) &= 2N_1 - 2N_2 + 4p\\ &= 2N_1 - 2N_2 + 6p\\ & \qquad\qquad\qquad\qquad \text{force poles}\\ &= 2N_1 - 2N_2 - 6p\\ &= 2N_1 - 2N_2 - 4p\end{aligned} \tag{12.84}$$

It should be noted that only the last two of the four possible right-hand members of eq. (12.84) need be considered, since the first two will give force poles which are too large to be significant in producing magnetic noise in the core. If $N_2 > N_1$ for this combination of slot harmonics, the force poles are

$$\begin{aligned}(2N_2 \pm p) - 2(N_1 \pm 5p) &= 2N_2 - 2N_1 - 4p\\ &= 2N_2 - 2N_1 + 6p\\ & \qquad\qquad\qquad\qquad \text{force poles}\\ &= 2N_2 - 2N_1 - 6p\\ &= 2N_2 - 2N_1 + 4p\end{aligned} \tag{12.85}$$

Again, only the first and third of the four possible right-hand members of eq. (12.85) need be considered as significant in producing magnetic noise in the core.

Proceeding in a similar manner and considering the slot harmonic associated with the fundamental to be one parent, considering the slot harmonic associated with the seventh space harmonic to be the other parent and considering $N_1 > N_2$, eq. (12.81) becomes

$$\begin{aligned}(2N_1 \pm 7p) - (2N_2 \pm p) &= 2N_1 - 2N_2 + 6p \\ &= 2N_1 - 2N_2 + 8p \\ &= 2N_1 - 2N_2 - 8p \\ &= 2N_1 - 2N_2 - 6p\end{aligned} \qquad \text{force poles} \qquad (12.86)$$

For this case, only the last two of the four possible right-hand members of eq. (12.86) are significant in producing magnetic noise in the core. If $N_2 > N_1$ for the combinations of slot harmonics above, the resulting force poles are

$$\begin{aligned}(2N_2 \pm p) - (2N_1 \pm 7p) &= 2N_2 - 2N_1 + 8p \\ &= 2N_2 - 2N_1 - 6p \\ &= 2N_2 - 2N_1 - 8p \\ &= 2N_2 - 2N_1 + 6p\end{aligned} \qquad \text{force poles} \qquad (12.87)$$

Only the second and third of the four possible right-hand members of eq. (12.87) are significant in producing magnetic noise in the core.

If the magnetic circuit of the machine has significant saturation, additional force waves can be produced with numbers of force poles which are sufficiently small as to produce magnetic noise. The normal space harmonics and slot harmonics thus far considered are produced by a common current, and each magnetomotive-force harmonic travels its respective harmonic wavelength in the same length of time as the fundamental magnetomotive force travels its fundamental wavelength. However, if significant saturation exists in the magnetic circuit, the fundamental of the rotating magnetomotive force will produce saturation harmonics, of orders 3, 5, and so on, in addition to the fundamental of the rotating flux wave. This occurs because of the nonlinearity between flux and magnetomotive force for the magnetic steel of the core. The resulting saturation harmonics are attached to the fundamental flux wave and rotate with it, with no relative motion between them. Thus saturation tends to complicate the prediction of magnetic noise. Although techniques have been devised for considering saturation harmonics, it is not completely clear from the technical literature how well predictions from such techniques correlate with test results in determining additional noise caused by saturation. It is a subject that probably deserves further work in correlating calculations with test results.

12.11.4 Frequency of the Force Wave

As discussed in Section 12.11.2, mechanical vibration of the core and resulting noise in the core occur when the exciting frequency of the force wave in hertz is in the region of the natural frequency in the bending mode of an annular section of the core, such as that shown in Fig. 12.7. Since only the force waves with a low number of force poles are significant in producing noise, it is only necessary in the usual case to determine the corresponding frequency of such waves.

Consider the force wave that results from the cooperation of the rotor-slot harmonic and the fundamental stator wave. There are N_2 rotor slots and, accordingly, this will cause a permeance variation which rotates with the rotor, which has $2N_2$ poles, or

$$N_{p2} = \frac{2N_2}{p} \quad \text{poles} \tag{12.88}$$

Then the frequency of alternations of this rotating permeance variation f_{v2}, as seen by the stator, is

$$f_{v2} = \frac{2N_2}{p}(1 - s)f_1 \quad \text{hertz} \tag{12.89}$$

where f_1 is the stator fundamental frequency and s is the slip of the rotor. The interaction of the variation of rotor-slot permeance as seen by the stator, with the fundamental of the stator magnetomotive-force wave, produces what is tantamount to the rotor-slot harmonic flux wave as seen by the stator. The frequencies of this resulting flux wave are

$$f_{s21} = \left[\frac{2N_2}{p}(1 - s) \pm 1\right]f_1 \quad \text{hertz} \tag{12.90}$$

The fundamental flux wave of frequency f_1, and the harmonic wave the frequency of which is given in eq. (12.90), represent two rotating flux waves present in the air gap. From eq. (12.80), they will cooperate to produce a rotating force wave, with frequencies equal to

$$f = \left\{ \left[\frac{2N_2}{p} (1 - s) \pm 1 \right] \pm 1 \right\} f_1 = \left[\frac{2N_2}{p} (1 - s) \right] f_1$$

$$= \left[\frac{2N_2}{p} (1 - s) + 2 \right] f_1 \quad \text{hertz} \qquad (12.91)$$

$$= \left[\frac{2N_2}{p} (1 - s) - 2 \right] f_1$$

It should be noted that the first equation of equation set (12.91) corresponds to the first equation of equation set (12.82) and of equation set (12.83), and so on, for the second equation and for the third equation of each of the three equation sets.

The exciting frequencies given in eq. (12.91) are the significant ones that can result in objectionable noise. It should be noted, however, that consideration of saturation harmonics which might be present can result in exciting frequencies that are somewhat lower and which could result in objectionable noise of an undetermined amount.

12.11.5 Numerical Example of Rotor-Slot Selection

The application of the concepts discussed in Sections 12.11.3 and 12.11.4 will be illustrated by a numerical example. Consider a four-pole polyphase induction motor with 60 stator slots. One component of core loss is reduced if the rotor slots are slightly less in number than the stator slots, as discussed in Chapter 14. For this example, assume that to reduce core loss, it is desired to use a few less rotor slots than stator slots if noise considerations will permit it. Accordingly, the use of 58 rotor slots is being investigated. Then $N_1 = 60$, $N_2 = 58$, $p = 4$, and $N_1 > N_2$. Substituting the values of N_1, N_2, and p into eq. (12.82) yields

$$2N_1 - 2N_2 = (2)(60 - 58) = 4$$

$$2N_1 - 2N_2 + 2P = (2)(60 - 58) + (2)(4) = 12 \quad \text{force poles} \qquad (12.92)$$

$$2N_1 - 2N_2 - 2p = (2)(60 - 58) - (2)(4) = -4$$

Also, substituting the values of N_1, N_2, and p into eq. (12.84) gives us

$$2N_1 - 2N_2 + 4p = (2)(60 - 58) + (4)(4) = 20$$

$$2N_1 - 2N_2 + 6p = (2)(60 - 58) + (6)(4) = 28$$

$$2N_1 - 2N_2 - 6p = (2)(60 - 58) - (6)(4) = -20 \quad \text{force poles} \qquad (12.93)$$

$$2N_1 - 2N_2 - 4p = (2)(60 - 58) - (4)(4) = -12$$

Finally, substituting the values of N_1, N_2, and p into eq. (12.86), we obtain

$$\left.\begin{aligned}2N_1 - 2N_2 + 6p &= (2)(60 - 58) + (6)(4) = 28\\ 2N_1 - 2N_2 + 8p &= (2)(60 - 58) + (8)(4) = 36\\ 2N_1 - 2N_2 - 8p &= (2)(60 - 58) - (8)(4) = -28\\ 2N_1 - 2N_2 - 6p &= (2)(60 - 58) - (6)(4) = -20\end{aligned}\right\} \text{ force poles} \qquad (12.94)$$

An inspection of equation sets (12.92) through (12.94) shows that the minimum number of force poles is 4, as determined by the first and last equations of equation set number 12.92.

The excitation frequencies that correspond to the two force-pole equations above are, respectively, the first and last of equation set (12.91). Then for the first equation the exciting frequency is

$$f = \left[\frac{2N_2}{p}(1 - s)\right]f_1 \quad \text{hertz} \qquad (12.95)$$

Assuming a value of slip s of 0.02 per unit and a value of line frequency f_1 of 60 H, one excitation frequency is

$$f = \left[\frac{(2)(58)}{4}(1 - 0.02)\right](60) = 1705 \quad \text{hertz} \qquad (12.96)$$

and the other exciting frequency is

$$f = \left[\frac{2N_2}{p}(1 - s) - 2\right]f_1 = \left[\frac{(2)(58)}{4}(0.98) - 2\right](60) = 1585 \quad \text{hertz} \qquad (12.97)$$

The existence of a four-pole force wave with frequencies in the vicinity of 1600 to 1700 H could cause undesirable noise if the stator punching and supporting frame structure are sufficiently compliant at these exciting frequencies. Thus the design engineer should either change the rotor slots, or if this were the first of a line of motors, at least to build a prototype model and test it.

12.12 ADDITIONAL EFFECTS OF HARMONICS

Harmonics can produce two more effects that are undesirable: additional losses and voltage ripple. The various rotating harmonic flux waves, sustained by magnetizing current, can produce corresponding currents on or near the surface of the rotor as well as in adjacent circuits. The resulting losses constitute what is called the rotating component of core loss. This component of loss, together with the fundamental core loss, gives the total core loss. Also, as additional current flows due to loading, additional losses occur in excess of normal I_2R, some of which is due to harmonics. Thus proper selection of rotor slots also affects the magnitude of core loss and load loss. These subjects are discussed more fully in Chapter 14 and voltage ripple is considered next.

In Section 12.9.5 it was stated that all of the harmonics, as well as the fundamental, of the stator flux wave induce corresponding voltages and hence corresponding currents in the rotor winding. Any of the resulting harmonic magnetomotive forces in the rotor can interact with the permeance variations of $2N_2$ poles and $2N_2/p$ harmonic order, caused by the rotor slots, to produce a rotating flux wave of harmonic order

$$(n_{s2})_1 = \frac{2N_2}{p} \pm n \quad \text{numeric} \tag{12.98}$$

For the rotor fundamental (i.e., n = 1), eq. (12.98) becomes

$$(n_{s2})_1 = \frac{2N_2}{p} \pm 1 \quad \text{numeric} \tag{12.99}$$

which corresponds, in harmonic order, to the rotor-slot harmonic given in eq. (12.57). The frequency f_2' of this wave relative to the rotor is

$$f_2' = \left(\frac{2N_2}{p} \pm 1\right) sf_1 \quad \text{hertz} \tag{12.100}$$

However, the rotor structure is traveling at (1 - s), in terms of frequency, so that the stator will see this flux wave at a frequency of $[s + (1 - s)]f_1 = f_1$ times the quantity inside the parentheses of eq. (12.100), or

$$f_{21}' = \left(\frac{2N_2}{p} \pm 1\right) f_1 \quad \text{hertz} \tag{12.101}$$

This flux wave will induce a voltage of the frequency given in eq. (12.101) in the stator winding, which will cause a small modulation on the supply voltage. Normally, such a voltage ripple is sufficiently small as to be of no significance. However, it can cause interference with communication circuits such as telephone lines if the ripple amplitude is sufficiently great. Such interference is called telephone influence and a frequency-weighted factor, which is a measure of this effect and which the electrical industry has adopted, is the telephone influence factor or (TIF). Although a maximum permissible value of TIF is usually specified for generators, in some special cases it is also specified for motors.

13

Reactance

13.1 Effect of Reactance on Polyphase Induction Motor Size and Performance 480

13.2 Separation of Total Winding Reactance into Leakage Reactance and Magnetizing Reactance 481

13.3 Magnetizing Reactance 484

13.4 Components of Leakage Reactance 486

13.5 Stator-Slot Leakage Reactance of a Rectangular Slot 487

13.6 Stator-Slot Leakage Reactance of a Nonrectangular Slot 497

13.7 Rotor-Slot Leakage Reactance of a Phase-Wound Rotor 499

13.8 Rotor-Slot Leakage Reactance of a Squirrel-Cage Rotor with Rectangular Slots 502

13.9 Rotor-Slot Leakage Reactance of a Single-Cage Rotor with Nonrectangular Slots 503

13.10 Rotor-Slot Leakage Reactance of a Multiple-Cage Rotor 505

13.11 End-Turn Leakage Reactance 508

- 13.11.1 Peripheral leakage-flux field 510
- 13.11.2 Axial leakage-flux field 513
- 13.11.3 Total end-turn leakage flux 517

13.12 Differential Leakage Reactance 519

- 13.12.1 Components of differential leakage reactance 519
- 13.12.2 Zigzag leakage reactance 519
- 13.12.3 Belt leakage reactance 523

13.13 Skew Leakage Reactance 527

13.14 Numerical Example of Running-Reactance Calculation 529

13.14.1 Calculation of the magnetizing reactance 531
13.14.2 Calculation of the stator-slot leakage reactance 532
13.14.3 Calculation of the end-turn leakage reactance 533
13.14.4 Calculation of the zigzag leakage reactance 533
13.14.5 Calculation of the belt leakage reactance 534
13.14.6 Calculation of the skew leakage reactance 535
13.14.7 Calculation of the rotor-slot leakage reactance 535
13.14.8 Total running reactance of the numerical example 535

13.15 Blocked-Rotor Reactance 536

13.15.1 Line frequency in the rotor circuit 537
13.15.2 Saturation of tooth tips due to high current values at blocked-rotor conditions 538
13.15.3 Calculation of blocked-rotor reactance 538

13.16 Numerical Example of Blocked-Rotor Reactance Calculation 540

13.16.1 Calculation of some necessary preliminary quantities 540
13.16.2 First iteration 542
13.16.3 Second iteration 546

13.1 EFFECT OF REACTANCE ON POLYPHASE INDUCTION MOTOR SIZE AND PERFORMANCE

Reactance has two very significant effects on the size and performance of induction motors. One effect is the limitation in possible power output rating for a given speed and frame size, and the other effect is the determination of specific performance characteristics for a given design. The power output, for a given speed and volume, and the specific performance of a given design are, quite clearly, of prime importance in the design process. Accordingly, the magnitude of the various components of reactance is of corresponding importance.

The exact equation for maximum torque is given in eq. (5.107) and the approximate equation for maximum torque is given in eq. (6.42). It can be seen from both of these equations that maximum torque is approximately proportional to the reciprocal of 2.0 times the sum of the leakage reactance of the stator winding and of the rotor winding, or with quantities in per unit, $T_m = 1/2(X_1 + X_2)$. Application requirements have established a minimum ratio of maximum torque to rated torque in the region 2.0 to 2.5, and this requirement has been incorporated into industry standards. To achieve this required value of maximum torque, the total leakage reactance must not exceed, say, 0.20 per unit. Then $T_m \cong 1/(2.0)(0.2) \cong 2.50$. Even a value of leakage reactance of 0.20 per unit may be too great in many cases. The reactance limitation on maximum torque also places a corresponding limit on rated torque and, at a given speed, on rated power output. Thus the magnitude of leakage reactance will, indeed, set a maximum limit on the power output available at a certain speed from a given amount of active machine material.

The effect of reactance on the determination of specific performance characteristics for a given design is apparent from a review of various equations that are associated with such performance characteristics. The stator and rotor currents, in complex form, are given in eqs. (5.16) and (5.22), respectively, and the magnetizing current is given in eq. (5.25). In each case the current magnitudes and angles can be determined from the corresponding equation, which is expressed in terms of stator leakage reactance X_1, rotor leakage reactance X_2, magnetizing reactance X_m, stator reactance R_1, rotor resistance R_2, slip s, and stator-bus voltage V_1. Net shaft horsepower HP_0 and net shaft torque are given in eqs. (5.33) and (5.87), respectively. Again, the equations for shaft power and shaft torque are expressed in terms of the same quantities, including X_1, X_2, and X_m.

Power factor is the ratio of the in-phase to the total stator current or stator volt-amperes. Thus the power-factor angle θ is a function of the out-of-phase or reactive volt-amperes [i.e., $\sin^{-1} \theta$ = (reactive volt-amperes)/(total volt-amperes)]. From the vector diagram shown in Fig. 7.2 it is apparent that the voltage vectors I_1X_1 and I_2X_2 and the current vector I_m are essentially out of phase with the voltage vector V_1. Accordingly, the corresponding volt-ampere components $I_1^2X_1$, $I_2^2X_2$, and I_mV_1 are also essentially out of phase. Thus the three reactances X_1, X_2, and X_m are very significant in determining the power factor of an induction motor.

It is apparent from the foregoing that reactance is of great importance in determining the size and performance of induction motors. It is appropriate to say that if the various components of reactance of a given machine are known, the essential performance of that machine is also known.

13.2 SEPARATION OF TOTAL WINDING REACTANCE INTO LEAKAGE REACTANCE AND MAGNETIZING REACTANCE

Figure 4.2 shows a simplified physical model of one phase of a polyphase induction motor. It was shown in Sections 4.4.1 through 4.4.4 that tests could be conducted on the physical model which would establish the equivalent circuit, shown in Fig. 4.3. An example was then given in Section 4.4.5, which resulted in the equivalent circuit shown in Fig. 4.4. This figure shows a magnetizing reactance component X_m and leakage reactance components X_1 and X_2 in the stator and in the rotor circuits, respectively. Thus this was the approach used to establish the existence of magnetizing reactance and of leakage reactance of the windings for the equivalent-circuit algorithm.

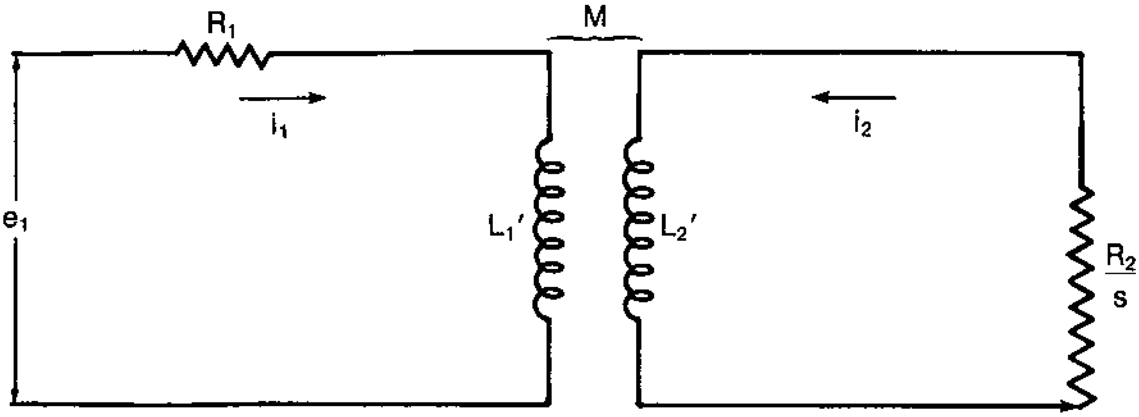

FIGURE 13.1 Actual circuit of one phase of the physical model of a polyphase induction motor.

The separate and unique existence of magnetizing reactance and of leakage reactance can be established from another point of view, which provides more physical insight when the subject of reactance alone is being considered. Figure 13.1 represents the electrical circuit of the physical model, shown in Fig. 4.2, where, for convenience, the resistance of the secondary winding R_2 is lumped with the resistance of the load $R_2(1 - s)/s$, to give R_2/s. The inductances L_1' and L_2' are the total measured inductances of the primary circuit and of the secondary circuit, with the opposite circuit open in each case, and M is the mutual inductance between the two circuits, all in henrys. The resistances R_1 and R_2 are the self-resistances of the primary circuit and of the secondary circuit in ohms. The differential equations of the voltages around the primary and the secondary circuits, respectively, are

$$iR_1 + L_1' \frac{di_1}{dt} - M \frac{di_2}{dt} = e \quad \text{volts} \tag{13.1}$$

$$-M \frac{di_1}{dt} + L_2' \frac{di_2}{dt} + i_2R_2 = 0 \quad \text{volts} \tag{13.2}$$

The equivalent circuit corresponding to the physical circuit above is shown in Fig. 13.2. In this circuit, R_1 and R_2 are the resistances of the primary and secondary windings in ohms, L_1 and L_2 are the actual leakage inductances of the primary and the secondary windings in henrys, and L_m is the actual mutual inductance between the primary winding and the secondary winding in henrys. The differential equations of the voltages around the primary and the secondary circuits, respectively, are

$$iR_1 + L_1 \frac{di_1}{dt} + L_m \frac{d(i_1 + i_2)}{dt} = e \quad \text{volts} \tag{13.3}$$

$$L_m \frac{d(i_1 + i_2)}{dt} + L_2 \frac{di_2}{dt} + i_2R_2 = 0 \quad \text{volts} \tag{13.4}$$

Rearranging eqs. (13.3) and (13.4) yields

$$i_1R_1 + (L_1 + L_m) \frac{di_1}{dt} + L_m \frac{di_2}{dt} = e \quad \text{volts} \tag{13.5}$$

$$L_m \frac{di_1}{dt} + (L_2 + L_m) \frac{di_2}{dt} + i_2R_2 = 0 \quad \text{volts} \tag{13.6}$$

Figure 13.1, and resulting eqs. (13.1) and (13.2), correspond to exactly the same physical situation as that shown in Fig. 13.2 and resulting eqs. (13.5) and (13.6), respectively. Accordingly, the coefficients of like terms of the corresponding differential equations are equal. Then, from eqs. (13.1) and (13.5),

$$L_1' = L_1 + L_m \quad \text{henrys} \tag{13.7}$$

$$-M = L_m \quad \text{henrys} \tag{13.8}$$

and from eqs. (13.2) and (13.6),

$$-M = L_m \quad \text{henrys} \tag{13.9}$$

$$L_2' = L_2 + L_m \quad \text{henrys} \tag{13.10}$$

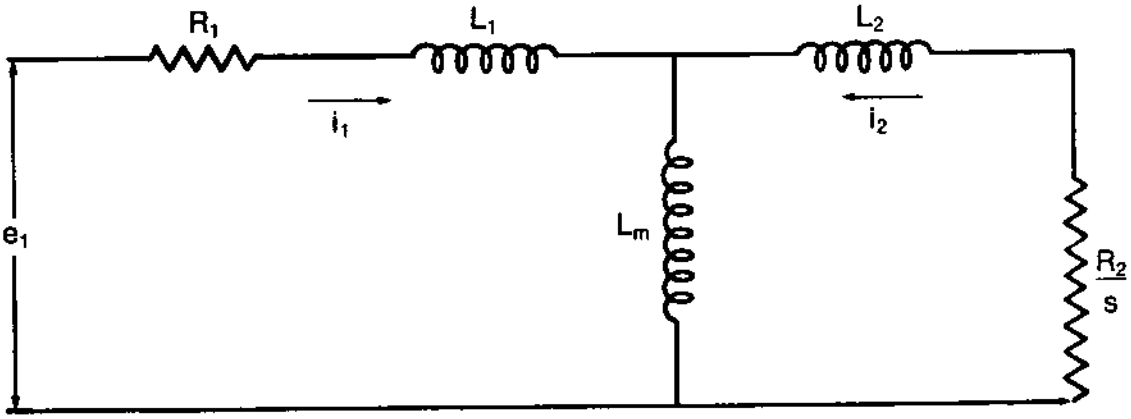

FIGURE 13.2 Equivalent circuit of one phase of a polyphase induction motor.

where the significance of the negative sign of M concerns the particular convention chosen for the positive direction of i_2 relative to the mutual-inductance coupling of M. From eq. (13.7),

$$L_1 = L_1' - L_m \quad \text{henrys} \tag{13.11}$$

and from eq. (13.10),

$$L_2 = L_2' - L_m \quad \text{henrys} \tag{13.12}$$

Also, from eqs. (13.8) and (13.9),

$$L_m = M \quad \text{henrys} \tag{13.13}$$

in magnitude. From the above it is apparent that (1) the leakage inductance L_1 of the stator winding is equal to the total inductance L_1' of that winding less the magnetizing inductance L_m, that (2) the leakage inductance of the rotor winding L_2 is equal to the total inductance L_2' of that winding less the magnetizing inductance L_m, and that (3) the coefficient of mutual inductance M of the actual phase circuit in Fig. 13.1 is equal to the magnetizing inductance L_m of the equivalent circuit in Fig. 13.2.

The corresponding reactances are equal to each of the inductances multiplied by ω. This is also true for L_2, of course, since the rotor angular velocity is ω, as seen by the stator. Then the equivalent-circuit reactances to be considered are

$$X_1 = \omega L_1 = 2\pi f L_1 \quad \text{ohms} \tag{13.14}$$

$$X_2 = \omega L_2 = 2\pi f L_2 \quad \text{ohms} \tag{13.15}$$

$$X_m = \omega L_m = 2\pi f L_m \quad \text{ohms} \tag{13.16}$$

The first reactance to be considered is magnetizing reactance.

13.3 MAGNETIZING REACTANCE

When rated phase voltage is applied to the terminals of the equivalent circuit, shown in Fig. 5.3, as well as to that shown in Fig. 13.2, magnetizing current I_m flows through the magnetizing branch of that circuit. This produces a voltage drop E_1 as viewed from the stator winding, and a voltage rise E_2 of equal magnitude as viewed from the rotor winding. Then

$$E_1 = I_m X_m \quad \text{volts} \tag{13.17}$$

Solving for X_m yields

$$X_m = \frac{E_1}{I_m} \quad \text{ohms} \tag{13.18}$$

It was shown in eq. (9.137) that

$$E_1 = 4.443K_pK_dN_{st}f\phi_{pm} \quad \text{volts/phase} \tag{13.19}$$

and in eq. (12.51) it was shown that

$$I_m = \frac{(296 \times 10^3)B_m pK_fK_s g}{N_{st}K_pK_d} \quad \text{amperes/phase} \tag{13.20}$$

Equation (13.20) is expressed in terms of flux/pole ϕ_{mp}, and eq. (13.19) is expressed in terms of maximum air-gap glux density B_m. Accordingly, eq. (13.20) should be modified in order to express it in terms of ϕ_{mp}, to be compatible with eq. (13.19). Considering the fundamental wave only, the average air-gap flux density is equal to $2/\pi$ multiplied by the maximum air-gap flux density, or

$$B_{av} = \frac{2}{\pi} B_m \quad \text{webers/meter}^2 \tag{13.21}$$

Also, the flux/pole is equal to the average air-gap flux multiplied by the area/pole of the air gap, or

$$\phi_p = \left(\frac{2}{\pi} B_m\right)\frac{\pi d\ell_c}{p} = \frac{2B_m d\ell_c}{p} \quad \text{webers} \tag{13.22}$$

Solving for B_m gives us

$$B_m = \frac{p\phi_{mp}}{2d\ell_c} \quad \text{webers/meter}^2 \tag{13.23}$$

where d is the diameter of the air gap and ℓ_c is the axial length of the core, with both quantities in units of meters. Then eq. (13.20) can be expressed in terms of flux/pole as

$$I_m = \frac{(148 \times 10^3)p^2\phi_{mp}K_fK_s g}{d\ell_c N_{st}K_pK_d} \quad \text{amperes/phase} \tag{13.24}$$

Substituting eqs. (13.19) and (13.24) into eq. (13.18) yields

$$X_m = \left(\frac{30}{10^6}\right)\frac{N_{st}^2 K_p^2 K_d^2 f d \ell_c}{p^2 K_f K_s g} \quad \text{ohms/phase} \qquad (13.25)$$

Equation (13.25) was formulated by use of MKS units. It can be converted to use units of inches by remembering that there are 39.37 inches in 1 meter. Then

$$X_m = \frac{76.2 N_{st}^2 K_p^2 K_d^2 f d \ell_c}{10^8 p^2 K_f K_s g} \quad \text{ohms/phase} \qquad (13.26)$$

An examination of eq. (13.26) shows how the value of magnetizing reactance will vary from one design to another. It will decrease as the radial length of the air gap g increases, and accordingly, the per unit magnetizing current I_m will decrease with a decrease in gap length for a given speed and power rating. Also, X_m will decrease as the second power of the number of poles. Since speed is inversely proportional to the number of poles, the magnetizing reactance is proportional to the square of speed, with other factors being constant. Accordingly, low-speed machines tend to have considerably more magnetizing current than high-speed machines, with other factors being constant. Since magnetizing current has a large out-of-phase component, it is essentially all reactive current. Accordingly, an increase in magnetizing current corresponds to a decrease in power factor, in general.

13.4 COMPONENTS OF LEAKAGE REACTANCE

As shown in eqs. (13.11) and (13.12), leakage inductance of the stator winding or of the rotor winding is equal to the total inductance of that winding less the mutual inductance of that winding with the other winding. Since reactance is equal to inductance multiplied by ω, leakage reactance is equal to the total reactance of the stator winding, or of the rotor winding, less the mutual reactance of that winding with the other winding. It is, in fact, caused by the "leakage flux," that is, the flux which links only that circuit and which does not link both circuits in common.

The leakage flux of an induction motor is equal to the sum of the stator leakage reactance X_1 and the rotor leakage reactance X_2. For purposes of subsequent discussion within this chapter, induction-motor leakage reactance is broken down to the following components:

1. Stator-slot leakage reactance
2. Rotor-slot leakage reactance
3. End-turn leakage reactance
4. Differential leakage reactance
    a. Zigzag leakage reactance
    b. Belt leakage reactance
5. Leakage reactance due to skew

Each component of reactance will be defined, in turn, as it is subsequently discussed.

It will be remembered that when the complete equivalent circuit, the simplified equivalent circuit, and the circle diagram were discussed, it was stated that leakage reactance at blocked-rotor conditions is less than that at full-speed operation. This results from saturation of a portion of the ferromagnetic paths to leakage flux, because of the large value of stator and rotor current at blocked-rotor conditions. Most of the blocked-rotor saturation occurs near the top of the rotor slot and, to a lesser extent, near the top of the stator slot. This effect will be discussed after the various slot leakage-reactance components have been discussed.

13.5 STATOR-SLOT LEAKAGE REACTANCE OF A RECTANGULAR SLOT

The leakage reactance of stator slots with parallel sides, such as are used for formed-coil windings, will first be derived. Following that, the leakage reactance of stator slots used for random windings will then be considered. Figure 13.3 shows a parallel-sided stator slot, which is occupied by the two coil sides T and B, together with the spatial relationship of this slot to adjacent parts of the magnetic core. The flux path of an elemental filament of leakage flux for both the top and the bottom coils are shown in the figure. Stator-slot leakage reactance of a given slot results from the total cross-slot flux of that slot, which links only that slot, in the manner shown in Fig. 13.3. The leakage reactance of the individual slot must be multiplied by the appropriate factors, of course, to obtain the stator-slot leakage reactance for the phase winding, and those factors will subsequently become apparent.

Figure 13.4 shows the pertinent depth and width dimensions, in general terms, for the same slot. Consider the bottom coil side B in that figure, in which an incremental filament of leakage flux is shown, which is dy meters wide and which is located y meters above the bottom of the conductors of coil B. If the unit length of the slot is considered, the cross-sectional area of the incremental flux path at y is

$$dA = dy \quad \text{meters}^2 \tag{13.27}$$

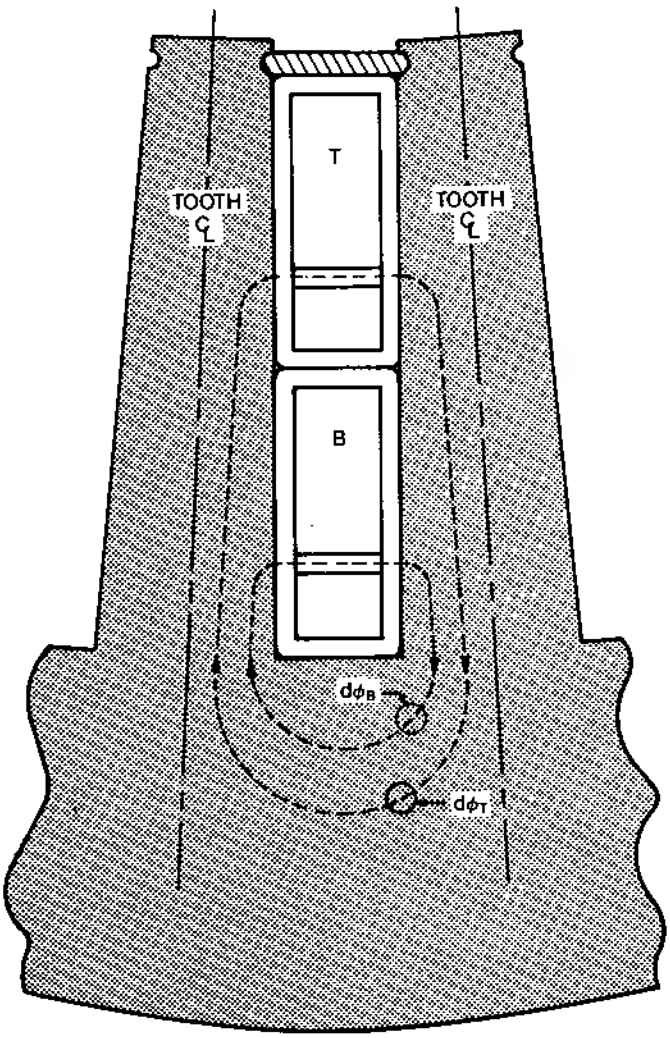

FIGURE 13.3 Incremental slot-leakage flux in the top coil and in the bottom coil of a stator slot.

The permeability of the steel core relative to the material within the slot is very great. If it is assumed that the ratio is infinite, then the length of the flux path as it links the slot is simply equal to the width of the slot w, or

$$\text{length of leakage flux path} = w \quad \text{meters} \tag{13.28}$$

The flux density of the incremental filament of leakage flux at point y is then

$$dB = \mu H = \frac{4\pi(NI)_y}{10^7 w} \quad \text{webers/meter} \tag{13.29}$$

where $(NI)_y$ is the magnetomotive force, in ampere turns, acting to force flux across the slot, at point y, and w is the length of the flux path along which the magnetomotive force acts.

There are N_c conductors per coil side, where N_c is the number of turns per coil. A current of I_t flows through each conductor; where I_t represents both conductor and coil current. Thus there are N_cI_t ampere-turns of magnetomotive force produced by each coil, for a winding with full-pitched coils which is acting to force leakage flux across the slot. The adjustment necessary to allow for fractional-pitched coils will be discussed subsequently. Then, at y the magnetomotive force is

$$(NI)_y = \frac{y}{d_1}(N_cI_t) \quad \text{ampere-turns} \tag{13.30}$$

Substituting eq. (13.30) into eq. (13.29) yields

$$dB = \frac{4\pi}{10^7 w}\frac{y}{d_1}(N_cI_t) \quad \text{webers/meter}^2 \tag{13.31}$$

If eq. (13.31) is multiplied by eq. (13.27), the result is the incremental flux $d\phi$ in webers associated with the incremental filament shown in Figs. 13.3 and 13.4. Then

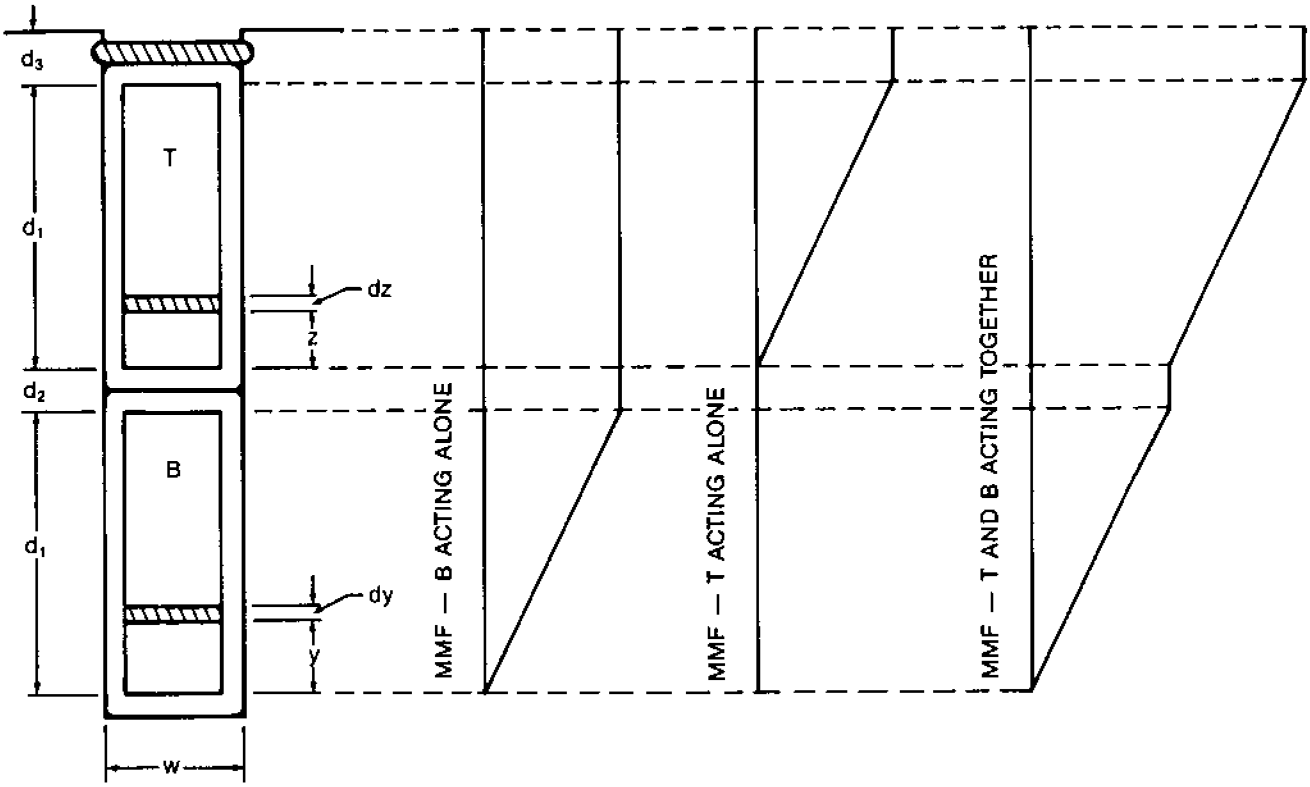

FIGURE 13.4 Distribution of the cross-slot magnetomotive force of two coil sides in a stator slot.

$$d\phi = \frac{4\pi}{10^7 w} \frac{y}{d_1} (N_c I_t)\ dy \quad \text{webers} \tag{13.32}$$

In general terms, leakage reactance is equal to

$$L = \frac{N\phi}{I} \quad \text{henrys} \tag{13.33}$$

where N is the number of turns linked by the leakage flux ϕ and $I = I_t$ is the current that sustains ϕ. The incremental leakage inductance associated with the incremental leakage flux given in eq. (13.32) is then

$$dL = N \frac{4\pi}{10^7 w} \frac{y}{d_1} N_c\ dy \quad \text{henrys} \tag{13.34}$$

If it is assumed that the current density is uniformly distributed in the conductors, the turns linked by the incremental leakage flux $d\phi$ at point y is proportional to y, or

$$N = \frac{y}{d_1} N_c \quad \text{turns} \tag{13.35}$$

Substituting eq. (13.35) into eq. (13.34), the incremental leakage inductance for the lower coil side B is

$$dL_B = \frac{4\pi}{10^7 w}\left(\frac{y}{d_1}\right)^2 N_c^2\ dy \quad \text{henrys} \tag{13.36}$$

Integrating from $y = 0$ to $y = d_1$ gives us

$$L_B = \frac{4\pi N_c^2}{10^7 w d_1^2} \int_0^{d_1} y^2\ dy = \frac{4\pi N_c^2}{10^7 w d_1^2} \frac{d_1^3}{3} \quad \text{henrys} \tag{13.37}$$

Rearranging eq. (13.37), we obtain

$$L_B = \frac{4\pi N_c^2}{10^7} \frac{d_1}{3w} \quad \text{henrys} \tag{13.38}$$

The flux and the flux density, due to coil side B only, are constant for the distance from the top of the conductors of coil side B to the top of the slot (see Fig. 13.4). Thus the expression for dL is a function of dy only. Then

$$dL'_B = \frac{4\pi N_c^2}{10^7 w} dy \quad \text{henrys} \tag{13.39}$$

Integrating from $y = d_1$ to $y = 2d_1 + d_2 + d_3 = B$ yields

$$L'_B = \frac{4\pi N_c^2}{10^7 w} \int_{d_1}^{B} dy = \frac{4\pi N_c^2}{10^7 w}(d_1 + d_2 + d_3) \quad \text{henrys} \tag{13.40}$$

Then the total self-leakage inductance of the lower coil side B is equal to the sum of eqs. (13.38) and (13.40), or

$$L_{BS} = \frac{4\pi N_c^2}{10^7 w}\left(\frac{4}{3} d_1 + d_2 + d_3\right) \quad \text{henrys} \tag{13.41}$$

The total self-leakage inductance of the top coil side T in Fig. 13.4 can be determined by proceeding in a homologous manner. Then the inductance of the increment dz located z distance above the bottom of the conductors of coil side T, corresponding to eq. (13.36) for coil side B, is

$$dL_T = \frac{4\pi}{10^7 w}\left(\frac{z}{d_1}\right)^2 N_c^2 \, dz \quad \text{henrys} \tag{13.42}$$

Integrating from $z = 0$ to $z = d_1$, we have

$$L_T = \frac{4\pi N_c^2}{10^7 w d_1^2} \int_0^{d_1} z^2 \, dz = \frac{4\pi N_c^2}{10^7 w d_1^2} \frac{d_1^3}{3} \quad \text{henrys} \tag{13.43}$$

or

$$L_T = \frac{4\pi N_c^2}{10^7} \frac{d_1}{3w} \quad \text{henrys} \tag{13.44}$$

The flux and the flux density due to coil side T only are constant from the top of the conductors of coil side T to the top of the slot (see Fig. 13.4). Again, the expression for dL is a function of dz only. Then

$$dL'_T = \frac{4\pi N_c^2}{10^7 w}\, dz \quad \text{henrys} \tag{13.45}$$

Integrating from z = d_1 to z = $d_1 + d_3$ gives us

$$L'_T = \frac{4\pi N_c^2}{10^7 w} \int_{d_1}^{d_1+d_3} dz = \frac{4\pi N_c^2}{10^7 w}(d_3) \quad \text{henrys} \tag{13.46}$$

The total self-leakage inductance of the top coil side T is then equal to the sum of eqs. (13.44) and (13.46), or

$$L_{TS} = \frac{4\pi N_c^2}{10^7 w}\left(\frac{d_1}{3} + d_3\right) \quad \text{henrys} \tag{13.47}$$

In common with any two inductively coupled circuits, there is a mutual inductance M_c between the bottom coil side and the top coil side. Consider the flux within the incremental filament dz in top coil side T due to current in bottom coil side B. This flux is equal to

$$d\phi_M = \frac{4\pi N_c I_t}{10^7 w}\, dz \quad \text{webers} \tag{13.48}$$

and it links $(z/d_1)N_c$ of the conductors of coil side T. Accordingly, this results in an incremental mutual inductance of

$$dM_c = \frac{4\pi N_c^2}{10^7 w d_1}\, z\, dz \quad \text{henrys} \tag{13.49}$$

Integrating from z = 0 to z = d_1, we obtain

$$M_C = \frac{4\pi N_c^2}{10^7 w d_1} \int_0^{d_1} z\, dz = \frac{4\pi N_c}{10^7 w d_1}\, \frac{d_1^2}{2} \quad \text{henrys} \tag{13.50}$$

or

$$M_c = \frac{4\pi N_c^2}{10^7 w} \frac{d_1}{2} \quad \text{henrys} \tag{13.51}$$

The flux from the top of the conductors in top coil side T to the top of the slot due to current in bottom coil side B is constant and the linkage is a function of dz only. Then

$$dM_c' = \frac{4\pi N_c^2}{10^7 w} dz \quad \text{henrys} \tag{13.52}$$

Integrating from $z = d_1$ to $z = d_1 + d_3$ yields

$$M_c' = \frac{4\pi N_c^2}{10^7 w} \int_{d_1}^{d_1+d_3} dz = \frac{4\pi N_c^2}{10^7 w} d_3 \quad \text{henrys} \tag{13.53}$$

and the total mutual inductance L_M of top coil side T due to current in bottom coil side B is equal to the sum of eqs. (13.51) and (13.53) for a full-pitched coil, or

$$L_M = \frac{4\pi N_c^2}{10^7 w} \left(\frac{d_1}{2} + d_3 \right) \quad \text{henrys} \tag{13.54}$$

The mutual inductance of bottom coil side B due to current in top coil side T is also equal to L_M, which can be shown by similar considerations. Then the total mutual inductance for the entire slot is equal to $2L_M$ for a full-pitched coil. For the more general case of a fractional-pitched coil for which there is a phase displacement between the current in the bottom coil side and the current in the top coil side, the total mutual reactance of the two coil sides in the slot L_{MS} is equal to

$$L_{MT} = \frac{4\pi N_c^2}{10^7 w} \left(\frac{d_1}{2} + d_3 \right) 2 \cos \theta_c \quad \text{henrys} \tag{13.55}$$

The total self-inductance of one stator slot is equal to the sum of the self-inductance of the bottom coil side L_{BS}, the self-inductance of the top coil side L_{TS}, and the total mutual inductance between the two coil sides, or

$$L = L_{BS} + L_{TS} + L_{MT} \quad \text{henrys} \tag{13.56}$$

Substituting eqs. (13.41), (13.47), and (13.55) into eq. (13.56) and rearranging gives us

$$L = \frac{4\pi N_c^2}{10^7}\left[\frac{4d_1}{3w} + \frac{d_2}{w} + \frac{d_3}{w} + \frac{d_1}{3w} + \frac{d_3}{w} + 2\left(\frac{d_1}{2w} + \frac{d_3}{w}\right)\cos\theta_c\right] \quad \text{henrys} \tag{13.57}$$

The vertical distance d_1 shown in Fig. 13.4 was chosen to delineate the current-carrying portion of a coil side, for ease of setting up the previous integration. However, use of the resulting equations in calculating motor reactance can be simplified by a simple change in symbols. The notation

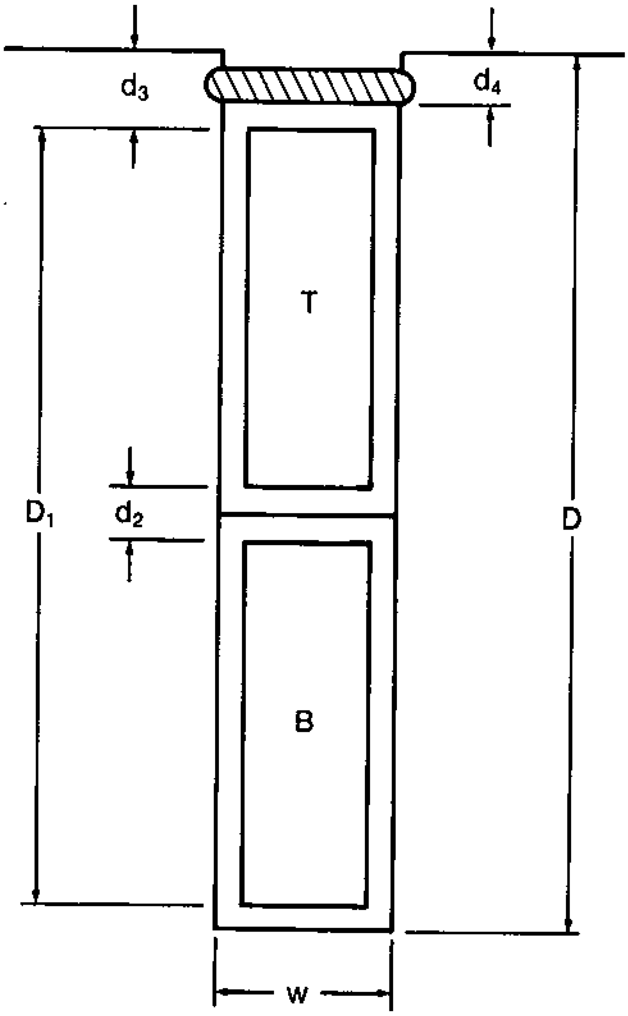

FIGURE 13.5 Dimensional nomenclature for a rectangular stator slot.

$2d_1 + d_2$ for the slot shown in Fig. 13.4 has been replaced by the notation D_1 for a corresponding distance of the slot shown in Fig. 13.5. Such a change in notation permits the determination of D_1 by subtracting the slot dimension d_4 and the vertical insulation allowance from the slot dimension D. Then, making the substitution

$$D_1 = 2d_1 + d_2 \quad \text{meters} \tag{13.58}$$

into eq. (13.57) and simplifying, we obtain

$$L = \frac{4\pi N_c^2}{10^7}\left[\frac{2d_3}{w}(1 + \cos\theta_c) + \frac{D_1 - d_2}{w}\,\frac{5 + 3\cos\theta_c}{6} + \frac{d_2}{w}\right] \quad \text{henrys} \tag{13.59}$$

Let

$$K_M = \frac{1 + \cos\theta_c}{2} \quad \text{numeric} \tag{13.60}$$

Substituting eq. (13.60) into eq. (13.59) and simplifying yields

$$L = \frac{4\pi N_c^2}{10^7}\left[4K_M\left(\frac{d_3}{w} + \frac{D_1}{3w}\right) + \frac{D_1}{3w}(1 - K_M) - \frac{d_2}{w}\left(K_M - \frac{2}{3}\right)\right] \quad \text{henrys} \tag{13.61}$$

Equation (13.61) is the total inductance of unit length of one slot and is based on the number of turns per coil N_c. Thus, to convert this equation to stator-slot leakage reactance/phase, the following operations should be performed:

1. Multiply by the series slots/phase = N_1/Cq
2. Express turns/coil N_c in terms of series turns/phase N_{st}, where $N_c = N_{st}qC/N_1$
3. Multiply by $\omega = 2\pi f$ to convert inductance L to reactance X
4. Multiply by the reciprocal of the number of parallel circuits, 1/C
5. Multiply by the slot length or core length ℓ_c

Performing the five operations above on the first factor in eq. (13.61), we obtain

$$X'_{s1} = \frac{4\pi}{10^7} \ell_c \frac{N_1}{Cq}\left(\frac{N_{st}qC}{N_1}\right)^2 2\pi f \frac{1}{C}$$

$$= \frac{8\pi^2 f \ell_c N_{st}^2 q}{10^7 N_1} \quad \text{ohms/phase} \qquad (13.62)$$

and the equation for stator-slot leakage reactance is

$$X_{s1} = \frac{8\pi^2 f \ell_c N_{st}^2 q}{10^7 N_1}\left[4K_M\left(\frac{d_3}{w} + \frac{D_1}{3w}\right) + \frac{D_1}{3w}(1 - K_M) - \frac{d_2}{w}\left(K_M - \frac{2}{3}\right)\right] \quad \text{ohms/phase} \qquad (13.63)$$

Equation (13.63) can also be written as

$$X_{s1} = \frac{32\pi^2 f \ell_c N_{st}^2 q}{10^7 N_1}\left[K_M\left(\frac{d_3}{w} + \frac{D_1}{3w}\right) + \frac{D_1}{12w}(1 - K_M) - \frac{d_2}{4w}\left(K_M - \frac{2}{3}\right)\right] \quad \text{ohms/phase} \qquad (13.64)$$

The quantities involving ratios of D_1, d_2, and d_3 to w contained in the right-hand set of brackets in eq. (13.64) are called slot permeance ratios. This is because the ratio of slot depth to slot width for unit length of slot is equal to the ratio of cross-sectional area to length of the leakage flux path, which is proportional to leakage flux permeance. The last two permeance ratios in eq. (13.64) are usually small in comparison to the first two. Thus they are frequently omitted in the technical literature and the resulting expression for the permeance ratios of a rectangular slot such as that in Fig. 13.5 is then

$$P_{s1} = K_M\left(\frac{d_3}{w} + \frac{D_1}{3w}\right) \quad \text{numeric} \qquad (13.65)$$

and the corresponding expression for slot-leakage reactance is

$$X_{s1} = \frac{32\pi^2 f \ell_c N_{st}^2 q}{10^7 N_1}\left[K_M\left(\frac{d_3}{w} + \frac{D_1}{3w}\right)\right] \quad \text{ohms/phase} \qquad (13.66)$$

Equation (13.66), which was derived by using the MKS system of units, can be converted to accept dimensions of inches by remembering that there are 39.37 inches in 1 meter. Then

$$X_{s1} = \frac{8.02f\ell N_c^2 N_{st} q}{10^7 N_1}\left[K_M\left(\frac{d_3}{w} + \frac{D_1}{3w}\right)\right] \quad \text{ohms/phase} \qquad (13.67)$$

13.6 STATOR-SLOT LEAKAGE REACTANCE OF A NONRECTANGULAR SLOT

The leakage reactance of rectangular slots used with formed coils is capable of exact mathematical analysis, whereas that of slots used with random coils is somewhat less capable of exact analysis, as will become apparent. Random-wound stator coils, which are applied to machines of lower power and/or voltage ratings, are normally used with semiclosed slots. Any given slot shape results from an effort to maximize the current-carrying space in the slot and at the same time to use uniformly the cross-sectional area of the tooth, which carries mutual flux. Thus the sides of such slots are not necessarily parallel, and the slot tends to approach a "pear" shape. Also, generous radii are used at any change in slot contour, to avoid damage to the individual conductors, as they are inserted into the slot during winding. Thus it is difficult, if not impossible, to set up a meaningful set of differential expressions for a random slot such as was done in eqs. (13.36), (13.42), (13.49), and (13.52) for a rectangular slot. An analytical expression for random-slot leakage reactance could be obtained by assuming that the slot shape is a truncated triangle, which, of course, it is not. However, the actual results will not necessarily be any more exact than to assume that the slot shape is a rectangle, which, also, it is not. Based on all of the above, a reasonable procedure is to assume that a random slot, in general, approaches a rectangular shape for the current-carrying portion of the slot, based on the width w_1.

Figure 13.6a shows a typical pear-shaped semiclosed slot with two random coil sides. Part (b) of the figure shows a somewhat idealized geometric version of the slot and coil sides, which tends to approach a rectangular slot. Even though the top coil side T has a slightly different shape than bottom coil side B, it is understood that both coil sides have the same number of turns.

With our previous knowledge of the rectangular-slot analysis available, the leakage reactance of the slot shown in Fig. 13.6b can be determined by inspection to a good approximation. The permeance ratio of the slot opening

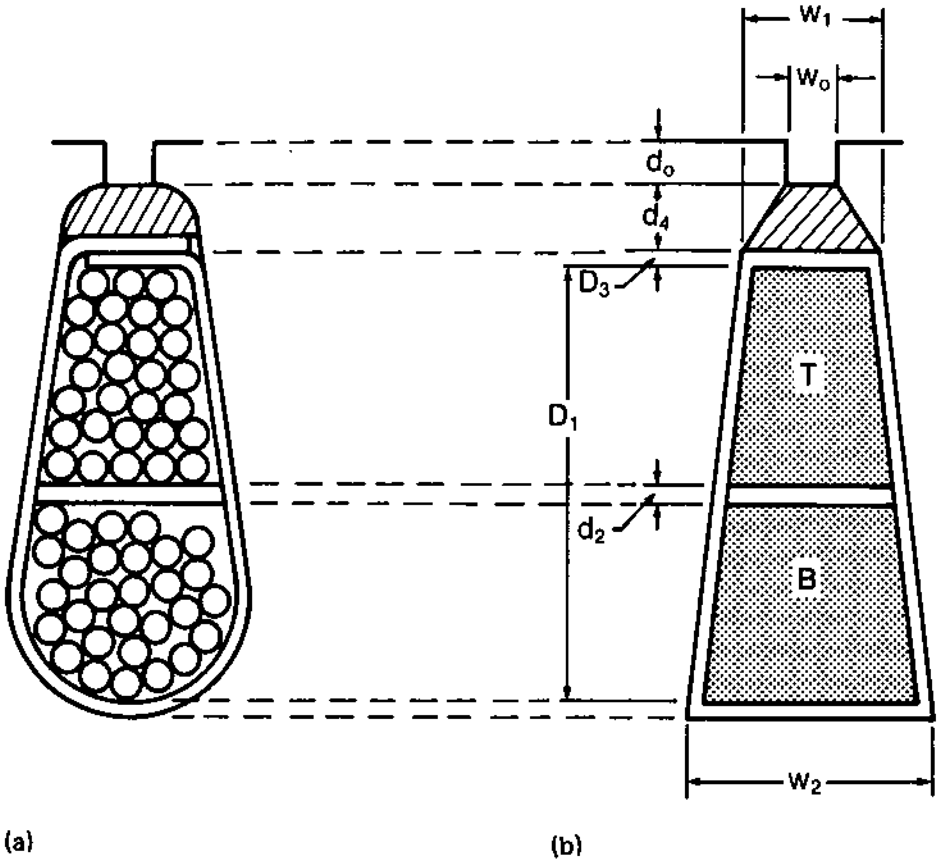

FIGURE 13.6 Dimensional nomenclature for a semiclosed stator slot with random coils: (a) typical shape of a random stator slot; (b) idealized shape of a random stator slot to facilitate calculation of reactance.

is equal to d_0/w_0. Also, the permeance ratio of that portion of the slot in which the wedge is located is equal to $2d_4/(w_0 + w_1)$, based on using the arithmetic average $(w_0 + w_1)/2$ of the leakage flux path length. The permeance ratio for the vertical slot distance D_3 is closely equal to D_3/w_1. The permeance ratio for the vertical slot distance D_1 is approximately equal to $D_1/3w_1$, based on using w_1 as the effective slot width throughout D_1. An effective slot width of $\sqrt{w_1 w_2}$ can also be used, but the use of a value w_1 results in slightly more total reactance and in slightly less calculated torque, which is a more conservative practice. Then, from the considerations above, the permeance ratios of the slot shown in Fig. 13.6b are approximately equal to

$$P_{s1} = K_M\left(\frac{d_0}{w_0} + \frac{2d_4}{w_0 + w_1} + \frac{D_3}{w_1} + \frac{D_1}{3w_1}\right) \quad \text{numeric} \qquad (13.68)$$

and the resulting slot-leakage reactance is equal to

$$X_{sl} = \frac{32\pi^2 f \ell_c N_{st}^2 q}{10^7 N_1}\left[K_M\left(\frac{d_0}{w_0} + \frac{2d_4}{w_0 + w_1} + \frac{D_3}{w_1} + \frac{D_1}{3w_1}\right)\right] \quad \text{ohms/phase} \qquad (13.69)$$

when MKS dimensional units are used, and is equal to

$$X_{sl} = \frac{8.02 f \ell_c N_{st}^2 q}{10^7 N_1}\left[K_M\left(\frac{d_0}{w_0} + \frac{2d_4}{w_0 + w_1} + \frac{D_3}{w_1} + \frac{D_1}{3w_1}\right)\right] \quad \text{ohms/phase} \qquad (13.70)$$

when inch dimensional units are used.

It is possible for any motor manufacturer to prepare a curve that provides a slot-taper factor versus the slot parameter w_1/w_2 from several specific random-slot shapes which that manufacturer might use and for which the factor is equal to 1/3 for the limiting case of parallel-sided slots. When using such a curve, the permeance ratio for the D_1 region of the slot should be equal to D_1/w_1 multiplied by the slot-taper factor. Also, it occasionally happens that for the wedge portion of the slot, corresponding to the distance d_4 in Fig. 13.6, some motor manufacturers use a curved transition in the slot, as shown in Fig. 9.6, as the slot width narrows. For such cases, the permeance ratio of the d_4 region of the slot can be determined by (1) the use of several small but finite rectangular elements along d_4, or by (2) orthogonal flux plotting. However, reasonable results can be obtained by judicious use of the nomenclature in Fig. 13.6 together with eq. (13.69) or (13.70).

13.7 ROTOR-SLOT LEAKAGE REACTANCE OF A PHASE-WOUND ROTOR

From the standpoint of calculating slot-leakage reactance, a phase-wound rotor slot is not significantly different from a rectangular stator slot. A rectangular stator slot is occupied by a bottom coil side and a top coil side and a phase-wound rotor slot is occupied by two side-by-side insulated bottom straps and two side-by-side insulated top straps (see Fig. 10.19). However, the mechanical purchase provided for the wedge is different for a phase-wound rotor slot, since it must withstand the effect of centrifugal force. Thus the permeance ratios for the phase-wound rotor slot must take this into consideration.

Figure 13.7 shows the two general types of phase-wound rotor slots used with formed rotor-winding straps, together with the necessary dimensional notation required to define the various permeance ratios along each of the two slots. From analogy with Figs. 13.5 and 13.6, the permeance ratios along the slot depth of Fig. 13.7 can be determined by inspection. They are

$$P_{s2} = K_{M2}\left(\frac{d_0}{w_0} + \frac{2d_4}{w_0 + w} + \frac{D_3}{w} + \frac{D_1}{3w}\right) \quad \text{numeric} \qquad (13.71)$$

where, again, K_{M2} is a factor that corrects for the phase-angle displacement between the current in the bottom half of the slot and in the top half of the slot. As for the corresponding factor K_M for the stator, K_{M2} is a function of the coil pitch of the particular winding under consideration and can be determined from the curve in Fig. 13.8. The rotor-slot leakage reactance as seen by the rotor and at rotor-circuit frequency is then

$$X'_{s2} = \frac{32\pi^2 f_2 \ell_c (N_{st2})^2 q}{10^7 N_2}\left[K_{M2}\left(\frac{d_0}{w_0} + \frac{2d_4}{w_0 + w} + \frac{D_3}{w} + \frac{D_1}{3w}\right)\right] \quad \text{ohms/phase} \qquad (13.72)$$

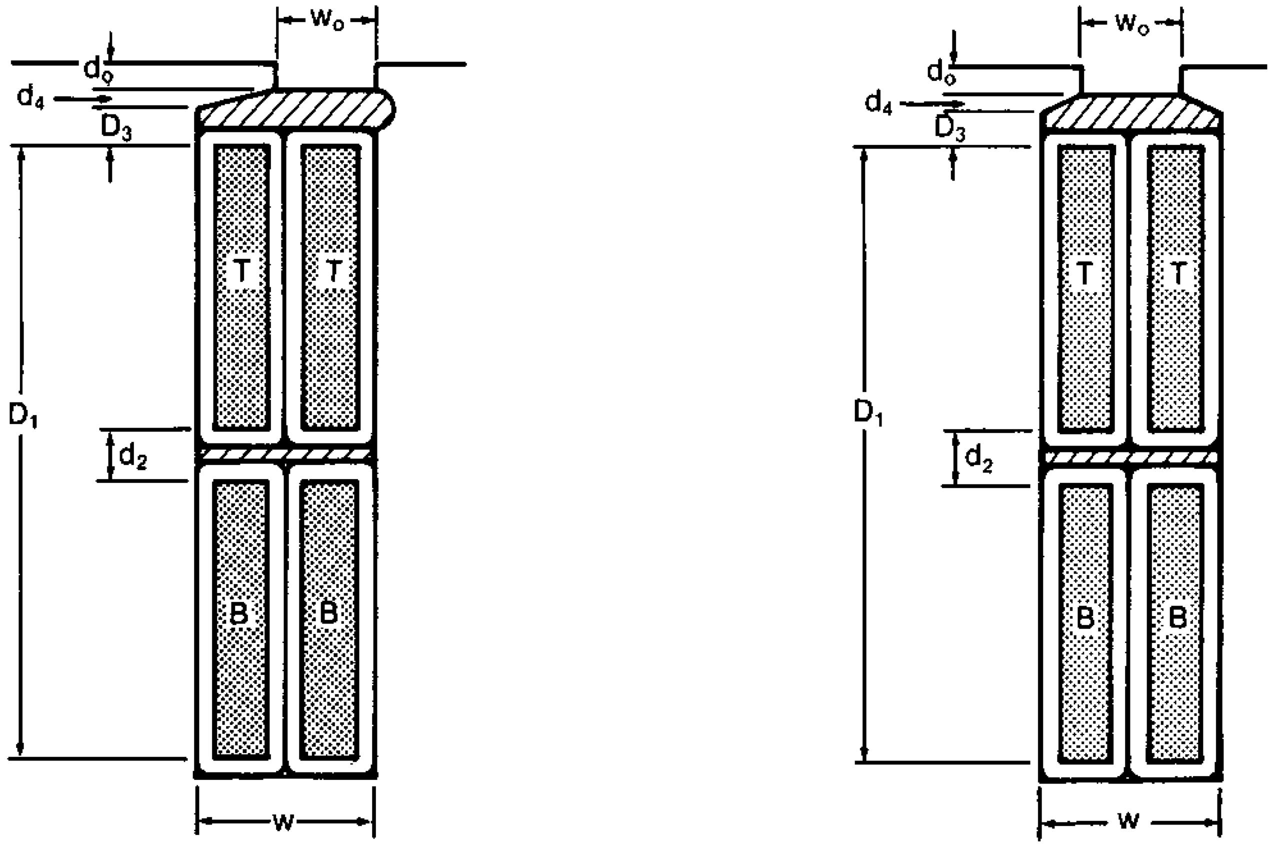

(a) (b)

FIGURE 13.7 Dimensional nomenclature for a rectangular wound-rotor slot: (a) offset opening and four-strap slot; (b) centered opening and four-strap slot.

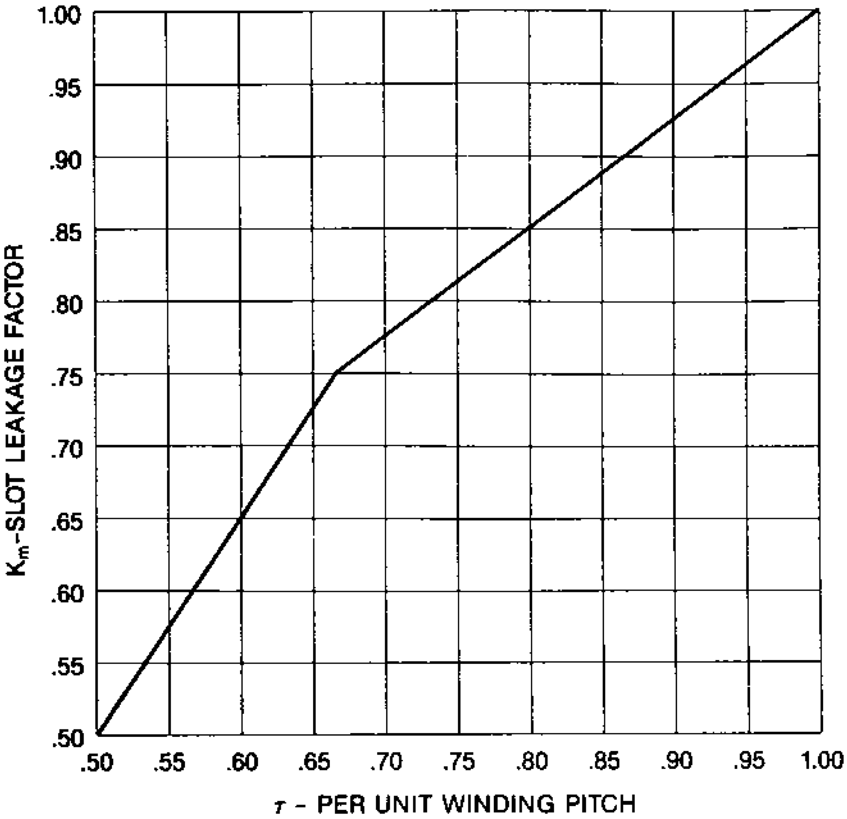

FIGURE 13. 8 Slot leakage factor or mutual factor K_M versus per unit pitch τ for use with a winding have 60-degree phase belts.

where

f_2 = rotor-circuit frequency, hertz
N_{st2} = series conductors/phase of the rotor winding
N_2 = number of rotor slots

The frequency of the rotor circuit is equal to the rotor slip s multiplied by stator frequency f, or to sf. However, the rotor structure is rotating at a speed of (1 - s) of synchronous speed, so that the frequency of the rotor circuit as seen by the stator is equal to sf + (1 - s)f = f hertz. Also, as shown in Section 4. 6 and as indicated in Table 4. 1, rotor impedance quantities are referred to the stator by mulfiplying them by the second power of the effective stator/rotor turns ratio [i. e., by $(N_{st}K_{p1}K_{d1})^2/(N_{st2}K_{p2}K_{d2})^2$]. Then the rotor-slot leakage reactance for a phase-wound rotor referred to the stator is

$$X_{s2} = \frac{32\pi^2 f_1 \ell_c N_{st}^2 q}{10^7 N_2}\left(\frac{K_{p1}K_{d1}}{K_{p2}K_{d2}}\right)^2\left[K_{M2}\left(\frac{d_0}{w_0} + \frac{2d_4}{w_0 + w} + \frac{D_3}{w} + \frac{D_1}{3w}\right)\right] \quad \text{ohms/phase} \qquad (13.\,73)$$

when slot dimensions are in MKS units, and is equal to

$$X_{s2} = \frac{8.02 f_1 \ell_c N_{st}^2 q}{10^7 N_2}\left(\frac{K_{p1}K_{d1}}{K_{p2}K_{d2}}\right)^2\left[K_{M2}\left(\frac{d_0}{w_0} + \frac{2d_4}{w_0 + w} + \frac{D_3}{w} + \frac{D_1}{3w}\right)\right] \quad \text{ohms/phase} \qquad (13.74)$$

when slot dimensions are in inches.

13.8 ROTOR-SLOT LEAKAGE REACTANCE OF A SQUIRREL-CAGE ROTOR WITH RECTANGULAR SLOTS

All the slots considered so far have had two coil sides in each slot to produce the magnetomotive force that causes leakage flux to flow across that slot. Squirrel-cage rotors, on the other hand, have only one conducting rotor bar in each slot to produce the corresponding magnetomotive force. As discussed in Chapter 10, the current density is uniform throughout the full depth of the rotor bar at running conditions when the actual rotor-circuit frequency is equal to 1 or 2 Hz. The resulting rotor-slot leakage reactance is called the "running" reactance. Under starting conditions, however, the current density is very nonuniform, with the current being crowded toward the top of the bar, due to the "deep bar" effect. This effect, together with the saturating effect of a high value of starting current, results in a significantly reduced value of rotor-slot leakage reactance which is called the "blocked-rotor" reactance. The running value of rotor-slot leakage reactance is considered next and the blocked-rotor value, later in this chapter. The first rotor-slot shape to be evaluated is the basic rectangular rotor bar.

Consider Fig. 13.9. The permeance ratio for the current-carrying bar portion of the slot is equal to $d_b/3w$, and for the portions of the bar along d_0 and d_4, it is equal to d_0/w_0 and $2d_4/(w_0 + w)$, respectively. Then the total permeance ratio is

$$P_{s2} = \frac{d_b}{3w} + \frac{d_0}{w_0} + \frac{2d_4}{w_0 + w} \quad \text{numeric} \qquad (13.75)$$

For a squirrel-cage rotor winding, $K_{p2}K_{d2} = 1.0$ and also $K_{M2} = 1.0$ since the current throughout the conducting bar is in phase. Then the rotor-slot leakage reactance referred to the stator for the slot shown in Fig. 13.9 is equal to

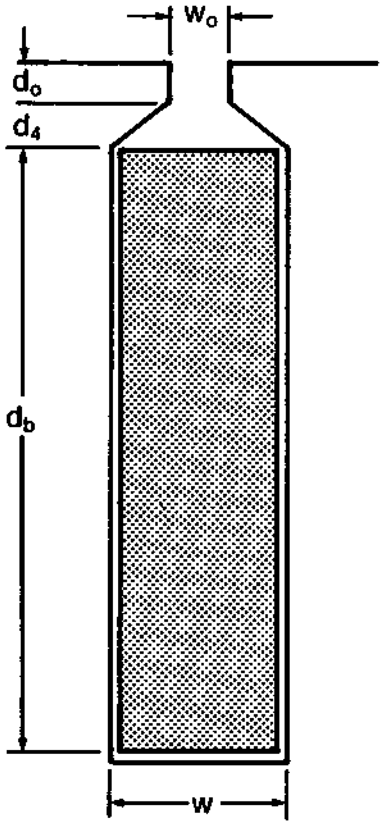

FIGURE 13.9 Dimensional nomenclature for a squirrel-cage rotor slot with a rectangular bar.

$$X_{s2} = \frac{32\pi^2 f_1 \ell_c N_{st}^2 q K_{p1}^2 K_{d1}^2}{10^7 N_2}\left(\frac{d_0}{w_0} + \frac{2d_4}{w_0 + w} + \frac{d_b}{3w}\right) \quad \text{ohms/phase} \tag{13.76}$$

when slot dimensions are in MKS units. It is equal to

$$X_{s2} = \frac{8.02 f_1 \ell_c N_{st}^2 q K_{p1}^2 K_{d1}^2}{10^7 N_2}\left(\frac{d_0}{w_0} + \frac{2d_4}{w_0 + w} + \frac{d_b}{3w}\right) \quad \text{ohms/phase} \tag{13.77}$$

when slot dimensions are in inches.

13.9 ROTOR-SLOT LEAKAGE REACTANCE OF A SINGLE-CAGE ROTOR WITH NONRECTANGULAR SLOTS

Many squirrel-cage induction motors of various power ratings and with normal starting-torque requirements utilize rotor-slot shapes similar to that

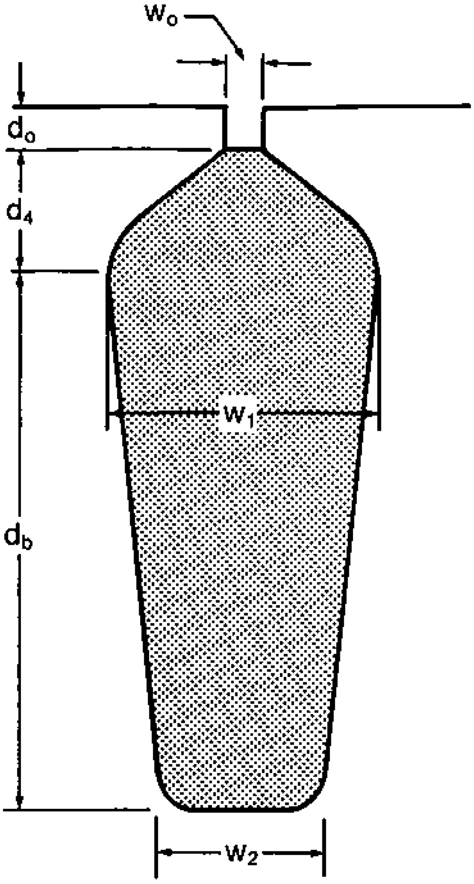

FIGURE 13.10 Dimensional nomenclature for a squirrel-cage rotor slot with a nonrectangular bar.

shown in Fig. 13.10. An opening w_0 at the top of the slot is shown in this figure. Such an opening may or may not be present in a given rotor design. If the rotor winding is made of cast aluminum, the opening would normally be omitted to simplify the casting process. In such cases the steel bridge over the top of the bar will become magnetically saturated at some value of bar current. The saturating value of bar current will depend on the depth of the bridge and the permeability of the steel. There will also be some saturation of the tooth steel adjacent to the slot opening under blocked-rotor conditions for designs that have slot openings, such as that shown in Fig. 13.10. This subject is considered in greater detail later in the chapter.

Accurate calculation of the various permeance ratios of the rotor slot shown in Fig. 13.10 is fraught with the problems discussed in Section 13.6 for the stator slot shown in Fig. 13.6. Such problems arise from the need to make optimum use of both the tooth space and the rotor-bar space for machines of low to medium power rating and with normal starting torque. This, then, results in a rotor bar with a pear-shaped cross section, and such a shape is not particularly amenable to exact calculation of the permeance ratio for the d_b portion of the slot. As for the stator slot shown in

Fig. 13.6, a reasonable procedure for the rotor slot shown in Fig. 13.10 is to assume that the d_b portion of the slot approaches a rectangular shape, based on using w_2 as the effective slot width throughout d_b. Again, an effective slot width of $\sqrt{w_1 w_2}$ can also be used, but the use of w_2 results in slightly more total reactance and in slightly less calculated torque.

From the above, the total permeance ratio for the rotor slot shown in Fig. 13.10 is equal to

$$P_{s2} = \frac{d_0}{w_0} + \frac{2d_4}{w_0 + w_1} + \frac{d_b}{3w_2} \quad \text{numeric} \tag{13.78}$$

The corresponding slot-leakage reactance is

$$X_{s2} = \frac{32\pi^2 f_1 \ell_c N_{st}^2 q K_{p1}^2 K_{d1}^2}{10^7 N_2}\left(\frac{d_0}{w_0} + \frac{2d_4}{w_0 + w_1} + \frac{d_b}{3w_2}\right) \quad \text{ohms/phase} \tag{13.79}$$

when slot dimensions are in MKS units and is equal to

$$X_{s2} = \frac{8.02 f_1 \ell_c N_{st}^2 q K_{p1}^2 K_{d1}^2}{10^7 N_2}\left(\frac{d_0}{w_0} + \frac{2d_4}{w_0 + w_1} + \frac{d_b}{3w_2}\right) \quad \text{ohms/phase} \tag{13.80}$$

when slot dimensions are in inches.

13.10 ROTOR-SLOT LEAKAGE REACTANCE OF A MULTIPLE-CAGE ROTOR

The rotor slots shown in Figs. 13.9 and 13.10 will provide a ratio R_{ac}/R_{dc} which results in adequate starting torque for many induction motor applications. However, for applications that require a greater-than-normal starting torque, in the range 150 to 250% of rated torque, a multiple-cage rotor winding is frequently used.

Figure 13.11 shows a triple-cage rotor bar for which the dimensions of the top cage T, the notched cage N, and the bottom cage B are shown. In the general case, the bar resistivity can be different for each of the three cages. Thus the top cage T could be made of brass or bronze, the bottom cage B could be made of copper, and the notched cage could be void of a conductor. This would tend to produce a high value of R_{ac} and a low value of R_{dc} and is used occasionally with fabricated-rotor windings. However, a more typical arrangement is to have all cages made of cast aluminum and

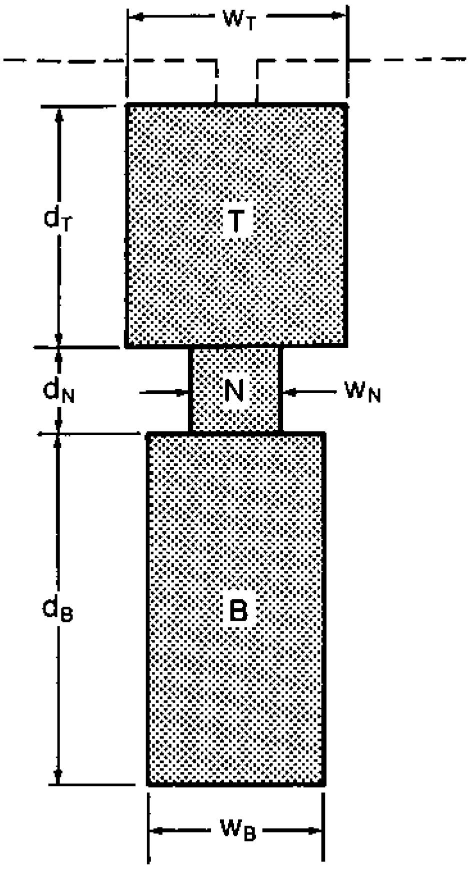

FIGURE 13.11 Dimensional nomenclature for a rotor slot with a triple cage.

thus to have one common resistivity for the three cages. Because of the cost advantages of the latter, it is the construction that is most frequently used for small to medium-sized induction motors.

The fundamental concept of the multiple-cage bar was discussed in Section 10.3.8. A generalized lattice network for analyzing the multiple-cage bar as well as any other bar shape under high-slip conditions was developed in Section 10.3.9. Also, a numerical example of calculation of R_{ac}/R_{dc} and X_{ac}/X_0 for a triple-cage rotor at blocked-rotor conditions was carried through in Section 10.3.11 and compared with a corresponding calculation made in Section 10.3.10 for a rectangular bar of the same depth and dc resistance. The procedure for calculating the running reactance at low rotor-circuit frequency is considered in this section.

Under blocked-rotor conditions the rotor-circuit frequency is equal to that of the stator. Thus if there are several bars in parallel in a given slot, the rotor current division between the various bars is determined by consideration of their total impedances, of which the reactive component is significant. Under normal running conditions, on the other hand, the actual rotor-circuit frequency is only about 2% of that of the stator. The rotor-circuit impedance is overwhelmingly resistive and the rotor current division is determined primarily by bar resistance. Thus it is a good approximation to assume that under normal operating conditions, the flow through the various bars within a slot divides in inverse proportion to the respective resistances. Then for the triple cage shown in Fig. 13.11, the three bar currents will divide in direct proportion to their areas, since all of the bars have the same length and the same resistivity. Accordingly, the leakage flux produced by the current in a given bar is proportional to the area of that bar. Also, the linkage of that flux with the bar is proportional to the bar area. Thus the flux linkage $N\phi$ is proportional to the second power of the bar area being considered.

Consider the triple cage shown in Fig. 13.11. The self-inductance of bar B with 1 A flowing in bar B is

$$L_B = \frac{4\pi}{10^7}\left(\frac{d_B}{3W_B} + \frac{d_N}{W_N} + \frac{d_T}{W_T}\right) \text{ henrys} \tag{13.81}$$

the self-inductance of bar N with 1 A flowing in bar N is

$$L_N = \frac{4\pi}{10^7}\left(\frac{d_N}{3W_N} + \frac{d_T}{W_T}\right) \text{ henrys} \tag{13.82}$$

and the self-inductance of bar T with 1 A flowing in bar T is

$$L_T = \frac{4\pi}{10^7}\frac{d_T}{3W_T} \text{ henrys} \tag{13.83}$$

The mutual inductance of bar N with bar T with 1 A following in bar N is

$$M_{NT} = \frac{4\pi}{10^7}\frac{d_T}{2W_T} \text{ henrys} \tag{13.84}$$

and the mutual inductance of bar B with bar N with 1 A flowing in bar B is

$$M_{BN} = \frac{4\pi}{10^7}\left(\frac{d_N}{2W_N}\ \frac{d_T}{2W_T}\right) \text{ henrys} \tag{13.85}$$

The resulting leakage reactance X_0 of the slot under running conditions is approximately equal to

$$X_0 = \frac{8\pi^2 f}{10^7}\left[\left(\frac{A_B}{A_B + A_N + A_T}\right)^2\left(\frac{d_B}{3W_B} + \frac{d_N}{W_N}\,\frac{d_T}{W_T}\right)\right.$$
$$+\left(\frac{A_N}{A_B + A_N + A_T}\right)^2\left(\frac{d_N}{3W_N} + \frac{d_T}{W_T}\right) + \left(\frac{A_T}{A_B + A_N + A_T}\right)^2 \frac{d_T}{3W_T}$$
$$\left. + \left(\frac{A_N + A_T}{A_B + A_N + A_T}\right)^2 \frac{d_T}{2W_T} + \left(\frac{A_B + A_N}{A_B + A_N + A_T}\right)^2\left(\frac{d_N}{2W_N} + \frac{d_T}{W_T}\right)\right] \quad \text{ohms/slot} \qquad (13.86)$$

The above is the approximate parallel leakage reactance of a triple-cage slot under running conditions. An additional permeance-ratio term such as d_0/w_0 should be added in series to the terms above inside the brackets to account for the bridge or slot lip over the top of the top bar, the configuration of which can vary from one cast-rotor design to another. Putting eq. (13.86) in terms of rotor-slot leakage reactance per phase yields

$$X_{s2} = \frac{32\pi^2 f_1 \ell_c N_{st}^2 q K_{p1}^2 K_{d1}^2}{10^7 N_2}\left[\left(\frac{A_B}{A_B + A_N + A_T}\right)^2\left(\frac{d_B}{3W_B} + \frac{d_N}{W_N} + \frac{d_T}{W_T}\right)\right.$$
$$+\left(\frac{A_N}{A_B + A_N + A_T}\right)^2\left(\frac{d_N}{3W_N} + \frac{d_T}{W_T}\right) + \left(\frac{A_T}{A_B + A_N + A_T}\right)^2 \frac{d_T}{3W_T}$$
$$\left. + \left(\frac{A_N + A_T}{A_B + A_N + A_T}\right)^2 \frac{d_T}{2W_T} + \left(\frac{A_B + A_N}{A_B + A_N + A_T}\right)^2\left(\frac{d_N}{2W_N} + \frac{d_T}{W_T}\right)\right] \quad \text{ohms/phase} \qquad (13.87)$$

if slot dimensions are in MKS units. If slot dimensions are in inches, the first factor on the right-hand side of eq. (13.87) should be replaced by the factor $8.02 f_1 \ell_c N_{st}^2 q K_{p1}^2 K_{d1}^2/(10^7 N_2)$.

13.11 END-TURN LEAKAGE REACTANCE

A considerable portion of the stator coil is located outside the stator core, as is apparent from the schematic sketch of a coil shown in Fig. 9.2. For a four-pole machine, the two extended ends of the coil (i.e., the end turns) can consist of 50% of the total coil length, and for a two-pole machine it can exceed that amount. All the flux that links the end turns and thus is not a part of the mutual flux is end-turn leakage flux. The path of the leakage flux around the current-carrying conductors of the end turns is essentially all in air and is impeded by the high reluctance of air. However, there is a considerable length of current-carrying conductors to produce the magnetomotive force that sustains this flux, with the result that end-turn leakage flux is a significant portion of total leakage flux for high-speed machines.

One coil side of a given coil is positioned in the bottom of one slot and the other coil side is positioned in the top of another slot, one coil throw away. The radial transition from the bottom to the top is made at the outer extremity of the end turn, at the coil "knuckle," and the circumferential transition from one slot to another one coil throw away is made by crossing other coil sides (see Fig. 9.1). This results in two layers of parallel coil sides, one layer of which makes an angle α with the vertical plane of the end of the core and the other layer of which makes the supplemental angle $\pi-\alpha$ with the same plane. The angle α is defined in Fig. 13.12. Thus the direction of the magnetomotive force and of the current which produces that magnetomotive force is very complex.

From the infancy of rotating electrical machinery in the late nineteenth century to the early-middle part of this century, the methods used to calculate end-turn leakage reactance were based on empirical formulas. As might be expected, no single empirical formula was satisfactory for a wide range of the pertinent variables, such as number of poles and stator diameter.

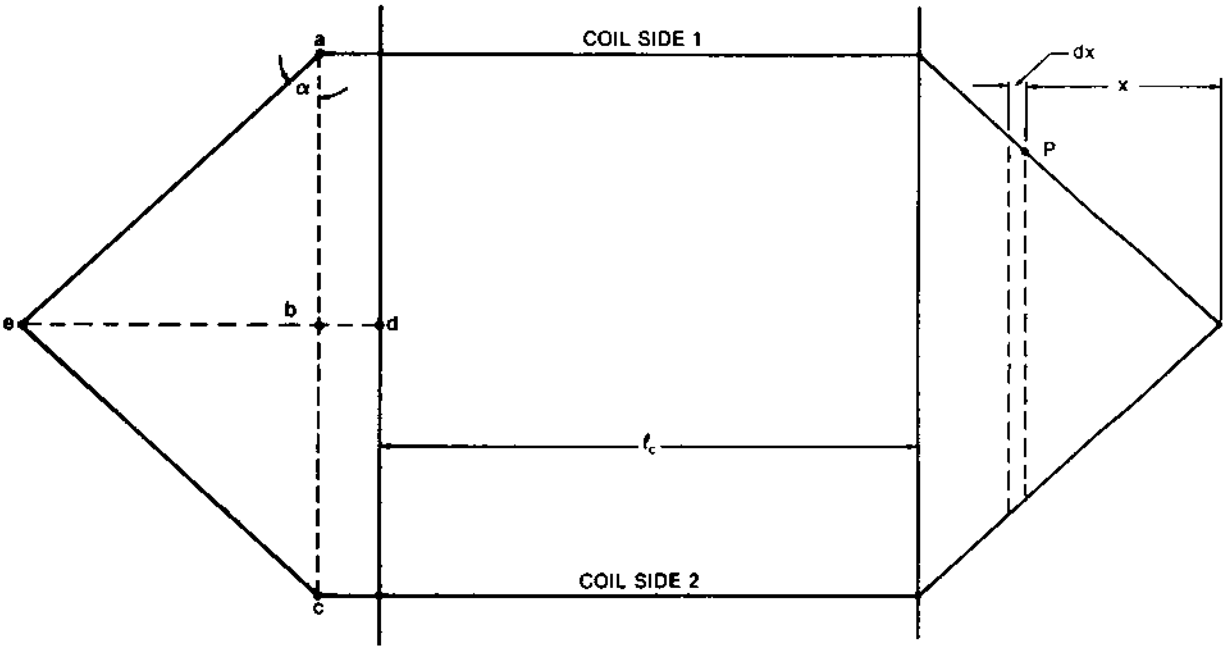

FIGURE 13.12 Geometric notation for a stator coil or for a wound-rotor coil.

However, in 1929, P. L. Alger presented a paper before the American Institute of Electrical Engineers which utilized an analytical approach to this subject. This paper, which has come to be regarded as a classic in the field of reactance, covered the general subject of leakage reactance, among which end-turn leakage reactance was included. Although the derivation of the end-turn leakage formula as presented in that paper is somewhat protracted, and although the resulting formula is then simplified, it is well worth the effort to consider its derivation, because of the insight it can give to end-turn leakage reactance. Accordingly, the following analysis is in general accordance with that presented by Alger in his classical paper.

The complex magnetic field associated with current flow in the end turns can be broken down into two distinct and separate fields. The first magnetic field is somewhat similar to the revolving magnetic field in the air gap between the stator and rotor cores. It is considered to flow in planes that are perpendicular to the axis of the shaft and is sustained by the axial component of end-turn current. Because of the direction of this magnetic field, it is called the "peripheral" leakage field. The second magnetic field is sustained by the circumferentially directed component of end-turn current. This field is considered to flow in radial planes and, accordingly, is called the "axial" leakage field. The concept of superposition will be used to consider the effect of each of the two leakage fields, and then to combine their individual effects to determine the total end-turn leakage reactance.

13.11.1 Peripheral Leakage-Flux Field

The axial component of end-turn current which produces the peripheral end-turn leakage field is obviously a function of end-turn geometry. Consider the left-hand end of the stator coil, shown in Fig. 13.12. The distance ac, in terms of the inside diameter of the stator d, number of poles p, and the per unit coil pitch τ, is

$$ac = \frac{\pi d \tau}{p} \quad \text{meters} \tag{13.88}$$

By definition, point b bisects line ac. Then distance ab is equal to

$$ab = \frac{ac}{2} = \frac{\pi d \tau}{2p} \quad \text{meters} \tag{13.89}$$

and distance be is equal to

$$be = \frac{\pi d \tau}{2p} \tan \alpha \quad \text{meters} \tag{13.90}$$

In his analysis Alger assumes that the distance de is approximately equal to the distance be and subsequently states that another assumption that was introduced tends to compensate for the assumption above. On this basis, the total axial length of the end-turn extension for both ends of the stator is

$$\text{total end-turn extension} = \frac{\tau\pi d}{p}\tan\alpha \quad \text{meters} \qquad (13.91)$$

The axial-length component above, together with the magnetizing reactance, will be used to calculate the peripheral leakage field that is sustained by the axial component of end-turn current.

The expression for magnetizing current for a three-phase stator was derived in eq. (13.25). If the right-hand side of that equation is multiplied by q/3 to make it applicable to a q-phase stator, and if the two factors K_f and K_s, which concern only steel cores, are omitted, the resulting expression is

$$X_m = \left(\frac{100}{10^7}\right)\frac{N_{st}^2 f \ell_c dq K_{p1}^2 K_{d1}^2}{p^2 g} \quad \text{ohms/phase} \qquad (13.92)$$

Rearranging eq. (13.92) to factor out the permeance multiplier for stator reactance gives us

$$X_m = \frac{32\pi^2 f \ell_c N_{st}^2 q}{10^7 N_1}\;\frac{0.317 N_1 d K_{p1}^2 K_{d1}^2}{p^2 g} \quad \text{ohms/phase} \qquad (13.93)$$

Equation (13.93) applies to a uniform air gap of length g. To adapt it to the end turns, which are essentially cylindrical in shape, it is necessary to multiply by an appropriate factor. Such a factor can be physically described as the ratio of the flux produced by a p-pole magnetomotive force with a sinusoidal distribution which is positioned around the periphery of a cylinder of air of diameter d, to the flux produced by the same magnetomotive force acting on a uniform air gap of length g. Alger, citing earlier authors, gave the following expression for the ratio:

$$\frac{\phi(\text{air cylinder})}{\phi(\text{uniform air gap})} = \frac{pg}{2d} \quad \text{numeric} \qquad (13.94)$$

Since the permeance multiplier in eq. (13.93) has ℓ_c in the numerator, the expression for the end-turn extension in eq. (13.91) should be divided by ℓ_c in order to maintain its original form when multiplied by the permeance multiplier. Then

$$\frac{\text{total length of end-turn extension}}{\ell_c} = \frac{\pi d\tau \tan\alpha}{p\ell_c} \quad \text{numeric} \qquad (13.95)$$

The product of eqs. (13.93), (13.94), and (13.95) is equal to the end-turn reactance due to the peripheral flux field. Performing the indicated multiplication and rearranging gives us

$$X_{ep} = \frac{32\pi^2 f\ell_c N_{st}^2 q}{10^7 N_1} \, \frac{\tau d N_1 K_d^2 \tan\alpha}{2p^2 \ell_c} \left[(0.317)\pi K_p^2\right] \quad \text{ohms/phase} \qquad (13.96)$$

The distribution factor K_d in eq. (13.96) has the same significance for the end turns as it does for the magnetic core portion of the stator winding, since the coil groups are of the same width in both cases. However, Alger concluded that compared to the leakage in the core region, associated with harmonics, the difference in the peripheral end-turn leakage field could be offset by setting $K_d = 1$ in eq. (13.96).

The pitch factor K_p along the length of the end turn varies from 0, at the outer extremity, to the same value as for the core portion, at the point where they join. Thus the significance of the pitch factor to the reactance of the end turns should now be evaluated. The factor $(0.317)\pi K_p^2$ is equal to K_p^2, and to evaluate it, the function K_p^2 must be integrated along the length of the end turn. From eq. (9.95) the pitch factor is defined as

$$K_p = \sin\frac{\tau\pi}{2} \quad \text{numeric} \qquad (13.97)$$

If x is the fractional distance of a point P along the end-turn projection, as shown in Fig. 13.12, the pitch factor at point P is then equal to

$$K_p' = \sin\frac{\tau\pi x}{2} \quad \text{numeric} \qquad (13.98)$$

Evaluating K_p^2 by integrating along the end-turn projection gives us

$$F(\tau) = \int_0^1 \sin^2\frac{\tau\pi x}{2}\, dx = \frac{1}{2\tau\pi}\left[\tau\pi x - 2\sin\frac{\tau\pi x}{2}\cos\frac{\tau\pi x}{2}\right]_0^1$$

$$= \frac{1}{2\tau\pi}(\tau\pi - \sin\tau\pi) \quad \text{numeric} \qquad (13.99)$$

and eq. (13.96) can be written as

$$X_{ep} = \frac{32\pi^2 f \ell_c N_{st}^2 q}{10^7 N_1} \, \frac{\tau d N_1 \tan\alpha}{2p^2 \ell_c} \, [F(\tau)] \quad \text{ohms/phase} \qquad (13.100)$$

with dimensions in MKS units.

13.11.2 Axial Leakage-Flux Field

The axial end-turn leakage field is produced by the peripheral component of current flowing in the end turns. The peripheral components of current, in the upper and the lower end-turn layers, are out of phase by $\tau\pi x$ radians. Then, at any point x in Fig. 13.12, the resultant is proportional to

$$(\text{resultant of peripheral current})_x \sim \cos\frac{\tau\pi x}{2} \quad \text{numeric} \qquad (13.101)$$

In his analysis Alger proceeds to take moments of the resultant peripheral current about the outer end of stator core to determine the centroid of this current. From eq. (13.91) the total end-turn extension is equal to $(\tau\pi d \tan\alpha)/p$ for the two ends and is equal to $(\tau\pi d \tan\alpha)/2p$ for one end. After some judgmental approximation in evaluating the result, the effective distance from the end of the core to the centroid of the peripheral current is determined to be

$$\text{distance from core to centroid of peripheral current} = \frac{\tau\pi d \tan\alpha}{4p}\left(1 + \frac{\tau^2}{5}\right) \quad \text{meters} \qquad (13.102)$$

At this point the assumption is made that the axial end-turn leakage reactance is the same as if the peripheral current were concentrated in one conductor of circular cross section located at each end of the machine at the above centroidal distance from the end of the core and running circumferentially around the end-turn region. Also, after some consideration, Alger makes the judgment that the effective cross-sectional diameter of each of these two equivalent conductors is equal to half of the end-turn extension on one end, or

$$\text{diameter of equivalent peripheral current} = \frac{\tau\pi d \tan\alpha}{4p} \quad \text{meters} \qquad (13.103)$$

Figure 13.13 shows the two equivalent peripheral-current conductors that produce the axial end-turn leakage flux.

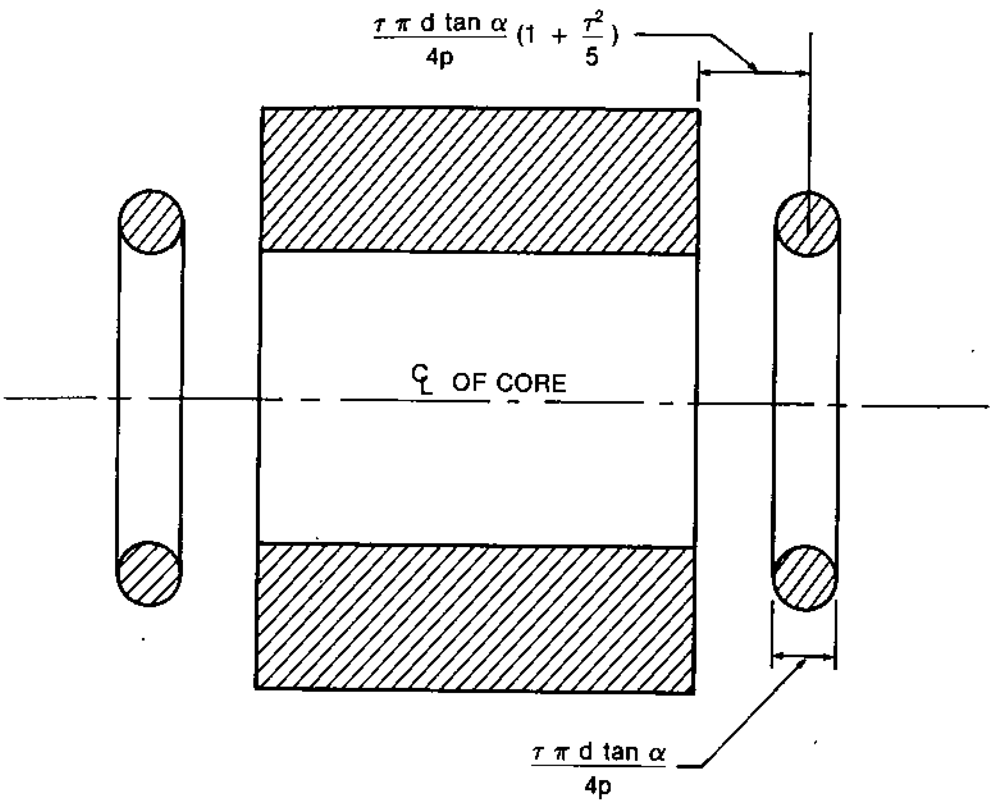
$\frac{\tau \pi d \tan\alpha}{4p}(1+\frac{\tau^2}{5})$
℄ OF CORE
$\frac{\tau \pi d \tan\alpha}{4p}$

FIGURE 13.13 Cross-sectional view of stator, showing idealized conductors which carry the peripheral component of end-turn current that sustains the axial component of end-turn leakage flux.

At a given instant of time, the magnitude of this fictitious current varies sinusoidally as it proceeds around the periphery of the end turns in a plane perpendicular to the axis of the shaft. Thus it is necessary to translate the currents that exist in the stator coils in one pole pitch of the stator core to the peripheral component that is effective in producing the axial component of end-turn leakage flux. If the currents in all of the stator coils within one pole pitch were maximum at the same instant, the maximum value of the peripheral current would be

$$(I_{ep})'' = \sqrt{2}\,\frac{I_1 N_{st} q}{p} \quad \text{amperes} \tag{13.104}$$

However, the actual current distribution in the stator coils follows a sinusoidal distribution for one pole pitch. Also, the coils are connected into phase groups, and very probably, the coil pitch is less than 1.0, requiring the use of K_d and K_p. Thus the maximum value of current in the equivalent conductor must be multiplied by $2/\pi$, K_p, and K_d, giving

$$(I_{ep})' = \sqrt{2}\,\frac{I_1 N_{st} q K_p K_d}{p}\,\frac{2}{\pi} \quad \text{amperes} \tag{13.105}$$

The effective value of this current is $1/\sqrt{2}$ of that given in eq. (13.105), or

$$I_{ep} = \frac{2 I_1 N_{st} q K_p K_d}{\pi p} \quad \text{amperes} \tag{13.106}$$

Alger's analysis considers that the two fictitious conductors shown in Fig. 13.13 constitute a single-phase transmission line. The resulting transmission-line model assumes that the iron core is removed and that the inboard sides of the end turns are positioned back to back, since the core is assumed to carry no end-turn leakage flux. The parameters of this transmission line are

$$\text{length} = \pi d \text{ meters} \quad \text{meters} \tag{13.107}$$

$$\text{conductor diameter} = \frac{\tau \pi d \tan \alpha}{4p} \quad \text{meters} \tag{13.108}$$

$$\text{separation between centers of conductors} = \frac{\tau \pi d \tan \alpha}{2p}\left(1 + \frac{\tau^2}{5}\right) \quad \text{meters} \tag{13.109}$$

The self-inductance of a single-phase transmission line is equal to

$$L = \left(2 \ln \frac{S}{D/2} + \frac{1}{2}\right)\left(\ell \times 10^{-7}\right) \quad \text{henrys} \tag{13.110}$$

per conductor, where

S = separation between conductor centerlines, meters
D = conductor diameter, meters
ℓ = length, meters

Substituting the parameters in eqs. (13.107), (13.108), and (13.109) into eq. (13.110) and simplifying yields

$$L = \left\{2 \ln\left[4\left(1 + \frac{\tau^2}{5}\right)\right] + \frac{1}{2}\right\}\frac{2\pi d}{10^7} \quad \text{henrys} \tag{13.111}$$

To avoid the use of the function $\ln\left[4(1 + \tau^2/5)\right] + 1/2$, Alger replaced it with the simpler function $(8.2 + \tau^2)/5$, which he considered equivalent, to give

$$L = \frac{4\pi d}{10^7}\,\frac{8.2 + \tau^2}{5} \quad \text{henrys} \tag{13.112}$$

Then the leakage reactance due to the axial end-turn flux, sustained by the peripheral component of end-turn current, is equal to

$$X_{ea} = 2\pi f L = \frac{8\pi^2 f d(8.2 + \tau^2)}{5 \times 10^7} \quad \text{ohms} \tag{13.113}$$

Since the equivalent transmission line for which L was calculated in eq. (13.112) consisted of both end turns and the entire periphery of the machine, the total reactive volt-amperes of the machine associated with X_{ea} is equal to

$$VAR'_{ea} = I_{ep}^2 X_{ea} \quad \text{volt-amperes} \tag{13.114}$$

The volt-amperes for one phase are equal to

$$VAR_{ea} = \frac{I_{ep}^2 X_{ea}}{q} \quad \text{volt-amperes/phase} \tag{13.115}$$

Substituting eqs. (13.106) and (13.113) into eq. (13.115) and simplifying the resulting expression gives us

$$VAR_{ea} = \frac{I_1^2 (32)\pi^2 N_{st}^2 K_p^2 K_d^2 q f d(1 + 0.12\tau^2)}{6.02 p^2} \quad \text{volt-amperes/phase} \tag{13.116}$$

Then dividing VAR_{ea} by I_1^2 to determine X_{ea}, omitting K_d^2 for the same reason that it was omitted, following eq. (13.96), and multiplying the numerator and denominator by $\ell_c N_1$, we obtain

$$X_{ea} = \frac{VAR_{ea}}{I_1^2} = \frac{32\pi^2 f \ell_c N_{st}^2 q}{10^7 N_1}\,\frac{K_p^2 d N_1 (1 + 0.12\tau^2)}{6.02 p^2 \ell_c} \quad \text{ohms/phase} \tag{13.117}$$

with dimensions in MKS units.

13.11.3 Total End-Turn Leakage Flux

The sum of the reactance due to the peripheral leakage flux field given in eq. (13.100), and the reactance due to the axial leakage flux field given in eq. (13.117), is equal to the total end-turn leakage reactance per phase. Then

$$X_e = \frac{32\pi^2 f \ell_c N_{st}^2 q}{10^7 N_1}\left[\frac{\tau d N_1 \tan\alpha \, F(\tau)}{2p^2 \ell_c} + \frac{K_p^2 d N_1 (1 + 0.12\tau^2)}{6.02 p^2 \ell_c}\right] \quad \text{ohms/phase} \qquad (13.118)$$

The expression in brackets in eq. (13.118) can be rearranged into

$$\frac{dN_1}{p^2 \ell_c}\left[\frac{\tau \tan\alpha \, F(\tau)}{2} + \frac{K_p^2 (1 + 0.12\tau^2)}{6.02}\right] \quad \text{numeric} \qquad (13.119)$$

Alger's analysis then replaces this expression with

$$\frac{dN_1}{p^2 \ell_c}\left[(0.3)(3\tau - 1)\right] \quad \text{numeric} \qquad (13.120)$$

This great simplification is achieved by setting α equal to its typical value of 60 degrees and then by determining eq. (13.120) as a numerically equivalent, but much simpler, function of coil pitch τ. Thus the total stator end-turn leakage reactance is equal to

$$X_e = \frac{32\pi^2 f \ell_c N_{st}^2 q}{10^7 N_1} \frac{(0.3)(3\tau - 1) d N_1}{p^2 \ell_c} \quad \text{ohms/phase} \qquad (13.121)$$

with dimensions in MKS units, and is equal to

$$X_e = \frac{8.02 f \ell_c N_{st}^2 q}{10^7 N_1} \frac{(0.3)(3\tau - 1) d N_1}{p^2 \ell_c} \quad \text{ohms/phase} \qquad (13.122)$$

with dimensions in inches.

Equations (13.121) and (13.122) give the end-turn leakage reactance of the stator winding. An equivalent equation can be derived for the end-turn leakage of a phase-wound rotor by applying the same approach to the rotor winding. The resulting equation is

$$X_{e2} = \frac{32\pi^2 f_1 \ell_c N_{st}^2 q}{10^7 N_2}\left(\frac{K_{p1}K_{d1}}{K_{p2}K_{d2}}\right)^2 \frac{(0.3)(3\tau_2 - 1)d_r N_2}{p^2 \ell_c} \quad \text{ohms/phase} \tag{13.123}$$

with dimensions in MKS units. If dimensions are in inches, the resulting equation is

$$X_{e2} = \frac{8.02 f_1 \ell_c N_{st}^2 q}{10^7 N_2}\left(\frac{K_{p1}K_{d1}}{K_{p2}K_{d2}}\right)^2 \frac{(0.3)(3\tau_2 - 1)d_r N_2}{p^2 \ell_c} \quad \text{ohms/phase} \tag{13.124}$$

τ_2 is the fractional coil pitch of the rotor winding and d_r is the average diameter of the rotor end turns. Equations (13.123) and (13.124) are referred to the stator side at stator frequency, as was done for the rotor-slot leakage reactance of a phase-wound rotor in eqs. (13.73) and (13.74).

The end-turn leakage reactance of squirrel-cage rotor windings is evaluated in various ways. Most of the polyphase induction motors that are manufactured have cast-aluminum rotor windings. As discussed in Chapter 10, the end rings of such rotor windings are immediately adjacent to the ends of the rotor core. This, of course, results in a negligible axial component of rotor end-turn current, which, in turn, results in a correspondingly small peripheral leakage-flux field. However, a peripheral component of end-turn current does exist, which, in turn, results in an axial leakage-flux field and hence in some additional end-turn leakage permeance. This additional leakage permeance, resulting from the end turns of squirrel-cage rotors, has been handled historically in several different ways: by (1) neglecting it, (2) developing a separate reactance equation to provide for it, and (3) lumping it into the stator end-turn leakage equation by use of an empirical factor or adjustment. In any case, the various motor manufacturers most immediately concerned will have arrived at their respective practices from the accumulated knowledge that comes from reconciling test results with design expectations over a prolonged period. Thus customers can reasonably expect that all components of leakage reactance will have been considered and that motor products will provide the torque and other performance characteristics specified.

13.12 DIFFERENTIAL LEAKAGE REACTANCE

13.12.1 Components of Differential Leakage Reactance

As discussed in Chapter 12, the air gap contains space-harmonic and slot-harmonic magnetomotive forces of various magnitudes, any one of which travels in one of the two directions around the air gap at a speed of (1/n)th of synchronous speed as a wave with n times the number of poles as the fundamental wave. Each such harmonic magnetomotive force produces a corresponding harmonic flux which also rotates around the air gap. Each harmonic flux wave induces a voltage of fundamental frequency in the winding which produces that harmonic. However, the voltage that a given harmonic wave induces in the opposing winding is not at slip frequency, so no useful torque results. The fundamental-frequency voltage that each harmonic wave induces in the winding that produces it contributes to leakage reactance, and the total of such leakage reactances constitute the differential leakage reactance.

For purposes of understanding and of calculating, differential leakage reactance is divided into zigzag leakage reactance and belt leakage reactance. The zigzag leakage reactance is derived as that reactance due to the harmonics that would be produced if the winding had only one slot per pole per phase (i.e., if there was only one slot per phase group) and if that slot carried the same effective uniformly distributed current as the total currents of the group. Accordingly, zigzag reactance is associated with the slot harmonics, with harmonic orders such as $2N_1/p \pm 1$ and $2N_2/p \pm 1$. Thus, this reactance is a function of the number of slots but is not affected by the coil pitch.

The belt leakage reactance is defined as the additional reactance due to currents being required to flow in actual phase groups, which are several slots wide. Incidentally, fractional-slot windings have phase groups that are variable in width, which can cause an additional, although small source of leakage reactance. Belt leakage reactance is associated with the space harmonics, with harmonic orders such as the fifth and seventh. This reactance is affected by the coil pitch, since the currents in the two coil sides in a given slot are affected by the coil pitch. However, belt leakage reactance is not affected by the number of slots.

13.12.2 Zigzag Leakage Reactance

Although there is more than one way to analyze zigzag leakage reactance, the method used here is in general accord with that presented by Alger, in his paper presented to the American Institute of Electrical Engineers in August 1928. As noted earlier, zigzag leakage reactance is associated with slot-harmonic fluxes, which induce fundamental-frequency voltage in the winding. The slot-harmonic fluxes are produced by corresponding slot-harmonic magnetomotive forces, just as the fundamental flux is produced by the fundamental magnetomotive force. The reactance associated with the fundamental flux is the magnetizing reactance X_m.

The point of departure in Alger's analysis is to consider a full-pitch winding with one slot per phase group [i.e., with $N_1/(pq) = 1.0$]. For such a winding, the belt leakage is zero and the differential leakage is equal to the zigzag leakage. Citing the previous work of Chapman, Alger gives the ratio of total winding inductance to the inductance of one coil of this winding as

$$\frac{\text{total winding inductance}}{\text{coil inductance}} = \frac{p}{N_1} \csc^2 \frac{\pi p}{2N_1} \quad \text{numeric} \tag{13.125}$$

Citing the same source, Alger gives the ratio of total useful winding inductance of the winding to the inductance of a coil as

$$\frac{\text{total useful winding inductance}}{\text{coil inductance}} = \frac{4N_1}{\pi^2 p} \quad \text{numeric} \tag{13.126}$$

The reciprocal of eq. (13.126) is

$$\frac{\text{coil inductance}}{\text{total useful winding inductance}} = \frac{\pi^2 p}{4N_1} \quad \text{numeric} \tag{13.127}$$

The product of eqs. (13.125) and (13.127) gives

$$\frac{\text{total winding inductance}}{\text{total useful winding inductance}} = \left(\frac{p}{N_1} \csc^2 \frac{\pi p}{2N_1}\right) \frac{\pi^2 p}{4N_1} \quad \text{numeric} \tag{13.128}$$

The product of eq. (13.128) and the magnetizing reactance is equal to the sum of magnetizing reactance and the differential reactance. However, in the case of this particular winding, by definition, the differential reactance is equal to the zigzag reactance. Then if the magnetizing reactance is subtracted from the product above, the result is equal to the zigzag reactance. Accordingly,

$$Z_{z1} = X_m\left(\frac{p}{N_1} \csc^2 \frac{\pi p}{2N_1}\right) \frac{\pi^2 p}{4N_1} - X_m = X_m\left(\frac{\pi^2 p^2}{4N_I^2} \csc^2 \frac{\pi p}{2N_1} - 1\right) \quad \text{ohms/phase} \tag{13.129}$$

The transcendental expression in eq. (13.129) can be evaluated by use of a power series. The series expansion of csc x is

$$\csc x = \frac{1}{x} + \frac{x}{6} + \frac{7x^3}{360} + \cdots \quad \text{numeric} \tag{13.130}$$

The series above converges sufficiently fast that use of the first two terms will give good accuracy, and this is particularly true when the angle x is not large, as is the case for $x = \pi p/2N_1$. Then, setting $\csc^2 x$ equal to the first two terms of the series in eq. (13.130), and expanding, we obtain

$$\csc^2 x = \left(\frac{1}{x} + \frac{x}{6}\right)^2 = \frac{1}{x^2} + \frac{x^2}{36} + \frac{1}{3} \quad \text{numeric} \tag{13.131}$$

Replacing x with $\pi p/(2N_1)$ in eq. (13.131), substituting eq. (13.131) into eq. (13.129), and simplifying yields

$$X_{z1} = X_m\left(\frac{\pi^2 p^2}{12N_1^2} + \frac{\pi^4 p^4}{576N_1^4}\right) \quad \text{ohms/phase} \tag{13.132}$$

An examination of eq. (13.132) shows that the coefficient of the fourth power term is 1/5 of that of the second power term, and that the fourth power term represents a small value raised to the fourth power. Thus that term can be neglected with no significant change in results. Accordingly,

$$X_{z1} = X_m \frac{\pi^2}{12}\frac{p^2}{N_1^2} \quad \text{ohms/phase} \tag{13.133}$$

An analogous analysis can be carried through for the rotor, to give

$$X_{z2} = X_m \frac{\pi^2}{12}\frac{p^2}{N_2^2} \quad \text{ohms/phase} \tag{13.134}$$

where N_2 is the number of rotor slots. The total zigzag leakage reactance of the complete machine is then equal to the sum of eqs. (13.133) and (13.134), or

$$X_z = X_m \frac{\pi^2}{12}\left[\left(\frac{p}{N_1}\right)^2 + \left(\frac{p}{N_2}\right)^2\right] \quad \text{ohms/phase} \tag{13.135}$$

which is essentially equal to

$$X_z = \frac{X_m}{1.2}\left[\left(\frac{p}{N_1}\right)^2 + \left(\frac{p}{N_2}\right)^2\right] \quad \text{ohms/phase} \tag{13.136}$$

Equations (13.133) and (13.134) give the actual distribution of zigzag leakage reactance between the stator and rotor windings. In practice, however, the total zigzag reactance is usually calculated using eq. (13.136), and half is allocated to the stator winding and half is allocated to the rotor winding. Equation (13.136) can be put into the usual reactance format by multiplying by the expression for X_m. If the right-hand side of eq. (13.25) is multiplied by q/3 to make it applicable to a q-phase stator, the resulting equation rearranged to factor out the usual permeance multiplier, and the resulting equation then substituted into eq. (13.136), the result is

$$X_z = \frac{32\pi^2 f \ell_c N_{st}^2 q}{10^7 N_1} \; \frac{0.317 N_1 d K_{p1}^2 K_{d1}^2}{p^2 g K_f K_s} \; \frac{1}{1.2}\left[\left(\frac{p}{N_1}\right)^2 + \left(\frac{p}{N_2}\right)^2\right] \quad \text{ohms/phase} \tag{13.137}$$

if dimensional units are in MKS units and

$$X_z = \frac{8.02 f \ell_c N_{st}^2 q}{10^7 N_1} \; \frac{0.317 N_1 d K_{p1}^2 K_{d1}^2}{p^2 g K_f K_s} \; \frac{1}{1.2}\left[\left(\frac{p}{N_1}\right)^2 + \left(\frac{p}{N_2}\right)^2\right] \quad \text{ohms/phase} \tag{13.138}$$

if dimensional units are in inches.

Some comments are in order concerning eqs. (13.137) and (13.138). For semiclosed slots, such as those used for random-wound stators and for squirrel-cage rotors, eqs. (13.137) and (13.138) give values which are near that of the actual zigzag leakage reactance. However, the use of open slots tends to increase the air-gap reluctance and hence the effective air-gap length, as will be discussed in Chapter 14. This, in turn, reduces the ratio of total flux to mutual flux produced by an individual coil, which causes the actual zigzag leakage reactance to be somewhat less than $X_m(1/1.2)[(p/N_1)^2 + (p/N_2)^2]$. Then for stators with open slots and for phase-wound rotors, the actual zigzag leakage reactance is somewhat less than indicated by eqs. (13.137) and (13.138). The magnitude of this decrease is mitigated to some extent by the fringing factor K_f, which is greater than unity, which occurs in the denominator of the expression for X_m in eqs. (13.137) and (13.138).

Anyone who is seriously interested in making an adjustment, empirical or otherwise, to eq. (13.137) or (13.138), with the goal of more fully utilizing the decrease in leakage reactance resulting from the use of open slots should observe one precaution. It is important not to assume that a machine has less leakage reactance than, say, that calculated by using eqs. (13.137) and (13.138) unless that assumption has been verified by testing. This is because of the inverse relationship of starting torque and maximum torque with leakage reactance. It can be reasonably assumed that the various electrical manufacturers will have verified their respective calculating procedures for leakage reactance, whatever these procedures might be, by suitable test programs. Thus this precaution concerns primarily field modifications or repair-shop modifications, not new machines.

13.12.3 Belt Leakage Reactance

As mentioned earlier, belt leakage reactance is associated with space harmonics in the magnetomotive-force wave which result from current flow being confined to several coils connected in series to form groups, each group of which is several coils wide. It was shown in Chapter 12 that the confinement of current to coil groups results in traveling space harmonics, with harmonic orders of 5, 7, 11, and so on. This train of harmonic magnetomotive-force waves acting on the average air-gap permeance produces a corresponding train of harmonic flux waves which rotate around the air gap at their respective harmonic speeds. These harmonic fluxes induce voltages in both the stator winding and the rotor winding. The voltages induced in the stator winding are of fundamental frequency and thus tend to contribute to leakage reactance. However, the frequency of these induced voltages within the rotor winding are such that if the rotor winding is short circuited, as occurs in a squirrel-cage winding, damping currents will flow. Such damping currents flowing in the rotor tend to react against, and to reduce, the corresponding harmonic currents in the stator. Thus the belt leakage reactance of a motor with a squirrel-cage rotor winding is very low. In fact, it is generally considered to be negligible and is not included as a component of total leakage reactance for such motors. On the other hand, because of the significant difference in harmonic order of the slot harmonics compared to the space harmonics, zigzag leakage reactance is generally present in squirrel-cage motors, as determined in Section 13.12.2.

The bars or coil sides of the windings of phase-wound rotors are not short circuited and, accordingly, wound-rotor motors do produce some amount of belt leakage reactance. Thus it is in order to derive the equation for this component of reactance for machines with phase-wound rotors. For a winding with a large number of coils, and hence with a large number of slots in the corresponding magnetic core, the belt leakage reactance is essentially equal to the magnetizing reactance of the space harmonics of both the stator and rotor windings. Accordingly, it is necessary to consider the magnetizing reactance of the space harmonics.

From Faraday's law as expressed in eq. (9.137), the relationship between the fundamental component of stator flux per pole ϕ_1 and the resulting fundamental component of induced voltage E_1 is

$$E_1 = 4.443 N_{st} K_{p1} K_{d1} \phi_1 f \quad \text{volts/phase} \tag{13.139}$$

and the corresponding relationship between the nth harmonic component of stator flux per pole ϕ_n and the resulting nth harmonic component of induced voltage E_n is

$$E_n = 4.443 N_{st} K_{pn} K_{dn} \phi_n f \quad \text{volts/phase} \tag{13.140}$$

Dividing eq. (13.140) by eq. (13.139) yields

$$\frac{E_n}{E_1} = \frac{\phi_n K_{pn} K_{dn}}{\phi_1 K_{p1} K_{d1}} \quad \text{numeric} \tag{13.141}$$

Also, from eq. (12.39), the relationship between the maximum value of the nth harmonic component of magnetomotive force H_n and the maximum value of the fundamental component of magnetomotive force H_1 is

$$\frac{H_n}{H_1} = \frac{1}{n} \frac{K_{pn} K_{dn}}{K_{p1} K_{d1}} \quad \text{numeric} \tag{13.142}$$

Since $B = \mu H$, eq. (13.142) can be written in terms of maximum value of air-gap flux density, as

$$\frac{B_{mn}}{B_{m1}} = \frac{1}{n} \frac{K_{pn} K_{dn}}{K_{p1} K_{d1}} \quad \text{numeric} \tag{13.143}$$

The ratio of the area per pole of the nth harmonic to the area per pole of the fundamental wave is 1/n. Then, since flux ϕ is equal to flux density B multiplied by the area per pole, the ratio of flux per pole for the nth harmonic ϕ_n to the flux per pole of the fundamental ϕ_1 is equal to 1/n times eq. (13.143), or

$$\frac{\phi_n}{\phi_1} = \left(\frac{1}{n}\right)^2 \frac{K_{pn} K_{dn}}{K_{p1} K_{d1}} \quad \text{numeric} \tag{13.144}$$

Substituting eq. (13.144) into eq. (13.141)

$$\frac{E_n}{E_1} = \left(\frac{1}{n}\right)^2 \left(\frac{K_{pn} K_{dn}}{K_{p1} K_{d1}}\right)^2 \quad \text{numeric} \tag{13.145}$$

In eq. (9.130) the distribution factor K_{dn} for any harmonic n was shown to be

$$K_{dn} = \frac{\sin(nN_g\alpha/2)}{N_g \sin(n\alpha/2)} \quad \text{humeric} \qquad (13.146)$$

where N_g is the number of slots per group and α is the electrical angle between slots. The distribution factor is the ratio of the chordal distance AB to the arc AB in Fig. 9.16. If the angle α is small (i.e., if the number of slots is large), eq. (13.146) approaches the quantity

$$K_{dn} = \frac{\sin(nN_g\alpha/2)}{nN_g\alpha/2} \quad \text{numeric} \qquad (13.147)$$

The product $N_g\alpha$ is equal to the electrical angle encompassed by one group of coils, which for the usual three-phase machine with a regular winding, is equal to $\pi/3$ electrical radians. Thus eq. (13.147) can be written as

$$K_{dn} = \frac{\sin(n\pi/6)}{n(\pi/6)} \quad \text{numeric} \qquad (13.148)$$

If the quantity $\sin(n\pi/6)$ is calculated for the fundamental and for the various space harmonics, the numerical value is equal to 0.50. Then, substituting eq. (13.148) into eq. (13.145) for K_{d1} and K_{dn},

$$\frac{E_n}{E_1} = \left(\frac{1}{n}\right)^4 \left(\frac{K_{pn}}{K_{p1}}\right)^2 \quad \text{numeric} \qquad (13.149)$$

Since the voltage induced in the winding is proportional to the magnetizing reactance, eq. (13.149) can be written as

$$\frac{X_{mn}}{X_{m1}} = \left(\frac{1}{n}\right)^4 \left(\frac{K_{pn}}{K_{p1}}\right)^2 \quad \text{numeric} \qquad (13.150)$$

Equation (13.150) gives the ratio of the magnetizing reactance for the nth space harmonic to that for the fundamental. Solving for X_{mn} and using the usual symbol X_m for X_{m1} yields

$$X_{mn} = X_m \left(\frac{1}{n}\right)^4 \left(\frac{K_{pn}}{K_{p1}}\right)^2 \quad \text{ohms/phase} \qquad (13.151)$$

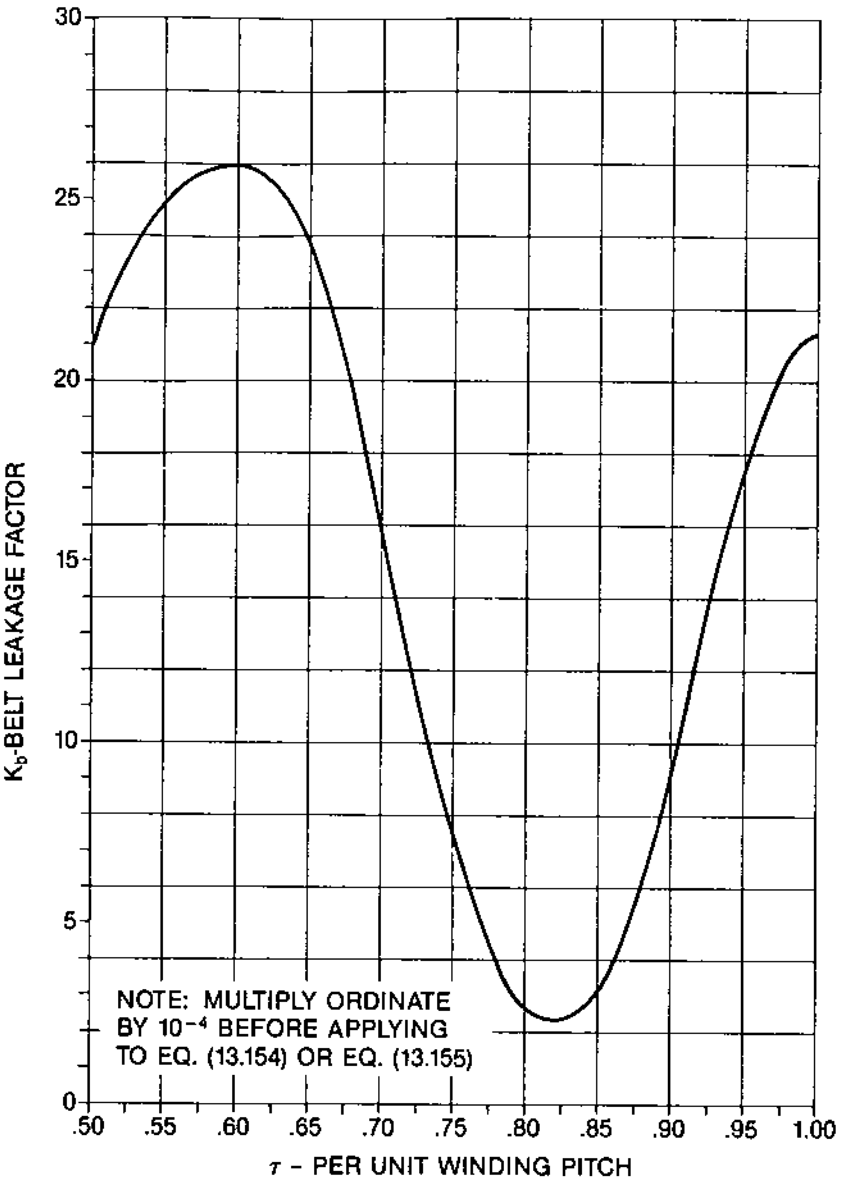

FIGURE 13.14 Belt leakage factor K_b versus per unit winding pitch τ for use with a winding having 60-degree phase belts.

which is the belt leakage reactance for the nth space harmonic produced by the stator winding. The total belt leakage of the stator winding is equal to the sum of eq. (13.151), for all space harmonics. Thus for a three-phase winding with a full-pitch coil, the stator belt leakage reactance is equal to

$$X_{b1} = X_m\left[\left(\frac{1}{5}\right)^4 + \left(\frac{1}{7}\right)^4 + \left(\frac{1}{11}\right)^4 + \cdots\right] \quad \text{ohms/phase} \qquad (13.152)$$

For a winding with a coil pitch other than 100%, the expression $(1/n)^4 \times (K_{pn}/K_{p1})^2$ from eq. (13.151) must be summed to cover all the space harmonics. Although this would appear to be a formidable numerical procedure, the work has been completed and the results published in various technical papers during the past 60 years or so. Thus for the usual case of a chorded winding, the summation above is determined as a function of the winding pitch from curves that are well established and accepted within the electrical industry. Such a curve is given in Fig. 13.14. The total belt leakage of a wound-rotor motor is equal to the sum of the belt leakage of the stator winding and of the rotor winding, or

$$X_b = X_m(K_{b1} + K_{b2}) \quad \text{ohms/phase} \qquad (13.153)$$

where K_{b1} and K_{b2} are the belt leakage factors determined from the curve in Fig. 13.14. Equation (13.153) was developed on the basis of a winding with a large number of slots. However, even though the belt leakage reactance is slightly greater than calculated by eq. (13.153), for a winding with a practical number of slots, the difference is of no significance.

Equation (13.153) can be put into the familiar format for leakage reactance by substituting the general expression for X_m into eq. (13.153) and then by factoring out the permeance multiplier. Accordingly,

$$X_b = \frac{32\pi^2 f \ell_c N_{st}^2 q}{10^7 N_1} \, \frac{0.317 N_1 d K_{p1}^2 K_{d1}^2}{p^2 g K_f K_s} (K_{b1} + K_{b2}) \quad \text{ohms/phase} \qquad (13.154)$$

if dimensions are in MKS units, and

$$X_b = \frac{8.02 f \ell_c N_{st}^2 q}{10^7 N_1} \, \frac{0.317 N_1 d K_{p1}^2 K_{d1}^2}{p^2 g K_f K_s} (K_{b1} + K_{b2}) \quad \text{ohms/phase} \qquad (13.155)$$

if dimensions are in inches.

13.13 SKEW LEAKAGE REACTANCE

As discussed in Section 10.3.12, rotor bars are frequently skewed to reduce some of the undesirable effects of slot harmonics. However, rotor-bar skewing causes a decrease in the voltage induced in the rotor winding, which can be understood by considering the voltage along a given rotor bar. As the rotating air-gap flux wave passes the rotor bar, the peak of the fundamental component of the flux wave will see portions of that bar at successively later times. This causes the fundamental component of the rotating flux wave to appear smaller, that is, for the ratio of mutual flux to total flux to be reduced, as seen by the rotor, with a reduction in the induced rotor voltage. As shown in eq. (10.150), the rotor voltage is reduced by a factor equal to the skew factor K_s. On the other hand, the voltage induced in the stator winding by the mutual flux is unaffected by rotor skew. Such a reduction in induced rotor voltage with no change in induced stator voltage is equivalent to a decrease in the ratio of effective rotor-winding turns to stator-winding turns by a factor equal to K_s.

The reduction in induced rotor voltage is real and it represents an actual physical condition that exists within the machine. However, from the standpoint of performance, a similar effect can be achieved by postulating the existence of an apparent leakage reactance in the rotor circuit, called the skew leakage reactance. This allows the normal magnetizing current I_m to flow in the stator winding and to excite the normal magnetizing reactance X_m, producing the normal induced voltage E_1 in the stator winding. The additional skew leakage reactance X_{sk}, added to the already existing rotor leakage reactance, also accounts for less apparent mutual reactance, relative to total self-reactance, as seen by the rotor current.

To arrive at the expression for the additional leakage reactance X_{sk}, it should be remembered that X_{sk} must just offset the reduction in effective rotor turns, which has been decreased by the factor K_s, due to skew. As shown in eq. (4.43), rotor leakage reactance must be multiplied by the second power of the turns ratio to refer it to equivalent-circuit conditions in the stator. Thus while the effective turns of the rotor have been reduced by the factor K_s, the compensating increase in rotor leakage reactance must be equal to $X_m - K_s^2 X_m$. Then skew reactance is equal to

$$X_{sk} = X_m(1 - K_s^2) \quad \text{ohms/phase} \tag{13.156}$$

In eq. (10.150), K_s was shown to be equal to $\sin(\alpha/2)/(\alpha/2)$, where α is the angle of skew in electrical radians or in electrical degrees as defined in Fig. 10.16. Then

$$X_{sk} = X_m\left\{1 - \left[\frac{\sin(\alpha/2)}{\alpha/2}\right]^2\right\} = X_m\left[1 - \frac{4\sin^2(\alpha/2)}{\alpha^2}\right] \quad \text{ohms/phase} \tag{13.157}$$

Again, eq. (13.157) can be put into the familiar leakage-reactance format by substituting the expression for X_m into eq. (13.157) and then factoring out the permeance multiplier, to give

$$X_{sk} = \frac{32\pi^2 f \ell_c N_{st}^2 q}{10^7 N_1} \frac{0.317 N_1 d K_{p1}^2 K_{d1}^2}{p^2 g K_f K_s}\left[1 - \frac{4\sin^2(\alpha/2)}{\alpha^2}\right] \quad \text{ohms/phase} \tag{13.158}$$

if dimensions are in MKS units, and

$$X_{sk} = \frac{8.02 f \ell N_c^2 q_{st}}{10^7 N_1} \frac{0.317 N_1 d K_{p1}^2 K_{d1}^2}{p^2 g K_f K_s} \left[1 - \frac{4 \sin^2(\alpha/2)}{\alpha^2} \right] \quad \text{ohms/phase} \qquad (13.159)$$

if dimensions are in inches.

13.14 NUMERICAL EXAMPLE OF RUNNING-REACTANCE CALCULATION

The various reactances that have been considered and the corresponding equations that have been derived so far in this chapter concern "running" reactance. Running reactance is based on the physical conditions that exist within the machine when it is operating at or near full speed. The frequency of the rotor circuit is in the vicinity of 1 to 2 Hz and the magnitudes of the stator and rotor currents are in the vicinity of rated values. Thus the full depth d_b of the rotor bar is effective in carrying current (i.e., there is no deep-bar effect in the rotor cage). Also, there is no saturation of the ferromagnetic paths of leakage flux, since only rated current flows in the stator and rotor windings. Use of the previously derived reactance equations in calculating running reactance will now be shown by a numerical example of running reactance. For this example it will be assumed that dimensions are in inches.

Consider a three-phase 60-Hz 2300-V eight-pole, 1000-hp induction motor with parameters as described below.

1. Stator and rotor slots
   a. $N_1 = 72$.
   b. $N_2 = 86$.
   c. Dimensions, as given in Fig. 13.15.
2. Stator winding
   a. Parallel circuits/phase C = 2.
   b. The phase windings are connected in wye to form the three-phase winding.
   c. 1-9 coil throw, which corresponds to $\tau = 8/9 = 0.889$ per unit.
   d. Turns/coil $N_c = 6$.
   e. Each turn consists of two rectangular copper strands, each 0.120 in. deep and 0.210 in. wide, covered with a 0.005-in. film, for use as turn insulation. The two strands that form each turn are located side by side.
   f. Ground insulation consists of 0.065-in.-thick mica-based insulation around the four sides of the coil.

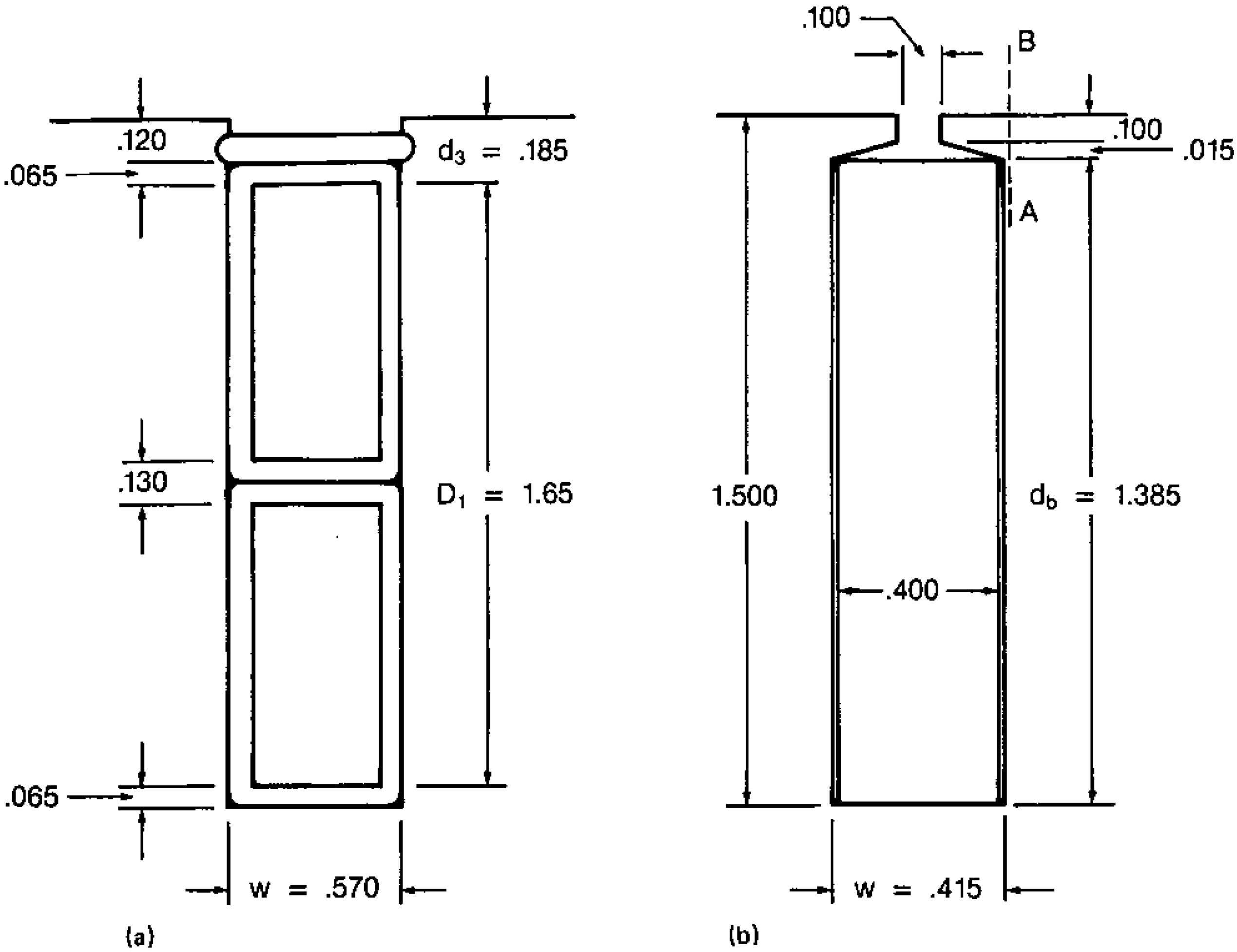

FIGURE 13.15 Dimensional information for the rotor and stator slots used in the numerical example: (a) stator slot; (b) rotor slot.

3. Rotor winding
   a. Each bar is 0.400 in. wide and 1.385 in. deep and is made of copper.
   b. The rotor-winding circuit is completed at each end of the rotor core by copper end rings.
4. Stator core
   a. Overall core length ℓ_c = 27 in.
   b. Stator punching outside diameter = 34 in.
   c. Stator punching inside diameter d = 26.4 in.
   d. There are 13 radial air ducts in the stator core, each 0.25 in. wide.
5. Rotor core
   a. Overall core length ℓ_c = 27 in.
   b. Rotor punching outside diameter = 26.3 in.
   c. Rotor punching inside diameter = 19.5 in.
   d. There are 13 radial air ducts in the rotor core, each 0.25 in. wide.
6. Air gap
   a. Radial length = 0.050 in.

Since dimensions are given in units of inches for this numerical example, the reactance equations appropriate for accepting such units will be used. However, the procedure would be similar and the results would be identical if the dimensions were in metric units and if the equations appropriate for accepting metric units were used.

The number of series turns/phase of the stator winding N_{st} will be required for calculating reactance. From eq. (9.136),

$$N_{st} = \frac{N_1 N_c}{qC} \quad \text{numeric} \tag{13.160}$$

Inserting the appropriate values from the list of machine parameters above into eq. (13.160) yields

$$N_{st} = \frac{(72)(6)}{(3)(2)} = 72 \quad \text{numeric} \tag{13.161}$$

13.14.1 Calculation of the Magnetizing Reactance

If the equation for magnetizing current as derived in eq. (13.25) is multiplied by q/3 to make it applicable to a q-phase stator, and if the terms that comprise the permeance multiplier for stator reactance are collected into a separate factor, the result is

$$X_m = \frac{32\pi^2 f \ell_c N_{st}^2 q}{N_1 \times 10^7} \; \frac{0.317 N_1 d K_{p1}^2 K_{d1}^2}{p^2 g K_f K_s} \quad \text{ohms/phase} \tag{13.162}$$

which is the general equation for magnetizing reactance using MKS units. If eq. (13.162) is divided by 39.37, the number of inches in 1 meter, the result is

$$X_m = \frac{8.02 f \ell_c N_{st}^2 q}{N_1 \times 10^7} \; \frac{0.317 N_1 d K_{p1}^2 K_{d1}^2}{p^2 g K_f K_s} \quad \text{ohms/phase} \tag{13.163}$$

which is the applicable form of the equation when dimensional units are in inches.

As mentioned earlier, the fringing factor K_f and the saturation factor K_s are considered in Chapter 14. At this point it is only necessary to know that K_f allows for the apparent electromagnetic increase in air-gap length due to fringing of the mutual flux lines crossing the air gap caused by slot and air-duct openings, and that K_s is the ratio of total magnetizing ampere-turns to air-gap ampere-turns. For this example it will be assumed that $K_f = 1.96$ and that $K_s = 1.15$. The pitch factor K_{p1} and the distribution factor K_{d1} of the stator winding are easily determined using procedures considered previously. Then substituting the appropriate values for this example into eq. (13.163) gives us

$$X_m = \left[\frac{(8.02)(60)(27)(72)^2(3)}{(72)10^7}\right]\left[\frac{(0.317)(72)(26.4)(0.985)^2(0.955)^2}{(8)^2(0.050)(1.96)(1.15)}\right] = 20.7 \quad \text{ohms/phase} \qquad (13.164)$$

This value of X_m can be expressed in per unit, based on the machine's own output kVA base. From Table 4.3, normal ohms Z_n is equal to $(V_{L-L})^2/(746\text{ hp})$ for such a kVA base. Then

$$Z_n = \frac{(V_{L-L})^2}{746\text{ hp}} = \frac{(2300)^2}{(746)(1000)} = 7.09 \quad \text{ohms/phase} \qquad (13.165)$$

and for this example,

$$X_m = \frac{20.7}{7.09} = 2.92 \quad \text{per unit} \qquad (13.166)$$

13.14.2 Calculation of the Stator-Slot Leakage Reactance

From eq. (13.67) the expression for stator-slot leakage reactance for a rectangular slot with dimensional units in inches is equal to

$$X_{s1} = \frac{8.02 f \ell_c N_{st}^2 q}{N_1 \times 10^7}\left[K_M\left(\frac{d_3}{w} + \frac{D_1}{3w}\right)\right] \quad \text{ohms/phase} \qquad (13.167)$$

The slot dimensions d_3, D_1, and w are shown in Fig. 13.15a. Also, from Fig. 13.8, $K_M = 0.920$ for a winding with a coil pitch τ of 88.9%. Substituting the appropriate values into eq. (13.167) yields

$$X_{s1} = \left[\frac{(8.02)(60)(27)(72)^2(3)}{(72)10^7}\right]\left[(0.920)\left(\frac{0.185}{0.570} + \frac{1.65}{(3)(0.570)}\right)\right] = 0.333 \quad \text{ohms/phase} \qquad (13.168)$$

In per unit, on the machine's own output kVA base, we have

$$X_{s1} = \frac{0.333}{7.09} = 0.0470 \quad \text{per unit} \tag{13.169}$$

13.14.3 Calculation of the End-Turn Leakage Reactance

From eq. (13.122) the expression for end-turn leakage reactance with dimensional units in inches is equal to

$$X_e = \frac{(8.02)f\ell_c N_{st}^2 q}{N_1 \times 10^7} \, \frac{(0.3)dN_1(3\tau - 1)}{p^2\ell_c} \quad \text{ohms/phase} \tag{13.170}$$

The per unit stator coil pitch τ is equal to 0.889. Substituting this and the other appropriate values into eq. (13.170) gives us

$$X_e = \frac{(8.02)(60)(27)(72)^2(3)}{(72)10^7} \, \frac{(0.3)(26.4)(72)[(3)(0.889) - 1]}{(8)^2(27)} = 0.154$$

$$\text{ohms/phase} \tag{13.171}$$

For this example it will be assumed that the end-turn leakage reactance of the rotor winding is small and can be considered to be lumped into (13.171). Then the per unit end-turn leakage reactance on the machine's own output kVA base is

$$X_e = \frac{0.154}{7.09} = 0.0217 \quad \text{per unit} \tag{13.172}$$

13.14.4 Calculation of the Zigzag Leakage Reactance

Zigzag leakage reactance can be calculated from eq. (13.136) if X_m is known, or from eq. (13.137) or (13.138) if X_m is not yet known. Since X_m has previously been calculated, eq. (13.136) is the proper choice. Then

$$X_z = \frac{X_m}{1.2}\left[\left(\frac{p}{N_1}\right)^2 + \left(\frac{p}{N_2}\right)^2\right] \quad \text{ohms/phase} \tag{13.173}$$

Substituting the appropriate values into eq. (13.173) yields

$$X_z \doteq \frac{20.7}{1.2}\left[\left(\frac{8}{72}\right)^2 + \left(\frac{8}{86}\right)^2\right] = 0.362 \quad \text{ohms/phase} \tag{13.174}$$

From an inspection of the expression in brackets in eq. (13.173), as well as from the mode of derivation of that equation, it is apparent that zigzag leakage reactance can be broken down to that due to stator slots and to that due to rotor slots. Then for the stator,

$$X_{z1} = \frac{X_m}{1.2}\left(\frac{p}{N_1}\right)^2 = \frac{20.7}{1.2}\left(\frac{8}{72}\right)^2 = 0.213 \quad \text{ohms/phase} \tag{13.175}$$

and similarly, for the rotor,

$$X_{z2} = \frac{X_m}{1.2}\left(\frac{p}{N_2}\right)^2 = \frac{20.7}{1.2}\left(\frac{8}{86}\right)^2 = 0.149 \quad \text{ohms/phase} \tag{13.176}$$

The values of ohms/phase in eqs. (13.174), (13.175), and (13.176) can be converted to per unit on the machine's own output kVA base by dividing by normal ohms. Then

$$X_z = \frac{0.362}{7.09} = 0.051 \quad \text{per unit} \tag{13.177}$$

and

$$X_{z1} = \frac{0.213}{7.09} = 0.030 \quad \text{per unit} \tag{13.178}$$

and

$$X_{z2} = \frac{0.149}{7.09} = 0.021 \quad \text{per unit} \tag{13.179}$$

13.14.5 Calculation of the Belt Leakage Reactance

As discussed in Section 13.12.3, a squirrel-cage rotor will permit currents to flow in the rotor winding which tend to nullify belt leakage reactance. Accordingly, X_b is insignificant in such machines and is assumed to be zero. Thus for this numerical example

$$X_b = 0 \quad \text{ohms/phase} \tag{13.180}$$

This is not the case, of course, for a machine with a phase-wound rotor.

13.14.6 Calculation of the Skew Leakage Reactance

Since the rotor bars were not skewed for this numerical example, skew leakage reactance does not exist. Then

$$X_{sk} = 0 \quad \text{ohms/phase} \tag{13.181}$$

13.14.7 Calculation of the Rotor-Slot Leakage Reactance

From eq. (13.77), the expression for rotor-slot leakage reactance for a rectangular rotor slot with dimensions in inches is equal to

$$X_{s2} = \frac{8.02 f_1 \ell_c N_{st}^2 q K_{p1}^2 K_{d1}^2}{N_2 \times 10^7} \left(\frac{d_0}{w_0} + \frac{2d_4}{w_0 + w} + \frac{d_b}{3w} \right) \quad \text{ohms/phase} \tag{13.182}$$

Substituting the appropriate winding and core parameters into the permeance-multiplier term and the rotor-slot dimensions from Fig. 13.15 into the permeance term, we obtain

$$X_{s2} = \left[\frac{(8.02)(60)(27)(72)^2(3)(0.985)^2(0.955)^2}{(86)10^7} \right] \left[\frac{0.100}{0.100} + \frac{(2)(0.015)}{0.100 + 0.415} + \frac{1.385}{(3)(0.415)} \right]$$
$$= 0.451 \qquad \text{ohms/phase} \tag{13.183}$$

Again this value can be converted to per unit on the machine's own output kVA base by dividing by normal ohms. Then

$$X_{s2} = \frac{0.451}{7.09} = 0.064 \quad \text{per unit} \tag{13.184}$$

13.14.8 Total Running Reactance of the Numerical Example

The total leakage reactance of the stator X_1 under running conditions is equal to

$$X_1 = X_{s1} + X_e + X_{z1} + X_{b1} \quad \text{ohms/phase} \tag{13.185}$$

Inserting the previously calculated values for this numerical example into eq. (13.185) gives us

$$X_1 = 0.333 + 0.154 + 0.213 + 0 = 0.700 \quad \text{ohms/phase} \tag{13.186}$$

The total leakage reactance of the rotor X_2 under running conditions is equal to

$$X_2 = X_{s2} + X_{z2} + X_{b2} + X_{sk} \quad \text{ohms/phase} \tag{13.187}$$

Again, inserting the values calculated previously for this numerical example into eq. (13.187), we obtain

$$X_2 = 0.451 + 0.149 + 0 + 0 = 0.600 \quad \text{ohms/phase} \tag{13.188}$$

In per unit on the machine's own output kVA base, X_1 and X_2 are, respectively, equal to

$$X_1 = \frac{0.700}{7.09} = 0.0987 \quad \text{per unit} \tag{13.189}$$

and to

$$X_2 = \frac{0.600}{7.09} = 0.0846 \quad \text{per unit} \tag{13.190}$$

The foregoing values of stator leakage reactance X_1, rotor leakage reactance X_2, and magnetizing reactance X_m are the reactance parameters used in the equivalent circuit, the vector diagram, and the circle diagram to predict performance under running conditions. However, to construct the circle diagram, the blocked-rotor leakage reactance is also required. Similarly, to calculate starting torque and blocked-rotor current from the equations derived from the equivalent circuit, the blocked-rotor leakage reactance is required.

13.15 BLOCKED-ROTOR REACTANCE

Under blocked-rotor conditions, slip is equal to 1.0 and the frequency of the rotor circuit is equal to that of the stator circuit. With slip s equal to unity, the rotor-circuit resistance function R_2/s is equal to R_2. At running conditions, on the other hand, the value of R_2/s is typically 50 to 100 times R_2.

Thus at blocked-rotor conditions, the resistive component of impedance is greatly reduced and the impedance of the stator and rotor circuits consists primarily of reactance. This results in stator currents which are from five to seven times their corresponding values at rated speed. This will subsequently become apparent when blocked-rotor current and blocked-rotor reactance are calculated for the numerical example. Also, under blocked-rotor conditions, rotor current increases by approximately the same ratio, and again, this will become apparent in the subsequent numerical example.

To summarize: Under blocked-rotor conditions, the rotor-circuit frequency is equal to the stator-circuit frequency, and currents on the order of five to seven times full-load value flow in the stator and rotor windings. Both of these conditions cause the blocked-rotor reactance to be less than the running reactance. The first condition can be handled in an analytical manner, as shown in Chapter 10. However, the second condition must be handled by utilizing an iterative process.

13.15.1 Line Frequency in the Rotor Circuit

Line frequency in the rotor circuit at blocked-rotor conditions tends to cause the rotor-bar current to be crowded toward the top of the bar. For a bar of 2 or 3 cm depth, such crowding becomes significant and is called the deep-bar effect. This concentration of current into the top of the rotor bar has two electromagnetic consequences. The ratio of ac to dc resistance of the bar is increased and the effective bar depth in producing slot-leakage permeance is decreased. The deep-bar effect was analyzed in Sections 10.3.5 and 10.3.6, and equations were derived that give the increase in resistance and decrease in leakage permeance of the bar as a function of frequency. Figure 10.9 provides a set of curves which give the results of these equations applied to rectangular bars. Also, in Sections 10.3.8 through 10.3.11, a generalized lattice network was derived and applied to specific examples. This method utilizes a finite-element electromagnetic approach to a rotor cage of any particular shape to determine the increase in cage resistance and the decrease in leakage permeance of the bars of the cage. The curves in Fig. 10.9 are restricted to rectangular bars or to bars that can be approximated as rectangles, although the general method is capable of being extended to cover trapezoidally shaped bars. However, as stated above, the finite-element method can be applied to bars of any shape; in Section 10.3.10 the method was applied to a rectangular-bar rotor and in Section 10.3.11 it was applied to a triple-cage rotor. Thus for any squirrel-cage rotor, the reduction in rotor-slot leakage reactance caused by line frequency in the rotor circuit can be determined by the methods presented in Chapter 10.

13.15.2 Saturation of Tooth Tips Due to High Current Values at Blocked-Rotor Conditions

Currents of from five to seven times rated which flow in the stator and rotor slots at blocked-rotor conditions increase the cross-slot magnetomotive force in the same proportion. This, in turn, causes a large increase in leakage flux resulting from that magnetomotive force to cross the slot. An inspection of Fig. 13.4 shows that the cross-slot magnetomotive force and the resulting cross-slot flux are at maximum values in the region near the top of the slot. Thus it would be expected that under blocked-rotor conditions, any overhanging portion of the adjacent tooth tips, such as the tooth steel to the left of vertical line AB in Fig. 13.15, would saturate to some extent. In actual practice, the tooth tips of semiclosed slots, such as those used with squirrel-cage rotors and with random-wound stators, do tend to saturate at blocked rotor. It is even possible under these conditions to have some tooth-tip saturation with open slots, although this is not usual. Tooth-tip saturation has the effect of increasing the width of the slot in the region where saturation occurs, and this, in turn, decreases the overall slot permeance. If the slot permeance is decreased, the slot leakage flux is also decreased. Then since inductance is equal to

$$L = \frac{N\phi}{I} \quad \text{henrys} \tag{13.191}$$

a decrease in cross-slot flux linkage per ampere results in a corresponding decrease in slot leakage reactance at blocked-rotor conditions. The question then arises as how to calculate or, more correctly stated, approximately calculate leakage reactance under blocked-rotor conditions when tooth-tip saturation is present and when reduction in effective bar height, discussed in Section 13.15.1 is also present.

13.15.3 Calculation of Blocked-Rotor Reactance

Saturation of the stator or of the rotor tooth tips will result in a corresponding decrease in slot leakage reactance of the stator or of the rotor, for the reason given above. A significant amount of tooth-tip saturation can also result in some amount of reduction in zigzag leakage reactance since, as discussed earlier, the width of the slot opening will tend to affect that component of reactance. However, the primary effect of saturation of leakage-flux paths is to reduce slot leakage reactance, and any reduction of zigzag reactance is of secondary importance in the usual case.

It should be noted that under blocked-rotor conditions, the magnitude of the magnetizing reactance is increased to some extent. This can be understood by considering the induced voltage E across the magnetizing reactance

X_m under such conditions. If the blocked-rotor current flowing in the stator winding is 6.0 per unit, and if the stator leakage reactance is 0.08 per unit, for example, the voltage drop from the stator bus to the magnetizing reactance branch of the equivalent circuit is equal to $(6.0)(0.08) = 0.48$ per unit. Thus the voltage across X_m is in the region of half of rated, which means that the magnetic circuit of the mutual flux is unsaturated. Hence, essentially all of the magnetizing ampere-turns are consumed in overcoming the air-gap reluctance, and the ampere-turns consumed in overcoming the reluctance of the ferrous flux paths in the stator and rotor cores are very small by comparison. Accordingly, the factor K_s defined by eq. (12.50) is very nearly equal to 1.0 at blocked rotor. Since this factor appears in the denominator of the expression for X_m [in equations (13.162) and (13.163) for example], the magnitude of X_m will increase by K_s. Thus if $K_s = 1.15$ and if $X_m = 4.0$ per unit under rated conditions, then $X_m = (1.15)(4.0) = 4.6$ per unit at blocked-rotor conditions.

The procedure that is used to calculate blocked-rotor leakage reactance is an iterative process. For the first iteration, the running value of reactance, but with the rotor-slot reactance reduced, to consider the reduced permeance from the deep-bar effect is used to calculate the stator and rotor currents for a value of slip equal to 1.0. Using the resulting current values, the cross-slot flux densities in the stator and in the rotor teeth are calculated. If the tooth-tip flux density is such as to indicate that saturation is occurring in either the stator or the rotor teeth, the affected slot openings are considered to be increased effectively for the extent of the saturated portion of the tooth steel. The stator-slot and/or the rotor-slot leakage reactance is recalculated based on the assumed new value of slot openings, and the calculations above repeated. The final iteration corresponds to the case in which the resulting tooth-tip flux density is just below that value at which saturation is assumed to occur for the steel used for the punching. The value of rotor and stator leakage reactance, which corresponds to the final iteration, is the blocked-rotor leakage reactance of the machine.

If it is found that the stator-slot and/or the rotor-slot openings have been significantly widened from saturation, it is the practice of some experienced engineers to reduce slightly the blocked-rotor value of zigzag leakage reactance. Although based on a rationale, such an adjustment of X_2 is essentially empirical and further complicates an already complicated iterative procedure. Probably, this additional step should only be used when a suitable test program clearly shows that such an adjustment of X_z is required in order to achieve acceptable agreement between calculated and test values of blocked-rotor characteristics. Also, any given procedure for making an empirical adjustment of X_2 should be considered valid only within the limit of the stator and rotor design parameters (i.e., slot combinations, punching diameters, air-gap lengths, poles, etc.) for which that procedure has been verified by the test program mentioned above.

13.16 NUMERICAL EXAMPLE OF BLOCKED-ROTOR REACTANCE CALCULATION

13.16.1 Calculation of Some Necessary Preliminary Quantities

The calculation of blocked-rotor leakage reactance will be illustrated by use of the same numerical example as was used in Section 13.14 to calculate running reactance. However, the values of magnetizing reactance X_m, induced voltage E, air-gap flux density B_g, and effective rotor-bar depth, all at blocked-rotor conditions, must first be determined since they will be required later to calculate blocked-rotor leakage reactance by iteration.

In eqs. (13.164) and (13.166), X_m was determined to be equal to 20.7 Ω per phase or to 2.92 per unit. The value of K_s, or the ratio of total magnetizing ampere turns to air-gap ampere turns, was taken to be 1.15 for the example. Then, for reasons discussed in Section 13.15.3, the value of X_m at blocked-rotor conditions is equal to

$$X_m = (1.15)(20.7) = 23.8 \quad \text{ohms/phase} \tag{13.192}$$

or, in per unit, is equal to

$$X_m = \frac{23.8}{7.09} = 3.36 \quad \text{per unit} \tag{13.193}$$

With from five to seven times rated current in the stator winding, the impedance drop from the stator bus to the magnetizing branch X_m is very significant. For the example, using a value of 6.0 per unit blocked-rotor current I_ℓ and a value of 0.0987 per unit stator leakage reactance from eq. (13.189), the impedance drop in the stator winding is essentially equal to

$$I_\ell X_1 = (6.0)(0.0987) = 0.592 \quad \text{per unit} \tag{13.194}$$

The voltage E_1 induced in the stator winding is equal to the bus voltage less the stator-winding impedance drop, or

$$E_1 = V_1 - I_1 Z_1 \quad \text{per unit} \tag{13.195}$$

which for this example at blocked-rotor conditions is equal to

$$E_1 = 1.0 - 0.592 = 0.408 \quad \text{per unit} \tag{13.196}$$

From eq. (9.138) the voltage induced in the stator winding is equal to

$$E_1 = \frac{4.443K_pK_dN_{st}f\phi_{pm}}{10^8} \quad \text{volts/phase} \tag{13.197}$$

when ϕ_{pm} is in units of maxwells. Solving for flux/pole ϕ_{pm} gives us

$$\phi_{pm} = \frac{E_1 \times 10^8}{4.443K_pK_dN_{st}f} \quad \text{maxwells/pole} \tag{13.198}$$

Substituting the appropriate quantities for the example into eq. (13.198) yields

$$\phi_{pm} = \frac{(0.408)(1328)(10^8)}{(4.443)(0.985)(0.955)(72)(60)} = 3.0 \times 10^6 \quad \text{maxwells/pole} \tag{13.199}$$

under blocked-rotor conditions. To determine the corresponding air-gap flux density, the air-gap area/pole A_g must first be found. This area is equal to

$$A_g = \frac{\pi d \ell_c}{p} \quad \text{inches}^2 \tag{13.200}$$

Substituting the appropriate quantities for the example into eq. (13.200) gives us

$$A_p = \frac{(\pi)(26.4)(27)}{8} = 280 \quad \text{inches}^2 \tag{13.201}$$

Flux/pole ϕ_{pm} divided by air-gap area/pole gives the average air-gap flux density. Since the fundamental of the air-gap flux wave has a sinusoidal space distribution, this quotient must be multiplied by $\pi/2$ to obtain the maximum air-gap flux density. As discussed in Chapter 14, flux densities in the air gap and in the teeth are normally given in terms of their maximum values, since the corresponding magnetic field strength H that forces the mutual flux through these parts is related to such values. Then the maximum air-gap flux density at blocked-rotor conditions is equal to

$$B_g = \frac{\phi_{pm}}{A_g}\frac{\pi}{2} \quad \text{maxwells/inch}^2 \tag{13.202}$$

Substituting eqs. (13.199) and (13.201), into eq. (13.202)

$$B_g = \left[\frac{(3.0)(10^6)}{280}\right]\frac{\pi}{2} = 16.8 \times 10^3 \quad \text{maxwells/inch}^2 \qquad (13.203)$$

By comparison, the maximum air-gap flux density at full-speed operation is equal to $(16.8 \times 10^3)/0.408 = 41.1 \times 10^3$ Mx/in.^{2}.

The rectangular copper rotor bar is 0.400 in. wide and 1.385 in. deep and the rotor slot is 0.415 in. wide. Then from Fig. 10.9, the quantity δd_b is equal to

$$d_b = 0.349 d_b\sqrt{Kf} = (0.349)(1.385)\sqrt{\left(\frac{0.400}{0.415}\right)(60)} = 3.68 \quad \text{numeric} \qquad (13.204)$$

and from the curve in Fig. 10.9, the ratio $\lambda_{ac}/\lambda_{dc}$ is equal to

$$\frac{\lambda_{ac}}{\lambda_{dc}} = 0.407 \quad \text{numeric} \qquad (13.205)$$

Accordingly, the effective rotor-bar height with a frequency of 60 Hz in the rotor circuit is equal to

$$d_b = (1.385)(0.407) = 0.564 \quad \text{inches} \qquad (13.206)$$

13.16.2 First Iteration

For the first iteration, the stator and rotor slot openings are tentatively assumed to have the same dimensions as shown in Fig. 13.15 (i.e., to have negligible saturation), but the reduction in rotor-bar depth due to the deep-bar effect is considered. From these assumptions the rotor-slot leakage reactance is recalculated, and using the new value of X_2, the stator and rotor currents are calculated approximately. Using the resulting values of currents, the flux densities in the stator and rotor tooth tips are calculated to determine (1) if saturation exists in these parts, and if so, (2) the amount of slot-width adjustment required to make in order to adjust for such saturation.

From eq. (13.77), rotor-slot leakage reactance is equal to

$$X_{s2} = \frac{8.02 f \ell_c N_{st}^2 q}{10^7 N_2}(K_{p1}K_{d1})^2\left(\frac{d_0}{w_0} + \frac{2d_4}{w_0 + w} + \frac{d_b}{3w}\right) \quad \text{ohms/phase} \qquad (13.207)$$

Substituting the appropriate quantities into eq. (13.207) and remembering that $d_b = 0.564$ in., at blocked-rotor conditions

$$X_{s2} = \left[\frac{(8.02)(60)(27)(72)^2(3)}{(10^7)(86)}\right]\left[(0.985)(0.955)\right]^2\left[\frac{0.10}{0.10} + \frac{(2)(0.015)}{0.515} + \frac{0.564}{(3)(0.415)}\right]$$

$$= 0.314 \quad \text{ohms/phase} \tag{13.208}$$

The corresponding value of X_2 for the first iteration is equal to

$$X_2 = X_{s2} + X_{z2} = 0.314 + 0.149 = 0.463 \quad \text{ohms/phase} \tag{13.209}$$

or in per unit,

$$X_2 = \frac{0.463}{7.09} = 0.065 \quad \text{per unit} \tag{13.210}$$

The value of X_2 above, the previously calculated full-speed value of X_1, and the value of X_m given in eq. (13.193) will be used to calculate I_1 and I_2 at blocked-rotor conditions.

Using eq. (5.16), setting $s = 1$, and neglecting R_1 and R_2, blocked-rotor stator current is equal to

$$I_{1\ell} = \frac{V_1}{j(X_1 + X_m) - (jX_m)^2/j(X_2 + X_m)}$$

$$= \frac{1.0}{j(0.0987 + 3.36) - (j3.36)^2/j(0.0650 + 3.36)}$$

$$= 6.15 \quad \text{per unit} \tag{13.211}$$

in magnitude. Also, using eq. (5.21), setting $s = 1$, and neglecting R_1 and R_2, the corresponding rotor current is equal to

$$I_{2\ell} = \frac{jV_1X_m}{[j(X_1 + X_m)][j(X_2 + X_m)] - (jX_m)^2}$$

$$= \frac{j(1)(3.36)}{[j(0.0987 + 3.36)][j(0.065 + 3.36)] - (j3.36)^2}$$

$$= 6.04 \quad \text{per unit} \tag{13.212}$$

in magnitude.

To check the amount of saturation in the stator teeth, per unit line current will be converted to amperes/phase and then to amperes/slot. Normal amperes on the machine's own , VA base is

$$I_n = \frac{(746)(1000)}{(\sqrt{3})(2300)} = 187.3 \quad \text{amperes/phase} \tag{13.213}$$

Then

$$I_{1\ell} = (6.15)(187.3) = 1152 \quad \text{amperes/phase} \tag{13.214}$$

The stator winding has two circuits/phase and, accordingly, the current in each circuit is equal to 1152/2 = 576 A per circuit. There are 6 turns/coil and 12 turns/slot, so that the current per slot is equal to

$$I_{1s} = (12)(576) = 6912 \quad \text{amperes/slot} \tag{13.215}$$

Using units of maxwells and inches, the relationship between flux density and magnetic field strength at the top of the slot is

$$B = \frac{4\pi(2.54)NI}{10w} = \frac{3.192NI}{w} \quad \text{maxwells/inch}^2 \tag{13.216}$$

Then the flux density across the top of the stator slot as well as that of the immediately adjacent parts of the tooth tips in Fig. 13.15a is equal to

$$B = \frac{(3.192)(6912)}{0.570} = 38,700 \quad \text{maxwells/inch}^2 \tag{13.217}$$

In eq. (13.203), the maximum air-gap density due to the mutual flux at blocked-rotor conditions, was determined to be $B_g = 16,800$ Mx/in.^{2}. The direction of the air-gap magnetic field and of the resulting mutual flux is complicated at the corner of a tooth, as will become apparent in Chapter 14. However, if the relative direction and phase relationship of the magnetic fields of the mutual flux and of the cross-slot leakage flux were such that they added algebraically, which is not the case, the flux density in the stator-tooth tips would only be 38,700 + 16,800 = 55,500 Mx/in.^{2}. Since this is about half of the value of flux density at which saturation is impending in a steel tooth, it can safely be concluded that the stator teeth are not saturating for this or any subsequent iteration.

To check the amount of saturation in the rotor teeth, rotor-bar current at rated load will be calculated and that value multiplied by per unit rotor current to give amperes/slot. From eq. (10.156), rotor bar current is equal to

$$I_b = \frac{2qI_{12}N_{st}K_{p1}K_{d1}}{N_2} \quad \text{amperes/bar} \tag{13.218}$$

where I_{12} is the load component of stator current. For the subject motor, this is equal to $[(746)(1000)]/[(\sqrt{3})(2300)] = 187.2$ A per phase. Substituting this and the other appropriate values into eq. (13.218) gives us

$$I_b = \frac{(2)(3)(187.3)(72)(0.985)(0.955)}{86} = 885 \quad \text{amperes/bar} \tag{13.219}$$

at rated load and speed. At blocked-rotor conditions, the rotor-bar current is equal to the product of eqs. (13.212) and (13.219), or

$$I_{b\ell} = (6.04)(885) = 5345 \quad \text{amperes/bar} \tag{13.220}$$

The amount of saturation in the rotor teeth can be checked by proceeding in a manner similar to that done for the stator teeth. Then the cross-slot flux density at the top of the slot is

$$B = \frac{3.192I_{b\ell}}{w_0} = \frac{(3.192)(5345)}{0.10} = 170.6 \times 10^3 \quad \text{maxwells/inch}^2 \tag{13.221}$$

Again, the contribution of the air-gap flux to saturation of the tooth tip must be evaluated. The rotor-tooth slot pitch (i.e., the distance from the beginning of one slot to the beginning of the next slot) is equal to $(d - 2g)(\pi)/N_2 = (26.3)(\pi)/86 = 0.961$ in. The tip width of the rotor tooth is then equal to $0.961 - 0.100 = 0.861$ in., and the air-gap flux density immediately above the tooth tends to approach $(0.961/0.861)(16,800) = 18,400$ Mx/in.^{2}. An inspection of the rotor tooth shown in Fig. 13.15b would indicate that a considerable component of the air-gap flux which enters the tooth overhang must have a tangential component in order to enter the other portions of the rotor tooth. However, considering the phase relationship as well as the direction between the two fluxes, somewhat less than 10,000 Mx/in.^{2} of the air-gap flux density should be added to the cross-slot flux density in determining saturation within the rotor-tooth overhang. Using this value as a conservative assumption, the flux density within the steel of the tooth overhang is equal to 10,000 Mx/in.^{2}, added to the value given in eq. (13.221), or to $170,600 + 10,000 = 180,600$ Mx/in.^{2}. Depending on the steel being used, a condition of ferromagnetic saturation will occur in the tooth tips at flux densities within the range 100,000 to 115,000 Mx/in.^{2}. It then becomes a reasoned judgment what value of flux density to use as a criterion for tooth-tip saturation. For purposes of this numerical example, a value of 110 Mx/in.^{2} will be used. Based on this criterion, it is apparent that the value of

180,600 Mx/in.^{2} calculated for the first iteration is considerably in excess of this criterion and that a state of saturation exists in some part of the rotor-tooth overhang.

13.16.3 Second Iteration

The second iteration consists in making an estimate of the effective width of the rotor slot opening w_0 caused by saturation, based on the results of the first iteration and of then essentially repeating the operations of that iteration. From eq. (13.221) it is apparent that the effective width of the rotor-slot opening w_0 is inversely proportional to the cross-slot flux density at the top of the slot. Since the actual slot opening of 0.10 in. resulted in 170,600 Mx/in.^{2} of cross-slot flux density, and since it is desirable to find an effective value of w_0 that will limit the cross-slot flux density to 100,000 Mx/in.^{2}, it would appear that the estimated effective value of w_0 should be (170.6/100) × (0.10) = 0.171 in. Although such a value would be close, it is not quite sufficient. As the value of w_0 is increased, it increases the opening of the d_4 part as well as the d_0 part of the slot. The reluctance across the slot opening is, indeed, increased as w_0 is increased, because of the increase in the length of the flux path. However, the reluctance is also slightly decreased because of a slight increase in cross-sectional area to the flux in the d_4 part of the slot overhang. Thus the estimated effective value of w_0 must be further increased to a slight extent to compensate for this.

Then, as a first-order approximation, the effective value of w_0 should be

$$w_0' = \left(\frac{170.6}{100.0}\right)(0.10) = 0.171 \quad \text{inches} \qquad (13.222)$$

However, this value is somewhat too small. As stated above, a further increase in the effective value of w_0 is justified to compensate for the increase in the cross-sectional area of the leakage flux path. Then, assume that $w_0' = 0.186$ for the second iteration. To determine the new dimensions for calculating X_{s2}, consider Fig. 13.15b. The slope of the line that forms the bottom of the overhang is equal to

$$\text{slope of bottom of overhang} = \frac{(0.015)(2)}{0.415 - 0.100} = 0.0953 \quad \text{numeric} \qquad (13.223)$$

Using the selected value of $w_0' = 0.186$ in., the decrease in each lip of the overhang is equal to

$$\text{decrease in length of overhang} = \frac{0.186 - 0.100}{2} = 0.043 \quad \text{inches} \qquad (13.224)$$

and the effective depth d_0' of the overhang is equal to

$$d_0' = 0.10 + (0.0953)(0.043) = 0.1041 \quad \text{inches} \tag{13.225}$$

Similarly, the effective depth of d_4 is equal to

$$d_4' = 0.015 - (0.0953)(0.043) = 0.0109 \quad \text{inches} \tag{13.226}$$

Substituting the values of w_0', d_0', and d_4' above into eq. (13.207) and keeping the other quantities identical to those in eq. (13.208), we obtain

$$X_{s2}' = \left[\frac{(8.02)(60)(27)(72)^2(3)}{(10^7)(86)}\right]\left[(0.985)(0.955)\right]^2\left[\frac{0.1041}{0.186} + \frac{(2)(0.0109)}{0.186+0.415} + \frac{0.564}{(3)(0.415)}\right]$$

$$= 0.218 \quad \text{ohms/phase} \tag{13.227}$$

The corresponding value of X_2 is

$$X_2' = X_{s2}' + X_{z2} = 0.218 + 0.149 = 0.367 \quad \text{ohms/phase} \tag{13.228}$$

and in per unit,

$$X_2' = \frac{0.367}{7.09} = 0.0518 \quad \text{per unit} \tag{13.229}$$

Substituting the value of X_2' above into eq. (13.212), while maintaining the other values to calculate $I_{2\ell}$ for the second iteration, gives us

$$I_{2\ell} = \frac{j(1)(3.36)}{[j(0.0987 + 3.36)][j(0.0518 + 3.36)] - (j3.36)^2} = 6.58 \quad \text{per unit} \tag{13.230}$$

in magnitude. From eq. (13.219) the rotor-bar current I_b is equal to 885 A per bar at rated speed and rated load. Then the rotor-bar current $I_{b\ell}$ at blocked-rotor conditions is equal to

$$I_{b\ell} = (6.58)(885) = 5823 \quad \text{amperes/bar} \tag{13.231}$$

and the cross-slot flux density at the top of the slot for the second iteration is equal to

$$B = \frac{3.192 I_{b\ell}}{w_0'} = \frac{(3.192)(5823)}{0.186} = 100{,}000 \quad \text{maxwells/inch}^2 \tag{13.232}$$

The flux density in the rotor-tooth tip adjacent to the slot, due to cross-slot leakage flux, is then equal to 100,000 Mx/in.^{2}. If that component of the air-gap flux previously considered appropriate to add is then added to the cross slot flux, the resulting flux density in the tooth-tip overhang is equal to 100,000 + 10,000 = 110,000 Mx/in.^{2}, which is also the value of the previously selected criterion which indicates that saturation has been reached. Thus an increase in the rotor-slot opening w_0 from 0.100 in. to 0.186 in. because of saturation of the tooth-tip overhang has resulted in a calculated value of flux density in that part, which is just at a condition of ferromagnetic saturation. This, then, indicates that the value of X_{s2} and the corresponding value of X_2 is appropriate for blocked-rotor conditions. Accordingly, the blocked-rotor reactance of the rotor $X_{2\ell}$ for this numerical example is equal to

$$X_{2\ell} = 0.367 \quad \text{ohms/phase} \tag{13.233}$$

and the blocked-rotor reactance of the stator is equal to

$$X_{1\ell} = X_1 = 0.600 \quad \text{ohms/phase} \tag{13.234}$$

For pedagogical reasons, the iterative process above was carried through in detail to illustrate the logic behind that process. Such a procedure would, of course, be programmed and the calculations performed on a digital computer in the usual case.

14

The Magnetic Circuit

14.1 Function and Role of the Magnetic Circuit 550

14.2 Diamagnetism and Paramagnetism 550

14.3 Ferromagnetic Materials 551

14.4 Magnetic Saturation 552

14.5 Magnetic Hysteresis Loss 553

14.6 Eddy-Current Loss 558

14.7 No-Load Core Loss 562

14.8 Load Loss 564

14.9 Core Structure 567

- 14.9.1 Producing the punching 567
- 14.9.2 Producing the core 569
- 14.9.3 Interlamination resistance and ring testing 575
- 14.9.4 Numerical example of a ring test 577
- 14.9.5 Magnetic dissymmetries and resulting shaft voltages 580

14.10 Effect of Slot and Air-Duct Openings and the Use of Carter's Coefficient 582

14.11 Calculation of the Magnetic Circuit 585

- 14.11.1 Derivation of the saturation curves for use with the teeth and the core yoke 585
- 14.11.2 Calculation of the magnetic circuit, with numerical example 587

14.1 FUNCTION AND ROLE OF THE MAGNETIC CIRCUIT

As discussed in previous chapters, when voltage is applied to the terminals of the stator winding, a three-phase rotating magnetomotive-force wave is produced, which acts on the average permeance of the air gap and produces a corresponding three-phase rotating flux wave. The rotating flux wave, in turn, induces a voltage E_2 in each phase of the rotor in accordance with Faraday's law. Since each phase of the rotor winding is closed, the induced rotor voltage will cause corresponding rotor currents to flow. These rotor currents, which also rotate, will interact with the rotating air-gap flux wave to produce a useful torque on the rotor structure, in accordance with Ampère's law. This, then, is the basis of motor action. There is no mechanical linkage between the stator, to which electrical power has been applied, and the rotor, which rotates as a result of the application of that electrical power. Obviously, only the electromagnetic field is effective in transferring electrical energy across the medium of air (or, in some cases, hydrogen or water), which comprises the air gap.

From the above, the electromagnetic field is central to motor action in a polyphase induction motor. The mutual flux, which links the stator winding and the rotor winding, flows through the closed path consisting of the stator core, the air gap, the rotor core, the air gap, and back to the stator core. In this chapter details of the mutual-flux path are considered in detail, the first of which relates to the magnetic properties of steel.

14.2 DIAMAGNETISM AND PARAMAGNETISM

To the best of present-day knowledge, magnetic fields are produced only by an electrical current (i.e., by a moving charge). Since all matter is electrical in composition, the source of magnetic properties of matter must start with the structure of the atom and with the first strata of subatomic particles (i.e., electrons, protons, and neutrons). For example, a proton has a positive charge and, accordingly, can be expected to have lines of electric-field force associated with the presence of such a charge, to form current loops. Then, as it spins on its own axis, it would further be expected that the particle should act as a loop of current-carrying conductor and produce a magnetic field with north and south polarity. Although admittedly elementary at first appearance, this explanation offers insight into these particles and explains the fact that they have magnetic fields not unlike those of bar magnets. The magnetic moment of the particles is called their "spin magnetic dipole moment." Since atoms are composed of such subatomic particles, each with individual magnetic fields, it would reasonably be expected that these particles would give the overall atom a net magnetic field, resulting from the combined effect of their individual magnetic fields. To a small extent, this does occur. In most cases, however, the individual particles appear to arrange themselves within the atom such as to cancel each other's magnetic dipoles.

In addition to the source of magnetic properties above, the complete atom can be considered as a system consisting of electrons that are orbiting around a central nucleus. Thus these orbiting electrons constitute a number of circular currents which result in a magnetic field for the complete atom. Magnetic fields resulting from orbiting electrons would be expected to be a significant source of magnetic characteristics for most elements. However, for many of the atoms, the electron orbits are oriented such as to cancel each other's magnetic fields, just as a similar orientation tends to cancel the spin magnetic moment mentioned above.

If the cancellation of the effect of spin magnetic dipole moment of the individual particles and of the orbital electrons is complete for a given atom, it will show no permanent magnetic moment. Elements that have such atoms, such as carbon, copper, and lead, are said to be diamagnetic. However, the atoms of several elements have a few electrons, called uncompensated electrons, the magnetic moments of which are not canceled. Such atoms exhibit a permanent magnetic moment and the corresponding elements are said to be paramagnetic. Paramagnetism tends to decrease with an increase in temperature of the material, because of thermal action. Diamagnetism, on the other hand, is unaffected by temperature.

14.3 FERROMAGNETIC MATERIALS

A few elements show an unusually strong paramagnetic effect; that is, they have sufficient uncompensated electrons within their atoms to exhibit very large magnetic moments. Such elements include the commercially important ones of iron, cobalt, and nickel, as well as a few less well known ones, such as gadolinium and dysprosium. All of these elements are called ferromagnetic elements. Iron and nickel are, of course, the significant ferromagnetic materials as far as industry is concerned. These elements, which are also called transition elements, have internal orbital shells which are not completely filled with orbital electrons. Presumably, as a result of this, the usual cancellation of electron spin magnetic moments is not complete in such cases, thus permitting relatively large values of magnetic moments to exist.

These large magnetic moments allow atoms within small volumes of the material to orient themselves locally such that the magnetic moments of the atoms within these volumes are aligned in the same direction. Such volumes, which contain locally oriented atoms, are called magnetic domains or, more simply, domains, and the length of a typical domain in one direction is of the order of 10^{-3} to 10^{-5} m. If a volume of ferromagnetic material such as iron in the demagnetized state is considered, the domains will be present but the direction of the magnetic moment of the various domains will be random relative to each other. If, however, a magnetic field is impressed across the material, the domains will tend to reorient themselves such that a greater number of the domains are oriented with their magnetic moments aligned in the direction of the applied field. As mentioned earlier, ferromagnetism is somewhat affected by temperature. If, for example, the volume of iron above, which contains some number of oriented domains, is sufficiently heated, the resulting thermal energy contained in the volume will cause a loss of orientation, and above this temperature, the material will behave like most other paramagnetic materials. The temperature at which this transition occurs is the Curie temperature, which is 770°C for iron and 358°C for nickel in their elemental states free of impurities.

14.4 MAGNETIC SATURATION

Using the aforementioned simplified model of domains within ferromagnetic materials, the well-known phenomenon of magnetic saturation can be more clearly understood. Assume that a unidirectional magnetic field is applied across a volume of iron and that the flux density B in the iron in webers/meter^2 is determined for various values of the magnetic field strength H in ampere-turns/meter as the field strength is increased. Figure 14.1 shows a plot of corresponding values of B and H for a sample of magnetic-core steel. Such a plot gives the familiar normal saturation curve of the material and is, of course, an important magnetic characteristic of that material.

If the steel is initially demagnetized, the myriads of domains are randomly aligned, giving the overall material a net magnetic field of zero in any direction. Then if a small value of magnetic field strength H is applied across the sample, a small percentage of the domains will tend to align themselves in the direction of the field, thereby increasing the value of B from zero to a small number. If the value of H is slightly increased, the value of B will increase in about direct proportion as more domains tend to align themselves with the field. Prior to application of the field, the direction of the magnetic moments was randomly distributed. The domains, which are most nearly in alignment with the field, are the first to align, at the lower values of H. This essentially direct proportionality between B and H will then continue as long as the domains can reorient from their original random positions and align with the field without being obstructed by other domains or by impurity particles. A point is eventually reached, however, where a given increment of H results in a diminishing increment of B because of mechanical interference. At this point, as a given domain tries to rotate in order to orient itself with the field, it will be partially blocked by another domain or impurity particle, thus requiring a considerably greater value of H to complete, or even partially complete, the orientation. This process gives rise to the characteristic shape of the saturation curve of a ferromagnetic material.

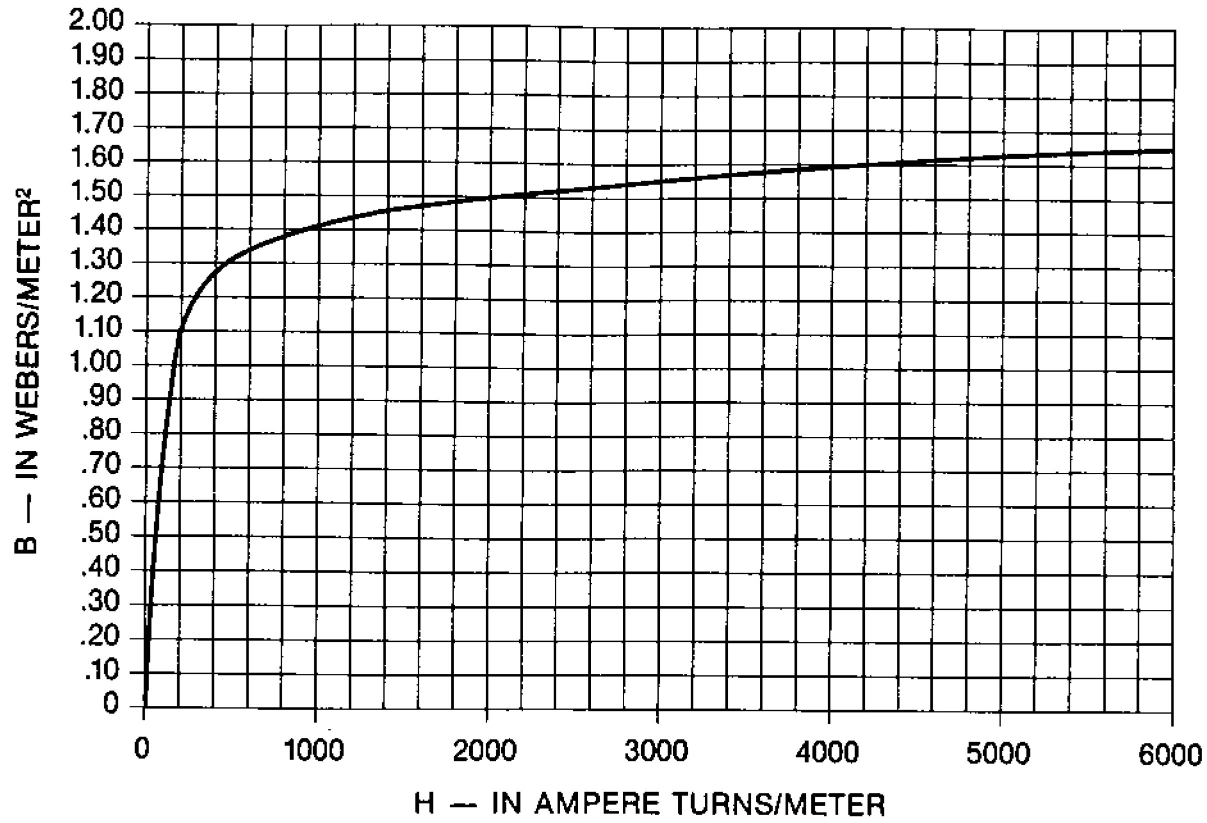

FIGURE 14.1 Normal dc saturation curve of steel.

14.5 MAGNETIC HYSTERESIS LOSS

It should come as no surprise that the relationship shown in Fig. 14.1 between flux density B and field strength H as H is cyclically varied is not fully reversible. If, starting at some point on the saturation curve, such as $B = 1.3\ \mathrm{Wb/m^2}$ and the corresponding value of H, it is decided to decrease H incrementally to zero and to plot corresponding points of B and H, the result would be similar to part ab of the curve in Fig. 14.2. Thus a value of flux density B equal to ob remains in the steel sample, with the magnetic field strength H reduced to zero. This value of B at point b, which is called the retentivity, results from the fact that not all of the magnetic moments of the domains have returned to a state of random direction from the state of general orientation with the field that existed at point a on the curve. If the magnetic field strength is sufficiently increased in the reverse direction to an amount equal to oc, the flux density will be reduced to zero. The magnetic field force oc corresponding to this condition is called the coercive force. A further increase in H in the reverse direction will cause the flux density to increase, but in the negative direction, such as exists at point d. This point has about the same numerical values of B and H as point a, but they are negative instead of positive. If the magnetic field strength is decreased from its negative value to zero and then increased in the positive direction, the corresponding values of B and H will form the curve of defa', where a' is essentially the same point as the original a. The curve abcda is called the hysteresis loop of the ferromagnetic material and the physical process is called magnetic hysteresis. The name of the process is taken from the classical Greek language and a reasonable translation is "to lag." An inspection of Fig. 14.2 would indicate that the choice of the name is appropriate.

From the previous description of domain magnetic-moment alignment, under the influence of a magnetic field, it could be reasonably assumed that the area within the hysteresis loop in Fig. 14.2 represents unrecoverable energy, or heat, which is lost during the cycle. That assumption is surely correct, as will now be shown. Consider a sample of steel which is formed into a closed ring of length L meters and cross section A meters^2, around which N turns of conductor are wrapped to form a coil. Let a unidirectional voltage be impressed across the terminals of the coil, to give a unidirectional current of i amperes. This will result in a magnetic field force of

$$H = \frac{Ni}{L} \quad \text{ampere-turns/meter} \qquad (14.1)$$

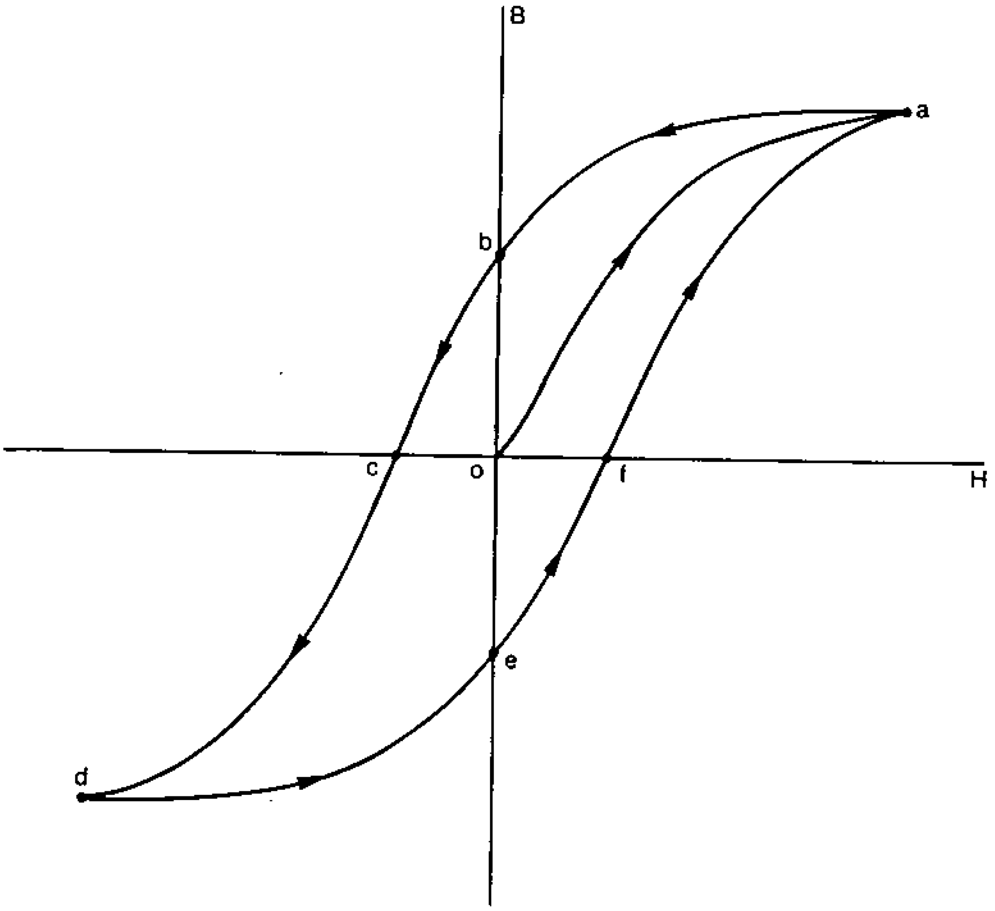

FIGURE 14.2 Typical magnetic hysteresis curve.

Solving eq. (14.1) for i, we obtain

$$i = \frac{HL}{N} \quad \text{amperes} \tag{14.2}$$

If the current i is changed by an incremental amount di, the magnetic field strength H will be changed by an amount dH. This, in turn, will cause the flux density B to change by an amount dB and the flux ϕ in the core will change by an amount $d\phi = A\ dB$. From Faraday's law, if the incremental change occurs in an incremental time dt, the voltage induced in the coil is equal to

$$e = -\frac{N\,d\phi}{dt} = -\frac{(AN)\,dB}{dt} \quad \text{volts} \tag{14.3}$$

assuming that there is no significant leakage flux from the coil (i.e., that all of the flux links all of the turns of the coil). This induced voltage is in such a direction as to oppose the change in current di that caused it. Accordingly, the voltage bus must provide a voltage that is numerically equal, but opposite in direction, to e. The resulting energy supplied by the source in time dt is then equal to

$$dJ = ei\ dt \quad \text{joules} \tag{14.4}$$

Substituting eqs. (14.2) and (14.3) into eq. (14.4) yields

$$dJ = AN\frac{dB}{dt}\frac{HL}{N}\ dt = ALH\ dB \quad \text{joules} \tag{14.5}$$

and

$$J = AL\int H\ db \quad \text{joules} \tag{14.6}$$

As the current i is increased, the energy supplied to the field as the flux density changes from B_e, corresponding to point e, to B_a, corresponding to point a, is

$$J_{ea} = AL\int_{B_e}^{B_a} H\ dB \quad \text{joules} \tag{14.7}$$

The integral above corresponds to the area between the B axis, or the ordinate, and the hysteresis curve between points e and a. When the flux density B decreases, the value of the integral in eq. (14.6) is negative, which indicates that the magnetic field is releasing energy. For a complete cycle of hysteresis, the energy supplied, J_{in}, from Fig. 14.3a is equal to

$$J_{in} = AL\left(\int_{B_e}^{B_a} H\,db + \int_{B_b}^{B_d} H\,dB\right) \quad \text{joules} \tag{14.8}$$

and the energy released, J_{out}, from Fig. 14.3b is equal to

$$J_{out} = AL\left(\int_{B_a}^{B_b} H\,db + \int_{B_e}^{B_d} H\,dB\right) \quad \text{joules} \tag{14.9}$$

It is apparent from Fig. 14.3 that more energy is supplied to the magnetic circuit than is released in the course of one hysteresis cycle. This difference results from the heat energy lost during the cycle, which corresponds to the area inside the hysteresis loop, or to eq. (14.6). If the hysteresis cycle is completed f times a second, the hysteresis power loss is equal to

$$P_h = ALf\int H\,dB \quad \text{watts} \tag{14.10}$$

Since A is in meters^2 and L is in meters, the product AL is equal to the volume of the steel sample in meters^3. The magnetic hysteresis loss per unit volume is then equal to

$$P_{hv} = \frac{P_h}{V} = f\int H\,dB \quad \text{watts/meter}^3 \tag{14.11}$$

Early in this century, Steinmetz conducted a study of various ferromagnetic materials, from which he determined that eq. (14.11) could be put into an empirical form for ready use as

$$P_h = K_h f B_m^x \quad \text{watts/meter}^3 \tag{14.12}$$

where

K_h = constant for a given material
$x \cong 1.6$ for most usual materials, at flux densities of 0.15 to 1.4 Wb/m^2
B_m = maximum value of flux density
P_h = hysteresis loss, in W/m^3

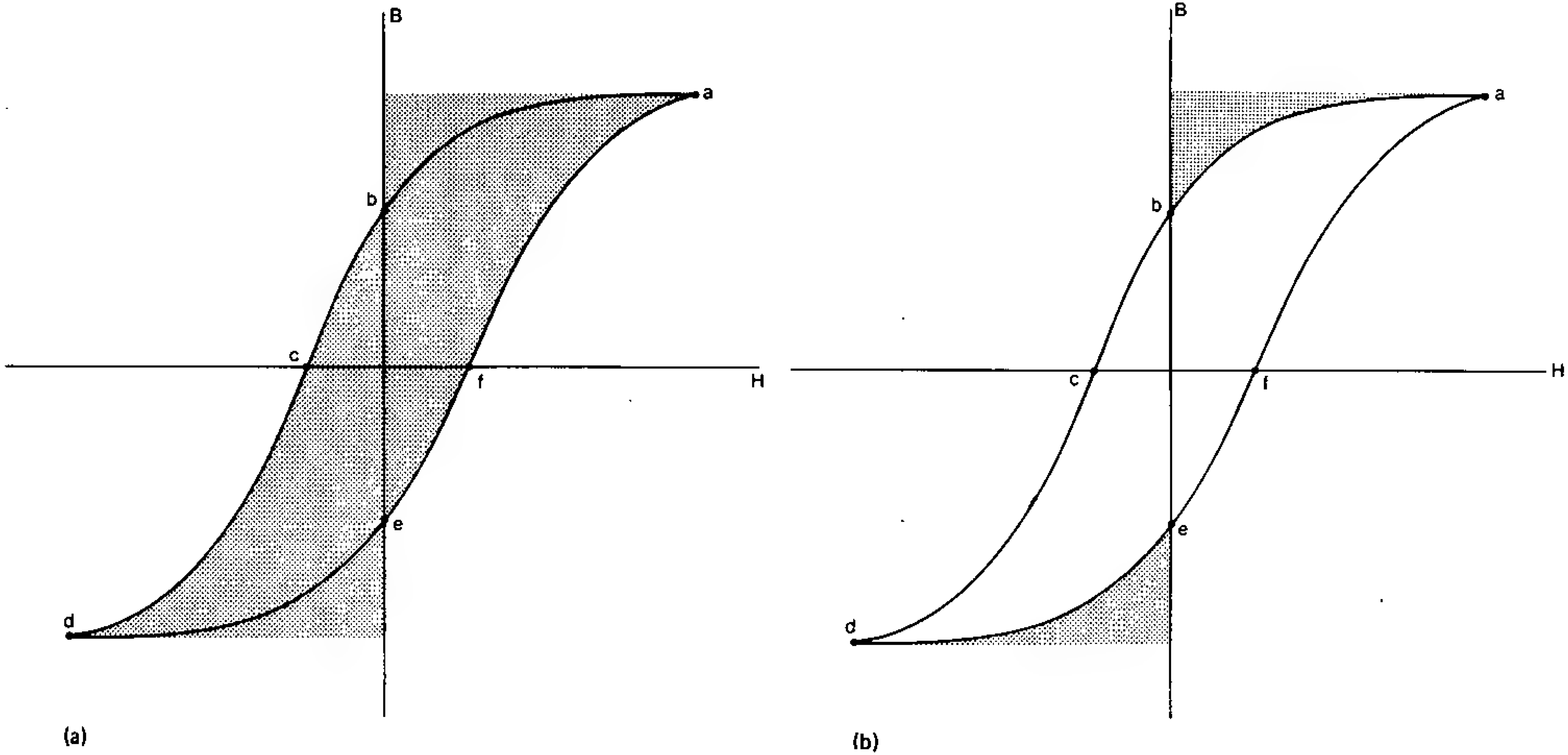
B
a
b
c
f
H
e
d
(a)
B
a
b
c
f
H
e
d
(b)

FIGURE 14.3 Energy exchange during one cycle of magnetic hysteresis: (a) energy supplied in one cycle; (b) energy released in one cycle.

For most magnetic steels used in polyphase induction motors, eq. (14.12) becomes

$$P_h = K_h f B_m^{1.6} \quad \text{watts/meter}^3 \tag{14.13}$$

Equation (14.13) was derived using MKS units and the resulting loss was expressed in terms of watts/meter^3. If a different system of units is used and the resulting loss is expressed in, say, watts/pound, the value of K_h will, of course, change. In the usual case, the hysteresis loss at a given value B_m' will be provided by the steel supplier for the grade of magnetic steel being used. Then a given motor manufacturer can store these data, together with corresponding data for eddy-current loss (which will be discussed later), in computer memory for future use. This information can subsequently be applied, at some value of maximum flux density B_m, by assuming that hysteresis loss varies as the 1.6 power of the ratio B_m/B_m' and that eddy-current loss varies as the second power of the same ratio, as will become apparent later. Hysteresis loss can be reduced, or controlled, (1) by use of special metallurgical processes at the mill, (2) by annealing the sheet steel and/or the punchings, and (3) by limiting the maximum value of flux density in the design.

14.6 EDDY-CURRENT LOSS

Magnetic hysteresis loss, discussed in the preceding section, results from internal friction as the magnetic domains rotate, in an attempt to maintain orientation of their magnetic moment with the field direction. Thus this loss is a magnetic loss. However, eddy-current loss, which is considered in this section, is not a true magnetic loss. It is, in fact, a resistive loss caused by eddy currents flowing through a conductor (i.e., the magnetic steel used for the magnetic core). Nevertheless, this loss is associated with the magnetic core and is therefore considered part of fundamental core loss.

The iron or iron alloy that is used for magnetic cores is an electrical conductor. Accordingly, the changing mutual flux within the core induces voltages in the core structure which, in turn, cause eddy currents to flow in that structure. The I^2R losses produced by these currents (1) contribute to heating, (2) reduce efficiency, and (3) cause some demagnetizing. All of these efforts are undesirable, and if appropriate design steps are not taken, they would be very significant and even overwhelming, at least for the stator core. Two mitigating design steps, both of which are important, are to build up the core from a stack of insulated laminations, which are from 0.35 to 0.65 mm thick, and to use a type of magnetic steel that has a relatively high resistivity. The need for both of these design steps will soon become apparent.

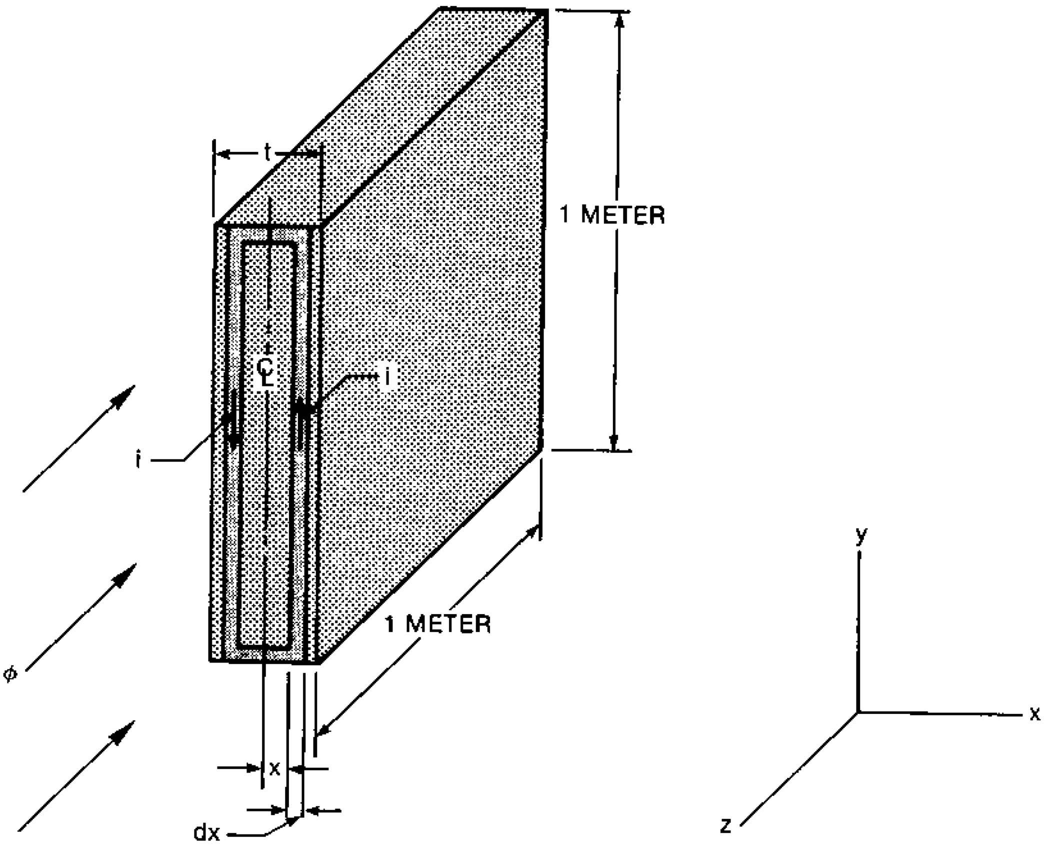

FIGURE 14.4 Eddy-current path in a sheet of steel.

Consider Fig. 14.4, which shows a rectangular prism of magnetic steel sheet, which has dimensions of t × 1 × 1 meters. This corresponds to a piece of stator-core lamination through which mutual flux, with a flux density of B, is flowing in the direction indicated in the figure. If this flux is increasing in the direction of the arrow, it will induce a current, as shown in the figure, the direction of which is such as to oppose this change in flux. The dimensionn t will be from 0.35 to 0.65 mm, for a typical stator-core configuration, so that the vertical dimension of the current path is three orders of magnitude greater than the t dimension. Thus the resistance r of the incremental current path is equal to

$$r = \frac{2y\rho}{z\,dx} \quad \text{ohms} \tag{14.14}$$

where ρ is the resistivity of the steel. But since $y = 1$ and $z = 1$, then

$$r = \frac{2\rho}{dx} \quad \text{ohms} \tag{14.15}$$

This elemental current path is linked by the flux ϕ, which is equal to

$$\phi = 2Bxy \quad \text{webers} \tag{14.16}$$

But again, $y = 1$, and

$$\phi = 2Bx \quad \text{webers} \tag{14.17}$$

The eddy-current impedance is predominantly resistive, so that any reactive component can be ignored. Thus the flow of current can be considered to be essentially limited only by resistance and, accordingly, the loss in the incremental current path is equal to

$$dP'_e = \frac{(d\phi/dt)^2}{r} \quad \text{watts} \tag{14.18}$$

Substituting eqs. (14.15) and (14.17) into eq. (14.18) yields

$$dP'_e = \frac{(dB/dt)^2 (2x)^2}{2\rho/dx} = \left(\frac{dB}{dt}\right)^2 \frac{2x^2}{\rho}\, dx \quad \text{watts} \tag{14.19}$$

and P'_e is equal to

$$P'_e = \left(\frac{dB}{dt}\right)^2 \frac{2}{\rho}\left(\int_0^{t/2} x^2\, dx\right) = \left(\frac{dB}{dt}\right)^2 \frac{t^3}{12\rho} \quad \text{watts} \tag{14.20}$$

The volume of the rectangular prism, shown in Fig. 14.4, is equal to $t \times 1 \times 1 = t$, meters^3. Accordingly, the eddy-current loss per unit volume is equal to

$$P_e = \frac{P'_e}{t} = \left(\frac{dB}{dt}\right)^2 \frac{t^2}{12\rho} \quad \text{watts/meter}^3 \tag{14.21}$$

If the flux change is sinusoidal, then

$$B = B_m \sin \omega t \quad \text{webers/meter}^2 \tag{14.22}$$

and

$$\left(\frac{dB}{dt}\right)^2 = B_m^2 \left(\frac{d \sin(\omega t)}{dt}\right)^2 = \omega^2 B_m^2 \cos^2 \omega t \quad \text{volts}^2 \tag{14.23}$$

However, the mean value of $\cos^2 \omega t$ over a cycle is equal to 0.50. Then eq. (14.21) becomes

$$P_e = \frac{\pi^2 f^2 B_m^2 t^2}{6\rho} \quad \text{watts/meter}^3 \tag{14.24}$$

The dimension t corresponds to the thickness of the sheet used for the laminations and it is apparent from eq. (14.24) that the thickness of the steel sheet should be kept to a minimum to limit eddy-current loss. Also, as mentioned earlier, the steel resistivity ρ should be a large value, to reduce the magnitude of eddy currents. This is accomplished by alloying 1.0 to 3.0% of silicon with the iron, to form what is called "silicon steel." This has the adverse effect of slightly reducing the permeability of the steel, but such an effect is outweighed by the significant reduction in losses in most cases.

The flux wave tends to be somewhat flattened relative to the magnetomotive-force wave, due to saturation. Thus, theoretically, eq. (14.24) should be multiplied by the square of the ratio of the form factor of the actual flux wave to the form factor (1.11) of a sine wave. From a practical standpoint, though, this is not usually done, as eq. (14.24) gives a value of P_e that is generally too low, for other reasons, and the values of both P_e and P_h are determined by test. This is because the rate of change of B, with respect to time (i.e., dB/dt) is greater than ωB in certain localized areas, as the domains change their magnetic moment alignment in order to reorient with the changing magnetic field. Thus, in practice, eddy-current as well as hysteresis loss is determined by test, usually conducted by the steel supplier at a specific value of flux density and at a specific frequency, such as 60 Hz. The two losses may be added together to give the fundamental core loss. However, they can be separated, since eddy-current loss varies as the second power of f, whereas hysteresis varies as the first power of f. In any case, eq. (14.24) is a valid equation to show the specific variables and their exponents which affect eddy-current loss.

Most of the discussion above concerning eddy-current loss, as well as that concerning hysteresis loss, applies specifically to the stator core and only generally to the rotor core. The rate of mutual-flux change in the stator core is equal to line frequency f, whereas it is equal to slip s multiplied by line frequency f to give sf in the rotor core. Thus except for wound-rotor motors, which may be required to operate for extended periods with relatively high rotor-circuit frequency, the fundamental component of core loss is small in the rotor core. However, harmonic flux waves which pass by the rotor surface cause a component of core loss called the rotational component which affects the rotor teeth as well as the stator teeth. This is discussed in Section 14.7.

14.7 NO-LOAD CORE LOSS

No-load core loss is equal to the total losses of the machine, operating at no-load, full-speed, and rated-voltage conditions, less the friction and windage losses and the no-load I^2R losses. It consists of the following components:

1. Fundamental core loss
   a. Hysteresis loss
   b. Eddy-current loss
2. Rotational core loss
   a. High-frequency rotor-surface and stator-surface losses
   b. High-frequency rotor-tooth and stator-tooth pulsation losses

The fundamental core loss, consisting of hysteresis loss and eddy-current loss, has been covered in Sections 14.5 and 14.6, and the expressions which give the variables that affect these two losses are given in eqs. (14.13) and (14.24), respectively. As mentioned previously, both hysteresis-loss and eddy-current loss data, in terms of watts per unit volume or watts per unit weight at a given value of B_m, are usually provided by the suppliers of magnetic steel. These data can also be provided by some number of independent testing laboratories from samples of magnetic steel taken from the user's stock. The fundamental component of core loss is then equal to

$$(CL)_f = K_t V_t (P_{ht} + P_{et}) + K_c V_c (P_{hc} + P_{ec}) \quad \text{watts} \tag{14.25}$$

where

K_t = empirical fundamental tooth factor, which is close to 1.0, dimensionless
V_t = volume of stator teeth, meters^3, centimeters^3, or inches^3
P_{ht} = hysteresis loss/unit volume in the stator teeth, based on stator-tooth maximum flux density, watts/meter^3, watts/centimeter^3, or watts/inch^3
P_{et} = eddy-current loss/unit volume in the stator teeth, based on stator-tooth maximum flux density, watts/meter^3, watts/centimeter^3, or watts/inch^3
K_c = empirical fundamental core factor, which is close to 1.0, dimensionless
V_c = volume of stator core, meters^3, centimeter^3, or inches^3
P_{hc} = hysteresis loss/unit volume in the stator core, based on stator-core maximum flux density, in watts/meter^3, watts/centimeter^3, or watts/inch^3
P_{ec} = eddy-current loss/unit volume in the stator core, based on stator-core maximum flux density, watts/meter^3, watts/centimeter^3, or watts/inch^3

Equation (14.25) is based on using hysteresis and eddy-current loss data, expressed in terms of watts/unit volume. Obviously, the same results would be obtained if P_{ht}, P_{hc}, P_{et}, and P_{ec} were expressed in terms of watts/kilogram, watts/gram, or watts/pound, and if V_t and V_c were expressed in weight terms of kilograms, grams, or pounds of tooth and core material. The factors K_t and K_c would, ideally, be equal to 1 in each case. Standardized hysteresis and eddy-current tests, such as the standard Epstein test, do not exactly duplicate operating conditions for a wide span of induction motor ratings. Thus K_t and K_c allow for minor empirical adjustments that might be required in order to correlate test results performed on the machine with loss data provided by the steel suppliers. However, for such correlation to be meaningful, the rotational component must first be added to the fundamental component of no-load core loss to give the total no-load core loss.

Let the stator-winding resistance/phase of a typical polyphase induction motor be measured accurately. Then let the machine operate at full-speed, no-load conditions while accurately measuring and recording stator current/phase and total input power at a specific value of stator voltage. Also, let these measurements be repeated from a low value of stator voltage to a value in the region of 1.25 of rated voltage. If the resulting total input wattage is plotted against stator voltage on linear graph paper, the watts will increase as a power function of voltage (approximately the second power). The intercept of the curve with the wattage axis obtained by extrapolating the plot gives the friction and windage losses of the machine. If voltage raised to the second power is plotted against wattage on linear graph paper, the resulting curve is essentially a straight line, and such a technique may result in a more accurate determination of the intercept and hence of friction and windage losses. Then let the friction and windage losses and the stator no-load-rated-voltage I^2R loss, adjusted to the temperature of the winding during test, be subtracted from the total input power to the machine at rated voltage. The result is the no-load core loss of the machine. This value of no-load core loss is considerably in excess of the fundamental component of core loss as determined by eq. (14.25). The difference, which is called the rotational component of no-load core loss, is frequently equal to, or in excess of, the fundamental core loss.

The rotational component of no-load core loss results from harmonic fluxes which are present in the air gap at no-load conditions. The current flowing in the stator winding at no-load conditions is essentially all magnetizing current, with a small component of in-phase current which sustains friction and windage and I^2R losses. As discussed in Chapter 12, the stator current is confined to a discrete number of coil sides located in slots, and is required to flow through coils which are connected in series to form phase groups. Such constraints on current flow result in a stepped magnetomotive-force wave similar to that shown in Figs. 12.2 and 12.3. The difference between the actual, stepped magnetomotive-force wave and true sine wave results in a series of traveling magnetomotive-force waves of odd harmonic order which are present in the air gap. These harmonic MMF waves, acting on the average air-gap permeance, produce corresponding traveling harmonic flux waves. Also, the presence of slot openings in the stator and in the rotor produce two effects. They are (1) to modulate the air-gap permeance and to produce permeance waves, as discussed in Chapter 12, and (2) to produce traveling slot-harmonic magnetomotive-force waves again, as discussed in Chapter 12. The slot-harmonic MMF waves also produce corresponding traveling harmonic flux waves. Thus there are a large number of traveling harmonic flux waves which pass the stator teeth and the rotor teeth.

The rotational component of no-load core loss is due primarily to the eddy currents set up in the tip region of the stator and rotor teeth and to additional losses in the teeth from pulsations resulting from the passing flux harmonics. There is also some loss which results from magnetic hysteresis in the rotor. From early in the twentieth century to the present, various engineers have analyzed the rotational component of core loss. Although there is general agreement on the variables involved, there is less than general agreement on the form the resulting equation should take. The essential result is that an empirical equation is developed by the particular organization that has a need for it, based on correlation of the pertinent design variables with test results. The pertinent variables, are the ratio of rotor-slot opening to air-gap length w_{20}/g, the ratio of stator-slot opening to air-gap length w_{10}/g, the number of stator slots N_1, the number of rotor slots N_2, the ratio of stator slots to rotor slots N_1/N_2, the maximum air-gap flux density B_g, the stator slot pitch τ_1, the rotor slot pitch τ_2, the air-gap length g, Carter's coefficient K_f, the resistivity of magnetic steel ρ_1 and others. That so large a number of variables should be involved is not surprising. The surprising fact is that considering the large number of variables that are involved, a workable empirical equation can be formulated which will give reasonable results. Since most of the organizations that have formulated these equations have not published them, it is not appropriate to give examples of the final form of such equations.

14.8 LOAD LOSS

Assume that the core loss and friction and windage losses of a polyphase induction motor have been determined accurately from tests, as discussed above. Let rated voltage be applied to the stator winding and let the connected load be such that it is exactly equal to the rating of the machine. Under such rated-load conditions, let the power input to the stator be measured accurately. Also, let the temperature of the stator and rotor windings be determined accurately by some means. With this information available, determine the sum of core loss, friction and windage losses, stator I^2R loss, and rotor I^2R loss, with the two I^2R losses being adjusted to correspond to the full-load operating temperatures of their respective windings. This sum of losses will then be found to be considerably smaller than the total power delivered to the stator less the total shaft power delivered to the connected load. This discrepancy in losses, which typically varies from 0.8 to 2.0% of the power rating of the machine, is called stray load loss or, more usually, load loss.

Adequate attention must be given to load loss when planning a line of motors or when designing a special one, to avoid undesirable surprises in the resulting heating and efficiency of such motors. The art and science of designing rotating electrical machinery had not progressed very far during the first part of the twentieth century before the phenomenon of load loss was recognized and its fundamental cause was understood in a general way. To allow for its anticipated effect on heating, efficiency, and power factor, a value equal to a fixed percentage of the machine's power rating, such as 1.0%, was assigned to this loss at the design stage. As might be expected, this practice became increasingly unsatisfactory, particularly for larger power ratings, as customers' expectations increased. The specific design variables soon came to be recognized, and by midcentury various electrical manufacturers were able to correlate their individual test results with empirical equations that involved these variables. Thus in a way similar to that done for the rotational component of no-load core loss, discussed in Section 14.7, acceptable values of load loss can be determined by use of empirical equations which are calibrated by test results. This similarity should be expected, since both core loss and load loss are related phenomena associated with the stator and rotor magnetic cores and their windings and are affected by the same design variables.

When a motor is operating at no-load conditions, stator current is essentially equal to magnetizing current, with a small component of in-phase current associated with the no-load losses of the machine. Thus the various air-gap flux harmonics which cause no-load core loss are based on these components of stator current. At full-load conditions the magnetizing component of current is essentially unchanged, but the in-phase component will have increased by an order of magnitude or more. Thus the harmonic fluxes that cause load loss are sustained by the load component of current. For the most part, these harmonic fluxes are the air-gap leakage fluxes produced by the stepped magnetomotive-force wave as increased load current flows through the windings of the machine. These harmonic fluxes produce losses on, or near, the surface of the stator and to a greater extent, rotor teeth, which are called surface load losses. Also, the harmonic fluxes produce pulsation losses within the rotor teeth and, to a lesser extent, within the stator teeth, which are called tooth-pulsation load loss. Both surface load loss and tooth-pulsation load loss are, in effect, high-frequency core losses.

Flux pulsations associated with tooth-pulsation losses will induce high-frequency voltages in the rotor winding and, to a lesser extent, in the stator winding. Corresponding high-frequency eddy currents will then flow in the copper as these currents try to oppose, and to nullify, the flux pulsations. The I^2R losses associated with such high-frequency eddy currents contribute to load loss. The rotating flux field associated with end-turn leakage flux can also induce fundamental-frequency voltages in metallic machine parts which are in close proximity, such as end shields and air deflectors. The I^2R losses of the resulting current in these parts also contribute to load loss.

The design variables that affect load loss are essentially the same ones that affect no-load core loss. They include air-gap length g, air-gap fringing factor K_f, ratio of rotor-slot opening to air-gap length W_{02}/g, ratio of stator-slot opening to air-gap length W_{01}/g, stator slot pitch τ_1, rotor slot pitch τ_2, number of poles p, number of stator slots N_1, number of rotor slots N_2, ratio of stator slots to rotor slots N_1/N_2, and a few others. The ratio N_1/N_2 is an important and sensitive design variable such that the losses increase rapidly as the ratio varies from a value near 1.0. This can be understood by remembering that N_1 relates to the stator slot pitch and that N_2 relates to the width of the rotor tooth tip. It is good design practice from the standpoint of load loss as well as of core loss to keep the ratio of N_1/N_2 within the limit of 0.83 to 1.20 if possible. Unfortunately, there are other design considerations, such as magnetic noise and perturbations on the speed-torque curve considered in Chapter 12, which may be affected adversely if the ratio N_1/N_2 is close to 1.0. As is typical of the design process, a balance must be achieved between the two opposing requirements.

In common with the rotational component of core loss, empirically determined load-loss equations, which correlate test results with design variables, are not generally available to the public domain. However, there should be no reason for customers or field application engineers to need such proprietory equations when applying, or using, original equipment. If, however, the stator of a given machine is being rewound for a different speed, or if the original rotor is being replaced with another one which has a different number of slots, there is a sound engineering reason to consider the effect of this change on load loss as well as on core loss. For such infrequently encountered cases, the customer or the repair shop should contact the manufacturer of the motor, giving the model number and the serial number, and should request all information that might be required for the modification, such as the effect on core loss and load loss. If the motor manufacturer requests payment for such a service, as he could reasonably be expected to do, the customer or the repair shop should accept these charges as appropriate for this type of service. In any case, such a charge is equivalent to a low-cost insurance policy for what otherwise could be a failed project if subsequent preventable problems should arise.

14.9 CORE STRUCTURE

14.9.1 Producing the Punching

It was shown in Section 14.6 that eddy-current loss varies as the second power of the thickness t of the core material, where t is measured in the axial direction of the core of the motor. Thus it was determined early in the history of induction motor production, as well as of other electrical machine productions, that magnetic cores with alternating flux should be built up from a large number of magnetic-steel laminations, with some amount of electrical insulation present on the contact surface between laminations. The usual practice is to use sheet steel with a thickness of from about 0.35 mm to about 0.65 mm or from about 0.014 in. to about 0.026 in. One circle of the lamination is formed (1) by several equal segments which form a complete circle, or (2) by one uninterrupted circle of steel. For both cases the individual piece is called a blank if the slots have not yet been formed, and a punching if the slots have been formed. For case 1, the piece is called either a segmental blank or a segmental punching, and for case 2, it is called either a single-segment blank or a single-segment punching. Single-segment punchings are used for most rotor cores as well as for small stator cores. Segmental punchings are used for essentially all medium-sized and large stator cores, in order to reduce the scrap ratio.

Punchings are produced on a punch press capable of developing sufficient force, using the specific shearing die for the blank or slot desired. The die used to produce blanks is called a blanking die, and the one used to produce slots is called a slot die. If the slots are produced one or so at a time, the slot die is called an index die (see Fig. 14.5). If, on the other hand, the blank and slots are both produced in one simultaneous punch-press operation; the combined die is called a compound die. Dies are made from alloy steel of very high physical strength and must be held to very close dimensional tolerances. Thus the production of dies is an expensive and time-consuming operation, and this is particularly true of a compound die. However, such a die significantly reduces the per unit shop cost and cycle time of producing punchings. Accordingly, compound dies are generally used for designs for which high volume is anticipated, whereas index dies are used for designs for which the volume is expected to be less.

A punch press operates by feeding sheet steel between the bottom member and the top member of the die set and then applying a force to shear the steel. The cut is a clean shear for 60 to 90% of the thickness of the cut and is a tear for the remaining 10 to 40%. The amount of tear is a function of the metallurgy of the steel and of the sharpness of the die set, since the quality of the shearing operation will very gradually deteriorate from one die sharpening to the next. Thus all punchings will have some amount of miniature burrs along the cut line, as well as mechanical stresses within

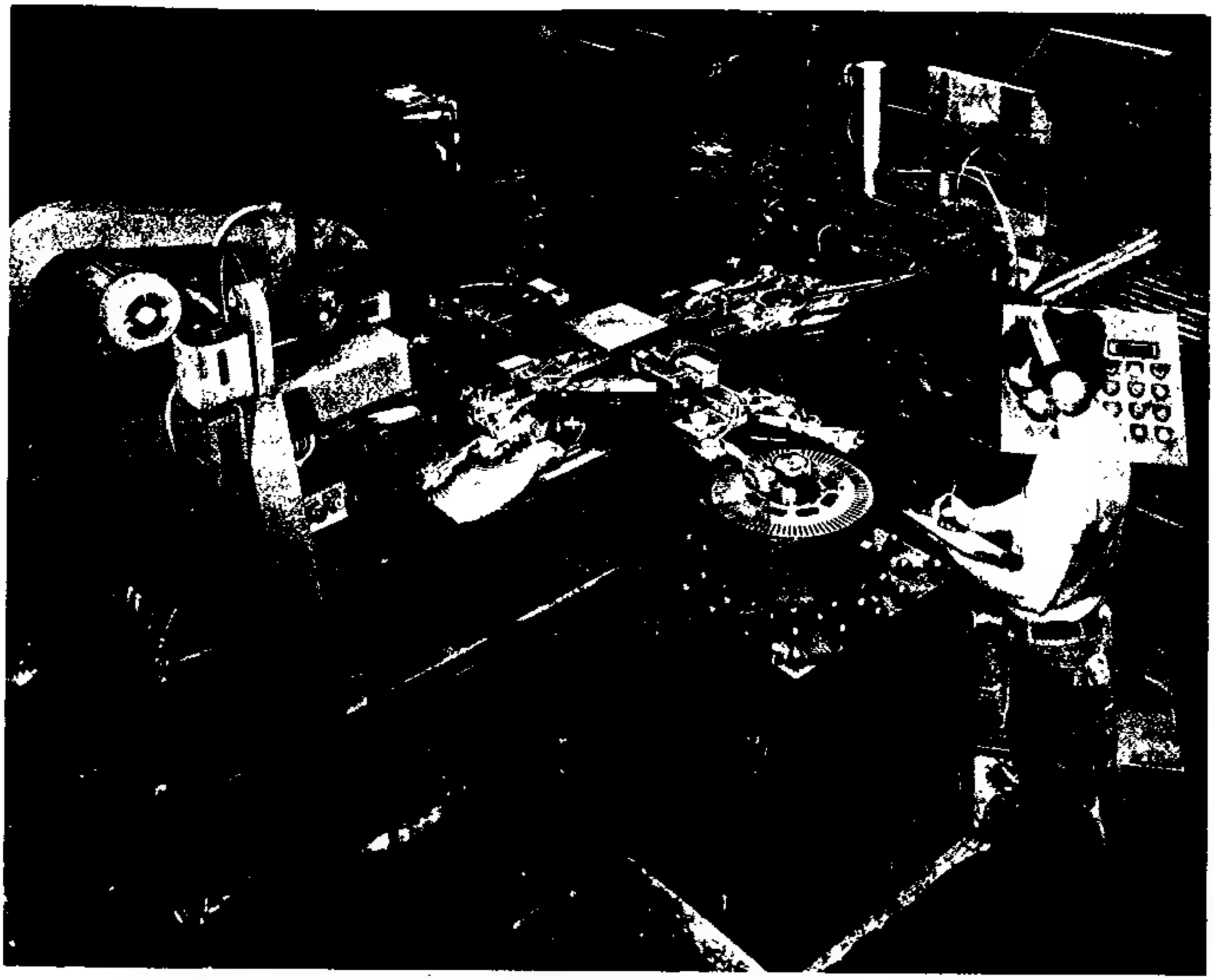

FIGURE 14.5 Automatic indexing punch press producing rotor punchings.

the material in the vicinity of the edges of the workpiece. The burrs will to some extent result in short circuiting of the insulation between punchings, causing more losses in the core, such that the original purpose for using thin laminations is, to a corresponding extent, nullified. Burrs can, to a significant extent, be removed by subjecting the punchings to a burr-removing operation, such as a rotary brush with strong wire bristles being passed over the punchings, particularly in the slot region. The residual stresses resulting from the punch-press operation will also increase the losses in the core if they are not removed. Such stresses can be greatly reduced by stress-relief annealing the punchings in an annealing oven at an appropriate time-temperature cycle. The operations of burr grinding and of stress-relief annealing add to the cost and cycle time of producing punchings, of course. Accordingly, these processes are not used for all designs of induction motors. However, the additional cost of either or both is not a very large percentage of the total cost of producing a laminated core structure and should be used when economically beneficial. The additional losses resulting from short-circuiting burrs and from unrelieved shearing stresses occur in the slot and tooth portion of the punching, thus affecting the temperature rise of the stator winding. More output per unit volume is usually possible if the punchings are free of burrs and of residual stresses, particularly for medium-sized and large machines.

14.9.2 Producing the Core

Single-segment punchings are used for the rotor and stator cores for most small induction motors and, frequently, the center scrap, which results from producing the stator punchings, provides the material for the blanks for producing the rotor punchings. However, as the size of the unit increases, the economics that support this practice tend to change. Because of centrifugal force and in some designs, for other reasons, it is desirable to utilize single-segment punchings for rotors to the maximum extent possible. However, since the fundamental component of core loss is very low in the rotor, except for some wound-rotor motors, lower-cost sheet steel can be used for rotor cores than for stator cores. Thus a point is reached at which it is economically desirable to use separate grades of steel for rotors and for stators. Then, to reduce the scrap ratio of the stator-core steel, it is necessary to use segmental punchings that lend themselves to "nesting" (i.e., fitting together in such a pattern as to give a minimum of scrap to usable steel). Accordingly, essentially all medium-sized and large stators utilize segmental punchings.

For optimum scrap ratio, the number of segments per circle is obviously a function of the ratio OD/ID of the stator punching. In turn, this ratio is a function of the number of poles, and the combination of these effects could result in a large number of possible segments. However, there are other economic reasons for standardizing the number of stator punching segments per circle across a product line. Some of these reasons are (1) standardization in the number of stator frame ribs which mate with the stator core, (2) standardization in the number of axial prewound-core straps, (3) standardization in methods and procedures, and (4) standardization in equipment in some cases. The result is that most segmental punchings practices are standardized across a product line. Typically, six segments per circle are used as standard, although other numbers of segments are also used.

With six punching segments per circle, there are obviously six joints between the segments around the circle. As the core is stacked, the beginning point of each successive layer of punchings should be rotated so that the joints between segments do not fall on top of the joints of the layer beneath it. This is done to maximize the strength and to minimize magnetic dissymmetries of the core, discussed further in Section 14.9.5. However, the procedure for segment rotation must be coordinated with standardization of the number of frame ribs and/or the number of axial straps of the prewound core. This is necessary because each punching has a mating seat punched on its OD to accommodate the frame rib or the prewound-core strap.

Figure 14.6 shows a symmetrical and an asymmetrical, or offset, arrangement, both of which can be used with a 60-degree punching segment. As the punching segments are stacked around the circle, the mating seats on the OD and the slots on the ID must be kept in alignment. Use of the symmetrical arrangement shown in part (a) of the figure will permit 12 joints between segments, equally distributed throughout the core. This is accomplished by starting the second layer of punchings at a point which is advanced 30 degrees beyond the starting point of the first layer. The third layer of punchings is then started at a point which is advanced 30 degrees beyond the starting point of the second, and so on. Use of this symmetrical arrangement of the seat is simple and, accordingly, it is frequently used. However, it permits only 12 joints with the 60-degree segment. Use of the asymmetrical arrangement shown in part (b) of the figure will permit 24 joints between segments, equally distributed throughout the core. Starting with side A of the punching on the left-hand side as shown in the figure, and proceeding in a clockwise direction, the first circle is completed. The starting point of the second layer is advanced 15 degrees clockwise beyond the starting point of the first layer. However, the punching is "flopped" (i.e., it is rotated such that side B is on the left-hand side) before it is applied. The starting point of the third layer is advanced 15 degrees clockwise beyond the starting point of the second layer. For this layer the punching is applied with side A on the left-hand side. The starting point of the fourth layer is advanced 15% clockwise beyond the starting point of the third layer, and for this layer, the punching is again flopped before it is applied. This stacking pattern is repeated until the desired core length ℓ_c has been achieved. Since the starting point of each layer is advanced 15 degrees, this pattern will give 360/15 = 24 joints, which will be equally distributed throughout the core structure. Figure 14.6 shows a six-segment punching, and the discussion above is based on such a configuration. However, the concept is applicable to other numbers of segments.

The condition imposed on the slots and teeth must also be fully considered when segmental punchings are designed and used. If, for example, the number of stator slots N_1 is equal to 72, there are 360/72 = 5 degrees between slots and 12 slots for each 60-degree segment. There will be as many teeth as there are slots, so that each segment will also have 12 teeth. It is generally considered undesirable to have the joint, or the edge of a segment, fall within the limits of a tooth, and such an occurrence results in what is called a "tooth sliver." For the example above, the slot positions relative to the edges of the 60-degree punching can be set up in such a way as to avoid tooth slivers, using the punching seat pattern shown in either part (a) or part (b) of Fig. 14.6. However, for some values of stator slots N_1, tooth slivers will occur. Consider the ratio

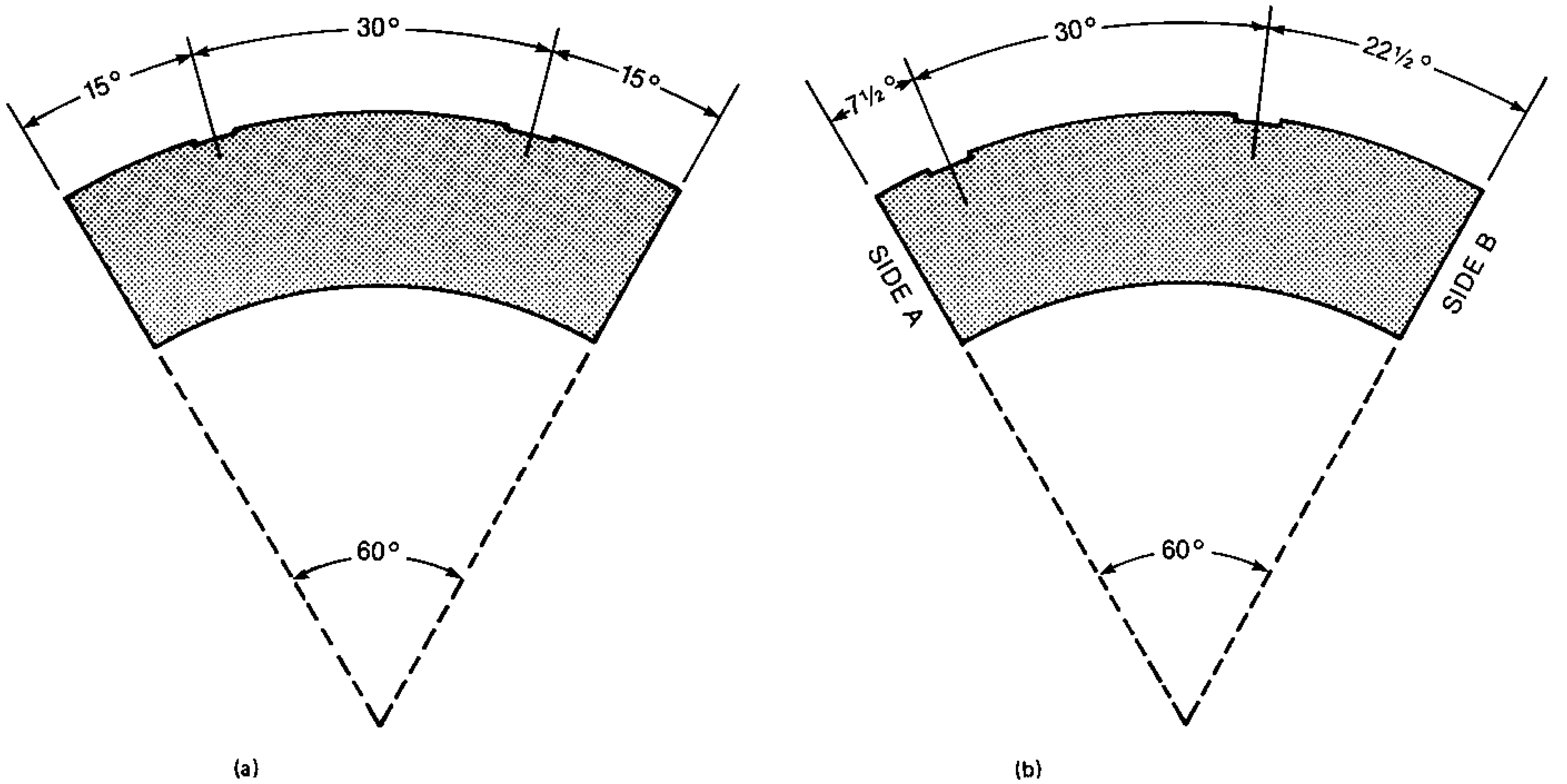
15°
30°
15°
60°
(a)
7½°
30°
22½°
SIDE A
SIDE B
60°
(b)

FIGURE 14.6 Angular positions of mating surfaces of punching, which accommodate frame ribs: (a) symmetrical rib seat; (b) asymmetrical rib seat.

$$\frac{N_1}{\text{number of segments/circle}} = I \quad \text{numeric} \tag{14.26}$$

If I is an even integer and is divisible by 4, the 7 1/2°-60°-22 1/2° pattern can be used, without causing tooth slivers, on a 60-degree segment. If I is an even integer and is not divisible by 4, the 7 1/2°-60°-22 1/2° pattern can be used, but tooth slivers may result. On other hand, the 15°-30°-15° pattern can be used for any case for which I is an integer, even or odd. However, use of the 15°-30°-15° pattern will result in a higher probability of magnetic dissymmetries, the effects of which cannot be ignored for larger machines. This subject is considered in Section 14.9.5

As discussed previously, the use of prewound stator cores offer advantages over stack-in-frame stator cores and some motor manufacturers use such construction to the maximum extent possible. For this construction, the stator core consists of a steel end plate on each end of the core, with the punchings being held between the two end plates by high compression. The compressive force between laminations is maintained by axially placed steel straps, located around the OD of the core, which mate with corresponding punchings seats, also located around the OD of the core. These axial straps are welded to the end plates, while the core is positioned around a central arbor and is under significant pressure, produced by a hydraulic press. Figure 14.7 shows a medium-sized prewound core with the arbor still in place but with the hydraulic press removed. An average retained interlaminational pressure of about 100 N/cm^2, or about 150 lb/in.^{2}, is desirable and this can usually be accomplished without any difficulty. For medium-sized to large machines, radial air ducts are located every 3 to 5 cm along the core. Such air ducts are from 6 to 10 mm wide in the axial direction, and are formed by inserting spacers, such as I-shaped straps of metal, positioned in a radial direction and welded to a circle of punchings at the appropriate locations. The space blocks are progressively inserted as the core is stacked. A medium-sized two-pole prewound stator with air ducts is shown in Fig. 14.8, and a small prewound stator core without air ducts is shown in Fig. 14.9.

If a prewound stator core is not used, the stator punchings are stacked directly into the frame. The frame will have been machined by having a fit turned on the ID of its axial ribs to receive the OD of the punchings. In addition, a circumferential key groove will have been turned near each end of the ribs, to accept the keys, which are located on the outboard sides of the two end plates and which retain the interlaminational pressure of the core. The machined frame ribs jointly act as an outside stacking mandrel against which the OD of the punchings seat. Otherwise, much of the information above concerning prewound-core stacking applies to stacking within the frame.

As noted earlier, most rotor cores are built up from single-segment punchings because of centrifugal-force considerations. Twenty-five years ago, essentially all medium-sized and large induction-motor rotors were

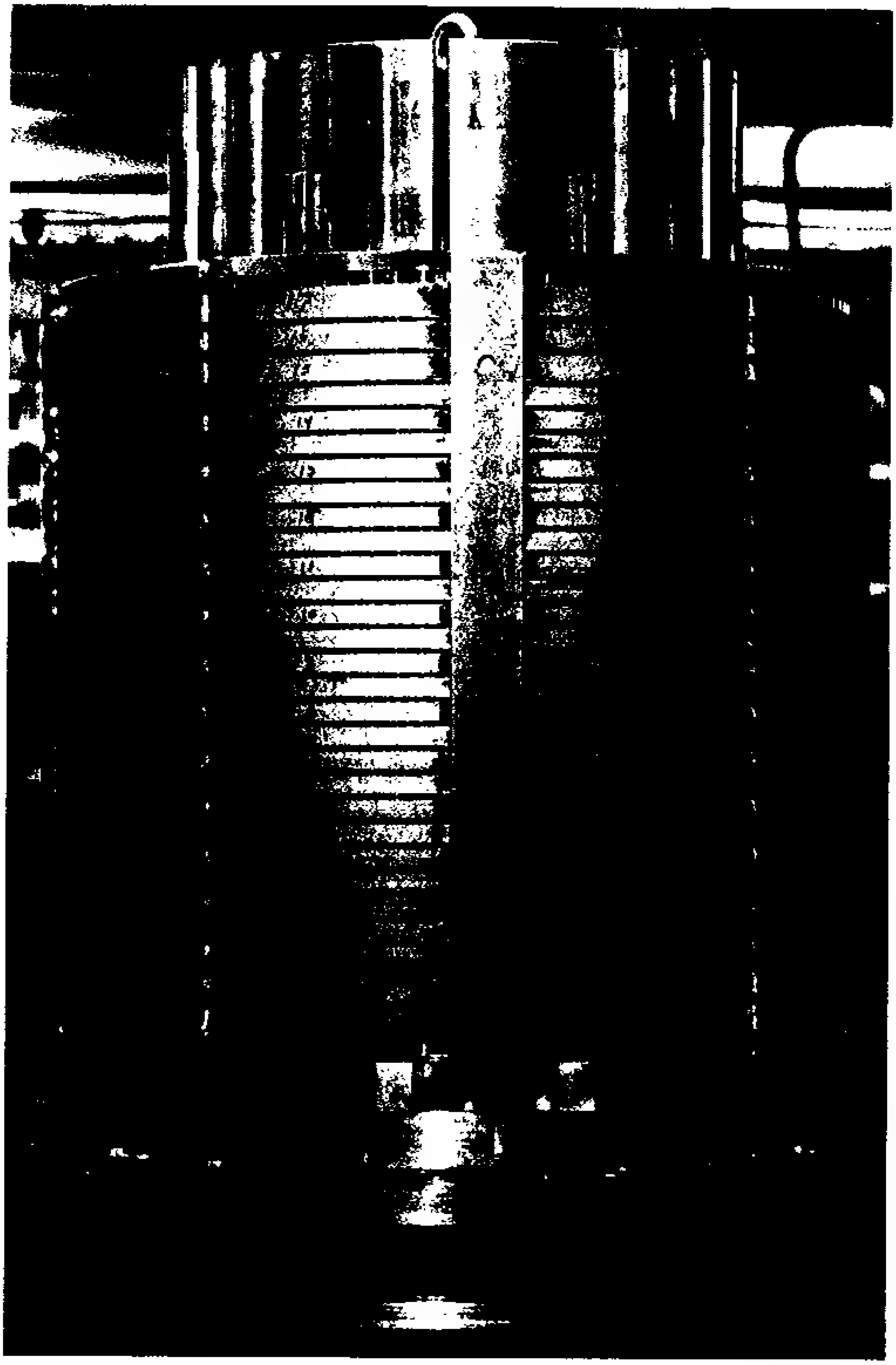

FIGURE 14.7 Medium-sized prewound core positioned around a stacking mandrel.

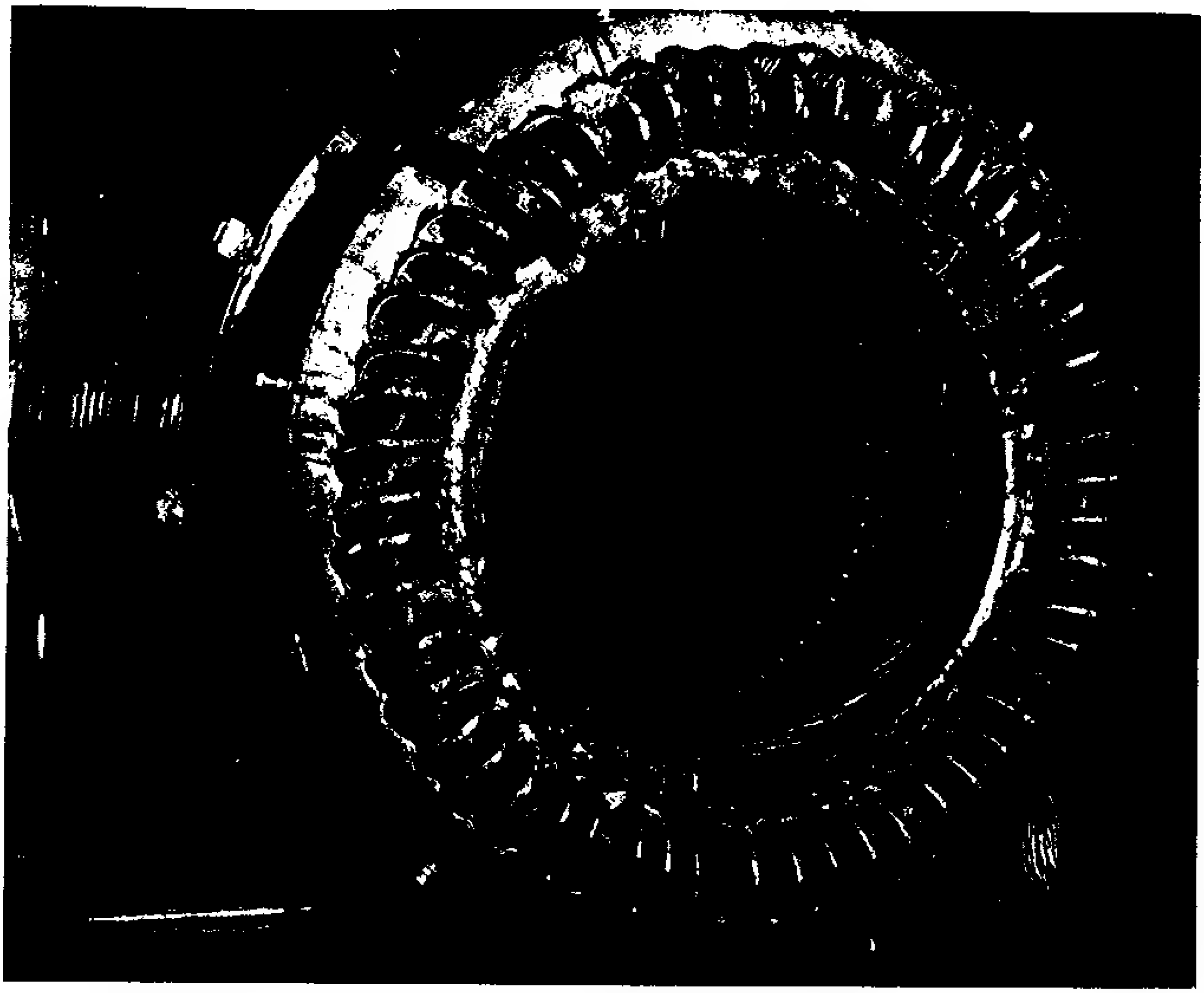

FIGURE 14.8 Medium-sized two-pole prewound stator core with radial air ducts.

stacked on an intermediate structure, called a "spider." The spider, which carried the rotor core, was then located over the shaft with a close fit. For the past 25 years, the design trend has been to eliminate the spider and to stack the punchings directly onto the shaft. Because of the small amount of fundamental core loss in the rotor core relative to the stator core, a lower grade of steel is used for rotor punchings. Also, since most rotor designs use single-segment punchings, there is available steel within the punching to replace the cast iron or steel of the spider. Further, if it were not so used, it is probable that the center steel from the rotor punching, which is called the "cookie," would be discarded as scrap. The rotor punchings shown in the punch-press operation in Fig. 14.5 are single-segment punchings that will be stacked directly onto the shaft. Figure 10.5 shows a completed rotor which also utilizes this type of punching.

14.9.3 Interlamination Resistance and Ring Testing

As discussed in Section 14.6, it is necessary to laminate magnetic cores of polyphase induction motors and to provide some amount of insulation on the surface of the steel laminations. Until about the middle of this century, this was accomplished by applying various formulations of organic varnish. Although the varnish buildup could be controlled to some extent by controlling the viscosity of the varnish, the buildup was typically in the range 0.012 to 0.018 mm (or 0.0005 to 0.0007 in./side). However, some buildups exceeded this range. For punchings with a thickness of 0.5 mm (0.020 in.) and using a conservative value of varnish buildup of 0.015 mm, the buildup would constitute about (2)(0.015)/0.5 = 0.06 per unit, or 6%, of the overall core length, not including radial air ducts. This amount of buildup corresponds to (0.06)(40) = 2.4 cm, for a 40-cm solid stack length, or to approximately 0.90 in. for a 15-in. solid stack length.

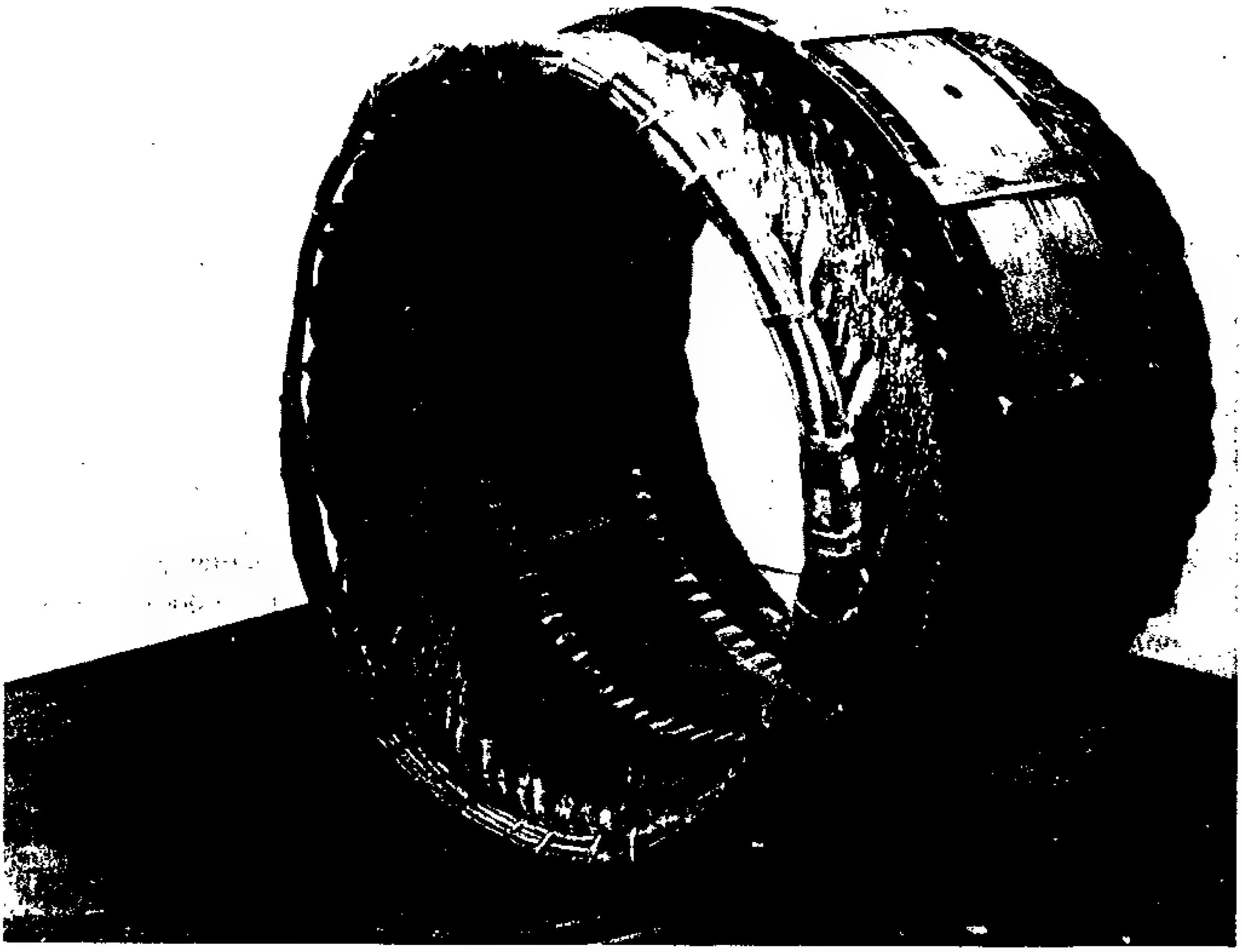

FIGURE 14.9 Small prewound core without radial air ducts.

The operating temperature of the core is a maximum in the region of the stator teeth and of the tips of the rotor teeth. Continued exposure of the punching varnish to temperatures equal to or in excess of 100°C tended to deteriorate the varnishes to some degree. Initial deterioration caused the punchings to lose some of their interlaminational pressure in the tooth region. As this effect progressed, the teeth would tend to loosen. This, in turn, had an unfavorable mechanical effect on the coil insulation in direct contact with the teeth, as might be expected. Also, as the varnish deteriorated, the interlaminational resistance decreased, causing an increase in heating from eddy currents. This, of course, caused a corresponding deterioration in the stator-coil insulation. Although most of the concern has been directed at the tooth region of the stator core, because of the proximity of the stator-coil insulation, similar conditions also developed in the yoke region of the core in some cases. From the 1950s on, the industry has been replacing organic varnish with inorganic materials for treatment of the punching surfaces. In some cases the material is applied at the mill, and in other cases it is applied by the motor manufacturer. In general, use of the more recent core-plating materials has significantly improved the interlaminational resistance of cores. This has resulted in some of the earlier problems being correspondingly reduced, although not totally eliminated.

Because of concern for the gradual deterioration of interlaminational insulation with time, and because of occasional mechanical damage to the stator core, a technique has been developed to check the quality of insulation between stator punchings in a general way. This technique is called a "ring test." The test, which is normally conducted in the field, consists of removing the rotor from the stator and then of wrapping a given number of turns of suitable cable around the yoke of the stator core to form an improvised coil which encircles the stator core in a radial plane. To accomplish this, the cable is threaded through the stator bore and around the back of the core yoke to form the turns of the coil. Sufficient voltage at rated frequency is then applied to the coil to produce the desired value of ampere turns. The desired value of ampere-turns is that amount which will produce a value of flux ϕ, with a flux density B, in the yoke portion of the core, equal to that under normal operating conditions.

The test is continued for sufficient time to permit the core to reach a stabilized temperature. The stator bore, as well as the back of the core, if it is accessible, is carefully scanned by means of an infrared heat indicator to determine if any core hot spots are present. As a precaution, the heat indicator should be used intermittently during the early part of the test to prevent any localized hot spot of severe intensity from developing. Field experience has shown that this test is very effective in determining if hot spots exist in the yoke portion of the core, as might be expected. Field experience has also shown that it is effective in determining if hot spots exist in the tooth portion of the core.

14.9.4 Numerical Example of a Ring Test

The application of a ring test to a stator core is best illustrated by a numerical example. The motor used for the example will be the three-phase 60-Hz 2300-V eight-pole 1000-hp induction motor, with parameters as described in Section 13.14.1 and in Fig. 13.15. Since dimensions are given in inches in Section 13.14, similar dimensions will be used in this example. For this machine, the depth of the stator core behind the slot, or the radial depth of the core yoke, is equal to

$$\text{radial depth of yoke} = \frac{\text{stator OD} - [\text{stator ID} + (2)(\text{stator slot depth})]}{2} \quad \text{inches} \qquad (14.27)$$

Substituting the appropriate quantities from Section 13.14 into eq. (14.27) yields

$$\text{radial depth of yoke} = \frac{34 - [26.4 + (2)(1.90)]}{2} = 1.90 \quad \text{inches} \qquad (14.28)$$

The solid length of the stator core is equal to

$$\text{solid stack length of core} = (\ell_c - \text{total axial air duct space})(0.95) \quad \text{inches} \qquad (14.29)$$

where the factor 0.95 is the stacking factor for the particular punchings used for the core. Again, substituting the appropriate quantities from Section 13.14 into eq. (14.29) gives us

$$\text{solid length of core} = [27 - (13)(1/4)][0.95] = 22.6 \quad \text{inches} \qquad (14.30)$$

The cross-sectional area of the yoke, or the cross-sectional area of the core, behind the slot is

$$\text{yoke cross-sectional area} = (\text{radial depth of yoke})(\text{solid length of core}) \quad \text{inches}^2 \qquad (14.31)$$

Then substituting eqs. (14.28) and (14.30) into eq. (14.31), we have

$$\text{yoke cross-sectional area} = (1.90)(22.6) = 42.9 \quad \text{inches}^2 \qquad (14.32)$$

The normal operating value of flux density B_{c1} in the yoke portion of the core for this design is

$$B_{c1} = 85.8 \times 10^3 \quad \text{maxwells/inch}^2 \tag{14.33}$$

If the actual value of B_{c1} cannot be determined, for a given field test, a reasonable value, in the range of 80,000 to 90,000 Mx/in.^{2}, or 1.25 to 1.40 Wb/m^2 should be assumed. The total circumferential flux, which is desired to be circulated around the yoke, from eqs. (14.32) and (14.33), is equal to

$$\phi = (B_{c1})(\text{yoke cross-sectional area}) = (85.8 \times 10^3)(42.9) = 3.68 \times 10^6 \quad \text{maxwells} \tag{14.34}$$

Using Faraday's law, in the form given in eq. (9.138), when ϕ is expressed in maxwells, the relationship between flux and voltage is

$$E = \frac{4.443 K_p K_d N_{st} f \phi_m}{10^8} \quad \text{volts/phase} \tag{14.35}$$

When performing the ring test, the only active winding is that produced by applying a voltage V at a frequency f to the circuit formed by wrapping N turns of the cable around the stator yoke. Then

$$V = \frac{4.443 N f \phi}{10^8} \quad \text{volts/coil} \tag{14.36}$$

where for conditions of the test it is considered that $K_p K_d = 1.0$. Solving for the number of turns N of the cable, which will be required at voltage V,

$$N = \frac{V \times 10^8}{4.443 f \phi} \quad \text{turns} \tag{14.37}$$

Using a single-phase voltage of 110 V at a frequency of 60 Hz, and using the value of ϕ calculated in eq. (14.34), we have

$$N = \frac{110 \times 10^8}{(4.443)(60)(3.68 \times 10^6)} = 11.2 \quad \text{turns} \tag{14.38}$$

Thus 11 turns of the cable, excited at 110 V, will be required to produce a yoke flux density which is equal to that which exists at normal operating conditions.

The current that flows through the improvised coil to produce the flux in the yoke is equivalent to the magnetizing current of an iron-core reactor. To determine the value of this current, the ampere-turns must first be determined. The magnetic field strength H, which corresponds to a flux density B of 85.8×10^3 Mx/in.^{2}, will depend on the specific steel used for the stator punchings of the motor being tested. For purposes of this illustration example, it will be assumed that a core flux density of 85.8×10^3 Mx/in.^{2} corresponds to a magnetic field strength of 12 A-t/in. The average circumferential length of the yoke is equal to

$$\text{average circumferential length of yoke} = (\text{stator OD} - \text{radial depth of yoke})(\pi) \quad \text{inches} \qquad (14.39)$$

Substituting the value of the stator OD from Section 13.14.1, and the value of the radial depth of the yoke from eq. (14.28) into eq. (14.39), we have

$$\text{average circumference of yoke} = (34 - 1.90)(\pi) = 100.8 \quad \text{inches} \qquad (14.40)$$

The total magnetomotive force M that is required to force the flux around the average circumference of the yoke is equal to

$$M = (H)(\text{average circumference of yoke}) \quad \text{ampere-turns} \qquad (14.41)$$

Then, using a value of H = 12 A-t/in. and substituting eq. (14.40) into eq. (14.41), the required magnetomotive force is

$$M = (12)(100.8) = 1210 \quad \text{ampere-turns} \qquad (14.42)$$

The magnetizing current is equal to

$$I = \frac{M}{N} \quad \text{amperes} \qquad (14.43)$$

Substituting eq. (13.38) rounded off to N = 11, and eq. (14.42) into eq. (14.43), we obtain

$$I = \frac{1210}{11} = 110 \quad \text{amperes} \qquad (14.44)$$

There will also be an energy component of current, of a few amperes, in quadrature with the exciting current I, which sustains the core loss in the yoke. However, this component of current will not significantly affect the value of I. Then the value of the volt-amperes required to perform the ring test is equal to

$$\text{exciting volt-amperes} = VI \quad \text{volt-amperes} \qquad (14.45)$$

Using the previously selected value of V = 110 V and the value of I as calculated by eq. (14.44) gives us

$$\text{exciting volt-amperes} = (110)(110) = 12,100 \quad \text{volt-amperes} \qquad (14.46)$$

Thus a single-phase transformer of at least 12 kVA capacity is required to conduct the ring test and to verify the condition of the stator-core interlaminational resistance.

14.9.5 Magnetic Dissymmetries and Resulting Shaft Voltages

In rotating electrical machines, a voltage can, and frequently does, appear along the shaft, as well as between the bearing journal of the shaft and its stationary bearing support. If this voltage is sufficient relative to the impedance of the bearing, measurable currents will flow through the bearing. These currents can be sufficiently large as to cause damage to sleeve bearings and to antifriction (ball and roller) bearings. Such flow of bearing current is prevented by inserting insulation between the bearing or bearing seat and the supporting structure (i.e., the bracket, end bell, end shield, or pedestal). The magnitude of shaft voltages is a function of various dissymmetries of the magnetic circuit and of the size of the machine. Thus to prevent shaft currents it is necessary (1) to minimize dissymmetries in the magnetic circuit at the design and manufacturing stage, and (2) to insulate the bearings of all machines above a given size.

There are three basic causes of the voltage above, which are (1) the flow of a unidirectional magnetic flux along the shaft and through the bearings, (2) the flow of an alternating magnetic flux along the shaft and through the bearings, and (3) the presence of an alternating magnetomotive force which links the shaft. Cause 1, due to the flow of unidirectional magnetic flux along the shaft and bearings, is produced by a unidirectional current linking the shaft of a dc machine such as can occur if the interpole connections are all in the same direction. This cause will not be considered further, since shaft voltages as they relate to induction motors are being addressed. Cause 2, due to the flow of an alternating magnetic flux along the shaft and bearings, is associated with spurious leakage flux, such as can occur on large two-pole motors, for example. Cause 3, due to an alternating magnetomotive force, which links the shaft, is the primary cause of shaft voltages in induction motors and is the cause considered below.

Magnetic dissymmetries in the core structure can arise from design features which are required for other reasons. As discussed in Sections 14.9.1 and 14.9.2, stator punchings are made in segments instead of complete circles for machines above a certain size. Thus there will be a gap between segments at each joint, and the reluctance of the gap is very much greater than an equal amount of steel punching. Depending on the ratio of segments to poles, the magnetomotive force required to force the mutual flux through the core path is not constant for all instants of time. This results in the magnetomotive force around the circle of the stator core not summing to zero at all instants of time. Such a condition is equivalent to having a net magnetomotive force around the circumference of the core, which varies with time. Since this alternating magnetomotive force links the shaft, it will induce a voltage in the shaft. Also, since the electrical circuit, consisting of the shaft, bearings, bearing support, and frame, is usually closed, current can flow through this circuit, including through the bearings.

Magnetic dissymmetries can also occur if the ratio $2N_1/p$ is an odd integer. They can also occur if the number of grooves punched into the OD of the stator core and used for mating seats does not have symmetry relative to the number of poles. Further, various manufacturing variations in the production of punchings, as well as efforts to correct manufacturing variations, such as turning or grinding the stator bore to "true up" a slightly eccentric stator ID, can result in magnetic dissymmetries. Regardless of its source, a magnetic dissymmetry can produce shaft voltage if it causes the magnetomotive force not to sum to zero around the circle of the stator core at all instants of time.

During the past century, most of the causes of shaft voltages associated with design parameters have been identified. Also, it has come to be recognized that as the size of the machine increases, spurious magnetic dissymmetries tend to increase. Accordingly, the following set of criteria are now generally accepted throughout the industry as being indicative of possible shaft voltage. Additional criteria are used occasionally, but they do not have the wide acceptance of the ones given below. If for design reasons, a given criterion cannot be avoided, the bearings should be insulated. These criteria are:

1. $\dfrac{\text{Number of punching segments}}{p} = \dfrac{3}{8}$, or $\dfrac{3}{4}$, or $\dfrac{3}{2}$
2. $\dfrac{2N_1}{p} = I$, where I is an odd integer
3. $\dfrac{(4)(\text{Number of punching segments})}{p} = I$, where I is an odd integer
4. $\dfrac{(2)(\text{Number of punching segments})}{p} = \dfrac{A}{B}$, where A is an odd integer,

   when the fraction A/B has been reduced to its lowest terms
5. All two-pole motors of approximately 1000 hp or greater
6. All induction motors of approximately 2500 hp or greater, for any number of poles

14.10 EFFECT OF SLOT AND AIR-DUCT OPENINGS AND THE USE OF CARTER'S COEFFICIENT

If the air-gap surface of the stator and the rotor were not interrupted with slot openings, the mutual flux lines which cross the air gap would be true radial lines, and the equipotential lines of the magnetic field would be true circles concentric with the stator ID and with the rotor OD. However, the stator slots and the rotor slots, as well as the radial air ducts, significantly distort the magnetic field of the air gap from this ideal geometric configuration. The ratio of the permeability of the steel punching to that of air is a very large number which for purposes of conceptual visualization, can be considered to be infinite. Thus the air-gap flux at the boundary between the steel and the air must enter the various punching surfaces at right angles to the steel. Also, the presence of the slots increase the air-gap reluctance in the region of the slot, thereby decreasing the flux density directly over the slot opening. The combination of the two factors above causes considerable fringing of the air-gap flux as it crosses the air gap. This, in turn, causes the air-gap flux to have a longer effective path than the actual mechanical gap between the rotor surface and the stator surface.

The mutual flux lines crossing the air gap and the magnetomotive-force equipotential lines in the air gap represent two sets of orthogonal trajectories from the viewpoint of complex-variable theory. That is, they always intersect at right angles within the region of the air gap, and thus they represent a Laplace region. Such a region is amenable to the powerful methodology available to complex-variable theory, including that of conformal mapping. At about the beginning of this century, Carter, a British engineer, used the concept of conformal mapping to determine the effective increase in air-gap length due to the aforementioned fringing effect of air-gap flux. It is not necessary to discuss conformal mapping to any significant extent at this point. It is only necessary to know that it consists of using a complex-variable equation, called a transformation equation, to transform from one coordinate plane to another. Such a transformation can result in a better understanding of flow phenomena, among other things. The particular transformation used by Carter was the Schwartz-Christoffel transformation.

In 1926, Carter presented an important paper before the Institute of Electrical Engineers in the United Kingdom. This paper covered earlier work, done at the turn of the century, as well as work done subsequent to that time. An important part of this paper concerned the fringing of air-gap flux due to slot openings, and the resulting increase in the average air-gap reluctance. Specifically, he showed that the effect of slot openings in either the stator or the rotor is described by the relationship

$$\sigma w = \frac{2}{\pi}\left\{ w \tan^{-1}\left(\frac{w}{2g}\right) - g \ln\left[1 + \left(\frac{w}{2g}\right)^2\right]\right\} \quad \text{meters} \qquad (14.47)$$

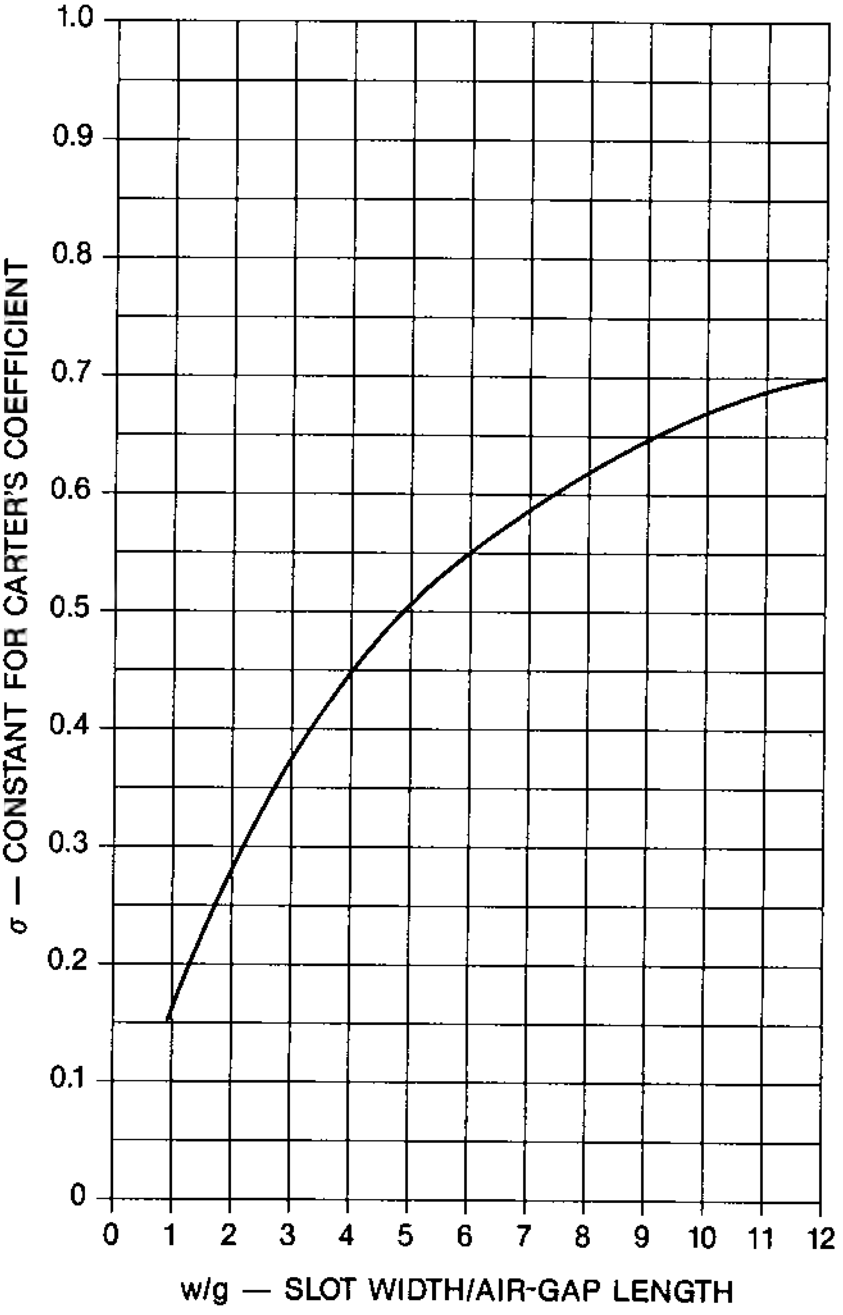

FIGURE 14.10 Carter's original curve of σ versus w/g.

where w is the width of the slot and g is the length of the air gap, with both in consistent units, and where σ is the per unit equivalent change in slot width. An increase in air-gap reluctance caused by flux fringing can be expressed as a decrease in effective area or as an increase in effective length. In his analysis, Carter converted the change in width dimension σw in eq. (14.47) to an equivalent increase in the length dimension. The equivalent relationship given by Carter is

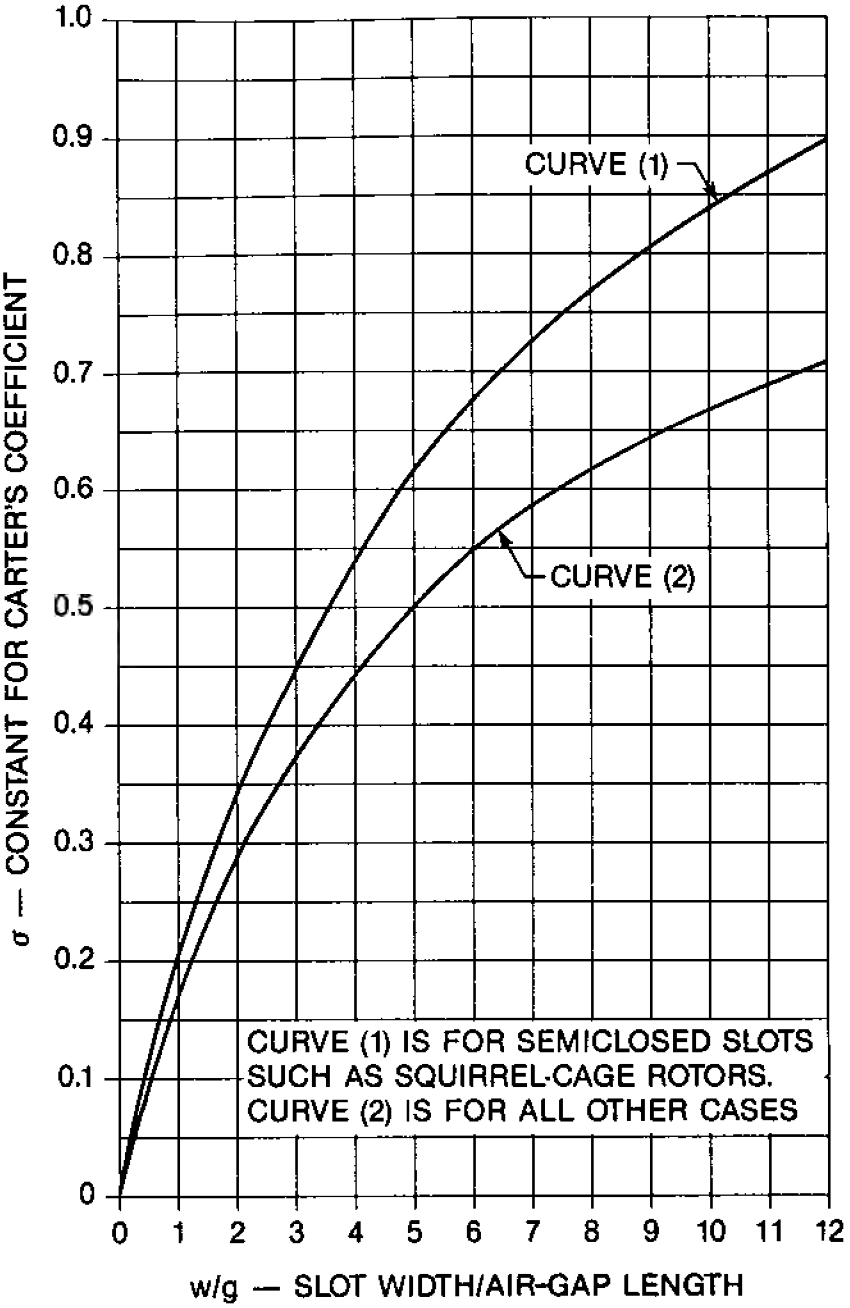

FIGURE 14.11 Typical curve of σ versus w/g.

$$\frac{t + w}{g'} = \frac{t + w - \sigma w}{g} \quad \text{numeric} \tag{14.48}$$

where t is the width of the tooth and g' is the effective length of the gap, with both expressed in the same dimensional units. Solving for g', we have

$$g' = \frac{t + w}{t + w - \sigma w}\, g \quad \text{meters} \tag{14.49}$$

Since t + w is equal to the slot pitch τ_s, eq. (14.49) can be written as

$$g' = K_f' g \quad \text{meters} \tag{14.50}$$

where K_f' is equal to

$$K_f' = \frac{\tau_s}{\tau_s - \sigma w} \quad \text{numeric} \tag{14.51}$$

The coefficient K_f is called Carter's coefficient, or the air-gap fringing coefficient, which must be determined and applied successively for the stator slots, for the rotor slots, and for the radial air ducts, to determine the total effective air gap.

If eq. (14.47) is divided by w, the result is that σ is expressed as a function of the slot opening w and the mechanical gap length g. This suggests that a curve of σ as a function of w/g could be plotted and then used repeatedly to calculate K_f. This is, in fact, what has been done. Carter's original curve of σ versus w/g as presented in his paper is shown in Fig. 14.10. Since Carter's original work, experience has indicated that his original curve should be somewhat modified to give more accurate results, in particular, for partially closed slots. This modification has been done at various times by various people over the ensuing years. The curves in Fig. 14.11 are typical of presently used curves, for which a modification has been made for the one used with semiclosed slots. Application of eq. (14.51) and of the curves in Fig. 14.11 will become apparent in Section 14.11 when it is used in calculating the magnetic circuit of an induction motor.

14.11 CALCULATION OF THE MAGNETIC CIRCUIT

14.11.1 Derivation of the Saturation Curves for Use with the Teeth and the Core Yoke

Neglecting the steps that result from the presence of slots, the wave shape of the magnetomotive-force wave is reasonably close to that of a sine wave, and this similarity increases as the ratio N_1/p increases. If there were no saturation in the ferrous portion of the mutual-flux path, the flux wave would, correspondingly, approach a sine-wave shape. However, some amount of saturation does exist in a typical polyphase induction motor, the usual amount accounting for from 10 to 20% of the total magnetizing ampere-turns. Such saturation has the effect of reducing the peak value of the flux wave. At an electrical angle of 0.929 rad, or 53.2 electrical degrees, however, the ordinate of the actual flux wave will be essentially equal to that of its fundamental component. This is because the third harmonic, associated with saturation, and the fifth and seventh harmonics tend to sum to a minimum value at this point. Since sin(53.2°) = 0.80, the ordinate of the fundamental component of the sine wave and the ordinate of the actual sine wave are both equal to 0.80 at this angle. This provides a useful technique for deriving the saturation curve for use in calculating the magnetomotive-force drop across the teeth and the yoke of the core.

The normal dc saturation curve, such as that shown in Fig. 14.1, provides the basic data from which the ac saturation curves are derived. A value of maximum flux density B is selected and this value is then multiplied by 0.8. This value corresponds to the value of the actual flux wave, and to its fundamental component, as discussed above. Then the value of magnetic field strength H which corresponds to (0.80)(B) is read from the normal dc saturation curve for the grade of steel being considered. This value of H is divided by 0.80 to give the average value of H that corresponds to the selected value of B. This values of H is then multiplied by $\sqrt{2}$ to give the equivalent maximum value of ampere-turns/meter or ampere-turns/inch for use with ac current. This effective value of H is then plotted against the selected value of B to give one point on the ac saturation curve. The process is repeated until the curve is completed. Figure 14.12 shows such

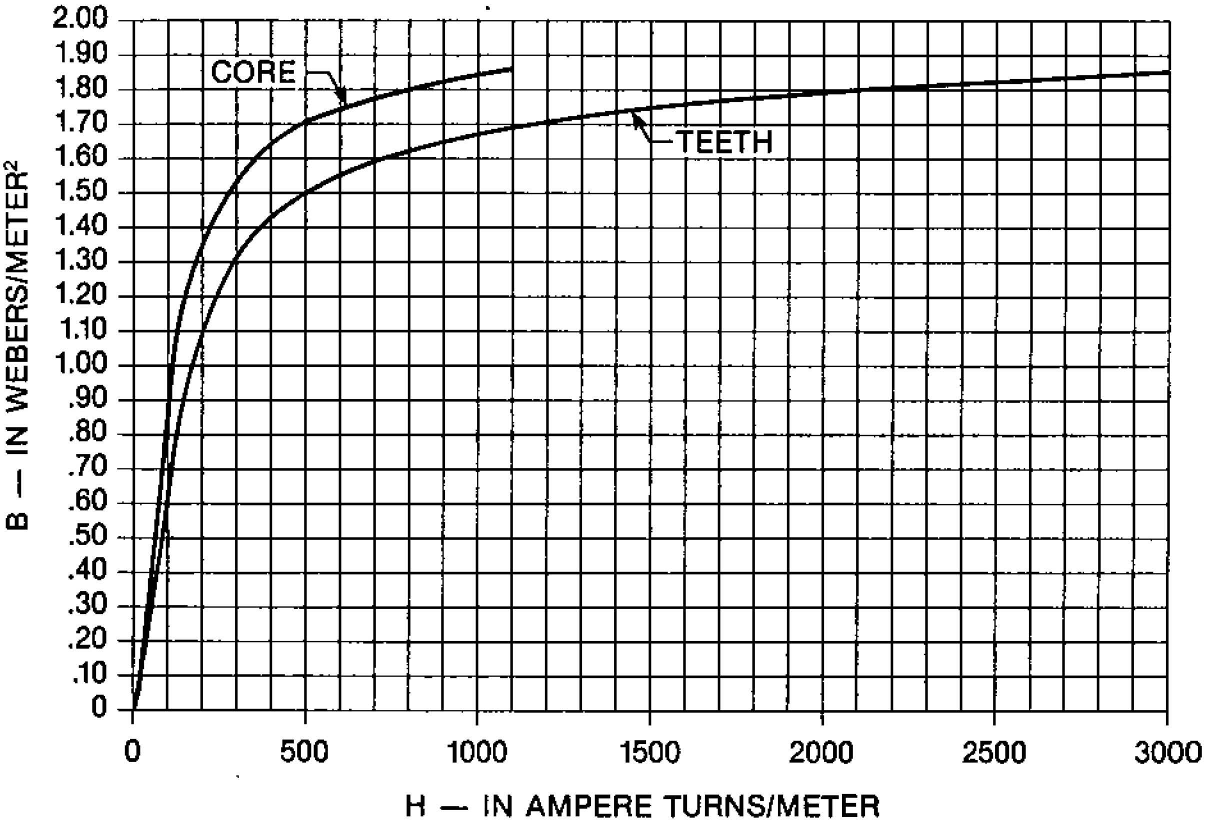

FIGURE 14.12 Ac saturation curve for use in calculating the magnetomotive-force drop in teeth and core yokes.

a "tooth" curve for use in calculating the magnetomotive-force drop through the stator and the rotor teeth.

The total flux/pole divides at the center of the pole at any instant of time, with one-half of the flux going in each direction of the yoke of the core. Thus the flux density is zero at the center of the core yoke and is a maximum at the interpolar point (Fig. 14.13). Thus, the flux density in the core yoke is the space integral of the air-gap flux wave, which has just passed through the teeth. To determine the core-yoke saturation curve (usually called the "core" saturation curve), half of a sine wave (i.e., a wave from 0 to 90 degrees) is divided into increments of equal angle, such as 15, 30, 45, 60, 75, and 90 degrees, and the corresponding values of sin θ calculated. The "tooth" magnetizing curve is then used to construct the "core" magnetizing curve. A given value of flux density B is selected, which corresponds to the maximum value of flux density at the interpolar point. Using the choice of increments above, the six values of incremental flux density are B sin(15), B sin(30), B sin(45), B sin(60), B sin(75), and B sin(90). The corresponding values of H for each of the increments above are then read from the tooth magnetizing curve. The six values of H are then averaged to give the value of H that corresponds to the selected value of B. Corresponding pairs of B and H, so determined, are then plotted, to give the core magnetizing curve. Figure 14.12 also shows such a curve.

Most of the ac magnetizing curves in general use are slightly modified from that determined by the procedure above. For medium-sized and larger machines, the same grade of steel will usually not be used for the rotor as is used for the stator. Also, some number of grades of steel will be carried in stock for use in production. Rather than have a separate set of tooth and core saturation curves for each particular grade of steel, it is common practice to have one or two sets of curves, each of which represents an average of two or more grades of steel. This is not as inaccurate a practice as might at first appear to be the case. For example, if 15% of the total magnetizing ampere-turns/pole are due to the steel portion of the mutual-flux path, and if a given magnetization curve for the steel is in error by, say, 10%, the total error is only (0.15)(0.10) = 0.015 per unit, or 1.5%, relative to the total ampere-turns. The stacking factor, which is used to determine the flux densities, is not accurately known within this limit of accuracy.

14.11.2 Calculation of the Magnetic Circuit, with Numerical Example

It was shown in Chapter 12 that magnetizing current flowing in each of the phase windings produces a rotating magnetomotive-force wave. This magnetomotive-force wave reacts on the average permeance of the air gap to produce a corresponding rotating flux wave. If this flux wave is viewed throughout the entire magnetic circuit at a given instant of time, it will

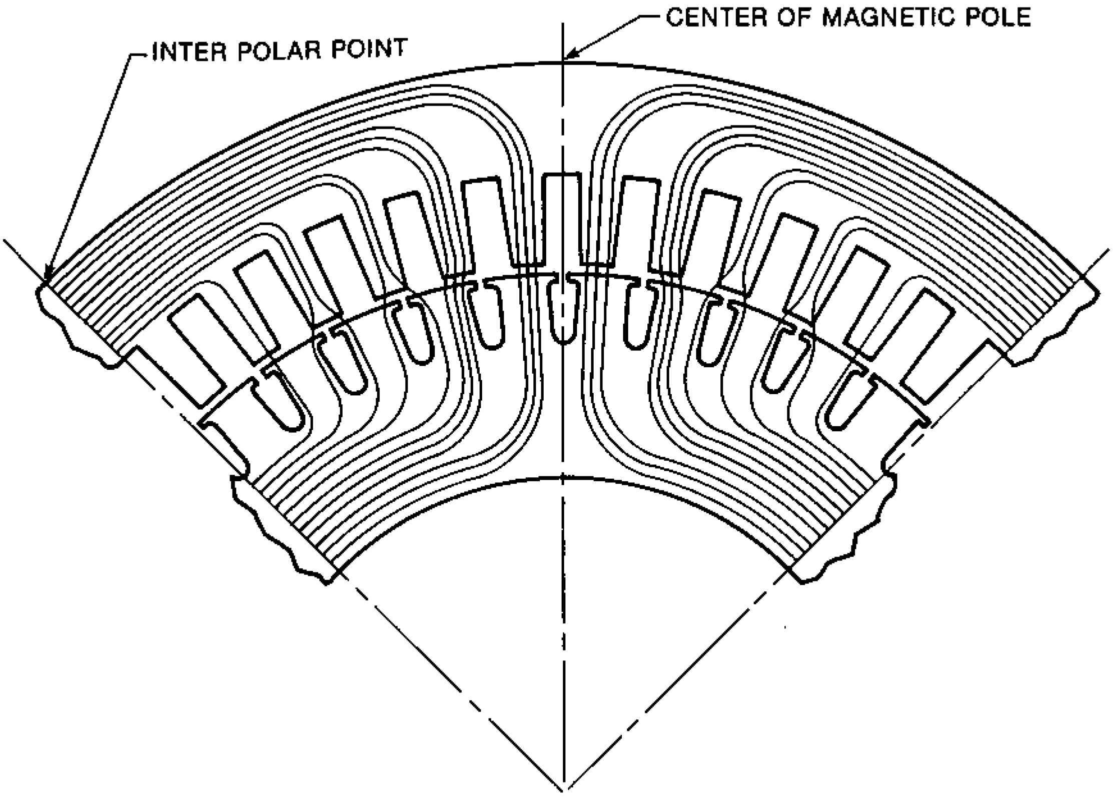

FIGURE 14.13 Pattern of flux in a four-pole induction motor.

appear as shown in Fig. 14.13. In this figure the mutual-flux flow lines are shown at a given instant of time for a four-pole motor. A four-pole magnetic structure was chosen for the illustration because it is representative of the flux pattern for one pole pitch. It is apparent that the flux resembles a sinusoidal distribution across the teeth encompassed by one pole pitch. It is also apparent that the flux/pole divides at the midpoint of the pole in the core yoke, with half of the flux going in each direction. Accordingly, the flux density is equal to the space integral in the core yoke. Thus it is equal to zero at the center of the pole and is a maximum at the interpolar point.

Calculation of the magnetic circuit can best be understood by use of a numerical example. The three-phase 60-Hz 2300-V eight-pole 1000-hp induction motor with design parameters as described in Section 13.14 will be used. Since dimensions are given in inches, that system of units will be used in the example. Mutual flux/pole is equal to

$$\phi_p = \frac{V_1 \times 10^8}{4.443 K_p K_d N_{st} f} \quad \text{maxwells} \tag{14.52}$$

Inserting the appropriate values, from Section 13.14, into eq. (14.52) gives us

$$\phi_p = \frac{(1328)(10^8)}{(4.443)(0.985)(0.955)(72)(60)} = 7.36 \times 10^6 \quad \text{maxwells} \qquad (14.53)$$

One pole pitch at the air gap spans a circumferential distance equal to the inside diameter of the stator d, multiplied by π and divided by the number of poles, or to

$$\text{pole pitch} = \frac{\pi d}{p} = \frac{(\pi)(26.4)}{8} = 10.37 \quad \text{inches} \qquad (14.54)$$

The gross length of the core ℓ_c is equal to 27 in. The area of the air gap/pole is then equal to

$$A_g = \frac{\pi d}{p} \ell_c = (10.37)(27) = 280 \quad \text{inches}^2 \qquad (14.55)$$

The mutual flux/pole, divided by the air-gap area/pole, is equal to the average air-gap flux density. However, as determined in Section 12.8, the air-gap flux density should be expressed in terms of its maximum value B_{gm}, which for simplicity is written as B_g. Thus the average value of air-gap flux density should be multiplied by $\pi/2$ to give the maximum value of its fundamental component, or

$$B_g = \frac{7.36 \times 10^6}{280} \frac{\pi}{2} = 41.3 \times 10^3 \quad \text{maxwells/inch}^2 \qquad (14.56)$$

As noted earlier, the relationship between flux density and magnetic field strength, when using units of maxwells and of inches, is

$$B = \frac{(3.192)(NI)}{\ell} \quad \text{maxwells/inch}^2 \qquad (14.57)$$

where ℓ is the length of the flux path. For the air gap of an induction motor, eq. (14.57) becomes

$$B_g = \frac{(3.192)(NI)_g}{g'} \quad \text{maxwells/inch}^2 \qquad (14.58)$$

Solving for $(NI)_g$, the ampere-turns/pole required to force the flux/pole across the air gap is

$$(NI)_g = \frac{B_g g'}{3.192} \quad \text{ampere-turns/pole} \tag{14.59}$$

where $g' = K_f g$. Thus it is necessary to determine the fringing factor for the air gap for this example. To do this, Carter's coefficient must be determined for the stator slots, the rotor slots, the stator ventilating air ducts, and the rotor ventilating air ducts. These four coefficients are then multiplied together to give K_f for the air gap.

From eq. (14.51), Carter's coefficient K_f' for a slot or for an air duct is equal to

$$K_f' = \frac{\tau}{\tau - \sigma w} \quad \text{numeric} \tag{14.60}$$

Using design parameters for the numerical example from Section 13.14. the stator slot pitch is

$$\tau_1 = \frac{\pi d}{N_1} = \frac{(\pi)(26.4)}{72} = 1.152 \quad \text{inches} \tag{14.61}$$

and the rotor slot pitch is

$$\tau_2 = \frac{\pi d_r}{N_2} = \frac{(\pi)(26.3)}{86} = 0.961 \quad \text{inches} \tag{14.62}$$

The ventilating air-duct pitch for both the stator and the rotor is equal to

$$\tau_{v1} = \tau_{v2} = \frac{\ell_c}{N_v + 1} = \frac{27}{13 + 1} = 1.929 \quad \text{inches} \tag{14.63}$$

where N_v is the number of ventilating ducts in the core. The stator-slot opening is equal to 0.570 in., and the mechanical air gap is equal to 0.50 in. Then $w/g = 0.570/0.050 = 11.4$. From curve 2 of Fig. 14.11, the constant σ is equal to 0.696 for the stator slot. Inserting $w = 0.570$, $\sigma = 0.696$, and $\tau = 1.152$ into eq. (14.60) gives us

$$K'_{s1} = \frac{\tau}{\tau - \sigma w} = \frac{1.152}{1.152 - (0.696)(0.570)} = 1.511 \quad \text{numeric} \tag{14.64}$$

The rotor slot opening is equal to 0.100 in., giving a value of $w/g = 0.100/0.050 = 2.0$. From curve 1 of Fig. 14.11, the constant σ is equal to 0.338 for the rotor slot. Inserting $w = 0.100$, $\sigma = 0.338$, and $\tau = 0.961$ into eq. (14.60), we have

$$K'_{s2} = \frac{\tau}{\tau - \sigma w} = \frac{0.961}{0.961 - (0.338)(0.100)} = 1.037 \quad \text{numeric} \qquad (14.65)$$

The radial ventilating air duct width w_v is equal to 0.250 in. in width, giving a value of $w/g = 0.250/0.050 = 5.0$. From curve 2 of Fig. 14.11, the constant σ is equal to 0.50. Inserting $w = 0.250$, $\sigma = 0.50$, and $\tau = 1.929$ into eq. (14.60), we obtain

$$K'_{v1} = K'_{v2} = \frac{\tau}{\tau - \sigma w} = \frac{1.929}{1.929 - (0.50)(0.250)} = 1.069 \quad \text{numeric} \qquad (14.66)$$

Then the fringing constant K_f for the numerical example is equal to

$$K_f = K'_{s1}K'_{s2}(K'_{v1})^2 = (1.511)(1.037)(1.069)^2 = 1.791 \quad \text{numeric} \qquad (14.67)$$

Thus the value of the effective air-gap length g' is equal to

$$g' = K_f g = (1.791)(0.05) = 0.0896 \quad \text{inches} \qquad (14.68)$$

Substituting eqs. (14.56) and (14.68) into eq. (14.59), the air-gap ampere turns/pole is

$$(NI)_g = \frac{B_g g'}{3.192} = \frac{(41.3 \times 10^3)(0.0896)}{3.192} = 1159 \quad \text{ampere-turns/pole} \qquad (14.69)$$

The average solid circumferential width of the stator teeth for one pole pitch, as reckoned at the midpoint of the stator teeth, is equal to

$$W_{t1} = \frac{(d + D)(\pi) - N_1 w}{p} \quad \text{inches} \qquad (14.70)$$

Using design parameters from Section 13.14, the solid stator-tooth width for one pole pitch is equal to

$$W_{t1} = \frac{(26.4 + 1.9)(\pi) - (72)(0.570)}{8} = 5.98 \quad \text{inches} \qquad (14.71)$$

Similarly, the average, solid circumferential width of the rotor teeth for one pole pitch, as reckoned at the midpoint of the rotor teeth, is equal to

$$W_{t2} = \frac{(d_r - \text{rotor-slot depth})(\pi) - (N_2)(\text{rotor-slot width})}{p} \quad \text{inches} \tag{14.72}$$

Using design parameters from Section 13.14, the solid rotor-tooth width for one pole pitch is equal to

$$W_{t2} = \frac{(26.3 - 1.50)(\pi) - (86)(0.415)}{8} = 5.28 \quad \text{inches} \tag{14.73}$$

The solid axial length of the stator core and of the rotor core is equal to

$$\ell_s = (\ell_c - N_v W_v)(\text{stacking factor}) \quad \text{inches} \tag{14.74}$$

Using design parameters from Section 13.14 for ℓ_c, N_v, and W_v, and using a typical stacking factor of 0.95, we obtain

$$\ell_s = [27 - (13)(0.25)](0.95) = 22.56 \quad \text{inches} \tag{14.75}$$

The average cross-sectional area of the stator-tooth steel for one pole pitch is equal to

$$A_{t1} = W_{t1}\ell_s \quad \text{inches}^2 \tag{14.76}$$

Substituting eqs. (14.71) and (14.75) into eq. (14.76) yields

$$A_{t1} = (5.98)(22.56) = 134.9 \quad \text{inches}^2 \tag{14.77}$$

Similarly, the average cross-sectional area of the rotor-tooth steel for one pole pitch is equal to

$$A_{t2} = W_{t2}\ell_s \quad \text{inches}^2 \tag{14.78}$$

and substituting eqs. (14.73) and (14.75) into eq. (14.78), we have

$$A_{t2} = (5.28)(22.56) = 119.1 \quad \text{inches}^2 \tag{14.79}$$

The mutual flux/pole, divided by A_{t1}, is equal to the average stator-tooth flux density. However, the magnetization curve for stator and rotor teeth relates maximum flux density, B_{t1} and B_{t2}, to magnetic field strength H. Accordingly, the average value of flux density in the teeth should be multiplied by $\pi/2$ to give the maximum value of flux density. Then for the stator teeth

$$B_{t1} = \frac{\phi_p}{A_{t1}} \frac{\pi}{2} \quad \text{maxwells/inch}^2 \tag{14.80}$$

Substituting eqs. (14.53) and (14.77) into eq. (14.80) gives us

$$B_{t1} = \frac{7.36 \times 10^6}{134.9} \frac{\pi}{2} = 85.7 \times 10^3 \quad \text{maxwells/inch}^2 \tag{14.81}$$

Similarly, the maximum value of flux density in the rotor teeth is equal to

$$B_{t2} = \frac{\phi_p}{A_{t2}} \frac{\pi}{2} \quad \text{maxwells/inch}^2 \tag{14.82}$$

and substituting eqs. (14.53) and (14.79) into eq. (14.82), we have

$$B_{t2} = \frac{7.36 \times 10^6}{119.1} \frac{\pi}{2} = 97.1 \times 10^3 \quad \text{maxwells/inch}^2 \tag{14.83}$$

The ampere turns/pole required to force the mutual flux/pole through the stator teeth or through the rotor teeth is equal to

$$(NI)_t = (H_t)(\text{length of tooth}) \quad \text{ampere-turns/pole} \tag{14.84}$$

where H_t is the magnetic field force H, at flux density B_t, as determined from an appropriate ac saturation curve. The saturation curve in Fig. 14.12 is in MKS units, and hence B_{t1} must be converted to webers/meter^2, in order to use it. This conversion can be made by remembering that 1.0 Wb/m^2 is equal to 64.5×10^3 Mx/in.^{2}. Thus, from eq. (14.81), $B_{t1} = 85.7 \times 10^3$ Mx/in.^{2}, which is equal to $(85.7 \times 10^3)/(64.5 \times 10^3) = 1.33$ Wb/m^2. Similarly, from eq. (14.83), $B_{t2} = 97.1 \times 10^3$ Mx/in.^{2}, which is equal to $(97.1 \times 10^3)/(64.5 \times 10^3) = 1.51$ Wb/m^2. Referring to the ac saturation curve given in Fig. 14.12, $H_{t1} = 310$ A-t/m and $H_{t2} = 515$ A-t/m. These values of H can be converted to ampere-turns/inch by dividing by 39.37, the number of inches/meter. Then $H_{t1} = 310/39.37 = 7.87$ A-t/in. and $H_{t2} = 515/39.37 = 13.1$ A-t/in. Accordingly, from eq. (14.84), the total ampere-turns required to force the mutual flux/pole through the stator teeth is equal to

$$(NI)_{t1} = (7.87)(1.9) = 15.0 \quad \text{ampere-turns/pole} \qquad (14.85)$$

and the total ampere-turns required to force the mutual flux through the rotor teeth is equal to

$$(NI)_{t2} = (13.1)(1.5) = 19.7 \quad \text{ampere-turns/pole} \qquad (14.86)$$

The radial depth behind the stator slot which is available to carry the mutual flux is equal to

$$\text{radial depth behind the stator slot} = \frac{\text{stator core OD} - [d + 2(\text{stator-slot depth})]}{2} \quad \text{inches} \qquad (14.87)$$

Substituting the appropriate design constants from Section 13.14 into eq. (14.87) gives us

$$\text{radial depth behind stator slot} = \frac{34 - [26.4 + (2)(1.9)]}{2} = 1.90 \quad \text{inches} \qquad (14.88)$$

Also, the radial depth behind the rotor slot which is available to carry the mutual flux is equal to

$$\text{radial depth behind the rotor slot} = \frac{[\text{rotor core OD} - 2(\text{rotor-slot depth})] - \text{rotor core ID}}{2} \quad \text{inches} \qquad (14.89)$$

and substituting the appropriate design constants from Section 13.14 into eq. (14.89), we obtain

$$\text{radial depth behind the rotor slot} = \frac{[26.3 - (2)(1.5)] - 19.5}{2} = 1.90 \quad \text{inches} \qquad (14.90)$$

The product of the radial depth behind the slot multiplied by the solid length of core ℓ_c is equal to the cross-sectional area of the steel of the core yoke which is available to carry one-half of the mutual flux/pole. This area is only required to carry half of the mutual flux/pole, because the flux divides at the center of the pole, with half flowing in each of the two circumferential directions. Then the stator-core yoke area available to carry flux is

$$A_{c1} = (\text{radial depth behind stator slot})(\ell_s) \quad \text{inches}^2 \tag{14.91}$$

and, similarly, the rotor-core yoke area, available to carry flux, is

$$A_{c2} = (\text{radial depth behind rotor slot})(\ell_s) \quad \text{inches}^2 \tag{14.92}$$

Substituting eqs. (14.88) and (14.75) into eq. (14.91) yields

$$A_{c1} = (1.90)(22.56) = 42.9 \quad \text{inches}^2 \tag{14.93}$$

Also, substituting eqs. (14.90) and (14.75) into eq. (14.92), we obtain

$$A_{c2} = (1.90)(22.56) = 42.9 \quad \text{inches}^2 \tag{14.94}$$

Since as discussed earlier, the mutual flux flowing in each direction of the core yoke from the midpoint of the pole to the interpolar point is the space integral of the flux passing through the teeth, one-half of the mutual flux/pole divided by A_{c1} is equal to the maximum flux density in the core yoke. Accordingly, for the stator core,

$$B_{c1} = \frac{\phi_p}{2A_{c1}} \quad \text{maxwells/inch}^2 \tag{14.95}$$

and for the rotor core,

$$B_{c2} = \frac{\phi_p}{2A_{c2}} \quad \text{maxwells/inch}^2 \tag{14.96}$$

Substituting eq. (14.53) and eq. (14.93) into eq. (14.95) yields

$$B_{c1} = \frac{7.36 \times 10^6}{(2)(42.9)} = 85.8 \times 10^3 \quad \text{maxwells/inch}^2 \tag{14.97}$$

and substituting eqs. (14.53) and (14.94) into eq. (14.96), we have

$$B_{c2} = \frac{7.36 \times 10^6}{(2)(42.9)} = 85.8 \times 10^3 \quad \text{maxwells/inch}^2 \tag{14.98}$$

The ampere-turns/pole required to force half of the mutual flux/pole through one of the two parallel paths of either the stator-core yoke or the rotor-core yoke is equal to

$$(NI)_c = (H_c)(\text{length of yoke path}) \quad \text{ampere-turns/pole} \tag{14.99}$$

The length of one of the parallel paths in the stator-core yoke is equal to

$$L_{c1} = \frac{(\text{stator OD - radial depth behind stator slot})(\pi)}{2p} + \frac{(\pi)(\text{radial depth behind stator slot})}{4} \quad \text{inches} \tag{14.100}$$

and the corresponding length of one of the parallel paths in the rotor-core yoke is equal to

$$L_{c2} = \frac{(\text{inside diameter of rotor core + radial depth behind rotor slot})(\pi)}{2p} + \frac{(\pi)(\text{radial depth behind rotor slot})}{4} \quad \text{inches} \tag{14.101}$$

Substituting the appropriate design parameters from Section 13.14 and the radial depth behind the stator slot from eq. (14.88) into eq. (14.100) gives us

$$L_{c1} = \frac{(34 - 1.90)(\pi)}{(2)(8)} + \frac{(\pi)(1.90)}{4} = 7.79 \quad \text{inches} \tag{14.102}$$

and substituting the appropriate design parameters from Section 13.14 and the radial depth behind the rotor slot from eq. (14.90) into eq. (14.101) gives us

$$L_{c2} = \frac{(19.5 + 1.90)(\pi)}{(2)(8)} + \frac{(\pi)(1.90)}{4} = 5.69 \quad \text{inches} \tag{14.103}$$

The ampere-turns/pole required to force the mutual flux/pole through the stator core or through the rotor core is equal to

$$(NI)_c = H_c L_c \quad \text{ampere-turns/pole} \tag{14.104}$$

From eq. (14.97), the density in the stator-core yoke is equal to 85.8×10^3 Mx/in.^{2} or to $(85.8 \times 10^3)/(64.5 \times 10^3) = 1.33$ Wb/m^2. From the corresponding ac saturation curve of Fig. 14.12, $H_{c1} = 185$ A-t/m, or to $185/39.37 = 4.70$ A-t/in. Then substituting this value of H_{c1} and the value of L_{c1} from eq. (14.102) into eq. (14.104) gives us

$$(NI)_{c1} = (4.70)(7.79) = 36.6 \quad \text{ampere-turns/pole} \tag{14.105}$$

From eqs. (14.97) and (14.98), it is apparent that $B_{c1} = B_{c2}$. For this particular case, H_{c1} is equal to H_{c2}, and thus H_{c2} is also equal to 4.70 A-t/in. Substituting this value of H_{c2} and the value of L_{c2} from eq. (14.103) into eq. (14.103) into eq. (14.104) yields

$$(NI)_{c2} = (4.70)(5.69) = 26.7 \quad \text{ampere-turns/pole} \tag{14.106}$$

The total ampere-turns/pole for the complete magnetic circuit is equal to the sum of that for the air gap, stator teeth, stator-core yoke, rotor teeth, and rotor-core yoke, or

$$(NI)_t = (NI)_g + (NI)_{t1} + (NI)_{c1} + (NI)_{t2} + (NI)_{c2} \quad \text{ampere-turns/pole} \tag{14.107}$$

Inserting the values from eqs. (14.69), (14.85), (14.86), (14.105), and (14.106) into eq. (14.107) yields

$$(NI)_t = 1159 + 15.0 + 36.6 + 19.7 + 26.7 = 1257 \quad \text{ampere-turns/pole} \tag{14.108}$$

To obtain the values above, the maximum flux densities were calculated for each part of the mutual-flux path, and the corresponding maximum value of ampere-turns was then determined. The maximum ampere-turns/pole for a distributed stator winding can be expressed in terms of the stator winding as

$$(NI)_t = \sqrt{2}\, I_m \frac{2}{\pi} \frac{N_{st} q K_{p1} K_{d1}}{p} \quad \text{ampere-turns/pole} \tag{14.109}$$

Solving for the magnetizing current I_m gives us

$$I_m = \frac{(1.11)(NI)_t p}{q N_{st} K_{p1} K_{d1}} \quad \text{amperes/phase} \tag{14.110}$$

Substituting the appropriate design parameters from Section 13.14 and the value of $(NI)_t$ from eq. (14.108) into eq. (14.110) yields

$$I_m = \frac{(1.11)(1257)(8)}{(3)(72)(0.985)(0.955)} = 54.9 \quad \text{amperes/phase} \tag{14.111}$$

Although magnetizing current can be calculated by other methods, the foregoing method of calculating it (i.e., directly from the total magnetizing ampere-turns) is the most accurate one in the usual case. This will subsequently become apparent.

The saturation factor K_s is defined as the ratio of total ampere-turns/pole to air-gap ampere-turns/pole.

$$K_s = \frac{(NI)_t}{(NI)_g} \quad \text{numeric} \tag{14.112}$$

Inserting the value of $(NI)_t$ from eq. (14.108) and the value of $(NI)_g$ from eq. (14.69) into eq. (14.112), we obtain

$$K_s = \frac{1257}{1159} = 1.085 \quad \text{numeric} \tag{14.113}$$

for the numerical example. The magnetizing reactance X_m was calculated in Section 13.14.1 for the same numerical example. It was assumed in that exercise that $K_s = 1.15$ and also that $K_f = 1.96$. However, as subsequently determined in Section 14.11.2, the actual value of $K_s = 1.09$ and the actual value of $K_f = 1.79$. Thus the actual value of the magnetizing reactance calculated in eq. (13.164) should be

$$X_m = (20.7)\,\frac{(1.96)(1.15)}{(1.79)(1.09)} = 23.9 \quad \text{ohms/phase} \tag{14.114}$$

As discussed earlier, magnetizing current is equal to the voltage E induced in the stator winding divided by X_m. However, it can be calculated with only a small error by dividing the bus voltage/phase V_1 by X_m. Then using the above-corrected value of X_m originally determined in eq. (13.164), the corresponding value of magnetizing current is equal to

$$I_m = \frac{V_1}{X_m} = \frac{1328}{23.9} = 55.6 \quad \text{ampere/phase} \tag{14.115}$$

which agrees to within 0.013 per unit with I_m as calculated by eq. (14.111). If the slightly lower numerical value of E_1 had been used instead of V_1 in eq. (14.115), the numerical agreement would have been within accumulated round-off error. However, it is customary to calculate I_m directly from the magnetic circuit, such as was done in eq. (14.111).

15

Application of Induction Motors

15.1 The Role of Application 600

15.2 Installation 601

15.3 Methods of Power Transmission 602

- 15.3.1 Couplings 602
- 15.3.2 Belt drives 604
- 15.3.3 Chain drives 608
- 15.3.4 Gear drives 609
- 15.3.5 Endplay considerations in coupled motor drives 610
- 15.3.6 Alignment of solid couplings 611
- 15.3.7 Alignment of flexible couplings 613
- 15.3.8 Alignment of belt drives, chain drives, and gear drives 613

15.4 Methods of Starting Squirrel-Cage Induction Motors 614

- 15.4.1 Considerations of reduced-voltage starting 614
- 15.4.2 Autotransformer starting 616
- 15.4.3 Series-resistor starting 618
- 15.4.4 Series-reactor starting 619
- 15.4.5 Wye-delta starting 620
- 15.4.6 Solid-state starting 621
- 15.4.7 Other methods of starting 621
- 15.4.8 Stall time of squirrel-cage motors 623

15.5 Wound-Rotor Motor Starting 624

15.6 Methods of Speed Control 627

- 15.6.1 Rheostat control of wound-rotor motors 628
- 15.6.2 Speed control by cascading two wound-rotor induction motors 630

15.6.3 Speed control of wound-rotor motors by use of auxiliary machines or devices 631
15.6.4 Speed control of squirrel-cage motors by stator voltage 633
15.6.5 Multispeed motors 635
15.6.6 Speed control of squirrel-cage motors by impressing constant volts/cycle on the stator winding 639
15.6.7 Speed control of squirrel-cage motors by use of a controlled slip coupling 642

15.7 Acceleration 644

15.7.1 Acceleration time and the speed-time curve 645
15.7.2 The speed-current curve and the current-time curve 646
15.7.3 Numerical example of constructing a speed-time curve and a current-time curve 647
15.7.4 Heating and stored energy during acceleration 650
15.7.5 Load WK^2 and frequency of starts 652

15.8 Braking 653

15.8.1 The role of electrical braking 653
15.8.2 Reverse-rotation braking 653
15.8.3 Regenerative braking 655
15.8.4 Multispeed braking 656
15.8.5 Dynamic braking 656

15.9 Power Requirement for a Duty-Cycle Application 658

15.1 THE ROLE OF APPLICATION

The end purpose of specifying, designing, manufacturing, testing, and installing a polyphase induction machine at the site is to fulfill a need. That need is usually one of delivering torque to driven equipment under a given set of operating conditions. This mandates that the load requirements of the driven equipment be determined and then translated into drive-motor requirements. However, induction machines are also used for generating power, for changing frequency, and as position and speed indicators. Since the power rating, speed, starting torque, maximum torque, environmental enclosure of the machine, and its integration with the local power system must be determined prior to placing the purchase order, it is apparent that application engineering considerations are required before any other actions are possible. Also, after the machine has been tested and shipped to the site, it must be installed on an adequate foundation or support, correctly aligned, and its balance and proper function verified. Although these on-site activities are classified as installation and service, usually done under the supervision of an engineer, they can be, and frequently are, considered to be part of the overall application engineering required for the successful culmination of a capital investment in new equipment.

15.2 INSTALLATION

Installation starts at the time that the motor arrives at the site. The customer will have received copies of the instruction book prior to shipment. Immediately upon arrival the unit should be thoroughly inspected for any damage that may have resulted from shipment. Any damage should be documented, in accordance with instructions in the installation book, such as by photographs and by a written description, and then reported to the supplier and to the carrier. The unit should also be handled at all times in accordance with the instruction book. If not put into service immediately, the unit should be stored appropriately. Again, the instruction book will provide storage instructions and if there is any question about such instructions, the supplier should be contacted and the question resolved. Damage can and occasionally does occur to windings, bearings, and other parts due to improper storage. Accordingly, improper storage can result in additional cost, subsequent delays in installation, and possible invalidation of the manufacturer's warranty.

The outline drawing or equivalent document which the customer will have received soon after the purchase order was placed, will specify the mounting dimensions of the machine and probably the minimum foundation or support stiffness that is required for adequate support, under normal operating conditions. If the outline drawing does not have this information, it should be determined from a competent source. The foundation or support must provide the correct horizontal and vertical alignment between the motor and the driven equipment, carry the weight, resist the reaction torque, absorb any cyclical or dynamical forces produced by the combined equipment, and prevent vibration amplification. A reinforced concrete foundation which extends downward sufficiently to have firm footing on suitable substratum is usually preferable. If it is necessary that the machine be located on structural steel or on a building floor, it is important that this support be capable of providing for the weight and stiffness requirements as stated on the outline drawing or as otherwise determined. Also, it is essential that the dynamics of the total structural system, from the motor to the substratum footing of the structure, be considered in the evaluation.

An induction motor will normally have two machined mounting feet on the bottom of the frame, one on each side, running for most or all of the length of the frame. Intermediate pieces of steel called foundation caps or sole plates are often used between the frame feet and the foundation. When such intermediate pieces are used, they act as spacers between the actual foundation and the motor and should be considered as part of the foundation.

When used, they should be evenly supported by the foundation, and should be held in a true horizontal plane at an elevation which is essentially equal to the bottom of the motor. The goal is to have the machined surfaces on the bottom of the frame feet fixed in a horizontal plane parallel with the shaft and to mate with the top of the foundation caps or sole plates at such an elevation as to have the centerline of the motor shaft equal the centerline of the shaft of the driven equipment. To achieve this, steel shims of various thicknesses are applied, as required, between the motor feet and the sole plates. After the shims are applied, the nuts are "snugged down" on the foundation bolts. These nuts are not tightened, however, until the motor has been aligned with the driven equipment. Alignment is dependent on the method used to transmit power from the motor shaft extension. Thus it is in order to consider the various methods of power transmission.

15.3 METHODS OF POWER TRANSMISSION

15.3.1 Couplings

The usual methods of power transmission from the shaft extension of the drive motor to that of the driven equipment are (1) couplings, (2) pulleys and flat belts, (3) sheaves and V belts, (4) sprockets and chains, and (5) gears. Couplings provide a direct connection between the motor and the driven equipment and therefore the motor speed must be selected to match that of the driven equipment. However, as transmission equipment, the coupling is relatively simple and economical. Belt drives, chain drives, and gear drives permit selecting the most economical speed of drive motor, which is frequently 1800 rpm, to match the speed of the driven equipment by choice of the diameters of the pulley, sheave, sprocket, or gear. These types of drives are also useful in delivering a large load-torque requirement at a given speed and, accordingly, they are useful in the general field of application engineering. The disadvantages are the greater initial, cost of the total equipment due to the additional components and the greater maintenance associated with the total system. Thus direct-coupling drives constitute the preponderance of the power transmission systems for polyphase induction motor drives.

There are two generic types of direct coupling systems: solid coupling and flexible coupling. The solid coupling system consists of two essentially identical coupling halves, which have machined mating surfaces called coupling faces in the vertical plane, and holes drilled through their horizontal centerlines to accommodate the two shaft extensions. Each coupling half is pressed, or shrunk, on its respective shaft extension, and in addition, axial keys are positioned in corresponding keyways. During installation, the two coupling faces are positioned together and then solidly fastened by means of bolts through horizontally drilled holes located on a diameter concentric with, but with a diameter somewhat less than, the OD of the flange.

The flexible coupling system consists of (1) two half couplings, (2) an intermediate member to provide flexibility, and for some specific types, a cylindrical cover. The flexible member can be of various designs, such as spline and sprockets, laminated disks, studs and rubber bushings, two sprockets held together by one concentric double-strand chain, and so on. Some types of flexible couplings will permit significant independent axial movement of each of the two shaft extensions, whereas other types will not. Those couplings that permit independent shaft movement are said to permit "end float." End-float couplings allow the motor shaft to correspond to "magnetic center" without being affected by the status of the shaft of the driven equipment. Such couplings also allow the rotating parts of the driven equipment, such as pump impellers, to expand axially when heated without preloading the motor bearings in an axial direction. Also, in some types of end-float couplings, the amount of possible end float can be controlled by placing axial pins within the coupling.

The advantages and disadvantages of the two generic types of couplings can be summarized in outline form as follows:

A. Solid couplings
  1. Advantages
    a. Simplicity.
    b. Economy.
    c. If the driven equipment has only one outboard bearing on integrated equipment, the coupling can transmit vertical support to the inboard side, where practical.
  2. Disadvantages
    a. Shaft bending stresses. A solid coupling makes the two shafts essentially equivalent to one long shaft, which requires that all bearings be aligned on one centerline. Any departure from this will produce bending stresses within the shaft.
    b. Axial preloading of bearings. If the two coupling faces are not each machined at right angles to the axis of alignment, and parallel to each other, the bearings will be radially preloaded. Also, if one foot height is lower than the other, the bearings will be preloaded. Further, if one coupling half is offset in a widthwise direction, the bearings will be preloaded.
    c. Axial thrust cannot be isolated between the motor and the driven equipment.

B. Flexible couplings
  1. Advantages
    a. Prevents bending stresses due to misalignment of the two shafts.
    b. Prevents axial preloading of bearings, due to malmachining of coupling halfs or due to misalignment.
    c. Can isolate axial thrust and absorb axial expansion.

2. Disadvantages
    a. More complicated.
    b. Cost.
    c. More maintenance required.
    d. Cannot support the weight of the driven-equipment rotating parts on integrated equipment.

15.3.2 Belt Drives

A flat belt and pulley, or a V belt and sheave, transmit torque by virtue of a difference in tension in the two sides of the belt. Consider Fig. 15.1, and let T_1 and T_2 be the tensions in the belt at point A and at point B, respectively. Let $\Delta\ell$ be the incremental length of the belt from point C to point D, and let this length subtend an angle $\Delta\alpha$ at the center of the pulley at point O. Also, let the belt tension at point C on one side of the increment be equal to T newtons and let the belt tension at point D on the other side of the increment be equal to $T + \Delta T$ newtons. If the radial pressure per unit length of the incremental arc $\Delta\ell$ is p newtons/meter^2, the total radial force N acting on $\Delta\ell$ is equal to

$$N = p\,\Delta\ell \quad \text{newtons} \tag{15.1}$$

Since the incremental arc $\Delta\ell$ is small and since the corresponding subtended angle $\Delta\alpha$ is also small, the normal force N associated with the length $\Delta\ell$ can be considered acting in the direction of OE, which bisects the angle $\Delta\alpha$. The coefficient of friction μ between the belt and the pulley is equal to

$$\mu = \frac{F}{N} \quad \text{numeric} \tag{15.2}$$

where F is the frictional force that acts along $\Delta\ell$. Solving eq. (15.2) for F gives us

$$F = \mu N \quad \text{newtons} \tag{15.3}$$

and substituting eq. (15.1) into eq. (15.2) gives us

$$F = \mu p\,\Delta\ell \quad \text{newtons} \tag{15.4}$$

Since $\Delta\alpha$ is small, this frictional force can be considered as acting at right angles to the line OE. Assume that the belt tension is such that slippage is impending. Accordingly, the components of force acting along line OE must balance. Then

$$T \sin\frac{\Delta\alpha}{2} + (T + \Delta T)\sin\frac{\Delta\alpha}{2} = p\,\Delta\ell \quad \text{newtons} \tag{15.5}$$

Similarly, the components of force acting at right angles to OE must also balance. Then

$$(T + \Delta T) \cos \frac{\Delta\alpha}{2} - T \cos \frac{\Delta\alpha}{2} = \mu p \, \Delta \ell \quad \text{newtons} \tag{15.6}$$

Simplifying eq. (15.6) gives us

$$\Delta T \cos \frac{\Delta\alpha}{2} = \mu p \, \Delta \ell \quad \text{newtons} \tag{15.7}$$

Solving eqs. (15.5) and (15.7) for p $\Delta \ell$, equating, and simplifying, we have

$$\frac{2T + \Delta T}{\Delta T} \tan \frac{\Delta\alpha}{2} = \frac{1}{\mu} \quad \text{numeric} \tag{15.8}$$

Solving eq. (15.8) for ΔT gives us

$$\Delta T = \tan \frac{\Delta\alpha}{2} \, \frac{2T\mu}{1 - \mu \tan(\Delta\alpha/2)} \quad \text{newtons} \tag{15.9}$$

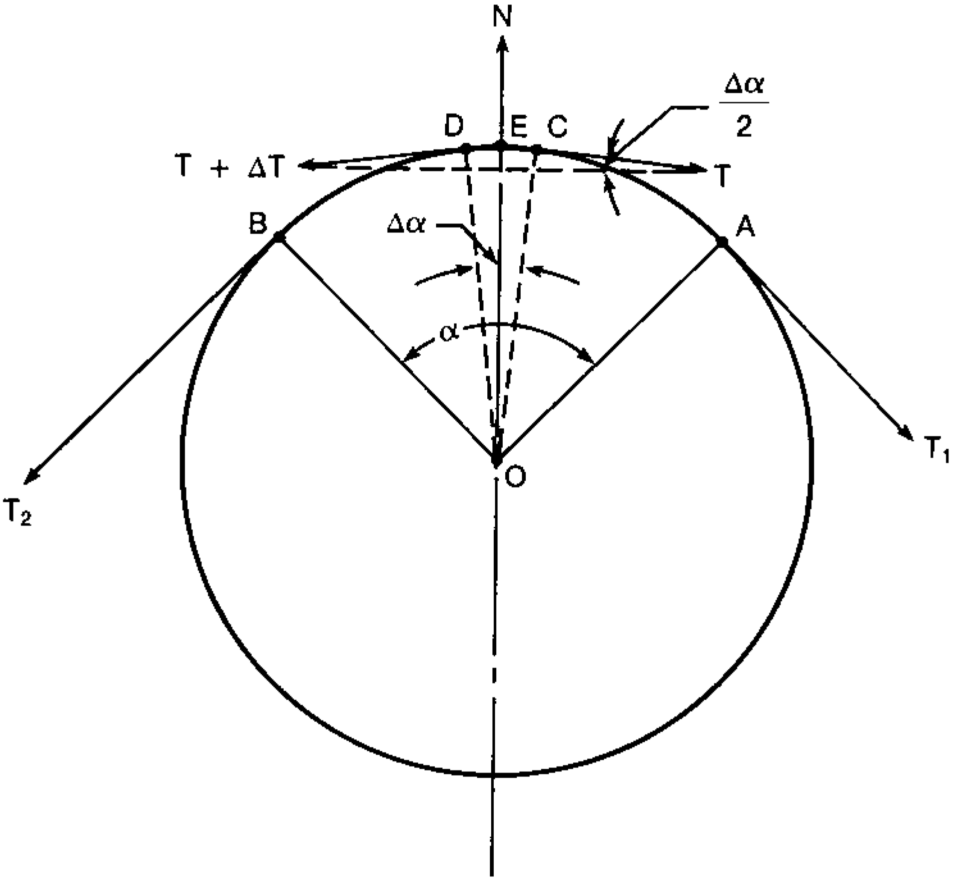

FIGURE 15.1 Difference in belt tension around the angle of embrace of the pulley of a belt drive.

Dividing both sides of eq. (15.9) by $\Delta\alpha$ yields

$$\frac{\Delta T}{\Delta\alpha} = \frac{\tan(\Delta\alpha/2)}{\Delta\alpha/2}\,\frac{T\mu}{1 - \mu\tan(\Delta\alpha/2)} \quad \text{newtons/radian} \tag{15.10}$$

Remembering that

$$\lim_{\Delta\alpha\to 0} \frac{\tan(\Delta\alpha/2)}{\Delta\alpha/2} = 1 \quad \text{numeric} \tag{15.11}$$

and taking the limit of eq. (15.10) as $\Delta\alpha \longrightarrow 0$,

$$\lim_{\Delta\alpha\to 0} \frac{\Delta T}{\Delta\alpha} = \frac{dT}{d\alpha} = \mu T \quad \text{newtons/radian} \tag{15.12}$$

or

$$\frac{dT}{T} = \mu\, d\alpha \quad \text{numeric} \tag{15.13}$$

Integrating eq. (15.13) yields

$$\ln T = \mu\alpha + k_1 \quad \text{newtons} \tag{15.14}$$

which can be written as

$$T = k_2\epsilon^{\mu\alpha} \quad \text{newtons} \tag{15.15}$$

To find the value of the constant of integration k_2, $T = T_1$ when $\alpha = 0$. Then the tension T_2, which corresponds to an angle of lap α, is equal to

$$T_2 = T_1\epsilon^{\mu\alpha} \quad \text{newtons} \tag{15.16}$$

and the ratio of tensions, on the two sides of the pulley, is equal to

$$\frac{T_2}{T_1} = \epsilon^{\mu\alpha} \quad \text{numeric} \tag{15.17}$$

The significance of eq. (15.17) is that the ratio of belt tension is equal to ϵ, the base of the natural logarithm raised to the $\mu\alpha$ power, where μ is the coefficient of friction between the belt and the pulley or sheave, and α is the angle of embrace of the belt around the pulley or sheave.

The belt will transmit torque from the motor shaft to the shaft of the driven equipment because of the difference between T_2 and T_1. This difference in tension is equal to the net force F acting around the angle of embrace α, or

$$F = T_2 - T_1 \quad \text{newtons} \tag{15.18}$$

If the effective radius of the motor pulley, or sheave, is R_m meters, the torque delivered by the motor is equal to

$$J_m = FR_m = (T_2 - T_1)R_m \quad \text{newton-meters} \tag{15.19}$$

and the power transmitted from the motor to the belt P_t is equal to

$$P_t = \frac{2\pi}{60}(\text{rpm})_m(T_2 - T_1)R_m \quad \text{watts} \tag{15.20}$$

where $(\text{rpm})_m$ is the drive-motor speed. Assuming negligible losses in the belt, the power transmitted from the belt to the driven equipment is also equal to (15.20), and the corresponding torque at the driven load is

$$J_d = \frac{60P_t}{2\pi(\text{rpm})_d} \quad \text{newton-meters} \tag{15.21}$$

Substituting eq. (15.20) into eq. (15.21) yields

$$J_d = \frac{(\text{rpm})_m}{(\text{rpm})_d}(T_2 - T_1)R_m = \frac{(\text{rpm})_m}{(\text{rpm})_d}J_m \quad \text{newton-meters} \tag{15.22}$$

where $(\text{rpm})_d$ is the speed of the driven equipment. Thus a belted-drive system can be regarded as a torque multiplier if the drive-motor speed is greater than the driven-equipment speed, as is normally the case.

As stated above, the difference in belt tensions $T_2 - T_1$, or the net force F, acting around the angle of embrace is effective in delivering torque to the belt. However, the lateral pull on the motor shaft extension is equal to the total lateral force that the shaft must resist (i.e., the sum of the two tensions). Thus the total force acting on the shaft is

$$F_s = T_1 + T_2 \quad \text{newtons} \tag{15.23}$$

Lateral belt pull can be a significant force and its effect must be considered at the design stage on the bearing, the shaft-extension end, and the bending stress in the shaft. Not all motors are designed to be suitable for belting. Thus if a motor that was initially sold as a coupled drive is subsequently considered for use as a belted drive, it is important that its suitability be verified. The owner should contact the manufacturer, who will then check the bearing on the shaft-extension end for bearing loading and the shaft for bending stress. When contacting the manufacturer, details of the proposed belted drive, including direction of belt pull, should be given. The direction of belt pull can be significant in determining the adequacy of the bearing on the shaft-extension end.

The following maximum values of belt-drive parameters are typical and can be used as a general guide. When applying belted drives, however, it is important to request and to use the recommendations of the belt manufacturer and of the motor manufacturer.

Type of belt	Maximum ratio of tensions	Maximum ratio of diameters	Maximum peripheral belt speed
V belt	7/1	8/1	1525 m/min or 5000 ft/min
Flat belt	4/1	5/1	1525 m/min or 5000 ft/min

The maximum peripheral belt speed should be verified by the belt manufacturer, though, since maximum permissible belt speed will vary somewhat. For flat belts, the distance between the centerline of the driving pulley and the driven pulley should be at least 2.5 times the diameter of the larger pulley, unless a belt-tension adjuster is used.

15.3.3 Chain Drives

For the preponderance of motor applications, direct-coupled drives and belted drives are used to transmit power. However, a small percentage of applications use chain drives for power transmission. For example, if it is desired to apply a motor to a low-speed application, and if belt slippage, such as can occur from occasional peak torques is not permissible, a chain drive could be a solution. For chain drives, sprockets replace pulleys or sheaves, and chains replace belts.

The teeth of the sprocket engage the cross members of the chain links, and thereby transfer a force from the teeth of the drive sprocket to the chain. Accordingly, the chain is impelled forward by the positive engagement of the teeth instead of by friction. The chain length should be such as to have a slight sag in the slack span when the pulling span is taut. It is sometimes stated that a chain drive is similar to a belted drive, except that the coefficient of friction μ is equal to 1.0. Although this is illustrative and useful when comparing the two types of drives, the analogy is not completely valid.

The distance between centerlines of the driving and the driven sprocket should be equal to or greater than the diameter of the larger sprocket plus the radius of the smaller one. The mechanical construction of, and the specific material used in, chains vary, depending on the type and the manufacturer. Accordingly, it is important to determine the maximum acceptable chain speed and sprocket ratio from the manufacturer of the specific type of chain being used. Lubrication of the chain is important and the lubrication and maintenance practices recommended by the chain manufacturer should be followed.

15.3.4 Gear Drives

One point of view is that a gear drive is a chain drive for which the chain link has been eliminated and the two "sprockets" placed together. The force is transmitted by the teeth of the drive pinion directly engaging the teeth of the driven gear. As for the chain drive, a gear drive can be considered to have a coefficient of friction of 1.0, and thus no slippage is possible. As for the chain drive, lubrication of the gear set is important and the lubrication and maintenance practices recommended by the gear manufacturer should be followed.

The number of conventional induction motors for which the driving pinion is mounted on the shaft extension of the motor is a very small percentage of total induction-motor applications, although some number do exist. However, so-called "gear motors" are manufactured and sold to some extent. Such drives consist of an induction motor and a reduction-gear set, enclosed within a transmission housing, which are compactly mounted to form one integral unit. Such units are generally limited to relatively low horsepower ratings and are normally used to provide torque at low speed. The manufacturers of this type of drive will supply necessary application information on their respective units. Similarly, sets of gears enclosed in a separate "gear box" and coupled to the drive motor and the connected load are also available, and manufacturers of this type of gear set will supply the necessary application information.

The primary applications for larger power ratings of gear drives are for ship propulsion and for use in certain slow-speed industrial mills. For such applications, it is not unusual for the set of gears to cost more than the drive motor. The application work, as well as the design and manufacture of the gears, is usually coordinated with that of the motor, so that a properly matched gear drive results; all large gear-drive applications should be handled in this manner. If for some reason it is decided to convert an existing medium-sized or large motor to a gear drive, qualified technical people should be consulted. Qualified people can be found in the application engineering organizations of motor manufacturers and gear manufacturers.

15.3.5 Endplay Considerations in Coupled Motor Drives

Endplay is an important consideration in coupling alignment. Thus it is in order to discuss endplay prior to considering alignment. Drive motors with so-called "antifriction" bearings (i.e., with ball or roller bearings) are normally designed to have the outer race of the opposite-drive-end bearing axially held by the bearing bracket or end shield. This permits the outer race of the drive-end bearing to move axially such as to allow for thermal expansion and contraction of the rotor relative to the stator. With one bearing axially held, such a machine does not have any endplay designed into the rotor. Also, it cannot accept any significant amount of external axial thrust from the driven equipment, unless that has been specified previously, at the design stage, and an appropriate bearing used which can carry both a radial and an axial load. Accordingly, a coupling that permits independent axial movement of the driven shaft relative to the motor shaft, such as a splined type, is recommended for drive motors with antifriction bearings. The exception would be for those drive motors for which the customer specified a capability for a given amount of axial thrust and the motor manufacturer provided an antifriction bearing with that capability.

Drive motors with sleeve bearings are designed to have approximately 6.5 to 12.5 mm (0.25 to 0.50 in.) of total endplay, with half in each direction

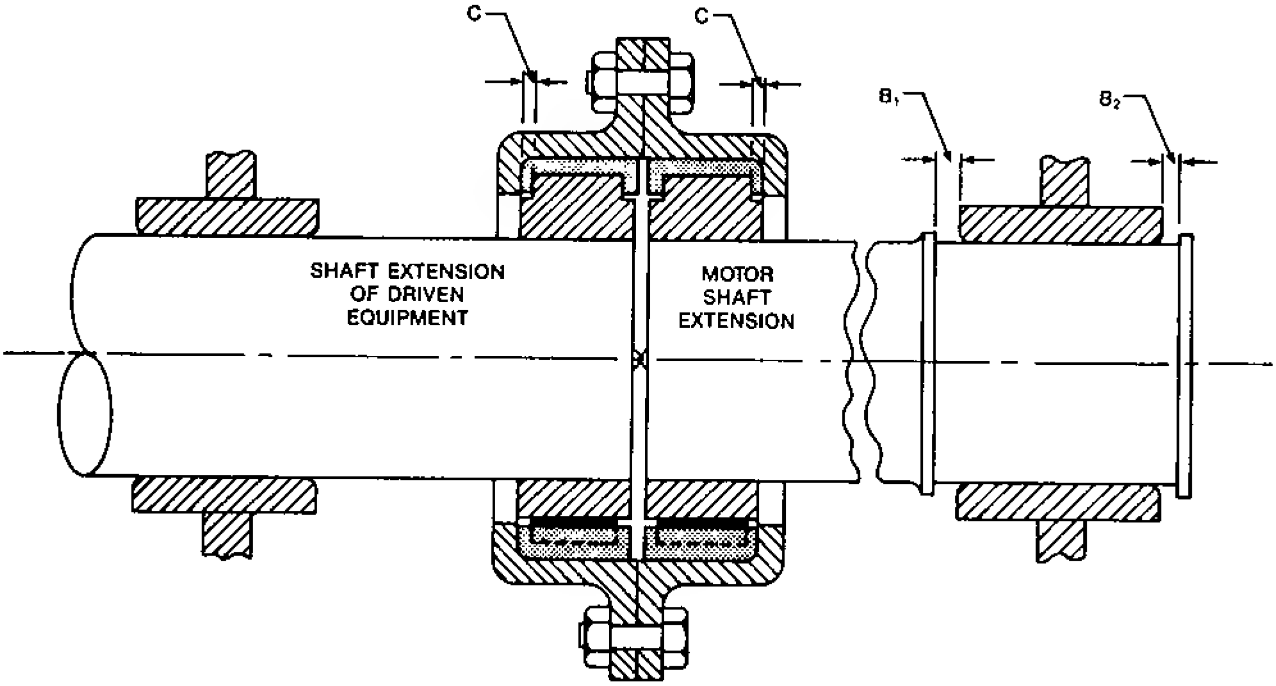

FIGURE 15.2 Schematic sketch of a generic limited end-float coupling.

from magnetic center. Thus the rotor will tend to operate on magnetic center, with approximately half of the endplay possible in either direction. Standard sleeve bearings are not normally designed to carry any significant external thrust. Thus if the driven equipment develops any axial thrust, such as from thermal expansion, hydraulic action, and so on, it is recommended that a limited end-float coupling be used. Again, in some cases, the drive motor will have been specified to have the capability for a specific amount of external thrust. Figure 15.2 is a schematic sketch of a generic limited end-float coupling. A system of clearances for a motor with a total endplay of 13 mm (approximately 1/2 in.) is as follows:

Relative positions of shaft	Dimensions					
	B_1		B_2		C	
	mm	in.	mm	in.	mm	in.
Shaft ends together	8.9	0.35	4.1	0.16	2.4	0.095
Shaft ends separated	4.1	0.16	8.9	0.35	0	0

15.3.6 Alignment of Solid Couplings

For purposes of simplification, alignment of solid couplings can be separated into two steps: parallel alignment and angular alignment. Parallel alignment will be considered first. With the machine positioned on its foundation as discussed in Section 15.2, the rotor is axially located in the center of its endplay. A dial indicator is then mounted on one coupling half, with its indicating probe touching the OD of the other coupling half (see Fig. 15.3a). It is important that this be a machined surface, as it usually is. The dial indicator is initially set at zero. Then the two coupling halves are rotated in unison, with no intentional relative motion between them. Dial indications are then read and recorded at the 3:00, 6:00, 9:00, and 12:00 o'clock angular positions. The shaft position is then adjusted such that the difference between the two lateral readings (i.e., 3:00 and 9:00 o'clock) and between the top and bottom readings (i.e., 12:00 and 6:00 o'clock) is less than 0.025 mm (0.001 in.). It can be expected that it will require several iterations to achieve this value. The vertical differences (i.e., at 12:00 and 6:00 o'clock) are corrected by adding or by removing shims of various thicknesses between the frame feet and the foundation. The lateral differences (i.e., at 3:00 and 9:00 o'clock) are corrected by lateral movement of the unit. It is not desirable to place too many shims in a given shim pack under any one foot, because too many shims can cause subsequent dynamical problems.

To put the motor into angular alignment, a dial indicator is mounted on one coupling half, with its indicating probe touching the vertical inboard side of the other coupling half (see Fig. 15.3b). Again, it is important that

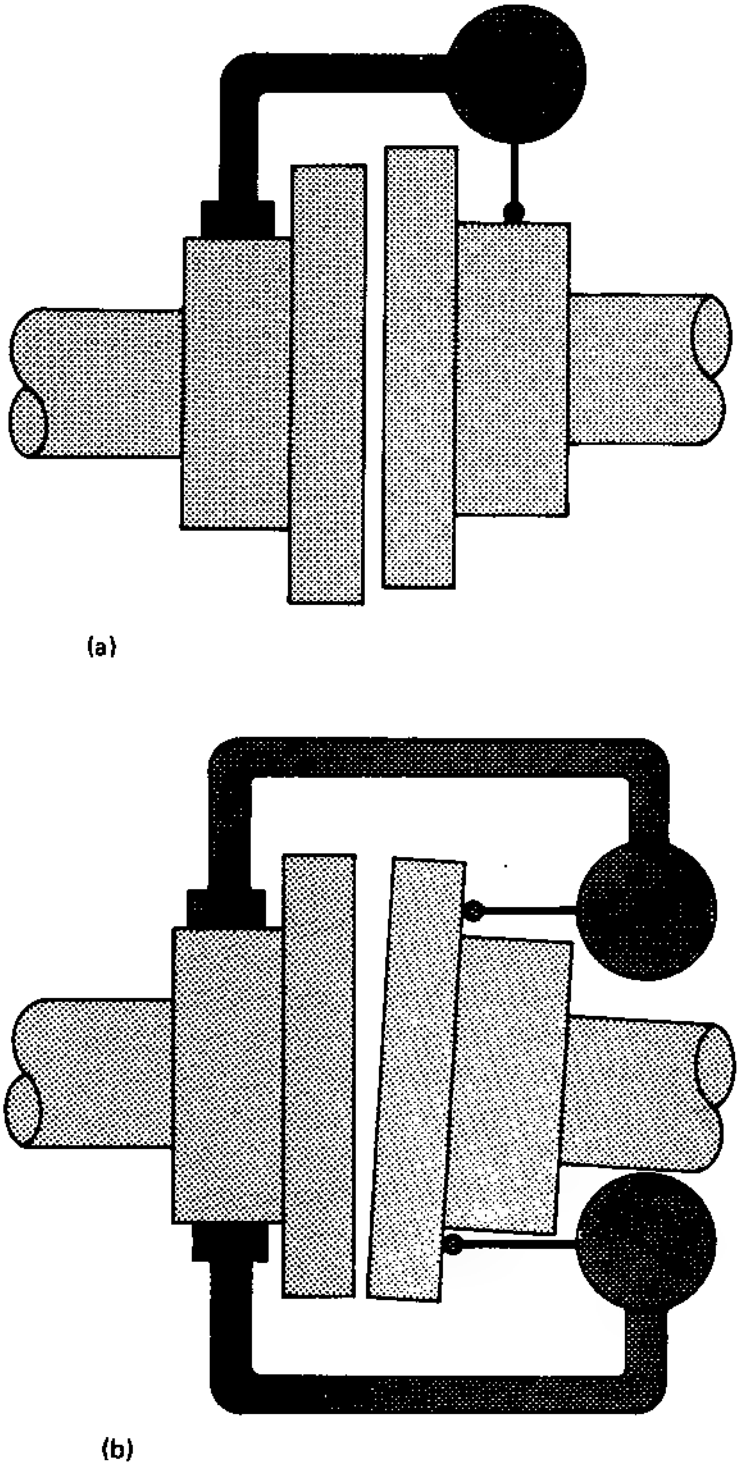

FIGURE 15.3 Dial indicator locations for aligning a motor drive with a solid coupling: (a) arrangement of dial indicator for making parallel alignment; (b) arrangement of dial indicators for making angular alignment.

this be a machined surface, as it usually is. A second dial indicator is mounted at an angular position, which is 180 degrees around the coupling, as shown in the figure. Each half-coupling is axially shifted to its maximum endplay and the dial indicators are then set at zero. The two half-couplings are held to maximum endplay and rotated in unison. The dial indications are read and recorded at 3:00, 6:00, 9:00, and 12:00 o'clock angular positions. The angular misalignment between the two coupling halves is determined from the difference in readings of the two dial indicators. Angular misalignment in the vertical plane is corrected by placing additional shims under the appropriate feet at one end of the motor. Angular misalignment in the horizontal plane is corrected by an appropriate lateral movement at one end of the motor. The alignment procedure should continue until the angular alignment is within about 0.04 mm (about 0.0015 in.). Again, this will require several iterations.

15.3.7 Alignment of Flexible Couplings

Although flexible couplings can compensate for some misalignment between the drive motor and driven equipment, it is not good practice to align such an installation in a casual manner. In fact, a flexible coupling should be aligned with the same diligence as is done for a solid coupling, and in all cases, the instructions of the coupling manufacturer and of the motor manufacturer should be followed. Limited end-float couplings should, in general, be given the same parallel and angular alignment as discussed in Section 15.3.6, as long as such procedures are not in conflict with the coupling manufacturer's instructions and if the two coupling halves can be made accessible to dial indicators.

In making the parallel and angular alignment, a machined, vertical surface may not be available to receive the dial-indicator probe on the inboard side of one of the half couplings. In that case, feeler gauges or block gauges can be substituted for the two dial indicators in conducting the angular alignment. In any case, the two half-couplings should be aligned to within 0.025 mm or (0.001 in.) parallel alignment and to within 0.040 mm (about 0.0015 in.) angular alignment.

15.3.8 Alignment of Belt Drives, Chain Drives, and Gear Drives

For most belt drives and for some chain drives, it is good practice to use slide rails with the drive motor, for ease of adjustment of belt tension. The slide rails should be leveled and adjusted in a manner similar to that discussed in Section 15.2 for foundation caps and sole plates. They should be positioned such that the horizontal centerline of the drive-motor shaft is parallel to the horizontal centerline of the driven-equipment shaft. Also, the vertical centerline of the pulley, sheave, or sprocket on the drive motor should be as close to the bearing bracket or end shield of the motor as possible consistent with full endplay. The equipment layout should be planned such as to permit reasonable access for belt or chain tension adjustment.

As stated above, it is important to align the pulley, sheave, or sprocket of the drive motor in the same vertical plane as that of the driven equipment. If this is not done properly, a periodic or continuous axial thrust can axially preload a motor bearing, which can result in premature bearing failure. Also, for a belt drive, the belt tension should be such as just to prevent slippage at full speed. Too great a belt tension will result in greater bearing loading than is normal, with more bearing heating and wear than is necessary. It is an incorrect practice to overly increase the belt tension in order to prevent some belt slippage and some "squealing" during the acceleration of high-inertia loads such as fans. As stated above, the belt tension should be set such as just to prevent slippage at full-load full-speed conditions. Thus for belt drives the belt should be allowed to slip during acceleration. Also, as stated in Section 15.3.3, for chain drives the chain should have a slight sag on its slack span when its loaded span is taut.

Gear motors, in which the drive motor and the gear set are integrally contained within an overall enclosure, have one pair of mounting feet and one shaft extension. Accordingly, the alignment of such a drive is similar to that of a direct-coupled drive motor, discussed previously in Sections 15.2 and 15.3.6. Gear sets that are enclosed in a separate housing to form independent "gearboxes" are normally coupled to the drive motor on one end, and to the driven load on the other end. Thus they are also aligned as discussed in Sections 15.2 and 15.3.6, but with the added complication that there are three, instead of two, separate units to be aligned. For the third type of gear drive, in which the pinion gear is mounted directly on the motor shaft, alignment of the drive motor is tantamount to alignment of the gear set. This requires that the two gears be so positioned in space relative to each other that their respective teeth engage and mesh correctly at their pitch diameters. Because of this, and because of the variation in tooth design as well as in other practices between various gear manufacturers, the gear set under consideration should be aligned in full accordance with the instructions of the particular manufacturer.

15.4 METHODS OF STARTING SQUIRREL-CAGE INDUCTION MOTORS

15.4.1 Considerations of Reduced-Voltage Starting

As discussed in earlier chapters, the magnitude of stator current of squirrel-cage induction motors at blocked-rotor conditions and at rated voltage is typically equal to 6.5 times its value at rated load and rated speed. This magnitude of current flowing through the impedance of the electrical system can result in a significant reduction in voltage levels within the local electrical distribution system. The amount of voltage drop will depend on the voltage regulation of the system, which is proportional to the starting kVA of the motor divided by the short-circuit kVA of the distribution system at that point. A given distribution system is said to be "stiff" or "soft," depending on whether the corresponding voltage dip in percent is small or is large enough to be significant.

A significant voltage dip, even of momentary duration, can result in significant problems. Such problems include momentary dimming of lights and malfunction of ancillary equipment, such as control and protective devices, associated with the distribution system. Thus there are good reasons to avoid large voltage drops within a given distribution system. Accordingly, most electric utilities have limitations on starting of motors within their systems. These limitations will permit the starting of a motor, up to a given horsepower rating, without any intermediate equipment, such as a reactor, to limit the starting current. This method of starting is called "full-voltage" or "across-the-line" starting. Above this maximum permissible horsepower rating, electric utilities have regulations that specify the maximum starting kVA/hp which is allowed. This requires that an intentionally reduced voltage be placed across the stator terminals during the starting period, in order to reduce correspondingly the starting kVA or demand seen by the distribution system.

There are some exceptions to the limitations on starting current. For example, the auxiliary motor drives associated with the generation plant of an electric utility are started at full voltage because of the huge source of kVA immediately available to supply the auxiliary motor bus. Also, many industrial plants utilize a sufficient amount of kVA, such that the added kVA increment associated with starting a large motor does not represent a significant percent of the plant's base kVA load at any particular time.

When a drive motor must be started at reduced voltage, an intermediate device or a temporary circuit must be utilized until the motor has essentially accelerated to rated speed. Such intermediate devices or temporary circuits include autotransformers, series reactance, series resistance, wye-delta connections, series-parallel connections, and part-winding starting connections. As discussed in earlier chapters, the torque developed by an induction motor is proportional to the second power of the applied voltage. Also, starting current is proportional to the first power of the applied voltage, except as affected by skin effect in the rotor bar and by saturation. However, all of the methods of starting at reduced voltage do not give the same value of the starting torque/starting current ratio for a given motor, as will subsequently become apparent. Since the motor torque must exceed the required load torque at all points along the speed-torque curve, a maximum value of this ratio is of considerable importance in starting induction motors.

When autotransformers, series reactors, or series resistors are placed in or out of the circuit, the switching can be such as to give short periods when the motor winding is disconnected from its source of voltage.

The same can occur when wye-delta, series-parallel, and part-winding starting connections are used. When the circuit is again closed following such an event, a circuit transient will generally result. This mode of switching is called open-circuit transition. Such electrical transients can be avoided by keeping the circuit closed during the switching period, and this mode of switching is called closed-circuit transition.

15.4.2 Autotransformer Starting

For this starting system, the input side of an autotransformer is connected to the motor bus and the output side of the autotransformer is connected to the stator terminals of the motor. A switching arrangement is provided, the function of which is to connect the motor to the autotransformer during the starting period, and directly to the motor bus during normal full-speed operation. Autotransformers for use with motors through about 50 hp are normally provided with taps at 65 and 80% of line voltage. For use with motors above 50 hp, through several hundred horsepower, they are normally provided with taps at 50, 65, and 80% of line voltage. However, taps at other voltages are generally available.

A simplified diagram of the basic circuit of an autotransformer for motor starting is shown in Fig. 15.4. The points L_1, L_2, and L_3 are

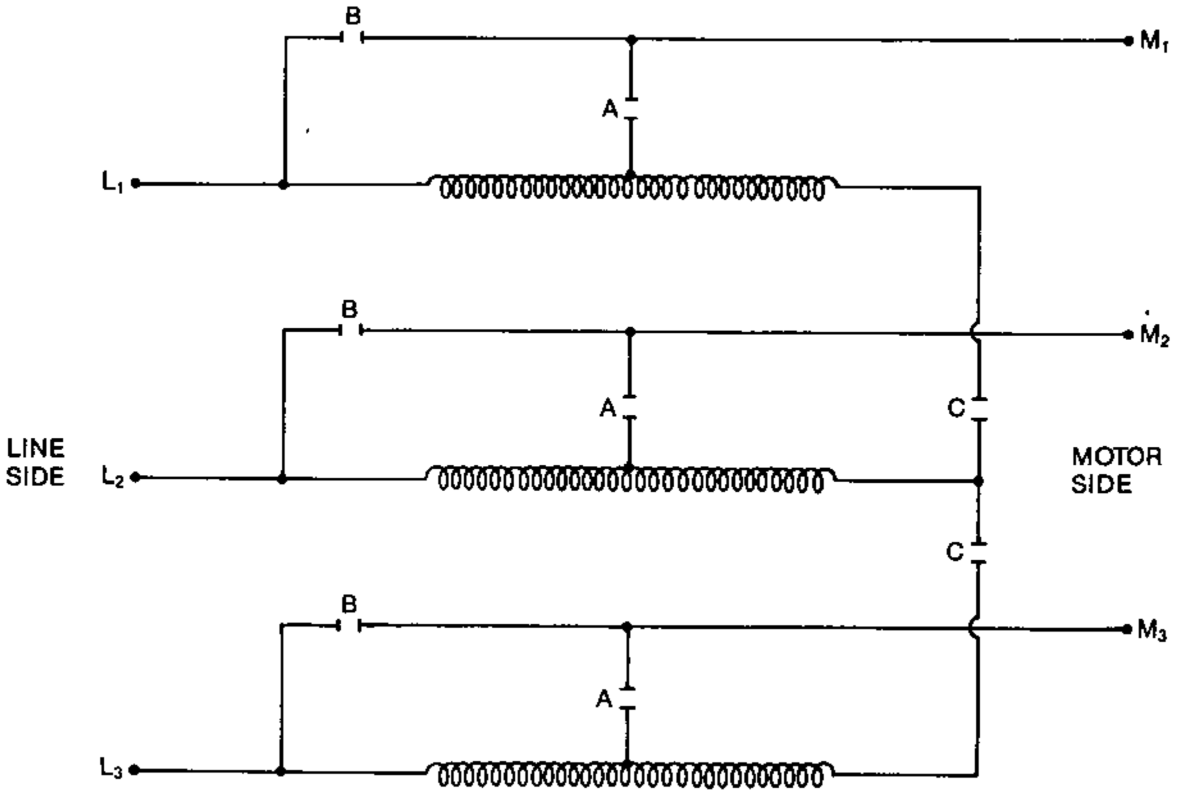

FIGURE 15.4 Simplified diagram of stator control for autotransformer starting of a motor.

TABLE 15.1 Open-Transition and Closed-Transition Switching Sequence for Starting a Squirrel-Cage Induction Motor with an Autotransformer

Event	Open-transition switching	Closed-transition switching
Apply reduced voltage to motor stator	Close contactors A and C	Close contactors A and C
Remove reduced voltage from motor stator	Open contactors A and C	Open contactor C
Apply full voltage to motor stator	Close contactor B	Close contactor B and then open contactor A

connected to the three-phase motor bus, and the points M_1, M_2, and M_3 are connected to the terminals of the phase windings of the motor. Table 15.1 gives the switching sequence for both open-transition and closed-transition starting. For open-transition starting, contactor sets A and C are closed, which applies reduced voltage to the terminals of the stator winding of the motor. This allows the motor to accelerate to full speed with reduced line current, but with reduced torque. When the motor has nearly accelerated to full speed, contactor sets A and C are opened to remove reduced voltage from the terminals of the stator winding. Immediately after that, contactor set B is closed, which places line voltage on the phases of the stator winding. This mode of starting requires that the stator winding be disconnected momentarily from a source of voltage before line voltage is applied. During that short period, the rotating rotor core still contains flux, and this "trapped" flux will continue to generate a voltage within the stator phase windings. It can be expected that when contactor set B is closed, line voltage and the voltage generated within the motor winding will be somewhat out of phase. This will cause a current transient and a torque transient, both of which are philosophically objectionable. However, open-transition starting is frequently used, particularly for motors of lower horsepower ratings.

To overcome the objections to switching transients, the concept of closed-transition starting was developed. The switching sequence for closed-transition starting, also known as the Korndorfer method of starting, is shown in Table 15.1. For this mode of autotransformer starting, contactor sets A and C are closed, applying voltage to the stator winding of the motor. The motor then accelerates to full speed, with reduced line current and reduced torque. When the motor has reached or nearly reached full speed, contactor set C is opened. This switching action opens the neutral point of the autotransformer and causes the phase windings of the stator to be connected to line voltage through the reactance associated with part of the autotransformer winding. Contactor set B is then closed, which directly connects the stator winding terminals to line voltage and at the same time short circuits the series-reactance connection between the winding and the stator bus. Finally, contactor set A is opened, which completely isolates the autotransformer and the above-mentioned series-reactance connection from both the motor and the motor bus. By use of closed-transition starting, the reduced-voltage source has been removed and the full-voltage source applied to the stator without, at any time, having the stator winding disconnected from a source of voltage. Thus the significant transient associated with a momentary open circuit is avoided. However, the cost of the control equipment is somewhat greater than for open-circuit transition starting.

Since the torque of an induction motor is proportional to the second power of the voltage applied to the stator, the motor torque is proportional to the second power of the per unit output voltage of the autotransformer during the starting period. Thus if a 0.80 voltage tap is used, the torque developed by the motor during acceleration is equal to $(0.80)^2 = 0.64$ per unit of that developed at full voltage. Also, since the current of an induction motor is proportional to the voltage applied to the winding during the starting period, the current that flows in the cables between the motor terminals and the output of the autotransformer is proportional to the first power of the per unit output voltage of the autotransformer. However, the current that flows in the cables between the bus and the input to the autotransformer is reduced by the turns ratio in comparison to the current on the motor side of the autotransformer. Thus the stator current as seen by the power distribution system is reduced by the second power of the per unit output voltage of the autotransformer. Then, since both the starting current and the starting torque are reduced by the second power of the per unit voltage impressed on the stator winding, the ratio of starting torque to starting current, or the torque-to-current effectiveness ratio, is the same as for full-voltage starting. This feature makes autotransformer starting of polyphase induction motors a very desirable method for many applications.

15.4.3 Series-Resistor Starting

For this starting system, a resistor is temporarily placed in series with each of the three stator-winding terminals, to limit the magnitude of starting kVA. Switching is provided either to (1) progressively short circuit the resistor, in increments, at successive points in time, or to (2) short circuit all of the resistor, at one time, after the motor has accelerated to a point on the speed-torque curve which approaches full speed. Use of the first method permits setting the switching system such that the maximum accelerating torque is developed, consistent with the local restriction on starting kVA. However, in many cases, starting in one step is satisfactory. This mode of starting does not result in any short periods in which the stator circuit is opened, and then closed, during the acceleration period. Thus this type of starting does not produce the aforementioned current and torque transients associated with open-circuit transition switching of an autotransformer.

For series-resistor starting, the stator line current drawn from the electrical distribution system is proportional to the net voltage impressed across the stator winding. On the other hand, the torque developed by the motor is proportional to the second power of that voltage. Thus the ratio of starting torque to starting current, or the torque-to-current effectiveness ratio, is less than for full-voltage starting or for autotransformer starting. However, the torque developed by series-resistance starting, as permitted by the typical electrical-utility restriction on starting kVA, is adequate for many applications.

As the power ratings of the motor increase, a point is eventually reached at which series-resistor starting becomes impractical. At this point, the I^2Rt energy losses correspond to a sufficient amount of heat, developed in a relatively short time, to create a heat dissipation problem within the restricted space normally available. Also, producibility considerations of resistor elements, properly insulated for such voltages as 2300 and 4000 V, can present manufacturing problems. Accordingly, this type of starting is generally limited to motors with voltage ratings of 550 V or less.

15.4.4 Series-Reactor Starting

Series reactors may be used in place of series resistors for reduced-voltage starting of induction motors. The series-reactor method has the disadvantage, however, that it is not possible to remove reactance in increments unless the reactor winding for each increment is on a separate magnetic core. Otherwise, this method is similar to series-resistor starting, including the associated switching arrangement. The ratio of starting torque to starting current, or the torque-to-current effectiveness ratio, is the same as for series-resistor starting and is less than for full-voltage starting or for autotransformer starting.

The series-reactor method has one advantage over the series-resistor method. As the motor accelerates to full speed, the rotor slip decreases, thereby increasing the value of R_2/s, the resistive component of the rotor circuit. Thus the starting reactor represents a fixed amount of reactance, which is in series with the motor circuit, the impedance of which is changing as the motor accelerates. At low speed, the impedance of the motor circuit is predominantly leakage reactance, whereas as the speed increases, the impedance increases in magnitude and becomes increasingly resistive. The net effect is that as the speed increases, the starting reactance becomes a smaller percentage of the total circuit impedance, and the voltage increases at the motor terminals. This permits both the torque and the line current of the motor to increase and to tend to approach the corresponding full-voltage values as the motor accelerates toward full speed.

Series-reactor starting is frequently used for motors with voltage ratings of 2300 V or greater, the power ratings of which are generally greater than are those for which series-resistor starting is used. The magnitude of reactance is frequently selected such as to limit the starting current to a value just equal to that allowed by the local power company. This will permit the maximum starting torque possible based on this mode of starting and on the local power company regulations.

15.4.5 Wye-Delta Starting

If a polyphase induction motor is designed to operate at rated voltage with a delta-connected stator winding, and if six stator leads are brought out to an external terminal board (i.e., one lead from each end of each phase winding), the motor is capable of wye-delta starting. It is apparent that if a delta connection results in rated voltage on each phase winding of a given machine, a wye connection will result in $1/\sqrt{3} = 0.577$ of rated voltage on each phase winding of the same machine. Accordingly, the stator winding can be externally connected in wye for starting, and then externally reconnected to delta, by switching, for full-speed operation. With the three-phase stator winding connected in wye, the phase voltage is $1/\sqrt{3} = 0.577$ of the rated value under full-speed operating conditions when the stator winding would be connected in delta. Thus during the starting period the phase current is reduced to 0.577 per unit of what it would be if rated voltage were impressed across the phase. However, with the stator winding connected in delta at full-speed operation, the line current is $\sqrt{3}$ times the phase current. Thus the starting line current is $(0.577)^2 = 0.333$ per unit of that of full-voltage line current with wye-delta starting.

With 0.577 per unit voltage across each phase, the flux is 0.577 per unit of what it would be with a delta connection at full-speed conditions. Accordingly, the starting torque is $(0.577)^2 = 0.333$ per unit of that at full voltage. Thus the ratio of starting torque to starting current, the torque-to-current ratio, is the same as for full-voltage starting and for autotransformer starting. However, a reduced-voltage value of starting torque, which is only 0.333 per unit of the full-voltage value of starting torque, may be too low a value for many applications. Also, the transfer from a wye-connected to a delta-connected stator is usually accomplished by open-transition switching. As discussed earlier, this results in a current transient and in a torque transient, both of which are generally undesirable. Schemes for switching have been developed in which the circuit is opened and closed through temporary resistors, which is tantamount to closed-circuit transition. As might be expected, this increases the complexity and cost of the associated control equipment. However, since the torque produced by wye-delta starting is only one-third of that of full-voltage starting, and since the motor must be designed to have a delta-connected stator winding for full-speed operation, this mode of reduced-voltage starting is infrequently used, aside from any consideration of switching.

15.4.6 Solid-State Starting

A starting system that can be expected to gain favor in future years is that which utilizes solid-state devices. The general approach is to use such devices as silicon-controlled rectifiers or thyristors in a three-phase full-wave bridge circuit and to control the phase angle between 0 and 180 degrees at which the SCRs are fired, to produce a controlled voltage at the terminals of the stator winding. Appropriate control circuitry can be designed to sense current amplitude and to regulate the current during acceleration of the motor to a value of from 250 to 400% of full-load value. Other schemes of control circuitry are possible utilizing timers, voltage ramps, speed signals, and so on.

Two disadvantages of solid state starting at the present time are cost and the production of harmonics. The cost of rectifier banks can be reduced to some extent by using a combination of rectifier diodes and SCRs instead of only SCRs. Also, the long-standing belief that the cost of solid-state devices will eventually be reduced is apparently occurring to some extent. Design efforts to reduce harmonic content usually result in greater cost of the starting system. Fortunately, the acceleration time during which harmonics are being produced is a very small percent of the total operating time for most applications. Thus the additional heating of the motor as well as any spurious effects on other control equipment caused by such harmonics can be tolerated for many applications. However, it is prudent and necessary to verify this with the motor manufacturer, as well as with other equipment suppliers, to remove completely any risk that might exist.

15.4.7 Other Methods of Starting

There are two other methods of starting, which have been used in the past, which are not now applied to any significant extent but which are of historical interest. These methods are series-parallel starting and part-winding starting. The series-parallel method will be the first to be discussed. Consider a given motor, the stator winding of which is designed to have two parallel circuits in each phase, for rated-speed, rated-voltage operation. If the same stator winding is reconnected to give a series circuit in each phase, it will produce the same flux/pole in the machine if it is excited at a voltage equal to two times rated voltage. This can be understood by examining eqs. (9.136) and (9.137). By changing the phase windings from two-parallel to series, the series turns/phase N_{st} is doubled, as can be seen from eq. (9.136). Also, if ϕ_{pm} is held constant and if N_{st} is doubled in eq. (9.137), the value of the induced voltage E_1 is also doubled. Thus if the actual rated voltage of the motor is 440 V line to line with the original connection of two circuits/phase, it will require 880 V line to line with a series circuit in each phase to maintain rated flux. Accordingly, if 440 V line to line is now applied to the motor, the flux/pole ϕ_{pm} is half of the rated value. This will result in a starting current that is only 50% and a starting torque that is only 25% of that at rated voltage.

To utilize the series-parallel method of starting, the motor must originally have been designed to have two circuits/phase for full-voltage operation, and the two ends of each circuit of each phase must be brought out of the machine for external connection. The series connection is then used for acceleration, and as the machine approaches full speed, the stator winding is switched to the two-parallel connection for full-speed operation. However, because the torque during the starting period is only 25% of that at full-voltage starting, this method of starting is not very practical for general-purpose applications. Nevertheless, there are some number of older machines still in service that use this method of starting.

The second method of reduced-voltage starting, which is infrequently used, is called part-winding starting. A three-phase induction motor that has a stator winding consisting of two identical wye-connected sections which are connected in parallel to form a two-parallel-wye stator winding for full-speed operation is a possible candidate for part-winding starting. Consider Fig. 15.5. One wye-connected section is defined by terminals 1, 2, and 3 and the other is defined by terminals 7, 8, and 9. The phase groups that make up one wye should be symmetrical with respect to the phase groups that make up the other wye.

If full three-phase bus voltage is applied to terminals 1, 2, and 3, one might expect that 50% of normal starting current would result. However,

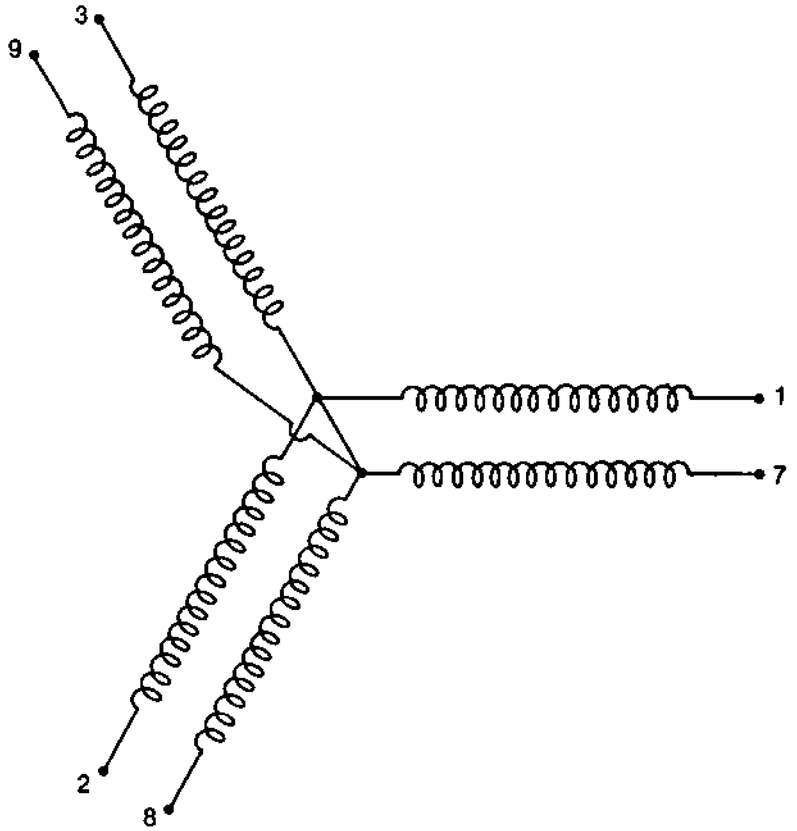

FIGURE 15.5 Stator-winding diagram for part-winding starting of a motor.

it must be remembered that only half of the coil sides positioned within the stator slots are excited and that normal mutual inductance between coil sides has been disrupted. The result is that starting current is approximately 65% of normal. The starting torque is generally less than 50% of normal and frequently will have cusps which are considerably lower than that amount. As the motor approaches full speed, switching contactors are closed such that terminals 7, 8, and 9 are connected simultaneously to the three-phase bus, placing terminal pairs 1 and 7, 2 and 8, and 3 and 9 on corresponding phases of the three-phase bus.

In applying a polyphase induction motor, it cannot be assumed that any motor with a two-circuit wye-connected stator winding, is suitable for part-winding starting. As stated above, the two wye-connected sections should be made up of symmetrically located coil groups. Also, appropriate terminals should be brought out external to the machine, as shown in Fig. 15.5. Further, perturbations on the speed-torque curve such as were discussed in Section 12.10 can be produced by this mode of starting. Occasionally, such perturbations are so severe as to be unacceptable for a given application. Thus it is important that the motor manufacturer be involved if part-winding starting is being considered for a given motor drive.

15.4.8 Stall Time of Squirrel-Cage Motors

It was shown in Section 10.3.16 that significant heating of a squirrel-cage rotor winding occurs during a change in speed of the rotor and any connected load, and the subject is considered further later in this chapter. However, significant rotor heating can also occur without a change in speed if power has been applied to the motor and if for some reason the motor does not accelerate. Blocked-rotor current for both the stator and rotor winding is typically 6.5 per unit of rated current at rated voltage. Under such conditions, the rate at which I^2Rt energy losses are being produced, in the rotor winding, is over 40 times the corresponding rate, at full-load, full-speed conditions at constant rotor resistance. However, the resistance of the rotor circuit, at blocked-rotor conditions, is typically 1.5 to 2.5 of that at full speed. Thus the energy-production rate at blocked rotor can be 80 times that at full-load full-speed conditions.

With "across-the-line" starting, the bus voltage will not be 1.0 per unit, of course. However, if the regulation of the motor bus is such that the voltage is 0.70 per unit of rated, with this kind of starting, the rate of energy production within the rotor winding is still equal to about 40 times that at full-load full-speed operation. Because of the relatively short time involved and because of reduced heat dissipation at blocked-rotor conditions, it can be reasonably assumed that all of the energy is effective in increasing the temperature of the rotor winding. Then, if the motor torque cannot "break away" the driven load for some reason, or if the rotor "crawls" at a reduced speed because of a cusp in the speed-torque curve, it is very clear that dangerous rotor-winding temperatures will be reached in a short time. The maximum time that a given motor can safely be stalled with full voltage applied to the stator terminals is called the maximum permissible stall time, or more usually, the "stall time" of that motor. It is apparent that if less than full voltage is applied to the motor, due to normal bus regulation or due to the use of reduced-voltage starting, the permissible stall time will increase as the voltage decreases. Thus if the rotor resistance is considered constant, the square of the ratio (actual blocked-rotor current)/(full-voltage blocked-rotor current) will have a hyperbolic relationship with stall time. Accordingly, an accurate stall-time curve can be made for a given motor which is applicable for blocked-rotor conditions. Further, the speed-time curve of a typical induction-motor application has an elongated S shape which tends to approach a straight line. Then, for most applications, it can be assumed that for an unhampered acceleration, speed varies linearly with time (although there are specific applications for which this assumption is not sufficiently close). Thus if the stall time and the acceleration time of a given motor application are known, timers can be used to activate relays, such as to protect the rotor winding of that motor during acceleration. The stall time of a specific motor should always be obtained from the motor manufacturer.

15.5 WOUND-ROTOR MOTOR STARTING

There are many applications for which wound-rotor motors are well suited and are preferred, aside from any consideration of starting. However, because of the use of a phase-wound rotor and because external connections are possible through collector rings and brushes to the rotor winding, wound-rotor motors provide prime starting characteristics and give a maximum ratio of starting torque to starting current. In fact, this type of motor is so well suited for starting that in applications that require drive motors with large power ratings, no other type of motor could be started without unacceptable disruption to the voltage levels of the local electrical distribution system. Also, as will be discussed subsequently, wound-rotor motors have the capability to accelerate connected loads that have very large values of rotational inertia.

If the brushes are shorted and if rated voltage is applied to the stator winding of an unloaded wound-rotor motor, it will produce a starting torque which is somewhat less than that of a squirrel-cage motor, and will accelerate to full speed. However, the starting current will be essentially equal to that of a squirrel-cage motor of the same rating. If, on the other hand, a given amount of external resistance is added to each phase of the rotor circuit, as discussed in Section 5.11, the added motor impedance will decrease the starting current, increase the starting torque, and not significantly affect the maximum torque (see Fig. 5.6). Additional increments of external rotor resistance will continue to decrease starting current and to increase starting torque until the starting torque is equal to the maximum torque. Beyond this point, if additional external resistance is added, both the starting torque and the starting current will decrease.

From the above it is apparent that wound-rotor motors can be used to accelerate a wide range of driven equipment by use of a controlled amount of external rotor resistance. Judicious selection of the resistance increments can give large accelerating torques and low line current with relatively few steps of external resistance. For motors of lower power ratings, a conventional type of resistor is used which has been designed to have adequate thermal capacity or sufficient heat dissipation ability. The number of steps and the ohmic value of each step is chosen so as to provide the ratio of torque to current that is required for the specific application. For motors of larger power ratings, a water barrel is frequently used. "Water barrel" is the colloquial name for a tank that contains a brine mixture. Brine is a conductor of current and also a conductor of heat. The amount of resistance exhibited is a function of how deeply the three solid-contact members are immersed into the liquid. If there is a significant amount of heat to be dissipated within the liquid, such as that produced by driven equipment which has high rotational inertia and which requires an appreciable length of time to accelerate, a fluid pump can be used to circulate the brine through a heat exchanger. Accelerating the motor and driven equipment by use of conventional or of liquid resistors is called resistor starting.

A second method of starting a wound-rotor application is that of using a combination of external resistance and reactance elements in the rotor circuit. The impedance of the reactance is proportional to the frequency of the rotor circuit, which decreases linearly with speed as the motor accelerates, without the need for step changes. The resistive component of the circuit is selected such as to give the required starting torque, and the reactive component is selected such as to combine with the resistive component to limit the accelerating current and to give the desired value of maximum torque. The result is a favorable ratio of starting torque to starting current throughout the speed-torque curve, without the need for steps, for most of the speed range. The accelerating torque is essentially constant for this mode of starting, up to about 85% speed, at which point the switching arrangement starts to short elements out of the static network, giving relatively constant torque up to full speed. The unusual smoothness of such an acceleration makes this mode of starting very suitable for such applications as hoists, draglines, and conveyors. This method is called reactor-controlled starting.

Figure 15.6 shows a typical static circuit for achieving this type of starting. This static circuit has three resistors and a reactor in each phase, which gives considerable adjustability in designing a circuit for constant-torque acceleration. All rotor-circuit contactors are open and all rotor-circuit impedance elements are in the circuit when voltage is applied to the

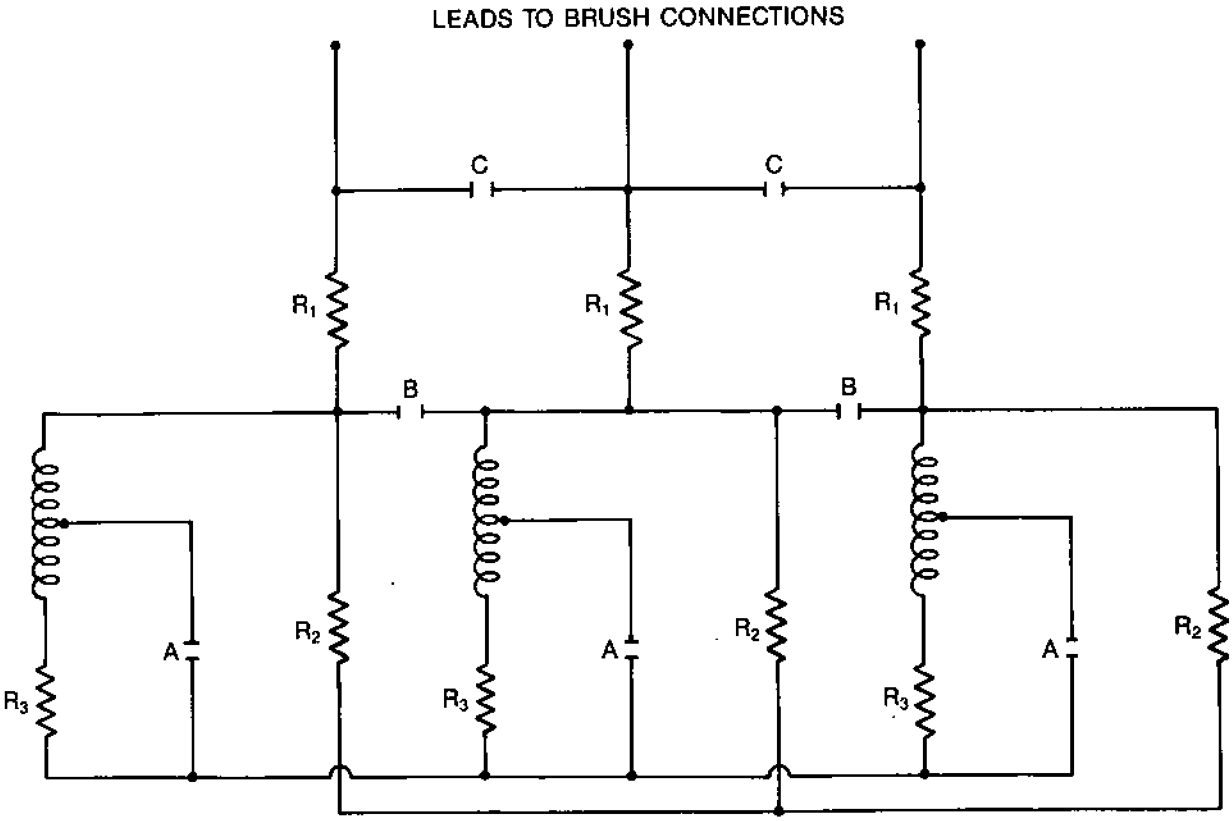

FIGURE 15.6 Rotor-control diagram for starting a wound-rotor motor using a resistor-reactor static network.

TABLE 15.2 Switching Sequence for Starting a Wound-Rotor Induction Motor Using a Static Resistor-Reactor Network in the Rotor Circuit

Event	Approximate speed (% of synchronous speed)	Switching
Remove resistor set R_3 and part of reactor from rotor circuit	85	Close contactor set A
Remove resistor set R_2 and remainder of reactor from rotor circuit	90-95	Close contactor set B
Remove resistor set R_3 from rotor circuit	95-97	Close contactor set C

stator. The switching sequence for the rotor-circuit control is given in Table 15.2. The motor accelerates with essentially constant torque to approximately 85% speed. At this point a signal from a tachometer or a timer closes contactor set A, which short circuits resistor set R_3 and part of each of the reactors in each rotor phase. Between 90 and 95% speed, contactor set B closes, which short circuits all the static circuit except for resistor set R_1 in each rotor phase. Finally, at between 95 and 97% speed, contactor set C closes, which short circuits the collector rings, leaving only the internal rotor-winding impedance in the rotor circuit. It will be noted that at no time in the sequence above is the rotor circuit open. Thus closed transition switching is used in this control system.

The disadvantage to wound-rotor starting is the cost of the capital investment. The cost of a wound-rotor motor is considerably greater than that of a squirrel-cage motor of the same power, speed, and stator-voltage rating. Also, the cost of the associated control is greater in most cases. Nevertheless, for a motor supplied from a constant-frequency voltage source, this type of motor is unsurpassed in its starting capabilities.

15.6 METHODS OF SPEED CONTROL

Because of lower cost, greater reliability, and lack of dependence on complicated control in comparison to other electrical drives, squirrel-cage induction motors are the most popular drive motor and have acquired the reputation of being the "workhorse" of industry. However, such machines are essentially constant-speed drive motors under normal operating conditions, whereas there are some number of industrial applications for which a variable-speed or an adjustable-speed drive motor is desirable, or even necessary. The alternative to a variable-speed ac electrical drive motor is a dc drive motor, which requires a considerably greater initial cost for a given amount of shaft power at a given base speed, which requires more costly control equipment, generally requires more maintenance, and requires a source of dc power which may not be available or which requires significant cost to put into place. Thus there has been considerable economic motivation through the years for the development of a variable-speed ac motor drive.

Early in the history of induction motors, the wound-rotor motor was developed, which permitted operation over a wide range of speed, but at the expense of efficiency due to increased slip loss at reduced speed. As stated earlier, though, wound-rotor motors are suited for more applications than variable-speed drives, and as discussed subsequently, methods have been devised to benefit from the slip loss of such machines, but at a significant increase in cost for the additional equipment. Accordingly, throughout the ensuing years, various methods have been developed to apply induction motors to variable-speed applications. Understandably, some of the earlier methods had disadvantages and were replaced by better methods developed subsequently. In this section we consider the more significant methods developed to apply polyphase induction motors to driven loads which require variable speed.

The operating speed of an induction motor can be changed by changing the synchronous speed or by changing the operating slip of the machine. From eq. (3.38), synchronous speed is equal to

$$n_s = \frac{60f}{p/2} \quad \text{rpm} \tag{15.24}$$

Thus synchronous speed can be varied by varying the frequency of the stator voltage or by changing the number of poles. Slip, which is proportional to the per unit I^2R loss in the rotor circuit, can be varied by varying the ohmic resistance of the rotor winding, by varying the stator voltage, and by inserting voltages of the desired frequency into the rotor circuit. Also, a squirrel-cage motor can drive a load through a slip coupling such as a hydraulic coupling, so as to give variable speed by controlling the slip of a coupling. Then any variable-speed induction motor for variable-speed operation must utilize one of the concepts above.

15.6.1 Rheostat Control of Wound-Rotor Motors

It was shown in Chapter 5 and illustrated in Fig. 5.6 that the speed-torque curve of a wound-rotor motor could be significantly changed by changing the ohmic value of the resistance in each phase of the rotor circuit. The slope of the speed-torque curve from the point of rated torque to the point of maximum torque will decrease as the rotor resistance increases. Accordingly, the point of intersection of the speed-torque curve of the drive motor and of that of the driven equipment, which defines the operating point, will also decrease as the rotor resistance increases. See Fig. 15.7, which shows the torque developed by the motor versus speed for three different settings of the external rheostat, as well as the load torque versus speed. The load shown in the figure requires a torque that varies as the second power of speed, such as for a fan or a pump. For such loads, the power requirements vary as the third power of speed. Thus if sufficient external rotor resistance is inserted to reduce the speed by 5%, the power requirements of the load decrease by about 14% [i.e., $(0.95)^3 = 0.857$]. Also, if sufficient rotor resistance is inserted to reduce the speed by 10%, the power requirements of the load is decreased by about 27% [i.e., $(0.90)^3 = 0.729$]. Thus for a load such as a fan or a pump, a relatively small decrease in speed is an effective way in which to reduce the rate of fluid flow.

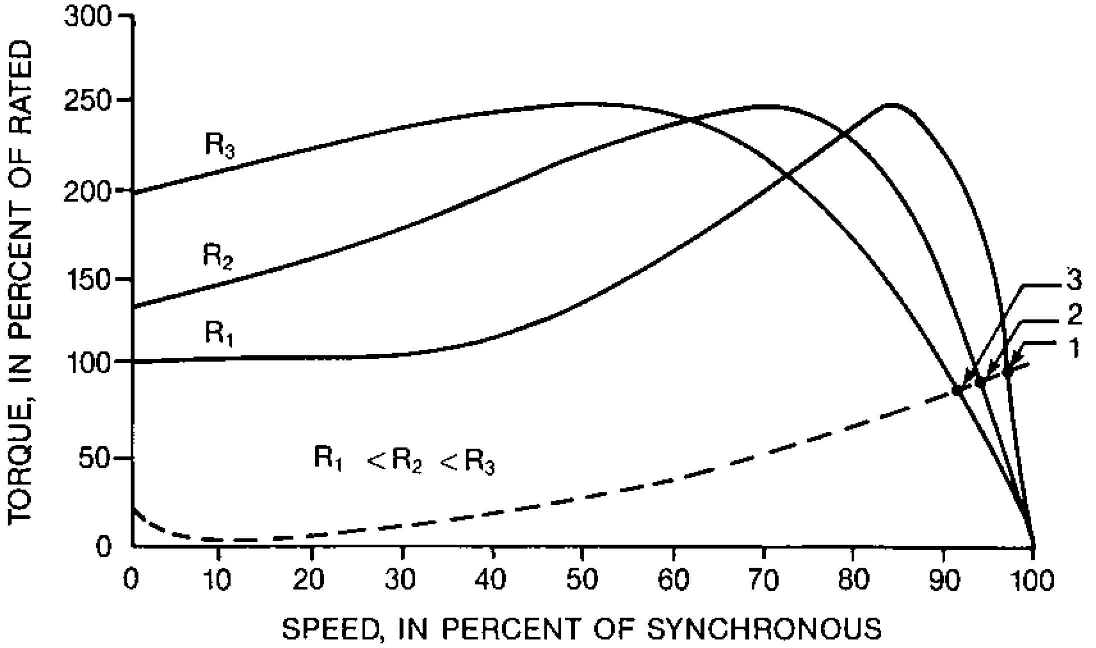

FIGURE 15.7 Speed variation of a wound-rotor motor by varying external rotor resistance.

As mentioned earlier, the reduction in speed of a wound-rotor motor is achieved at the expense of efficiency. Thus to reduce the speed by 5%, efficiency is reduced to about 95% of that at full speed. However, for such a variable torque load, the power requirements have decreased 85.7% of that at full speed. Similarly, to reduce the speed by 10%, the efficiency is reduced to about 90% of that at full speed, and the power requirements have decreased to 72.9% of that at full speed. There are variable-torque variable-speed applications for which the additional rotor loss of a wound-rotor motor is acceptable. For such applications the sum of the initial cost and the annualized operating costs should be equal to or less than alternative methods of providing for the requirements of the drive.

There are other specific applications, such as some material-handling equipment, which require high starting torque, high intermediate-speed torques, and low starting current throughout the duty cycle, for which wound-rotor motors are, not infrequently, the most economical type of drive motor. Also, as discussed in Section 15.5, it is occasionally necessary to utilize a wound-rotor motor for some large motor applications, because only such a motor will produce a sufficiently favorable ratio of torque to line current during the starting period. Aside from such application considerations as the above, however, the inherent inefficiency of wound-rotor motors at reduced speeds causes such motors to be uneconomical for many variable-speed applications.

15.6.2 Speed Control by Cascading Two Wound-Rotor Induction Motors

Assume that a wound-rotor motor and a squirrel-cage motor are mechanically coupled, that the stator winding of the wound-rotor motor is connected to a suitable bus, and that the rotor circuit of the wound-rotor motor is connected through its collector and brushes to the stator winding of the squirrel-cage motor. Such a connection of the two motors is called a cascaded, or a concatenated, connection and produces a combined motor system, with an effective number of poles equal to the sum or the difference of the two individual motors. Let voltage from the bus be applied to the stator winding of the wound rotor machine. Then the combined motor set will have a synchronous speed n_s equal to

$$n_s = \frac{60f}{(p_1 + p_2)/2} \quad \text{rpm} \tag{15.25}$$

or to

$$n_s = \frac{60f}{(p_1 - p_2)/2} \quad \text{rpm} \tag{15.26}$$

where p_1 and p_2 are the numbers of poles, respectively, of the two motors. The particular speed at which the set operates depends on the phase connections between the two machines, and to change from one speed to the other, it is only necessary to reverse any two of the three leads.

If, for example, a four-pole and a six-pole motor were cascaded, the combined set would exhibit ten-pole and two-pole synchronous speeds. Also, by disconnecting the electrical connections between the two machines (but not necessarily disconnecting the mechanical coupling) and by applying bus voltage to one or the other stator winding, the set would have a four-pole or six-pole synchronous speed. Accordingly, such a set has the capability to operate at an operating speed which is slightly less than 720, 1200, 1800, and 3600 rpm, assuming that both machines have been designed to withstand the mechanical stresses at such speeds. Further, if the second machine is also a wound-rotor motor, and a rheostat is connected to the rotor winding of that machine, a more refined degree of speed control, between base speeds, is possible.

The rotor winding of the wound-rotor motor used in a cascaded motor set should be designed to be adequate for the power rating of the second motor, which it supplies. Also, the voltage ratings of the wound rotor of the first motor should generally match the voltage rating of the stator winding of the second motor. The magnetizing current of the second motor must be transferred through the rotor and stator windings of the first motor. Thus the first motor must be sized to handle the additional kVA resulting from this additional out-of-phase current. Cascaded motor sets have not been used to any great extent in variable-speed applications in recent years. However, there are some number of such sets still in operation throughout industry.

15.6.3 Speed Control of Wound-Rotor Motors by Use of Auxiliary Machines or Devices

As discussed in Chapter 5, if the power input to the stator is P_1 and the sum of stator losses and friction and windage losses equal L, the power that is dissipated in the rotor winding as I^2R loss is essentially equal to $(P_1 - L)s$, where s is slip in per unit. Also, the reduction in speed, below synchronous speed n_s is proportional to s, so that rotor speed n is equal to

$$n = (1 - s)n_s \quad \text{rpm} \tag{15.27}$$

Thus in controlling the speed of a wound-rotor motor by use of a rheostat connected to the rotor circuit, speed reduction is proportional to I^2R loss in the rotor circuit, but at the expense of efficiency. As discussed in Section 15.6.1, this loss may be in acceptable proportion, relative to the total shaft power delivered, for variable-torque applications such as fan drives and pump drives. However, for constant-torque and constant-power loads, the additional rotor I^2R losses reach unacceptable proportions if the reduction in speed is significant. This was recognized early in the evolution of the induction motor, and some number of systems have been devised to utilize the additional rotor energy losses associated with speed reduction. All of the resulting systems provided a scheme for injecting a voltage at the desired slip frequency into the rotor winding of the wound-rotor drive motor. This injected voltage is intended to replace the original voltage associated with the I^2R voltage drop along the external rheostat. The various systems for accomplishing this can essentially be classified into two generic types. Simplified illustrations of these two generic types are shown in Fig. 15.8.

For the generic type, shown in part (a) of the figure, the wound-rotor motor is coupled to auxiliary rotating equipment, represented symbolically as system A. The function of system A is to impress the rotor-output voltage of the wound-rotor motor across the input terminals of auxiliary rotating equipment, and to utilize the power, which would otherwise appear as I^2R loss in a rheostat, to assist in driving the mechanical load. The accessory equipment contained within the box represents a system to receive collector-ring voltage at slip frequency, and to convert it to a torque that is compatible with the speed of the wound-rotor drive motor. Such accessory equipment can consist of rotary converters and/or dc motors, adjustable-ratio transformers, and perhaps, other equipment. Because of the high initial cost, additional maintenance, additional foundations, greater space, and general lack of availability of some of the required equipment, this type

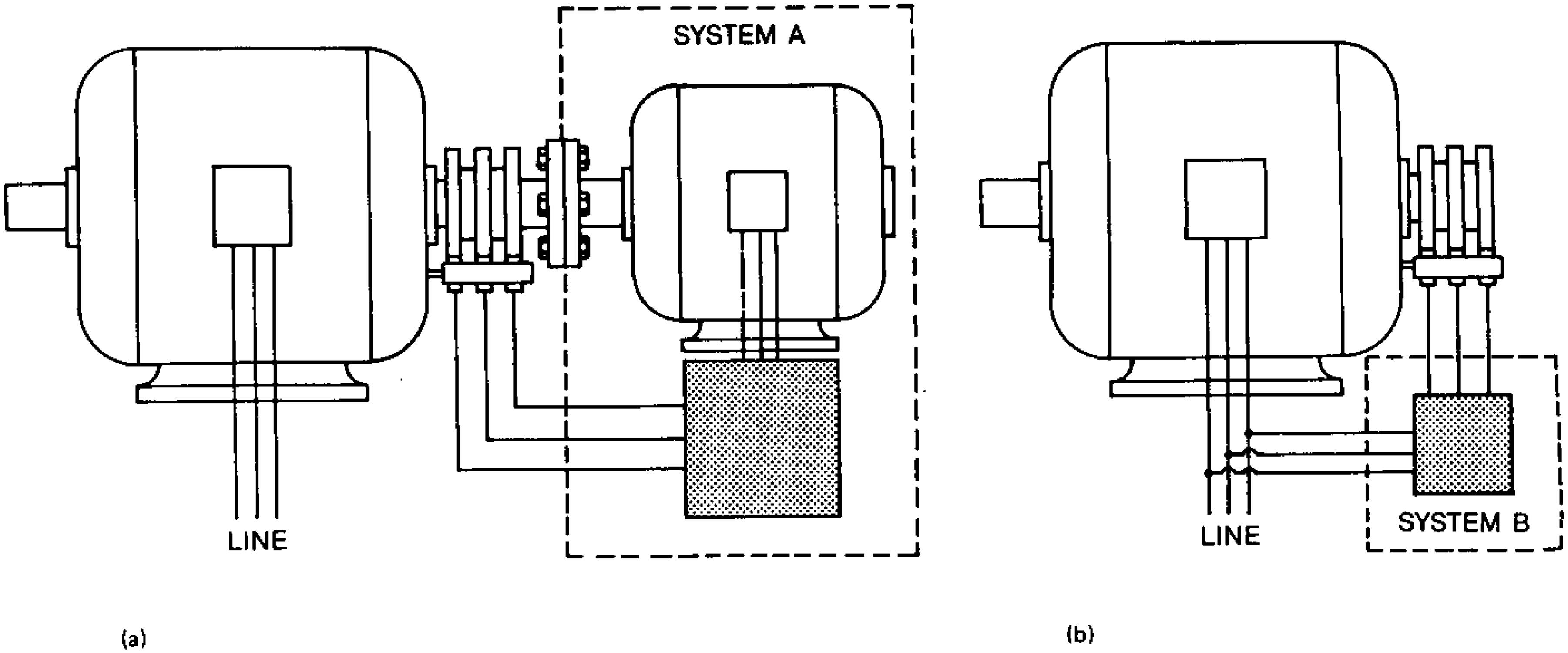
SYSTEM A
LINE
SYSTEM B
LINE
(a)
(b)

FIGURE 15.8 Speed variation of a wound-rotor motor, by injecting a slip-frequency voltage into the rotor circuit: (a) wound-rotor motor with accessory motors and other equipment: (b) wound-rotor motor and static equipment.

of variable-speed drive is no longer available. However, it provided an important variable-speed ac drive for large power rating for some number of years, and a few such drives are still in use.

For the generic type, shown in Fig. 15.8b, the rotor-output voltage at slip frequency is delivered to system B, represented by the box. The function of system B is to receive the rotor-output voltage at slip frequency and to return it to the line at line voltage and line frequency. Schemes have been devised to accomplish this function which also utilize auxiliary rotating equipment and in recent years, which utilize solid-state equipment such as certain types of cycloconverters. Again, because of about the same reasons as for system A, this type of variable-speed drive utilizing auxiliary rotating equipment is not used to any significant extent at present. Also, the present cost of the system using a cycloconverter or equivalent is sufficiently high that it is not attractive for most applications.

15.6.4 Speed Control of Squirrel-Cage Motors by Stator Voltage

Since the torque developed by an induction motor is proportional to the second power of the stator voltage, the speed-torque curve can be reduced along the torque scale by reducing the stator voltages. Figure 15.9 shows a set of speed-torque curves of a squirrel-cage induction motor for three values of impressed stator voltage. Curve D of the figure shows the speed-torque curve of a load, which varies as the second power of speed, such as for a centrifugal pump load or a fan load. Since power is proportional to torque × speed, the amount of power delivered to the load varies as the third power of the speed for this type of load. The application has a speed of 98% of synchronous speed at full voltage, as indicated by the curve. If the stator voltage is reduced to 80% of the rated value, the drive operates at 95.7% of synchronous speed. Thus the power delivered to the load has decreased to $(95.7/98)^3 = 0.931$, or 93.1% of that at full speed. If the stator voltage is reduced to 65% of rated value, the drive operates at 92.7% of synchronous speed, and the power delivered to the load has decreased to $(92.7/98)^3 = 0.846$, or 84.6% of that at rated speed. If the pump or fan load is assumed to have essentially constant efficiency throughout the speed range being considered, the water or air horsepower (i.e., the rate at which work is done on the water or on the air) has been reduced by $1 - 0.931 = 0.069$ per unit, or 6.9%, and by $1 - 0.846 = 0.154$ per unit, or 15.4%, respectively, for the two voltage changes considered.

The rate of fluid flow can be expected to be approximately proportional to the fluid horsepower. Thus the rate of flow is reduced by about 7%, at 80% of rated volts, and by about 15% at 65% of rated volts. This method of speed control, used to vary the rate of flow of a pump or fan, is a reasonable

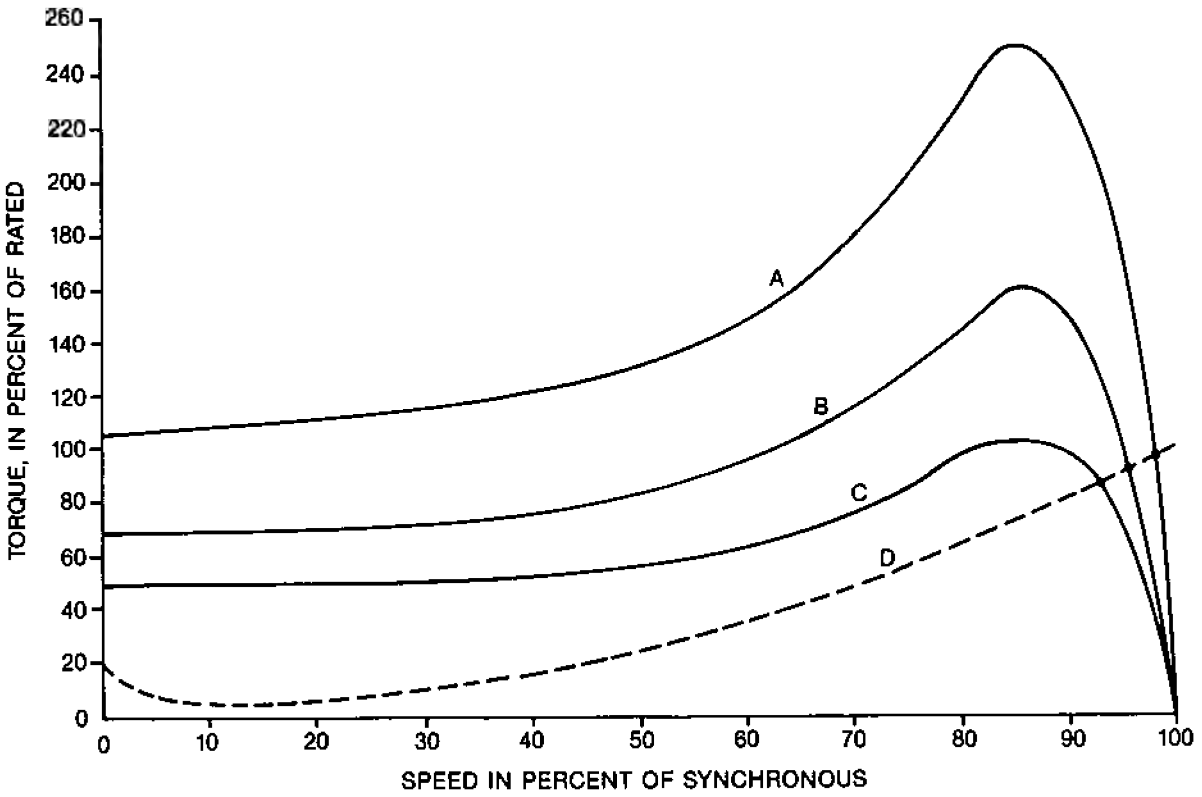

FIGURE 15.9 Speed-torque curve of an induction motor at different stator voltages. A, motor torque at 100% voltage; B, motor torque at 80% voltage; C, motor torque at 65% voltage; D, load torque.

one providing that flow changes of the foregoing magnitudes are desired. However, the maximum torque of the motor must be so specified that the motor torque is always greater than the load torque by a reasonable margin at the minimum voltage being considered. This method of speed control is not generally applicable to constant torque or to constant power loads. This is because the speed-torque curve of the load may not properly intersect the speed-torque curve of the motor such as to ensure a stable operating point, because of the reduced motor torque at reduced voltage.

An autotransformer with one or more voltage taps is frequently used to supply the stator voltage for this type of drive. Before this mode of speed control is selected, an authentic motor speed-torque curve should be obtained from the potential motor manufacturer, and an authentic pump or fan speed-torque curve should be obtained from the potential manufacturer of the driven equipment. Then the two speed-torque curves should be compared at the various operating speeds to ensure that there is adequate motor-torque margin over the load torque. In making this comparison, it is important that the reduced-voltage values be realistic (i.e., that they consider the regulation of the bus and the reactance drop through any autotransformer).

15.6.5 Multispeed Motors

It is possible to specify, design, and produce polyphase induction motors that can operate at two, three, or four specific base speeds. This is accomplished by designing one or more sets of windings within one magnetic structure, the number of poles of which can be changed by means of external connections. Performance characteristics such as efficiency and power factor are somewhat lower at any given speed than that of a single-speed motor of the same speed. Also, the frame size as well as cost is greater than that of a single-speed motor which has a speed equal to the lowest speed of the multispeed motor. However, there are many applications that require adjustable speed for which multispeed motors constitute a reasonable choice. Accordingly, a considerable number of such drives have been produced and installed.

Most of the multispeed motors that have been installed are included within the NEMA frame sizes. Motor manufacturers have established the following three classifications of output characteristics, based on the load requirements: (1) variable-torque variable-horsepower, (2) constant-horsepower variable-torque, and (3) constant-torque variable-horsepower. These classifications are more commonly called (1) variable-torque, (2) constant-horsepower, and (3) constant-torque. From a design standpoint, this type of drive motor can be grouped into three types: (1) single-winding two-speed, (2) two-winding three-speed, and (3) two-winding four-speed. In essentially all cases, a squirrel-cage rotor winding is used. Although a phase-wound rotor could theoretically be used, this is essentially never done, because of the additional complications and cost relative to any incremental benefits provided by such a choice.

The single-winding two-speed type of multispeed motor has a single winding that is designed to have the capability by means of external reconnection to produce either p or 2p poles. Thus the motor will exhibit two synchronous speeds which differ by a ratio of 2 to 1, each of which can be selected by external connection. To understand how this can be achieved, first consider Fig. 9.17. Let coil group 1-2 be connected to group 5-6 to form circuit (1-2)-(5-6), as shown in Fig. 15.10a. Also, let group 3-4 be connected to group 7-8, but with reversed polarity, to give circuit (4-3)-(8-7), also shown in Fig. 15.10a. If these two circuits are connected in parallel, with ends 1 and 4 joined together at one end, and ends 6 and 7 joined together at the other end, and if the resulting parallel circuit is excited, a conventional four-pole magnetic pattern will result, with two N poles and two S poles. If, on the other hand, circuit (1-2)-(5-6) is connected in series with circuit (7-8)-(3-4), as shown in Fig. 15.10b, by joining ends 6 and 7, with ends 1 and 4 forming the two terminals of the series circuit, and if the resulting series circuit is excited, the four groups will produce four N poles. Since individual magnetic poles of one polarity cannot separately exist, four corresponding S poles must appear automatically, as a consequence, at the

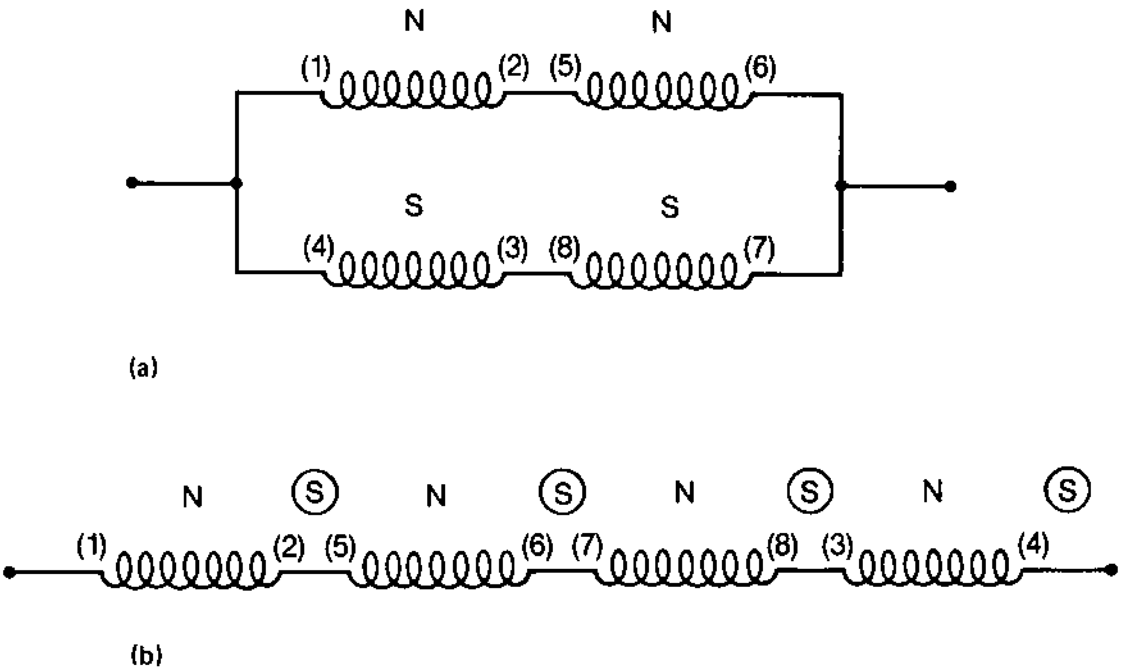

FIGURE 15.10 Illustration of phase connections for a one-winding two-speed motor using consequent poles for the lower speed: (a) phase groups connected to give a conventional two-circuit connection of the phase winding; (b) phase groups connected to give a consequent-pole series connection of the phase winding.

interpolar regions. Such poles are called consequent poles and the connection that produces them is called a consequent-pole connection. By externally connecting the three phases in delta, using the eight-pole series-circuit phase connection, a functional 900-rpm consequent-pole winding will result. Also, by connecting the three phases in wye using the four-pole two-circuit phase connection, an 1800-rpm conventional winding will result, as would be expected. The consequent-pole connection results in 120-degree phase belts, and the conventional connection results in the usual 60-degree phase belts. The use of 120-degree phase belts for the eight-pole connection can result in the presence of even-order harmonics in the stator magnetomotive-force wave. However, steps are usually taken at the design stage to prevent this from becoming a problem.

By use of the preceding series-parallel concept of group connection within the phase, and by judicious choice of either a wye or a delta connection between phases to form the three-phase winding, the correct value of flux/pole can be achieved at each speed, to provide the torque that is required for the application being considered. However, to keep flux densities within acceptable limits, the active material of the machine must be increased beyond that normally used for the low-speed machines. As mentioned earlier, the various motor manufacturers have standardized two-speed motor applications as variable-torque, constant-torque, and constant-horsepower applications. The stator connections, as well as the stator-lead identification, have also come to be standardized and published for the convenience of customers, such that there is essentially a common practice throughout the industry. Figure 15.11 shows the connections and the stator-lead identification for both speeds for the three application classifications of single-winding two-speed motors. Variable-torque motors are used for applications for which the torque increases with speed, such as for fans, centrifugal pumps, and centrifugal compressors. Constant-torque motors are used for applications for which the torque is essentially constant with speed, such as for reciprocating compressors, hoists, conveyors, and other material-handling equipment. Constant-horsepower motors are used for applications for which the load horsepower is essentially constant with speed, such as for machine tools.

Two-winding three-speed and two-winding four-speed motors are extensions of the single-winding two-speed motor concept using two separate windings. The separate stator windings of such a motor utilize a common magnetic core. The dimensions of the stator slots must be such as to accommodate the coil sides of both windings. The number of stator slots must be such as to give a balanced stator winding for each of the two windings. Thus the use of 72 stator slots with a four-pole and with a six-pole winding would result in $72/(4 \times 3) = 6$ slots/pole/phase and in $72/(6 \times 3) = 4$ slots/pole/phase, both of which would result in balanced windings in accordance with the criteria developed in Section 9.15. Also, the number of rotor slots must be such as to be compatible with the number of stator slots used with both stator windings. Such compatibility should consider perturbations on the speed-torque curve as discussed in Section 12.10, and electromagnetically induced noise and vibration as discussed in Section 12.11.

The configuration of the two independent windings and their spatial relationship to each other can be described in terms of two design concepts, which have been used. One concept, the four-tier method, requires a slot that is sufficiently deep as to accept the two separate windings one on top of the other, with the high-speed winding usually located at the bottom of the slot. This requires that each slot contain four coil sides, of course. The other concept, the two-tier method, requires that the two separate windings be interwoven such that one slot will contain a coil side from each of the two windings. This then requires that the coil span of the two windings be equal, in terms of the number of slots embraced, and that the number of slots be increased. The four-tier method is generally favored over the two-tier method. Because the coils of the idle winding are subjected to electromagnetic induction when the active winding is excited, care must be exercised when designing the winding connections and when selecting the switching sequence that current does not flow in closed circuits within the idle winding. Failure to prevent this will result in overheating of that winding, with probable damage.

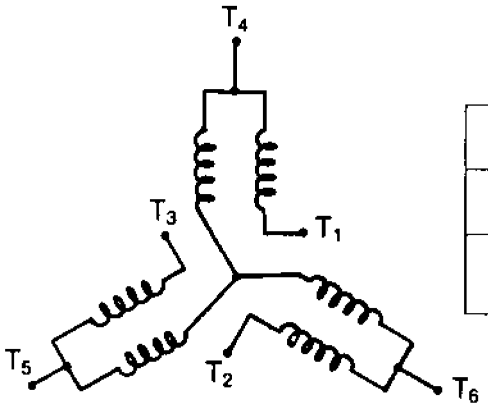

SPEED	LINE	OPEN	TOGETHER	CONNECTION
LOW	T_1, T_2, T_3	T_4, T_5, T_6	—	SERIES WYE
HIGH	T_6, T_4, T_5	—	T_1, T_2, T_3	2-PARALLEL WYE

(a)

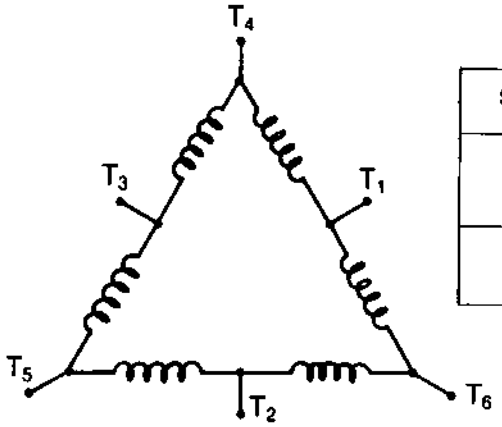

SPEED	LINE	OPEN	TOGETHER	CONNECTION
LOW	T_1, T_2, T_3	—	T_4, T_5, T_6	2-PARALLEL WYE
HIGH	T_6, T_4, T_5	T_1, T_2, T_3	—	SERIES DELTA

(b)

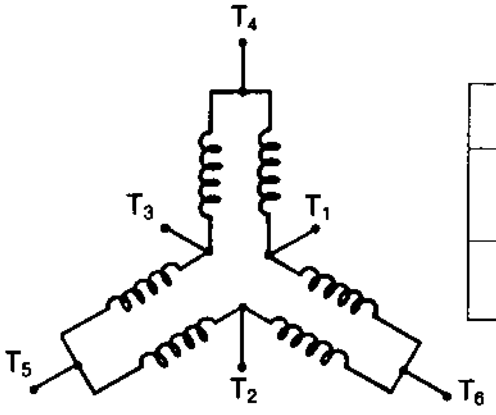

SPEED	LINE	OPEN	TOGETHER	CONNECTION
LOW	T_1, T_2, T_3	T_4, T_5, T_6	—	SERIES DELTA
HIGH	T_6, T_4, T_5	—	T_1, T_2, T_3	2-PARALLEL WYE

(c)

FIGURE 15.11 Stator connections for single-winding two-speed motors: (a) variable-torque winding connections; (b) constant-horsepower winding connections; (c) constant-torque winding connections.

For a three-speed two-winding motor, two speeds are achieved by use of one winding, which can be connected for conventional-pole mode and then reconnected for consequent-pole mode. The third speed is achieved by the second winding, which is always operated in conventional-pole mode. Thus such a motor, with a four-pole/eight-pole winding and a six-pole winding, can exhibit synchronous speeds of 900, 1200, and 1800 rpm. A four-speed two-winding motor can exhibit four synchronous speeds, by use of conventional-pole mode and consequent-pole mode, on both windings. Thus such a motor, with a four-pole winding and a six-pole winding, can exhibit synchronous speeds of 600, 900, 1200, and 1800 rpm. Two-winding three- and four-speed machines have been standardized, across the industry, to the same extent as have single-winding two-speed motors. Thus two-winding motors can be specified, designed, and applied for variable-torque loads, constant-horsepower loads, or constant-torque loads, with a basis for common understanding of performance, lead identification, and so on, among the various parties involved. Connection diagrams for two-winding motors for all three types of load applications, and for both three-speed and four-speed motors, are generally available. These diagrams are presented in a format similar to the single-winding diagrams in Fig. 15.11, except that the two-winding diagrams are expanded to cover both three or four speeds for each type of load application.

15.6.6 Speed Control of Squirrel-Cage Motors by Impressing Constant Volts/Cycle on the Stator Winding

As determined earlier, the flux/pole of an induction motor is equal to

$$\phi = \frac{V_1}{4.443K_pK_dN_{st}f} \quad \text{webers} \tag{15.28}$$

for which K_p, K_d, and N_{st} are determined by the stator winding and hence are constant for a given design. Accordingly, eq. (15.28) can be written as

$$\phi = K\frac{V_1}{f} \quad \text{webers} \tag{15.29}$$

From eq. (15.29) it is apparent that flux/pole remains constant as the stator voltage V_1 is varied if the ratio of the magnitude of the stator voltage to the frequency of that voltage is kept constant. From eq. (7.40) torque is equal to the vector cross product of ϕ and I_2, or

$$T = \phi \times I_2 \quad \text{newton-meters} \tag{15.30}$$

Then, at constant volts/cycle, the torque produced by an induction motor should be essentially unchanged for a given value of I_2. Otherwise stated, the torque characteristics should be essentially constant as the stator voltage changes, provided that the frequency changes in direct proportion. As discussed earlier, and as is apparent from eq. (15.24), the rotor speed will also change in direct proportion to the frequency. Thus variation of stator voltage while maintaining constant volts/cycle can provide an important method of induction-motor speed control with desirable torque characteristics. The shape of the speed-torque curve will resemble that shown in Fig. 5.5 but will be displaced to the left progressively as the magnitude of the voltage and the frequency is decreased. At 50% volts and 50% frequency, for example, the shape of the speed-torque curve would remain the same but will be compressed to the left with synchronous speed occurring at 50% instead of at 100% of rated-frequency speed.

If a variable-voltage source had been available which had constant volts/cycle characteristics, which had adequate kVA capability, and which was reasonable in both cost and maintenance, the use of a squirrel-cage induction motor with such a voltage source would be the preferred variable-speed electrical drive. Unfortunately, the lack of availability of such a voltage source has prevented this concept of variable-speed drive from achieving its full potential. In the past, various kinds of frequency changers with variable-voltage capability have been used to some extent for applications with low shaft-power requirements. However, systems that produce constant volts/cycle have been developed in recent years which utilize solid-state devices and which appear promising. As these systems continue to be technically improved, as their maximum kVA capability is increased, and as their cost/kVA decreases with increase in size and with increase in usage, it is probable that such devices will be applied at an accelerated rate by application engineers.

In overall concept, this system operates by receiving normal, fixed-frequency voltage from the line, and by use of solid-state devices such as diodes, thyristors, and/or SCRs delivers a voltage of variable magnitude at essentially constant volts/cycle to the motor terminals. The various available systems can be classified into three categories: (1) link converters, (2) cycloconverters, and (3) all others. At present it would appear that the link converter is the most promising system. For one type of such a system, normal, fixed-frequency voltage from the line is rectified to provide a dc voltage bus of constant value, which is then appropriately inverted to form the ac voltage wave. In the conversion, each half wave is typically divided into six pulses of varying width. By varying the widths of the pulses along the wave, in accordance with a prescribed program, a given amplitude of voltage at constant volts/cycle can be synthesized. The amplitude as well as the frequency of the ac voltage output is controlled by the relative time duration on the positive and negative terminals of the dc bus. Thus it is apparent that a reasonably sophisticated commutating circuit is necessary to provide the desired conduction periods of the thyristors, to give the necessary pulse width and polarity sequence required to achieve the desired voltage amplitude of the constant volts/cycle output.

The cycloconverter performs a direct ac-to-ac conversion between the normal line-voltage bus and the motor terminals. For one type of cycloconverter, the variable-frequency output voltage is produced from fixed-frequency line voltage. This is accomplished by synthesizing the required output voltage wave by appropriate external control of the gates of the thyristors or SCRs. Again, it is apparent that the commutating circuit is an important factor in the successful operation of such conversion equipment. This type of conversion does not have as wide a range of working frequency as does the link converter. However, it is more amenable to reverse/power flow than is the link converter.

Depending on the capabilities of the conversion equipment, a motor can be started in any one of several ways. It can be started from the normal fixed-frequency voltage bus in the conventional way, brought up to full speed and then transferred to the conversion equipment. Also, it can be started as a constant-frequency motor using the conversion equipment at a given fixed frequency within its operating range. In addition, a motor can be started at the lowest frequency of which the conversion equipment is capable, and brought up to speed at constant volts/cycle. When starting with the conversion equipment, an important consideration is to develop the torque required to accelerate the load and not exceed the current capability of the equipment. Such a current limitation can be due to inability to commutate the higher current as well as to the rating of the thyristors. It is common practice to hold the motor voltage at rated value for operation above rated frequency and rated speed. This requires that the commutating circuit be capable of performing in this mode. Increasing the motor frequency at a fixed stator voltage causes the maximum torque to decrease. Thus the motor operates as a constant-horsepower drive under these conditions.

Conversion equipment produces a voltage that is rich in harmonics. Such harmonics in the voltage wave are called "time" harmonics, to differentiate them from the "space" harmonics produced by the spatial distribution of the magnetomotive-force wave, which was considered in Chapter 12. Each of the various time harmonics can be regarded as a separate voltage of relatively small amplitude and with a frequency corresponding to the order of the harmonic. The net effect of impressing such harmonics on the stator winding is to produce undesirable spurious effects such as additional heating. It can be expected that as constant volts/cycle systems are increasingly applied to induction motors and as operating experience is accumulated, the industry will develop some type of standard motor derating factor for use in properly sizing the drive motor. Until such time as that is accomplished, however, it is important that there be adequate communications between all parties involved in this kind of application, to ensure that the effects of time harmonics are adequately considered. Thus prior to ordering the equipment, in specifying equipment for such an installation, an application engineer should verify that the harmonic content of the voltage out of the inverter is obtained from the manufacturer of the particular equipment that will be used. This information, in turn, should be given to the motor manufacturer. The motor manufacturer can then size the motor frame based on the required shaft power and speed, for the speed range desired, as well as on the additional heating, and so on, caused by the time harmonics in the voltage supply.

15.6.7 Speed Control of Squirrel-Cage Motors by Use of a Controlled Slip Coupling

As mentioned previously, the output of fluid-handling equipment such as fans, centrifugal compressors, and centrifugal pumps can be varied by relatively small changes in speed. Accordingly, this type of industrial equipment is frequently driven by a squirrel-cage motor through a controlled-slip coupling. Hydraulic couplings, eddy-current couplings, and salient-pole magnetic couplings are three frequently used types of such couplings. Fluid handling equipment such as centrifugal pumps requires a load torque that varies as the second power of the speed. Thus if base speed is considered synchronous speed, at which the load-torque requirement is 100%, and if the coupling slip is adjusted to 7% of base speed, the load-torque requirement will decrease to $(0.93)^2(100) = 86.5\%$ of full-load torque. Since power is proportional to the product of torque and speed, the horsepower requirement of the pump will decrease to $(0.93)^3(100) = 80.4\%$ of full-load horsepower, assuming that the efficiency of the pump has not significantly changed. As discussed earlier, the water flow of the pump is approximately proportional to the water horsepower. Then a 7% decrease below base speed has reduced the pump flow by 20%. The reduction in speed is achieved at the expense of slip loss. However, since the centrifugal pump unloads as the third power of the per unit speed, the actual slip loss is not great. This can be understood by considering the relationship between speed and the slip loss produced by the coupling to a greater extent.

Since the load torque of a centrifugal pump, centrifugal compressor, or fan varies as the second power of the speed, it can be expressed as

$$T = kn^2 \quad \text{per unit} \qquad (15.31)$$

where n is speed in per unit. If the per unit slip of the coupling is equal to s, eq. (15.31) can be written as

$$T = k(1 - s)^2 \quad \text{per unit} \qquad (15.32)$$

The slip loss in the coupling is equal to

$$L_s = Ts = k(1 - s)^2 s \quad \text{per unit} \tag{15.33}$$

To determine the value of slip s that results in maximum slip loss, differentiate eq. (15.33), equate to zero, and solve for s. Then

$$\frac{d[k(1 - s)^2 s]}{ds} = \frac{d[k(s - 2s^2 + s^3)]}{ds} = k(1 - 4s + 3s^2) = 0 \quad \text{numeric} \tag{15.34}$$

or

$$3s^2 - 4s + 1 = 0 \quad \text{numeric} \tag{15.35}$$

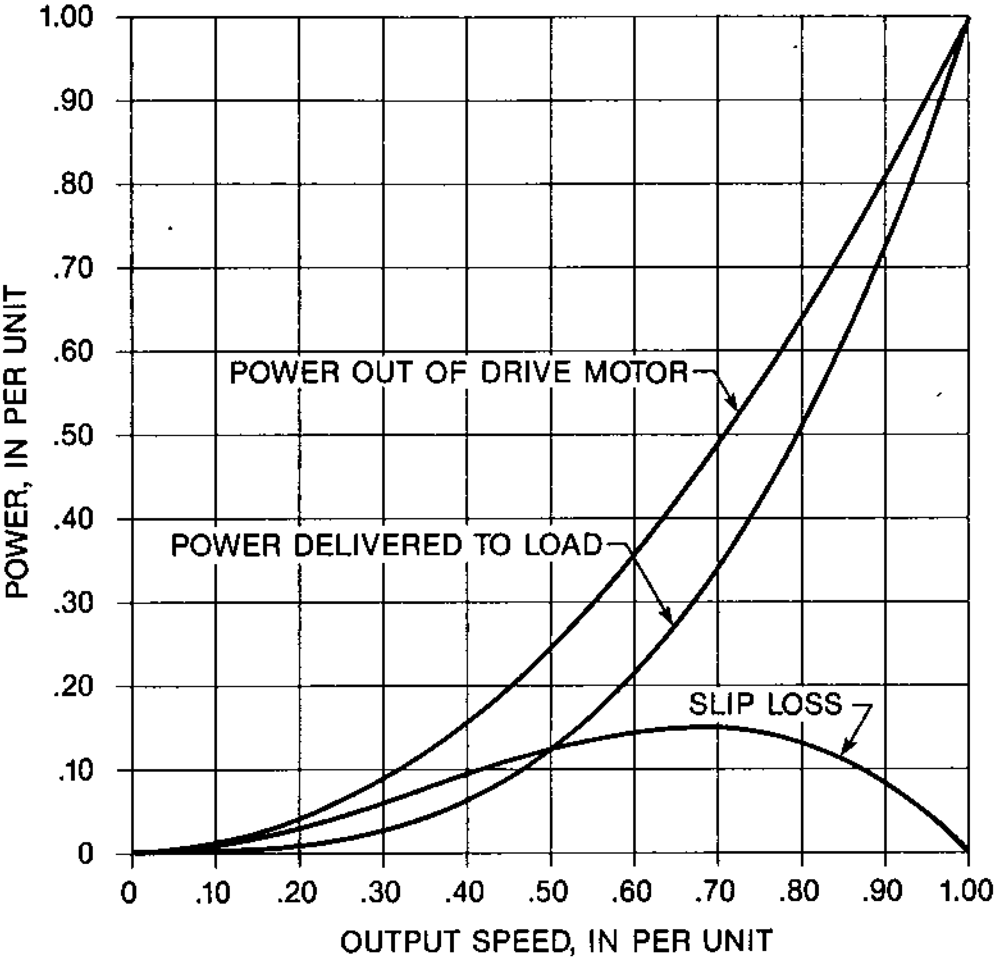

FIGURE 15.12 Relationship of slip loss, power delivered to the load, and power out of the drive motor versus output speed of a slip coupling.

Solving for s gives us

$$s = \frac{4 \pm \sqrt{16 - 12}}{6} = 1, \frac{1}{3} \quad \text{per unit} \tag{15.36}$$

Thus maximum loss in the hydraulic coupling, which is of interest to the application engineer, occurs when the slip is 1/3 per unit, or at 2/3 of rated speed. The magnitude of slip loss developed by the slip coupling is given in eq. (15.33). Substituting eq. (15.36) into eq. (15.33), to determine the maximum value of slip loss, we have

$$L_{sm} = k\left(1 - \frac{1}{3}\right)^2 \left(\frac{1}{3}\right) = 0.148k \quad \text{per unit} \tag{15.37}$$

In per unit notation, the constant of proportionality k is equal to 1.0. Thus the maximum value of coupling slip loss is equal to 0.148 per unit, or 14.8%, of the full-speed power requirement of the pump and it occurs at 66.7% of full speed. Figure 15.12 shows slip loss, power delivered to the load, and power out of the drive motor as a function of speed for a variable-torque load such as a centrifugal pump.

If the power rating of the driven equipment is large, the resulting slip loss, at a reduced speed, may be sufficient that a heat exchanger might be required even though the per unit value of the slip loss is small. For example, consider a 2000-hp draft fan driven by a squirrel-cage motor through a hydraulic coupling. Let base power be taken as 2000 hp, and let base speed be taken as the synchronous speed of the motor. Then let the hydraulic coupling be set to deliver a speed of 0.95 per unit. This will result in approximately $(0.95)^3 = 0.857$ per unit gas flow being produced by the draft fan. From Fig. 15.12 the slip loss is 0.045 per unit at 0.95 per unit speed. This amount of slip loss corresponds to (2000)(0.045) = 90 hp or to 67 kW, so that the loss produced in the oil of the hydraulic coupling would probably be removed by an oil-to-water heat exchanger.

15.7 ACCELERATION

In starting an induction motor and its connected load, a quantity of electrical energy, which can be considerable, is drawn from the local electrical distribution system during the time that the motor and load are accelerating. A portion of this energy is used to accelerate and rotational inertia of the rotor and connected load during the acceleration period. As discussed subsequently, this results in energy being stored as $(1/2)I\omega^2$ in the rotating system. An essentially equal amount of energy is dissipated, as I^2Rt, in the rotor circuit during the acceleration period. An amount of energy that is proportional to the ratio of the stator resistance to the rotor resistance is also dissipated in the stator circuit during this period. The energy that is stored as $(1/2)I\omega^2$ is subsequently released (1) as heat energy during coast down, or (2) as heat energy or as electrical energy during braking, or (3) as work done on a duty-cycle load. Some of the items above are considered in this section. The remainder of the items are considered subsequently in this chapter.

15.7.1 Acceleration Time and the Speed-Time Curve

Newton's second law of motion applied to rotation is

$$T = I\alpha = I\,\frac{d\omega}{dt} \quad \text{newton-meters} \tag{15.38}$$

where

T = accelerating torque, newton-meters
I = rotational inertia, of the rotor and load, kilogram-meters^2
α = angular accleration, radians/second^2
ω = angular velocity, radians/second

The differential equation for acceleration time can be obtained by rearranging eq. (15.38). Thus

$$dt = \frac{I}{T}\,d\omega \quad \text{seconds} \tag{15.39}$$

Also, ω can be expressed in terms of rotor speed, in rpm, as

$$\omega = \frac{2\pi n}{60} \quad \text{radians/second} \tag{15.40}$$

Differentiating eq. (15.40) with respect to n gives us

$$d\omega = \frac{2\pi n}{60}\,dn \quad \text{radians/second} \tag{15.41}$$

Substituting eq. (15.41) into eq. (15.39) yields

$$dt = \frac{2\pi}{60}\,\frac{I}{T}\,dn = \frac{1}{9.55}\,\frac{I}{T}\,dn \quad \text{seconds} \tag{15.42}$$

Thus acceleration time is equal to

$$t = \frac{I}{9.55} \int \frac{dn}{T} \quad \text{seconds} \tag{15.43}$$

where it is understood that acceleration torque T is a function of rotor speed n.

In actual practice, the speed-torque curve of a polyphase induction motor is not easily expressed as a mathematical function, except in a general way. Accordingly, the integration above is performed by summing using finite elements of speed change Δn and the corresponding values of accelerating torque T_n for the various speed increments chosen. Then eq. (15.43) can be written as

$$t = \frac{I}{9.55} \sum_{n=1}^{n} \frac{\Delta n}{T_n} \quad \text{seconds} \tag{15.44}$$

Equation (15.44) was derived using the MKS system of units, with I expressed in kilogram meters^2. The equation can be put into a form to use the FPS system of units by remembering that 1 kilogram-meter^2 = 23.7 pound-feet^2 and that 1 newton-meter = 0.738 pound-foot. Then

$$t = \frac{WK^2}{308} \sum_{n=1}^{n} \frac{\Delta n}{T_n} \quad \text{seconds} \tag{15.45}$$

where WK^2 is expressed in pound-feet^2 and T_n is expressed in pound-feet. Then the time required for an induction motor rotor and connected load to accelerate to full speed can be calculated from eq. (15.44) or (15.45), depending on the system of units being used, if the speed-torque curve of the motor and the WK^2 of the motor rotor and connected load are known.

It should be noted that the acceleration torque T_n at any speed is the net torque, or the torque produced by the motor, less the load torque at that speed. In Fig. 15.9, for example, if 80% of rated voltage is impressed on the motor terminals during starting, the acceleration torque is the vertical distance, or the difference in ordinates, between curves B and D at the various speeds. If the accumulative value of t is plotted versus speed n for the successive value of Δn, the result is the speed-time curve. Such a curve is frequently helpful in setting protective relays, which are used during acceleration.

15.7.2 The Speed-Current Curve and the Current-Time Curve

The shape of the speed-current curve shown in Fig. 5.5 is typical of a general-purpose squirrel-cage motor or of a wound-rotor motor with the collector brushes short circuited. The stator current is essentially constant for the greater portion of the speed. As the rotor speed approaches full speed, the stator current decreases until at the speed that corresponds to maximum torque, the current is approximately 70% of blocked-rotor current. Beyond that point the stator current decreases rapidly and approaches zero at synchronous speed. Full-load current corresponds to full-load speed, of course. A speed-current curve is easily constructed by the engineering departments of the various motor manufacturers. If the motor being considered is a standard NEMA design, standard speed-current curves will probably be available immediately. On the other hand, if the motor is of special design, or if it is larger than those included within the NEMA frame sizes, it is probable that the engineering department will be required to produce such a curve. In either case, however, the curve is obtainable and is frequently useful to the application engineer.

Another curve, which may be even more useful to the application engineer and which is derived from the curve above, is the current-time curve. It is apparent that if the speed-time curve discussed in Section 15.7.1 is available and if a speed-current curve, as just discussed, is available, a current-time curve can also be determined. Thus the time that corresponds to a given speed can be determined from the speed-time curve. Similarly, the current that corresponds to the same speed can be determined from the speed-current curve. From this information the corresponding current and time values can be plotted as a point on a current-time coordinate system. Proceeding in this manner for selected speed points on the two parent curves, a complete current-time curve can be constructed. Such a curve is useful to the application engineer in setting relays associated with motor starting.

15.7.3 Numerical Example of Constructing a Speed-Time Curve and a Current-Time Curve

Assume that an application engineer is applying a 1000-hp 1200-rpm squirrel-cage induction motor to a fan load and requires a speed-time curve and a current-time curve. The engineer has previously determined that the voltage at the terminals of the motor will be approximately 65% of rated value during the starting period. The following information has been obtained from the motor manufacturer and from the fan manufacturer.

Rotational inertia of rotor, $I_m = 26.4\ \text{kg}\cdot\text{m}^2$, or $WK^2 = 626\ \text{lb-ft}^2$
Rotational inertia of fan, $I_f = 395\ \text{kg}\cdot\text{m}^2$, or $WK^2 = 9362\ \text{lb-ft}^2$
Motor speed-torque curve, curve C of Fig. 15.9
Fan speed-torque curve, curve D of Fig. 15.9
Speed-current characteristics of motor, at rated voltage, are as follows:

Percent speed	0	20	40	60	70	80	85	98
Percent current	650	650	645	630	620	550	460	100

If base speed is 1200 rpm and if base power is 1000 hp (using USA horsepower instead of metric horsepower), base torque is equal to

$$T = \frac{P}{2\pi(n/60)} = \frac{(1000)(746)(60)}{(2\pi)(1200)} = 5936 \quad \text{newton-meters} \qquad (15.46)$$

The average accelerating torque (i.e., the net torque between curves C and D) from zero speed to 30% speed is equal to approximately 38%. Thus for this increment, $\Delta n = (0.30)(1200) = 360$ rpm and $T_n = (0.38)(5936) = 2256$ N·m. Substituting the values above as well as the given value of I into eq. (15.44) gives us

$$(\Delta t)_1 = \frac{I}{9.55}\frac{\Delta n}{T_n} = \left[\frac{(26.4 + 395)}{9.55}\right]\left(\frac{360}{2256}\right) = 7.04 \quad \text{seconds} \qquad (15.47)$$

Taking the speed interval from 30% to 50% speed as the second interval, the average accelerating torque is equal to 37% and Δn is equal to (50 - 30) = 20%. Then the value of $(\Delta t)_2$ is equal to

$$(\Delta t)_2 = \left(\frac{421.4}{9.55}\right)\left[\frac{(0.20)(1200)}{(0.37)(5936)}\right] = 4.82 \quad \text{seconds} \qquad (15.48)$$

Similarly, taking the speed interval from 50% to 75% speed as the third interval, the average accelerating torque is equal to 28% and Δn is equal to (75 - 50) = 25%. Then the value of $(\Delta t)_3$ is equal to

$$(\Delta t)_3 = \left(\frac{421.4}{9.55}\right)\left[\frac{(0.25)(1200)}{(0.25)(5936)}\right] = 8.92 \quad \text{seconds} \qquad (15.49)$$

Similarly, taking the speed interval from 75% to 93% speed as the fourth interval, which is the last interval at reduced voltage, the average accelerating torque is equal to 27% and Δn is equal to (93-75) = 18%. Then the value of $(\Delta t)_4$ is equal to

$$(\Delta t)_4 = \left(\frac{421.4}{9.55}\right)\frac{(0.18)(1200)}{(0.27)(5936)} = 5.95 \quad \text{seconds} \qquad (15.50)$$

The time increment $(\Delta t)_4$ completes the acceleration to 93% speed, which is the intersection of curves C and D. At about this point, a relay will be activated by a timer or by a tachometer signal, which will place rated voltage on the motor terminals. Then the last increment is from 93% to 98% speed, which is the operating speed with the fan load. For this increment, T_n is equal to the average ordinate between curves A and D, or to 66% and Δn is equal to (98-93) = 5%. The value of $(\Delta t)_5$ is equal to

$$(\Delta t)_5 = \left(\frac{421.4}{9.55}\right)\left[\frac{(0.05)(1200)}{(0.66)(5936)}\right] = 0.07 \quad \text{seconds} \tag{15.51}$$

From eq. (15.47), the total time required for the drive motor to accelerate the fan load from standstill to 30% speed is equal to $(\Delta t)_1 = 7.04$ seconds. From eqs. (15.47) and (15.48), the total time required to accelerate to 50% speed is equal to $(\Delta t)_1 + (\Delta t)_2 = 7.04 + 4.82 = 11.86$ seconds. Similarly, from eqs. (15.47), (15.48), and (15.49), the total time required to accelerate to 75% speed is equal to $(\Delta t)_1 + (\Delta t)_2 + (\Delta t)_3 = 7.04 + 4.82 + 8.92 = 20.78$ seconds. Similarly, from eqs. (15.47), (15.48), (15.49), and (15.50), the total time required to accelerate to 93% speed is equal to $(\Delta t)_1 + (\Delta t)_2 + (\Delta t)_3 + (\Delta t)_4 = 7.04 + 4.82 + 8.92 + 5.95 = 26.73$ seconds. Finally, by adding $(\Delta t)_5$ to the sum of $(\Delta t)_1$ through $(\Delta t)_4$, the total time required to accelerate to full speed is equal to $26.73 + 0.07 = 26.80$ seconds. When the application engineer plots the coordinates above, the result is the speed-time curve for this application, shown as curve 1 of Fig. 15.13.

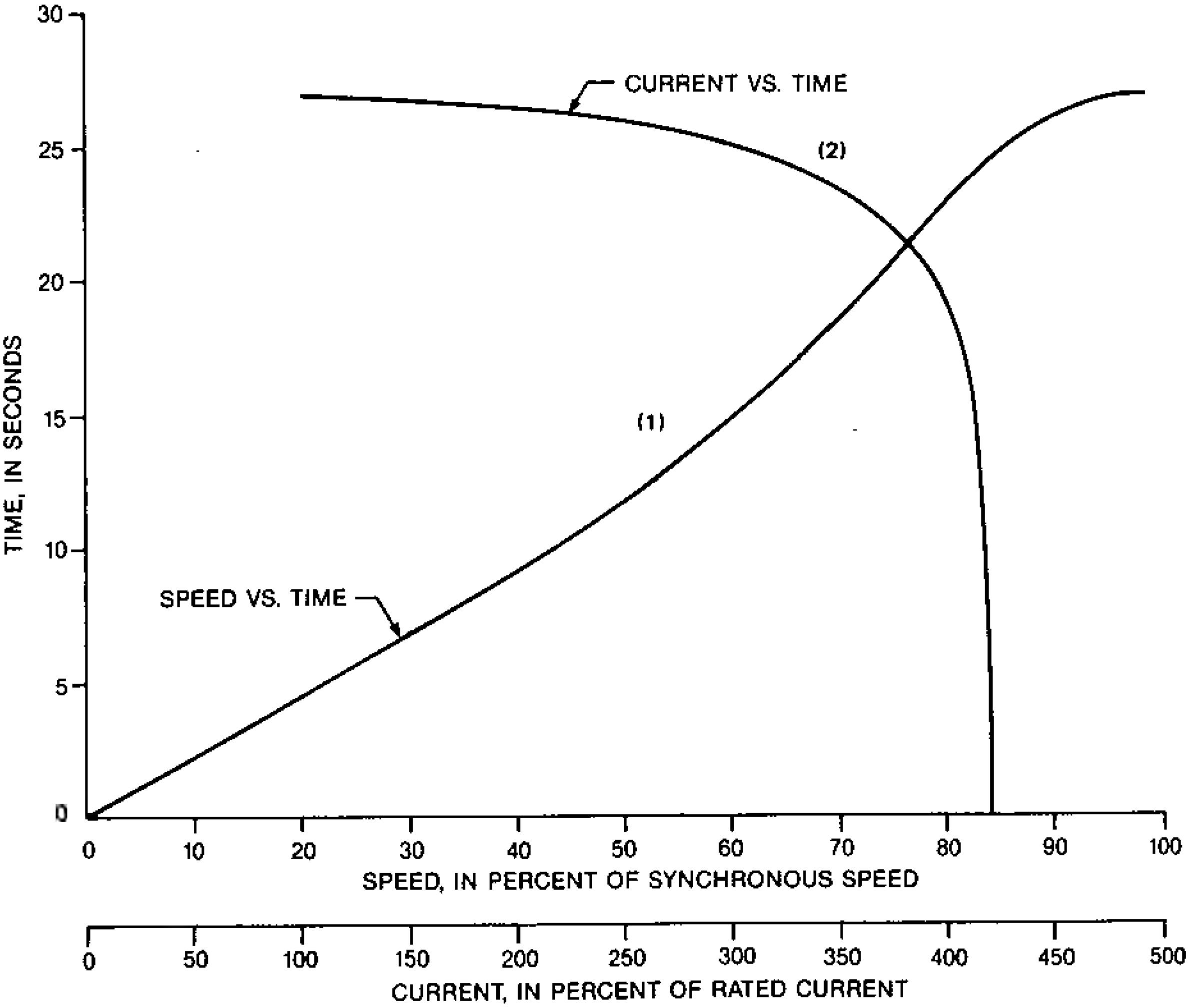

FIGURE 15.13 Speed-time and current-time curves for a 1000-hp six-pole induction motor starting a draft fan at 65% normal voltage.

With the speed-time curve just constructed, and with the speed-current data included with the application data at the beginning of this section, the application engineer can also construct a current-time curve. From the application data for rated voltage, the stator current is equal to 650% at zero speed, which corresponds to (0.65)(650) = 423% current at 65% voltage. Thus one point on the current-time coordinates is 423% current at zero time. Similarly, the full-voltage current is also 650% at 20% speed, which results in 423% current at 65% voltage at 20% speed. From curve 1 of Fig. 15.13, 20% speed corresponds to 4.7 seconds. Then a second point on the current-time coordinates is 423% current at 4.7 seconds. Proceeding in a similar manner, the full-voltage current is 645% at 40% speed, which results in (0.65)(645) = 419% current at 65% voltage at 40% speed. Again, from curve 1 of Fig. 15.13, 40% speed corresponds to 9.3 seconds. This gives a third point on the current-time coordinates, which is 416% current at 9.3 seconds. If successive coordinate points are determined to the extent of the given speed-current data, a current-time curve can be drawn for the application. When the application engineer plots the points above, the result is the current-time curve shown as curve 2 of Fig. 15.13.

15.7.4 Heating and Stored Energy During Acceleration

It was shown in Section 10.3.16 that the heat energy dissipated within the rotor circuit during acceleration is equal to

$$\mathcal{E} = -I\omega_s^2 \int_{s_1}^{s_2} \frac{T_m}{T_m - T_L}\, s\, ds \quad \text{joules} \qquad (15.52)$$

where

ω_s = angular velocity, at synchronous speed, radians/second
I = rotational inertia, kilogram-meters^2
T_m = torque developed by the motor, newton-meters
T_L = load torque, newton-meters
s = slip, per unit
s_1 = slip at beginning of the speed change, per unit
s_2 = slip at end of the speed change, per unit

If the load torque is small in comparison to the motor torque during acceleration, eq. (15.52) reduces to

$$\mathcal{E} = -I\omega_s^2 \int_{s_1}^{s_2} s\, ds \quad \text{joules} \qquad (15.53)$$

Integrating between zero speed and full speed, or between slip $s_1 = 1$ and slip $s_2 \simeq 0$,

$$\mathcal{E} = \frac{1}{2} I\omega_s^2 \quad \text{joules} \tag{15.54}$$

For this typical case of acceleration, the energy that is dissipated within the rotor circuit during the starting period is equal to $(1/2)I\omega_s^2$. This term will be recognized as the expression for kinetic energy stored in a rotating system, which has rotational inertia equal to I and an angular velocity of ω_s. Thus the energy dissipated within the rotor circuit during one start is equal to the kinetic energy stored in the rotating motor rotor and connected load. This relationship provides a convenient way in which to calculate rotor-circuit heating during startup. Since $\omega_s = 2\pi(\text{rpm})_s/60$, eq. (15.54) can be expressed as

$$\mathcal{E} = \frac{1}{2} I \left[\frac{2\pi(\text{rpm})_s}{60}\right]^2 = \frac{I(\text{rpm})_s^2}{182.4} \quad \text{joules} \tag{15.55}$$

with I expressed in kilogram-meters^2. Equation (15.55) can be expressed in terms of WK^2, in pound-feet^2, by remembering that there are 23.7 pound-feet^2 in 1 kilogram-meter^2. Then

$$\mathcal{E} = \frac{0.231 WK^2 (\text{rpm})_s^2}{10^3} \quad \text{joules} \tag{15.56}$$

If the load torque is significant relative to the motor torque during the starting period, the integral in eq. (15.52) can be evaluated by summing discrete intervals, similar to that done in calculating acceleration time. For many cases, however, the load torque can be neglected, although there are exceptions to this generalization. Equations (15.55) and (15.56) give the energy stored in the rotating system and the heat dissipated in the rotor winding. This stored energy is important for braking and for duty-cycle calculations. The heat dissipated in the rotor winding is important for determining rotor-winding heating, as discussed in Section 10.3.16.

It should be noted that there is also stator-winding heating due to acceleration, although it is not usually as severe as for the rotor winding. During acceleration the stator current is six to seven times normal at full voltage. Thus the rate at which $i_1^2R_1t$ energy is being produced is from 35 to 50 times normal for a full-voltage acceleration. Because of the relatively short time required to accelerate, most of this energy loss is effective in increasing the temperature of the stator winding. The stator-winding heating can be determined by use of the current-time curve. Select the average value of stator current for a chosen increment of time. Then square this value of current, using amperes/phase, and multiply by the time interval in seconds, by the stator resistance R_1, and by the number of phases. Repeat this for all the time increments that comprise the starting period. The sum of the various resulting energy values, divided by the volume of stator-winding copper and by the volumetric specific heat of the copper, gives the transient temperature rise of the stator winding during acceleration. An approximate method to determine the energy dissipated in the stator winding, during acceleration, is to multiply eq. (15.55) or (15.56) by the ratio R_1/R_2, where R_2 is the weighted average of R_2 during the starting period.

15.7.5 Load WK^2 and Frequency of Starts

Essentially all of the energy $\mathcal{E}$ dissipated within the rotor circuit during one acceleration is effective in causing a transient increase in rotor-winding temperature. As discussed in Section 10.3.16, the amount of heat transfer is small during the acceleration period. As is apparent from eq. (15.56), the amount of energy dissipated is directly proportional to the amount of WK^2 that the motor must accelerate. Also, during the adjustment of driven equipment, or for other reasons, it is occasionally necessary to make more than one start in succession. If the WK^2 to be accelerated is large, and if several starts are attempted in rapid succession, injurious temperatures can be attained in the rotor winding as well as in the stator winding.

The WK^2 of a rotating system increases approximately as the fifth power of its linear dimension. This is because the weight W is proportional to the third power of the linear dimension for homologous increases in size. Also, the radius of gyration R when raised to the second power is proportional to the second power of the linear dimension. Thus as motors and their connected loads increase in size, the magnitude of the energy $\mathcal{E}$ which must be dissipated in one acceleration increases disproportionately. This effect can result in motors of a given horsepower and speed rating being built in larger-than-normal frame sizes just to have an adequate volume of rotor-winding copper to limit the winding temperature during acceleration.

Accordingly, industry-wide standards have been put in place for large motors which define the normal accelerating capability of a standard motor. The NEMA Standard MG 1-20.42 Load WK^2 for Polyphase Squirrel-Cage Induction Motors is the applicable document for squirrel-cage motors for horsepower and speed ratings greater than 500 hp at 1800 rpm, and greater than equivalent sizes at other horsepower and speed ratings. This standard specifies the maximum value of WK^2 which a given motor of a specific horsepower and speed rating can accelerate without injurious temperature rise under specified voltage conditions. The load torque during acceleration is assumed to be no more severe than that which varies as the second power of speed, such as for a fan. Under these conditions the motor must be capable of two successive starts, with the motor windings initially at ambient temperature and with the motor and connected load coasting to rest between the two starts (i.e., no braking). If the motor is initially at its rated temperature, the motor is considered capable of only one start at that particular time.

15.8 BRAKING

15.8.1 The Role of Electrical Braking

It is desirable in some number of applications to have a method of braking the motor and connected load. This need can result from safety considerations or it can result from a repeated duty cycle such as a mine-hoist application. Braking can be accomplished by a mechanical brake or by use of electrical equipment. For both cases the speed of the rotating systems is reduced by virtue of the transformation of the kinetic energy of rotation [i.e., $(1/2)I\omega^2$] into another form of energy. For a mechanical braking system, it is transformed into heat due to friction. Mechanical brakes are used (1) for preventing rotation or for maintaining a fixed position at standstill, (2) for braking rotating systems with low speed and low WK^2, and (3) for emergency backup protection in case of power failure. Induction motors offer the opportunity for the utilization of electrical braking on a broader application basis.

Figure 12.5 shows the three modes of operation of a polyphase induction motor: motoring, generating, and reverse-rotation braking. Two of these three modes of operation, generating and reverse-rotation braking, result in a decelerating torque being developed by the motor. Also, a polyphase induction motor can produce a braking torque by replacing the ac voltage on the stator winding with dc voltage. Such a method is called dynamic braking. For all forms of electrical braking, the thermal and the mechanical suitability of the motor for the specific application must be considered. In some number of applications, a drive motor with an oversized frame relative to the required motor horsepower is selected, in order to have adequate thermal capacity for braking. In other applications, wound-rotor motors are selected in order to enhance dynamic-braking capability or to externally dissipate rotor loss associated with braking.

15.8.2 Reverse-Rotation Braking

The direction of rotation of the magnetic field of a given motor is determined by the phase sequence of the applied voltage. By reversing any two phase connections between the bus and the stator winding, the phase sequence and hence the direction of rotation of the magnetic field will be reversed. Thus if a motor is operating at full speed and if any two stator leads are reversed, the magnetic field will suddenly start rotating in the opposite direction of the rotor at twice rated speed. This mode of operation will effectively brake the speed of the rotor and is called reverse-rotation braking, or in colloquial terms, "plugging" (see Fig. 12.5.).

Reverse-rotation braking can be understood in terms of the changes in slip as the motor brakes. At normal full-speed operation, the slip is small, such as 0.01 to 0.03 per unit. As soon as the direction of rotation of the magnetic field is reversed, the slip is equal to 2. Near the end of the braking action, as the rotor approaches zero speed, the slip approaches 1. Thus during reverse-rotation braking, $s_1 = 2$ and $s_2 = 1$. Substituting these values of slip into eq. (15.53) gives us

$$\mathcal{E} = -I\omega_s^2 \int_{s_1}^{s_2} s\, ds = -I\omega_s^2 \int_1^2 = s\, ds \quad \text{joules} \tag{15.57}$$

Integrating eq. (15.57) yields

$$\mathcal{E} = -\left(\frac{1}{2} I\omega_2^2\right)\left[(2)^2 - (1)^2\right] = -\left(\frac{1}{2} I\omega_s^2\right)(3) \quad \text{joules} \tag{15.58}$$

Thus the energy dissipated in the rotor, while the braking action is decelerating the rotor from full speed to zero speed, is three times that for one normal acceleration. As would be expected, this method of braking results in a short stopping time. The energy loss within the stator winding is about equal to, or slightly greater than, one normal acceleration.

Because of the short braking time and relative simplicity of reverse-rotation braking, it is used on many applications. Braking action can be used on any part or all of the reverse-braking speed range (see Fig. 12.5.). However, all motors are not designed to be suitable for this type of braking because of the large amount of heat energy that is dissipated in the rotor circuit in a short period of time. Thus when ordering a new motor, for which reverse-rotation braking is intended, it is important that the specifications so state. Also, if an existing motor is to be used on a new application involving this type of braking, it is also important that the suitability of the motor for such duty be verified by the motor manufacturer.

Plugging of a wound-rotor motor results in an induced voltage in the rotor winding which is equal to two times that at blocked-rotor conditions. Obviously, the rotor must be insulated for double voltage with normal margin in order that it be used for this type of duty. Again, this should be part of the specifications for a new motor and should be verified by the motor manufacturer of a motor being reapplied, for which plugging is a part of the duty. Also, adequate external resistance should be inserted in the rotor to ensure that a sufficient amount of the energy $\mathcal{E}$ in eq. (15.58) is dissipated outside the rotor to limit the rotor-winding temperature to a safe value. The insulated windings of phase-wound rotors can safely withstand less than half of the transient temperature rise that an uninsulated squirrel-cage rotor winding can safely withstand.

15.8.3 Regenerative Braking

From an inspection of Fig. 12.5 it is apparent that if an induction motor is driven above synchronous speed, it will generate. To perform in this mode, the machine will draw reactive power from the line for its excitation and will deliver real power to the line. Thus any induction motor that is driven above synchronous speed by an overhauling torque, and which is connected to the line, will act as a generator. Use of any portion of the generating region of the speed-torque curve shown in Fig. 12.5 will result in such generation. Since mechanical energy is taken from the rotating system, transformed into electrical energy, and then delivered to the electrical distribution system, a braking action is accomplished. This method of braking is called regenerative braking. Obviously, regenerative braking will not occur below the synchronous speed of the machine. Also, to have stable operation, the overhauling torque must be compatible with the braking torque of the machine. As for any method of braking, the motor must be thermally adequate for the particular braking duty to which it is applied. Further, the motor must be suitable for the maximum overspeed encountered in the braking duty.

To understand the magnitude of energy taken from the rotating system and delivered to the line, consider an application for which the speed is to be reduced from twice synchronous speed to synchronous speed. Thus during this braking action, the initial slip is equal to -1 and the final slip is equal to zero, or $s_1 = -1$ and $s_2 = 0$. Substituting these values into eq. (15.53) yields

$$\mathcal{E} = -I\omega_s^2 \int_{s_1}^{s_2} s\,ds = -I\omega_s^2 \int_{-1}^{0} s\,ds \quad \text{joules} \tag{15.59}$$

Integrating eq. (15.59) gives us

$$\mathcal{E} = -\left(\frac{1}{2}\,I\omega_s^2\right)[(0)^2 - (-1)^2] = \left(\frac{1}{2}\,I\omega_s^2\right)(1) \quad \text{joules} \tag{15.60}$$

Thus, in reducing the overspeed from twice synchronous speed to synchronous speed, the amount of energy taken from the rotating system and returned to the line through the machine is equal to $(1/2)I\omega_s^2$. This will be recognized as being equal to the energy dissipated within the rotor circuit for one normal acceleration from zero speed to full speed.

15.8.4 Multispeed Braking

Multispeed braking is a special case of regenerative braking. As discussed in Section 15.6.5, a multispeed motor can have two, three, or four synchronous speeds. Thus a specific four-speed motor might have synchronous speeds of 600, 900, 1200, and 1800 rpm, and the duty cycle to which it is applied might require that the motor operate at 1800 rpm for a portion of the cycle, and that it immediately operate at 1200 rpm for the next portion of the cycle. If the control is set up to switch immediately to the 1200-rpm connection at this point, with the motor rotating at approximately 1800 rpm, the motor is then subjected to a slip of -1.5 per unit. Accordingly, the speed of the rotating system can be reduced to 1200 rpm in a short time by regenerative braking.

Other combinations are also possible for the case above. For example, if the motor is operating at 1800 rpm on the high-speed connection, the speed of the rotating system can be reduced to 600 rpm by immediately switching to the 600-rpm connection. This subjects the motor to a slip of -3 per unit at this point. Thus regenerative braking appears to offer practical possibilities for applications that use multispeed motors. However, as for all braking applications, the thermal and mechanical adequacy of the particular motor must be verified.

15.8.5 Dynamic Braking

If dc voltage is applied to the stator winding of an induction motor, such as across two of the three stator loads, the magnetic poles will be fixed in time and in space. Thus the induction motor becomes an inverted (or inside-out) synchronous generator, for which the induction-motor stator now becomes the field and the induction-motor rotor becomes a rotating armature. For a squirrel-cage motor the armature is short circuited, and for a wound-rotor motor the armature can be connected to an external load. An induction motor operating in this mode provides an opportunity for braking, and such braking is called dynamic braking.

Either squirrel-cage or wound-rotor motors can be used for dynamic braking. However, squirrel-cage motors are less effective than wound-rotor motors, for this duty. The shape of the speed-torque curve of a squirrel-cage motor with dc excitation on the stator is similar to that of a normal motor with the speed scale reversed. Thus the maximum value of dynamic-braking torque occurs relatively near zero speed, whereas the maximum value of motoring torque occurs relatively near synchronous speed. Accordingly, a typical squirrel-cage motor will exhibit relatively small braking torque between 100% speed and 15 to 20% speed, but will exhibit significant braking torque between 15 and 20% speed and low speed. For this reason, the use of squirrel-cage motors on applications that require dynamic braking is normally limited to power ratings of about 100 hp or less.

Wound-rotor motors are very amenable to dynamic braking. By use of various amounts of external resistance in the rotor circuit, the point of maximum braking torque can be made to coincide with whatever braking speed the application might require. Thus the ability to select the speed range in which maximum braking torque occurs by means of external resistance, and the ability to use the same external resistance as a sink for absorbing the energy that results from the braking action, makes dynamic braking with wound-rotor motors a prime means of braking. For some braking applications, the starting resistor is sufficient for braking. For other applications, such as for mine hoists with significant loads, a separate resistor may be required.

Since an induction motor becomes an alternator when dc excitation is applied to the stator, this method of braking is fundamentally different from the methods considered previously. Stator heating results only from I^2Rt losses associated with a fixed amount of dc current flowing in the stator winding. Rotor heating is, in effect, armature heating of the alternator in delivering load. For a squirrel-cage machine the load is the rotor resistance. For a wound-rotor machine the load is the sum of the rotor-winding resistance and that of the external resistor, and with a judicious choice of the external resistor, most of the resulting loss will appear outside the machine. The magnitude of the energy that must be dissipated in the load is that generated by controlling the speed of an overhauling torque for a given period of time, or by changing the speed of a rotating system, both of which can be calculated.

The dc excitation can be applied to the stator winding with the stator phases connected in three different ways, depending on whether the stator winding is wye connected or delta connected. If the stator is wye connected, dc voltage can be connected to any two stator leads. The use of a dc braking current of about 1.5 times full-load ac motor current will result in a maximum braking torque of about 1.5 per unit of rated motor torque. However, proportionally more dc excitation current is required at lower values of excitation. Also, if the stator is wye connected, two of the three stator leads can be connected together to form one connection to the dc voltage bus and the third stator lead used for the other connection to the dc voltage bus. Also, if the stator is delta-connected, any two stator leads can be connected to the dc voltage bus. For these two connections, a dc braking current of about 1.5 times full-load ac motor current will result in a maximum braking torque of about 1.2 per unit of rated motor torque. Again, proportionally more dc excitation current is required at lower values of excitation. For all three of the above-mentioned connections, dc excitation current flowing in the stator winding will result in magnetic poles that are fixed in space and in unequal current loading in the stator windings. It is important that the amount of dc excitation current not be sufficient to cause sufficient magnetic pull between the rotor and stator as to cause pullover with the rotor rubbing the stator. For all dynamic-braking applications, the application engineer should determine the dc excitation current required for the desired braking torque and any design restrictions on the maximum limit on dc excitation to avoid pullover.

15.9 POWER REQUIREMENT FOR A DUTY-CYCLE APPLICATION

Some applications, such as driving a centrifugal pump at constant speed against an essentially constant pressure head, require a specific amount of motor power on a continuous basis. However, some applications require a different amount of motor power during different periods. If such a pattern of duty is repeated, as frequently occurs for an industrial application, the application is called a duty cycle. Such duty cycles can include shutdown periods and/or braking periods. A method frequently used to size a drive motor for a duty cycle is the rms horsepower method.

Figure 15.14 shows a graphical representation of a duty cycle using a graphical format that is frequently employed in laying out the activities within the cycle. It will be noted that there are four activities, which require different amounts of power and which are of different durations. Also, there is one activity, with a duration of t_5 minutes, during which the motor is shut down. Since heating is approximately proportional to the second power of the power output for a given motor, the motor heating will obviously be different for each of the five activities shown in Fig. 15.14. The power output for a given motor frame is limited by heating and by reactance, the latter of which is inversely related to maximum torque. Thus to select the power rating of the drive motor for a given duty cycle, the rms power requirements of that cycle are determined. Then, assuming a drive motor of that power rating, (1) the maximum torque which that motor would normally produce is compared with the maximum torque that the duty cycle requires and (2) the motor's safe temperature limit is compared with that activity within the duty cycle which has the greatest value of $(\mathrm{hp})^2t$. Concerning criterion 1, the maximum torque of the motor at the voltage that exists at the motor terminals must exceed the maximum torque requirement of any activity, with some margin. Also, concerning criterion 2, a given motor will have a short-time overload capacity. However, the duty-cycle activity that produces the greatest heating [i.e., the maximum value of $(\mathrm{hp})^2t$] should be evaluated. If the time interval of that activity is at all significant, the application engineer should verify with the potential motor manufacturer that a motor of the rms hp rating can be safely overloaded by that amount for that period. Adjustments should be made in the rms hp rating if required after consideration of criteria 1 and 2. Frequently, but not always, these criteria do not require an increase in rating over the initial calculation of rms hp rating.

The calculation of the rms hp requirement of a typical duty cycle can be illustrated by an algebraic example. Consider Fig. 15.14. The power

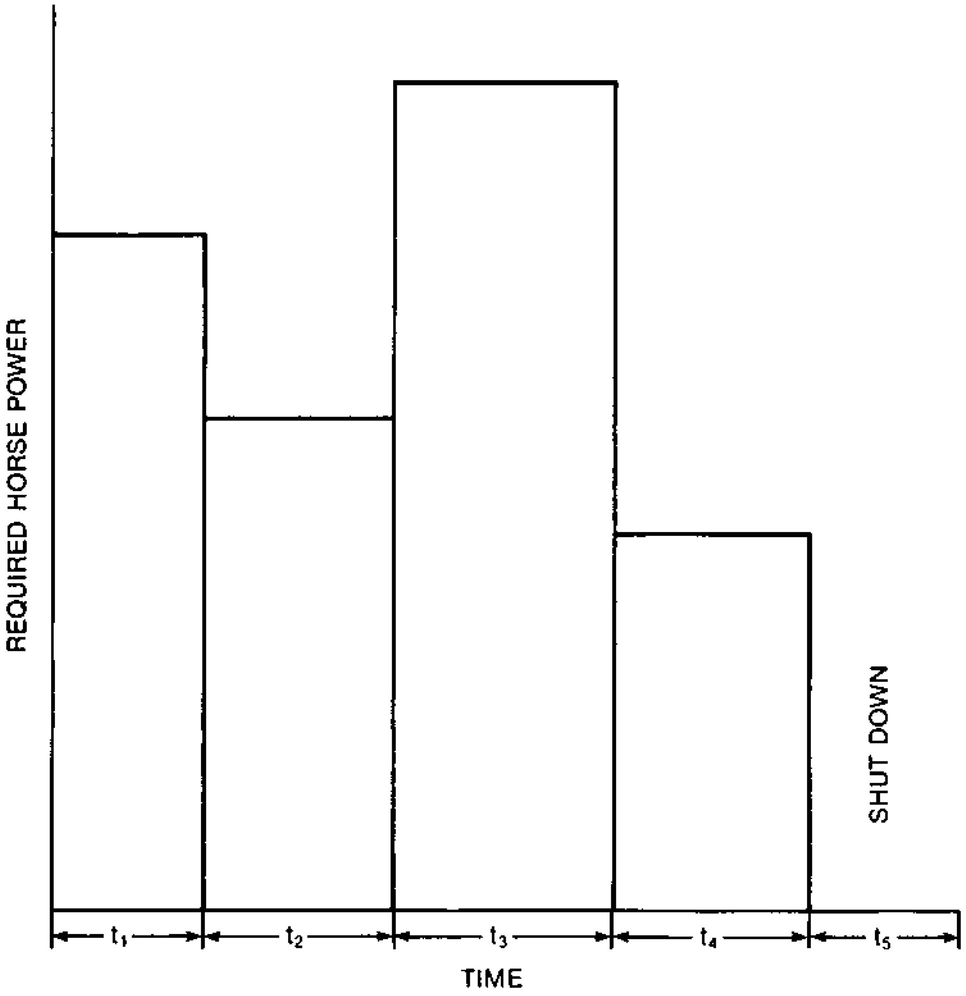

FIGURE 15.14 Graphical representation of a duty-cycle application.

duration and the time interval of four activities are shown. The fifth and last activity of the duty cycle consists of shutting down the drive for t_5 minutes. During this period the motor is not producing losses, to add further to heating. It could be argued, then, that for purposes of sizing the drive motor, the duty cycle time should be limited to the sum of t_1, t_2, t_3, and t_4. However, since the motor is not rotating during the fifth activity, cooling air is not flowing through it and the heat energy already in the machine parts is not being effectively transferred during this period. The conventional way in which this is handled is to divide the shutdown time by 3 or 4 when calculating the rms hp rating of the duty cycle. Then the duty cycle, given in Fig. 14, requires a drive motor with a rms power rating of

$$\mathrm{hp} = \sqrt{\frac{(\mathrm{hp}_1)^2 t_1 + (\mathrm{hp}_2)^2 t_2 + (\mathrm{hp}_3)^2 t_3 + (\mathrm{hp}_4)^2 t_4}{t_1 + t_2 + t_3 + t_4 + t_5/4}} \quad \text{horsepower} \qquad (15.61)$$

List of Symbols

A	area, meters^2 or inches^2; also a constant
A_c	cross-sectional area of core yoke, to carry flux, meters^2 or inches^2
A_g	cross-sectional area/pole of air gap, meters^2 or inches^2
A_r	cross-sectional area of end ring, meters^2 or inches^2
A_t	average cross-sectional area/pole of teeth, meters^2 or inches^2
a	ratio of effective stator turns to effective rotor turns
B	flux density, webers/meter^2 or maxwells/inch^2; also a constant
B_c	maximum flux density in core, webers/meter^2 or maxwells/inch^2
B_t	maximum flux density in teeth, webers/meter^2 or maxwells/inch^2
C	capacitance, farads; also number of parallel circuits/phase
CL	core loss, watts
D	loss density, watts/meter^2, or watts/inch^2; also electric flux density, coulombs/meter^2 or coulombs/inch^2; also depthwise slot dimension, meters or inches; also outside diameter of stator, meters or inches; also a constant
D_r	mean diameter of end ring, meters or inches
d	diameter of stator bore, meters or inches; also depthwise slot dimension, meters or inches
d_r	outside diameter of rotor, meters or inches
E	induced voltage, volts or per unit; also electric field strength, volts/meter or volts/inch
E_r	open-circuit voltage between collector rings, line-to-line volts or per unit
e	instantaneous value of induced voltage, volts
F	force, newtons or pounds; also magnetomotive force, ampere-turns
f	frequency, hertz
F&W	friction and windage losses, watts or horsepower
g	actual length of the air gap, meters or inches; also loss density, watts/meter^3 or watts/inch^3; also electrical gradient, volts/meter or volts/inch
g'	effective length of gap, meters or inches

H	magnetic field strength, ampere-turns/meter or ampere-turns/inch
hp	horsepower
h	magnetic field strength, ampere-turns/meter or ampere-turns/inch
I	rotational inertia, kilogram-meters^2; also current, amperes or per unit
I_1	stator current/phase, amperes or per unit
I_2	rotor current/phase, amperes or per unit
I_{12}	load component of rotor current, referred to the stator, amperes or per unit
I_b	rotor-bar current, amperes/bar
I_ℓ	blocked-rotor current, amperes/phase or per unit
I_m	magnetizing current/phase, amperes or per unit
I_r	end-ring current, amperes/ring; also current through collector ring, amperes/ring or per unit
i	instantaneous value of current, amperes
J	energy, joules; also torque, newton-meters or pound-feet
j	imaginary operator; also current density, amperes/meter^2 or amperes/inch^2
K	dielectric constant; also a constant; also radius of gyration, meters or feet
K_b	belt leakage factor
K_d	winding distribution factor
K_f or K_f'	air-gap fringing factor, also called Carter's coefficient
$K_M = K_s$	slot-reactance mutual factor
K_p	coil-pitch factor
K_s	skew factor; also saturation factor
L	inductance, henrys; also loss, watts
LL	load loss, watts
L_1	stator-winding leakage inductance, henrys
L_2	rotor-winding leakage inductance, henrys
L_m	magnetizing inductance, henrys
ℓ	length, meters or inches
ℓ_c	core length, meters or inches
M	mutual inductance, henrys
m	mass, kilograms
mmf	magnetomotive force, ampere-turns
N	number of turns; also number of harmonic poles; also a constant
N_1	number of stator slots
N_2	number of rotor slots
N_c	number of turns/coil
N_g	number of series coils/phase
N_{st}	number of series turns/phase
N_v	number of radial ventilating ducts
n	rotational speed, rpm or per unit; also harmonic order

n_s	synchronous speed, rpm or per unit
P	power, watts or horsepower; also permeance, webers/ampere-turns
P_e	eddy-current loss, watts/meter^3 or watts/inch^3
PF	power factor, per unit
P_h	hysteresis loss, watts/meter^3 or watts/inch^3
p	number of poles; also pressure, pascals or pounds/inch^2
Q	electric charge, coulombs
q	number of phases; also electric charge, coulombs
R	resistance, ohms or per unit; also reluctance, ampere-turns/weber; also a vector resultant
R_1	resistance of stator winding, ohms/phase or per unit
R_2	resistance of rotor winding, ohms/phase or per unit
r	resistance, ohms or per unit
s	slip, per unit
T	torque, newton-meters or pound-feet
T_L	load torque, newton-meters or pound-feet
T_m	motor torque, newton-meters or pound-feet
t	time, seconds; also thickness, meters or inches
V	voltage, volts; also velocity, meters/second or feet/second; also volume, meters^3 or inches^3
V_1	voltage impressed on stator winding, volts/phase or per unit
V_2	voltage measured across slip rings, line-to-line volts or per unit
V_s	sparking potential of a gas, volts
VA	volt-amperes
v	instantaneous voltage, volts; also velocity, meters/second or feet/second
W	power, watts; also weight, kilograms or pounds
WK^2	(weight)(radius of gyration)^2, used in the FPS system of units, pound-feet^2
w	power, watts; also widthwise slot dimension, meters or inches
X	reactance, ohms; also spatial dimension, meters or inches; also symbol for vector cross product
X_b	belt leakage reactance, ohms/phase or per unit
X_e	end-turn leakage reactance, ohms/phase or per unit
X_m	magnetizing reactance, ohms/phase or per unit
X_{s1}	stator-slot leakage reactance, ohms/phase or per unit
X_{s2}	rotor-slot leakage reactance, ohms/phase or per unit
X_{sk}	skew leakage reactance, ohms/phase or per unit
X_z	zigzag leakage reactance, ohms/phase or per unit
x	spatial dimension, meters or inches; also reactance, ohms
Y	admittance, siemens
y	admittance, siemens; also spatial dimension, meters or inches
Z	impedance, ohms
Z_ℓ	blocked-rotor impedance, ohms/phase or per unit

Z_0	characteristic impedance or surge impedance of a winding, ohms
Z_{oc}	open-circuit impedance, ohms
Z_s	conductors/slot
Z_{sc}	short-circuit impedance, ohms
z	spatial dimension, meters or inches
α	angle, radians or degrees; also attenuation factor of a winding, relative to a surge, radians/meter or radians/foot; also angular acceleration, radians/second^2
β	angle, radians or degrees; also wavelength factor of a winding, relative to a surge, radians/meter or radians/foot
γ	angle, radians or degrees; also propagation constant of a winding relative to a surge, radians/meter or radians/feet
Δ	increment, when used with a variable such as t, to give Δt
δ	depth of penetration, 1/meters or 1/feet; also defect angle of a dielectric material, radians or degrees
ϵ	permittivity, farads/meter; also base of the natural logarithm
η	efficiency
θ	power-factor angle, radians or degrees; also any angle, radians or degrees
θ_c	phase angle between currents in the top and in the bottom coil sides, radians or degrees
λ	permeance, webers/ampere-turn
μ	permeability, henrys/meter; also coefficient of friction
$\mathcal{E}$	energy stored in a rotating system, joules
ρ	resistivity, ohms-meters or ohm-inches
σ	factor in Carter's coefficient
τ	pitch, or distance between successive elements of an iterative structure, meters or inches
ϕ	flux, webers or maxwells
ϕ_p	flux/pole, webers or maxwells
ψ	flux linkage, webers or weber-turns, or maxwells or maxwell-turns
ω	angular velocity, radians/second

Bibliography

Alexander, D. F. (1928). Fractional Pitch Windings for Induction Motors, Electric Journal, 25: 77-82.

Alger, P. L. (1928). The Calculation of the Armature Reactance of Synchronous Machines, AIEE Transactions, 47: 493-512.

Alger, P. L. (1930). Induction Motor Performance Calculations, AIEE Transactions, 49: 1055-1066.

Alger, P. L. (1947). The Air-Gap Reactance of Polyphase Machines, AIEE Transactions, 66: 1331-1343.

Alger, P. L. (1970). *Induction Machines, Their Behavior and Use*, Gordon and Breach, Science Publishers, New York.

Bahbouth, S., Roye, D., Perret, R., and LeHuy, H. (1980). Heating of a Static Inverter Fed Induction Machine, *IEEE Conference Record of IAS 15th Annual Meeting*, pp. 540-544.

Bendz, W. I. (1938). Comparison of Methods of Stopping Squirrel-Cage Induction Motors, AIEE Transactions, 57: 499-505.

Bewley, L. V. (1930). Induced Voltage of Electric Machines, AIEE Transactions, 49: 456-466.

Bitter, F. (1934). Recent Theories of Magnetism, AIEE Transactions, 53: 1246-1250.

Bloomquist, W. C., and Boice, W. K. (1945). Application of Capacitors for Power Factor Improvement of Induction Motors, AIEE Transactions, 64: 274-278.

Boehne, E. W. (1930). Voltage Oscillations in Armature Windings Under Lightening Impulses, AIEE Transactions, 49: 1587-1607.

Bragg, L. (1945). Magnetic Materials, Journal of the IEE, 92: 444-451.

Calvert, J. F. (1938). Amplitude of Magnetomotive Force Harmonics for Fractional Slot Windings, Part I, AIEE Transactions, 57: 777-785.

Carter, F. W. (1926). The Magnetic Field of the Dynamo-Electric Machine, Journal of the IEE, 64: 1115-1138.

Clayton, A. E. (1923). A Mathematical Development of the Theory of the Magnetomotive Force of Windings, Journal of the IEE, 61: 749-787.

Cobine, J. D. (1941). Gaseous Conductors, McGraw-Hill Book Company, New York.

Cochran, P. L. (1953). Dynamic Braking Characteristics of Wound Rotor Motors, AIEE Transactions, 72, part 3: 992-996.

Cochran, P. L. (1965). Protecting Motor Windings from Surges, Power, 109: 89-90.

Cochran, P. L. (1969). Class F Rating for Industrial Generators, Power, 133: 86-87.

Cole, G. H. (1924). Effect of Punching Strains on the Magnetic Properties of Electrical Sheet Steel, Electric Journal, 21: 55-61.

Concordia, C. (1946). Rotating Electric Machine Time Constants at Low Speeds, AIEE Transactions, 65: 882-887.

Concordia, C., Carey, S. B., and Kron, G. (1942). The Doubly Fed Machine, AIEE Transactions, 61: 286-289.

Cotton, H. (1923). The Operation of Induction Motors in Cascade, AIEE Transactions, 61: 284-293.

Cummings, P. G. (1986). Estimating Effect of System Harmonics on Losses and Temperature Rise of Squirrel Cage Motors, IEEE Transactions, IA-22, no. 6: 1121-1126.

Devins, J. C., and Sharbaugh, A. H. (1961). The Fundamental Nature of Electrical Breakdown, Electro-Technology, February: 104-122.

Dreese, E. E. (1930). Synchronous Motor Effects in Induction Motors, AIEE Transactions, 49: 1033-1040.

Gilman, R. E. (1920). Eddy Current Losses in Armature Conductors, AIEE Transactions, 39, part 1: 997-1048.

Gilman, R. E. (1924). Eddy Current Losses in Armature Conductors, AIEE Transactions, 43: 246-249.

Graham, Q. (1927). The M.M.F. Wave of Polyphase Windings with Special Reference to Sub-synchronous Harmonics, AIEE Transactions, 46: 19-28.

Graham, Q. (1940). Dead Spots in Squirrel-Cage Motors, AIEE Transactions, 59: 637-642.

Guillemin, E. A. (1949). The Mathematics of Circuit Analysis, John Wiley & Sons, Inc., New York.

Hague, B. (1917). The Mathematical Treatment of the Magnetomotive Force of Armature Windings, Journal of the IEE, 55: 489-514.

Harrell, F. E., and Hough, W. R. (1935). DC Braking of Induction Motors, AIEE Transactions, 54: 488-493.

Hellmund, R. E. (1907). Zig-Zag Leakage of Induction Motors, AIEE Transactions, 26, part 2: 1505-1524.

Hildebrand, L. E. (1930). Quiet Induction Motors, AIEE Transactions, 49: 848-852.

Hildebrand, L. E. (1939). Duty Cycles and Motor Ratings, AIEE Transactions, 58: 478-483.

Hoxie, G. L. (1903). The Induction Motor and Its Engineering Capabilities, Journal of the Franklin Institute, 156: 183-214.

Kalb, W. C. (1945). Maintenance of Good Brush Performance, AIEE Transactions, 64: 819-825.

Kilgore, L. A. (1931). Calculation of Synchronous Machines—Reactance and Time Constants Affecting Transient Characteristics, AIEE Transactions, 50: 1201-1213.

Kilgore, L. A. (1935). Effect of Saturation on Machine Reactance, AIEE Transactions, 54: 545-550.

Kincaid, C. W. (1923). Induction Motor Secondary Windings, Electrical Journal, 20: 410-419.

Kincaid, C. W. (1929). Characteristics and Curves of the Double Deck Induction Motor, Electrical Journal, 26: 22-25.

Kincaid, C. W., and Alexander, D. F. (1926). Polyphase Induction Motors with Double Squirrel Cage Windings, Electrical Journal, 23: 15-19.

Koch, C. J. (1932). Measurement of Stray Load Loss in Polyphase Induction Motors, AIEE Transactions, 51: 756-761.

Kron, G. (1930). Generalized Theory of Electrical Machines, AIEE Transactions, 49: 668-683.

Kron, G. (1931). Induction Motor Slot Combinations, AIEE Transactions, 50: 757-767.

Lawrence, R. R. (1940). Principles of Alternating Current Machinery, McGraw-Hill Book Company, New York.

Liwschitz, M. M. (1941). Damping and Synchronizing Torques of the Double Fed Asynchronous Machine, AIEE Transactions, 60: 923-924.

Liwschitz, M. M. (1942). Field Harmonics in Induction Motors, AIEE Transactions, 61: 797-803.

Liwschitz, M. M. (1944). Differential Leakage with Respect to the Fundamental Wave and to the Harmonics, AIEE Transactions, 63: 1139-1150.

Liwschitz, M. M. (1946). Differential Leakage of a Fractionsl-Slot Winding, AIEE Transactions, 65: 314-320.

Liwschitz, M. M., and Formhals, W. H. (1947). Some Phases of Calculation of Leakage Reactance of Induction Motors, AIEE Transactions, 66: 1409-1413.

Mathes, K. N. (1985). Thermal Aging of Electrical Insulation—Technology and Standardization, Electrical Insulation, 1: 29-35.

McLauchlin, N. W. (1915). The Magnetic Behavior of Iron Under Alternating Magnetization of Sinusoidal Wave Forms, Journal of the IEE, 53: 809-819.

Middendorf, W. H. (1958). Calculation of Induction Motor Torque and Power, AIEE Transactions, 73, part 3: 1055-1058.

Middendorf, W. H. (1962). An Approach to Induction Motor Synthesis, AIEE Transactions, 81, part 3: 64-69.

Middendorf, W. H. (1976). Methods for Improving Design Procedures, IEEE Transactions, E-19: 148-153.

Miner, D. F. (1941). *Insulation of Electrical Equipment*, McGraw-Hill Book Company, New York.

Moon, P. H. (1931). The Theory of Thermal Breakdown of Solid Dielectrics, AIEE Transactions, 50: 1008-1021.

Moon, P. H., and Norcross, A. S. (1930). Three Regions of Dielectric Breakdown, AIEE Transactions, 49: 755-765.

Morgan, E. L. (1947). An Application of the Theory of the Complex Variable to the Mapping of Some Potential Functions, Journal of the Franklin Institute, 243-244: 309-322.

Morgan, T. H., Brown, W. E., and Schumer, A. J. (1939). Reverse-Rotation Test for Determination of Stray Load Loss in Induction Machines, AIEE Transactions, 58: 319-364.

Morrill, W. J. (1940). Harmonic Theory of Noise in Induction Motors, AIEE Transactions, 59: 474-480.

Murnaghan, F. D. (1927). Maxwell's Theory of the Layer Dielectric, AIEE Transactions, 46: 259-266.

Nowacki, L. M. (1934). Induction Motors as Selsyn Drives, AIEE Transactions, 53: 1721-1726.

Peek, F. W. (1915). The Effect of Transient Voltages on Dielectrics, AIEE Transactions, 34, part 2: 1857-1909.

Reddick, H. W., and Miller, F. H. (1948). *Advanced Mathematics for Engineers*, John Wiley & Sons, Inc., New York.

Reist, H. G., and Maxwell, H. (1909). Multispeed Induction Motors, AIEE Transactions, 28: 601-609.

Robinson, R. C. (1943). The Calculation of Unbalanced Magnetic Pull in Synchronous and Induction Motors, AIEE Transactions, 62: 620-624.

Robinson, R. C. (1947). The Horsepower Output of Polyphase Induction Motors, AIEE Transactions, 66: 770-775.

Rosenberg, E. (1918). Magnetic Pull in Electric Machines, AIEE Transactions, 37, part 2: 1425-1469.

Rudge, W. J., Wiesman, R. W., and Lewis, W. W. (1933). Protection of Rotating AC Machines Against Traveling Wave Voltages Due to Lightning, AIEE Transactions, 52: 434-440.

Savage, R. H. (1945). Carbon Brush Contact Films, General Electric Review, 48: 13-20.

Sokolnikoff, I. S., and Sokolnikoff, E. S. (1941). *Higher Mathematics for Engineers and Physicists*, McGraw-Hill Book Company, New York.

Spooner, T. (1925). Squirrel-Cage Induction Motor Core Losses, AIEE Transactions, 44: 155-160.

Spooner, T., and Kinnard, I. F. (1924). Surface Iron Losses with Reference to Laminated Materials, AIEE Transactions, 43: 262-280.

Stein, J. M. (1947). The Magnetomotive Force of Two-Layer Windings of Rotating Machines, AIEE Transactions, 66: 756-758.

Steinmetz, C. P. (1892a). On the Law of Hysteresis, AIEE Transactions, 9: 3-51.

Steinmetz, C. P. (1892b). On the Law of Hysteresis and Other Phenomena of the Magnetic Circuit, Part II, AIEE Transactions, 9: 621-729.

Steinmetz, C. P. (1894). On the Law of Hysteresis (Part III) and the Theory of Ferric Inductances, AIEE Transactions, 11: 570-608.

Steinmetz, C. P. (1897). The Alternating Current Induction Motor, AIEE Transactions, 14: 185-217.

Steinmetz, C. P. (1911). Mechanical Forces in Magnetic Fields, AIEE Transactions, 30: 367-385.

Steinmetz, C. P., and Lamme, B. J. (1913). Temperature and Electric Insulation, AIEE Transactions, 32, part 1: 79-89.

Stevenson, A. R. (1926). Fundamental Theory of Flux Plotting, General Electric Review, 29: 797-804.

Wagner, K. W. (1922). The Physical Nature of the Breakdown of Solid Dielectrics, AIEE Transactions, 41: 288-298.

Wall, T. F. (1912). The Development of the Circle Diagram for the Three Phase Induction Motor, Journal of the IEE, 48: 499-507.

Ware, D. H. (1945). Measurement of Stray-Load Loss in Induction Motors, AIEE Transactions, 64: 194-197.

Weber, C. A. M., and Lee, F. W. (1924). Harmonics Due to Slot Openings, AIEE Transactions, 43: 687-693.

Whitehead, J. B. (1924). Gaseous Ionization in Built-Up Insulation, Part II, AIEE Transactions, 43: 116-122.

Whitehead, J. B. (1927). Lectures on Dielectric Theory and Insulation, McGraw-Hill Book Company, New York.

Whitehead, J. B., and Banos, A. (1932). Prediction of the A-C Characteristics of Dielectrics, AIEE Transactions, 51: 392-402.

Whitehead, J. B., and Marvin, R. H. (1929). Anomalous Conduction as a Cause of Dielectric Absorption, AIEE Transactions, 48: 299-313.

Whitehead, S. (1932). Dielectric Phenomenon, D. Van Nostrand Company, Princeton, N.J.

Williams, J. W. (1931). Recent Dielectric Constant Theory and Its Relation to Electric Insulation, Journal of the Franklin Institute, 211: 581-606.

Wooldridge, W. J. (1911). Hysteresis and Eddy Current Exponents for Silicon Steel, AIEE Transactions, 30, part 1: 215-217.

Index

Absorption, effect of, 378, 379
Acceleration
  current-time relationship during, 646-650
  heating from, 650-653
  speed-current relationship during, 646-650
  time of, 645, 646
Adjusted circle diagram
  concept of, 160, 161
  how constructed, 166-169
Adjusted voltage, definition of, 119
Air-gap permeance harmonics, source of, 451-453
Algorithms
  comparison of results, 175
  used for analysis, 33, 34
Ampère
  differential form of law, 6, 7
  law of, 5, 6
  vector form of law, 7
Asynchronous crawling, how produced, 456-458
Attenuation factor, definition of, 413

Balanced winding, determination of, 238-242
Bearing currents, source of, 359
Belt leakage factor, curve of, 526
Belt leakage reactance, derivation of, 523-527
Belt tension, derivation of, 604-608
Belted drives, alignment of, 613, 614
Bivot and Savart, work of, 5
Blocked-rotor current
  by test, 148-150
  equation for, 92
Blocked-rotor impedance, by test, 165, 166
Blocked-rotor losses, by test, 148-150, 163, 164
Blocked-rotor reactance
  example of calculation, 540-548
  method of calculation, 536-539
Braking
  by dc voltage on stator winding, 656-658
  by regeneration, 655
  by reverse-rotation voltage on stator winding, 653-655
  with multispeed motors, 656

Capacitance
  definition of, 366

[Capacitance]
  energy associated with, 369
  equation for, 368, 369
  to ground, 398-400
Carter's coefficient, derivation of, 582-585
Chain drives
  alignment of, 614
  description of, 608, 609
Characteristic impedance (see Surge impedance)
Charging current
  example of calculation, 402-404
  for high-potential testing, 401, 402
Circle diagram
  derivation of, 142-147
  from test data, 147-150
  interpretation of, 150, 151
  limitations of, 158-160
  status of, 142
Coils, types of, 180-185, 190, 191
Collector rings and brushes
  current flow in, 345-347
  electrical loss of, 351-353
  friction loss of, 349-351, 353
  how constructed, 347-349
Conductors
  definition of, 196, 197, 361
  materials used, 194-196
  properties of, 194, 195
Core loss
  components of, 67, 72, 73, 562-564
  effect on the equivalent circuit, 41, 42
  energy component of current, 42, 73, 74
  how modeled, 70
Corona, causes of, 396, 397
Couplings
  alignment of, 610-613
  types of, 602-604
Creepage, definition of, 424
Cut-out coils (see Failed stator coils)

DC motor, configuration of, 2
Deep-bar effect
  definition of, 278, 279
  derivation of, 278-292
  example of, 292-295
Demagnetizing ampere turns, due to rotor current, 44, 45, 127
Diamagnetism, definition of, 550, 551
Dielectric breakdown
  of gasses, 383, 384
  of liquids, 384, 385
  of solids, 385-387
Dielectric constant
  definition of, 363
  typical values of, 377
Dielectric loss
  dissipation factor of, 383
  equation for, 382
  loss factor of, 382
  vector diagram of, 381
Differential leakage reactance, concept of, 519
Distribution factor
  of the fundamental, 225-229
  of space harmonics, 229-231
Duty cycle
  concept of, 658
  selecting motor rating for, 658, 659

Eddy-current loss, in magnetic core, 558-561
Efficiency
  at full load, 70-75
  at part load, 76-81
  from the vector diagram, 137-139
Electric flux density, definition of, 364
Electrical gradient
  definition of, 364
  of two different materials in contact, 370, 371

End-turn leakage reactance
  concept of, 508-510
  derivation of, 510-518
Energy
  conversion by drive motor, 1, 13
  use by society, 1
Equivalent circuit
  calculation with actual quantities, 46-50
  calculation with per-unit quantities, 50-57
  choice of, 120, 121
  comparison of results, 118
  formulation of, 60-64
  to refer quantities from one side to the other, 46-50
Equivalent-circuit impedance, definition of, 45, 46
Equivalent T-network, determination from physical model, 36-41

Fabricated rotor winding, how produced, 269-273
Failed stator coils, operating with, 259-261
Faraday
  derivative form of law, 10, 11
  integral form of law, 12
  velocity form of law, 8, 9
  work of, 7, 8
Ferromagnetism, definition of, 551
Formed coils
  definition of, 190, 191
  how produced, 191, 192
  where applied, 190, 191
Formed-coil windings, how produced, 193, 194
Foundation, requirements of, 601, 602
Fourier series
  definition of, 429-431
[Fourier series]
  results of, 431
Fractional-slot windings
  definition of, 236, 237
  permissible configurations of, 236-238
Friction and windage
  as a retarding torque, 83
  at low speed, 85
  how represented, 72
  source of, 68, 69
Fringing factor, 591 (see also Carter's coefficient)

Gauss's theorem, as applied to an electric field, 365
Gear drives
  alignment of, 614
  description of, 609, 610

Induced rotor current
  how produced, 23, 24
  magnitude induced in rotor bar, 25
  magnitude induced in rotor coil, 26
  phase angle of, 25-27
Induced voltage
  in the rotor coils, 22, 23
  in the rotor winding, 18-21
  in the stator coils, 217-220
  in the stator phase winding, 231, 232
Insulation
  resistance of, 420-424
  strength of, 388-395
  temperature classes of, 419-420
Insulator, definition of, 361
Integral-slot windings
  definition of, 232, 233
  permissible configurations, of, 232-236

Iterative impedance (see Surge impedance)

Kirchoff's voltage equations, for the equivalent circuit, 64

Lattice network
  concept of, 298, 299
  derivation of, 299-305
  for calculating the ac resistance of a multiple-cage rotor bar, 309-312
  for calculating the ac resistance of a rectangular rotor bar, 305-309
Leakage reactance, concept of, 481-484, 486, 487
Load loss
  components of, 73
  explanation of, 564-566
  model for, 70
  procedure for use in equivalent circuit, 73, 74

Magnetic circuit, calculation of, 587-598
Magnetic core, how constructed, 567-574
Magnetic domains, definition of, 551
Magnetic hysteresis
  definition of, 553, 554
  loss from, 556, 557
Magnetic noise
  caused by magnetic force waves, 467-469
  compliance of stator core, 469-472
  definition of, 466
  frequency of, 475, 476
  how produced, 472-475
Magnetic pull
  definition of concentric component, 246-250
  definition of unbalanced component, 246
  derivation of concentric component, 246-250
  derivation of unbalanced component, 250-255
  effect of winding configuration, 255, 256
  example of calculation, 257-259
Magnetic saturation, explanation of, 552
Magnetizing current
  calculation of, 597, 598
  derivation of, 446-449
  of the vector diagram, 124
  one definition of, 61
Magnetizing reactance, derivation of, 484-486
Magnetomotive force
  graphical construction of wave shape, 441-445
  of a coil, 434
  of cooperating groups, 436
  of a phase winding, 438
  of the stator winding, 440
Maximum power, from the circle diagram, 153
Maximum power factor, from the circle diagram, 153, 154
Maximum torque
  equation for, 87-89
  example of calculation, 89, 90
  slip at, 85-87
Motor action
  definition of, 13, 14
  first requirement for, 14-18
  requirements for, 178
  second requirement for, 18-24
  third requirement for, 24-27
Multiple cage winding, concept of, 295-298

No-load current, from test, 147, 148, 162, 163
No-load losses, from test, 147, 148, 162, 163

Oersted, work of, 5
Output power, from the complete equivalent circuit, 67-70

Paramagnetism, definition of, 550, 551
Paschen's law
  definition of, 384
  in curve form, 385
Performance
  by the adjusted circle diagram, 170-176
  by the conventional circle diagram, 154-158
Permittivity, definition of, 362
Per-unit quantities, definition of, 50-54
Physical model representation, of the induction motor, 35, 36
Pitch factor
  for the fundamental, 220-223
  for space harmonics, 223, 224
Polarization, effect on dielectric constant, 374-377
Population, of polyphase induction motors, 3
Power factor
  at full load, 70-75
  at part load, 76-81
  from the vector diagram, 137, 139
Power-station auxiliary motors
  prevalence of, 4
  range of ratings, 4
Power transformation analysis, from the vector diagram, 128-131
Propagation constant, definition of, 409, 410

Radial decentering force (see Magnetic pull)
Random coils
  definition of, 185
  how produced, 186, 187
  where applied, 185, 186
Random windings, how produced, 187-190
Ratings, range of, 3
Reactance
  effect on output, 480, 481
  effect on performance, 480, 481
Ring testing of magnetic cores
  how performed, 576-580
  why required, 575, 576
Rotating magnetic field
  production of, 14-18
  strength of, 17
Rotor bars, transient temperature rise of, 326-328
Rotor-circuit frequency, relation to slip, 63
Rotor current, from the complete equivalent circuit, 66, 67
Rotor end rings, transient temperature rise of, 326-328
Rotor harmonics, source of, 453
Rotor skew
  concept of, 312
  effect on slot harmonics, 312
Rotor-slot harmonics, characteristics of, 451
Rotor-slot leakage reactance, derivation of, 499-508
Rotor winding, types of, 265, 266
Running reactance, example of calculation, 529-536

Saturation curve, derivation of ac curve from the normal dc curve, 585-587
Shaft voltages
  causes of, 580
  how prevented, 581
Siemens, discovery by, 361, 380
Simplified equivalent circuit
  adjusted voltage for, 119
  background of, 98
  magnetizing current from, 99
  maximum torque from, 105-109
  numerical example of, 111-118
  phase current from, 98-101
  power output from, 101-103
  starting torque from, 109, 110
  torque output from, 104, 105
Single-phase representation, of the induction motor, 34
Skew factor
  derivation of, 312-315
  example of, 315
Skew leakage reactance, derivation of, 527-529
Slip, definition of, 62
Slot-leakage factor, 501
Slot-loss factor
  equations for, 209, 210
  example of, 210-217
Space harmonics
  characteristics of, 449, 450
  equivalent circuit of, 446
  of a three-phase stator winding, 440
Speed control
  background of, 627, 628
  by cascading two machines, 630, 631
  by constant volts/cycle on stator circuit, 639-642
  by injecting a voltage into rotor circuit, 631-633
  by multispeed motors, 635-639
[Speed control]
  by slip couplings, 642-644
  by varying stator voltage, 633, 634
  of wound-rotor motors, 628, 629
Speed-current curve, explanation of, 95, 96
Speed-torque curve
  explanation of, 93-95
  of generating region, 456
  of motoring region, 455
  of reverse-rotation region, 455, 456
  of a wound-rotor motor, 94, 95
  perturbations of, 453, 454
Squirrel-cage rotor windings
  mechanical stresses in, 274, 275
  production of, 266-269
  resistance of, 316-322
  thermal stresses in, 275, 276
  types of, 276, 277
Stall time, definition of, 623, 624
Starting
  by autotransformer, 616-618
  by part-winding connections, 622, 623
  by series-parallel connections, 621, 622
  by series reactor, 619, 620
  by series resistor, 618, 619
  by solid-state circuitry, 621
  by wye-delta connections, 620
  frequency of, 652, 653
  limitations on, 614-616
  of wound-rotor motors, 624-627
Starting current, equation for, 92
Starting torque
  equation for, 90, 91
  for a wound-rotor motor, 91, 92
Stator coils, definition of, 179, 180
Stator connection diagram, 245, 246

Stator current
  from the complete equivalent circuit, 64, 65
  from the vector diagram, 127
Stator-slot harmonics, characteristics of, 450, 451
Stator-slot leakage reactance, derivation of, 487-499
Strands
  circulating currents between, 205-209
  definition of, 196, 197
  eddy-current losses in, 197-205
Surge impedance
  definition of, 408, 409
  typical values of, 414
Synchronous crawling torques
  how prevented, 462
  how produced, 462
Synchronous locking torques
  how prevented, 459
  how produced, 458, 459
Synchronous motor, configuration of, 2

Tesla, invention of polyphase induction motor, 4, 5
Time harmonics, definition of, 641, 642
Torque
  alternating component of, 29
  alternate derivation of, 134-137
  constant component of, 29-31
  derivation of equation for, 81-85
  from adjusted circle diagram, 169, 170
  from the circle diagram, 151-153
  from the vector diagram, 132, 133, 139
  production of, 2, 3, 13, 14, 28-32
[Torque]
  relationship to power and speed, 81, 83
Tracking, definition of, 424
Tractive force, equation of, 250
Transient temperature rise, from change in speed, 322-328
Turns, definition of, 196, 197
Turns ratio
  definition of, 43
  effect on the equivalent circuit, 43-46

Unbalanced winding, analysis of, 242-245

Vector cross product
  definition of, 7
  use in expressing torque, 134
Vector diagram
  construction of, 126, 127
  derivation of, 123-126
  interpretation of, 127, 128
  viewpoint of, 125, 126
Vector dot product, application to power transformation, 128-131
Voltage ripple, how calculated, 478
Voltage surges
  behavior of, 414, 415
  causes of, 405
  control of, 415-419
  impedance to, 408, 409
  velocity of, 414

Wavelength factor, definition of, 413
Windage noise, definition of, 466

Wound-rotor windings
  banding of end turns, 353-355
  description of, 333-340
  distribution factor for, 341, 342
  effect of centrifugal force in design of, 330, 331
  pitch factor of, 342
  phase current in, 343, 344
[Wound-rotor windings]
  phase resistance of, 344, 345
  types of wave windings, 331-333
  voltage induced in, 342

Zigzag leakage reactance, derivation of, 519-523

about the book . . .

Generously illustrated with over 1600 display equations and more than 145 drawings, diagrams, and photographs, ***Polyphase Induction Motors*** is a handy, single-source reference suited to readers with a wide span of educational backgrounds and technical experience.

Comprehensive both in scope and depth—*destined to become the primary source of polyphase induction motor analysis*—this indispensable manual covers all significant aspects of the field . . . reviews fundamental laws of physics such as Ampère's Law and Faraday's Law, emphasizing basic explanations of motor behavior . . . derives all important equations and relationships required to analyze, design, and apply polyphase induction motors . . . uses the worldwide SI or international MKS system of units to derive working equations, and displays them in terms of SI units, as well as practical units still widely used in the United States . . . shows how to apply working equations to real-life situations with numerical examples . . . and more.

Integrating important theory and technique, this very useful sourcebook is essential reading for electrical and electronics, applications, manufacturing, mechanical, power, production, design, development, project, chemical, and petroleum engineers; electric motor manufacturers, electric utilities' staff, and government power authorities; and undergraduate and graduate students in the above disciplines.

about the author . . .

PAUL L. COCHRAN is a Private Consultant in Schenectady, New York. His roster of clients has included the General Electric Company, Schenectady, New York, and Electric Power Research Institute, Palo Alto, California, among other organizations. Mr. Cochran retired from the General Electric Company in 1982, where he had served as an employee for 27 years in various engineering and managerial capacities including production, design, development, and project engineer, technical leader, and manager of an engineering unit and subsection. He received a General Manager's Award and various other General Electric awards, as well as several patent awards. Mr. Cochran is a life senior member of the Institute of Electrical and Electronics Engineers, and a member of the American Society of Mechanical Engineers, and New York Academy of Sciences. He received the B.S. degree (1943) in electrical engineering from the University of Illinois at Urbana-Champaign, and M.S. degree (1950) in electrical engineering from the University of Pittsburgh in Pennsylvania.

Printed in the United States of America ISBN: 0—8247—8043—4

marcel dekker, inc./new york · basel